APPENDIX A
ACRONYMS AND ABBREVIATIONS

A. ACRONYMS

ACM	alternative conceptual model
BDCF	biosphere dose conversion factor
BWR	boiling water reactor
CCDF	complementary cumulative distribution function
CDF	cumulative distribution function
CDSP	co-disposed
CSNF	commercial spent nuclear fuel
CSNF-SS	commercial spent nuclear fuel-stainless steel
CSNF-Z	commercial spent nuclear fuel-Zircaloy (zirconium-based cladding)
DI	document identifier
DIRS	Document Input Reference System
DLL	dynamically linked library
DOE	U.S. Department of Energy
DS	drip shield
DSNF	DOE spent nuclear fuel
DTN	data tracking number
EBS	engineered barrier system
ECRB	Enhanced Characterization of Repository Block
EF	early failure (only used in modeling cases)
EIS	Environmental Impact Statement
EPA	U.S. Environmental Protection Agency
EPRI	Electric Power Research Institute
ESF	Exploratory Studies Facility
FD	fault displacement (only used in modeling cases)
FEHM	Finite Element, Heat and Mass (Model)
FEIS	Final Environmental Impact Statement
FEP	feature, event, or process
GM	ground motion (only used in modeling cases)
GLUE	generalized likelihood uncertainty estimation
HLW	high-level radioactive waste
IAEA	International Atomic Energy Agency
IDPS	in-drift precipitated salts
IMARC	Integrated Multiple Assumptions and Release Code
INEEL	Idaho National Engineering and Environmental Laboratory
IRT	International Review Team
IVRT	Independent Validation Review Team
LA	License Application

ACRONYMS (Continued)

LaBS	lanthanide borosilicate
LHS	Latin hypercube sample
MIC	microbially influenced corrosion
MINC	Multiple Interacting Continua
MOX	mixed oxide fuel
MSTHM	Multiscale Thermohydrologic Model
NEA	Nuclear Energy Agency
NRC	U.S. Nuclear Regulatory Commission
NSNF	naval spent nuclear fuel
NWTRB	Nuclear Waste Technical Review Board
OCRWM	Office of Civilian Radioactive Waste Management
ODBC	Open Database Connectivity
OCB	outer corrosion barrier
PA	Performance Assessment
P&CE	Physical & Chemical Environment (as in P&CE container)
PDF	Parameter Documentation Form
PEF	Parameter Entry Form
pdf	Probability Density Function
PGA	peak ground acceleration
PGV	peak ground velocity
PMA	Performance Margin Analysis
PIF	Parameter Identification Form
PRCC	Partial Rank Correlation Coefficient
PSHA	Probabilistic Seismic Hazard Analysis
PVEF	Parameter Value Entry Form
PVF	Parameter Verification Form
PVHA	probabilistic volcanic hazard analysis
PWR	pressurized water reactor
QA	quality assurance
QARD	Quality Assurance Requirements and Description
RAM	random access memory
RMEI	reasonably maximally exposed individual
RST	residual stress threshold
SAR	Safety Analysis Report
SCC	stress corrosion cracking
SCM	Software Configuration Management
SD	standard deviation
SME	subject matter expert
SNF	spent nuclear fuel

ACRONYMS (Continued)

SNL	Sandia National Laboratories
SRC	Standardized Regression Coefficient
SRRC	Standardized Rank Regression Coefficient
SZ	saturated zone
TAD	Transportation, aging, and disposal
TDMS	Technical Data Management System
TH	thermal-hydrologic
THC	thermal-hydrologic-chemical
TSPA	Total System Performance Assessment
TSPA-LA	Total System Performance Assessment for the License Application
TSPA-SR	Total System Performance Assessment for the Site Recommendation
TSPA-VA	Total System Performance Assessment for the Viability Assessment
TWP	Technical Work Plan
UTM	Universal Transverse Mercator grid
UZ	unsaturated zone
WAPDEG	waste package degradation model
WP	waste package
YMP	Yucca Mountain Project

INTENTIONALLY LEFT BLANK

A2. ABBREVIATIONS

acre-ft	acre-foot
atm	atmospheres
C	Celsius
Ci	curie
cm	centimeter
F	Fahrenheit
fco_2	fugacity of CO_2
f_{ff}	flow focusing factor
ft	foot
G	constant of gravity
g	gram
gal	gallon
GB	gigabytes
Gbps	gigabytes per second
GHz	gigahertz
GWd	gigawatt-day
hr	hour
Hz	hertz
in.	inch
K	Kelvin
K_d	distribution coefficient (mL/g)
kg	kilogram
kJ	kilojoules
km	kilometer
kVA	kilovolt ampere
kW	kilowatt
L	liter
lb	pound
log( )	logarithm
ln()	natural logarithm
m	meter
Mbps	megabits per second
mg	milligram
MHz	megahertz
mi	mile
mL	milliliter
M_L	local magnitude

ABBREVIATIONS (Continued)

mm	millimeter
M_{max}	maximum magnitude
M_{min}	minimum magnitude
mol/L	molarity
mol/kg	molality
mph	mile per hour
mrem	millirem
mSv	millisievert
mT	metric tons
MTHM	metric tons of heavy metal
MW	megawatt
M_w	moment magnitude
µm	micrometer (micron)
nm	nanometer
Pa	pascal
pCi	picocurie
pCO_2	negative log of the partial pressure of CO_2
Pco_2	partial pressure of CO_2
pH	scale of acidity and alkalinity (hydrogen ion concentration notation)
pO_2	negative log of the partial pressure of O_2
Po_2	partial pressure of O_2
ppb	parts per billion
ppm	parts per million
psi	pounds per square inch
rem	roentgen equivalent man
s or sec	second
TB	terabyte
t, τ	time
W	watt
yr	year

APPENDIX B
DATA TRACKING NUMBERS FOR THE TSPA-LA MODEL

B1. INTRODUCTION

Appendix B describes the interrelationships among the Total System Performance Assessment for the License Application (TSPA-LA) Model output data tracking numbers (DTNs) for the TSPA-LA Model. Figure B-1 shows the information flow among the output DTNs submitted to the Technical Data Management System (TDMS).

The DTNs contain work products (e.g., Microsoft Excel spreadsheets, TSPA Model files, etc.) that are not captured directly in the *Total System Performance Assessment Model/Analysis for the License Application*. The DTNs have been submitted to TDMS.

The following sections contain brief descriptions of the contents of the DTNs. The respective ReadMe.doc file located in each DTN provides more detailed information on the contents of each DTN. Figures B-1 and B-2 provide an overview of the relationships between the DTNs.

B2. DESCRIPTIONS OF THE DATA TRACKING NUMBERS

The following text supports Figures B-1 and B-2. Each block on Figures B-1 and B-2 is described below.

B2.1 MODEL DEVELOPMENT RECORDS PACKAGE

Reference Figure B-1, Block 1, and Figure B-2, Block 105—This records package documents each of the model changes that were generated since v3.007 of the Model, which is documented in DTN: MO0506MWDTLMV3.000_R0 [DIRS 174809]. In order to clearly demark the first step toward building a 10,000-year/peak dose model, the versioning started with v4.000. This records package contains v4.000 through v4.047 of the Groundwater Model and v.E1.000 through vE1.003 of the Eruptive Model. All model versions generally follow the same folder content. For example, the content for a typical folder would contain a Master Folder and the specific case folders that were appropriate at that stage of model development. Examples of case folders are as follows: (1) HI 1Myr, (2) Ign 1Myr, (3) Nominal 1Myr, and (4) Seismic EF 10kyr. Each Master Folder generally contains the following:

- One or more change approval forms
- Change checklist
- Checking checklist
- Conceptual checklist
- Conceptual description
- GoldSim model file
- GoldSim version report
- Additional information directory (optional)

This records package feeds output DTN: MO0709TSPAREGS.000_R0 [DIRS 182976], which contains the final versions of the Groundwater Model (v5.000) and the Eruptive Model (vE1.004). This records package also feeds output DTN: MO0708TSPAPOST.000_R0 [DIRS 182986], which contains the Post Implementation Verification Tests.

B2.2 V4.042 AND VE1.003 RECORDS PACKAGE

Reference Figure B-1, Block 2—Block 2 is on Figure B-1 to clearly indicate which versions of the model were used for this activity. The justifications for the versions used are discussed in Section 7.2.

B2.3 TSPA-LA MODEL POST IMPLEMENTATION VERIFICATION TESTS: OUTPUT DTN: MO0708TSPAPOST.000_R0 [DIRS 182986]

Reference Figure B-1, Block 3—This DTN contains the model cases and supporting checking documentation for the post-implementation verification tests discussed in Section 7.2.

B2.4 PLOTS AND FIGURES FOR THE TSPA-LA DOCUMENT: OUTPUT DTN: MO0709TSPAPLOT.000_R0 [DIRS 183010]

Reference Figure B-1, Block 4 and Figure B-2 Block 109—This DTN contains the official version of the sigma plot files for all the plots used in this document. In addition, any checklists used for checking of the plots will also be included.

B2.5 TSPA-LA PARAMETER SENSITIVITY ANALYSIS: OUTPUT DTN: MO0709TSPASENS.000_R0 [DIRS 182982]

Reference Figure B-1, Block 5—This DTN contains analyses to evaluate the significant uncertain parameters in the TSPA-LA Groundwater and Eruptive Models that are documented in output DTN: MO0709TSPAREGS.000_R0 [DIRS 182976].

B2.6 TSPA-LA MODEL CASES THAT EVALUATE NAVAL SPENT NUCLEAR FUEL: OUTPUT DTN: MO0707NAVYFUEL.000_R0 [DIRS 182991]

Reference Figure B-1, Block 6—This DTN contains the TSPA-LA Model cases, including checking documentation, that were run to evaluate the representation of naval spent nuclear fuel in the TSPA-LA Model as discussed in Section 7.5.3.

B2.7 TSPA-LA GW & E WITH FINAL DOCUMENTATION: OUTPUT DTN: MO0708GWEFINAL.000_R0 [DIRS 182977]

Reference Figure B-1, Block 7—This is the version of the TSPA-LA Groundwater and Eruptive Model (v5.000 and vE1.004) that is used to generate the GoldSim Player Files that supports the TSPA-LA. The differences between the GoldSim files in this DTN versus output DTN: MO0709TSPAREGS.000_R0 [DIRS 182976] are that this DTN contains only the master files for v5.000 and E1.004. These master files have been modified to update the explanatory text. The explanatory text that is in output DTN MO0709TSPAREGS.000_R0 [DIRS 182976] should be ignored, since it is not current. The enclosed master files have not been run; therefore, there are no results in this DTN. The value in providing un-run files is the files can be opened on most current model personal computers. The value in adding the documentation is an interested party can read the embedded text to obtain an overview of how the model is constructed. Also included is a data-only copy of the TSPA Input Database. The value of the data-only version of the TSPA Input Database is an interested party can review the input parameters to quickly

determine the numerical value of a parameter as well as the product that the value is documented within. In most cases, the product is an output DTN from a model and/or analysis report.

B2.8 TSPA GENERATED INPUTS AND POST-PROCESSED INPUTS: OUTPUT DTN: MO0708TSPAGENT.000_R0 [DIRS 183000]

Reference Figure B-1, Block 8—This DTN contains inputs that fall into two categories: (1) TSPA-LA Model-generated inputs and (2) Post-Processed inputs. TSPA-LA Model-generated inputs do not have any external inputs used to create the input values. Post-Processed inputs do have external inputs supplied by supporting Analysis and Model Reports. These external inputs must be Post-Processed for use in the TSPA-LA Model.

B2.9 DECAY OF WASTE FORM INVENTORIES FROM FINAL EMPLACEMENT TO CLOSURE: OUTPUT DTN: MO0707EMPDECAY.000_R0 [DIRS 182995]

Reference Figure B-1, Block 9—This DTN contains the GoldSim files used to decay the TSPA-LA waste form inventories from their time of emplacement to repository closure (i.e., the start of postclosure). The decayed inventory is an input to the TSPA-LA Model. This calculation is discussed in more detail in Section 6.3.7.1.2.1.

B2.10 PREWAP PROCESSING OF MSTHM FILES: OUTPUT DTN: MO0707PREWAPMS.000_R0 [DIRS 183002]

Reference Figure B-1, Block 10—This DTN contains the Multiscale Thermohydrologic Model (MSTHM) input files that are processed by PREWAP software and the resultant output files that are an input to the TSPA-LA Model. The DTN includes a description of how PREWAP was run. This calculation is discussed in more detail in Section 6.3.2.3.

B2.11 TSPA-LA REPRESENTATION OF DOE SPENT NUCLEAR FUEL: OUTPUT DTN: MO0707TSPADSNF.000_R0 [DIRS 182992]

Reference Figure B-1, Block 11—This DTN contains the TSPA-LA Model cases, including checking documentation, that were run to evaluate Categories 2 through 11 of U.S. Department of Energy spent nuclear fuel as discussed in Section 7.5.4.

B2.12 TSPA RESULTS FOR SEIS: DTN: MO0708TSPASEIS.000_R0 [DIRS 183009]

Reference Figure B-1, Block 12—This DTN contains the identical GoldSim files that are included in the Regulatory Compliance output DTN MO0709TSPAREGS.000_R0 [DIRS 182976] plus some additional supporting information such as the sigma plot files, and an evaluation of the important uncertain parameters.

B2.13 TSPA-LA MODEL (GROUNDWATER AND ERUPTIVE) USED FOR REGULATORY COMPLIANCE: OUTPUT DTN: MO0709TSPAREGS.000_R0 [DIRS 182976]

Reference Figure B-1, Block 13—This is the version of Groundwater (v5.000) and Eruptive (vE1.004) Models that is used for Regulatory Compliance that is presented in Section 8. This DTN contains all the modeling cases and supporting checking documentation.

B2.14 UZ KD CORRELATION MATRIX FOR THE TSPA-MODEL: OUTPUT DTN: MO0707UZKDCORR.000_R0 [DIRS 183003]

Reference Figure B-1, Block 14—This DTN contains two MathCad worksheets that are used to produce two unsaturated zone Kd (distribution coefficient (mL/g)) correlation matrices that are used as an input to the TSPA LA Model, as well as a description of the calculation. This calculation is discussed in more detail in Section 6.3.9.3.

B2.15 TSPA-LA PREPROCESSING OF PERCOLATION FLUXES FOR THE DRIFT WALL CONDENSATION SUBMODEL: OUTPUT DTN: MO0707PERCFLUX.000_R0 [DIRS 183001]

Reference Figure B-1, Block 15—This DTN contains the GoldSim files used to extract the percolation fluxes from the MSTHM files and provide one-dimensional percolation flux tables, which are inputs to the Drift Wall Condensation Submodel in the TSPA-LA Model (Section 6.3.3.2.3).

B2.16 TSPA LA WASTE PACKAGE AND DRIP SHIELD DEGRADATION: OUTPUT DTN: MO0707WPDRIPSD.000_R0 [DIRS 183005]

Reference Figure B-1, Block 16—This DTN contains the TSPA-LA Waste Package (WP) and Drip Shield Degradation Inputs.

B2.17 TSPA LOCALIZED CORROSION ANALYSIS: OUTPUT DTN: MO0709TSPALOCO.000_R0 [DIRS 182994]

Reference Figure B-1, Block 17—This DTN contains the GoldSim run that is used to confirm that localized corrosion is addressed by the Compliance Model that is documented in output DTN MO0709TSPAREGS.000_R0 [DIRS 182976].

B2.18 TSPA-LA MODEL GROUNDWATER AND ERUPTIVE STABILITY ANALYSIS: OUTPUT DTN: MO0709TSPASTAB.000_R0 [DIRS 182983]

Reference Figure B-1, Block 18—This DTN contains the GoldSim runs that confirm that the Compliance Model is statistically stable as discussed in Section 7.3.1.

B2.19 TSPA-LA MODEL VALIDATION AND ANALYSES CASES: OUTPUT DTN: MO0708TSPAVALI.000_R0 [DIRS 182985]

Reference Figure B-1, Block 19—This DTN contains GoldSim files that address the following subjects that support model validation:

- Single Realizations (Discussed in Section 7.7.1)
- Accuracy of Expected Dose (Discussed in Section 7.3.2)
- FEHM Particle Stability (Discussed in Section 7.3.5)
- Validation of the number of Timesteps (Discussed in Section 7.3.3)
- Spatial Discretization (Discussed in Section 7.3.4)
- Statistical Stability (output DTN MO0709TSPASTAB.000_R0 [DIRS 182983])

B2.20 TSPA LA MODEL IMPACT ANALYSIS: OUTPUT DTN: MO0709TSPALAMO.000_R0 [DIRS 182981]

Reference Figure B-1, Block 20—This DTN contains GoldSim Files that are evaluating errors and potential future improvements to the Compliance Model contained in output DTN MO0709TSPAREGS.000_R0 [DIRS 182976].

B2.21 CO-DISPOSED SEISMIC DAMAGE CALCULATION: OUTPUT DTN: MO0708CDSPSEIS.000 [DIRS 183007]

Reference Figure B-1, Block 21—This DTN contains the calculations related to the co-disposed WP damage frequency and damage (area) crack fraction distributions for both an intact and degraded state of the WP.

B2.22 SEISMIC FREQUENCY CALCULATION OF WASTE PACKAGE CONTAINERS, OUTPUT DTN: MO0708FREQCALC.000_R0 [DIRS 183006]

Reference Figure B-1, Block 22—In the TSPA-LA, to calculate the expected dose for the Seismic Ground Motion Modeling Case for 10,000 years, a number of simplifications were made in the implementation of the seismic consequences abstraction. Among these simplifications were omitting damage to transportation, aging, and disposal canisters and rupture and puncture of WPs. As documented in the TSPA-LA Section 7.3.2, the use of these simplifications is justified by analysis relying on calculations of the frequency of these various events. This DTN contains the calculations that support the analysis reported in Section 7.3.2.

B2.23 SIMPLIFIED TSPA ANALYSIS: OUTPUT DTN: MO0708SIMPLIFI.000_R0 [DIRS 182980]

Reference Figure B-1, Block 23—This DTN contains the source and executable code for the Simplified TSPA Analysis, the spreadsheets used to develop aspects of that model, input files required to execute the model, and output files for the four modeling cases executed with the model. This DTN is discussed in more detail in Section 7.7.2.

B2.24 TSPA-LA WASTE PACKAGE AND DRIP SHIELD STANDALONE: OUTPUT DTN: MO0709TSPAWPDS.000_R0 [DIRS 183170]

Reference Figure B-1, Block 24—A streamlined version of the v5.000 model file (v5.000_GS_9.60.100.gsm) was made to model the WP and DS degradation. This stand-alone model runs more quickly and is used to perform analyses of WP and DS degradation mechanisms and to generate plots for use in the TSPA-LA. Two versions of the standalone model were created, one for DS only degradation calculations and one for WP degradation calculations. The DS only model did not require the WAPDEG software and the run time was even more reduced.

B2.25 TSPA PERFORMANCE MARGIN ANALYSIS (PMA) GENERATED INPUTS AND POST PROCESSED INPUTS, CORROBORATIVE DTN: MO0708TSPAPROC.000_R0 [DIRS 182979]

Reference Figure B-2, Block 100—This DTN contains inputs that fall into two categories: (1) TSPA LA PMA generated inputs and (2) Post-Processed inputs. TSPA-LA PMA-generated inputs do not have any external inputs used to create the input values. Post-Processed inputs do have external inputs supplied by supporting analysis and/or model reports. These external inputs must be Post-Processed for use in the TSPA-LA Model.

B2.26 FRACTION OF WASTE PACKAGES CONTAINING STAINLESS STEEL CLADDING AND INITIAL ROD FAILURES FOR THE COMPLIANCE CASE: OUTPUT DTN: MO0702PAFRACSS.000_R1 [DIRS 181588]

Reference Figure B-2, Block 101—This DTN contains values for the percentage of WPs containing stainless steel and the fraction of rods assumed failed upon receipt at the repository.

B2.27 COMMERICAL SPENT NUCLEAR FUEL DISSOLUTION RATE PARAMETER DESCRIPTION FOR PMA CORROBORATIVE DTN: SN0707PMACSNFD.001_R0 [DIRS 183045]

Reference Figure B-2, Block 102—This DTN contains Excel spreadsheets describing the parameter distribution effective surface area long-term dissolution scaling factor (F1), and radiolysis scaling factor (F2).

B2.28 IN-PACKAGE CHEMISTRY ABSTRACTION FOR PERMANCE MARGIN ANALYSIS: CORROBORATIVE DTN: SN0704PMAIPCAB.001_R1 [DIRS 182602]

Reference Figure B-2, Block 103—This DTN contains the in-package chemistry abstraction files for the TSPA performance margin analysis. They are used to predict ph and ionic strength in the pore water of degradation products inside commercial spent nuclear fuel and co-disposed WP.

B2.29 SATURATED ZONE FLOW AND TRANSPORT ABSTRACTION FOR THE PERFORMANCE MARGIN ANALYSIS: CORROBORATIVE DTN: SN0704PMASZFTA.001_R1 [DIRS 184395]

Reference Figure B-2, Block 104—This DTN contains input, output, and radionuclide breakthrough curves from the Saturated Zone Flow and Transport Abstraction Model and parameters for the Saturated Zone 1-D Transport Model.

B2.30 V4.044 FROM RECORDS PACKAGE

Reference Figure B-2, Block 106—This records package is the same records package described in Section B2.1.

B2.31 COMPLIANCE MODEL TSPA-GENERATED DTNS

Reference Figure B-2, Block 107—This block represents the DTNs listed from Figure B-1. The contents of each of these DTNs are described in their respective sections.

B2.32 PERFORMANCE MARGIN ANALYSIS: CORROBORATIVE DTN: MO0709MARGANAL.000_R0 [DIRS 182978]

Reference Figure B-2, Block 108—This DTN contains all the runs used for the Performance Margin Analysis.

B2.33 NEW EXTENDED-RANGE SEEPAGE LOOK-UP TABLE FOR SEEPAGE INTO 5.5-M-WIDE CENTER PORTION OF COLLAPSED DRIFT PLUS SUPPORTING FILES: CORROBORATIVE DTN: LB0704PASEEP02.001_R1 [DIRS 181093]

Reference Figure B-2, Block 110—This DTN contains a seepage look-up table that gives seepage results (i.e., seepage percentage and seepage rate) as a function of seepage-relevant parameters capillary strength, permeability, and percolation flux.

B2.34 UZ TRANSPORT MODEL, UNCERTAINTY DISTRIBUTION PARAMETERS AND FEHM FILES FOR PMA ANALYSIS: CORROBORATIVE DTN: MO0704PAUZFEHM.000_R0 [DIRS 182790]

Reference Figure B-2, Block 111—This DTN contains the PMA UZ Transport Model FEHM files.

B2.35 GLASS DEGRADATION MODEL FOR PERFORMANCE MARGIN ANALYSIS (PMA): CORROBORATIVE DTN: SN0704PMAGDEGM.001_R2 [DIRS 183955]

Reference Figure B-2, Block 112—This DTN contains a revised expression for calculating releases of radionuclides from high-level radioactive waste glass as it dissolves when contacted by water. Release rates for radionuclides are calculated as the product of three terms:

- Surface area of glass contacted by water
- Glass dissolution rate
- Mass Fraction of each radionuclide in the glass

B2.36 ALTERNATIVE UNCERTAINTY EVALUATION FOR THE SOLUBILITIES OF PUO2 (HYD, AGED), NPO2, NP2O5, NANPO2CO3, SCHOEPITE, NA-BOLTWOODITE, AND NA4UO2 (CO3)3, CORROBORATIVE DTN: SN0704PMASOLUB.001_R1 [DIRS 182787]

Reference Figure B-2, Block 113—This DTN contains spreadsheets and EQ3/6 input/output files used in the evaluation of alternative uncertainties for the solubility of NP(IV), NP(V), PU(IV), AND U (VI) solubility-controlling solids.

B2.37 SUPPORTING DATA AND CALCULATIONS FOR WATER BALANCE EVALUATION, CORROBORATIVE DTN: SN0704PMAWBCAL.001_R2 [DIRS 182335]

Reference Figure B-2, Block 114—This DTN contains supporting data files and excel spreadsheets for evaluation of water mass balance calculations.

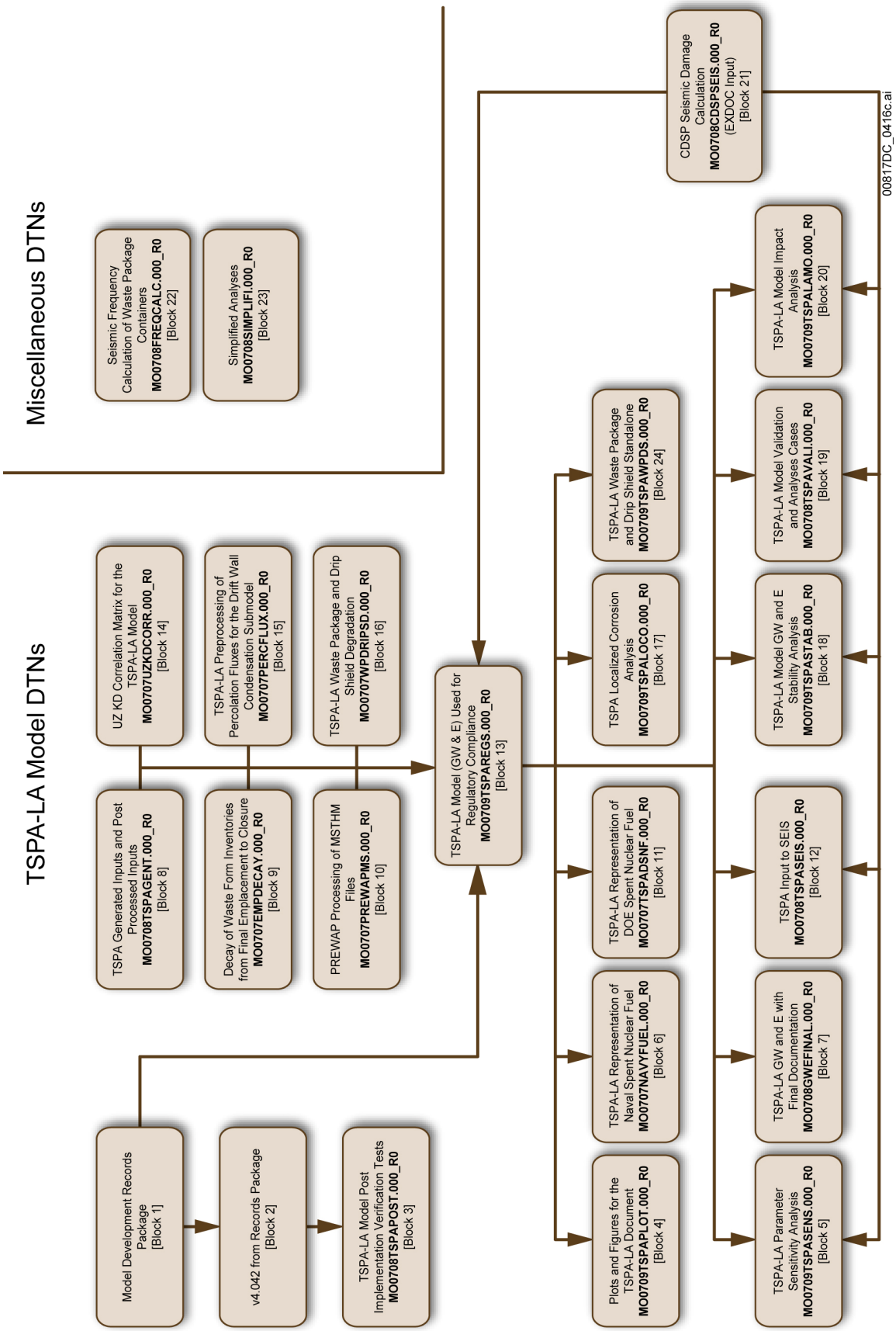

Figure B-1. Road Map of TSPA-LA Model Data Tracking Numbers

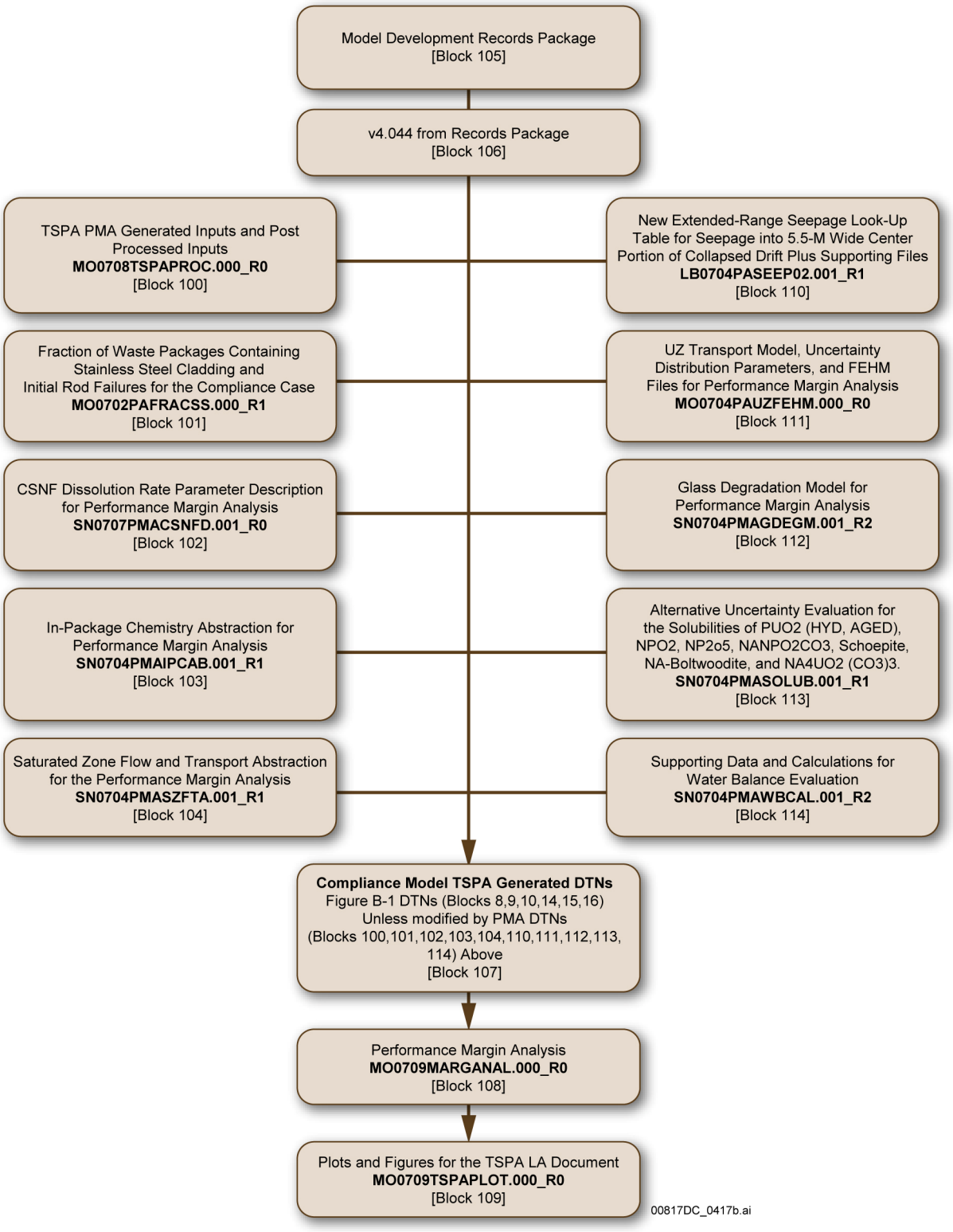

Figure B-2. Road Map of Performance Margin Analysis Data Tracking Numbers

APPENDIX C
PERFORMANCE MARGIN ANALYSIS

C.1 PURPOSE AND OBJECTIVE

The judicious use of conservative assumptions has played an important role in enhancing the confidence and defensibility of the Total System Performance Assessment for the License Application (TSPA-LA) Model. As discussed in Section 6.3, conservative assumptions in the TSPA-LA were generally introduced in the formulation of the TSPA-LA submodels and in the derivation of selected submodel parameter ranges in order to simplify the model formulations or compensate for the epistemic uncertainties that are difficult to quantify. Conservative assumptions must be used judiciously; more importantly, the use must ensure that the potential radiological risks are not underestimated. Individual conservatisms introduced at the submodel level can be attenuated differently to the system-level performance measures (i.e., projected annual dose). Thus, the objective of this Performance Margin Analysis (PMA) is to evaluate the significance of the major explicit and implicit conservatisms of the type identified in Section 5.0 and Section 6.3. Specifically, the PMA was designed to:

1. Confirm that when propagated individually through the TSPA-LA Model, the conservatisms introduced at submodel levels are conservative with respect to the total system performance measures (e.g., mean annual dose).

2. Quantify the extent to which the conservatisms, individually and collectively, overestimate the projected annual dose relative to the model projections presented in the performance demonstration (Section 8.0). The delta in annual dose between the TSPA-LA Model and the PMA is a measure of the performance margin.

3. Assess whether the evaluated conservatisms introduce any inappropriate risk dilution in the TSPA-LA results presented in support of the LA (e.g., reduce the peak total mean annual doses).

The PMA is comprised of an exclusive set of TSPA calculations from those conducted for the TSPA-LA (Section 8.0). The PMA calculations were intended to gauge both individual and collective impacts of major conservatisms embedded in the TSPA-LA model and thereby give a perspective on the potential performance margin included in the TSPA-LA dose projections.

Most of the conservatisms in the TSPA-LA Model were introduced during submodel development and/or derivation of parameter uncertainty characterizations as discussed in Section 6.3. For the most part, these conservatisms are implemented to bound the effects of processes that promote radionuclide release and transport. Other conservatisms were also introduced as a result of not taking credit for processes or conditions, which may potentially enhance containment and isolation. Additional submodels were developed for inclusion in the PMA for the specific purpose of evaluating implicit conservatism. It is important to state, that while these additional submodels and data were developed in accordance with applicable quality assurance (QA) requirements, in some cases they represent new models with limited technical foundation, verification, and validation. Consistent with the requirements of SCI-PRO-006, *Models,* Section 6.2.1.O, PMA submodels may use software (Section C3) that is controlled but not qualified.

The PMA was conducted by first modifying selected submodels and parameters of the TSPA-LA Model, including the addition of submodels and parameters for PMA, and then repeating a select set of modeling cases that were run for the TSPA-LA. The PMA results are compared to the mean annual dose results of the TSPA-LA Model. Thus, the PMA is one aspect of the validation work supporting the TSPA-LA Model (Section 7.0).

C.2 QUALITY ASSURANCE

Technical Work Plan for: Total System Performance Assessment FY 07-08 Activities (SNL 2008 [DIRS 184920]) describes applicable Quality Assurance requirements for the TSPA-LA. Consistent with the requirements of the TWP, this section details measures taken to ensure appropriate controls were in place for the PMA.

C2.1 CONFIGURATION MANAGEMENT

The development of the PMA required the same organization, control, and accountability that was necessary for the development of the TSPA-LA Model (Section 2.0). The PMA used the same configuration management processes that were used for the TSPA-LA Model. Those configuration management processes included software control, change control for making modifications to the TSPA-LA Model, control of inputs to the TSPA-LA Model, and error tracking and evaluation. Refer to Section 2.1 (Configuration Management) for details on these configuration management processes.

The PMA utilized software that was used for the TSPA-LA Model runs as well as additional software specifically for the PMA. All of the software used for the PMA was placed under Software Configuration Management (SCM) control. Refer to Section C.3 (Use of Software) for details on the controlled and baselined software used, qualification status, and any limitations on the use of software for the PMA.

Changes to the TSPA-LA Model for the purpose of the PMA were implemented upon receipt of written approval from the TSPA Department Manager, TSPA Model Calculations Lead, and TSPA Configuration Management Lead.

As in the TSPA-LA Model, the input parameter values used in the PMA are controlled through the TSPA Input Database. The database provides the parameter values and distributions necessary for the PMA. The TSPA Input Database categorizes, stores, and retrieves fixed and distributed values of the model parameters and allows authorized analysts to review and update the values. The TSPA Input Database has strict user controls that feature read and write access and audit trails that ensure the security, integrity, and traceability of the information used in the PMA.

C.3 USE OF SOFTWARE

Software that was necessary for the development and execution of the TSPA-LA Model is documented in Section 3.0. Three additional qualified software items, listed in Table C.3-1, were used specifically to support the development and execution of the PMA for the TSPA-LA. One was used to provide supporting information, and the other was directly implemented in the TSPA-LA Model and coupled to the GoldSim simulation software. These three items are

qualified and have been placed under the control of SCM per IM-PRO-003. The qualified software used to support the PMA, including qualified software used in the TSPA-LA, is listed in Table C.3-2, along with their unique software tracking numbers (STNs). Qualification documentation for each piece of software is available in SCM as well as the Records Processing Center. All qualified software was obtained from SCM, was appropriate for use in this analysis, and each was used within the software's range of validation.

TSPA-LA software was installed on TSPA-LA department computers in accordance with a qualified process. The installation process for each software code listed in Table C.3-2 was followed to ensure that there was a proper, qualified (i.e., in accordance with governing project procedures and controlled by SCM) installation by personnel authorized by SCM (Section 3.0).

The discussion below describes the three qualified software codes listed in Tables C.3-1 and C.3-2 that are in addition to or replaces qualified software used in the TSPA-LA Model (i.e., FEHM, TSPA_dB, and iTough). Each software discussion identifies the following information: (1) name of software; (2) brief description of software; (3) relationship to the PMA (i.e., used for PMA model development only, PMA model development and final component, or final component only); (4) location of software documentation; and (5) statement regarding use of software within the range of validation.

In addition, two unqualified software items were used in the development of the saturated zone (SZ) breakthrough curves that were used for post-processing, which was required to include the redox conditions in the SZ (Section C6.7). The two codes are listed in Table C3-3. Per SCI-PRO-006, *Models*, Section 6.2.1.O unqualified, non-exempt software may be used to corroborate model results. The PMA is a corroborative effort and the use of unqualified software is permissible.

C3.1 FEHM

C3.1.1 Description of Software

The finite element heat and mass transfer code (FEHM) used in the PMA documented in this report has the following general capabilities:

- Is called from another program that conforms to the external interface method and function calls described in the *User's Guide, GoldSim Probabilistic Simulation Environment* (GoldSim Technology Group 2007 [DIRS 183214])
- Provides GoldSim with the ability to perform calculations not included in the standard capabilities of GoldSim
- Calculates the transport of radionuclides through the unsaturated zone (UZ)
- Transfers information to and from the GoldSim software when the PMA is running.

C3.1.2 Relationship to the Performance Margin Analysis

The computer software code, which implements the UZ transport abstraction model for the TSPA-LA Model is based, is FEHM V2.24-01 [DIRS 179419]. The software used for the UZ PMA is FEHM V 2.25-00 (STN: 10086-2.25-00 [DIRS 182477]). The qualification status of this and other software is indicated in the electronic Document Input Reference System (DIRS) database. This version of FEHM has updates (relative to V2.24-01) that incorporate the colloid diversity model and the feature to enable the water table rise to be provided as input, either through the input file or through the interface between FEHM and GoldSim (GoldSim 2007 [DIRS 181903]).

C3.1.3 Software Documentation

The software qualification documents for the version of FEHM mentioned in Section C3.1.2 are listed in Table C3-4.

C3.1.4 Range of Validation

The range of validation for FEHM V 2.25-01 (STN: 10086-2.25-00 [DIRS 182477] listed in Section C3.1.2 is defined by the documented functionality (i.e., requirements) and range(s) of acceptable inputs. The requirements are located in the respective documents listed in Table C3-4. The range(s) of acceptable inputs are discussed in the respective design and user documents listed in Table C3-4.

C3.2 TSPA_INPUT_DBV2.2

C3.2.1 Description of Software

All versions of TSPA_Input_DB used in the TSPA-LA Model documented in this report are a Microsoft Access database that is used as a quality-controlled storage area for the TSPA-LA Model input parameters. The parameter values are maintained as originally entered (i.e., no manipulations or post-processing of the parameter values are performed). The database is capable of interfacing via open database connectivity (ODBC) for automated download to the TSPA-LA Model.

C3.2.2 Relationship to the Performance Margin Analysis

TSPA_Input_DB V2.2 (STN: 10931-2.2-00 [DIRS 181061]) was used for the TSPA-LA Model development and TSPA-LA Model validation and analysis cases. TSPA_Input_DB V2.2 (STN: 10931-2.2-01 [DIRS 181062]) was also used for the TSPA-LA Model validation and analysis cases. For the PMA, a new copy of the TSPA_Input_DB was created to store additional PMA input values and data files, TSPA_PMA_Input_DBv2.2. The PMA downloads input from both the TSPA-LA Model DB and the PMA DB. The TSPA_PMA_Input_DBv2.2 uses the same software (TSPA_Input_DB V2.2, STN: 10931-2.2-01 [DIRS 181062]); however, it is populated with the data that are specific to the PMA (Section 4.0).

C3.2.3 Software Documentation

The software documents for the versions of the TSPA_Input_DB mentioned in Section C3.2.2 are listed in Table C3-5. This documentation is the same for the TSPA_PMA_Input_DBv2.2 since it uses the same software as the TSPA_LA_Input_DBv2.2.

C3.2.4 Range of Validation

The ranges of validation for the versions of TSPA_Input_DB listed in Section C3.2.2 are defined by the documented functionality (i.e., requirements) and range(s) of acceptable inputs. The requirements are located in the respective requirements documents listed in Table C3-54. The range(s) of acceptable inputs is discussed in the respective design and user documents listed in Table C3-5. This range of validation is the same for the TSPA_PMA_Input_DBv2.2 since it uses the same software as the TSPA_LA_Input_DBv2.2.

C3.3 ITOUGH2 V5.0

C3.3.1 Description of Software

iTOUGH2 V5.0 (STN: 10003-5.0-00 [DIRS 160106]) is a computer program that provides inverse modeling capabilities for the TOUGH2 code.

C3.3.2 Relationship to the Performance Margin Analysis

iTOUGH2 V5.0 (STN: 10003-5.0-00 [DIRS 160106]) implemented for the Seepage Model for Performance Assessment (SMPA) simulations conducted to develop the PMA seepage look-up table for collapsed drifts, based on the same methodology and procedure as the TSPA-LA simulations for collapsed drifts described in *Seepage Model for PA Including Drift Collapse* (BSC 2004 [DIRS 167652]). Systematic seepage simulations were then conducted using iTOUGH2 V5.0 to calculate steady-state seepage rates for the 5.5-m wide center section of the 11-m wide collapsed drift for twelve realizations of heterogeneous permeability fields and 2,550 combinations of seepage-relevant parameters.

C3.3.3 Software Documentation

The software documents for the version of iTOUGH2 V5.0 mentioned in Section C3.3.2 are listed in Table C3-6.

C3.3.4 Range of Validation

The range of validation for the versions of iTOUGH2 V5.0 listed in Section C3.3.2 is defined by the documented functionality (i.e., requirements) and range(s) of acceptable inputs. The requirements are located in the respective requirements documents listed in Table C3-6. The range(s) of acceptable inputs is discussed in the respective design and user documents listed in Table C3-6.

C3.4 UNQUALIFIED SOFTWARE

Per SCI-PRO-006, *Models*, 6.2.1.O unqualified, non-exempt software may be used to corroborate model results. The PMA is a corroborative effort and the use of unqualified software is therefore permissible. The two codes used to support this analysis were placed under configuration control, and following the configuration management plan (Appendix C2) are included in the PMA output. These codes were only used in the PMA to generate the input data used for the Saturated Zone Transport Abstraction (Appendix C6.7).

C.3.4.1 SZ_Post_NonQ

SZ_Post_NonQ, Version 3.1 (STN: LL2000) is the code that was used for post-processing radionuclide transport simulation results to produce breakthrough curve files for irreversible colloids.

C.3.4.2 Reduce_Track_NonQ

Reduce_Track_NonQ, Version 00 (STN LL2001) is the code that was used to compute the average track length through the reducing zone of the SZ. The output of the software was used to determine the path length of the reducing zone for use in the one-dimensional SZ transport model.

C.4 INPUTS

This PMA utilizes the TSPA-LA Model with changes to certain inputs and models for the purpose of quantifying the performance margin inherent in the TSPA-LA Model. Therefore, most of the inputs are already given in Section 4, Volume I (Inputs), along with a description of how the inputs are managed. This section presents those inputs that have been changed from those used in the TSPA-LA Model and additional inputs necessary to support the PMA. Table C4-1 lists the input parameters to the TSPA-LA Model that have been changed or deleted for the PMA. Table C4-2 lists input parameters that have been added to the TSPA-LA Model for the PMA. The PMA contains both qualified and unqualified data. The data traceability, as described in Sections C4.1 (Performance Margin Analysis Input Database) and C.4.2 (Parameter Entry Forms), provides a mapping from the PMA parameters to the data source.

C.4.1 PERFORMANCE MARGIN ANALYSIS INPUT DATABASE

Section 4.7, Volume I, provides a summary of the TSPA Input Database. The PMA utilizes both the TSPA Input Database (TSPA_Input_DB, Output DTN: MO0708GWEFINAL.000 [DIRS 182977]) and a PMA-specific input database (TSPA_PMA_Input_DB, Corroborative DTN: MO0709MARGANAL.000 [DIRS 182978]). The TSPA Input Database and the PMA Input Database are used to support the PMA by providing the parameter values and distributions necessary for the PMA. Additional detail on its design and operation can be found in the software documents listed in Section C.3. The database is used to categorize, store, and retrieve fixed and distributed values of the PMA parameters.

C.4.2 PARAMETER ENTRY FORMS

All parameter names, values, and references used in support of the PMA are documented in Parameter Entry Forms (PEFs) and contained in the PMA Input Database. PEFs document both parameters that were downloaded from the PMA Input Database and parameters that were entered directly into the PMA. Table C.4-3 lists the direct inputs that are specific to the PMA and associates each with a reference (source) and a PEF number. The PEFs listed in Section 4.0 (Volume I) and in Table C.4-3 collectively contain all parameters used as input to the PMA. Each PEF references the specific locations of the parameters within a reference document or DTN to aid in the traceability of the direct inputs. The original signed PEFs are in the records package for this document; however, the TSPA Input Database and the PMA Input Database can be used to generate any PEF, as described in Section 4.7 (Volume I).

C.5 ASSUMPTIONS

The assumptions that support the TSPA-LA are documented either in Section 5, Sections 6.3 through 6.6, or in related process model reports. All these assumptions except those listed in Table C5-1 remain the same for the PMA. Those listed in the table were identified to be conservative and potentially significant to the overall performance of the repository. In the PMA, these assumptions were replaced with less conservative ones based on additional data and alternative model analyses or eliminated by development of process models or abstractions. It is important to reiterate, that while these additional submodels and data were developed in accordance with applicable quality assurance (QA) requirements, in some cases they represent models with limited technical foundation, verification, and validation. Consistent with the requirements of SCI-PRO-006, *Models,* Section 6.2.1.O, PMA submodels may use software (Section C3) that is controlled but not qualified. Detailed descriptions of the changes are documented in Section C.6.

C.6 PERFORMANCE MARGIN ANALYSIS DESCRIPTION

C6.1 METHODOLOGY

In the TSPA-LA Model projections presented in the performance demonstration (Section 8.0), postclosure performance is analyzed for time periods of 10,000 years and 1,000,000 years after closure. Because of the inherent uncertainties in making such long-term projections, the TSPA is largely based on a probabilistic modeling approach that accounts for uncertainties in parameters and in future conditions. In the PMA, the postclosure performance is analyzed over a selected set of modeling cases with the removal of a selected set of conservatisms included in the TSPA-LA. The objective of the PMA is to carefully and quantitatively evaluate the significance of these conservatisms that would be otherwise difficult to address given the range of uncertainties and long-term projections inherent in a model of this magnitude. The methodology used to accomplish this task included two primary steps:

- Identify the modeling cases that produce the most significant releases and dominate the projected doses

- Identify the sources of uncertainty and/or conservatisms that are most influential in producing the spread of the distribution of projected doses for these modeling cases.

The TSPA-LA includes four scenario classes: Nominal, Early Failure, Seismic, and Igneous. Detailed descriptions of the technical basis of these scenario classes, and their associated modeling cases, are presented in Sections 6.3 through 6.6 of Volume I. Section 8.0 presents the postclosure performance assessment results to support the LA for a nuclear waste repository at Yucca Mountain. The TSPA-LA demonstration of performance for the individual protection standard is based on the total mean annual dose computed by summing the results for seven modeling cases: (1) Nominal, (2) Waste Package EF, (3) Drip Shield EF, (4) Igneous Intrusion, (5) Volcanic Eruption, (6) Seismic GM, and (7) Seismic FD (Section 8.1). As required by the disposal standards for the TSPA-LA, the postclosure performance is quantified for time periods of 10,000 years and 1,000,000 years after closure. Likewise, the PMA was conducted over the 10,000-year and 1,000,000-year postclosure periods for comparison with the TSPA-LA. Drawing from the evaluation presented in Section 8.0, the PMA was exercised using five modeling cases (the Seismic GM Modeling Case includes the effects of the nominal processes when run for 1,000,000 years postclosure). The Volcanic Eruption Modeling Case was not evaluated in the PMA because none of the changes included in the PMA have any impact on the Volcanic Eruption Modeling Case. To demonstrate the performance margin inherent in the TSPA-LA, the mean of the projected total annual doses to the RMEI (i.e., sum of the expected annual doses projected for each scenario class) is used to evaluate the performance margin for the period within 10,000 years after disposal and over the period after 10,000 years through the period of geologic stability (Section 8.1, Equation 8.1.1-1). The PMA total mean annual dose was calculated replacing the selected set of TSPA-LA modeling cases (identified above) with PMA results. The TSPA-LA results for the Volcanic Eruption Modeling Case were combined with the PMA results to calculate the PMA total mean annual dose. The method used to calculate the total mean annual doses for the TSPA-LA Model and the PMA is presented in Appendix J. The total mean annual dose was evaluated to assess the potential performance margin embedded in the TSPA-LA Model (presented in Section C7).

The next step in the PMA process was to identify potentially conservative assumptions embedded in the TSPA-LA Model that may be significant contributors to the dose. Table C5-1 lists the conservative assumptions embedded in the parameters and submodels of the TSPA Model that were changed or modified for evaluation of their potential to impact the performance margin for the TSPA. The identification of these conservatisms came from the underlying model reports and from professional judgment of subject matter experts. In order to assess the effect of the listed conservatisms in the TSPA-LA Model, changes to submodels and parameter values were formulated. The changes to the TSPA inputs for the PMA primarily focus on the following:

- Include additional coupling between physical and chemical processes
- Reduce discontinuities in scale between submodels
- Represent the expected performance in existing models by reducing the uncertainty distributions in cases where conservative bounding values were assumed

- Include alternative conceptual models (ACMs) that have been screened out in favor of a more conservative model.

In the subsections that follow, each conservatism in the TSPA-LA Model that was assessed for the PMA is discussed along with the changes implemented in the TSPA-LA Model, the basis for the changes, and how those changes were implemented.

The PMA was conducted by first modifying selected submodels and parameters of the TSPA-LA Model. In some cases, the addition of new submodels and parameters was necessary for the PMA changes to the TSPA-LA Model. The second step was to repeat the selected set of modeling cases that were run for the TSPA-LA. The significance of the individual conservatisms was evaluated by examining the results for each modeling case (Section C.7, Results). The collective impact of the major assumptions was quantified by combining the PMA projections for annual dose for all modeling cases and then comparing the total mean dose curves against those of the TSPA-LA Model.

For the most part, the changes were incorporated in the submodels included in the TSPA-LA Nominal Modeling Case (Volume I, Section 1.5.1). More specifically, the changes for the PMA are embedded in the following model components:

- Drift-Scale UZ Flow (C6.2)
  - Reduction of seepage flux to waste package (WP) based on a reduced hydrologic cross-section for the representation of collapsed drift geometry (Drift Seepage Submodel)
- Waste Package and Drip Shield Degradation (C6.3)
  - Modification of corrosion rates based on fluoride ion concentration threshold instead of fixed and pervasive condition of aggressive corrosion
  - Implementation of a lower WP Alloy 22 (UNS N06022) general corrosion rate based on weight loss coupon data instead of crevice corrosion data
  - Implementation of stress corrosion cracking (SCC) of Alloy 22 using a higher representative yield stress threshold
  - Inclusion of a mechanistic approach to the calculated distribution of breached area as a result of localized corrosion on the WP outer barrier
- Engineered Barrier System (EBS) Flow (C6.4)
  - Inclusion of a detailed in-package water balance to account for the mass fluxes of water through the WPs
- Waste Form Degradation and Radionuclide Mobilization (C6.5)

  - Modification of the in-package chemistry model that accounts for the extent of material degradation and the availability of water inside a waste package
  - Inclusion of long-term degradation rate models for commercial spent nuclear fuel (CSNF) and high-level (radioactive) waste (HLW) glass waste forms
  - Inclusion of credit for initial clad failure fractions in place of assuming all cladding is failed at time of emplacement; applied to first 20,000 years only
  - Reduction of uncertainties for thermodynamic properties of neptunium, uranium, and plutonium

- UZ Transport Submodel (C6.6)
  - Enhanced matrix diffusion effects on radionuclide transport
  - Addition of colloid diversity model and retardation of irreversibly sorbed radionuclides
  - Addition of detailed model for water table rise

- SZ Transport Submodel (C6.7)
  - Addition of discrete interface for redistribution of the diffusive mass relaeased from the UZ matrix to SZ fractures
  - Addition of colloid diversity model and retardation of reversible and irreversibly sorbed radionuclides
  - Addition of enhanced radionuclide sorption in potential reducing zone
  - Implementation of an alternative distribution for flowing interval porosity
  - Inclusion of correlation between flowing interval porosity and groundwater specific discharge

- Seismic Scenario Class (C6.8)
  - Inclusion of an Alternative Conceptual Model for the crack-area density model in the Seismic Damage Abstraction.

It should be acknowledged that this list of modifications by no means is exhaustive; some other assumptions in the TSPA-LA Model may also benefit from additional detail or be conservative; for example, the assumption of complete WP failure in an igneous intrusion case and possible reduction of waste package damage due to the depth of the repository in a seismic ground motion case. The exclusion of these examples from the PMA is generally based on the consideration of lack of sufficient technical data for supporting such analyses. A discussion of each conservatism listed above and how it has been addressed with a modification to the above submodels follows.

C6.2 DRIFT-SCALE UNSATURATED ZONE FLOW

C6.2.1 Conceptual Model

In the TSPA-LA model, seepage abstraction accounts for the possible collapse of drifts in lithophysal units using a specific seepage look-up table (SNL 2007 [DIRS 181244], Section 6.4.2.4). This collapsed-drift look-up table was generated from seepage simulations conducted with the seepage model for performance assessment (BSC 2004 [DIRS 167652]), assuming a rubble-filled circular opening with an 11-m diameter as the final state after collapse. In the TSPA-LA seepage component, the total flow of liquid water from the fractured formation into the rubble-filled opening is considered seepage, independent of the actual seepage location, and subsequent TSPA-LA components, such as those for radionuclide mobilization and transport, use this total seepage rate. Use of an 11-m diameter results in a treatment that over-predicts the seepage flux over the 5.5-m drift, since the mostly gravity-driven flow in the rubble-filled opening would effectively prohibit contact of water with the WPs or waste forms for off-center seepage locations. This treatment of seepage was chosen in the TSPA-LA model to account for possible uncertainties in the seepage modeling approach for collapsed drifts.

The lithophysal rocks at Yucca Mountain are relatively deformable with a low compressive strength (SNL 2007 [DIRS 176828], Section 6.7.1). As a result, drifts located in lithophysal units are expected to collapse in case of severe, possibly repeated seismic events (SNL 2007 [DIRS 166107]). During collapse, either sudden or gradual, the rock mass above an underground opening is expected to disintegrate into a number of fragments that fall down and begin to fill the open space. Because there are large voids between the rock fragments, the bulk porosity of the fragmented rubble is expected to be much larger than the intact rock. Examination of the mean volume as presented in Section 6.6 and shown on Figure 6.6-7 shows that rock volume in the lithophysal units will accumulate fairly rapidly. When this occurs, the broken rock provides backpressure, which prevents further collapse of the rock mass (SNL 2007 [DIRS 166107], Section 6.4.2.5). After complete drift collapse, the original opening has increased in size, but is filled, either partially or fully, with fragmented rock blocks with sizes on the order of centimeters or decimeters with large voids between them. The solid wall rock surrounding the rubble-filled opening will remain largely intact, with a potential increase in permeability and a reduction in capillary strength due to the dynamic motion and the stress redistribution. For convenience, the rubble-filled opening is referred to as a 'collapsed drift,' although technically there is no drift after collapse. In collapsed drifts, seepage is defined as the flow of water from the intact fractured formation into the rubble-filled drift. The simulated profiles of collapsed drifts (see Appendix R of SNL 2007 [DIRS 166107]) were approximated, for seepage purposes, as rubble-filled openings of circular shape with a diameter of 11 m, which represents the largest diameter predicted.

For the TSPA-LA Model, seepage simulations were conducted for the selected collapsed-drift conditions, for the full set of seepage parameter combinations (with capillary strength values ranging from 100 Pa to 1,000 Pa, mean permeability values ranging from -14 to -10 (in $\log_{10} m^2$), and percolation flux values ranging from 1 mm/year to 1,000 mm/year, and a seepage look-up table was developed for use in the TSPA (BSC 2004 [DIRS 167652], Section 5). A capillary strength parameter of 100 Pa was assumed for the fragmented rock material within the collapsed drift (BSC 2004 [DIRS 167652], Section 5). Simulations conducted with the Seepage Model for

Performance Assessment indicated that, for the conditions at Yucca Mountain, the seepage into collapsed drifts is smaller than the percolation flux arriving at the drift crown (i.e., despite the changes in drift size and shape, most of the flux is diverted around the rubble-filled opening). However, the seepage rates have significantly increased compared to the intact-drift (SNL 2007 [DIRS 181244], Section 6.4.2.4.2). The larger the drift size, the more seepage can be expected because (1) the total amount of percolation flux arriving at the drift increases with the horizontal size, and (2) flow diversion is less effective for a larger drift.

As mentioned above, the total flow of liquid water from the fractured formation into the rubble-filled opening is considered seepage in the TSPA seepage component, independent of the actual seepage location. The possibility that only a fraction of the seepage water may actually come into contact with the WPs in the center of the drifts is currently not considered in the TSPA. The larger the horizontal extent of a drift, the higher the possibility that seepage water would bypass the center section of the drift in case seepage occurs at off-center ceiling locations.

Figure C6-1 schematically illustrates the potential migration paths of water within the rubble-filled opening depending on its seepage location along the ceiling. Water flow in the rubble is expected to be primarily gravity-driven, because of the coarseness of the rubble material and the large voids between them, corresponding to a weak capillarity. As a result, flow paths should be mostly vertical and highly focused (i.e., dispersion should be limited and the cross-sectional area of the flow should be rather small). This assessment is supported by laboratory experiments examining unsaturated flow behavior in packs of rock blocks with up to a 20 cm size (Tokunaga et al., 2005 [DIRS 180513]). These experiments demonstrated that single point infiltration of water at the top would branch out laterally no more than a few rock blocks, and that merging and splitting of flow paths would stabilize after about five rock layers in the vertical, to be followed by a dynamic stationary state exhibiting dominantly gravity-driven vertical flow. The observed final flux distributions were remarkably reproducible among numerous different rock packings and infiltration rates. Thus, one may assume that lateral dispersion of flow in rubble-filled collapsed drifts is limited and that the contact of seepage water with the WP or waste form should only be possible for seepage locations near the center of the collapsed opening.

It follows that the TSPA-LA Model for seepage—allowing all water entering a collapsed drift to influence drip shield (DS)/WP degradation and radionuclide mobilization/transport—is conservative (Section 6.3.3.1). A less conservative TSPA seepage model would be to assume that only water that enters the drift in the 5.5-m wide center section should be considered seepage (i.e., only then would it be considered in subsequent TSPA components with an impact on DS/WP degradation and radionuclide mobilization/transport). Water that seeps outside of this center section would be neglected because it would bypass drift shields and waste packages in the drift center. To evaluate the importance of the above conservatism, an alternative seepage look-up table for collapsed drifts, developed from revised Seepage Model for Performance Assessment simulations, was included in the PMA. The alternative (or PMA) look-up table gives seepage only when the seepage location is in the 5.5-m wide center section of the rubble-filled opening (Figure C6-1). The conceptual model of water fluxes within the EBS remains the same as the TSPA-LA Model, but with a reduced seepage flux.

The Seepage Model for Performance Assessment simulations conducted to develop the PMA seepage look-up table for collapsed drifts are based on the same methodology and procedure as the TSPA-LA simulations for collapsed drifts described in *Seepage Model for PA Including Drift Collapse* (BSC 2004 [DIRS 167652]). In both simulations, the seepage rate for a certain simulation case is calculated by adding up the seepage fluxes between rock and drift elements. In the PMA Seepage Model for Performance Assessment simulations, seepage is calculated by adding up only those rock-drift fluxes that occur in the 5.5-m wide center section of the 11-m wide collapsed drift. In contrast, the TSPA-LA Seepage Model for Performance Assessment simulations added up as seepage any rock-drift flux that occurred over the entire 11-m wide collapsed drift. The revision involves a change in the post-processing calculation for the seepage simulations, not a change in the simulation methodology and procedure. Thus, the technical basis for the Seepage Model for Performance Assessment simulations, including the model concept, numerical methods, discretization, assumptions, inputs, parameters, validation work, and limitations, has not changed from the description given in *Seepage Model for PA Including Drift Collapse* (BSC 2004 [DIRS 167652], Sections 3, 4, 5, and 6).

The revised Seepage Model for Performance Assessment simulation runs were conducted using various script files and model input files given in the data tracking number (DTN): LB0307SEEPDRCL.001 [DIRS 180511]. This DTN contains supporting files for mesh generation and seepage simulation for the TSPA-LA Seepage Model for Performance Assessment runs. Minor modifications were made to script files and model input files to accommodate the necessary changes. Systematic seepage simulations were then conducted using iTOUGH2 V5.0 to calculate steady-state seepage rates for the 5.5-m wide center section of the 11-m wide collapsed drift for twelve realizations of heterogeneous permeability fields and for 2,550 combinations of seepage-relevant parameters. These parameter combinations are the same as before; they include a variation of capillary-strength values (100 Pa to 1,000 Pa in steps of 100 Pa), mean permeability values (-14 to -10 in steps of 0.25, given in log10 with permeability in the unit m^2), and percolation flux values (1, 5, 10, 20, 50, and 100 through 1,000 mm/year in steps of 100 mm/year).

The seepage results from the PMA simulations, including all necessary supporting files for the iTOUGH2 model, are given in corroborative DTN: LB0704PASEEP01.001_Rev01 [DIRS 181223]. The necessary steps to conduct the simulations and perform some post-processing operations are explained in the Readme file and its Appendix provided in this DTN. Summary results of seepage rates and seepage percentages, for individual realizations as well as averaged over all realizations, are given in file LookupTableSeepageCollapsedDriftCenter.xls. Seepage rates and seepage percentages are provided for a reference drift section of a 5.5-m width (in the center of the collapsed drift) and 5.1-m length, the latter corresponding to the approximate length of a WP plus the 0.1 m spacing between canisters. The seepage rate gives the total amount of water seeping into the reference drift section per unit of time (in kg/yr/WP). The seepage percentage is defined as the ratio of seepage rate divided by percolation rate across a reference area multiplied by 100. Here, the reference area is given by the 5.5-m wide and 5.1-m long drift section over which seepage is calculated. Note that in the TSPA-LA collapsed-drift look-up table, seepage percentage was calculated using a reference area of 11 m wide and 5.1 m long (i.e., the total width of the collapsed drift was used). This is an important point when converting seepage rate into seepage percentage and vice versa. Example results from the

revised Seepage Model for Performance Assessment simulations are compared with the TSPA-LA seepage simulations for intact and collapsed drifts on Figure C6-2.

Figure C6-2 gives contours of the simulated seepage rate as a function of the capillary-strength parameter and the mean fracture permeability (in log10) for a selected percolation flux of 5 mm/year. In all cases, as expected, the seepage rate increases with decreasing capillary strength and decreasing permeability. Compared to the intact drift case, both collapsed drift simulations arrive at higher seepage rates because flow diversion is less effective for a larger opening. When comparing the two collapsed-drift cases, seepage collected over the 11-m total width of the rubble-filled opening is much higher than seepage collected over the 5.5-m wide center section. For example, for the parameter case with a permeability value of -12.5 in log10 m^2 and a capillary strength of 500 Pa, the average seepage rate into an intact drift is less than 5 kg/yr/WP, the average seepage rate into the 11-m wide collapsed drift is above 50 kg/yr/WP, and the average seepage rate collected over the 5.5-m wide center section of an 11-m wide collapsed drift is about 20 kg/yr/WP.

C6.2.2 Model Implementation

Section 6.3.3 details the Drift Scale UZ Flow Submodel for the TSPA-LA. Implementation of the PMA seepage model follows the same process described in Section 6.3.3 with the exception of the data contained in the Seepage Model for Performance Assessment file. The PMA seepage look-up table developed in Section C6.2.1 covers a percolation flux range from 1 mm/yr up to 1,000 mm/yr. As pointed out in *Abstraction of Drift Seepage* (SNL 2007 [DIRS 181244]), this upper limit may be exceeded in the TSPA calculations because revised infiltration estimates have resulted in larger percolation fluxes for certain climate and infiltration conditions. If a sampled parameter value within TSPA would fall outside of the Seepage Model for Performance Assessment range, the outlier value would need to be truncated to the respective upper limit. To avoid (or limit) such truncations, the PMA seepage look-up table developed above is modified to comprise an extended percolation flux range. The data manipulations necessary to develop these extended-range tables are identical to those previously performed for seepage look-up tables in corroborative DTN: LB0702PASEEP01.001_R0 [DIRS 179511], as documented in *Abstraction of Drift Seepage* (SNL 2007 [DIRS 181244]). The modification of the look-up tables is based on the notion that the resulting seepage percentages from the Seepage Model for Performance Assessment are identical for simulation cases that have the same ratio of percolation flux $q_{perc,ff}$ (in mm/yr) over permeability k (in m^2). This is because the steady-state capillary pressure and saturation conditions are determined by the ratio of percolation flux over permeability, not by the individual flux and permeability values.

The new extended-range look-up table for seepage into the 5.5-m wide center section of a collapsed drift is provided in corroborative DTN: LB0705PASEEP02.001 [DIRS 181093]. The new look-up table is given in file:

ResponseSurfaceSMPA_Collapsed_DriftCenter_ExtendedFlux.dat

In the PMA, this file replaces the collapsed-drift look-up table provided in DTN: LB0702PASEEP01.001_R0 [DIRS 179511]. Seepage rates for the PMA are interpolated from the new look-up table.

C6.3 WASTE PACKAGE AND DRIP SHIELD DEGRADATION

C6.3.1 Conceptual Model

Drip Shield General Corrosion Rates

The DS design utilizes Titanium Grade 7 for the plate and Titanium Grade 29 for the frame materials. The general corrosion degradation of the DSs is evaluated for both the underside and topside surface of the DS. General corrosion (or passive corrosion) is the uniform thinning of the material at its open-circuit corrosion potential (E_{corr}), and it can potentially occur when a liquid film exists on the surface of the DS. The titanium general corrosion model is based upon corrosion rates for Titanium Grade 7 determined by weight-loss measurement after 2.5 years of controlled exposure. The rate data supports two environmentally distinct corrosion rates, one for a relatively aggressive aqueous environment, the other corresponding to a rather benign environment. The detailed description of the corrosion model for the TSPA-LA can be found in *General Corrosion and Localized Corrosion of the Drip Shield* (SNL 2007 [DIRS 180778]).

The aqueous environments for DS corrosion are defined on the basis of dissolved fluoride concentrations. The 'steady-state' passive current density measurements of Titanium Grade 7 from a series of long-term (approximately 20 days) potentiostatic polarization tests showed that the passive corrosion rate of the alloy is low and not much affected by chloride ion concentration and pH; however, the passive corrosion rate increases significantly with an increase in the fluoride ion concentrations of water contacting the alloy (Brossia and Cragnolino 2001 [DIRS 162420], Figure 10; Brossia and Cragnolino 2004 [DIRS 180832], Figures 8 to 10). The critical (or minimum) fluoride ion concentration that causes a marked increase in the passive corrosion rate is about 0.5 millimolar (mM), and the passive corrosion rate increase levels off at about 0.01 molar (or 10 mM) fluoride ion concentration (Brossia and Cragnolino 2004 [DIRS 180832], Figure 9). The passive corrosion behaviors of Titanium Grade 2 and Grade 7 were about the same for the environments tested by the above investigators. Thus, for the PMA modeling purpose, an environmental condition that could lead to elevated fluoride ion concentrations in the water contacting DS is defined as an 'aggressive environmental condition' for the DS general corrosion. Any other environmental condition is defined as a 'benign environmental condition.' The critical (or minimum) fluoride ion concentration that causes a marked increase in the passive corrosion rate is set to 0.5 mM or 9.5 mg/L.

The chemical composition of the seepage water that enters the drifts will change in response to evaporation, mineral precipitation, or both. Throughout the thermal period (depending on the relative humidity in the drifts), evaporative concentration of seepage can occur in the EBS. Evaporation increases aqueous species concentrations, mineral precipitation, and the concentration of the most soluble components in brines. In accordance with the geochemical divide theory, the composition of the seepage water changes according to the sequence of minerals that should precipitate from that solution as a function of initial water composition, thermal conditions, relative humidity, and gas composition where the evaporation occurs (SNL 2007 [DIRS 177412], Section 6.3.3.1). An aggressive corrosion environment would only be present when the topside surface of the DS is exposed to dripping water with an evaporative concentration of seepage. However, for simplicity, the TSPA-LA Model applies the aggressive environment DS general corrosion rate to the topside surface of DSs when they are exposed to

seepage dripping, regardless of the changes in water chemistry due to the thermal evolution of the repository. The aggressive environment DS general corrosion rate is also applied to the topside surface of DSs for locations in the repository that are not exposed to dripping seepage. The benign environment DS general corrosion rate is applied to the underside surfaces of the DS at all locations. This treatment results in an earlier failure of DSs. Note that fluoride concentrations in the initial (i.e., with no evaporation) pore waters are all significantly lower than the critical value of 9.5 mg/L for aggressive corrosion (SNL 2007 [DIRS 177412], Table 4.1-3).

The temporal evolution of the physical and chemical environmental conditions within the waste emplacement drifts of the repository, including the DS and WP surfaces, is documented in *Engineered Barrier System: Physical and Chemical Environment* (SNL 2007 [DIRS 177412]). The near-field chemistry model defines four starting waters as representative of the potential range of the Topopah Spring pore-water compositions (SNL 2007 [DIRS 177412]). As water percolates down through from the surface, it interacts with the rock. The water-rock interactions modify the water composition. The normal compositions due to water-rock interactions are further modified by the repository heating as the water passes through the thermal field in the TSw. Ultimately, this thermally altered water is what enters the drift and controls the chemical conditions in the drift. Output seepage water compositions span the natural variability of pore-water compositions in repository units. The data in Table 4.1-3 of *Engineered Barrier System: Physical and Chemical Environment* (SNL 2007 [DIRS 177412]) show that fluoride concentrations in the 34 pore water samples from the Topopah Spring Tuff used to define the four starting waters all range from 0.36 to 4.8 mg/L, with the majority between 1-2 mg/L. Therefore, it is likely that the benign conditions will prevail in the repository after the radiation heat attenuates and the repository returns to near ambient conditions. In the PMA, the chemical environment for DS general corrosion is determined explicitly from the incoming seepage water compositions calculated by the EBS Chemical Environment Submodel (Section 6.3.4). For DSs whose topside surface is exposed to dripping seepage water, the general corrosion environment (e.g. aggressive or benign) is determined as a function of the seepage water chemistry. When the fluoride concentration exceeds 0.5 mM, an aggressive environment is assumed to be present on the topside of the DS. As seepage water compositions return to near ambient conditions, the fluoride concentration drops below 0.5 mM and the environment is switched to benign conditions.

Weight-loss Data for General Corrosion of the Waste Packages

The Alloy 22 general corrosion rates used in the TSPA-LA Model are represented by one of three cumulative distribution functions (CDFs) determined from the five-year crevice geometry samples (Section 6.3.5.1.3 and SNL 2007 [DIRS 178519], Sections 6.4.3). The observed general corrosion rates of the crevice specimens are higher than those of the 'plain' weight-loss specimens (SNL 2007 [DIRS 178519], Figure 6-22). This may have been caused by the difference in surface-polishing treatments between these two groups of test specimens (Wong et al. 2004 [DIRS 174800]). The weight-loss specimens were polished on both sides while the crevice specimens were polished only on one side. Thus, the unpolished surface of the crevice specimens retained the finishing given at the mill (by the primary metal producer) at the time of their immersion into the test electrolytes (i.e., the crevice specimens were tested without removing the mill-annealed oxide coating from their surface) (SNL 2007 [DIRS 178519], Section 6.4.3.2). It is possible that the removal of this mill-annealed oxide film from the

unpolished side of the crevice specimens during post-test specimen cleaning caused a greater amount of weight-loss for these specimens. This, in turn, could have resulted in derivation of higher general corrosion rates for the crevice specimens.

The PMA includes an alternative model using the corrosion rates of weight-loss samples to derive the R_o distribution for use in the general corrosion model of WP outer barrier (Alloy 22). These rates are documented in *General Corrosion and Localized Corrosion of Waste Package Outer Barrier* (SNL 2007 [DIRS 178519], Section 6.4.3.5.2). The weight-loss data is fit to a Weibull distribution using maximum likelihood estimators (i.e., using the same methods applied to the crevice sample data). The results of this fitting procedure found that the scale parameter, *b*, and a shape parameter, *c*, are 3.447 nm/yr and 1.318, respectively (SNL 2007 [DIRS 178519], Section 6.4.3.5.2 and Appendix VI). A plot of the general corrosion rate distribution resulting from fitting the five-year exposed weight-loss sample data and the data themselves is shown on Figure C6-3. A comparison of the weight-loss data with the crevice sample data shows that the weight-loss data show less corrosion relative to the TSPA-LA general corrosion model (Figure C6-4). This evaluation of the effects of the exclusion of the weight-loss data from the TSPA-LA was conducted using two alternative PMA modeling cases that evaluated the affects on the Seismic GM and Nominal Modeling Cases. The PMA results discussed in Section C.7.1 and Section C.7.2 do not include the weight-loss data in the WP general corrosion submodel calculations. Evaluation of this data is contained in Section C7.3, General Corrosion of the Waste Packages.

Localized Corrosion WP Failure Area

Localized corrosion is a phenomenon in which corrosion progresses at discrete sites or in a non-uniform manner (SNL 2007 [DIRS 178519], Sections 6.4.4). The area of the Alloy 22 WP outer barrier that is contacted by seepage is potentially subject to localized corrosion (SNL 2007 [DIRS 178519], Sections 6.3.5 and 6.4.4.8.3). In the TSPA-LA Model, it is assumed the maximum available area for localized corrosion (i.e., the area of the WP wetted by seepage) is the area of the WP damaged by localized corrosion (SNL 2007 [DIRS 178519], Section 6.3.5.2.2). Therefore, the entire surface area of the WP is removed as a barrier to water inflow and transport of radionuclides from a localized corrosion damaged WP.

In the PMA, the results of an ACM are used to establish a minimum WP area subject to crevice corrosion processes from localized corrosion (SNL 2007 [DIRS 178519], Sections 6.4.4.8.3). The ACM considers a minimum WP creviced surface area based on the WP-to-emplacement pallet contact area (SNL 2007 [DIRS 178519], Sections 6.4.4.8.3). The calculated minimum WP-pallet contact area is 1.924×10^4 mm^2 (SNL 2007 [DIRS 178519], Sections 6.4.4.8.3). Therefore, the minimum creviced area is about 0.05 percent of the total WP surface area of 36.074 m^2 for the transportation, aging, and disposal (TAD) canister-bearing WP configuration. The maximum available area for localized corrosion is the area of the WP wetted by seepage. In the absence of specific information regarding local environments on the WP, for the PMA the area of the WP failed by localized corrosion was assumed to have a log-uniform distribution that was sampled between the range of the entire WP surface area that is exposed to seepage (100 percent) and the calculated ACM minimum of 0.05 percent of the WP surface area (SNL 2007 [DIRS 178519], Section 6.4.4.8.3).

Alloy 22 Residual Stress Threshold

The damage abstractions for the seismic scenario will define the total damaged area on the WP barrier. The presence of high residual tensile stress has the potential to result in potential SCC. This combined mechanical-corrosion failure mechanism is expected to be a cause of damage to the WP and DS from impact processes caused by vibratory ground motions and by rockfall induced by vibratory ground motions. The areas that exceed the residual tensile stress threshold are considered damaged areas. The damaged or deformed area that exceeds a residual stress threshold is conceptualized to result in a tightly spaced network of stress corrosion cracks (SNL 2007 [DIRS 176828], Sections 6.1.4). Application of a residual tensile stress threshold for seismic failures is non-mechanistic in the sense that detailed calculations for potential crack initiation and potential crack propagation are not used to determine the actual failure time after a seismic event. Rather, a network of stress corrosion cracks is considered to immediately form once the residual tensile stress threshold is exceeded, providing potential pathways for radionuclide transport and release (SNL 2007 [DIRS 176828], Sections 6.1.4). The residual tensile stress threshold is often referred to as the residual stress threshold, with the understanding that the principal residual stress must always be tensile to initiate the potential for SCC. The structural response calculations for the WP exposed to seismic induced vibratory ground motions were evaluated for three values of the residual stress threshold for Alloy 22: 90 percent, 100 percent, and 105 percent of the yield strength of Alloy 22 (SNL 2007 [DIRS 176828], Sections 6.1.4). The residual stress threshold range for Alloy 22 is provided in *Stress Corrosion Cracking of the Waste Package Outer Barrier and Drip Shield Materials* (SNL 2007 [DIRS 181953], Section 6.2.2 and Table 8-1). The SCC threshold stress initiation criterion for Alloy 22 is defined as 1.05 YS(T) (at-temperature yield strength) (SNL 2007 [DIRS 181953], Section 8.1.1). The Alloy 22 residual stress threshold associated with the initiation of SCC was established by applying a safety factor to the maximum long-term applied stress without failure. Results obtained from the constant-load tests were used because the conditions were shown to be conservative relative to the expected repository environment and failure was not observed in this data (SNL 2007 [DIRS 181953], Section 6.2.2). In addition, to appropriately reflect uncertainty, a range from 0.9 YS(T) to 1.05 YS(T) with a uniform distribution between these values was selected for use in the TSPA-LA Model (SNL 2007 [DIRS 181953], Section 6.2.2). For the PMA, a range from 100 percent to 105 percent of the yield strength of Alloy 22 was used to evaluate damage to the WP outer barrier during a seismic event. The narrower range of uncertainty is justified for use in the PMA since the residual stress threshold for Alloy 22 was defined at 105 percent already including a safety factor of 2.0 (SNL 2007 [DIRS 181953], Section 6.2.2). The seismic damage abstraction calculates the probability of nonzero damage to a WP as a function of the sampled residual stress threshold. A lower residual stress threshold results in a greater probability of damage to the WP (SNL 2007 [DIRS 176828], Table 6-11 and Table 6-26). Application of the reduced range for residual stress threshold in the PMA will decrease the number of WP damaged during a seismic event.

C6.3.2 Model Implementation

Drip Shield General Corrosion Rates

The temporal evolution of the physical and chemical environmental conditions within the waste emplacement drifts of the repository, including the DS and WP surfaces, is documented in

Engineered Barrier System: Physical and Chemical Environment (EBS P&CE) (SNL 2007 [DIRS 177412]). The EBS Chemical Environment Submodel is described in Section 6.3.4. There are 396 in-drift precipitated salts (IDPS) look-up tables for seepage water composition spanning combinations of Pco_2 and temperature for each of four starting water types, 11 water-rock interaction parameter bins, and nine combinations of three Pco_2 values and three temperatures. The IDPS tables for TSPA-LA use are part of DTN: SN0701PAEBSPCE.001_R1 [DIRS 180523], and the guidance for using these inputs is provided in EBS P&CE (SNL 2007 [DIRS 177412], Section 6.15).

The local calculations of the EBS Chemical Environment Submodel determine the Pco_2 pH, $[Cl^-]$, and $[NO_3^-]$ of the crown seepage water. The TSPA-LA Model only requires pH, ionic strength, $[Cl^-]$, and $[NO_3^-]$ of the crown seepage water. The look-up tables included in the EBS Chemical Environment Submodel only include these parameters extracted from the chemical parameters contained in the 396 IDPS look-up tables (DTN: SN0701PAEBSPCE.001_R1 [DIRS 180523]). To correlate the DS general corrosion environment with the fluoride concentrations in the seepage waters, the fluoride concentration needed to be extracted for use in the PMA. Each IDPS look-up table is defined for a specific starting water type, temperature, and Pco_2. The tables are defined for Pco_2 values of 10^{-2}, 10^{-3}, and 10^{-4} bar and temperature values of 30°C, 70°C, and 100°C. There are 99 tables for all possible combinations for each of the four starting waters. For any combination of temperature and Pco_2 values, the fluoride concentration of the seepage water increases with decreasing relative humidity (e.g., evaporative water compositions prevail). Table C6-1 contains the minimum relative humidity below which the fluoride concentration exceeds 0.5 mM for the 99 possible combinations for each of the four starting waters.

To calculate the DS surface general corrosion environment for each repository subregion, the DS surface temperature, drift Pco_2, and DS relative humidity are fed into the look-up table. When the DS relative humidity exceeds the minimum value defined in Table C6-1, the benign environment for DS general corrosion is applied to the topside surface of the DS for all locations. When the relative humidity is below the minimum value, aggressive conditions are applied to the topside of the DS in all locations. For the underside of the DS, the general corrosion rate corresponding to the benign environment is applied for the entire simulation, identical to the TSPA-LA Model.

The EBS Thermal-Hydrologic (TH) Environment Submodel (Section 6.3.2) contains the DS temperatures and relative humidity values used to evaluate the DS corrosion environment for the PMA. The PREWAP_LA V1.1 software (PREWAP_LA V1.1, STN: 10939-1.1-00 [DIRS 181053]) creates environment-history files containing the WP and DS temperature and relative humidity histories as well as the drift wall temperature.

Weight-Loss Data for General Corrosion of the Waste Packages

For each percolation subregion, the WAPDEG V4.07 software simulates corrosion degradation of WPs by patch penetration (due to general corrosion) (Section 6.3.5.1.3). The model implementation is identical to the TSPA-LA Model, with the exception that only one rate distribution is chosen for each realization. This distribution is sampled by the WAPDEG V4.07 software for every patch on each WP. Two additional external files were added to the TSPA

PMA_dB, *WDlnR_ESC_WL_cdf* and *WDlnR_ASC_WL_cdf*, which represent the weight loss general corrosion rate CDFs (corroborative DTN: MO0708TSPAPROC.000 [DIRS 182979]). The first data set represents the scaled rate used in the WP/DS Degradation Submodel WP general corrosion calculations (Section 6.3.5), and the second data set is used to calculate the average WP thickness in the Seismic Damage Abstraction (Section 6.6). The development of the WAPDEG input vector and associated files is documented in corroborative DTN: MO0708TSPAPROC.000 [DIRS 182979]. This evaluation of the effects of the exclusion of the weight-loss data from the TSPA-LA was conducted using two alternative PMA modeling cases that evaluated the affects on the Seismic GM and Nominal Modeling Cases. The PMA results discussed in Section C.7.1 and Section C.7.2 do not include the weight-loss data in the WP general corrosion submodel calculations. Evaluation of this data is contained in Section C7.3, General Corrosion of the Waste Packages.

Localized Corrosion Waste Package Failure Area

The implementation of the localized corrosion WP failure area affects only the Drip Shield EF Modeling Case. However, localized corrosion of the WP outer barrier was simulated for all modeling cases in the Nominal, Early Failure and Seismic Scenario Classes. The Localized Corrosion Initiation and Propagation Submodel (Section 6.3.5.2.3) calculates the likelihood of localized corrosion on the WP outer surfaces which will lead to WP failure as a function of the EBS Chemical Environment, Seepage, and EBS TH Submodels. The primary output from the Localized Corrosion Initiation and Propagation Submodel is the fraction of CSNF WPs and CDSP WPs that fail by localized corrosion due to seepage, as a function of time, in each percolation subregion. These fractions are used to define the number of WPs that fail by localized corrosion during the simulation time and their average breach areas as a function of time. Localized corrosion is not included in the Nominal, Seismic GM and Waste Package EF cases because the DSs remain intact over the time frame in which the seepage water composition was calculated to potentially initiate localized corrosion. For the Igneous Scenario, both the DS and the entire WP is assumed to be destroyed; therefore, localized corrosion is not included.

Modifications to the TSPA-LA Model to include the PMA distribution of localized corrosion WP failure areas for the Drip Shield EF Modeling Case are outlined here. A new stochastic parameter was added to the model in the *Epistemic_Params* container (*f_WP_failed_area_EF_DS_PMA_a*) with a log-uniform distribution [0.0005-1]. The Drip Shield EF Modeling Case parameter *f_WP_Dam_EF_DS* in the EBS submodel container *\Global_Inputs_and_Calcs\ Global_Events \Global_EF\ Model_Input_EF* was modified to select the distribution for the fraction of the WP surface area failed from localized corrosion during a Drip Shield EF Modeling Case. These parameters feed the EBS Flow and EBS Transport Submodel calculations (Section 6.3.6 & Section 6.3.8) with the appropriate advective and diffusive areas used to calculate radionuclide release and transport.

Alloy 22 Residual Stress Threshold

The implementation of the Alloy 22 residual stress threshold involves both the Nominal and Seismic GM Modeling Cases. Modifications to the TSPA-LA Model to include the PMA value for the residual stress threshold of Alloy 22 are outlined here.

In the *Epistemic_Params* container, the Alloy 22 residual stress threshold parameter (*Stress_Thres_SCC_a*) was changed from a uniform distribution between 315.9 MPa to 368.55 MPa (equivalent to 0.90 to 1.05 stress threshold) to 351 MPa to 368.55 MPa (or 1.00 to 1.05 stress threshold values). These parameters feed the Nominal WP and DS Degradation Submodel calculations (Section 6.3.5) and the Seismic Damage Abstraction (Section 6.6).

C6.4 ENGINEERED BARRIER SYSTEM FLOW

C6.4.1 Conceptual Model

Water, whether in liquid or vapor state, can be transported in and out of a breached WP by both diffusive and/or advective percolation through failed areas on the outer layers of WPs. Accurate knowledge of these water mass fluxes is inherently important to constrain the amount of water that would interact with waste components. At an early stage of the repository, when a significant amount of heat generated by radiation still remains, this transport will be affected by the temperature gradient across WP barriers; that is, higher temperatures inside a WP will tend to prevent water vapor condensation onto waste components. The amount of water available inside a WP will ultimately determine the extent of waste degradation and the subsequent release and transport of radionuclides from the WPs. Waste degradation may modify the water potential inside a WP by releasing hydroscopic salts into water, affecting water vapor transport across the WP barriers. The objective of this PMA is to obtain an estimate of the quantity of water available inside a breached WP for waste degradation, and radionuclide transport. This analysis involves coupling the thermal evolution, waste degradation, and water transport. The amount of water is modeled as a function of relative humidity in the EBS, dripping rate, distribution of failed openings on the WP outer layers, and extent of waste degradation. In general, the model is somewhat similar to those developed for water or moisture transport in soils or in other analogous subsurface unsaturated porous media. Walton (1994 [DIRS 127454]) also applies a similar approach in an attempt to describe the potential effect of evaporation on the water chemistry interacting with WP components. The following processes are included in the model:

- In-package water condensation or evaporation as controlled by thermal evolution
- Water diffusion and advection through failed openings on WPs
- Water consumption by chemical reactions
- Capillary and osmotic effects on water saturation in alteration products
- Dripping water run-off onto WP surface.

In the TSPA-LA Model, the failure patches of the WP outer layer are assumed to have no resistance to advective seepage flows (SNL 2007 [DIRS 177407], Section 6.3.3.2.5). The TSPA-LA Model also assumes that the condensation of water vapor inside a WP is controlled by water sorption onto corrosion products (SNL 2007 [DIRS 177407], Section 6.3.4.3.2) and no water will be consumed by corrosion reactions (SNL 2007 [DIRS 177407], Section 5.4).

Different from the TSPA-LA model, the PMA water balance analysis: (1) assumes that a failure patch will be filled with porous corrosion products, which will provide additional resistance to water percolation into a breached WP; (2) accounts for water consumption by reactions; and (3) fully couples hydrologic effects (e.g., the sheet flow on the WP surface and capillarity effect of porous corrosion products) and chemical processes (e.g., water consumption and salt release by reactions; the depression of water activity with increasing dissolved salt concentration). The modeling system for in-package water balance is shown in Figure C6-5.

Water Potentials

It is assumed that water vapor inside a WP will remain in equilibrium with liquid water in pore space of waste degradation products, and the pore space of the alteration products will be the only space for holding liquid water. Additional liquid water beyond the capacity of pore space will percolate through the whole WP. This assumption is justified if the failed openings are distributed equally on both the upper and lower surface of the WP. This assumption maximizes the water flux out of the WP.

By analog to unsaturated soils, it is also assumed that the total water potential (ψ, in bars) inside the pores of waste degradation or metal corrosion products is determined by both the matrix potential of water (ψ_m, in bars) in the porous degradation products and the osmotic potential (ψ_o, bars) due to the presence of dissolved salts in the pore water (Nassar and Horton 1989 [DIRS 179400]):

$$\psi = \psi_m + \psi_o . \qquad \text{(Eq. C6.4-1)}$$

The matric potential is related to water saturation degree (s_w) by a water retention function. For simplicity, Campbell's function (Campbell 1974 [DIRS 179405]) is adopted:

$$\psi_m = \psi_e (s_w)^{-b} \qquad \text{(Eq. C6.4-2)}$$

where ψ_e and b are constants. ψ_e can be further related to the particle size of the porous material (Campbell and Shiozawa 1992 [DIRS 180398]): $\psi_e = 0.0003 d^{-1.5}$ in the unit of m (1 m water head = 0.0978 bar), where d is the mean particle diameter (mm). For a non-isothermal case, Equation C6.4-2 needs to be corrected for the effects of elevated temperature and dissolved salt on water surface tension. Since the capillarity and matric potential in an unsaturated porous medium are proportional to the surface tension of water (Dullien 1979 [DIRS 179404]) and also because the surface tension of water linearly decreases with the temperature and increases with dissolved salt concentration (m, molality) over the parameter ranges of interest (Belton 1935 [DIRS 180397]; Matubayasi et al. 1999 [DIRS 179401]), such effects can be captured by modifying Equation C6.4-2 into:

$$\psi_m = \psi_e (s_w)^{-b} [1 - \alpha (T_{in} - T_0)](1 + \beta m) \qquad \text{(Eq. C6.4-3)}$$

where α and β are constants; T_{in} is the temperature inside the WP (K); and T_0 is the reference temperature (298.15 K).

For a simple electrolyte solution, the osmotic potential of water can be calculated using the van't Hoff relation (Papendick and Campbell 1981 [DIRS 179398], p. 17):

$$\psi_o = \omega \eta m \rho_{water} R T_{in} \quad \text{(Eq. C6.4-4)}$$

where ω is the osmotic coefficient; η is the number of osmotically active species per molecule of solute (e.g., 2 for NaCl); and R is the gas constant (82.06 cm^3.atm/mole/K). The osmotic coefficient weakly depends on salt concentration (Papendick and Campbell 1981 [DIRS 179398], p. 17; Robinson and Stokes 1965 [DIRS 108567]):

$$\omega = 0.006m^2 + 0.0251m + 0.9102 \quad \text{(Eq. C6.4-5)}$$

(corroborative DTN: SN0704PMAWBCAL.001 [DIRS 182335]). Equation C6.4-4 has been widely used in modeling salt and moisture distributions in soils (Papendick and Campbell 1981 [DIRS 179398]). For simplification, NaCl is chosen to represent dissolved salts in WPs.

The total water potentials calculated from Equations C6.4-1 to C6.4-5 can then be related to the relative humidity inside a WP (RH_{in}) by (Harris 1980 [DIRS 179403]):

$$RH_{in} = \frac{\rho_{in}}{\rho_s(T_{in})} = e^{-\frac{\psi v_w^0}{RT_{in}}} \quad \text{(Eq. C6.4-6)}$$

where ρ_{in} is the water vapor density inside the WP (kg/m^3); ρ_s is the saturated water vapor density of pure water (kg/m^3); and v_w^0 is the molar volume of water (m^3/mole), which is assumed to be constant over the temperature range of interest. ρ_s (kg/m^3) can be calculated as a function of temperature T (K) by (corroborative DTN: SN0704PMAWBCAL.001 [DIRS 182335]; Kimball et al. 1976 [DIRS 179402]; and Nassar and Horton 1989 [DIRS 179400]):

$$\rho_s(T) = 10^{-3} e^{19.83 - 5000/T} \quad (kg/m^3). \quad \text{(Eq. C6.4-7)}$$

The analysis result for a special case indicates that water saturation is sensitive to the temperature difference across the outer layers of the WP and dissolved salt concentration. In this analysis, vapor density is assumed to be in equilibrium between the inside of the WP and drift. One degree difference in temperature may effectively reduce water vapor condensation on waste components (corroborative DTN: SN0704PMAWBCAL.001 [DIRS 182335]).

Water Consumption by Chemical Reactions

The reactions during the degradation of waste forms and WP materials consume water. Based on inventory estimates (SNL 2007 [DIRS 180506], Table 6-9), four major components are included in the calculation of water consumption: CSNF, N-reactor, HLW glass, and Stainless Steel Type 316. The degradation of each component can be represented by an overall stoichiometric reaction:

1 kg waste component i + n_i^w (mole) H_2O → n_i^s (m^3) solids + n_i^{salt} (mole) salt (Eq. C6.4-8)

where stoichiometric coefficients n_i^w, n_i^s, and n_i^{salt} can be evaluated with EQ3/6 (STN: 10813-8.1-00 [DIRS 176889]) calculations (Table C6-2).

Mass Balance Equations

The water balance inside a breached WP can be described by:

$$\frac{dQ}{dt} = \rho_{water}\left(F_{in}^{adv} - F_{out}^{adv}\right) + \frac{D\phi^{5/3}A}{L}(\rho_{out} - \rho_{in}) - M_w \sum_i n_i^w S_i R_i \qquad \text{(Eq. C6.4-9)}$$

with

$$Q = \frac{V_s\phi}{1-\phi}\left[s_w\rho_{water} + (1-s_w)\rho_{in}\right] + V_{void}\rho_{in} \qquad \text{(Eq. C6.4-10)}$$

where Q is the mass of water as either liquid or vapor inside the WP (kg); t is the time (year); V_s is the total volume of degradation products (m^3) inside the WP; ϕ is the porosity of degradation products, assumed to uniformly distribute over [0.35, 0.5]; ρ_{water} is the density of liquid water (kg/m^3); V_{void} is the volume of void space outside the fuel rods and corrosion rinds (m^3); F_{in}^{adv} and F_{out}^{adv} are the advective fluxes of liquid water into and out of the WP (m^3/year); ρ_{out} is the water vapor density outside the WP (kg/m^3) calculated by multiplying the relative humidity on the waste package outer surface to the saturated water vapor density at a given temperature; D is the molecular diffusivity of water vapor in air (m^2/year); A is the cross-sectional area of failure patches on the outer layers of the package for water vapor transport (m^2); L is the thickness of the outer layers (m); M_w is the molecular weight of water (kg/mole); S_i is the surface area of waste component i (m^2); and R_i is the degradation rate of component i (kg/m^2/year). The left-side term of Equation C6.4-9 represents the accumulation rate of water mass inside the WP. The three terms on the right side of the equation represent the water flux by advective flows, water flux by vapor diffusion, and water consumption rate, respectively.

The factor $\phi^{5/3}$ includes the effect of tortuosity (e.g., Nassar and Horton 1989 [DIRS 179400]). The molecular diffusivity of water vapor in air can be calculated by (Kimball et al. 1976 [DIRS 179402]):

$$D = 722 * (T_{in} + T_{out})/2/273.15)^{1.75} \ (m^2/\text{year}) \qquad \text{(Eq. C6.4-11)}$$

where T_{out} is the temperature in the drift (K). It is assumed in Equation C6.4-9 that no significant advective vapor flow will be induced by water evaporation or consumption. This assumption is justified for two reasons: First, for water vapor to advectively flow out, the gas pressure inside the WP must be higher than the ambient pressure. This would be possible only when a large volume of liquid water were introduced into a hot (>100°C) WP. However, this is unlikely because water seepage will not occur until the drift temperature is below the boiling temperature of water. Below the boiling point, it is not possible for evaporation inside the WP to generate air

pressures larger than those outside in the drift since the saturated water vapor pressure is always lower than 1 atm (Lide 2006 [DIRS 178081]). Second, water consumption by chemical reactions could create a pressure gradient between the inside and outside of the WP, which may induce an incoming advective gas flow. This is unlikely because water vapor partial pressure only accounts for a small fraction of total gas pressure (e.g., <10 percent for temperatures < 40°C) (Lide 2006 [DIRS 178081]), and the total pressure gradient created by reactions, if any, will be small in magnitude. This small gradient will be further compensated by the in-package accumulation of non-reactive air components that will be brought in by advective flows. Furthermore, as discussed below, with 10 percent of the WP surface failed, vapor diffusion can only transport up to 756 liters of water into a WP per year. Such a large diffusive flux is expected to overwhelm water-consuming reactions, resulting in an even smaller total pressure gradient.

Similarly, the mass balance for other quantities can be formulated as follows:

$$\frac{dV_s}{dt} = \sum_i n_i^s S_i R_i \qquad \text{(Eq. C6.4-12)}$$

$$\frac{dW_i}{dt} = -S_i R_i \qquad \text{(Eq. C6.4-13)}$$

$$\frac{dV_{void}}{dt} = \sum_i \left(\frac{1}{\rho_i^{waste}} - n_i^s \right) S_i R_i \qquad \text{(Eq. C6.4-14)}$$

$$\frac{dM_{salt}}{dt} = 1000(F_{in}^{adv} m_{seep} - F_{out}^{adv} m) + \sum_i n_i^{salt} S_i R_i \qquad \text{(Eq. C6.4-15)}$$

$$m = \frac{M_{salt}(1-\phi)}{\rho_{water} V_s s_w \phi} \qquad \text{(Eq. C6.4-16)}$$

where W_i is the total mass of material component *i* inside a WP (kg); M_{salt} is the total mass of salt dissolved in the pore water (moles); m_{seep} is the concentration of dissolved salt in the seepage water; and ρ_i^{waste} is the density of waste component *i* (kg/m^3). The initial values of V_s and M_{salt} are set to zero. The initial value of W_i is set to the initial inventory of material component *i*. The initial void space, V_{void}, is estimated to be 6.72 m^3 for a CSNF package and 8.49 m^3 for the co-disposed (CDSP) WP (corroborative DTN: SN0704PMAWBCAL.001 [DIRS 182335]).

Advective Water Influx (F_{in}^{adv}): A Sheet-Flow Model

For a dripping case, it is crucial to evaluate the advective water influx term (F_{in}^{adv}) in Equation C6.4-9. The evaluation assumes that:

- A drip falling on the WP surface will form a rivulet with a thickness of h (m) and a surface area of A_w (m^2), which will move down across the package surface.
- Upon the rivulet flowing over the failure openings of WP, a certain fraction of water will be able to percolate into the package through filling corrosion products, with the rest running off the package surface.
- The corrosion products filling the failure openings can be treated as a porous medium for water percolation. It should be recognized that little is known about the hydraulic permeability of corrosion products. Based on the observations on the rust of ancient ferrous artifacts exposed to atmospheric corrosion, porous corroded material could have the pore size ranging from a few nanometers to tens of microns with the porosity generally less than 15 percent (Dillman et al. 2004 [DIRS 171480], Table 7). For the PMA purpose, the hydraulic permeability of corrosion products is assumed to be 10^{-14} to 10^{-10} m^2, equivalent to that of silty sand (Freeze and Cherry 1979 [DIRS 101173]). The porosity of corrosion products is chosen to be 0.35 to 0.5. Since the values chosen here are likely higher than actual ones, the PMA water balance may overestimate the water flux percolating through WPs.

The velocity of a rivulet movement (v, m/s) can be described by (Ruschak et al. 2001 [DIRS 180747]; Lin et al. 2003 [DIRS 180748]):

$$v = \frac{\rho_{water} g h^2 \sin(\frac{\pi}{2} - \theta)}{3\mu} \qquad \text{(Eq. C6.4-17)}$$

where g is the gravity acceleration (9.81 m/s^2); θ is the angle as shown on Figure C6-5; and μ is the viscosity of water (Pa s = $kg \cdot m^{-1} \cdot s^{-1}$). The evolution of the rivulet can be described by:

$$\frac{d(A_w h)}{dt} = -\phi A_w f K_c^s \sin\theta \qquad \text{(Eq. C6.4-18)}$$

$$\frac{d\theta}{dt} = -\frac{v}{2\pi R_{wp}} \qquad \text{(Eq. C6.4-19)}$$

where f is the fraction of failed openings on the WP total surface area; K_c^s is the hydraulic conductivity of the corrosion products filling the failure openings at water saturated conditions (m/s); and R_{wp} is the radius of the WP. Equation C6.4-18 describes the volume change of water rivulet due to water percolation into the WP through the failure openings under the water head of $\sin\theta$ $(= L\sin\theta / L)$. Equation C6.4-19 converts the linear velocity of water rivulet to the radian velocity. For simplification, it is assumed that the thickness of water film will remain

approximately constant $\left(\frac{dh}{dt}=0\right)$ as the rivulet moves across the surface of the WP. The uncertainty related to this approximation is captured by uniformly sampling *h* over the range of 0.1 mm to 3 mm. This sampling range is constrained from both laboratory and natural analog observations (Katz et al. 1995 [DIRS 180396]; Alekseenko et al. 1998 [180383]). Then, Equation C6.4-18 reduces to:

$$\frac{d(A_w)}{dt}=\frac{-\phi A_w f K_c^s \sin\theta}{h}. \qquad \text{(Eq. C6.4-20)}$$

By combining Equations C6.4-17, C6.4-19, and C6.4-20, the following relation is obtained:

$$\frac{dA_w}{d\theta}=\frac{6\pi R_{wp}\phi A_w f K_p^s \tan\theta}{h^3}=\lambda A_w \tan\theta \qquad \text{(Eq. C6.4-21)}$$

with

$$\lambda=\frac{6\pi R_{wp}\phi f K_p^s}{h^3} \qquad \text{(Eq. C6.4-22)}$$

where K_p^s (= $\mu K_c^s/\rho_{water}g$) is the permeability of the corrosion products (m^2). By integrating Equation C.6.4-21 for A_w over [θ_0, 0], one obtains:

$$\frac{A_w}{A_w^0}=(\cos\theta_0)^{\lambda} \qquad \text{(Eq. C6.4-23)}$$

where A_w^0 is the initial area of the water film and θ_0 corresponds to the angle θ at the dripping location onto the WP surface. Assuming that the dripping is uniformly distributed over the footprint of the WP, one can calculate the fraction of dripping water that can enter a WP:

$$f_{in}^{adv}=1-\int_{\pi/2}^{0}(-\sin\theta_0)(\cos\theta_0)^{\lambda}d\theta_0=\frac{\lambda}{1+\lambda}. \qquad \text{(Eq. C6.4-24)}$$

For a given dripping rate Q_d (m^3/wp/year), the quantity of water that can enter a breached WP can then be calculated by:

$$F_{in}^{adv}=f_{in}^{adv}Q_d. \qquad \text{(Eq. C6.4-25)}$$

Equation C6.4-17 was originally established for a smooth surface but later extended to a rough surface (e.g., by correcting the water film thickness for surface roughness (Myers 2002 [DIRS 181017]). Given the maximum general corrosion rate of Alloy 22 (23 nm/year) (SNL 2007 [DIRS 178519]), the layer thickness of corrosion products on WP surfaces will remain less than 0.5 mm over at least the first 20,000 years. Thus, the validity of the proposed sheet-flow model is justified. Furthermore, the thickness of water film is generally found to be

on the scale of a few millimeters for various systems (Katz et al. 1995 [DIRS 180396]; Alekseenko et al. 1997 [DIRS 180383]). For the PMA, this thickness is chosen to range from 0.1 mm to 5 mm.

As illustrated on Figure C6-6, the fraction of seepage water that can enter a WP, calculated with Eq. C6.4-24, is relatively small, and the majority of the water will run off over the package surface. Consider an extreme case where the DS is completely neutralized and the maximum seepage rate is 1,000 liters/WP/year. For a typical water film thickness of 1 mm, the water influx F_{in}^{adv} is estimated to be < 1 liter/WP/year, which is small compared to the possible maximum vapor diffusion flux ($D\phi^{5/3}A\rho_d / L$) ~756 liters/WP/year under the same conditions with 10 percent of water package surface failed. Thus, vapor diffusion can potentially become a major source of water supply for waste degradation

Advective Water Out-Flux (F_{out}^{adv})

Assuming that the advective water flux is induced by the gravitational force only, the advective water flux out of the WP (F_{out}^{adv}) in Equation C6.4-9 can be calculated by:

$$F_{out}^{adv} = A_{out} K_c(s_w) \text{ for } s_w < 1 \qquad \text{(Eq. C6.4-26)}$$

where A_{out} is the opening area at the lower part of the WP surface. In reality, water drainage would create a gradient in the degree of water saturation that would prevent further drainage; thus, the water flux calculated from Equation C6.4-26 tends to be greater than would be expected. The hydraulic conductivity K_c is a function of water saturation s_w (Campbell 1974 [DIRS 179405]):

$$K_c = K_c^s (s_w)^{2b+3} \qquad \text{(Eq. C6.4-27)}$$

where b is the Campbell constant in Equation C6.4-2. For s_w = 1 (i.e., the pores of the degradation products are not sufficient for holding all incoming water), the extra water is assumed to percolate through the WP without any accumulation in the void space. From Equations C6.4-9 and C6.4-10, the advective flow F_{out}^{adv} can then be calculated by:

$$\begin{aligned} F_{out}^{adv} = F_{in}^{adv} &+ \frac{1}{\rho_{water}} \left[\frac{D\phi^{5/3} A}{L} (\rho_{out} - \rho_{in}) - M_w \sum_i n_i^w S_i R_i \right] \\ &+ \frac{1}{\rho_{water} \Delta t} \left[Q(t - \Delta t) - \frac{V_s \phi \rho_{water}}{1 - \phi} - V_{void} \rho_{in} \right] \end{aligned} \qquad \text{(Eq. C6.4-28)}$$

where $Q(t - \Delta t)$ is the mass of water accumulated at the previous timestep. The above formulation implies that, even for a non-dripping case (F_{in}^{adv} = 0), an advective out-flux is possible if the water inside a WP contains high enough hygroscopic salts, which may create a significant water vapor density gradient ($\rho_{out} - \rho_{in}$) across the outer layers of a WP barrier and

cause water condensation inside the package. This may happen for HLW packages since the HLW releases could generate a considerable amount of salt during dissolution, as indicated in Table C6-2.

Solid-Water Ratio

The volume ratio of solid to water ($r_{s/w}$) is an important parameter for establishing the chemical conditions inside a WP. This ratio can be calculated by:

$$r_{s/w} = \frac{1-\phi}{s_w \phi}. \qquad \text{(Eq. C6.4-29)}$$

After the thermal event, s_w will remain more or less constant and so will the solid-water ratio, possibly leading to relatively narrow in-package chemical conditions.

Temperature Difference across Waste Package Outer Barrier Layers

As discussed above in this section, the temperature difference between the inside and the outside of a WP may have a significant effect on the water potential inside the WP. For a steady-state heat conduction, this temperature difference (ΔT) can be estimated by:

$$\Delta T = T_{in} - T_{out} = \frac{1000 Q_h L}{2\pi D_c R_{wp}} \qquad \text{(Eq. C6.4-30)}$$

where Q_h is the linear thermal load (kW/m) and D_c is the thermal conductivity of the package materials (W/m/K). Equation C6.4-30 is derived by equating the linear thermal load to the heat flux across the package outer layer. As shown on Figure C6-7, the temperature difference across the outer barrier layers of the WP will be less than 2°K and diminish quickly after ~100 years. Note that the thermal load used in the calculation is the average value over the whole repository. These values are close to the thermal loads for CSNF WPs because they constitute a dominant fraction of the overall inventory. The HLW generally has a lower thermal load than the CSNF, and the temperature difference across the outer layers of HLW WPs is expected to be smaller. Therefore, in the PMA, the temperature difference (ΔT) between the inside and the outside of a WP is set to zero.

C6.4.2 Model Implementation

The water balance model presented in the previous section is solved iteratively using a Newton-Raphson method. The iteration algorithm is implemented in GoldSim with a looping container. The water balance model feeds (1) water saturation to the waste form and EBS water volume calculation, (2) advective water out-fluxes to both the In-Package Chemistry Submodel and Radionuclide Transport Submodel, and (3) the ionic strength to both the radionuclide solubility model and the colloid transport model.

Let us consider a discretization in time for Equation C6.4-9 using a first order backward difference in time. Let the solution be known at time level *n* and the solution be required at time level *n+1*. A fully implicit discretization of Equation C6.4-9 is

$$\frac{V_s\phi}{1-\phi}\left[s_w^{n+1}\rho_{water}+\left(1-s_w^{n+1}\right)\rho_{in}^{n+1}\right]+V_{void}\rho_{in}^{n+1}-\frac{V_s\phi}{1-\phi}\left[s_w^{n}\rho_{water}+\left(1-s_w^{n}\rho_{in}^{n}\right)\right]-V_{void}\rho_{in}^{n}$$

$$=\Delta t\left\{\rho_{water}\left(F_{in}^{adv}-F_{out}^{adv}\left(s_w^{n+1}\right)\right)+\frac{D\phi^{5/3}A}{L}\left(\rho_{out}-\rho_{in}^{n+1}\right)-M_w\sum_i n_i^w S_i R_i\right\} \quad \text{(Eq. C6.4-31)}$$

Similarly, a discretization of Equation C6.4-15 yields

$$M_{salt}^{n+1}=M_{salt}^{n}+\Delta t\rho_{water}\left(F_{in}^{adv}m_{seep}-F_{out}^{adv}m\right)+\Delta t\sum_i n_i^{salt}S_iR_i\,. \quad \text{(Eq. C6.4-32)}$$

Equation 6.4-16 is used to eliminate the variable m from Equation C6.4-32, yielding moles of salt as a function of water saturation

$$M_{salt}^{n+1}=\frac{M_{salt}^{n}+\Delta t\rho_{water}F_{in}^{adv}m_{seep}+\Delta t\sum_i n_i^{salt}S_iR_i}{1+\dfrac{\Delta t(1-\phi)F_{out}^{adv}\left(s_w\right)}{V_s s_w\phi}}\,. \quad \text{(Eq. C6.4-33)}$$

When the moles of salt are calculated from Equation C6.4-33, then the salt concentration is computed from Equation C6.4-16.

The discretized water balance (Equation C6.4-31) and water vapor density (Equation C6.4-6) are nonlinear algebraic equations in s_w^{n+1} and ρ_{in}^{n+1}. In order to solve these nonlinear system equations, together with auxiliary Equations C6.4-16 and C6.4-33, a Newton-Raphson method is applied. Consequently, the mass balance equation, Equation C6.4-10, is written as

$$F_1(s_w^{n+1},\rho_{in}^{n+1})=\frac{V_s\phi}{1-\phi}\left[s_w^{n+1}\rho_{water}+\left(1-s_w^{n+1}\right)\rho_{in}^{n+1}\right]+V_{void}\rho_{in}^{n+1}$$

$$-\frac{V_s\phi}{1-\phi}\left[s_w^{n}\rho_{water}+\left(1-s_w^{n}\rho_{in}^{n}\right)\right]-V_{void}\rho_{in}^{n}$$

$$-\Delta t\left\{\rho_{water}\left(F_{in}^{adv}-F_{out}^{adv}\left(s_w^{n+1}\right)\right)+\frac{D\phi^{5/3}A}{L}\left(\rho_{out}-\rho_{in}^{n+1}\right)\right.$$

$$\left.-M_w\sum_i n_i^w S_iR_i\right\}=0\,. \quad \text{(Eq. C6.4-34)}$$

The water vapor density equation, Equation C6.4-6, is written in the form

$$F_2\left(s_w^{n+1},\rho_{in}^{n+1}\right)=\rho_{in}^{n+1}$$

$$-\rho_s(T_{in})exp\left\{-\frac{v_w^0}{RT_{in}}\left[\frac{\psi_e}{(s_w^{n+1})^b}(1-\alpha(T_{in}-T_0))(1+\beta m)+\omega\eta m\rho_{water}RT_{in}\right]\right\}=0. \quad \text{(Eq. C6.4-35)}$$

The mole salt accumulated (Equation C6.4-33) and salt concentration (Equation C6.4-16) is updated at each Newton-Raphson iteration.

Let the solution vector be denoted

$$\mathbf{x}=\begin{pmatrix} s_w^{n+1} \\ \rho_{in}^{n+1} \end{pmatrix} \quad \text{(Eq. C6.4-36)}$$

and the vector equation written as

$$\mathbf{F}(\mathbf{x})=\begin{pmatrix} F_1(\mathbf{x}) \\ F_2(\mathbf{x}) \end{pmatrix}=\mathbf{0}. \quad \text{(Eq. C6.4-37)}$$

The Newton-Raphson iteration is

$$\mathbf{x}^{(k+1)}=\mathbf{x}^{(k)}-\mathbf{J}^{-1}(\mathbf{x}^{(k)})\mathbf{F}(\mathbf{x}^{(k)}) \quad \text{(Eq. C6.4-38)}$$

where the initial iteration is taken to be the value at the n-time level

$$\mathbf{x}^{(0)}=\begin{pmatrix} s_w^n \\ \rho_{in}^n \end{pmatrix}. \quad \text{(Eq. C6.4-39)}$$

The Jacobian matrix is

$$\mathbf{J}(\mathbf{x})=\begin{pmatrix} \frac{\partial F_1}{\partial s_w} & \frac{\partial F_1}{\partial \rho_{in}} \\ \frac{\partial F_2}{\partial s_w} & \frac{\partial F_2}{\partial \rho_{in}} \end{pmatrix}. \quad \text{(Eq. C6.4-40)}$$

The elements of the Jacobian matrix are computed as

$$\frac{\partial F_1}{\partial s_w}=\frac{V_s\phi}{1-\phi}(\rho_{water}-\rho_{in})+\Delta t\rho_{water}\frac{\partial F_{out}^{adv}}{\partial s_w}, \quad \text{(Eq. C6.4-41)}$$

$$\frac{\partial F_1}{\partial \rho_{in}}=\frac{V_s\phi}{1-\phi}(1-s_w)+V_{void}+\Delta t\frac{D\phi^{5/3}A}{L}, \quad \text{(Eq. C6.4-42)}$$

$$\frac{\partial F_2}{\partial s_w}=(F_2(s_w,\rho_{in})-\rho_s(T_{in}))\left\{-\frac{v_w^0}{T_{in}R}\left[-\frac{b}{s_w^{b+1}}\psi_e[1-\alpha(T_{in}-T_0)](1+\beta m)\right.\right.$$

$$+\frac{\psi_e}{s_w^b}(1-\alpha(T_{in}-T_0))\beta\frac{\partial m}{\partial s_w}+\omega\eta\rho_{water}RT_{in}\frac{\partial m}{\partial s_w}\Bigg]\Bigg\} \quad \text{(Eq. C6.4-43)}$$

$$\frac{\partial F_2}{\partial \rho_{in}}=1 \quad \text{(Eq. C6.4-44)}$$

where

$$\frac{\partial F_{out}^{adv}}{\partial s_w}=A_{out}K_c^s(2b+3)s_w^{2b+2} \quad \text{(Eq. C6.4-45)}$$

$$\frac{\partial m}{\partial s_w}=-\frac{M_{salt}(1-\phi)}{\rho_{water}V_s\phi s_w^2}+\frac{1-\phi}{\rho_{water}V_s\phi s_w}\frac{\partial M_{salt}}{\partial s_w} \quad \text{(Eq. C6.4-46)}$$

$$\frac{\partial M_{salt}}{\partial s_w}=-\Delta t\rho_{water}\left(F_{out}^{adv}\frac{\partial m}{\partial s_w}+m\frac{\partial F_{out}^{adv}}{\partial s_w}\right). \quad \text{(Eq. C6.4-47)}$$

Combining Equations C6.5-46 and C6.5-47, one obtains:

$$\frac{\partial m}{\partial s_w}=-\frac{\frac{M_{salt}(1-\phi)}{\rho_{water}V_s\phi s_w^2}+\frac{\Delta t(1-\phi)}{V_s\phi s_w}m(s_w)\frac{\partial F_{out}^{adv}}{\partial s_w}}{1+\frac{\Delta t(1-\phi)}{V_s\phi s_w}F_{out}^{adv}(s_w)}. \quad \text{(Eq. C6.4-48)}$$

The iteration is repeated until a convergence criterion is satisfied:

$$\max\left(s_w^{(k+1)}-s_w^{(k)},\rho_{in}^{(k+1)}-\rho_{in}^{(k)}\right)<\varepsilon. \quad \text{(Eq. C6.4-49)}$$

In the model simulation, ε is set to 10^{-8}, which is small enough since s_w varies from 0.05 to 1.0 and ρ_{in} from 0.0 to 1.2 kg/m^3.

C6.5 WASTE FORM DEGRADATION AND RADIONUCLIDE MOBILIZATION

C6.5.1 Conceptual Model

In-Package Chemistry

The TSPA-LA Model for in-package chemistry is documented in *In-Package Chemistry Abstraction* (SNL 2007 [DIRS 180506]). In the TSPA-LA, the pH inside a breached waste package is uniformly sampled over the range constrained from equilibrium with two major buffering mineral phases. The PMA, however, assumes that over the constrained range the in-package pH has a triangular distribution with the most probable value calculated as function of the extent of waste degradation, the pore water volume in waste degradation products, and the rate of water percolation through a waste package. As in the TSPA-LA Model, the predicted pH

is used to calculate concentrations of radionuclides and colloids. Unlike the TSPA-LA Model, the PMA in-package chemistry model no longer calculates the ionic strength inside a WP; this parameter is now provided by the water balance model (Section C6.4).

As in the TSPA-LA Model, the PMA in-package chemistry model is a batch reactor model that calculates the result of mixing the components within the waste-form cells of the WP with water and atmospheric gases to predict equilibrium solution compositions (SNL 2007 [DIRS 180506]). This model is applied to a total of three well-mixed reaction cells in two types of WPs: CSNF WPs and CDSP WPs. The CDSP WPs are represented by the WPs comprised of two multicanister overpacks (MCO) and two defense high-level waste (DHLW) glass logs. The three cells are:

1. CSNF cell 1. This cell contains all materials within and including the baskets inside the CSNF WP, excluding the guides. This includes the fuel basket assembly of neutron moderator material and thermal shunts, fuel basket tubes, and CSNF assemblies.

2. CDSP cell 1A. This cell comprises two containers of defense high-level waste (DHLW) glass and their canisters, as designed for the 2MCO/2DHLW WP.

3. CDSP cell 1B. This cell comprises two MCO containers of N reactor fuel and their canisters, as designed for the 2MCO/2DHLW WP.

The two CDSP cells are modeled separately because the CDSP waste forms are physically separated and their initial distribution within the WP is highly heterogeneous. Justification details are provided in *In-Package Chemistry Abstraction* (SNL 2007 [DIRS 180506], Section 6.3.1.1). Material volumes, properties, degradation rates, and surface areas are obtained from files *Rates CSNF Cell 1.xls, Rates 2DHLW cell.xls*, and *Rates 2MCO Cell 1b.xls* in DTN: SN0702PAIPC1CA.001_R2 [DIRS 180451]. Compositions of Stainless Steel 304B4 and HLW glass are taken from *304B4 Comp and Reaction.xls* and *CDSP_HLWGlass_Sensitivity r2.xls* in DTN: SN0702PAIPC1CA.001_R2 [DIRS 180451]. Other material compositions are obtained from Tables 6-4 and 6-6 of SNL (2007 [DIRS 180506]) and from Table 3 of the referenced document (CRWMS M&O 2001 [DIRS 153263]).

A modification of the *data0.ymp.R5* database, named *data0.R5f*, was used for all EQ3/6 simulations. Most of the modifications were incorporated in the *data0.R5f* database generated in *In-Package Chemistry Abstraction* (SNL 2007 [DIRS 180506], Section 6.3.1.1) and documented in DTN: SN0702PAIPC1CA.001 [DIRS 180451]. This database was further modified (but not renamed) by adding missing molar volumes for $NiMoO_4$ and Nontronite-H, two minerals that can account for a significant fraction of V_s in the PMA in-package chemistry simulations. The molar volume of $NiMoO_4$ is from Ehrenberg et al. (1995 [DIRS 180746]). The molar volume of Nontronite-H is assumed to be equivalent to the molar volume of Nontronite-Na, whose molar volume was already in the database. The modified database, *data0.R5f,* and its associated binary file, *data1.R5f,* are included in corroborative DTN: SN0704PMAIPCPM.001 [DIRS 180745].

The scope of the PMA in-package chemistry calculations is similar to that of the TSPA-LA model. The same three waste-form cells are considered for in-package chemistry (SNL 2007 [DIRS 180506], Section 1.0). The ranges of independent parameters, such as the partial pressure

of CO_2 (g) (10^{-4} to $10^{-1.5}$ bars), temperature (25°C), and flow rate (0 to >100 L/yr), are also similar. The primary difference between the two models is that in the PMA, liquid water is assumed to be restricted to the pores of the degradation products. The minimum ratio of the volume of degradation products, V_s, to the volume of liquid water, V_w, is set at V_s/V_p, where V_p is the volume of pore space. In these simulations V_s/V_p is 1.5, corresponding to a porosity of 0.4. Thus, V_s/V_w is 1.5 when the pores are fully saturated with water. The high range of V_s/V_w (≥ 1.5) in the PMA in-package chemistry model is accomplished by decreasing the amount of water in the simulations.

The PMA calculations for in-package chemistry consist of two parts: The first part is used to construct the functional dependence of pH on waste degradation kinetics for the cases where vapor diffusion is a dominant mechanism for water transport through a breached WP; The second part is to establish the relationship between the water chemistry and the flux of liquid water that percolates the WP. The calculation results are documented in two corroborative DTNs: (1) SN0704PMAIPCPM.001 [DIRS 180745] contains the process model simulations and results, and (2) SN0704PMAIPCAB.001 [DIRS 182602] contains the abstractions.

Diffusion-Dominated Cases—For the diffusion-dominated cases, liquid influx (q) was set to zero in the EQ3/6 simulations. One liter of pure water (to simulate water from water vapor) was reacted at a fixed pCO_2 with cell materials for a period of time to allow degradation products to accumulate. The actual amount of time was immaterial because the equilibrium pH and ionic strength in this model are only a function of the following variables: (1) pCO_2, (2) the relative amount of materials degraded (defined by ratios of k_{wf}, k_{ss}, and k_{al}), and 3) the ratio of the volume of water in the cell, V_w, to the total amount of degradation. The total amount of degradation can be represented by the total volume of degradation products, V_s.

A simulated ten years of reaction and accumulation was used as a starting point from which V_s/V_w was adjusted. To adjust V_s/V_w, H_2O was incrementally removed from the cell. Because the PMA in-package chemistry application considers water only in the pores of the degradation products and the porosity of the degradation products is assumed to be 0.4, the useful range of process model outputs is limited to V_s/V_w greater than or equal to 1.5. At 1.5, the pores are saturated with water. Above 1.5, the pores are unsaturated.

The simulations were performed over large ranges of pCO_2, relative degradation rates, and V_s/V_w so that the effects of these variables could be captured in the vapor influx abstraction. Table C6-3 shows the ranges simulated for each cell. The k_{ss}/k_{wf} ratio was varied from low values to high values in each cell except for the 2MCO cell. Because stainless steel will degrade much more slowly than N reactor fuel, the maximum k_{ss}/k_{wf} ratio simulated was 0.01 in the 2MCO cell. More finely discretized values of k_{ss}/k_{wf} were simulated in the CSNF and 2DHLW cells where pH outputs were highly sensitive to k_{ss}/k_{wf}. H_2O removal in the simulations was terminated at high values of V_s/V_w (e.g., greater than 20) or when the ionic strength reached ~4 molal. Application of the model over this ionic strength range is sufficiently accurate for the purposes of the in-package chemistry model (SNL 2007 [DIRS 180506], Section 6.3.1.1).

Liquid-Advection Dominated Cases—Liquid influx occurs when q is finite. This rate was varied in the liquid influx process model simulations to determine its effect (in combination with variations in degradation rates and pCO_2) on pH. In addition, the composition of the liquid

influx was varied. For condensed water, pure water was used. For seepage, the SD9 pore water of the TSPA-LA model was used as the incoming liquid. The composition of the SD9 water is from pore water sample SD-9/1184.7-1184.8/UC in DTN: GS030408312272.002 [DIRS 165226].

With respect to V_s and V_w, the liquid influx model assumes all water is located in the pores of the degradation products, all pores are filled with water, and the porosity of the degradation products is 0.4. Thus, for the liquid influx simulations, V_s/V_w was maintained at 1.5. Because EQ3/6 requires a constant volume of 1 liter of water for steady-state flow-through calculations, initialization of the cell was more involved than for the vapor influx model. To achieve an initial V_s/V_w of 1.5, degradation was simulated until V_s increased to 1.5 liters. In addition, because degradation reactions consume H_2O, additional H_2O was added to maintain 1 liter of water. From this point, flow-through of condensate or seepage was initiated and kinetically simulated for approximately 9 pore volumes for a given pCO_2, liquid influx rate, and set of degradation rates. By 9 pore volumes, the pH and ionic strength essentially level off and the system is approximately at steady state, as shown in the example on Figure C6-8.

Simulations were performed over large ranges of pCO_2, relative degradation rates, and liquid influx rates so that the effects of these variables could be captured in the liquid influx abstraction. Table C6-3 shows the ranges simulated for each cell. The ranges of k_{ss}/k_{wf} simulated span the variation in pH generated from the reactions, as determined in the diffusion-dominated simulations. The values of q simulated are generally in the range where flushing of the cell with seepage or condensed water controls the steady-state pH and ionic strength.

The degree to which the reactions or liquid influx rate affects the steady-state pH and ionic strength is controlled by the ratio of kinetic reaction rates to the liquid influx rate. This ratio is generally known as the Damkohler number. High values of this ratio (e.g., >100 when dimensionless) imply that the concentrations of the pertinent aqueous components are controlled by the kinetic reactions (i.e., dissolution reactions of structural materials and waste forms), while low values (e.g., <0.01 when dimensionless) imply that concentrations are controlled by the composition of the liquid influx. There are additional processes that affect pH and ionic strength, namely the heterogeneous equilibrium reactions involving precipitation and dissolution of degradation products. These processes are assumed to be instantaneous; thus, regardless of the Damkohler number, the steady-state pH and ionic strength will be affected by these equilibrium reactions.

Time-invariant pH and ionic strength is calculated using the EQ3/6 flow-through mode when the Damkohler number is extremely low or extremely high. When it is extremely low, as in the liquid influx simulations performed using the parameter values in Table C6-4, the composition of the liquid influx and the equilibrium reactions control the pH. When the Damkohler number is extremely high, the time-invariant pH is approximated by the vapor influx model where the liquid influx rate is zero (Table C6-3). In the middle range between extreme Damkohler numbers, the flushing rate is low but relevant. In this range, a long period of time is required to achieve 9 pore volume flushes, the point at which steady state values are approximated. This large amount of time causes V_s to substantially increase. At the same time, V_w stays constant due to a limitation of the EQ3/6 flow-through mode. Because V_s substantially increases and V_w stays

constant in the simulations, the V_s/V_w ratio also substantially increases, which conflicts with the developed liquid influx model that sets the V_s/V_w ratio at 1.5. Consequently, estimates of pH and ionic strength between the two Damkohler number extremes are obtained by interpolation.

The PMA in-package chemistry outputs of the vapor influx and liquid influx models are not a function of time. The absolute amounts of materials degraded and volumes of degradation products and water in the cell (V_s and V_w) are immaterial to the pH and ionic strength calculations. The vapor influx model is essentially an equilibrium model. For a given combination of pCO_2 and relative degradation ratio of stainless steel to waste form, a unique pH and ionic strength are determined for each V_s/V_w analyzed. The liquid influx model is a steady-state model. As long as steady state is achieved, a unique steady-state pH and ionic strength can be determined for a given combination of pCO_2, liquid influx rate, and set of relative degradation rates.

Commercial Spent Nuclear Fuel Cladding

Cladding prevents the environment from interacting with the fuel pellets by limiting the water or moist air from contacting and interacting with the fuel pellets and reduces radionuclide transport by reducing the diffusion area. All CSNF currently in use in the United States (both pressurized water reactor and boiling water reactor fuel) consists of assemblies of Zircaloy tubing filled with UO_2 fuel pellets (SNL 2007 [DIRS 180616], Section 6.1[a]). The cladding is completely sealed and only fuel with failed cladding can interact with water or moist air. Some cladding could be damaged before it is received at the repository. The distribution of failed cladding as-received has an expected value of 0.1 percent (SNL 2007 [DIRS 180616], Section 4.0[a]). After repository closure, additional cladding failure will occur due to mechanical causes. Mechanical failure occurs from events associated with seismic activities such as rockfall or rock overburden. The seismic events and associated rockfall can occur at any time and are addressed in a specific seismic scenario (Section 6.6). However, in the TSPA-LA model, no credit is taken for CSNF cladding as a barrier in all scenario classes (Section 5.0, Assumption 5.1.3). The as-received condition of the CSNF cladding is used in the PMA to evaluate the impact of this assumption.

The PMA repository performance is evaluated using the set of scenario classes defined in Section 6.1.2. Unfailed (not perforated) cladding is assumed to remain intact for the 10,000-year regulatory period in the absence of mechanical damage mechanisms from seismic ground motion and/or rockfall since the intact cladding only starts to split when the cladding fails and only after waste package failure (SNL 2007 [DIRS 180616], Section 6.2.4]). Any further cladding failure is the result of physical processes, including mechanical damage to the intact cladding caused during seismic events (SNL 2007 [DIRS 180616], Section 6.2.3[a]). Therefore, applying the assumption that all CSNF cladding failed for the 10,000-year Nominal and Early Failure Scenario Classes in the TSPA-LA Model is bounding. In the PMA analysis, the as-received cladding condition is assumed to be the only cladding failed for CSNF for the Nominal and Early Failure Scenario Classes during the first 10,000 years postclosure. WP failures do not occur in the Nominal Scenario Class during the first 10,000 years postclosure; therefore, the assumption in the TSPA-LA Model that all cladding is failed has no impact on dose. In the Seismic GM Modeling Case, DSs do not fail during the first 10,000 years postclosure. The probability of CSNF WP failure under an intact DS with intact internals is nonzero only for large events (Section 6.6.1.2.2.2 and Figure 6.6-10(a)). The probability of occurrence of a large enough event

in the first 10,000 years postclosure is small since these types of seismic events occur, on average, every 23,000 years. In the Seismic FD Modeling Case, the WP failures are caused by the shearing of WPs (Section 6.6.1.1.2) and cladding is likely to be failed as well. The as-received failed fuel rods undergo instantaneous clad splitting when the WP fails. The exposed fuel is available for waste form degradation. No cladding credit is taken for stainless steel clad fuel. The as-received cladding condition and stainless steel cladding distribution is provided by *Cladding Degradation Summary for LA* (SNL 2007 [DIRS 180616], Section 6.2[a] and Section 7.0[a]).

Degradation Rate of Commercial Spent Nuclear Fuel

CSNF constitutes a major portion of the total waste inventory. The degradation rate of this waste form is therefore expected to have a significant impact on the overall performance of the Yucca Mountain repository. In the TSPA-LA model, this rate is calculated as a function of temperature, oxygen fugacity, total carbonate concentration, and pH (BSC 2004 [DIRS 169987]). In the PMA, the functional dependence on water chemistry remains the same as in the TSPA-LA model. However, the distribution range of the effective surface area of CSNF is modified, and two additional scaling factors are included to capture the effect of long-term dissolution and the decrease in radiolysis, based on the synthesis of literature data.

Dissolution Kinetics—Oxidative dissolution of CSNF undergoes numerous chemical and physical transformations. The factors that have major impacts on waste dissolution are listed in Table C6-5. The PMA specifically considers the following factors: the effective surface areas, the effect of long-term dissolution, and the changes in radiolysis. In the PMA, the matrix dissolution rate of CSNF is calculated as:

$$\log(F) = Log(A) - Log(f_1) - Log(f_2) + a_0 + a_1 IT + a_2.pCO_3 + a_3.pO_2 + a_4.pH \qquad \text{(Eq. C6.5-1)}$$

where F is the fractional dissolution rate of the fuel (d^{-1}); A is the effective surface area of the fuel (m^2/mg); f_1 is the scaling factor for the effect of long-term dissolution; f_2 is the scaling factor for the attenuation of gamma and beta radiations; IT is the inverse temperature (K^{-1}); pCO_3 is the negative base 10 logarithm of total carbonate (molar); and pO_2 is the negative base 10 logarithm of oxygen partial pressure (atm). The PMA uses the same functional form as the TSPA-LA model for the rate dependence on temperature, pCO_3, pO_2, and pH, and thus the last five terms in Equation C6.5-1 (a_0 through a_4) remain the same as in the TSPA-LA model. These five terms were determined from short-term and far-from-equilibrium flow-through tests with rates normalized to surface areas obtained either by geometric or Brunauer-Emmett-Teller (BET) methods (BSC 2004 [DIRS 169987]). The first three terms on the right side of Equation C6.5-1 are described below in this section.

Effective Surface Area (A)—The effective surface area refers to the portion of total surface area that is directly contacted by water and participates in fuel dissolution. The effective surface area is always less than the total surface area for several reasons. First of all, the spent fuel contains various impurities such as plutonium, zirconium, and molybdenum; these metal cations tend to accumulate on the surface of the spent fuel during dissolution and block reactive surface sites (Grandstaff 1992 [DIRS 113255]). Some elements in groundwater (e.g., calcium and silicon) can also exert a similar effect on a surface site (Santos et al. 2006 [DIRS 182015]; Santos et al.

2006 [DIRS 182052]). These impurities usually have high affinities for sorption to the dissolution surface and form a protective surface layer, which could result in a large decrease in dissolution rate (Wilson and Gray 1990 [DIRS 115085]). Furthermore, not all surfaces of fuel grains are accessible by reactants. In many cases, the rate of a dissolution reaction is limited by the diffusion of chemical species either toward or away from the reaction front, and the reaction front does not necessarily coincide with grain boundaries (Finch et al. 1999 [DIRS 127332]). In addition, fuel dissolution takes place at a solid-water interface; as the water saturation decreases, the contact area between fuel and water also decreases (Kuechler and Noack 2007 [DIRS 182054]; Sverdrup and Warfvinge 1988 [DIRS 182056]). For all these reasons, accurately determining the effective surface area for a chemical reaction, particularly in environments with variable degrees of saturation, is generally subject to large uncertainties.

In the TSPA-LA Model, the effective surface area is determined from a combination of geometrical calculation, particle size distribution, BET measurements, and fractional release measurements (BSC 2004 [DIRS 169987]). The TSPA-LA Model chooses the geometric-specific surface of the cracked fragments in irradiated pellets as a most probable value for the effective surface area. The lower and upper limits are constrained from the fractional release measurements and particle size distributions, respectively. The distribution of log (A m^2/mg) for the TSPA-LA model is assumed to be triangular with a low of -7.3, apex of -6.7, and maximum of -5.4. This distribution is conservative, especially for the upper limit, because it assumes that all the surfaces of individual fuel fragments are accessible by reactants. Such scenarios are unlikely, since fuel dissolution takes place at a reaction front rather than pervasively on the surface of each individual particle, as discussed above.

To remove these conservatisms in the TSPA-LA model, the PMA derives the effective surface area from the fractional release rate measurements in fuel rod segment tests and further assumes this to be the most probable value. This assumption is reasonable because the fractional release rate is a parameter that is directly measured in leaching experiments. The reliability of these measurements has been confirmed by their consistency with the fuel fragment tests (BSC 2004 [DIRS 169987], Tables 6-10 and 6-11). The effective surface area therefore should be chosen to reflect these measurements. Second, dissolution rates depend on the physical configuration of the fuel, and the rod segment tests may more accurately mimic the likely state of spent fuels in a breached WP.

Based on the above discussion, the PMA used the following equation to calculate the effective surface area for spent fuel dissolution:

$$A = A_s . s_w \qquad \text{(Eq. C6.5-2)}$$

where A_s is the effective surface area under water-saturated conditions, and s_w is the water saturation in spent corrosion products calculated in the Water Balance Model (Section C6.4.1). The distribution of log (A_s) is assumed to be right triangular with values at the low and apex end of -7.3 and at the upper bound of -6.7. A right triangular distribution is assumed here as to weigh more on the low value as it was determined from leaching experiments. The upper limit is chosen to be the geometric-specific surface of the cracked fragments in irradiated pellets. A relationship similar to Equation C6.5-2 has been proposed for modeling mineral dissolution in

soils (Kuechler and Noack 2007 [DIRS 182054]; Sverdrup and Warfvinge 1988 [DIRS 182056]).

Scaling Factor for Long-Term Dissolution (f1)—The dissolution rate of spent fuel in a leaching test generally decreases with time (Hanson et al. 2004 [DIRS 182008]; Jégou et al. 2004 [DIRS 182066]). This decrease could be caused by the accumulation of impurities or the formation of coating layers on the dissolving surface of the fuel. For example, precipitation of a schoepite layer may slow down spent fuel dissolution (De Windt et al. 2006 [DIRS 182065]). Hanson et al. (2004 [DIRS 182008]) conducted flow-through dissolution tests using solutions with pH in the range 2 to 7 on a moderate burnup Light Water Reactor spent fuel. They found that the release rates of cesium, strontium, technetium, and plutonium all systematically decreased with time. Over a testing period of 140 days, the release rates for Cs were reduced by a factor of 3 to 10 (Hanson et al. 2004 [DIRS 182008], Figure 1). Therefore, for the PMA, it is recommended that the scaling factor for long-term dissolution be chosen to be 3 to 10 with a uniform distribution over this range. Note that this distribution range is considered conservative because the dissolution rate is expected to decrease further for longer time periods.

Scaling Factor for the Change In Radiolysis (f2)—It has been observed that the rate of UO_2 dissolution is enhanced by both gamma and beta radiolysis even in oxygenated solutions (Shoesmith and Sunder 1992 [DIRS 113368]; Shoesmith 2000 [DIRS 114445]). Note that the dose rate from these radiations in CSNF will diminish after a few hundred years. This implies that laboratory measurements on relatively fresh fuels have inevitably included the enhancing effect of gamma and beta radiolysis and have likely over-estimated the CSNF dissolution rates that are used for long-term performance assessments. To remove this conservatism, the PMA uses a scaling factor (f_2) to account for the diminishing effect of gamma and beta radiations on the CSNF dissolution rate.

In an oxygenated solution, the dissolution rate of UO_2 is found to linearly decrease with the dose rate of external gamma radiation on a log-log scale (Shoesmith and Sunder 1992 [DIRS 113368]; Shoesmith 2000 [DIRS 114445]). The gamma dose rate at the surface of fresh fuel is estimated to be ~10^3 Gy/h, which diminishes to approximately 10 Gy/h after about 800 years (Shoesmith 2000 [DIRS 114445], Figure 6). This decrease in gamma-dose rate is sufficient to reduce the dissolution rate of spent fuel by a factor of ~10 (Shoesmith 2000 [DIRS 114445], Figure 32; Shoesmith and Sunder 1992 [DIRS 113368], Figure 6). It is therefore recommended for the PMA that the scaling factor for the change in radiolysis be set to 5 to 10 with a uniform distribution over this range.

Degradation Rate of High-Level Waste Glass

The glass-degradation model developed in this section provides an expression for calculating releases of radionuclides from a single canister of HLW glass as it dissolves when contacted by water. Key parameters used by the TSPA-LA Model for glass degradation are based on short-term experimental dissolution rate data for a variety of HLW glasses. Because laboratory dissolution rates tend to be many times faster than long-term field rates reported for natural glasses, the TSPA-LA model for glass degradation may be conservative, especially at long times (e.g., greater than several hundred years) following breach of a WP.

Dissolution Mechanism of High-Level Glass—The TSPA-LA model for the dissolution of HLW glass (BSC 2004 [DIRS 169988], Section 6.3) is based on the transition-state theory, which was applied to the dissolution of borosilicate waste glass by Grambow (1985 [DIRS 163257]). Transition-state theory is founded on the concept of an activated complex that is transitional between two or more stable complexes but that has a configuration through which one species (species-1 of a certain configuration) must pass in order to achieve the configuration of a second species (species-2). Although species-2 has a lower free energy than species-1, the energy of the activated complex (or transition-state energy) is higher than both, and the energy difference between species-1 and the activated complex represents the activation energy (E_a) for the reaction, *species-1* ⇨ *species-2* (Lasaga 1981 [DIRS 160187]).

In the case of glass dissolution, Grambow (1985 [DIRS 163257]) proposed that the rate-limiting step, the transition state with the greatest activation energy, is the transition from a partly hydrolyzed complex that is part of the glass (surface) to a fully hydrolyzed complex dissolved in the water. Because silica comprises the essential structural framework of borosilicate glasses, the rate-limiting reaction proposed by Grambow (1985 [DIRS 163257]) is: ≡Si-O-Si(OH)$_3$ + H_2O → ≡Si-OH + Si(OH)$_{4(aq)}$, where [≡Si-O] represents a surface complex that is part of the structural framework. Thus, the rate-limiting step for glass dissolution is the detachment of orthosilicic acid from the glass surface, and the activation energy for that detachment is E_a.

At infinite dilution (and ignoring transport-limiting effects such as diffusion), the detachment of orthosilicic acid will proceed at a forward rate. The forward rate (k_f) depends on the activation energy of the rate-limiting step (E_a), temperature, pH, and glass composition. The forward rate constant, k_f, is defined by the following equation (BSC 2004 [DIRS 169988], Equation 11, p. 6-14):

$$k_f = \vec{k}_0 \times 10^{n \cdot pH} \times \exp\left(\frac{-E_a}{RT}\right). \qquad \text{(Eq. C6.5-3)}$$

The intrinsic rate constant, k_0, depends only on the glass composition (E_a and η are assumed to be independent of glass composition and temperature).

Experimental evidence indicates that, as the concentration of dissolved silica in the solution contacting the glass increases, the (apparent) rate of glass dissolution decreases (the dissolution rate is commonly determined from the rate of release into a solution of silica or boron). Grambow (1985 [DIRS 163257]) then proposed that as the silica concentration in solution approaches saturation with respect to amorphous silica, the rate at which orthosilicic acid detaches from the glass surface will be approximately equal to the rate at which it condenses back onto the surface.

Employing the concept of a mineral saturation index, Q/K, in which K is a solubility constant and Q is the ion activity product in solution, the (apparent) dissolution rate will slow as Q/K approaches unity (i.e., saturation). Grambow (1985 [DIRS 163257]) suggested that because the dissolution of the glass matrix is controlled by the detachment of orthosilicic acid, the value for Q is taken as the activity of orthosilicic acid in solution, and the corresponding value of K is the activity of orthosilicic acid in that same solution saturated with respect to amorphous silica [$SiO_{2(am)}$]. Thus, the precipitation of silica on the glass surface represents the re-attachment

(condensation) of orthosilicic acid and accounts for the common observation of silica-rich layers on surfaces of experimentally altered glasses.

Because glass does not have an equilibrium solubility, the value for K is essentially arbitrary and, recognizing this, Grambow (1985 [DIRS 163257]) proposed including a long-term rate (k_{long}) to account for the fact that the glass matrix will continue to dissolve at some constant (but slow) rate even when the solution is fully saturated with respect to amorphous silica. Thus, taking into account the silica saturation and long-term rate, the following general rate equation can be applied to glass dissolution:

$$rate_G = k_f \left(1 - \frac{Q}{K}\right) + k_{long} \quad \text{(Eq. C6.5-4)}$$

where k_f is defined in Equation C6.5-3.

The term (1-Q/K) has been called the reaction affinity (Grambow 1985 [DIRS 163257]) and is related to the Gibbs free energy of the reaction (ΔG_r) through the saturation index:

$$\Delta G_r = RT \ln\left(\frac{Q}{K}\right) \quad \text{(Eq. C6.5-5)}$$

where R is the gas constant and T is temperature in Kelvin (note that the equilibrium constant, K, is also a function of temperature). As Q/K approaches unity, the Gibbs free energy of reaction—and the reaction affinity—approaches zero.

The long-term rate constant, k_{long}, introduced by Grambow (1985 [DIRS 163257]) must have a functionality similar to that of the forward rate constant, k_f; however, determining the dependence of k_{long} on pH, temperature, and glass composition requires appropriate long-term dissolution-rate data. Although long term is not uniquely defined, it is assumed for the purposes of repository-relevant time scales to be on the order of a few thousand to several tens of thousands of years (or even longer). Such long-term dissolution rates are unavailable from laboratory experiments but can be inferred from observations of natural glasses (e.g., basaltic glasses) that have been altered in nature (Gordon and Brady 2003 [DIRS 176673]). Unfortunately, it is impossible to determine from such observations a reliable rate dependence on pH and temperature because sufficient knowledge about such environmental variables is rarely obtainable for ancient natural systems. In fact, these environmental variables are subject to change over time, both long term and short term (e.g., T can fluctuate diurnally and annually as well as over considerably longer time frames).

In order to implement the Grambow model in the TSPA-LA model (BSC 2004 [DIRS 169988], Equation 13, p. 6-14) combines k_0 and (1-Q/K) into an effective rate constant, k_E:

$$rate_{glass} = k_E \times 10^{n \cdot pH} \times \exp\left(\frac{-E_a}{RT}\right) \quad \text{(Eq. C6.5-6)}$$

where values for k_E, η, and Ea are determined by fitting experimental data; specifically, data for dissolution rates measured in the laboratory. All three parameters are assumed constant for all temperatures between 25°C and 90°C (the temperature range over which experimental data used to develop the model are obtained). Dependence of k_E on glass and solution compositions is accounted for by evaluating k_E from a variety of experiments conducted on various glasses under a range of experimental conditions. Furthermore, k_E used in the current rate model is assigned different values depending on which pH range, either acid or alkaline, is being considered. This is based on the inherent assumption that the reaction affinity, (1-Q/K), takes on different values above and below pH 6.8.

It is readily apparent that the long-term rate constant proposed by Grambow (1985 [DIRS 163257]), k_{long}, is not included in the dissolution-rate equation in the TSPA-LA Model. Although it is well documented that the rate of glass dissolution slows as Q approaches K, this dependency is also unavailable in Equation C6.5-6 (BSC 2004 [DIRS 169988], Equation 13, p. 6-14). Therefore, it is not possible to model a reduction in the dissolution rate through the affinity term. By using Equation C6.5-6 to model glass dissolution, there is no change in the glass dissolution rate over time (despite a preponderance of evidence to the contrary). Instead, the reaction affinity is incorporated into k_E by fitting rate data from glass-corrosion experiments conducted under a variety of experimental conditions where Q/K assumes various values and k_E is treated as an epistemic uncertainty represented by two triangular distributions, one for each pH condition (i.e., pH less than 6.8 and greater than 6.8 at 25°C). The experimentally determined range of k_E values is intended to reflect the potential range of silica saturation expected under repository-relevant conditions: from Q/K near zero, where $k_E \approx k_f$, to Q/K near one (approaching saturation), for which $k_E << k_f$. However, because the range of k_E values is treated as a random variable with a distribution (given by the range of k_E values), there is no rule by which lower values of k_E are preferentially used as an HLW glass log reacts with water that contains increasing silica concentrations as a function of contact time. In addition, the current glass dissolution model does not account for the concentration of dissolved silica in natural groundwater and pore waters expected to enter the repository.

Natural Glasses—Dissolution rates of HLW glasses intended for permanent disposal in a geologic repository are currently modeled as dissolving at rates derived solely from laboratory experiments. In an effort to estimate rates at which HLW glasses are likely to dissolve in a geologic repository over the timescales of interest for geologic disposal (several thousands to tens of thousands of years), a comparison of dissolution rates determined for naturally occurring glasses can provide a range of likely long-term HLW glass dissolution rates more consistent with those observed in the natural environment over repository relevant timescales.

Considerable evidence exists from the study of naturally occurring minerals and glasses in their native environments that the rates at which solids dissolve (or corrode or alter) in nature appears to be substantially slower than rates determined in laboratory experiments (e.g., White and Brantley 2003 [DIRS 168088]; Gordon and Brady 2003 [DIRS 176673]). It is common for initial dissolution rates of minerals and glasses to slow over laboratory timescales; however, even the slowest laboratory rates may be one or more orders of magnitude faster than dissolution rates of analogous materials after thousands of years of weathering in nature. A full explanation for such differences remains a topic of debate; however, Grambow (2006 [DIRS 181381]) notes that, "The main reasons are the progressive *depletion of reactive surface sites*, the *accumulation*

of leached layers, the *formation of secondary precipitates*, the *low permeability and high mineral/fluid ratios*, and *increased solute concentration over time*." (emphasis added). These are primarily time-dependent processes. Grambow (2006 [DIRS 181381]) further notes that "it has been estimated that it would take about 1,000 years for the laboratory-measured rates to decrease to rates observed in the field." He goes on to say that, "Linear, long-term glass dissolution rates are used as a worst-case, upper limit of future behavior."

A primary goal of the PMA is to introduce a reasonable time dependence into the overall model for the rate of glass dissolution, such that the long-term dissolution rate approaches that observed for many natural glasses (primarily of basaltic composition, as these are considered to be reasonable chemical analogues of HLW glasses, largely due to their similar silica and alkali contents) (Byers et al. 1985 [DIRS 163209]; Crovisier et al. 1985 [DIRS 163211]; Lutze et al. 1987 [DIRS 125923]; Grambow et al. 1985 [DIRS 163258]; Gordon and Brady 2003 [DIRS 176673]; and Crovisier et al. 2003 [DIRS 180488]).

Dissolution Rate—In the PMA, the rate expression for HLW dissolution at timestep (t_i) is given by:

$$rate_G(t_i) = k_f \left(1 - \frac{Q}{K}\right)_{t_i} \quad \text{(Eq. C6.5-7)}$$

where the forward rate is calculated with Equation C6.5-3. The intrinsic rate constant ($\vec{k}_0$) in Equation C6.5-3 is assigned a value of 1×10^7 g/m^{-2}·d^{-1}.

Separate sets of parameter values are used to calculate forward reaction rates in acidic and basic solutions, and the pH value at which the acid and basic rates are equal (pH_{eq}) depends on temperature, as given by the following relationship:

$$pH_{eq} = 7.3\text{-}0.02 \times T\,(°C) \quad \text{(Eq. C6.5-8)}$$

which, for 25°C, gives a value for pH_{eq} equal to 6.8 (pH_{eq} equals 5.5 at 90°C).

Constant values of $\eta = -0.49$ and $E_a = 31$ kJ/mol are used for acidic solutions ($pH < pH_{eq}$), and constant values of $\eta = 0.49$ and $E_a = 69$ kJ/mol are used for basic solutions ($pH > pH_{eq}$) (values are from BSC 2004 [DIRS 169988], Table 8-1). Substituting these constant values into Equation C6.5-6 yields the forward rate as a function of pH and temperature:

$$k_{f\_acidic} = 1 \times 10^7 \times 10^{-0.49 \cdot pH} \times \exp(-31/RT) \quad \text{(Eq. C6.5-9a)}$$

$$k_{f\_alkaline} = 1 \times 10^7 \times 10^{0.49 \cdot pH} \times \exp(-69/RT). \quad \text{(Eq. C6.5-9b)}$$

The forward rates calculated with Equations C6.5-9a or C6.5-9b (depending on pH range) are substituted for k_f in Equation C6.5-7 in order to calculate the degradation rate for the applicable range of pH. The pH and temperature are variables in the glass dissolution model and their values are obtained from another model; R is the gas constant.

Reaction Affinity—The reaction affinity at timestep (t_i) in Equation C6.5-7 is split into two parts representing both short and long-term water chemistry respectively:

$$\left(1-\frac{Q}{K}\right)_{t_i} = \left(1-\frac{Q}{K}\right)_{Final} + \left(1-\frac{Q}{K}\right)_{Initial} \times e^{-\left(\frac{T_R}{T_{RC}}\right)} \qquad \text{(Eq. C6.5-10)}$$

where T_R is the thickness of the reaction rind before the current timestep (in millimeters) and T_{RC} is the rind thickness at which solute transport begins to dominate the concentration of silica (and, therefore, Q) at the surface of the dissolving glass. The value of $(1 - Q/K)_{t_i}$ is constant for a given timestep and is incremented for each successive timestep (beginning after water first contacts the glass following the breach of a WP), with subsequent values decreasing exponentially over the course of a realization and approaching a value that represents near-saturation conditions within the alteration rind. Alternatively, as noted above, the time dependence of the reaction affinity is a measure of how the Gibbs free energy of reaction is expected to decrease over time, and the rate at which the reaction affinity term approaches zero corresponds to the rate at which the reaction approaches equilibrium. Because glass can never reach equilibrium with water, the final value of the reaction affinity, $(1\text{-}Q/K)_{Final}$, is chosen to ensure that the glass dissolution rate never equals zero but merely slows to a long-term rate.

The initial value of (1-Q/K) in J-13 groundwater is 0.5 ([Si] = 0.001 M), whereas (1-Q/K) is unity (Q = 0) for water condensed from humid air. Because the release of glass constituents occurs for pristine glass exposed to silica-saturated waters, the initial value of the reaction affinity for exposure to groundwater is taken as being greater than that of J-13. $(1\text{-}Q/K)_{Final}$ corresponds to the long-term reaction affinity for which Q is assumed to be approximately equal to the concentration of dissolved silica in the corrosion rind. Therefore, the value of the reaction affinity, $(1\text{-}Q/K)_{Final}$, is assumed to be near (but not at) saturation with respect to amorphous silica (log[Si] ≈ -2.7 (Stumm and Morgan 1996 [DIRS 125332], pp. 667 and 668). Long-term reaction rates reported for natural basalt glasses after approximately 1,000 to 3,000 years of sub-aerial weathering are on the order of 10^{-5} to 10^{-8} $g \cdot m^{-2} \cdot d^{-1}$ for reaction temperatures commonly reported to be between approximately 0°C and 10°C (Gordon and Brady 2003 [DIRS 176673]). These rates are used to constrain the long-term affinities for HLW degradation. Therefore, the values of reaction affinity can be chosen as:

Humid Air: $(1\text{-}Q/K)_{HA\_Initial} = 1.0$
Groundwater: $(1\text{-}Q/K)_{GW\_Initial} = 0.8$
Long-term reaction affinity: $(1\text{-}Q/K)_{Final} = 5 \times 10^{-4}$ (most probable value).

The exponential factor, T_R/T_{RC}, establishes the rate at which the affinity term approaches the long-term value, $(1\text{-}Q/K)_{Final}$. The parameter T_R is the total thickness of the reaction rind formed since the beginning of the realization (prior to the current timestep, (t_i)) and T_{RC} is the rind thickness at which solute transport (e.g., diffusion) begins to dominate silica concentration at the surface of the dissolving glass and, thereby, begins to dominate the reaction affinity term. The rate dependence establishes that the reaction affinity will (nearly) reach its minimum value, $(1\text{-}Q/K)_{Final}$, after the reaction rind has achieved a thickness approximately five times T_{RC} after which the glass dissolves at a constant long-term (minimum) rate.

The reaction affinity derived from Equation C6.5-10 is substituted into Equation C6.5-7 for $(1 - Q/K)_{t_i}$ in order to calculate the dissolution rate for each timestep, (t_i), and is incremented after each timestep. The long-term rate is simply

$$R_{long} = k_f(1-Q/K)_{Final.} \quad \text{(Eq. C6.5-11)}$$

For example, a value of $(1-Q/K)_{Final}$ equal to 0.005 (which corresponds to a final Gibbs energy of reaction equal to -0.00134 kJ/mol) results in a long-term dissolution rate (R_{long}) that is 0.5 percent of the forward rate. The glass dissolution rate model given by Equations C6.5-7 through C6.5-11 is valid over the pH range 1 to 14, over the temperature range 10°C to 150°C, and over the relative humidity range 44 percent to 100 percent.

Reactive Surface Area—As noted above, the reaction rate must be multiplied by a surface-area term in order to scale the normalized rate to dissolution of a specific glass sample (HLW glass log). As in the TSPA-LA model, the PMA calculates the reactive surface area, $S(t_i)$ (in square meters), of the mass of glass that reacts during a given timestep, (t_i), as follows:

$$S(t_i) = f_{exposure} \times S_{SP} \times M(t_{i-1}) \quad \text{(Eq. C6.5-12)}$$

where

S_{SP} = the specific surface area of the glass (2.70×10^{-3} m^2/kg). S_{SP} is a constant value calculated from the internal geometry of an average glass canister and is calculated from the nominal dimensions and initial mass of glass, based on a weighted average of anticipated waste glasses in short and long canisters.

$f_{exposure}$ = a dimensionless multiplier that accounts for the reactive surface area being greater than S_{SP} due to cracking caused by thermal effects and handling. The value of $f_{exposure}(t_i)$ is sampled over a triangular distribution with both the low and the most probable values of 4 and the high value of 17.

$M(t_{i-1})$ The mass of (undissolved) glass at timestep t_{i-1}.

***M_d*: Mass of Glass Dissolved**—The mass of glass that will have degraded at the end of the current timestep is calculated with:

$$\Delta M_D(t_i) = rate_G(t_i) \times \Delta t_i \times S(t_i) \quad \text{(Eq. C6.5-13)}$$

where $rate_G(t_i)$ is the rate of glass dissolution applied during timestep (t_i), $S(t_i)$ is the surface area available at the beginning of timestep (t_i), and Δt_i is the duration of timestep (t_i).

The mass of undissolved glass that remains at the end of the current timestep, $M(t_i)$, is calculated by:

$$M(t_i) = M(t_{i-1}) - \Delta M_D(t_i) \quad \text{(Eq. C6.5-14)}$$

where $M(t_{i-1})$ is the total mass of undissolved glass prior to the current timestep.

Glass Alteration Layer: Reaction Rind—A description of the reaction rind is given in *Defense HLW Glass Degradation Model* (BSC 2004 [DIRS 169988], Appendix D), including equations to calculate the volume, thickness, and water content of the alteration layer, in terms of the mass of HLW glass that dissolves in a single canister. The volume of the alteration layer is given by:

$$V_R \text{ (in m}^3\text{)} = 3.7 \times 10^{-4} \times M_D(t) \text{ kg.} \qquad \text{(Eq. C6.5-15)}$$

The volume of pore water within the alteration layer is:

$$V_w \text{ (in m}^3\text{)} = 6.3 \times 10^{-5} \times M_D(t) \text{ kg.} \qquad \text{(Eq. C6.5-16)}$$

The thickness of the alteration layer, T_R, is determined from Equation C6.5-17 (BSC 2004 [DIRS 169988], *cf.* Equation D-17, Appendix D, p. D-8):

$$\text{TR (in meters)} = 0.30 - [0.090 - (3.0 \times 10\text{–}5) \times \text{MD}(t)]/2. \qquad \text{(Eq. C6.5-17)}$$

Relative Humidity—As in the TSPA-LA model, glass degradation is not applied (i.e., $rate_G(t_i) = 0$) if the relative humidity is below 44 percent. For relative humidity greater than or equal to 44 percent, the same rate expression (Equation C6.5-7) is used to calculate the degradation rate whether the glass is exposed to humid air, dripping water, or is immersed. At temperatures between 100°C (100 percent relative humidity for water at 0.1 MPa total pressure) and 125°C (44 percent relative humidity), Equation C6.5-7 is used with the pH fixed at 10 (consistent with the TSPA-LA model).

As a cautionary note, Anovitz et al. (2006 [DIRS 180487]), who studied hydration of obsidian over a wide range of relative humidities, state in their *Conclusions* that,

> "... if nuclear waste storage glasses behave in a manner similar to obsidian, large reductions of relative humidity (below about 20 percent relative humidity) will be needed before significant reductions in the rate of glass corrosion due to water diffusion, including the rate of perlite formation, are observed. This should be true even in a vapor-dominated atmosphere, where water-mediated corrosion due to leaching is expected to be minimal."

However, Anovitz et al. (2006 [DIRS 180487]) also acknowledge that the extent to which their data, obtained on an alkali aluminosilicate glass, might apply to glasses of vastly different compositions is not clear.

The PMA developed here can be considered a reasonable approximation of expected glass dissolution over time, and yet may be moderately conservative in several aspects, based on discussions below in this section; therefore, no adjustment is recommended to change the lower limit of relative humidity for initiating glass degradation from that already used in the TSPA-LA glass degradation model.

Model Values for k_0, $(1\text{-}Q/K)_{Final}$, and T_{RC}—The glass degradation model in the PMA introduces a time dependence to the reaction affinity (through a growing reaction rind); whereas,

with the exception of k_0, all other model parameters and assumptions are identical to those in the TSPA-LA model. A value for the intrinsic rate constant, k_0, is required for this model because, in order to reintroduce the reaction affinity term, (1-Q/K), the parameter k_E in the TSPA-LA model has been separated into its constituent factors [$k_E = k_0(1\text{-}Q/K)$]. The value for k_0 recommended is essentially equal to the value of k_E used for the acid leg rate equation in the TSPA-LA model (i.e., $k_{E\_acid} = 1.15 \times 10^7$ g m^{-2} d^{-1}; BSC 2004 [DIRS 169988], Table 8-1). The value for k_0 recommended is 1×10^7 g m^{-2} d^{-1}. Because k_0 is considered an intrinsic property independent of pH and temperature (Grambow 1985 [DIRS 163257]), k_0 is the same for both pH legs in the model. One result of this constancy in k_0 is to eliminate a discontinuity in the calculated dissolution rate across pH legs that arise from different values of k_E being used for acid versus basic pH legs. Such a discontinuity has never been observed in experiments on glass dissolution.

The most probable value for the final reaction affinity, $(1\text{-}Q/K)_{Final}$ ($= 5 \times 10^{-4}$), is chosen such that the long-term rate (defined by Equation C6.5-11) is approximately equal to long-term reaction rates reported for basaltic glass in nature (Gordon and Brady 2003 [DIRS 176673], Table 4, field rates). Considerable variability in reported rates for natural glasses, combined with uncertainty about the effectiveness of the reaction rind to limit access of water to the glass surface under the variety of potential conditions over repository relevant timescales, the reaction affinity term is assumed to have a log-normal distribution centered on the most probable value, with a minimum value of 10^{-5} and a maximum value of 10^{-2}. Such a distribution results in long-term dissolution rates that bracket those reported in Table 4 of Gordon and Brady (2003 [DIRS 176673]) for natural basaltic glasses.

The value for T_{RC}, the critical reaction-rind thickness, is the thickness of the reaction rind for which mass transport through the reaction rind begins to dominate the exchange of glass constituents between the bulk glass and solution and, therefore, begins dominating control on the reaction affinity, (1-Q/K). The role of the reaction rind in this model is to establish the long-term dissolution rate, which occurs when $T_R \approx 5T_{RC}$. For the purposes of the model, the reaction rind is considered to include any precipitated phases (amorphous silica and clays) on the glass surface, as well as depleted and leached zones below the surface of reacted glass. The value of T_{RC} used in the model is based on observations of reaction rinds from a variety of glass dissolution experiments. McLoughlin et al. (2006 [DIRS 181382]) measured the reaction rind thicknesses of three archeological glasses after 32 years of burial in a soil. These measurements represent the longest-term reaction rinds formed under well constrained conditions of pH (9.5 to 9.7) and temperature (0.7°C to 18.9°C). The three glasses examined by McLoughlin et al. (2006 [DIRS 181382], Figures 4, 5, 6, and 7) displayed different reaction rind (and depleted zone) thicknesses, from less than 10 to greater than 30 micrometers, with differences attributed to differences in glass composition. Based on diffusion constants from Grambow and Müller (2001 [DIRS 171412], fig. 7), a 30 micrometer thick reaction layer is sufficiently thick that diffusion will dominate glass alteration. However, McLoughlin et al. (2006 [DIRS 181382]) notes that, whereas two of the three glasses with thinner reaction rinds appeared to have reached steady state, the one glass with the thickest layer had apparently not, despite the observation that this 30 μm layer was substantially depleted in alkalis and alkaline earths and strongly enriched in silica. The composition of this latter glass is more like that of a HLW glass than is the composition of the least reacted glass studied by McLoughlin et al. (2006 [DIRS 181382]). The minimum value for the critical reaction rind thickness, T_{RC}, for the model is therefore chosen to

be the thickness of the thickest reaction layer reported by McLoughlin et al. (2006 [DIRS 181382]): 30 micrometers [0.03 mm]. This is an estimate of a rind thickness for which diffusion just begins to dominate the reaction affinity term. The model applies to the entire glass surface available for dissolution. In reality, the reaction rind is likely to vary in both thickness and extent, so another factor of approximately three is applied to T_{RC} to arrive at the most probable value of 0.1 mm. The maximum value for T_{RC} is 0.3 mm, considered to be well beyond the rind thickness necessary to establish diffusion as the predominant mechanism controlling the reaction affinity term.

Comparing Model Predictions Against Long-Term Glass Corrosion—Ojovan et al. (2005 [DIRS 180494]) reported dissolution rates for a low-level (radioactive) waste (LLW) glass that has been buried in water-saturated soil for 16 years. The dissolution rates gradually diminished from 9.4 x 10^{-7} g/cm^2/day over the first year to 2.2 x 10^{-7} g/cm^2/day over 16 years of tests. Radionuclide Cs losses obey a square root time dependence indicating a diffusion-controlled release mechanism. The main parameters, which control the corrosion of waste glass in the near-surface repository, are the effective diffusion coefficient of radiocaesium and the rate of glass hydrolysis. Diffusion is predicted to be dominant for about 16 years after which diffusion and hydrolytic dissolution are expected to be similarly important. This mixed stage is predicted to continue for about 260years after which hydrolytic dissolution will be the dominant mechanism. Figure C6-9 illustrates the PMA for HLW glass dissolution developed here for temperature and pH conditions equivalent to those reported by Ojovan et al. (2005 [DIRS 180494]) (6.5°C and pH 7.6). In order to best fit the LLW glass data, the T_{RC} value of 0.3 mm and the $f_{exposure}$ of 17 were used. Dissolution-rate data reported by Ojovan et al. (2005 [DIRS 180494]) are shown as filled triangles (1 year and 16 years), and steady-state rates that they expect to occur after approximately 262 years of burial are shown as well (hollow triangle). Also shown on Figure C6-9 are dissolution rates for natural basalt glasses (filled squares) reported in Table 4 of Gordon and Brady (2003 [DIRS 176673]) that correspond to temperatures of approximately 10°C. The long-term dissolution rate predicted by the PMA developed here is also shown on Figure C6-9 (dashed line); however, that model rate is not achieved until after about two million years at this temperature. The long-term rate shown on Figure C6-9 is also within a factor of five of the long-term reaction rate for basaltic glasses in seawater (0.1 μm yr^{-1}) estimated by Grambow et al. (1985 [DIRS 163258], Figure 3). The fit of the PMA to the data of Ojovan et al. (2005 [DIRS 180494] is excellent; however, model rates remain well above dissolution rates estimated for natural basaltic glasses, and the time for the model rates to reach a rate comparable to the estimated long-term rates of natural basalts is about 1,000 times longer than achieved in nature. Such a result suggests that, while a reasonable approximation of long-term LLW glass dissolution, the PMA developed here remains conservative with respect to observed natural basaltic glass degradation rates and, by inference, with respect to anticipated HLW glass degradation rates.

Uncertainty Associated with Uranium(VI), Plutonium(IV), Neptunium(IV), and Neptunium(V) Solubility Limits

The objective of this submodel update in the PMA is to reconsider the uncertainties assigned to the solubilities of some actinide-bearing solids considered in *Dissolved Concentration Limits of Radioactive Elements* (SNL 2007 [DIRS 177418]). The uncertainties for the solubilities of solids controlling the concentrations of the radionuclides uranium(VI) (solids: schoepite,

Na-boltwoodite, $Na_4UO_2(CO_3)_3$); Pu(IV) (solid: PuO_2(am) or PuO_2(hyd,aged)); neptunium(IV) (solid: NpO_2); and neptunium (V) (solids: Np_2O_5 and $NaNpO_2CO_3$) have been assessed by comparisons between the EQ3/6 code predictions using the thermodynamic database *data0.ymp.R5* (DTN: SN0612T0502404.014 [DIRS 178850]) and solubility data available in the peer-review scientific literature. In cases where solubility data are limited or not available, uncertainties in log K values advanced by the source (in this case, the thermodynamic data compilation by the Organization for Economic Cooperation and Development/Nuclear Energy Agency compilation of thermodynamic data) are used as the basis for the uncertainty evaluations of the affected phases. These Organization for Economic Cooperation and Development/Nuclear Energy Agency uncertainties are mainly based on their evaluation of thermodynamic data of the relevant solid and aqueous species.

In general, solubility data for actinide solids are scant. In many cases data are given at specific redox conditions and solution compositions, thus restricting their use to specific chemical conditions. Still, some of the available solubility data can be used to evaluate and reasonably bound the predicted actinide solubilities using the computer code EQ3/6 and thermodynamic database *data0.ymp.R5* (DTN: SN0612T0502404.014 [DIRS 178850]). The analysis report, *Dissolved Concentration Limits of Radioactive Elements* (SNL 2007 [DIRS 177418]) assessed uncertainties on the solubility of the above-mentioned solids. The assessment was mainly based on potential sources of uncertainty effecting solubility and/or solubility calculations. These include uncertainties due to: (1) thermodynamic data in the solubility calculations, (2) variations in solution chemistry, (3) temperature effects, and (4) calculations of activity coefficients at different ionic strengths. The assessment of uncertainty due to thermodynamic data is captured by the parameter ε_1. This parameter is estimated from the uncertainty rolled in the log K computed from the uncertainties in thermodynamic data of the individual chemical species composing the solubility reaction. The uncertainty in water chemistry is represented by ε_2, which explicitly accounts for the effect of F^- concentration in solution. Finally, the uncertainty in the activity coefficients is defined by the difference between those predicted by the EQ3/6 code using the b-dot activity coefficient model and mean salt activity coefficients calculated by the method of Truesdell and Jones (1974 [DIRS 170136]). The uncertainty due to temperature effects is assessed in the analysis report *Dissolved Concentration Limits of Radioactive Elements* (SNL 2007 [DIRS 177418]) but is implemented in a qualitative discussion of its magnitude relative to the bounding nature of the model results. In general, the appropriate treatment of all these uncertainties as to unequivocally discern their effects on solubility calculations is a difficult problem. Equally important is how these uncertainties could have downstream effects on EQ3/6 or other geochemical code calculations given the wide range of water compositions estimated for the near-field environment. Examination of these downstream effects of uncertainties in geochemical code calculations is often difficult, given the complexities of how these propagate when, for example, solubilities are determined as a function of pH. For instance, substantial changes in the aqueous speciation due to the presence of carbonate in solution with increasing pH can have a significant effect on solubility. Moreover, the selection of different sets of aqueous species representing a given chemical system (sometimes the case between different thermodynamic databases) could also influence uncertainty propagation in solubility calculations. In addition, the effects of ionic strength on activity coefficients can also affect uncertainty, particularly when the relative proportion of highly charged aqueous species in solution could be large. A rigorous assessment of parameter uncertainty, whether it involves the

retrieval of thermodynamic data or a model output, could encompass an extensive statistical analysis using techniques involving sampling approaches (e.g., jackknife, bootstrap, Markov Chain Monte Carlo) and evaluations of residuals by regression methods among others (Meinrath et al. 2000 [DIRS 180861]; Meinrath 2001 [DIRS 180862]; Weber et al. 2006 [DIRS 180902]). An additional complexity is the nature of uncertainty propagation in the determination of thermodynamic parameters from analytical measurements (e.g., log K data) and, consequently, how these propagate within an aqueous speciation model intrinsic to the chemical system of interest (Criscenti et al. 1996 [DIRS 100720]).

An uncertainty evaluation comprising some form of rigorous statistical approach as mentioned above could translate into a large effort given the rather diverse applications of geochemical models in the Yucca Mountain Project. For example, geochemical calculations are utilized in the evaluation of water chemistries during waste degradation, water/rock interactions in the near-field, and in the assessment of solubilities of actinide solids. One potential limitation in using any of the aforementioned statistical approaches to evaluate uncertainty is that the solubility data needed in the assessments of uncertainties may be limited or non-existent, therefore precluding the useful applicability of these methods. As a result, addressing explicitly the effect of all these uncertainties not only goes beyond the scope of the current effort but could end up being impractical given the large number of parameters in geochemical modeling and their dependencies on solution concentration. However, for a relatively simple system, estimation of uncertainties in geochemical calculations based simply on data (e.g., solubilities) should reasonably correspond to that derived from propagated uncertainties evaluated using other rigorous statistical approaches. This is because the actual uncertainty in the result depends more on the weighted uncertainties of the chemical species that contribute significantly to the result (Criscenti et al. 1996 [DIRS 100720], p. 3552, 3rd Para.). *Dissolved Concentration Limits of Elements with Radioactive Isotopes* (SNL 2007 [DIRS 177418]) captures the extent of various uncertainties by combining them additively (in log-space) to generate an uncertainty envelope encompassing some of the above-mentioned effects. However, because these uncertainties would not simply be additive, this method probably overestimates the actual uncertainty in any single result. It is the purpose of this PMA work to use a more simplistic method to reasonably bound uncertainties based on comparisons with solubility data or use those advanced by a sanctioning body such as the Organization for Economic Cooperation and Development/Nuclear Energy Agency in their thermodynamic data compilations when solubility data are lacking.

The uncertainty advanced in this work, to a large extent, is similar to the ε_1 uncertainty parameter in *Dissolved Concentration Limits of Elements with Radioactive Isoptopes* (SNL 2007 [DIRS 177418]). The approach taken here is mainly based on direct comparisons with available solubility data. In cases where solubility data for a given solid can be evaluated in a sufficiently large number of observations as a function of pH, then a statistically based approach is used to estimate the standard error of the EQ3/6 code prediction. This is the case for the phase PuO_2(hyd,aged). In cases where solubility data are either limited or simply not available for a particular phase, the uncertainty advanced by the Organization for Economic Cooperation and Development/Nuclear Energy Agency data compilation on the relevant solid is used in the evaluation. In such cases, comparisons with available solubility data for a similar phase (i.e., a hydrated form of the evaluated phase) are used to constrain the uncertainty bounds. Although the latter cannot be considered an explicitly valid comparison because of obvious differences in the exact composition of the solid, it is by itself a reasonable approach to evaluating the

uncertainty limits based on the solubility of a similar phase. It is also assumed that the resulting uncertainty envelope appropriately represents the bounds as a function of pH. There was no attempt to propagate explicit uncertainties in the values of pH and ionic strength because (1) solubility and related uncertainty data for the solids of interest are not abundant, and (2) it would require a more involved analysis in the characterization of uncertainty propagation as a result of changes in aqueous speciation. Overall, it was noted that moderate changes in ionic strength (e.g., 0.5 to 1 molal) did not result in significant changes in the predicted solubilities as to invalidate the recommended uncertainty envelope.

Explicit representation of uncertainty to relatively large values of ionic strength (i.e., values much larger than 1 molal) is not currently possible except for a few actinide solids for which solubility data exist but require the use of a different activity coefficient model (i.e., Pitzer model). At this point, it is assumed that ionic strength effects are relatively insignificant and captured within the recommended uncertainty. This is based on analyses regarding the behavior of the model at various ionic strengths. An example of this is the prediction of $NaUO_2(CO_3)_3$ solubility (Figure C6-15) up to an ionic strength of 4 molal using the b-dot approach. The predicted solubility is well represented by the EQ3/6 results in comparison with the solubility data. However, one must be cautious in extending this result to other cases given that the main electrolyte is NaCl, which is symmetrical, and the b-dot activity coefficient prediction does not suffer much from the expected breakdown with increasing ionic strength. Mixed (unsymmetrical) electrolytes with large proportions of aqueous species having valences larger than unity could result in the breakdown of the b-dot activity coefficient model.

Solution chemistry could be considered a major contributor in the uncertainty estimates. The variations in solution chemistry for the different sets of solubility data, specifically in the case of PuO_2(hyd,aged), appear to be captured by the recommended uncertainty limits. In the PMA, the effect of solution chemistry is assumed to be captured within the recommended uncertainty limits. No additional uncertainties are assigned beyond what is determined on the basis of comparisons with reported solubilities, or uncertainties evaluated based on information in the Organization for Economic Cooperation and Development/Nuclear Energy Agency data compilations. It should be noted that direct propagation of the pH uncertainty is not treated here within the uncertainties evaluated for the solubility prediction. Such uncertainties due to the independent parameters of the solubility-limited dissolved concentration models are evaluated explicitly within the TSPA calculation based on the abstractions that constrain those parameter values.

Uncertainty Estimate of PuO_2(am) Solubility—The solubility of PuO_2(am) at 25°C at pH ~3 to ~8.5 has been addressed by various experimental studies. Notice that PuO_2(hyd,aged) is sometimes used instead of PuO_2(am) in the spreadsheet given its designation in the *data0.ymp.R5* (DTN: SN0612T0502404.014 [DIRS 178850]) thermodynamic database. The uncertainty evaluation of PuO_2(am) solubility was assessed based on comparisons with the solubility data by Rai et al. (2001 [DIRS 168392]), Rai et al. (1984 [DIRS 122768]), Efurd et al. (1998 [DIRS 108015]), Nitsche et al. (1993 [DIRS 155218]), and Nitsche et al. (1994 [DIRS 144515]) and obtained at a temperature of 25°C. The selected value for log fO_2(g) of -7 is used in this evaluation. The basis for using this log fO_2(g) is to obtain an Eh-pH range in the generation of the solubility curve using the EQ3/6 reaction path calculations that closely corresponds to that in the study of Rai (1984 [DIRS 122768]). The corresponding values

calculated in Eh units (Volts) from those reported by Rai (1984 [DIRS 122768]) in pe units range from 0.957 at pH 2.3 to 0.864 at pH 3.8 (Corroborative DTN: SN0704PMASOLUB.001 [DIRS 182787] 'Recommended_Uncertainties_Pu_Np_U_Rev01.xls, worksheet: T.Bernot_PuO2 Solub_data_ Comp). This range in particular is closely reflected by the resultant Eh-pH trajectory that is represented by the curves on Figure C6-10. It must be noted that a few observations from Rai (1984 [DIRS 122768]) for corresponding Eh values at pH higher than 3.8 are slightly lower than those expected from a linear Eh-pH relation. Although these data deviated from the Eh-pH trend of the EQ3/6 reaction path calculation, they were still considered in the uncertainty evaluation. The chosen log $fCO_2(g)$ in this evaluation equals -3.5 assuming equilibrium with air. The similarity in solubility trends as a function of pH between data obtained from different sources adds further confidence in the use of the data. Finally, a comparison with a recent set of solubility data from Fujiwara et al. (2002 [DIRS 180468]), although obtained under different experimental conditions, indicates good agreement with other data sets strengthening the confidence in the selected data.

The EQ3/6 runs were conducted with a solution composition having ~0.4 molal NaCl in agreement with Rai et al. (1984 [DIRS 122768]) solubility experiments. Runs with relatively more dilute NaCl concentrations yield similar solubility curves except in the high pH range (e.g., pH > 8). Given the nature of the solubility with respect to its variation as a function of pH, the solubility values for both EQ3/6 predictions and experimental observation were transformed to a logarithmic (base 10) scale. A log normal distribution is assumed and is evaluated by plotting the difference of the log-transformed values (log predicted–log observed) for total plutonium concentrations as a function of pH (Figure C6-11). This plot shows that most of the data lie below the solubility curve with a slight skewing of the data at low pH. Still, the apparent skewing does not preclude the use of a log normal distribution to capture the range of observed solubilities for this phase at this low pH range. The sum of log transformed differences squared divided by the number of experimental observations given by Equation C6.5-18 was calculated with respect to the actual predicted solubility value computed by EQ3/6 at a given pH value:

$$\textit{Sum of Squared Differences} = \frac{\sum\left(log[Pu]_{obs} - log[Pu]_{pred}\right)^2}{40}. \qquad \text{(Eq. C6.5-18)}$$

where $log[Pu]_{obs}$ and $log[Pu]_{pred}$ correspond to the observed and predicted log of total plutonium concentration, respectively. The value of 40 represents the total number of observed measurements used in the analysis. This formulation is slightly different from that used to calculate a variance that uses an average of the data. The standard error of the EQ3/6 prediction (not to be confused with standard deviation in this case) of the whole solubility data population is calculated by taking the square root of Equation C6.5-18 (see spreadsheet Recommended_Uncertainties_Pu_Np_U_Rev01.xls, worksheet PuO2(hyd,aged)_summary, corroborative DTN: SN0704PMASOLUB.001 [DIRS 182787]):

$$\textit{Standard Error} = \sqrt{\frac{\sum\left(log[Pu]_{obs} - log[Pu]_{pred}\right)^2}{40}} \qquad \text{(Eq. C6.5-19)}$$

The value obtained from Equation C6.5-19 is ±0.79 and is applied to the whole pH range for which the solubility curve is computed. To evaluate the confidence interval of the solubility

curve, the estimated standard error (±0.79) is applied to the mean of the log solubility in molal units and compared to the reported solubilities as seen on Figure C6-11. Overall, an uncertainty of ±0.79 appears to capture most of the data, generally within the lower confidence bound. Notice on Figure C6-10 that no data lie outside the upper confidence bound for the pH range comprised by the reported solubilities. It should be noted that many of the experimental solubilities used in this analysis correspond to chemical conditions that are different with respect to each other. For example, the solubility data sets include solubilities measured in NaCl and $NaClO_4$ electrolyte matrices (Rai et al. 2001 [DIRS 168392]) and in J-13 water composition (Nitsche et al. (1993 [DIRS 155218]). Moreover, the Eh-pH relations in these studies are relatively variable and in many cases deviate from the assumed trend in the reaction path model with a fixed log $fO_2(g)$ value. In addition, the lower uncertainty bound appears to capture a large fraction of the solubility data by Fujiwara et al. (2002 [DIRS 180468]) that was obtained under more reduced conditions and in solutions with higher ionic strength. Therefore, even with these variations in solutions chemistry and redox potentials, the selected confidence interval is sufficiently adequate as to reasonably capture most of the observed solubility data for this phase. It should be noted that the data by Fujiwara et al. (2002 [DIRS 180468]) are used for comparison purposes only and did not take part in the uncertainty analysis. The EQ3/6 runs were conducted without suppressing any aqueous species. It was noted that some code run results at ionic strength values close to or slightly larger than unity results in the shift of the solubility curve at pH>8. The recommended uncertainty distribution for the solubility of this phase is given in Table C6-8. For a log normal distribution with the mean set at zero, the value for σ based on the computed standard error is ±0.79 and truncated at $\pm 1\sigma$.

Uncertainty Estimate of NpO_2 Solubility—The log K value for NpO_2 in the thermodynamic database *data0.ymp.R5* (DTN: SN0612T0502404.014 [DIRS 178850]) is based on thermochemical measurements on the solid and not from solubility data. On the other hand, solubility data only exist for amorphous and/or hydrated forms of NpO_2. The study of Rai and Ryan (1985 [DIRS 137138]) reports the solubility of $NpO_2{*}H_2O$ with and without carbonate in solution. The log K value for the reaction $NpO_2 + 4H^+ = Np^{++++} + 2H_2O$ is determined from the Gibbs energies of formation for each component in the reaction. The log K value evaluated by the Organization for Economic Cooperation and Development/Nuclear Energy Agency (Guillaumont et al. 2003 [DIRS 168382], Section 10.2.2.2.1, p. 297, 1st paragraph) for the reaction $NpO_2 + 2H_2O = Np^{++++} + 4OH^-$ is -65.75 ±1.07. Converting this reaction in the form consistent with the EQ3/6 thermodynamic database requires combining the above expression with the one for H_2O dissociation having the stoichiometric coefficients multiplied by 4. Assuming the uncertainties for the log K value of the water dissociation reaction are negligible relative to those of the NpO_2 reaction, the adopted uncertainty from the Organization for Economic Cooperation and Development/Nuclear Energy Agency source is ±1.07 log solubility in molality units. The comprehensive evaluation by the Organization for Economic Cooperation and Development/Nuclear Energy Agency thermodynamic data compilation (Guillaumont et al. 2003 [DIRS 168382], Section 10.2.2.2) renders this source as sufficiently adequate as to justify the use of this uncertainty value in this work. For comparison with a similar phase, the solubility data of Rai and Ryan (1985 [DIRS 137138]) are shown with the predicted solubility curve calculated by EQ3/6 (Figure C6-12). The log $fO_2(g)$ value used in the EQ3/6 calculations is -0.7, which results in more oxidized conditions relative to those of the Rai and Ryan (1985 [DIRS 137138]) experiments. Therefore, the predicted solubility of this anhydrous phase is upper

bound at this redox condition. The differences are relatively small for most of the data, and the uncertainty bounds capture all the data in the pH range of 6.9 through 7.7 (Figure C6-12). The EQ3/6 runs were conducted without suppressing any aqueous species. It should be noted that these solubility data were not used in the uncertainty analysis since it pertains to a different phase, but it is used for qualitative purposes remarking how the uncertainty bounds capture the solubility of the hydrated Np(IV) oxide solid. The recommended uncertainty distribution for the solubility of this phase is given in Table C6-8. For a triangular distribution in the range a through c, a equals -1.07, b is set to zero, and c is 1.07. A triangular distribution is recommended to emphasize the average, and the limits (a and c) provide for truncation of the distribution at values different from those in the implementation of a normal distribution. In addition, this type of distribution seems to be appropriate given the limited amount of data used in the comparison.

Uncertainty Estimate of Np_2O_5 Solubility—The log K value for Np_2O_5 in the thermodynamic database *data0.ymp.R5* (DTN: SN0612T0502404.014 [DIRS 178850]) is also based on thermochemical measurements on the solid and not from solubility data. Like in the case of NpO_2, there are some solubility studies on hydrated forms of Np_2O_5 by Efurd et al. (1998 [DIRS 108015]). Pan and Campbell (1998 [DIRS 180455]) reported solubilities for Np_2O_5 in CO_2-free solutions that are about a log unit more soluble than that calculated using the Organization for Economic Cooperation and Development/Nuclear Energy Agency thermodynamic data and those given by Efurd et al. (1998 [DIRS 108015]). A discussion in the Organization for Economic Cooperation and Development/Nuclear Energy Agency source (Guillaumont et al. 2003 [DIRS 168382], p.585) mentions the solubility data from Pan and Campbell (1998 [DIRS 180455]), but they select the constant based on thermochemical measurements and estimations. Guillaumont et al. (2003 [DIRS 168382], Section 10.2.2.1, p. 297) make remarks on the agreement of their selected log K value based on thermochemical data with the log K value given by Efurd et al. (1998 [DIRS 108015]) based on solubility data, even if it is for a hydrous phase. The recommended uncertainty for the Organization for Economic Cooperation and Development/Nuclear Energy Agency log K value is ±2 for the solubility reaction adopted in the *data0.ymp.R5* (DTN: SN0612T0502404.014 [DIRS 178850]) thermodynamic database $Np_2O_5 + 2H^+ = 2NpO_2^+ + H_2O$. This uncertainty interval is rather large and it appears to be mainly based on the uncertainty of the thermochemical data for the solid. The Organization for Economic Cooperation and Development/Nuclear Energy Agency compilation of Guillaumont et al. (2003 [DIRS 168382], Section 10.2.2.1, p. 297) selected their log K value on the grounds that it is in good agreement with that obtained in the study of Efurd et al. (1998 [DIRS 108015]). The same rationale is adopted in this evaluation but recommends an uncertainty of ±1 for the calculated solubility of this phase in molality units (Figure C6-13). The reason for recommending an uncertainty value half of that advanced by Guillaumont et al. (2003 [DIRS 168382], Section 10.2.2.1, p. 297) is because it is considered sufficient to encompass the data by Efurd et al. (1998 [DIRS 108015]). However, the upper bound underestimates Pan and Campbell (1998 [DIRS 180455]) solubility data by ~1 log unit. Guillaumont et al. (2003 [DIRS 168382], Section 10.2.2.1, p. 297) does not provide any arguments on why the solubility data of Pan and Campbell (1998 [DIRS 180455]) were not used in their analysis to constrain solubilities even when the authors report Np_2O_5(cr) as the equilibrium phase in their experiments. The solubility data given by Pan and Campbell (1998 [DIRS 180455]) at pH values larger than 9, do not follow the expected trend of increasing solubility with pH. A possible explanation for this is that these solubility experiments were conducted under CO_2-free

conditions and Np-carbonate complexation would not be expected in the alkaline pH range. Although Pan and Campbell (1998 [DIRS 180455]) noticed this behavior in the solubility data, they did not offer an explanation for the cause of such trend except to say that it opposes the observed increase in solubility in the alkaline pH range. The data by Nitsche et al. (1993 [DIRS 155218]) tabulated in Efurd et al. (1998 [DIRS 108015]) is shown in the graph since it was also considered by Efurd et al. (1998 [DIRS 108015]) for comparison with their results. The study by Nitsche et al. (1993 [DIRS 155218]) reports X-ray diffraction analysis of the solids for the solubility experiments at 25°C and concludes that better agreement of the X-ray diffraction patterns is obtained for hydrated Na-Np(IV)-carbonate phases. Therefore, the relevance of these data to the solubility of Np_2O_5 is small but it is shown for comparison purposes only. No suppressions were used in the EQ3/6 runs. The recommended uncertainty distribution for the solubility of this phase is given in Table C6-4. For a triangular distribution in the range a through c, a equals -1, b is set to zero, and c is 1. A triangular distribution is recommended to emphasize the average, and the limits (a and c) provide for truncation of the distribution at values different from those in the implementation of a normal distribution. In addition, this type of distribution seems to be appropriate given the limited amount of data used in the comparison.

Uncertainty Estimate of $NaNpO_2CO_3$ Solubility—The log K value for $NaNpO_2CO_3$ selected by the Organization for Economic Cooperation and Development/Nuclear Energy Agency compilation (Guillaumont et al. 2003 [DIRS 168382], Section 10.6.2.1.1, p. 305) is based on the solubility study at various CO_3^{--} concentrations in NaCl solutions. The adopted uncertainty of ±0.5 is that evaluated by the Organization for Economic Cooperation and Development/Nuclear Energy Agency Guillaumont et al. (2003 [DIRS 168382], Section 10.6.2.1.1) for the log K, which is applied to the log of the solubility in molality units to be obtained from the EQ3/6 predictions. The available solubility data for this phase has already been evaluated by OECD (2001 [DIRS 159027]) and Guillaumont et al. (2003 [DIRS 168382], Section 10.6.2.1.1) for the retrieval of thermodynamic data for this phase. The recommended uncertainty distribution for the solubility of this phase is given in Table C6-8. Note that this uncertainty of ±0.5 given by the Organization for Economic Cooperation and Development/Nuclear Energy Agency Guillaumont et al. (2003 [DIRS 168382], Section 10.6.2.1.1) is at the 95 percent confidence level. The recommended distribution is log normal truncated at 2σ.

Uncertainty Estimate of Schoepite ($UO_3 \cdot 2H_2O$) Solubility—Evaluation of log K values for schoepite has been largely determined from solubility studies. However, the log K value adopted in the thermodynamic database *data0.ymp.R5* (DTN: SN0612T0502404.014 [DIRS 178850]) from the Organization for Economic Cooperation and Development/Nuclear Energy Agency compilation (Guillaumont et al. 2003 [DIRS 168382], Section 9.3.2.1.5.1, p. 179) is derived from thermochemical measurements as evaluated by Grenthe et al. (1992 [DIRS 101671]). Guillaumont et al. (2003 [DIRS 168382], Section 9.3.2.1.5.1) considered the log K value calculated using the thermodynamic data advanced by Grenthe et al. (1992 [DIRS 101671]) adequate based on comparisons with various log K values determined from solubility data. At this point, the evaluation of schoepite solubility has been reasonably extensive in the Organization for Economic Cooperation and Development/Nuclear Energy Agency thermodynamic data reviews by Grenthe et al. (1992 [DIRS 101671]) and Guillaumont et al. (2003 [DIRS 168382], Section 9.3.2.1.5.1). The uncertainties advanced by Guillaumont et al. (2003 [DIRS 168382], Section 9.3.2.1.5.1) for their tabulated reaction log K of ±0.4 is applied to the solubility of this phase in molality units is adopted in this evaluation. This uncertainty is less

than that advanced by *Dissolved Concentration Limits of Radioactive Elements* (SNL 2007 [DIRS 177418]) for the log K value of this solid. The uncertainty analysis in this report for the U(VI)-bearing phases (schoepite, Na-boltwoodite, and $Na_4UO_2(CO_3)_3$) is somewhat different in the sense that it combines the uncertainty of two solids when their solubility overlaps as a function of pH and fCO_2. However, this 'crossover' uncertainty (as referred in the aforementioned report) is not treated explicitly in their report (SNL 2007 [DIRS 177418]) and a total uncertainty of ±0.99 units is then applied to all log total uranium concentrations. In the analysis described here, all uncertainties are explicitly assigned to each U(VI)-bearing phase. For the PMA implementation, the sampling of uncertainties among schoepite, Na-boltwoodite, and $Na_4UO_2(CO_3)_3$ will be perfectly correlated to ensure the continuity of uranium solubility in mineral phase transitions. The recommended uncertainty distribution for the solubility of this phase is given in Table C6-8. For a triangular distribution in the range a through c, a equals -0.4, b is set to zero, and c is 0.4. A triangular distribution is recommended to emphasize the average, and the limits (a and c) provide for truncation of the distribution at values different from those in the implementation of a normal distribution. Also, this type of distribution seems to be appropriate given the limited amount of data used in the comparison.

Uncertainty Estimate of Na-Boltwoodite ($NaUO_2SiO_3OH·1.5H_2O$) Solubility—Thermodynamic data for Na-boltwoodite have been largely based on the solubility data. However, the log K value in the thermodynamic database *data0.ymp.R5* (DTN: SN0612T0502404.014 [DIRS 178850]) is based on the Gibbs energy of formation for this phase given in the Organization for Economic Cooperation and Development/Nuclear Energy Agency compilation (Guillaumont et al. 2003 [DIRS 168382], p. 443). It should be noted that this value estimated in the work by Chen et al. (1999 [DIRS 106346]) and Guillaumont et al. (2003 [DIRS 168382], p. 442 to 443) does not select this datum in their tabulations even when it is discussed in this volume. The main reason for not selecting this value in Guillaumont et al. (2003 [DIRS 168382], p. 441 to 443) is the need of more work or further re-evaluation of the thermodynamic data for this solid. The more recent study of the solubility of this phase by Ilton et al. (2006 [DIRS 178810]) calculates a log K value at 25°C (log K = 5.86 ±0.24) that is in good agreement with that adopted in the thermodynamic database *data0.ymp.R5* (log K = 6.08 (DTN: SN0612T0502404.014 [DIRS 178850])). Moreover, this value is in good agreement with that advanced by the solubility study of Nguyen et al. (1992 [DIRS 100809], Table 6, p. 374) of log K ≥5.82(±0.16). It should be noted that the uncertainty range given by Ilton et al. (2006 [DIRS 178810]) is not represented on Figure C6-14, and the size of the symbol is arbitrary.

As seen on Figure C6-14, the EQ3/6 solubility predictions, as a function of pH tend to over-predict the solubility at pH 6.7 to 7.5 where transitions from predominantly uranyl-hydroxy-carbonate to uranyl-carbonate-aqueous species occur. At pH above 7.5, the difference between predicted and observed solubilities is relatively small, and the predicted solubility trend conforms well to that of the experimental data. The recommended uncertainty distribution for the solubility of this phase is given in Table C6-8. For a triangular distribution in the range a through c, a equals -0.5, b is set to zero, and c is 0.3. Note that a slightly larger uncertainty of-0.5 is assigned to the unsaturated side of the solubility curve where a larger difference between predicted and observed data exists at pH ~6.6 to 7. This was determined by examination of an uncertainty range that captures the bulk of the data at undersaturated conditions relative to the EQ3/6 code prediction. Similarly, the uncertainty value 0.3 was

obtained in the same manner. To avoid confusion, there is little or no relationship of the recommended uncertainty in this evaluation with the one given by Ilton et al. (2006 [DIRS 178810]). Since these larger differences apply to two points lying outside the lower solubility bound, the predicted solubility curve in this narrow pH range could be considered conservative. Additional solubility data could provide better reconciliation of these differences as well as data scatter as a function of pH. Differences in predicted solubility values are anticipated considering that the log K value retrieved by Ilton et al. (2006 [DIRS 178810]) of K = 5.86 is somewhat smaller than that adopted in the thermodynamic database *data0.ymp.R5* (DTN: SN0612T0502404.014 [DIRS 178850]) with a log K value equal to 6.0800 at 25°C. Even with these differences in log K data of 0.22 log units, the predicted solubilities along with assigned uncertainties are in good agreement with their solubility data. Although these differences in log K values can cause the discrepancy between predictions and observations, other factors such as analytical uncertainties and solution chemistry can also have non-negligible effects on this deviation. Once more, the limited amount of experimental data along with its uncertainty makes it difficult to explain these discrepancies. Even with the limited amount of data and their associated uncertainties, solubility predictions do not show trends of either gross under- or over-prediction beyond the uncertainty range advanced by Ilton et al. (2006 [DIRS 178810]). It should be noted that Ilton et al. (2006 [DIRS 178810]) used variable concentrations of bicarbonate in their solubility experiments. Even with this variation in solution chemistry, the solubility predictions and associated uncertainties appear to reasonably capture this effect as a function of pH. A triangular distribution is recommended as to weigh more on the average and their limits (a and c) provide for truncation of the distribution at values different from those in the implementation of a normal distribution. In addition, this type of distribution seems to be appropriate given the limited amount of data used in the comparison.

There is an overlap in solubilities between schoepite and Na-boltwoodite in the TSPA implementation of the solubility model. For the PMA implementation, the larger uncertainty between schoepite and Na-boltwoodite will be applied when the solubilities of these two phases overlap.

Uncertainty Estimate of $Na_4UO_2(CO_3)_3$ Solubility—The log K value for $Na_4UO_2(CO_3)_3$ selected by the Organization for Economic Cooperation and Development/Nuclear Energy Agency compilation (Guillaumont et al. 2003 [DIRS 168382], Table 3-2, p. 75) traces back to another Organization for Economic Cooperation and Development/Nuclear Energy Agency compilation by Grenthe et al. (1992 [DIRS 101671]) for uranium. The log K value in the thermodynamic database *data0.ymp.R5* (DTN: SN0612T0502404.014 [DIRS 178850]) is based on the thermodynamic data given by Grenthe et al. (1992 [DIRS 101671]) who retrieved the thermodynamic parameters for this phase using data from the solubility study by Blake et al. (1956 [DIRS 180470]). Therefore, it is not surprising to obtain a good agreement between prediction and observed solubility (Figure C6-15). Consequently, this comparison is more of a confirmation of the predictive capability of the EQ3/6 code calculation along with the adopted thermodynamic data of aqueous species for this phase. Figure C6-15 shows that there is some level of discrepancy between the EQ3/6 prediction and experimental data. Further discussion on this is given below.

The Organization for Economic Cooperation and Development/Nuclear Energy Agency compilation (Guillaumont et al. 2003 [DIRS 168382]) selects a log K value for this phase. Given

the sanctioning status of such compilation of thermodynamic data, its use in this work is justified for its intended use. The EQ3/6 results tend to under predict the solubility at low NaCl concentration, but the difference between prediction and reported solubility tend to decrease with increasing NaCl concentration. Although the b-dot activity coefficient model should not be used at ionic strengths exceeding 1 molal, the electrolyte considered in the model and experiment (i.e., NaCl) is symmetric and the accuracy of the extrapolation should not suffer significantly as opposed to unsymmetrical electrolytes. Additional solubility data in a $NaClO_4$ solution (Blake et al. 1956 [DIRS 180470], Table II) shows that the differences in solubility between two different electrolytes are overall minimal, and the range is captured by the recommended uncertainty range. The recommended uncertainties for the log value of solubility in molality units are given in Table C6-8. For a triangular distribution in the range a through c, a equals-0.3, b is set to zero, and c is 0.3. The limits (a and c) provide for truncation of the distribution at values different from those in the implementation of a normal distribution.

The uncertainty values were assessed by examining a range that can capture the bulk of the solubility data relative to the EQ3/6 model prediction as depicted on Figure C6-15. The source (Grenthe et al. 1992 [DIRS 101671], p. 327) advances a lower uncertainty of ±0.16 for the log K value of the reaction $Na_4UO_2(CO_3)_3 = 4\ Na^+ + UO_2(CO_3)_3^{---}$ from the analysis of Blake et al. (1956 [DIRS 180470]) data. Figure C6-15 indicates that there is some level of discrepancy between the EQ3/6 prediction and experimental data. Examination of the sources of thermodynamic data for uranium(VI) hydroxide and carbonate aqueous species in the thermodynamic database *data0.ymp.R5* (DTN: SN0612T0502404.014 [DIRS 178850]) indicates that all are consistent with the source Grenthe et al. (1992 [DIRS 101671]). This is also the case for the solid $Na_4UO_2(CO_3)_3$ as already discussed above. Thermodynamic data U(VI) hydroxide aqueous species were not updated in Guillaumont et al. (2003 [DIRS 168382]). However, thermodynamic data for uranium (VI) carbonate complexes were updated, but the differences in the Gibbs energies of formation and resulting log K values for the corresponding reactions are relatively minor. In fact, the differences are within the uncertainties given by both authors. Knowing that thermodynamic data for the solid and aqueous species used in the solubility calculation are consistent with one source (i.e., Grenthe et al. (1992 [DIRS 101671])), then it is unlikely that the discrepancy is due to inconsistency in the thermodynamic data. A possible factor influencing this deviation is the different activity coefficient models used in the retrieval of thermodynamic parameters in the source data and that used in the EQ3/6 solubility calculation. The retrieval of thermodynamic data in the studies by Grenthe et al. (1992 [DIRS 101671]) and Guillaumont et al. (2003 [DIRS 168382]) use the specific ion interaction theory and the EQ3/6 code uses the b-dot equation. Differences in activity coefficient estimations between the two approaches as a function of NaCl concentration were not assessed here, but it is assumed that these would be relatively minor. Another difference is that the tabulated solubility data by Blake et al. (1956 [DIRS 180470]) is given in molarity units. However, the difference in solution density would be rather small, even up to 4 molal NaCl, and the resulting correction to molality units would be too small except in fairly concentrated electrolytes. It should be noted that the retrieval of the log K value for $Na_4UO_2(CO_3)_3$ by Grenthe et al. (1992 [DIRS 101671]) was based on the solubility runs in the $NaClO_4$ electrolyte solutions and a better agreement should be expected with these data. In summary, it is not evident why there is systematic deviation from the predicted solubility and the solubility data except to say that it is relatively small. The regression by Grenthe et al. (1992 [DIRS 101671]) to obtain the infinite dilution log K value for this phase using the specific ion interaction theory

indicates that there are indeed minor deviations from the solubility data as specified in their computed uncertainties. Therefore, some sort of discrepancy would also be expected from the EQ3/6 solubility predictions. Interestingly, the Gibbs energy of formation and log K for the reaction $Na_4UO_2(CO_3)_3 = 4Na^+ + UO_2(CO_3)_3^{----}$, plus their corresponding uncertainties, are identical between the sources Grenthe et al. (1992 [DIRS 101671]) and Guillaumont et al. (2003 [DIRS 168382]) even when the values for Gibbs energy of formation for $UO_2(CO_3)_3^{----}$ in each source are slightly different.

Since the current EQ3/6 prediction tends to underestimate part of the experimental data of Blake et al. (1956 [DIRS 180470]), it seems reasonable to adopt an uncertainty of ±0.3 to capture the bulk of the solubility data relative to the predicted solubility curve. This uncertainty is approximately twice that advanced by Grenthe et al. (1992 [DIRS 101671]) of ±0.16. The lower uncertainty in the latter is expected since it is based on the analysis of solubility data and is not relative to a model prediction as evaluated in this work. The use of a triangular distribution is recommended as to weigh more on the average, and the limits (a and c) provide for truncation of the distribution at values different from those in the implementation of a normal distribution. For the PMA implementation, the sampling of uncertainties among schoepite, Na-boltwoodite, and $Na_4UO_2(CO_3)_3$ will be perfectly correlated.

C6.5.2 Model Implementation

In-Package Chemistry

The calculations of in-package pH are abstracted into lookup tables for the PMA. The set of independent variables for the PMA in-package chemistry abstractions is different from those in the TSPA-LA model. The variables q and pCO_2 are retained and additional parameters for degradation rates, degradation amounts, and volumes of water and degradation products are used. In addition, the PMA in-package chemistry abstractions do not utilize the time since breach parameter.

The type of output in the PMA in-package chemistry abstractions is also modified in one respect. Instead of calculating the maximum and minimum pH, the most likely pH value is calculated. The TSPA-LA Model relies on major buffer reactions to establish the maximum and minimum pH but refrains from predicting the most likely pH.

The PMA in-package chemistry abstractions are split into three flow regimes: vapor diffusion-dominated cases, liquid advection cases, and the cases in between. The diffusion dominated regime is represented by the vapor influx abstraction described in Section C6.5.1. The outputs for this regime are primarily controlled by degradation and heterogeneous equilibrium reactions. The high-flow liquid influx regime is represented by the high-flow liquid influx abstraction (Section 6.5.1). Its outputs are primarily controlled by heterogeneous equilibrium reactions and liquid influx composition. The abstraction for the cases in between is an interpolation between the vapor influx and high-flow liquid influx abstractions. Its outputs are controlled to varying degrees by degradation reactions, heterogeneous equilibrium reactions, and liquid influx composition.

Diffusion-Dominated Cases—The vapor influx abstraction consists of a look-up table for each combination of pCO_2 and k_{ss}/k_{wf} in each cell in Table C6-3. The look-up tables provide pH, ionic strength, and concentrations of uranium, plutonium, neptunium, and fluorine as a function of V_s/V_w. Only pH is used in the PMA. The k_{ss}/k_{wf} ratio is represented in the look-up tables as R_{sw}, which is the ratio of the cumulative moles of stainless steel degraded in the cell, n_{ss}, to the cumulative moles of waste form degraded, n_{wf}. For the process model, these ratios are equivalent because they are held constant for the entire simulation. In the PMA simulation, these ratios will not always be the same because the rate ratio is an instantaneous ratio while the mole ratio is cumulative. In the PMA, instantaneous rates change with time and will go to zero when the associated material is completely degraded. It is appropriate to use the ratio of the moles of degraded materials to determine pH and ionic strength in this case because dissolved materials are not flushed out of the pore space under vapor influx conditions. Instead, the water composition in the pore space should reflect the cumulative degradation of materials in the cell.

V_s/V_w increases for each successive row in the look-up tables because each row represents an equilibrium condition after an additional aliquot of water is removed. Many of the rows at the tops of these tables are not applicable to the PMA because V_s/V_w is less than 1.5 until a sufficient amount of water is removed. V_s is calculated by EQ3/6 and included in the output. V_w is estimated from the mass of solvent in the EQ3/6 output assuming a density of 1 kg/L and negligible volume effects from dissolved constituents.

Liquid-Advection Dominated Cases—The high-flow liquid influx abstraction provides look-up tables to determine steady-state pH when the degradation rates are low compared to the flush rate (i.e., when the Damkohler number is low enough that degradation rates do not considerably affect the steady-state pH). To determine quantitatively the range of the high-flow liquid influx abstraction, process model steady-state results were plotted (in **Da.xls* spreadsheets in corroborative DTN: SN0704PMAIPCPM.001 [DIRS 180745]) as a function of an empirical Damkohler ratio, Da:

$$Da = \frac{(k_{ss} + k_{wf})}{q/V_p} \qquad \text{(Eq. C6.5-20)}$$

where the numerator is the sum of the degradation rates of the stainless steel and waste form in the cell and the denominator is the flush rate or turnover rate (q/V_p). Da has units of moles. The flush rate is used in the denominator instead of q because it is a much better indicator of how fast aqueous components are removed from the cell as the pore volume changes with time.

The EQ3/6 simulations indicate that below a Da value of 0.1, degradation rates negligibly affect the steady-state pH and ionic strength for each cell and at each pCO_2. Thus, when TSPA determines that Da is less than or equal to 0.1, then the pH and ionic strength values in the look-up tables of the high-flow liquid influx abstraction are defined to be the most likely pH and ionic strength values in the cell at the given time. These most likely values are used in combination with the uncertainties defined in the section below to determine the sampled pH values in TSPA calculations.

Intermediate Cases—For the cases with intermediate liquid flow rates, the pH is calculated through a linear interpolation between the output values in the vapor diffusion abstraction and

those in the liquid advection abstraction. This abstraction applies when Da is between 0.1 and 100. The detail of the interpolation process is explained in the Low-Flow Abstraction worksheet of *IPC PMA Flow Abstraction r1.xls*. The advective flux of liquid water is provided by the water balance model in Section 6.4. For simplicity, at the high advective flow end, only the lookup tables calculated with condensed water (deionized water) are used, since the difference in the predicted pH between the condensed water and the seepage water is insignificant.

Uncertainties—The output uncertainty is determined based on uncertainties in the inputs, uncertainties in the model, and ranges observed in sensitivity simulations. These uncertainties are adopted from the TSPA-LA model. The in-package chemistry model for TSPA-LA was designed to determine the maximum and minimum pH values in the vicinity of the waste form. The TSPA-LA model does this by identifying and quantifying the major pH-buffering reactions that cannot be overcome by possible sources of acid or base. The secondary minerals that accumulate in each In-Package Chemistry cell are primarily responsible for the buffer capacities, which are quantified by titrating accumulated minerals with hypothetical additions of acid and base. The hypothetical additions are extreme and exceed anticipated sources so that maximum and minimum pH limits are determined with a high degree of confidence.

Sensitivity analyses confirm that the established maximum and minimum pH limits are reasonable (SNL 2007 [DIRS 180506], Section 6.6). Sensitivity simulations for each of the three In-Package Chemistry cells involved varying liquid flux rates from 0.1 to 1,000 L/yr, varying degradation rates of the In-Package Chemistry cell materials and waste forms from minimum to maximum values, and varying the composition of the liquid influx among a range of compositions. Sensitivity analyses for liquid flux rate and degradation rates included variations in liquid flux composition.

For the PMA In-Package Chemistry abstraction, the maximum and minimum pH values determined in the TSPA-LA model are used to bound the pH uncertainty. The pH distribution is defined as triangular with the most probable value equal to the pH value determined in the PMA In-Package Chemistry abstraction (corroborative DTN: SN0704PMAIPCAB.001 [DIRS 182602]) and the maximum and minimum values equal to the values established in the TSPA-LA model (SNL 2007 [DIRS 180506], Section 6.10.1).

Commercial Spent Nuclear Fuel Cladding

In the PMA, the Cladding Degradation Submodel is invoked in both the Waste Package EF and Drip Shield EF Modeling Cases. Since no WP failures are predicted to occur during the first 10,000 years postclosure, the Cladding Submodel was not used in the Nominal Scenario Class. Input parameters include the fraction of predisposal failures (as-received failure fraction) and the fraction of CSNF WPs containing stainless-steel-clad fuel. The groups of WPs represented in the TSPA have an initial percentage of failed rods defined by the log uniform distribution with a range 0.01 percent to 1 percent (SNL 2007 [DIRS 180616], Table 7-1[a]). In addition, 1.0 to 2.0 percent (uniformly distributed) of the WPs are predicted to contain stainless-steel-clad fuel rods and the total amount of stainless-steel-clad fuel is fixed at 1.0 percent of the total CSNF (SNL 2007 [DIRS 180616], Table 7-1[a]).

The early failed WPs are partitioned into three fuel groups. The CDSP WPs containing HLW glass and DSNF canisters are assigned to the one fuel group. The CSNF WPs containing only Zircaloy-clad fuel are assigned to a second fuel group. The CSNF WPs containing both Zircaloy and stainless-steel-clad fuel are assigned to a third fuel group. In the PMA, each WP is assigned an initial fraction of failed cladding, sampled from a log-uniform distribution (f_2). This parameter represents epistemic uncertainty and is sampled once per realization. It applies to all Zircaloy-clad CSNF fuel. The third group contains both Zircaloy-clad and stainless-steel-clad fuel. The stainless-steel-clad fuel is modeled with cladding that is completely degraded. The fraction of WPs containing stainless-steel-clad fuel is sampled from a uniform distribution, representing epistemic uncertainty. This parameter is sampled once per realization. The fraction of total CSNF inventory that is stainless-steel clad is not uncertain. The ratio of these two parameters gives the fraction of stainless-steel-clad fuel in each of the WPs in the third fuel group. This fraction is added to the predisposal failure fraction assigned to the Zircaloy-clad fuel to give the total initial fraction of failed rods in each of the WPs in the third fuel group, f_3.

The structure of the TSPA-LA Model file does not permit the modeling of two SNF fuel groups. Therefore, the two groups are combined and the resulting cladding failure fraction, F_{fail}, is taken to be a weighted sum of the individual failure fractions for the two WP groups:

$$F_{fail} = \frac{N_2 . f_2 \ + N_3 . f_3}{N_2 + N_3} \qquad \text{(Eq. C6.5-21)}$$

where N_2 and N_3 are the number of WPs assigned to the second and third fuel groups, respectively, and f_2 and f_3 are the clad failure fractions for the second and third fuel groups, respectively.

Degradation Rate of Commercial Spent Nuclear Fuel

As discussed in Section C6.5.1, the functional dependence of the dissolution rate on water chemistry in the PMA remains the same as in the TSPA-LA model. The distribution range of the effective surface area of CSNF is modified, and two additional scaling factors are included to account for the effect of long-term dissolution and the temporal evolution of gamma and beta radiation fields. The distributions of the three parameters are recommended as listed in Table C6-6.

Degradation Rate of High-Level Waste Glass

The conceptual model for HLW glass dissolution described in Section C6.5.1 is based on chemical and physical feedback caused by formation of an increasing reaction rind on the surface of the glass. The rate at which the reaction rind forms is a function of solution chemistry (primarily pH and temperature), with the most aggressive conditions leading to the most rapid formation of the rind. Conceptually, such conditions should lead to the most rapid reductions in dissolution rate; however, the modeled rate at which the rind thickness provides feedback is a function of the timestep (Δt_i), so that the longer the timestep, the longer a fixed dissolution rate is applied to the mass of glass remaining. Under aggressive chemical conditions and relatively

long timesteps, this can lead to a physically unrealistic mass of glass being dissolved in a single timestep. This potential effect can be mitigated by separating the glass into two components, each of which dissolves at a different rate. The 'fast fraction' is that portion of the mass of a glass log that is assumed to dissolve at the forward rate (for which the reaction affinity term is unity), and the 'slow fraction' is the remaining portion of glass, assumed to dissolve at the long-term rate.

Depending on the value of the final reaction affinity, $(1\text{-}Q/K)_{final}$, the long-term reaction rate, $R_{long} = k_f(1\text{-}Q/K)_{final}$, is achieved once the reaction rind has attained between 5 and 15 times the critical reaction-rind thickness, T_{RC}, with the larger thickness required when the lowest value of $(1\text{-}Q/K)_{final}$ is used (Figure C6-16). Therefore, we can calculate the maximum mass of one glass log necessary to achieve a reaction-rind thickness sufficient to impose the long-term rate on the remaining mass of glass:

$$\text{Rate}_{glass} \leq 1.1R_{long} \text{ when } T_R = 15T_{RC.} \quad \text{(Eq. C6.5-22)}$$

The mass of glass dissolved is given by the volume of glass dissolved times the glass density:

$$M_D = V_{MD} \times \rho. \quad \text{(Eq. C6.5-23)}$$

The volume of dissolved glass is equal to the surface area of the glass log (assumed equal to $2\pi r_o L_o$, from the current document) times the rind thickness:

$$V_{MD} = 2\pi r_o L_o \times T_{R.} \quad \text{(Eq. C6.5-24)}$$

So that

$$M_D = = 2\pi r_o L_o \times T_R \times \rho \quad \text{(Eq. C6.5-25)}$$

Letting $r_o = 0.3$ m, $L_o = 3.9$ m, $\rho = 2{,}700$ kg/m^3, and $T_R = 15T_{RC}$ gives

$$M_D = 2\pi(0.3)(3.9) \text{ m}^2 \times 15T_{RC} \text{ m} \times 2{,}700 \text{ kg/m}^3 \quad \text{(Eq. C6.5-26)}$$

$$M_D \text{ (kg)} = 110T_{RC} \text{ m}^3 \times 2{,}700 \text{ kg/m}^3 = 297{,}000 \times T_{RC}. \quad \text{(Eq. C6.5-27)}$$

The proportion of a glass log that must be dissolved in order to approach the long-term rate is

$$M_D/M_0 = (297{,}000/2710) \times T_{RC} = 110 \text{ m}^{-1} \times T_{RC} \text{ m} \quad \text{(Eq. C6.5-28)}$$

where M_0 is the initial mass of an average glass log (2710 kg) and T_{RC} is the critical rind thickness in meters.

For the distribution of T_{RC} used in the PMA glass degradation model (Table C6-7), this gives a distribution for the proportion of glass to be assigned as the fast fraction; that is, the fraction of glass that dissolves at the forward rate (k_f). The fraction of glass where the long-term rate ($R_{long} = k_f(1\text{-}Q/K)_{final}$) is applied is simply one minus the fast fraction; this is the slow fraction. The intrinsic reaction rate constant k_0 in Equation C6.5-3 is set to $1\text{x}10^7$ g/m^2/d as discussed in the Conceptual Description. Multiplying the forward and long-term rates (g/m^2/d) by the specific

surface area (and the appropriate exposure factor) gives the fractional degradation rate (d^{-1}) used in the PMA. Thus,

Forward fractional rate: $rate_{forward} = S_{SP} \times f_{exposure} \times k_f$ (Eq. C6.5-29)

Long-term fraction rate: $rate_{long\text{-}term} = S_{SP} \times f_{exposure} \times k_f \times (1\text{-}Q/K)_{final}$. (Eq. C6.5-30)

These are the fractional degradation rates applied to the fast and slow fractions, respectively.

Uncertainty Associated with Uranium(VI), Plutonium(IV), Neptunium(IV), and Neptunium(V) Solubility Limits

As discussed in the Conceptual Description, the PMA provides uncertainties on selected actinide solid solubilities that are based on available experimental solubility and thermodynamic data reported in the scientific literature or in specialized data compilations. The recommended uncertainties and associated distributions for the relevant actinide solids in log solubility (given in molality units) were in essence based on comparisons of EQ3/6 code predictions with measured solubilities. EQ3/6 run outputs are given in corroborative DTN: SN0704PMASOLUB.001 [DIRS 182787]. In cases where solubility data were either not available or too limited for a valid statistical comparison, the uncertainties were then based on the evaluations of thermodynamic data described in the Organization for Economic Cooperation and Development/Nuclear Energy Agency compilations for the actinide solid of interest. The assigned uncertainty bounds were implemented in a continuous form as a function of pH and fCO_2. No additional uncertainty was assigned to explicitly capture the effects of any particular component given the lack of solubility data for many of these actinide solids as a function of solution chemistry. The recommended PMA solubility uncertainties are given in Table C6-8.

C6.6 UNSATURATED ZONE TRANSPORT

C6.6.1 Conceptual Model

The UZ Transport Model component of the PMA modifies certain elements of the TSPA-LA model thought to be conservative by using an alternate conceptual model. The resulting representation of the UZ transport consists of a different set of computer input files, a different version of the FEHM code, and accompanying documentation that allows a complete TSPA analysis model run to be performed with the changes defined herein in place. Many of the modeling assumptions and implementation details for the PMA are identical to those of the TSPA-LA model. Those components that have been changed to implement the PMA include: the colloid diversity model for colloid-facilitated radionuclide transport, the use of an alternate conceptual model and a matrix diffusion enhancement factor that represents the effects of small-scale fractures, and a new approach and parameter distribution for water table rise under future climate conditions.

Colloid Diversity Model (CDM) for Colloid-Facilitated Transport

In the TSPA-LA model (SNL 2008 [DIRS 184748], Section 6.4.5), radionuclides assumed to be affected by colloid-facilitated transport are handled using a composite of three individual components: 1) the reversibly sorbed species, 2) a fraction that is governed by irreversible

attachment to colloids that undergo retardation due to colloid attachment/detachment processes, and 3) a 'fast fraction' of colloids that were assumed to transport conservatively (without any filtration or retardation). The fast fraction was calculated by assuming that the CDF of observed filtration rate constants (from the same lab and field experiments and using the same weighting approach) reflects a typical population of colloids with filtration rate constants that are distributed according to the CDF of observed rate constants. The rate constant CDF was then extrapolated to estimate the cumulative probability associated with a rate constant less than or equal to the reciprocal of a specified groundwater travel time, and the resulting probability was taken to be the value of the fast fraction associated with that travel time. The fast fraction was calculated for a combined UZ/SZ groundwater travel time of 100 years and was assumed to apply to all TSPA realizations. The remaining colloids containing radionuclides (one minus the fast fraction) were all assumed to transport with a single retardation factor that is randomly sampled from the retardation factor CDFs developed from the experimental data, but truncated at the low end to avoid retardation factors of one (which were accounted for in the fast fraction). Details of the approach are provided in *Particle Tracking Model and Abstraction of Transport Processes* (SNL 2008 [DIRS 184748]).

This approach is modified in the PMA to address technical issues that could underestimate performance of the natural barriers for colloid-facilitated radionuclides. Principally, the model is considered to be conservative because it does not account, except in a coarse way, for the inherent variability of transport properties of individual colloids in a colloid population. In the PMA, the treatment of colloid-facilitated contaminant transport represents the variability of mobility of individual colloids as a process that is inherent to the colloid population, rather than as observations that lead to uncertainty in the transport properties within a conventional, single-valued parameter. The process of retardation via attachment and detachment of colloids on immobile surfaces is often modeled with time and space invariant parameters; here it is modeled assuming a diverse population of transport properties that account for the inherent variability of colloid size, surface charge and chemical properties, mineralogy, and the concomitant impact on colloid mobility. The critical concept is the assumption that the transport properties of colloids in nature are heterogeneous. Therefore, a single set of colloid transport parameters is insufficient to capture the composite transport behavior of a contaminant that is sorbing or is intrinsically bound to colloidal material. The colloid diversity treatment is formulated to account for these heterogeneities.

Robinson et al. (2007 [DIRS 180698]) introduced an approach called the 'colloid diversity' model, in which colloids are assigned a wide range of retardation factors (rather than single retardation factors for volcanics and alluvium) reflecting the diversity in retardation factors inherent in the experimental data. Instead of this variability being transformed into parameter uncertainty, the variability itself is built into the model. With regard to the implementation in the PMA, transport of species taken to be affected by colloid-facilitated transport is still handled by subdividing the species into up to three components: the reversibly sorbed component; the irreversibly sorbed component, which undergoes colloid retardation; and the fast fraction, a portion of the inventory assumed to irreversibly sorb radionuclides, with no colloid retardation. For isotopes of plutonium and americium, all three components are simulated; whereas for isotopes of cesium, protactinium, thorium, and tin, only the reversibly sorbed species are included. For all three components, the colloid diversity model changes the way the simulation

is performed. The implementation of each of these components in the colloid diversity model is outlined below.

Fast Fraction—As in the TSPA-LA model, the fast-fraction ('If') species travel through the system unaffected by sorption, filtration, or diffusion processes. The computational approach describing the fast fraction is identical to that developed in *Particle Tracking Model and Abstraction of Transport Processes* (SNL 2008 [DIRS 184748]), except that the size exclusion option is not active. Instead, it is assumed that all processes related to the transport of colloids through the system are governed by the colloid diversity model, which assigns specific characteristics to each individual colloid that determines its subsequent transport behavior. For the specific case of the fast-fraction species, this subpopulation is defined as the fraction of all individual colloids that transport with an effective retardation factor of 2 (the minimum value possible in this model analysis) for a given realization. Thus, in contrast with the TSPA-LA model, individual colloid transport processes in the TSPA-LA model are assumed to be subsumed in the colloid diversity model. Also, in contrast to the TSPA-LA model, the proportion of the mass that is assigned to the fast fraction varies from one realization to the next, and depends on the colloid diversity model parameters of that realization.

Irreversibly Sorbed Fraction—This fraction, represented by the 'Ic' species, applies only to isotopes of plutonium and americium and is subject to the colloid diversity model. This approach, implemented in FEHM V 2.25 (STN: 10086-2.25-00 [DIRS 182477]), assigns each particle in an Ic species a unique value of the retardation factor R_{coll} by sampling from the statistical distribution function defining R_{coll} for that particular species. Transport of the colloidal particles through the system is subject to spreading due to the variability of R_{coll} among the total population of colloids for each specific radioisotope. In the SZ part of the colloid diversity model, an option exists to be able to employ a stratified sampling strategy in which particles throughout the entire range of R_{coll} values are assigned, with weights established in order to reproduce the desired distribution. This approach can dramatically improve the numerical accuracy of the solution when the range of R_{coll} values spans several orders of magnitude. For the UZ, this option is not available in FEHM V 2.25 because difficulties associated with the simulation of decay chains make this implementation considerably more complex. Instead, in the UZ, uniform weighting and sampling from the distribution is used. This current limitation should not significantly impact the UZ PMA because TSPA simulations use a large number of particles (10^5 or more).

Observations and data used in the development of the R_{coll} distribution in the TSPA-LA Model were revisited. Those data are interpreted with respect to the forward and reverse rate constants, k_f and k_r, respectively. These parameters are related to R_{coll} using the following expression:

$$R_{coll} = 1 + \frac{k_f}{k_r}. \qquad \text{(Eq. C6.6-1)}$$

As in the TSPA-LA Model, the colloids associated with the Ic species are assumed not to undergo diffusion. In addition, the size exclusion and filtration at matrix interfaces is also not applied. Instead, the size exclusion and filtration processes are implicitly included in the colloid diversity model through the use of new parameters defining the CDF for the colloid retardation

factor. Therefore, it is assumed that transport processes such as these are all subsumed within the colloid diversity approach to modeling transport. Alternatively, the analysis could have been developed such that the size exclusion process or the filtration at matrix interfaces had been left as individual processes explicitly simulated. However, this approach would not have been consistent with the approach embodied in the colloid diversity model, which foregoes a process-by-process depiction of colloid transport in favor of a phenomenological approach involving retardation factors that can be parameterized so that it is consistent with lab and field observations.

Reversibly Sorbed Species—These species transport through the system subject to reversible sorption on the colloids and on the rock matrix. When the mass is in the aqueous phase, diffusion can also occur. As in the TSPA-LA model, these species are governed by a transport equation that was developed in *Particle Tracking Model and Abstraction of Transport Processes* (SNL 2008 [DIRS 184748], Section 6.4.5, Equation 6-15a):

$$\left(\frac{R_f + K_c R_{coll}}{1 + K_c}\right)\frac{\partial C}{\partial t} = D_{eff}\frac{\partial^2 C}{\partial z^2} - v\frac{\partial C}{\partial z} - \frac{q}{b(1 + K_c)} \qquad \text{(Eq. C6.6-2)}$$

where R_f is the retardation factor of the dissolved contaminant (assumed to be 1 for the fractured medium and governed by the retardation factor for sorption in the matrix), K_c is the sorption partition coefficient onto colloids, C is concentration, v is velocity, D_{eff} is the effective dispersion coefficient, q is the flux term to or from the matrix due to diffusion, and b is the fracture half aperture. The factor multiplying the time derivative is the effective retardation factor for a reversibly sorbed species. This mathematical expression is identical to that used in the TSPA-LA model, and the parameters K_c, R_f, and b are determined in an identical fashion as the TSPA-LA model. The one significant difference in the PMA for reversibly sorbed species is that the colloid diversity approach is used to determine an effective colloid retardation factor that is used in Equation C6.6-2. This parameter, which we call $\overline{R}_{coll}$ to distinguish it from the retardation factor of individual colloids, is now discussed. The first assumption is that the colloid diversity model governs the range of transport properties of colloids involved in the transport of reversibly sorbed species. The assumption of reversible equilibrium sorption means that radionuclide sorbs and desorbs rapidly on and off the colloids, resulting in an effective colloid retardation factor $\overline{R}_{coll}$ governing the behavior. We further assume that, in the absence of detailed data to the contrary, the equilibrium sorption coefficient for sorption of a radionuclide onto colloids is independent of that of the colloid's retardation factor (R_{coll}). These simplifications lead to the following expression for the effective colloid retardation factor for reversibly sorbed species:

$$\overline{R}_{coll} = \int_{R_l}^{R_u} \eta(R_{coll})\, dR_{coll} \qquad \text{(Eq. C6.6-3)}$$

where R_l and R_u are the minimum and maximum values of R_{coll} in the distribution and $\eta(R_{coll})$ is the density function for R_{coll}; that is, $\eta(R_{coll})dR_{coll}$ is the fraction of the colloid population possessing a value of R_{coll} between R_{coll} and $R_{coll} + dR_{coll}$. Thus, when the assumptions outlined above are made, the effective value of colloid retardation factor reduces to the mean value in the population. This relationship is implemented in FEHM V 2.25 so that the value varies from realization to realization, subject to the distribution of R_{coll} discussed below.

Development of Parameter Uncertainty Distributions

In the PMA, the development of the retardation factor distributions has been modified to better address the considerable uncertainty in the colloid experimental data, and particularly in the extrapolation of these data to TSPA time and distance scales. The retardation factor distributions, and also the fast fractions, are now realization-dependent because they are travel time dependent. In the TSPA-LA model, colloid retardation factor distributions for colloids with irreversibly-sorbed radionuclides were developed by constructing CDFs of retardation factors observed in lab and field experiments, with field data being given twice the weight as lab data because of their more relevant distance and time scales. These CDFs were assumed to be uncertainty distributions for the retardation of colloids due to attachment-detachment processes occurring for colloids carrying radionuclides. In the development below, the same data used previously are re-examined using the colloid diversity model approach to develop the parameter uncertainty distributions for the PMA. Note that as in the TSPA-LA model, data collected under saturated conditions are assumed to be appropriate for both the UZ and SZ systems.

Figure C6-17 shows plots of colloid filtration rate constants (k_f, hr^{-1}) and fractional recoveries as a function of groundwater travel time in laboratory and field tracer tests conducted in saturated fractured volcanics. These plots reflect the same data that were used to develop filtration rate constant and retardation factor distributions for saturated volcanics (BSC 2004 [DIRS 170006]). Figure C6-18 shows plots of retardation factors (R_{coll}) and detachment rate constants (k_r, hr^{-1}) as a function of travel time for the same experiments as Figure C6-17. These two parameters are inherently more uncertain than k_f values because the detachment rate constants are poorly constrained in most of the experiments, and the retardation factors are calculated using the detachment rate constants. Figures C6-19 and C6-20 are analogous plots to Figures C6-17 and C6-18 for saturated alluvium experiments. Again, the data are the same used to develop filtration rate constant and retardation factor distributions for alluvium in *Saturated Zone Colloid Transport* (BSC 2004 [DIRS 170006]), except new data points (output DTN: LA0705PR150304.001 [DIRS 181744]) are added for field experiments in the saturated alluvium south of Yucca Mountain (labeled YMP 22S Field in the plots).

The important points from all these plots are:

- Although the experiments involved a wide range of colloid compositions and sizes and significantly different distance scales, there is a clear tendency for both filtration rate constants and fractional recoveries to decrease as travel times increase.

- There is no clear correlation of retardation factors with time scale, although there appear to be trends within some data sets, including the Schijven data sets.

- Detachment rate constants appear to have a weak negative correlation with time/distance scales, and with the exception of three of the C-wells field data points, the detachment rate constants never exceed 1/travel time. Note that the nonconforming C-wells data points are all associated with attempts to fit a double-peaked breakthrough curve that was unique to all the data sets and required splitting the colloid mass into separate 'pathways' that had different detachment rate constants (SNL 2007 [DIRS 177394], Appendix D). These complications may be the reason that these data points do not conform to the general trend. This result is considered to be a factor in assessing the uncertainty of the parameters in the colloid diversity model but does not invalidate the approach.

Figure C6-21 shows the k_f values and fractional recoveries for the fractured volcanics, where data points associated with the same colloids in the same flow system (but with different travel times) are connected by lines. The field data in these plots are colored and the lab data are black. These plots show that there is an even better case for k_f values and recoveries decreasing with increasing time scales when different types of colloids and different flow systems are not viewed as a single data set. Figure C6-22 shows analogous plots for saturated alluvium. Only a few experiments contradict the general trends. In some cases, the colloids used in the experiments were so nonreactive that they were essentially fully recovered at the two different travel times studied (e.g., the natural colloids and 190-nm CML microspheres in the alluvium lab experiments), suggesting that the travel times were not long enough to discern a trend (although such a trend could only be downward with increasing time).

Because the colloid 'fast fraction' is essentially equivalent to the fractional recovery of colloids that are not retarded, it was decided that the best approach to obtaining a distribution of filtration rate constants for a colloid diversity model was *not* to simply construct a CDF of all experimental filtration rate constants (as was previously done) but rather to deduce a distribution that yielded a recovery versus travel time dependence consistent with the plots of Figures C6-21 and C6-22. It was also desirable from an implementation standpoint to have a single rate constant and retardation factor distribution rather than separate ones for the volcanics and alluvium. Figure C6-23 shows the log recovery data as a function of log time for both the volcanics and the alluvium on a single plot along with linear regression fits to each individual data set as well as a single linear regression fit to the combined data set. The upper and lower 95 percent confidence intervals, associated with the latter fit, are shown as the light dashed lines, and the 95 percent confidence intervals associated with the slope of the linear fit are shown as the dark dashed lines. The combined fit was forced to pass through the origin (forcing a fractional recovery of 1.0 at a time of 1 hour). The individual alluvium fit has a much steeper negative slope than the individual volcanic fit, mainly because of several laboratory alluvium tests involving natural smectite colloids and 190-nm fluorescent carboxylate modified polystyrene latex (CML) microspheres that had essentially complete fractional recoveries and several low recovery data points corresponding to virus transport over different distance/time scales in a sandy aquifer in the Netherlands (Schijven et al., 1999 [DIRS 162423]). The latter data are the only data that are not specific to the Nevada Test Site. These data were included

because they were previously used in the absence of any site-specific alluvium field data (a data gap that has since been addressed by data from a crosshole tracer test at Nye County Site 22, labeled YMP 22S Field on Figures C6-19 and C6-20), and they also serve to illustrate trends of decreasing recovery and filtration rate constant with time and distance under natural-gradient conditions.

The CDF of all filtration rate constants (assuming twice the weight for field data versus lab data) was previously shown to follow a linear trend on a log-log plot of probability versus rate constant (top figures of Figures C6-17 and C6-19), so a CDF P, with intercept b and slope m, of the following form was assumed to represent the diversity of rate constants in a colloid population:

$$\log_{10} P = b + m \cdot \log_{10}(k_f). \qquad \text{(Eq. C6.6-4)}$$

Equation C6.6-4 has a long tail at the low probability end of the distribution, consistent with a small fraction of colloids having small filtration rate constants and, hence, equilibrium retardation factors approaching unity.

Figure C6-24 shows the fractional recovery versus travel time superimposed over all the data from Figure C6-23 for three CDFs that approximately match (1) the best linear fit (passing through the origin) to the combined data set, (2) the CDF of all rate constants (with twice the weight given to field data), and (3) the best fit to the 2 highest recovery data points associated with the field tracer test in the fractured volcanics at the ER-20-6 site, which had the highest recoveries of any of the field tests. Fits (1) and (3) were chosen to represent the lower and upper bound CDFs, respectively, for the colloid diversity model.

Although it would seem justified to use CDFs that result in lower recoveries than (1), which is effectively only the 'mean' CDF that is consistent with the data, the use of CDFs with lower recoveries than (1) resulted in negligible recoveries/fast fractions for travel times exceeding a few years. Because most of the data (including all the field data) are associated with synthetic organic colloids (microspheres and viruses) rather than inorganic colloids, this approach was considered prudent. The approach also inherently de-emphasizes the virus data from a shallow sandy aquifer in favor of colloids in more relevant settings. Furthermore, the approach implicitly weights the field data sets more heavily than the lab data sets because the field data exert more influence on the slope of the best-fitting line through the data (owing to their greater distance from the origin) and also because the upper bound CDF is based on a fit to the field data set with the highest recoveries. Finally, the observations of the colloid-facilitated transport of plutonium over ~1 km in ~30 years from a nuclear test cavity at the Nevada Test Site (Kersting et al., 1999 [DIRS 103282]) provides a good argument for weighting the data such that the filtration rate constant CDFs emphasize the higher recovery data. The CDFs associated with (1), (2), and (3) above are plotted along with the actual CDF of the filtration rate constants (with twice the weight given to field data) on Figure C6-25.

To generate CDFs of colloid retardation factors based on the filtration rate constant CDFs, it is necessary to assume (1) some uncertainty in the latter CDFs (captured as slope and/or intercept uncertainty), and (2) a distribution of colloid detachment rate constants. To address (1), it is

assumed that the slope of the filtration rate constant CDF versus k_f on a log-log scale is subject to an uncertainty distribution given by a triangular distribution with values [0.17, 0.51, 0.85], which correspond to the negative of the slopes of the three lines on Figure C6-24. Because the intercept has a lesser effect on the filtration rate constant CDF than the slope, it was assumed to be fixed at a value of 0.2. To address (2), uncertainty in the detachment rate constants are assumed to be governed by a triangular distribution with a minimum value of 0.01/travel time (hr^{-1}), mode of 0.1/travel time (hr^{-1}), and maximum of 1/travel time (hr^{-1}) for any specified travel time. The latter serves as a reasonable upper bound for detachment rate constants, which were shown on Figures C6-18 and C6-20 to never exceed 1/travel time except for the C-wells tracer test involving two tracer peaks. The mode of 0.1/travel time is greater than many of the data points on Figures C6-18 and C6-20, but this value, extending down to the minimum of 0.01/travel time, is justified because of the poorly constrained nature of the detachment rate constants.

Figure C6-26 shows the resulting minimum, central, and maximum CDFs of colloid retardation factors associated with a 100-year travel time. The minimum CDF corresponds to a slope of 0.85 for the k_f CDF and a value of 0.01/travel time (hr^{-1}) for k_r, and the maximum CDF corresponds to a value of 0.17 for the k_f CDF slope and a value of 1/travel time (hr^{-1}) for k_r. The central CDF corresponds to the modes of the distributions of slope and k_r. Clearly, there is a great deal of uncertainty associated with the retardation factor CDFs. This uncertainty reflects the considerable scatter in the available data sets as well as the uncertainty associated with the extrapolation of the data to much longer time and distance scales. The large retardation factors associated with each of the CDF realizations will result in some filtration of colloids that are essentially permanent, which is a desirable effect that is considered to improve the colloid diversity model.

Because there are no colloid transport data associated with the UZ, it is assumed that the same retardation factor CDFs apply to both the UZ and SZ, and the CDFs ideally should be based on the combined UZ and SZ travel time in a given TSPA realization. This assumption may be conservative because of filtration and retardation processes that could be present in the UZ that do not occur in the SZ, such as colloid attachment to air-water interfaces, thin-film straining, and imbibition into the matrix during wetting-drying cycles.

Another implementation issue for the PMA concerns the independent/decoupled nature of the UZ and SZ systems. This implementation, rather than a single, unified UZ/SZ system, poses problems for simulating transport of colloids using the colloid diversity model. If the same retardation factor CDF is sampled once for the UZ and again for the SZ, there will be a strong tendency to eliminate the portion of the distribution with small retardation factors. That is, the probability of sampling small retardation factors in both the UZ and SZ and thus obtaining a small combined retardation factor is exceedingly small. The consistent approach is one in which fast-moving colloids in the UZ remain fast moving in the SZ.

To ensure that the fast portion of the colloid distribution is not under-sampled, leading to non-conservative results, the fast fraction species is retained, even though, in principle, this fraction could fall out naturally from the colloid diversity approach. Instead, for the PMA, the fast fraction is defined as the cumulative probability associated with a retardation factor of 2, the

minimum value in the distribution. Then, for the Ic species, a method is required that yields the appropriate overall CDF for the combined UZ/SZ system. Two approaches are taken to confront this issue. In both cases, the travel time used to establish the CDF for retardation factor is taken to be that of the SZ. In the first approach, the colloid diversity model for the Ic species is applied only to the SZ system, whereas for the UZ, the Ic species is conservatively taken to be governed by all R_{coll} values equal to 2. This assumption is valid if the travel time is dominated by the SZ portion of the flow path. However, if the travel times are equal to one another, then the process of individually sampling the CDFs in the UZ and SZ can be overcome by altering the CDF such that the composite behavior is the one that is desired. It can be shown that this altered CDF can be obtained by using a CDF that is sampled independently for both the UZ and SZ that has the retardation factors from the original CDF (combined UZ and SZ) but assigns the square root of the cumulative probabilities as the cumulative probability associated with each retardation factor. Figure C6-27 presents an example calculation that demonstrates that this approach reproduces the original combined UZ and SZ CDF when the distribution is randomly sampled twice.

Water Table Rise for Future Climate

In the TSPA-LA model, future climate conditions are simulated assuming that the system instantaneously changes from one steady state flow field to another at the time the climate changes. Future climates, termed the monsoonal and glacial-transition climate states, are represented by adopting a flow field in which infiltration rates are elevated compared to the present-day conditions for that realization. In the UZ flow model area, the present-day water table varies from less than 730 m to greater than 980 m above mean sea level (BSC 2004 [DIRS 169855] Figure 6.2). Within the repository fingerprint, the present-day water table varies from around 730 m to 850 m above mean sea level (BSC 2004 [DIRS 169855] Figure 6.2). Note that the bottom boundary for the flow models of all climate states is the present day water table. For use in conjunction with FEHM's multi-species particle tracking model the flow-field files for the monsoon, glacial-transition, and post-10,000-year climate flow fields from the UZ Flow Model Abstraction are post-processed to approximate the affects of a rising water table. The rising water table is approximated by constraining the water table to a minimum elevation of 850 m above mean sea level (SNL 2008 [DIRS 184748] Section 6.4.8). That is for future climates, any locations where the present-day water table is below 850 m it is set to 850 m and any locations where the present-day water table is above 850 m, the water table is not adjusted from the present day level (see BSC 2004 [DIRS 169855]). In the TSPA-LA model, the rise of up to 120 m above a nominal level of 730 m was adopted without uncertainty. This approach was considered to be conservative with respect to the UZ transport times, because 850 m was considered to be an upper bound, and the higher water table shortens the travel distance and travel times through the UZ. In the PMA, the water table elevation is taken as an uncertain parameter with a distribution that results in most realizations being conducted with a minimum water table elevation that is less than 850 m. This change should lead to an analysis that is less conservative with respect to UZ transport times than the TSPA-LA Model and one which incorporates the uncertainty in water table elevation.

A workshop was conducted on August 23, 2006, to quantify uncertainty in past water table rise at Yucca Mountain for use in the TSPA Model for future climatic conditions. This was accomplished by convening a group of Project participants who are technical experts in the areas of hydrology, geochemistry, mineralogy, and statistics/uncertainty to represent and consider the

multiple lines of evidence regarding this process. The workshop consisted of a series of presentations on previous studies and new geochemical information relevant to past water table rise at Yucca Mountain, followed by a quantitative assessment of uncertainty in water table rise by the entire group:

- James Paces (USGS)
- Leonid Neymark (USGS)
- Kenneth Rehfeldt (LANL)
- Robert Roback (LANL)
- Schön Levy (LANL)
- Srikanta Mishra (INTERA)
- Bill Arnold (SNL)
- Drew Coleman (DOE).

It was noted in the technical presentations that:

- The water table rise parameter for this discussion is defined as being the average water table rise in the area beneath the repository and is to be applied as a uniform increase in the water table elevation in the site-scale UZ transport model.

- A 'warm-up' exercise, in estimating the 90 percent confidence intervals for answers to a set of random questions by the participants, was conducted and confirmed a common outcome in which participants routinely underestimate their uncertainty in the answers.

- Differences in scale at which measurements are made and the scale of model parameters complicate the assessment of uncertainty for some parameters.

- Discussion among the participants concluded that uncertainty in water table rise is primarily epistemic (related to lack of knowledge) uncertainty.

- Previous studies relevant to water table rise include evidence from calcite morphology, Sr isotopes, zeolite mineralogy, paleospring deposits, packrat middens, and numerical models. More recent data indicate reevaluation the conclusions from the original analysis may be necessary.

- Large-scale areas of recharge occur generally to the north and east of Yucca Mountain and areas of natural discharge occur to the south.

- Schematic analyses indicate that with wetter climatic conditions and greater groundwater flow rates, the rise in the water table would be expected to be greater at locations upstream from springs, than at the springs.

- The original estimates of maximum standing water level rise published in 1991 (about 60 m to 100 m) were based on visual examination of cuttings from well H-6 (Levy 1991 [DIRS 100053]).

- Modeling studies by Czarnecki (1985 [DIRS 160149]) resulted in simulated water table rise of about 130 m.

- The three-dimensional regional-scale groundwater flow model of D'Agnese et al. (1999 [DIRS 120425]) simulated steady-state flow for full-glacial conditions (21,000 years ago), used increased precipitation estimates from an atmospheric general circulation model, and head-dependent sinks at inferred potential discharge locations. These studies indicated water table rise of 60 m to 150 m beneath the repository.

- CRWMS M&O (1997 [DIRS 101111]) gave a general endorsement of estimated water table rise in the range of 80 to 120 m, based on geochemical and existing paleodischarge evidence.

During and following these presentations, there were discussions among the participants about the uncertainties and persuasiveness of various lines of evidence regarding past water table rise beneath the repository. It was generally acknowledged by the group that no single line of evidence was definitive, but individual participants expressed greater or lesser confidence in different types of information. In particular, James Paces expressed doubt in the reliability of results from the numerical modeling of groundwater flow. Bill Arnold stated that it was unpersuasive to extrapolate the maximum rise in the water table at paleospring deposits to the area beneath the repository. Because the interpretation of water table rise based on patterns of zeolitic alteration by Schön Levy depends on the difference in water levels across the Solitario Canyon Fault, Dr. Levy acknowledged some uncertainty in the quantitative estimates in her presentation.

Next, each workshop participant completed a subjective probability assessment worksheet provided by Srikanta Mishra. This worksheet contains a table with seven quantiles to be filled in by each participant individually. The results of these subjective assessments of water table rise are shown as the light-colored curves on Figure C6-28.

Following completion of the worksheets, the results were entered into a spreadsheet, displayed graphically on a projector, and discussed by the entire group. In particular, each participant discussed the rationale used for the upper bound, lower bound, and median value. It was recognized that the lower bounds chosen by James Paces and Schön Levy differed significantly from the values chosen by other participants. Similarly, the upper bound chosen by James Paces was significantly different than the values from other participants.

Srikanta Mishra explained that there were two options available for defining the aggregate uncertainty in water table rise among the participants. The first option involved allowing each participant to reconsider his or her individual uncertainty distribution and then mathematically 'averaging' the results. The second option was to agree upon a consensus uncertainty distribution. The group decided to use the second option and a consensus uncertainty distribution was constructed through a process of graphical display, discussion, and trial-and-error variations in the quantile values. The resulting consensus uncertainty distribution in water table rise for use in the PMA is shown as a dark solid line on Figure C6-28.

However, for the PMA, this distribution is slightly modified for the following reason. It is desirable to use the FEHM input files for the TSPA-LA model that assigned the water table node bins so that these files do not have to be reworked. However, those files (DTN: MO0704PAFEHMBR.001_R3 [DIRS 184647]) assumed that the water table would be elevated no higher than 120 m higher than the minimum value in the present-day water table (730 m). Therefore, any water table elevations in the new analysis that extend beyond 730+120=850 m would be problematic because a grid node higher than this value would not be flagged as a repository node, leading to mass leaving the UZ system but not recorded in the output. To prevent this from happening while still enabling the use of the water table bins developed previously, it is required that the water table elevation be restricted to no more than 120 m. However, the 'consensus distribution developed earlier, extends to 150 m water table rise. To accommodate this limitation, the distribution is adjusted to linearly extend the high end of the CDF to unity at 120 m. The revised distribution is plotted as a dashed curve alongside the original 'consensus' curve on Figure C6-29. This is the CDF that is used in the PMA to capture uncertainty in water table rise. This necessary change to the distribution to accommodate limitations in the water table bins developed previously opens the possibility of roughly 5 percent of the realizations that would have been given a water table elevation between 850 m and 880 m being forced to be no greater than 850 m. For the purposes of examining the sensitivity of the UZ breakthrough curves to water table elevation, this change is an acceptable compromise. This is especially true if the dependence of transport results to the water table elevation is modest.

The distribution required for use in the PMA is the water table elevation, rather than the water table rise. These data are labeled 'Water Table Elevation' in the Excel spreadsheet in corroborative DTN: MO0704PAUZFEHM.000 [DIRS 182790] and is paired with the 'Consensus Quantile' column to define the CDF to be used in the PMA. It is computed by adding the water table elevation to the nominal value of the present-day repository beneath the repository, 730 m (SNL 2008 [DIRS 184748], Section 6.4.8). Figure C6-29 is the CDF to be used for water table elevation.

Matrix Diffusion Submodel

This section describes the changes to the diffusion model to be used in the PMA, compared to the TSPA-LA model. Changes include the addition of a diffusion-enhancement factor and the use of the Discrete Fracture Model as an alternate conceptual model for fracture/matrix interaction.

Effective Matrix Diffusion Coefficient

In the TSPA-LA Model (SNL 2008 [DIRS 184748]), the diffusion coefficient is based on a segregation of the rock units below the repository into three groups of similar properties, and a diffusion coefficient for each radioelement is computed as the product of the diffusive tortuosity τ_D and the free-water diffusion coefficient D_{free}:

$$D_{eff} = \tau_D D_{free} . \qquad \text{(Eq. C6.6-5)}$$

In the model, the diffusive tortuosity differs for each of the three rock units but is independent of radioelement; whereas the free-water diffusion coefficient is a property of the radioelement. Values for these parameters are developed in DTN: LB0702PAUZMTDF.001_R1 [DIRS 180776]. Studies have shown that laboratory based matrix-diffusion coefficients may underestimate field-scale matrix diffusion coefficients used to simulate field tests (SNL 2008 [DIRS 184614] Section 6.8 [a] and BSC 2006 [DIRS 178275] Section 6.4.1). Wu et al. (2001 [DIRS 156399]) and Liu et al. (2003[DIRS 162470]) indicated that the existence of many small-scale fractures may be the major reason for relatively large diffusion coefficient calculated from field data. For the PMA, the effect of a presumed increase in the effective diffusion coefficient D_{eff} due to the effects of small-scale fractures is modeled by applying a multiplication factor to this expression:

$$D_{eff} = f_d \tau_D D_{free} \quad \text{(Eq. C6.6-6)}$$

where f_d is the enhancement factor for matrix diffusion. In the PMA implementation of this enhancement factor, the GoldSim model is used to generate values of f_d and τ_D subject to the parameter uncertainty distribution described herein for f_d and in DTN: LB0702PAUZMTDF.001 [DIRS 180776] for τ_D, and the product of these two terms is passed to FEHM in the parameter input table.

To assign a parameter uncertainty distribution for f_d, the modeling efforts to reconcile the results of UZ transport field tests have been examined. In Section 7.8 of *UZ Flow Models and Submodels* (SNL 2007 [DIRS 184614]), a flow and transport field test and model are presented for a percolation and tracer test conducted along a fault in Alcove 8/Niche 3. A Multiple Interacting Continua model was developed for simulating flow and transport during the test. The fault was explicitly included, along with finely discretized grid spacings in the matrix adjacent to the fault. An analysis is presented of the influence of matrix diffusion and the parameter ranges required to match the breakthrough curves of two conservative, diffusing tracers with different diffusion coefficients in free water. *UZ Flow Models and Submodels* (SNL 2007 [DIRS 184614], Figure 7.8-9) shows that in order to obtain a good match to the tracer tests, the interface area had to be increased by a factor of 45 above that of the original data. Likewise, in *Radionuclide Transport Models Under Ambient Conditions* (SNL 2007 [DIRS 177396], Section 7.3), the same analysis is provided, and in both reports, a discussion on the need for adjusting the interface area is provided. In Liu et al. (2004 [DIRS 169948]), this need to enhance the diffusion coefficient or interface area is described in the form of an increase in the matrix diffusion coefficient, but the description in the paper postulates that the increase could be due to the increase in available surface area for diffusion as a solute encounters a greater number of fractures during its transit through a fractured medium.

Analysis of Alcove 8/Niche 3 Flow and Transport Tests (BSC 2006 [DIRS 178275]) describes a second round of testing at this field site, away from the location of the fault zone tested previously. The test, called the large-infiltration-plot test, consisted of flow and transport studies similar to those in the fault zone, to examine the behavior of rock in a relatively unfaulted zone, although the rock mass contained numerous fractures. A numerical model using the Multiple Interacting Continua conceptualization was developed to simulate the flow and transport

behavior. Like the discrete fracture representation above, the Multiple Interacting Continua approach employs a grid that includes fine discretization near the fractures, which in this case are represented as an equivalent continuum. From the standpoint of matrix diffusion, the Multiple Interacting Continua model is similar to that of the discrete fracture model in that it captures fine gradients in solute concentration away from the fractures. Although this test yielded seepage flow information, unfortunately no tracer breakthrough was observed during the test. Therefore, a transport model of this test could only be used to bound the diffusion coefficient. It was noted in transport simulations that if the laboratory based matrix diffusion coefficient was used, tracer breakthrough was predicted by the model. Transport models with diffusion coefficients increased by a factor of 45 (the same as that found in the fault zone test) resulted in predicted concentrations that were low enough that they would probably go undetected in the experiment (i.e., the concentrations would be within the background levels). From this result, the study concluded that this modeling exercise corroborated the reasonableness of the factor of 45 for the test.

The use of an enhancement factor of the diffusion coefficient (or, equivalently for an individual fracture zone, the interface area) is an attempt to parameterize a commonly used transport model formulation to explain the observed field results. In the PMA, to include this effect, it should be recognized that other parameters besides the diffusion coefficient influence the matrix diffusion coefficient, including the fracture aperture, spacing, and Active Fracture Model parameter γ. Therefore, it could be argued that uncertainties in these transport parameters already capture the uncertainty in the phenomena that lead to the need to increase the diffusion coefficient. In other words, it is possible that the difference between field-scale effective diffusion coefficients and lab-scale values is actually a geometric effect related to fracture area that is already included in the TSPA-LA Model analysis in the form of uncertainty in aperture. Alternatively, the enhancement factor may represent features such as the effects of small-scale fractures not simulated by the model, in which case the enhancement parameter needs to be explicitly included. An additional piece of information is available from an analysis of the Alcove 1 tracer test (Liu et al. 2003 [DIRS 162470]), which suggested that a multiplier of the diffusion term in the range of 2 to 4 provided a reasonable match to the data. The range of values determined from these tests, combined with the uncertainty in the tracer test interpretations themselves, suggest that a lower bound of the enhancement factor should be set to 1 (no enhancement considered), whereas the upper bound should be set to 45 to match the value obtained in the analysis of the fault test and corroborated as reasonable for the large-infiltration-plot test. Given the lack of systematic measurements to provide further constraints on this distribution, it is reasonable to assume a uniform distribution of the enhancement factor from 1 to 45.

Since the analyses leading to the value of 45 were obtained using models with fine discretization near the flowing fracture(s), this parameter uncertainty distribution is only compatible with the Discrete Fracture Model conceptual model incorporated in the UZ component of the PMA. The TSPA-LA model uses a dual-k conceptualization, for which higher values of the scale factor would likely be needed to match the field data. No attempt has been made to estimate the enhancement factor with a dual continuum transport model, so the uncertainty distribution developed herein is only compatible with the Discrete Fracture Model conceptual model for fracture/matrix interaction.

Discrete Fracture Model Fracture/Matrix Interaction Model Conceptualization

The matrix diffusion in the PMA is implemented with the Discrete Fracture Model. The TSPA-LA Model was developed using the dual-permeability (*k*) conceptualization because the only Mountain-scale, process model simulations available for comparison were performed with the dual continuum model option in T2R3D [DIRS 146654]. *Particle Tracking Model and Abstraction of Transport Processes* (SNL 2008 [DIRS 184748]) also developed a set of breakthrough curves using a discrete fracture representation of transport in the matrix. The choice of conceptual model used for the simulation is simply made by invoking the Discrete Fracture Model transfer function curves. For the PMA, the Discrete Fracture Model transfer function is selected because it is desirable to eliminate the conservatism that the dual-k model represents (greater breakthrough at short travel times), and because the Discrete Fracture Model transfer function is compatible with the enhancement factor uncertainty distribution developed in the previous section.

The Discrete Fracture Model transfer function has been used in a variety of tests to ensure that it performs as expected. A series of comparisons of the FEHM particle tracking model (with the Discrete Fracture Model transfer function) show favorable comparisons to a discrete fracture model with a completely different numerical formulation (SNL 2008 [DIRS 184748], Section 7.2.1). In a two-dimensional cross section model, the Discrete Fracture Model results showed reasonable comparison, especially at late travel times, to a Multiple Interacting Continua transport model and to a particle tracking model that employed a completely different numerical algorithm (SNL 2008 [DIRS 184748], Section 7.2.2). Finally, in the three-dimensional model validation runs presented in *Particle Tracking Model and Abstraction of Transport Processes* (SNL 2008 [DIRS 184748], Section 7.2.3), the Discrete Fracture Model runs, when compared to the validated dual-k transport model runs, exhibited behavior that is understandable given the nature of these two conceptual models: later first arrivals in the breakthrough curves, with convergence of the two breakthrough curves at long travel times. This series of model runs provides confidence that the particle-tracking model with the Discrete Fracture Model transfer function is behaving as expected and is suitable for use in the PMA.

The underlying mathematical development and the theoretical considerations related to the use of transfer functions to represent fracture/matrix interactions in the TSPA abstraction model for UZ transport are described in *Particle Tracking Model and Abstraction of Transport Processes* (SNL 2008 [DIRS 184748], Section 6.4.3). The inputs associated with this data are direct inputs to the UZ component of the PMA. They are invoked from within an FEHM data input file specified in the fehm_PMATSPA.mptr input file for the UZ transport abstraction.

The method for generating the transfer functions is described in detail in *Particle Tracking Model and Abstraction of Transport Processes* (SNL 2008 [DIRS 184748], Appendix C). The differences in the transfer-function parameter matrix from the analysis and/or model reports to the TSPA-LA model were discussed in *Particle Tracking Model and Abstraction of Transport Process* (SNL 2008 [DIRS 184748]. The treatment of this parameter in the PMA is identical to that used in the TSPA-LA model.

C6.6.2 Model Implementation

Colloid Diversity Model for Colloid-Facilitated Transport

The implementation of the colloid diversity model in the PMA is accomplished with the following steps. For the PMA, Steps 1 to 6 are evaluated within the SZ, as discussed in Section C6.7.2. Steps 7 and 8 apply only to the UZ PMA implementation.

1. For a given realization, determine the median SZ travel time, τ (hr), from the calculation of the If species in each Monte Carlo realization and store each travel time in a table.

2. Use τ (hr) as the total travel time through the UZ and SZ, equivalent to assuming that, for the purposes of assigning the colloid diversity distribution parameters, the SZ travel times are much longer than UZ travel times.

3. Randomly sample a triangular distribution with parameters (0.17, 0.51, 0.85) and use the resulting value as the slope m in Equation C6.6-4 to define a CDF for the colloid filtration rate constants (hr^{-1}). Use a value of b = 0.2 for all realizations.

4. Randomly sample from a triangular distribution [$log_{10}(0.01/\tau$ (hr^{-1})), $log_{10}(0.1/\tau$ (hr^{-1})), and $log_{10}(1/\tau$ (hr^{-1}))], and use the resulting value as the log_{10}(colloid detachment rate constant).

5. Transform the filtration rate constant CDF to a retardation factor CDF using Equation C6.6-1, which yields, after applying Equation C6.6:

$$\log_{10} P = b + m \cdot \log_{10}\left[k_r (R_{coll} - 1)\right]. \quad \text{(C6.6-7)}$$

6. Compute the fast fraction as the cumulative probability associated with a retardation factor of 2.

7. Define a new retardation factor CDF that can be independently sampled for the UZ and SZ by using the CDF from Step 5 with cumulative probabilities equal to the square root of the probabilities of the CDF from Step 5. This approach is executed by choosing this option in FEHM V 2.25. Alternatively, apply the colloid diversity model to the Ic species of the SZ system, and apply a uniform value of 2 for the Ic species in the UZ. The latter approach is used in the PMA.

8. Compute the value of $\overline{R}_{coll}$ for the reversibly sorbing species using Equation C6.6-3. This is done by supplying the retardation factor distribution parameters to FEHM V 2.25 and selecting the appropriate option in the input for the reversible species.

Water Table Rise for Future Climate

To implement this change for the PMA, the water table elevation under future climate conditions is now passed from GoldSim to FEHM during the simulation. FEHM V 2.25 now has the provision, which is invoked in the PMA, to change the flow field representation during the

simulation to accommodate the water table elevation at runtime. This requires that the template for information passing between GoldSim and FEHM be changed from that described in Table 6-2 of SNL 2008 [DIRS 184748] to accommodate the passing of an additional variable, called wt_elevation (corroborative DTN: MO0704PAUZFEHM.000 [DIRS 182790]).

Matrix Diffusion Submodel

The enhancement factor for the effective matrix diffusion coefficient for the PMA is implemented by the addition of a GoldSim stochastic element to the TSPA-LA Model. The stochastic element is used to sample a uniform distribution between 1 and 45 to choose a scaling factor, f_d, which is applied to the effective matrix diffusion coefficient as noted in Equation C6.6-6. The new effective matrix diffusion coefficient values will become part of a FEHM external file that is generated during a preprocessing PMA run (Sections 6.3.9.3 and F.2.1.1.13).

The switch to the Discrete Fracture Model fracture/matrix interaction alternative conceptual model is readily implemented in the TSPA-LA Model by replacing the FEHM external input file uz_tfcurves_nn_dualk_4680.in (DTN: MO0704PAPTTFBR.002_R0 [DIRS 180442]: Particle Tracking Transfer Functions) used in the TSPA-LA model with the alternate file uz_tfcurves_nn_dualk_4680.in (DTN: MO0704PAPTTFBR.002_R0 [DIRS 180442]: Particle Tracking Transfer Functions). This procedure is readily implemented using the MFCP-LA DLL that copies the desired Transfer Function curves file into a generically named file found in the FEHM external multi-species particle tracking files (Section F.2.1.11).

C6.7 SATURATED ZONE FLOW AND TRANSPORT

C6.7.1 Conceptual Model

Radionuclide Mass Flux from the UZ to the SZ

In the SZ TSPA TSPA-LA Model (Section 6.3.10), the radionuclide mass reaching the water table in both the matrix and fractures of the UZ released from the UZ Transport Model is transferred to flow through the fractures in the SZ radionuclide transport model. This is equivalent to assuming that the radionuclide mass instantly diffuses out of the UZ matrix and into the SZ fractures at the interface between the UZ and SZ. This approximation reduces the transport time expected if mass diffused from UZ matrix into SZ matrix. The analysis described in this section documents modification of the TSPA-LA Model by introducing matrix transport at the interface between the UZ and SZ. The modified model channels the radionuclide mass release from the UZ to the SZ three-dimensional and one-dimensional transport models and accounts for transport in the matrix.

In the SZ TSPA-LA Model (Section 6.3.10), the source of radionuclides in the SZ is modeled as the radionuclide mass released from the UZ at the water table (i.e., the interface between UZ and SZ). The UZ radionuclide transport model calculates the rate and spatial distribution of radionuclide releases to the SZ. The area beneath the repository is subdivided into four source regions, and the released mass from the UZ is directed to one of these four regions to be transported to the SZ. For the SZ three-dimensional transport model, the UZ released

time-varying radionuclide mass is combined with the SZ unit-source radionuclide breakthrough curves in a convolution integral to model radionuclide transport to the accessible environment. For the SZ one-dimensional transport model, the UZ radionuclide mass release is directly used as the source to the one-dimensional transport model within the TSPA Model. Radionuclide ingrowth is calculated in the one-dimensional transport model.

The UZ Transport Model primarily uses the dual-continuum approach that models transport in both the fractures and rock matrix. The dual-continuum approach is implemented using a numerical grid that consists of fracture and matrix cells, with each fracture cell connected to a corresponding matrix cell. Thus, in the dual-continuum numerical grid, the radionuclide mass released at the water table is through both fracture and matrix cells. The TSPA-LA Model combines the releases from the UZ fracture and matrix cells and directly feeds the output to both the SZ three-dimensional and one-dimensional transport models. For the PMA analysis, the radionuclide mass releases from the UZ matrix cells will be separated from the releases through fracture cells. The release from the matrix cells at the water table will then be routed through a sub-model that will simulate diffusion from the UZ matrix into the SZ fractures. This is done by introducing new GoldSim cell pathways in the TSPA Model. A GoldSim cell pathway is an element in the Contaminant Transport Module of GoldSim that is used to transport contaminant species. A network of cells, are mathematically equivalent to a finite difference network of nodes. The submodel contains a discretized scheme with five cells in series (to reduce numerical dispersion) at the UZ/SZ boundary that is used to transport mass from the UZ matrix to the SZ fractures (Figure C6-32). The new cells simulate transport by diffusion in a dual porosity environment. The output of the new cells is directed to both the SZ three-dimensional and one-dimensional transport models. The mass is applied to the four SZ regions. No change is made to the mass flux from the fractures of the UZ as the UZ-SZ interface accurately handles the mass flux transfer from the UZ fractures to the SZ.

Colloid Transport of Irreversibly Sorbed Radionuclides

In the SZ Flow and Transport Model Abstraction, radionuclides are transported in the SZ as solutes in groundwater or sorbed onto colloids (SNL 2008 [DIRS 183750], Section 6.3). For transport through colloids, the radionuclides are either reversibly or irreversibly sorbed onto colloids. The latter mode of colloid transport is the subject of this section. The TSPA SZ transport model simulation of colloid transport with irreversibly sorbed radionuclides has been applied to the radionuclides plutonium and americium (SNL 2008 [DIRS 183750], Section 6.5.2.11). A large fraction of the colloids are retarded by sorption while a small fraction, known as fast-fraction, are transported unretarded. In the TSPA-LA Model (SNL 2008 [DIRS 183750], Section 6.5.2.11), transport of irreversible colloids for the retarded fraction in both the volcanic units and alluvium is calculated using single retardation factors per realization (one for the volcanic units and another for the alluvium). Current data analysis shows that use of single retardation factors for all non-fast-fraction colloids in the volcanic rocks and alluvium does not fit experimental observations (corroborative DTN: LA0705PR150304.001 [DIRS 181744). Moreover, the TSPA-LA colloid model does not account for scale dependence of filtration rate or retardation factors. The data have been gathered from lab and field experiments (i.e., relatively small distances) and consideration of length (distance) scales may be more appropriate than directly applying them to large scale modeling grids.

In the PMA, colloid filtration (retardation) in the SZ is modeled with a colloid diversity model. The details of the colloid diversity model for both UZ and SZ is summarized in Section C6.6. In this model, colloids are assigned a wide range of retardation factors within a given TSPA realization in recognition of their diverse sizes, shapes, compositions, and surface properties (Robinson et al. 2007 [DIRS 180698]). In addition, the development of the colloid retardation factor distributions will be modified to better address the considerable uncertainty in the colloid transport experimental data and, particularly, in the extrapolation of these data to the TSPA time and distance scales. The retardation factor distributions, and also the fast fractions, will now be travel time dependent. This colloid diversity approach is implemented in the SZ three-dimensional and one-dimensional models.

The PMA implementation of a distribution of colloid retardation factors in the three-dimensional SZ transport model is accomplished with a modification of the FEHM software code (V. 2.25). For the SZ one-dimensional transport, the colloid diversity model is implemented by duplicating the GoldSim SZ 1-D pipe setup into 10 sets of pipes each with a different retardation factor, derived from the distribution of retardation factors, applied to each set of pipes. A GoldSim pipe pathway is an element in the Contaminant Transport Module that is used to simulate advectively dominated one-dimensional conduit. Implementation details with steps to be followed are given in Section C6.7.2. The SZ one-dimensional model implementation consists of a set of GoldSim pipe pathways with three pipe segments representing each of the four source regions. The three pipe segments represent the distance from the UZ-SZ boundary to the accessible environment. The lengths of each pipe segment are given in *Saturated Zone Flow and Transport Model Abstraction* (SNL 2008 [DIRS 183750], Table 6-6[a]).

Redox Conditions and Impacts on Radionuclide Transport

Potential variations in redox conditions in the SZ could have an impact on the migration of redox-sensitive radionuclide species released from the repository at Yucca Mountain (BSC 2006 [DIRS 178672]). For example, under reducing geochemical conditions, the solubility limit can be much lower and the sorption coefficient can be much higher for radioelements such as technetium and neptunium. Potential precipitation from lower solubility limits and retardation from enhanced sorption would lead to longer transport times in the SZ if groundwater flow paths from beneath the repository encountered reducing conditions before reaching the boundary of the accessible environment.

The base-case conceptual model of SZ transport developed for the TSPA-LA Model is implicitly taken to be oxidizing conditions in the SZ, based on the uncertainty distributions for sorption coefficients of technetium and neptunium (SNL 2008 [DIRS 183750]). In the TSPA-LA Model, technetium is modeled with no sorption (i.e., no retardation) in both the volcanic units and the alluvium. The objective is to modify the SZ Flow and Transport Abstraction Model and the SZ one-dimensional transport model for the PMA to simulate the transport of technetium and neptunium with enhanced sorption in zones of reducing geochemical conditions. Uncertainty in the transport of these redox-sensitive species is evaluated with regard to the location and size of a potential reducing zone in the SZ and uncertainty in the sorption coefficients within the reducing zone.

Redox conditions in the SZ, as measured by the reduction/oxidation potential of groundwater samples, are variable in the area near and downgradient from Yucca Mountain. Although apparent non-equilibrium redox conditions are observed in many wells, an approach based on a preponderance of evidence can be used to identify oxidizing and reducing locations in the SZ (BSC 2006 [DIRS 178672], Section 2.1). Measurements of dissolved oxygen, Eh from inert platinum electrode, and total iron concentration, along with manganese and nitrite/nitrate redox couples, are used to infer redox conditions in wells.

Results of the analysis of redox conditions in the SZ indicate that oxidizing conditions prevail in most characterized locations in the SZ but that there are several wells to the east and south of Yucca Mountain with reducing conditions. The assessment of redox conditions in wells near Yucca Mountain is summarized on the map shown on Figure C6-30 (BSC 2006 [DIRS 178672], Figure 2.1-2). The area of inferred reducing conditions, including Wells b#1, H-4, WT-17, and WT-12, is located along potential groundwater flow pathways in the SZ from beneath the proposed repository and it is this area in the tuff that is of greatest potential significance to the transport of redox-sensitive radionuclides. A working hypothesis is that the zone of observed reducing conditions is related to the presence of minor primary pyrite in the Tram Tuff and its reaction with dissolved oxygen in groundwater (BSC 2006 [DIRS 178672], Section 2.1). The solubility of both technetium and neptunium have much lower under reducing conditions, relative to oxidizing conditions (BSC 2006 [DIRS 178672], Section 2.2). Precipitation of these radioelements in the SZ could occur if their concentrations in upstream oxidizing groundwater exceeded the solubility limit as flow enters the reducing zone. Although the conceptual model of transport of redox-sensitive species acknowledges the possibility of precipitation of these radionuclides under reducing conditions in the SZ, a simplified approach that does not implement the precipitation process is used in the numerical modeling. This is because radionuclide concentrations are not explicitly simulated in the SZ Flow and Transport Abstraction Model and because enhanced sorption is probably the dominant process with regard to radionuclide retardation in reducing zones.

Experimental results and surface complexation modeling indicate that values of sorption coefficients for technetium and neptunium are significantly higher under reducing conditions (BSC 2006 [DIRS 178672], Section 2.3). The conceptual model used in the PMA is that the resulting enhanced sorption for these redox-sensitive radioelements would occur in the tuff matrix of the fractured volcanic units in reducing zones within the SZ. As with all radionuclides, diffusion from the fractures into the rock matrix must occur for the enhanced sorption of technetium and neptunium onto the tuff in the SZ (SNL 2008 [DIRS 183750], Section 6.3). For the purposes of the PMA and associated enhanced sorption of technetium and neptunium, reducing conditions are defined as geochemical conditions in which the Eh is less than approximately 100 mV (BSC 2006 [DIRS 178672], Section 2.3).

Flowing Interval Porosity (Fracture Porosity in Volcanic Units)

The flowing interval porosity is defined as the volume of the pore space through which significant groundwater flow occurs, relative to the total volume. It characterizes the flowing intervals rather than all fractures. Estimates of this parameter were based on theoretical models, pumping tests, and tracer data. For the TSPA-LA model, a cumulative distribution in the range 10^{-5} to $10^{-1}$was used (SNL 2008 [DIRS 183750], Table 6-8). To define the lower bound value,

estimates of fracture porosity of intact cores of volcanic rock were used. More details can be found in *Saturated Zone Flow and Transport Model Abstraction* (SNL 2008 [DIRS 183750], Section 6.5.2.5).

It has been pointed out that the lower bound might be low for bulk average parameter value (i.e., average value over the volcanic zone) that is being applied at the km scale (i.e., the model domain) (SNL 2008 [DIRS 183750], Section 6.5.2.5). A study of the cumulative distribution function plot for parameter flowing interval porosity in the *Saturated Zone Flow and Transport Model Abstraction* (SNL 2008 [DIRS 183750], Figure 6-13) shows that less weight is given to the bottom of the distribution (i.e., low flowing interval porosity) than the rest of the distribution. The 0.5 probability value of 10^{-3} is considered to be representative of the smallest values of fracture porosity estimated from the exploratory studies facility data and field tests (SNL 2008 [DIRS 183750], Section 6.5.2.5). Guimera and Carrera (2000 [DIRS 156830]) analyzed 90 tracer experiments performed in low-permeability fractured rocks The experimental data indicate that most of the porosity data were in the range of 10^{-4} to 10^{-2}, and few points were below porosity of 10^{-4}. The tracer tests represent distances in the range of 2 m to 346 m with an average distance of 41 m. Applying the measured porosity data to km scale would probably result in an even higher lower bound bulk porosity. As a result, using a lower bound porosity value of 10^{-4} would be appropriate for the purpose of this study. Therefore, for the PMA, the lower bound is raised from 10^{-5} to 10^{-4}.

In the TSPA-LA Model, the ground water specific discharge (which is the function of permeability) and flowing interval porosity are uncorrelated variables (SNL 2008 [DIRS 183750], Section 6.5.2). In a fractured flow aquifer, there are theoretical and geometric arguments that suggest the two parameters are at least partially correlated. As fracture density and apertures increase, one would expect both flowing interval porosity and permeability to also increase. An uncorrelated model could generate parameter combinations (large specific discharge and small flowing interval porosity) that are not physically consistent. A correlation factor applicable for Yucca Mountain conditions is considered in PMA for simulation of flow and transport in the SZ.

The relationship between permeability and porosity has been the subject of numerous studies. One of the most widely accepted relationships is the Kozeny-Carman equation that relates permeability to porosity and other characteristics of the porous medium (Bear 1972 [DIRS 156269], p. 166). The Kozeny-Carman equation is a porous medium modification of the cubic law relationship. Experimental data are not currently available for the development of a permeability-porosity correlation for the SZ volcanic and alluvial units; therefore, a literature review was conducted to find experimental data that are applicable to the Yucca Mountain setting. For this study the work of Guimera and Carrera (2000 [DIRS 156830]) that used experimental data performed in low-permeability fractured rocks has been adapted. The Guimera and Carrera study (2000 [DIRS 156830]) used data from 90 tracer experiments to explore correlations among parameters controlling flow and transport. The authors reported that the data from the first arrival time was more applicable to a permeability-porosity relationship. Most of the porosity data were in the range of 10^{-4} to 10^{-2}, and few points were below a porosity of 10^{-4} (Guimera and Carrera 2000 [DIRS 156830], Figure 1). For the PMA study, the literature data compiled by Guimera and Carrera (2000 [DIRS 156830]) was used. The data set was copied into an Excel spreadsheet and Rank Correlation performed. Rank correlation was used

because that is the method used in the TSPA-LA Model. The resulting correlation value was 0.64.

C6.7.2 Model Implementation

Radionuclide Mass Flux from the UZ to the SZ

To simulate matrix diffusion at the UZ and SZ boundary, an SZ submodel has been set up in GoldSim within the TSPA-LA Model. The PMA submodel allows routing of the radionuclide mass release from UZ matrix cells at the water table through an intermediate stage before reaching the SZ Transport Model. This approach does not change the transfer of radionuclide mass release at the water table from UZ fracture cells to the SZ. The PMA submodel simulates radionuclide transport by diffusion in a dual porosity environment. The submodel is represented by an SZ matrix block with total dimensions of 250 m × 250 m × 10 m (thickness) (Figure C6-31). The grid dimensions are the horizontal grid dimensions and the thickness of the first layer below the water table, used in the SZ three-dimensional flow and transport models (SNL 2007 [DIRS 177392], Section 6.3) and are appropriate for use for the purpose of the PMA.

The diffusive length and diffusive area for the model are evaluated as shown in Equations C6.7-5 and C6.7-6. The evaluation is done in the same way as with the SZ matrix diffusion model in the TSPA-LA model (Section 6.3.10).

$$\text{Diffusive length} = \text{FISVO}/2 \qquad \text{(Eq. C6.7-1)}$$

$$\text{Diffusive area} = \text{block length} \times \text{block thickness} \times (\text{block length}/\text{FISVO}) \times 2 \qquad \text{(Eq. C6.7-2)}$$

where FISVO is the flowing interval spacing (SNL 2008 [DIRS 183750], Section 6.5.2.4), and the block dimensions are as shown on Figure C6-31 and Table C4-2. The diffusive length is the distance to the middle of the flowing interval spacing. The diffusive area represents the cross-sectional area for diffusion, which includes two faces. Using a single block to model radionuclide transport by diffusion could introduce numerical dispersion. The alternative is to discretize the block into a number of cells that would diminish numerical dispersion. For this work, a five-cell discretization scheme has been considered. Figure C6-32 shows a conceptual model of the dual-porosity system with the discretization scheme. In the figure it is assumed that FISVO equals the total block length, which is 250 m. The figure shows half of the block length on either side of the fracture. The horizontal arrows show the direction of SZ matrix diffusion. Figure C6-33 shows the discretized system representation with five matrix cells as implemented in TSPA. In this model, the mass flux from the UZ is divided by five and applied to each SZ matrix cell. The total mass flux passes through the last cell to the SZ. The water volume and the matrix volume of each cell have also been divided by five. Since the five cells are in series, the diffusive length is divided by 5, while the diffusive area is the same for all the discretized cells. The output of the new scheme is simultaneously directed to the SZ convolution integral (three-dimensional) and the SZ one-dimensional transport system. The model has been applied to the four SZ regions.

Additional changes have also been made in other parts of the SZ transport section and the UZ transport section of the TSPA Model to allow flow of information between the new model and other sections of the TSPA Model.

Colloid Transport of Irreversibly Sorbed Radionuclides

The implementation of the colloid diversity model for the SZ is summarized below. The first four steps were followed for both the SZ three-dimensional and one-dimensional transport models.

1. For a given realization, determine the median SZ travel time, τ, using the mass breakthrough curves for the fast fraction of irreversible colloids. τ is an average of the median travel times of the four SZ regions and is given in hours.

2. Use τ as the total travel time through the SZ.

3. Randomly sample a triangular distribution defined by [0.17, 0.51, and 0.85] and use the resulting value as the slope m in Equation C6.7-1 to define a CDF for the colloid filtration rate constants. Use a value of b = 0.2 for all realizations.

4. Randomly sample a triangular distribution defined by [$\log_{10}(0.01/\tau)$, $\log_{10}(0.1/\tau)$, and $\log_{10}(1/\tau)$], and use 10 raised to the resulting value as the colloid detachment rate constant.

5. In the next step, the one-dimensional transport model is discussed. For the one-dimensional model, first calculate the probability *P* using the following procedure:

    a. Get the minimum probability value that corresponds to the minimum retardation factor, which is selected for this study to be equal to 2:

$$P_{\min} = 10^{b}\left[(R_l - 1)k_{\det}\right]^{m} = 10^{b}\, k_{\det}^{m} \qquad \text{(Eq. C6.7-3)}$$

where

P_{min} = minimum probability value

R_l = lower bound retardation factor = 2

    b. Divide the probability space into ten equal parts:

$$P_{diff} = (1.0 - P_{\min})/10 \qquad \text{(Eq. C6.7-4)}$$

where

P_{diff} = is the interval between two probability points, to get 10 equal parts

    c. Get 10 uncertainty uniform distributions with bin size as shown below. First the probability space is divided into ten bins (intervals). The range of each bin is as given below. Once the bins are defined the next step is to make a uniform distribution for each bin with

        i. $P_{\min}$ to $P_{\min} + P_{diff}$

ii. $P_{\min} + P_{diff}$ to $P_{\min} + 2P_{diff}$

iii. $P_{\min} + 2P_{diff}$ to $P_{\min} + 3P_{diff}$

iv. $P_{\min} + 3P_{diff}$ to $P_{\min} + 4P_{diff}$

v. $P_{\min} + 4P_{diff}$ to $P_{\min} + 5P_{diff}$

vi. $P_{\min} + 5P_{diff}$ to $P_{\min} + 6P_{diff}$

vii. $P_{\min} + 6P_{diff}$ to $P_{\min} + 7P_{diff}$

viii. $P_{\min} + 7P_{diff}$ to $P_{\min} + 8P_{diff}$

ix. $P_{\min} + 8P_{diff}$ to $P_{\min} + 9P_{diff}$

x. $P_{\min} + 9P_{diff}$ to $P_{\min} + 10P_{diff}$.

6. Retardation factors R_{f1} to R_{f10}: For each bin, randomly sample across the probability range assuming a uniform distribution between the lower and upper probability limits of the bin. Once the detachment rate constant (Step 4 above) and the sampled probabilities for each bin are evaluated, the retardation factor for each bin is calculated using Equation C6.7-4.

7. For the one-dimensional SZ transport model, use 10 one-dimensional pipe sets with retardation factors calculated using Step 6. Note that a pipe set for the 1-D SZ Model is as defined in the Conceptual Description. The mass flux is divided equally to the 10 pipe sets. The calculated 10 retardation factors, which are realization dependent, replace the TSPA-LA parameters CORVO and CORAL (SNL 2008 [DIRS 183750], Section 6.5.2.11). The parameters CORVO and CORAL are the single colloid retardation factors in the volcanic units and alluvium defined in *Saturated Zone Flow and Transport Model Abstraction* (SNL 2008 [DIRS 183750], Section 6.5.2.11). For the PMA, no distinction is made between the volcanic units and alluvium values of colloid retardation for irreversibly sorbed radionuclides.

8. For the three-dimensional SZ Flow and Transport Model, use the detachment rate constant, slope m, y-intercept b, and minimum and maximum retardation factor values to implement the CDM. As with the one-dimensional model, the minimum retardation factor is 2.0. The maximum retardation factor is derived using Equations C6.7-1 and C6.7-3 in conjunction with the maximum probability value of 1.0. For the three-dimensional model, the CDM is implemented in the particle tracking 'sptr' module of the code FEHM V. 2.25 (STN: 10086-2.25-00 [DIRS 182477]). Each simulation is conducted using a user-defined number of particles (500 in this case). FEHM generates 500 retardations (one for each particle) using the minimum and maximum retardations as two of the retardation coefficient values. The remaining 498 retardation values are derived by dividing the range of the retardation into 499 equal intervals ($LogR_{Interval}$) in log space, where

$$\log R_{Interval} = \log 10(R_{\max} / R_{\min}) / 499. \qquad \text{(Eq. C6.7-5)}$$

The retardation values are then found by taking the antilogs of these values. Except for the particles assigned the minimum and maximum retardation, the value of each particle is

then weighted based upon the difference between probabilities ($P_{i-1/2}$ and $P_{i+1/2}$) of retardation (from Equations C6.7-1 and C6.7-3) representing the midpoints (in log space) between a selected retardation (R_i) and the retardation an the interval below it (R_{i-1}) and the retardation an interval above (R_{i+1}) where i = 2 - 499. The weighting factor Wi can be defined as:

$$W_i = (P_{i+1/2} - P_{i-1/2}) . \quad \text{(Eq. C6.7-6)}$$

The weighting factors for the minimum retardation and the maximum retardation are in turn defined as follows:

$$W_1 = (P_{1+1/2} - P_1) \quad \text{(Eq. C6.7-7)}$$

and

$$W_{500} = (P_{500} - P_{500-1/2}) . \quad \text{(Eq. C6.7-8)}$$

The normalized weighting factors, w_i, used in the model are then defined as

$$w_i = \frac{500 W_i}{\sum_{j=1,500} W_j} . \quad \text{(Eq. C6.7-9)}$$

Redox Conditions and Impacts on Radionuclide Transport

The PMA for the effects of potential reducing conditions on the transport of redox-sensitive species is implemented in the PMA by modifying the SZ Flow and Transport Abstraction Model and the SZ one-dimensional transport model to incorporate these effects. A zone of uncertain dimensions is defined in the three-dimensional SZ flow and transport abstraction model to represent the location of reducing conditions. A separate value for the sorption coefficients in the volcanic matrix is assigned within this zone, relative to the values assigned to the volcanic units and alluvium under oxidizing conditions. The SZ one-dimensional transport model is modified by subdividing the GoldSim pipe elements such that separate pipe segments exist for oxidizing and reducing conditions. The length of the pipe segment with reducing conditions is assigned to approximate the flow path length through the reducing zone in the three-dimensional SZ Flow and Transport Abstraction Model for each realization.

Uncertainty in radionuclide transport related to potential reducing conditions in the SZ is incorporated into the PMA by defining uncertainty distributions for key parameters and sampling from these uncertainty distributions in the Monte Carlo realizations. These uncertainty distributions are summarized in Table C6-9.

The potential reducing zone in the SZ is approximated by a rectangular area that includes several wells in which reducing conditions have been inferred from groundwater samples. This zone is elongated in the north-south direction and encompasses Wells b#1, H-4, WT-17, and WT-12, as shown on Figure C6-30. The potential zone extends over the elevation from 200 m to ~730 m (where the water table is located) in that area. The eastern boundary of the reducing zone varies

from a maximum of 550,000 m to a minimum of 548,200 m (in Universal Transverse Mercator [UTM] coordinates), corresponding to a maximum width of 2,800 m and a minimum width of 0 m. The southern boundary of the reducing zone varies from a minimum of 4,069,200 m to a maximum of 4,073,300 m UTM, and the northern boundary varies from 4,077,300 m to 4,080,000 m. These ranges of geographical uncertainty in the boundaries of the reducing zone include the potential for misinterpretation of redox conditions in one to all of the wells used to infer the location of the reducing zone. The implementation of the SZ reducing zone in the PMA utilizes the synthesis and conclusions of *Impacts of Solubility and Other Geochemical Processes on Radionuclide Retardation in the Natural System – Rev 01* (BSC 2006 [DIRS 178672]) as direct input but also incorporates a potentially large degree of uncertainty in those conclusions. The unitless uncertain parameters for the boundaries of the reducing zone given in Table C6-9 are used as multiplying factors to the ranges given above in meters in defining the boundaries of the reducing zone for each realization.

The elements technetium and neptunium can exist in several oxidation states in groundwaters depending on the redox potential (Eh) of the groundwater, and their mobility highly depends on their oxidation states. Under oxidizing conditions, technetium exists primarily in the +7 oxidation state while neptunium exists primarily in the +6 oxidation state. Under sufficiently reducing conditions (Eh = < 100 mv) in near-neutral groundwaters (pH = 7.0 +/-2), both technetium and neptunium exist primarily in the +4 oxidation state. Although sorption experiments under reducing conditions have not been carried out for these two elements using samples from Yucca Mountain, sorption coefficients for these elements under reducing conditions have been reported in the literature. Lieser and Bauscher (1988 [DIRS 172722]) have reported on sorption coefficients for technetium under reducing conditions, and Lieser and Muhlenweg (1988 [DIRS 106684]) reported on sorption coefficients for neptunium under reducing conditions. These estimates of the sorption coefficients were obtained using sediment samples from the Gorleben site in Germany. The sediments were composed mainly of quartz with lesser amounts of other minerals including orthoclase, plagioclase, kaolinite, muscovite, calcite, chlorite, and dolomite. This mineralogy is not unlike the mineralogy of many of the tuffs at Yucca Mountain (BSC 2006 [DIRS 178672], Section 2.3.2). The surface areas of the Gorleben samples ranged from 0.011 to 0.025 m^2/g. Although several different groundwater compositions were used in the experiments including two with chemistry similar to groundwaters at Yucca Mountain, the sorption coefficients obtained for technetium and neptunium under reducing conditions did not show much sensitivity to groundwater composition. The sorption coefficients obtained by Lieser and Bauscher (1988 [DIRS 172722]) for technetium under reducing conditions averaged about 1,000 +/- 200 mL/g. For neptunium, Lieser and Muhlenweg (1988 [DIRS 106684]) obtained sorption coefficients ranging from 1,060 to 1,600 mL/g.

The uncertainty distributions for the sorption coefficients of technetium and neptunium under reducing conditions (Table C6-9) are based primarily on the experimental results of Lieser and Bauscher (1987 [DIRS 172722]) and Lieser and Muhlenweg (1988 [DIRS 106684]), respectively. These results show that the average value of the sorption coefficient under reducing conditions is about 1,000 mL/g for both technetium and neptunium. The uncertainty distributions are inclusive of the Lieser and Bauscher (1987 [DIRS 172722]) and Lieser and Muhlenweg (1988 [DIRS 106684]) values of sorption coefficients measured under reducing conditions. The values of sorption coefficients from these uncertainty distributions are likely underestimates because the tuffs and sediments at Yucca Mountain have surface areas 100-1,000

times larger than the surface areas of the Gorleben sediments (SNL 2007 [DIRS 177392], Appendix A). In addition, surface complexation modeling for neptunium sorption on quartz, as a function of Eh, quantitatively confirmed the high values of the sorption coefficient from the experimental sources (BSC 2006 [DIRS 178672], Section 2.3.2).

The SZ Flow and Transport Abstraction Model for the TSPA-LA model (DTN: SN0702PASZFTMA.001_R0 [DIRS 179504]) formed the basis for the model developed for the SZ PMA. Parameter values for the SZ Flow and Transport Abstraction Model were resampled, including the additional parameters related to the impacts of the reducing zone listed in Table C6-9. The resampled parameters for the reducing zones model, are included in the file SZ_Sampled_Vectors_PMA.txt in corroborative DTN: SN0704PMASZFTA.001_R1 [DIRS 184395]. The main input files to the FEHM software code used in the SZ Flow and Transport Abstraction Model were modified to include a zonal definition for the reducing zone to describe the coordinates. The input files controlling radionuclide transport in the FEHM code for technetium and neptunium were modified to assign the value of the sorption coefficients under reducing conditions to all volcanic hydrogeologic units within the reducing zone. A complete set of simulated radionuclide breakthrough curves was generated by the SZ Flow and Transport Abstraction Model for technetium and neptunium, as in the case for the TSPA-LA model runs (SNL 2008 [DIRS 183750], Section 6.6).

The structure of the SZ one-dimensional transport model was modified to insert additional pipe segments to represent the reducing zone within the volcanic units. Figure C6-34 shows the unmodified GoldSim structure used for the TSPA-LA model. The SZ three-dimensional model uses an external software (SZ_Convolute [DIRS 181060]) to calculate flow and transport through the SZ. The element *SZ_External* is a call to SZ_Convolute [DIRS 181060], which simulates the breakthrough of radionuclides 18 km away from the repository. The mass flux returned from SZ_Convolute [DIRS 181060] for each source region is then fed to cell *SZOUT*. A small volume and large flow rates (inflow and outflow) are assigned to *SZOUT,* which ensures that all mass entering *SZOUT* is flushed into cell *Sink* at every timestep. The one-dimensional transport model represents a network of four pathways, one for each source region. Each pathway consists of three GoldSim pipe segments. The first two pipes in each of the four pathways represent two distinct volcanic sections of the SZ and the third pipe simulates flow and transport through the saturated zone. The mass fluxes exiting the last pipe of each of the four one-dimensional model pathways are collected in element *Sink*. The *Sink* cell represents an unlimited volume into which all radionuclide mass exiting the two flow and transport models can flow without constraints. The total mass flux exiting the SZ from the one-dimensional model is calculated as a sum of the four mass fluxes exiting the last pipes.

Since the reducing zone path length could extend from Pipe_ax to parts of Pipe_bx on Figure C6-34, where x represents the source regions, the PMA divides both Pipe_ax and Pipe_bx into two parts, as shown on Figure C6-35, to accommodate variable path length of reducing zones. The resampled parameter values used in the SZ Flow and Transport Abstraction Model are also applied to the modified SZ one-dimensional transport model for consistency. The resulting modified version of the SZ one-dimensional transport model is inserted into the GoldSim model for PMA. The tabulated data representing the reducing zone path length for the one-dimensional transport model is given in the EXCEL spreadsheet

RZ_1-D_Average_Length.xls in corroborative DTN: SN0704PMASZFTA.001_R1 [DIRS 184395].

Flowing Interval Porosity (Fracture Porosity in Volcanic Units)

Based on the discussion above, the cumulative distribution (log_{10}-transformed) of the flowing interval porosity was revised and given in Table C6-10. This new distribution was used in the generation of the SZ breakthrough curves that feed TSPA and was also used for the SZ one-dimensional transport model. The correlation factor of 0.64 between the parameters flowing interval porosity and groundwater specific discharge multiplier was used during parameter sampling (corroborative DTN: SN0704PMASZFTA.001_R1 [DIRS 184395]).

C6.8 SEISMIC SCENARIO CLASS

The Seismic Scenario Class describes future performance of the repository system in the event of seismic activity that could disrupt the repository system (Section 6.6). The Seismic Scenario Class represents the direct effect of vibratory ground motion and fault displacement associated with seismic activity. The Seismic Scenario Class considers the effects of the seismic hazards on DSs and WPs because damage to or failure of these components has the potential to initiate or increase releases of radionuclides by forming new diffusive or advective transport pathways. The Seismic Scenario Class estimates the mean annual dose due to seismic activity by accounting for the probability of occurrence of activity expressed in terms of its mean annual exceedance frequency. The estimate of mean annual dose takes into account the relevant processes that affect system performance.

C6.8.1 Conceptual Model

Seismic Crack Area Density for Alloy 22

The seismic crack density model of the WP estimates the crack opening area on a WP damaged by a seismic event. The cracks within the damaged area are assumed to be caused as a result of stresses induced by a seismic event. The areas of the WP outer barrier that exceed the residual tensile stress threshold are considered damaged area (Section 6.6). The damaged or deformed area that exceeds a residual stress threshold is conceptualized to result in a tightly spaced network of stress corrosion cracks (SNL 2007 [DIRS 176828], Sections 6.1.4). In order to assess the potential for radionuclide release through these cracks, it is necessary to assess the possible number of cracks in the damaged area and the opening areas of these cracks.

The TSPA-LA Model samples a uniform distribution from 3.27×10^{-3} to 1.31×10^{-2} for the crack area density for WP seismic damage area. This distribution includes an upper bound allowing for uncertainties, such as the potential for crack overlap and deviations from a regular array of identically shaped cracks, to be appropriately accounted for (SNL 2007 [DIRS 181953], Section 6.7.3.3). This crack density model, used in the seismic damage analyses, includes the use of lower yield strength values for Alloy 22 (Haynes International 1988 [DIRS 101995], p. 15) leading to greater calculated damaged area. The yield strength is considered conservative because the process of crack initiation and through-wall crack propagation will result in significant reduction in the residual stress (SNL 2007 [DIRS 181953], Section 6.7.3.3). The yield strength of the material should be used as a reasonable estimate for the stress component in

the crack area density calculation (SNL 2007 [DIRS 181953], Section 6.7.3.3). The crack length used in the calculation of the lower bound allows for cracks, if they lie in the same plane, to just touch without overlapping (SNL 2007 [DIRS 181953], Section 6.7.3.1). The upper bound considers a crack length that allows for significant overlap (SNL 2007 [DIRS 181953], Section 6.7.3.2). For both the upper and lower bounds, the room temperature range of crack area density was used in the TSPA-LA as this choice yields higher crack area densities (SNL 2007 [DIRS 181953], Section 6.7.3.3). Additionally, because the hexagonal array used in the crack area density model for TSPA-LA represents a high effective density (close spacing) of individual cracks, this hexagonal geometry, with crack center spacings set at the plate thickness is considered a conservative representation (SNL 2007 [DIRS 181953], Section 6.7.2).

An alternative model for the crack area density considers a damaged area with a circular geometry circumscribed by a single through-wall crack and yields crack area density at a room temperature of 7.22×10^{-3} (SNL 2007 [DIRS 181953], Section 6.7.4). This is considered a limiting realistic case (SNL 2007 [DIRS 181953], Section 6.7.2). For the PMA, the crack area density was changed to a constant value equal to the lower bound used in the TSPA-LA Model, 3.27×10^{-3}. This lower bound more closely resembles the ACM results.

C6.8.2 Model Implementation

Seismic Crack Area Density for Alloy 22

The implementation of the crack area density affects only the Seismic GM Modeling Cases. The seismic crack area density model of the WP estimates the crack opening area on a WP damaged by a seismic event. In the *Epistemic_Params* container, the selector element, *WP_Crack_Area_Density*, was added to select between the TSPA-LA Model value (a uniform distribution from 3.27×10^{-3} to 1.31×10^{-2}) represented by the stochastic parameter, *WP_Crack_Area_Density_a*, and a constant value of 3.27×10^{-3}, used for the PMA included in the data element *WP_Crack_Area_Density_PMA*. The crack area density parameter only affects diffusive releases from WPs damaged during a Seismic GM Modeling Case. These parameters feed the Seismic Damage Abstraction calculations (Section 6.6).

C.7 RESULTS

Detailed probabilistic projections developed for the PMA are presented and explained in the subsequent sections. The *mean value* of the projected PMA annual doses to the RMEI is used as the primary metric for comparison with the TSPA-LA Model. The mean annual dose is quantified using four scenario classes: Nominal, Early Failure, Seismic, and Igneous. Detailed descriptions of the technical basis of these scenario classes and their associated modeling cases are presented in Sections 6.3 through 6.6 of Volume I of this report. In addition, a detailed discussion of the TSPA-LA Model dose is documented in Section 8.0 of this report.

The projection of total mean annual dose for the Individual Protection Standard is based on summing the expected annual doses over seven modeling cases: (1) Nominal, (2) Drip Shield EF, (3) Waste Package EF, (4) Seismic GM, (5) Seismic FD, (6) Igneous Intrusion, and (7) Volcanic Eruption. As required by the disposal standards, the postclosure performance is quantified for time periods of 10,000 years and 1,000,000 years after closure. Drawing from the evaluation

presented in Section 8.2, the PMA is exercised over modeling cases that are anticipated to have significant contributions to annual dose over the specified regulatory time periods. As discussed in Section C6.1, the performance margin of the TSPA-LA model can be largely quantified with results from the Seismic GM and Igneous Intrusion modeling cases since these two cases dominate the projected mean annual doses to the RMEI for time periods after a few hundred years (Sections 8.1 and 8.2). The results of this scenario class and modeling case screening for the performance margin analysis are summarized below:

- Nominal Modeling Case *included* (included in the Seismic GM Modeling Case)
- Drip Shield EF Modeling Case *included*
- Waste Package EF Modeling Case *included*
- Seismic GM Modeling Case *included*
- Seismic FD Modeling Case *included*
- Igneous Intrusion Modeling Case *included*
- Volcanic Eruption Modeling Case *excluded.*

The Seismic GM Modeling Case includes the effects of the nominal processes when run for 1,000,000 years after closure.

C7.1 PERFORMANCE MARGIN IN TOTAL ANNUAL DOSE PREDICTIONS

As described in Section 6.1.2 (Volume I), probabilistic projections of the expected (in the statistical sense) total annual dose to the RMEI are computed as a combination of the calculated expected annual doses for each of the four scenario classes; the expectation is taken over all aleatory (i.e., randomly occurring in time) uncertainties.

The main result of the simulation process is a plot of a set of expected annual dose histories. On each plot, dose curves for the mean, median, 5th and 95th percentiles are superimposed. The mean annual dose history was computed by taking the *arithmetic average* of the 300 expected annual dose values for individual time planes along the curves. Similarly, the *median* dose history was constructed from points obtained by sorting the 300 expected values from lowest to highest, and then averaging the two middle values. Curves for the 5th and 95th percentiles are also plotted to illustrate the spread in the expected annual dose histories; 90 percent (or 270 of the 300 epistemic realizations) of the projected dose histories fall between these two percentile curves. The plots obtained from the PMA are shown on Figure C7-1 for 10,000 years and on Figure C7-2 for 1,000,000 years.

The largest *mean* annual dose to the RMEI is estimated by the PMA to be about 0.02 mrem for the 10,000-year disposal period. Similarly, the largest *mean* annual doses to the RMEI after 10,000 years but within the period of geologic stability is estimated by the PMA to be about 1.0 mrem. To provide importance of the epistemic uncertainty of the performance projections, the annual dose histories corresponding to the 5th- and 95th- percentiles are also shown in the plots.

Important performance margin insights can be gained by comparison of the mean annual dose curves between the PMA and the TSPA-LA, which are shown on Figure C7-3 for 10,000 years

and on Figure C7-4 for 1,000,000 years. From those dose curves, the following general observations can be drawn about the PMA:

- The PMA mean annual doses are generally nearly an order of magnitude lower than the mean annual dose from the TSPA-LA Model over the first 250,000 years.

- The largest PMA mean annual doses calculated over 10,000 years are an order of magnitude lower than the largest mean annual dose from the TSPA-LA Model.

- The largest PMA mean annual doses calculated over 1,000,000 years are lower by a factor of two than the largest mean annual dose from the TSPA-LA Model.

As shown on Figures C.7-5(b) and C.7-6(b), the major contributors to the mean annual dose in the PMA ranked from highest to lowest, are: ^{99}Tc, ^{129}I, ^{14}C, ^{237}Np, ^{239}Pu, ^{240}Pu, and ^{234}U for the first 10,000 years and ^{226}Ra, ^{242}Pu, ^{237}Np, ^{129}I, ^{233}U, ^{135}Cs, ^{99}Tc, ^{229}Th, and ^{230}Th for the time period of 1,000,000 years. These radionuclides typically have a combination of unique characteristics such as: (1) large initial inventories in the nuclear waste, (2) moderate to high solubililities, (3) relatively long half-lives (e.g., $\geq 10^5$ years), and (4) low to non-sorbing properties. The dominant radionuclides identified in the PMA are similar to those found in the TSPA-LA Model (Figures C.7-5(a) and C.7-6(a)), indicating that the modifications made for the PMA do not alter the fundamental behavior of the repository system and thus add additional confidence in the TSPA-LA Model results. The lower annual doses estimated by the PMA, however, confirm that the conservatisms identified in Table C5-1 have potentially significant impacts on the repository performance. The PMA also confirms that, when propagated through the TSPA-LA Model, the conservatisms addressed in this analysis are conservative with respect to the total system performance measures (e.g., peak mean annual dose).

Additional insights into the performance margin can be gained by disaggregating the total annual doses into the mean annual dose curves for individual modeling cases, which are shown on Figure C7-7 for 10,000 years after closure and on Figure C7-8 for 1,000,000 years after closure. From those dose curves, the following general observations can be made about the projected postclosure performance for the PMA:

- The Igneous Intrusion Modeling Case is the dominant contributor to the calculated mean annual dose for both 10,000 years and 1,000,000 years.

- Mean annual doses for the Drip Shield EF, Seismic FD, and Volcanic Eruption Modeling Cases are relatively small and are estimated to be on the order of 10^{-4} mrem or less for both 10,000 years and 1,000,000 years after closure.

- Mean annual dose projected for the Waste Package EF Modeling Case is on the order of 10^{-3} mrem or less and is the second largest contributor to the calculated total mean annual dose until 10,000 years after closure.

- Mean annual dose projected for the Seismic GM Modeling Case is on the order of 10^{-1} mrem or less and is the second largest contributor to the calculated total mean annual dose for 1,000,000 years after closure.

In the TSPA-LA Model, the Seismic GM Modeling Case dominates the mean annual dose for the 10,000-year time period; whereas for 1,000,000 years, the Seismic GM and Igneous Intrusion Modeling Cases contribute equally to the total mean annual dose to the RMEI (Section 8.1.1.2). The PMA, however, shows that the Igneous Intrusion Modeling Case dominates the mean annual dose for the 10,000-year time period; whereas for 1,000,000 years, the Seismic GM and Igneous Intrusion Modeling Cases start to dominate after 200,000 years. The remaining cases combined have a negligible contribution.

Although the Igneous Intrusion Modeling Case dominates the calculated annual dose in the PMA, it is important to note, for the purpose of risk insights, that the mean annual frequency for a dike to intersect the repository is estimated to be 1.7×10^{-8} per year (Section 8.1.1.3). This frequency is only slightly greater than the NRC frequency threshold (10^{-8}) for unlikely FEPS that can be omitted by regulation.

C7.2 PERFORMANCE MARGIN ANALYSIS—MODELING CASE RESULTS

It is necessary to disaggregate the PMA results by modeling case to quantify the extent to which the conservatisms, individually and collectively, affect the projected annual dose, relative to the TSPA-LA Model projections presented in Section 8.1. In this section, the PMA results are examined for each individual modeling case in comparison with the TSPA-LA results.

Drip Shield EF Modeling Case—In this modeling case, the defective drip shields are assumed to fail at the time of repository closure (Section 6.4.1, Volume I). WPs under an early-failed DS are assumed to experience localized corrosion as soon as seepage contacts the WP, since the area of the Alloy 22 WP outer barrier that is contacted by seepage is potentially subject to localized corrosion (Section 6.4, Volume I). The mean annual dose histories calculated in the PMA are presented on Figures C7-7(a) and C7-8(a), together with those obtained in the TSPA-LA calculations. It can be clearly seen in the figures that the TSPA-LA Model predicts a higher mean annual dose than the PMA by more than one order of magnitude over both 10,000-year and 1,000,000-year time frames. The radionuclides that contribute most to the PMA Drip Shield EF Modeling Case mean annual dose are shown on Figures C7-9(a) and C7-10(a). In the first 10,000 years after repository closure, soluble radionuclides ^{99}Tc, ^{14}C, and ^{129}I are the primary contributors to the Drip Shield EF Modeling Case mean annual dose; while over the 1,000,000-year time period, the mean annual dose is dominated by ^{242}Pu, ^{129}I, ^{126}Sn, ^{237}Np, ^{135}Cs, and ^{233}U. Compared to the TSPA-LA Model, Figures C7-11(a) and C7-12(a), the total dose contributions from soluble radionuclides, are reduced in the PMA results for the Drip Shield EF Modeling Case by more than one order of magnitude for the first 10,000 years, while the contributions from solubility-controlled radionuclides, such as plutonium, neptunium, and uranium, are reduced by about two orders of magnitude. In the TSPA-LA Drip Shield EF Modeling Case, the entire area of the Alloy 22 WP outer barrier that is contacted by seepage is assumed to be failed since it is potentially subject to localized corrosion (Section 6.4, Volume I). In the PMA, the localized corrosion failure area is uncertain and generally much smaller than the entire WP surface area (Section C6.3). In addition, unfailed (not perforated) CSNF cladding is assumed to remain intact for the 10,000-year regulatory period in the absence of mechanical damage mechanisms from seismic ground motion and/or rockfall (Section C.6.5). The lower dose results in the PMA are primarily controlled by these changes.

Waste Package EF Modeling Case—In the Waste Package EF Modeling Case, an early-failed WP is considered breached at the beginning of the simulation, and its entire surface area is considered degraded (Section 6.4.2, Volume I). General corrosion of the DSs due to nominal corrosion processes (Section 6.3.5.1.2) is included in the Waste Package EF Modeling Case. The mean annual dose histories calculated in the PMA are presented on Figures C7-7(b) and C7-8(b), together with those obtained in the TSPA-LA calculations. The figures indicate that the TSPA-LA Model slightly exceeds the mean dose as compared to the PMA over the first 9,000 years, after which the TSPA-LA model exceeds the PMA predicted dose by one order of magnitude. The radionuclides that contribute most to the PMA Waste Package EF Modeling Case mean annual dose are shown on Figures C7-9(b) and C7-10(b). In the first 10,000 years after repository closure, soluble radionuclides ^{99}Tc, ^{14}C, and ^{129}I are the primary contributors to the Waste Package EF Modeling Case mean annual dose; while over the 1,000,000-year time period, the mean annual dose is dominated by ^{242}Pu, ^{129}I, ^{99}Tc, ^{237}Np, ^{135}Cs, and ^{239}Pu. Compared to the TSPA-LA Model Figures C7-11(b) and C7-12(b), the total dose contributions from soluble radionuclides are slightly reduced in the PMA results for the Waste Package EF Modeling Case over the first 9,000 years; while the contributions from solubility-controlled radionuclides, such as plutonium, neptunium, and uranium, are reduced by one to two orders of magnitude over most of the 1,000,000-year time period. In the Waste Package EF Modeling Case, releases from the waste packages by diffusion control the dose results as diffusive transport of dissolved radionuclides through the WP using the entire surface area is sufficiently high that there are minimal differences between the PMA and TSPA-LA mean annual dose results over the first 9,000 years. In the PMA unfailed (not perforated) CSNF, cladding is assumed to remain intact for the 10,000-year regulatory period (Section C.6.5), which explains the sudden increase in the dose in the TSPA-LA when the CSNF WP begins to release radionuclides; whereas there is no corresponding increase in the PMA results at approximately 9,000 years. The lower dose results in the PMA over the 1,000,000-year time period are primarily controlled by a cumulative effect from reductions in the saturation used to calculate the diffusive releases and a reduction in the WF degradation rates (Section C7.3).

Seismic GM Modeling Case—This modeling case represents DSs and WPs that fail from mechanical damage associated with seismic vibratory ground motion (Section 6.6, Volume I). Depending on the timing, sequence, and intensity of the ground motion events, the DSs and WPs can accumulate damage and/or cause a failure. In the case of the DSs, seismic ground motions could cause damage or failure by: (1) buckling and rupture, (2) exceeding residual stress threshold, and (3) deformation or rupture by large block rockfall. Similarly, the WPs could be damaged or fail by: (1) local strain that exceeds ultimate tensile strength, (2) deformations creating residual stresses that induce SCC, and (3) lithostatic loading from rubble that causes a rupture of the outer barrier by WP internals. Both the DSs and WPs are also degraded by the nominal corrosion processes (e.g., general corrosion and localized corrosion). The total mean annual dose history for the Seismic GM Modeling Case calculated in the PMA is presented on Figures C7-7(c) and C7-8(c), together with those obtained in the TSPA-LA calculations. Comparison of the total mean annual dose curves shown in the figure indicate that the TSPA-LA Model results exceed the PMA mean annual dose by three orders of magnitude over the first 10,000 years. The difference between the PMA and the TSPA-LA model dose results decreases over the time period from 10,000 years to 700,000 years after repository closure. The radionuclides that contribute most to the PMA Seismic GM Modeling Case mean annual dose are shown on Figures C7-9(c) and C7-10(c). In the first 10,000 years after repository closure,

soluble radionuclides ^{14}C, ^{99}Tc, and ^{129}I are the primary contributors to the PMA Seismic GM Modeling Case mean annual dose; while over the 1,000,000-year time period, the mean annual dose is dominated by ^{129}I, ^{99}Tc, ^{79}Se, ^{135}Cs, ^{36}Cl, ^{242}Pu, and ^{237}Np. Compared to the TSPA-LA Model Figures C7-11(c) and C7-12(c), the total mean annual dose contributions from soluble radionuclides are reduced in the PMA results by three orders of magnitude over the first 10,000 years, while the contributions from solubility-controlled radionuclides, such as plutonium, neptunium, and uranium, are reduced by a factor of one to two orders of magnitude over most of the 1,000,000-year time period. The CDSP WPs are the primary container damaged during the 10,000-year period in both the PMA and the TSPA-LA modeling cases. The CSNF WPs are much more resistant to seismic damage than the CDSP WPs (Section 6.6, Volume I). The predominate mechanism causing damage to the CDSP and CSNF WPs in the TSPA-LA Seismic GM Modeling Case consisted of small cracks (SCC) when the residual stress threshold on the WP outer barrier was exceeded (Section 8.2.4.1). In the PMA, the residual stress threshold necessary for SCC is higher than the TSPA-LA (Section C6.8), as well as a reduction in the SCC density on damaged WPs (Section C6.8). The lower dose results in the PMA are primarily controlled by these changes.

Seismic FD Modeling Case—This modeling case includes disruption of the WPs and DSs by the displacement of faults. As described in Section 6.6.1 (Volume I), the characterization of the fault is based on data from known faults in the vicinity of the site area. The disruption in this modeling case is conceptualized as a sudden discontinuity in the profile of the repository. The location and magnitude of the fault displacement determines the number of DSs and WPs that are disrupted. The total mean annual dose history for the Seismic FD Modeling Case calculated in the PMA is presented on Figures C7-7(d) and C7-8(d), together with those obtained in the TSPA-LA calculations. Comparison of the total mean annual dose curves shown on the figures indicate that the TSPA-LA Model results exceed the PMA mean annual dose by one to two orders of magnitude over both the first 10,000 years and the first 1,000,000 years after repository closure. The radionuclides that contribute most to the PMA Seismic FD Modeling Case total mean annual dose are shown on Figures C7-9(d) and C7-10(d). In the first 10,000 years after repository closure, soluble radionuclides ^{14}C, ^{99}Tc, and ^{129}I are the primary contributors to the PMA Seismic FD Modeling Case mean annual dose; while over the 1,000,000-year time period, the mean annual dose is dominated by ^{129}I, ^{99}Tc, ^{242}Pu, ^{79}Se, ^{239}Pu, ^{237}Np, and ^{135}Cs. Compared to the TSPA-LA Model Figures C7-11(d) and C7-12(d), the total mean annual dose contributions from soluble radionuclides are reduced in the PMA by about a factor of 10 for the first 10,000 years, while the contributions from solubility-controlled radionuclides, such as plutonium, neptunium, and uranium, are reduced by a factor of one to two orders of magnitude over the most part of the 1,000,000-year time period. The Seismic FD Modeling Case includes the destruction of both the WP and DS (Section 6.6, Volume I). The radionuclide releases in both the TSPA-LA and PMA are controlled by the advective releases from the EBS. The PMA is primarily driven by a reduced seepage flux to WP based on a smaller hydrologic cross section used for the representation of collapsed drift geometry (Section C.6.2) and the result of the PMA predicting much lower advective water flux percolating through breached WPs (Section C.6.4). A discussion of these affects in Section C.7.3 follows.

Igneous Intrusion Modeling Case—As described in Section 6.5.1 (Volume I) in this modeling case, a simulated magmatic dike intersects the footprint of the repository causing failure of the EBS. Radionuclide releases attributed to the intrusion and transport away from the repository

are analyzed in a manner analogous to that for the Nominal Modeling Case but differ in the conceptualization of the EBS failure. The modeling case assumes that all the WPs in the repository are completely destroyed, exposing the waste forms to percolating groundwater with subsequent degradation, radionuclide mobilization, and transport. The total mean annual dose history for the Igneous Intrusion Modeling Case calculated in the PMA is presented in Figures C7-7(e) and C7-8(e), together with those obtained in the TSPA-LA calculations. Comparison of the total mean annual dose curves shown on the figures indicates that the TSPA-LA Model results systematically exceed the PMA mean annual dose by a factor of two to a factor of ten for both the first 10,000 years and the first 1,000,000 years after repository closure. The radionuclides that contribute most to the PMA Igneous Intrusion Modeling Case total mean annual dose results are shown on Figures C7-9(e) and C7-10(e). In the first 10,000 years after repository closure, soluble radionuclides ^{99}Tc, ^{129}I, and ^{14}C are the primary contributors to the PMA Igneous Intrusion Modeling Case mean annual dose; while over the 1,000,000-year time period, the mean annual dose is dominated by ^{226}Ra, ^{242}Pu, ^{237}Np, ^{233}U, and ^{239}Pu. The domination of ^{226}Ra is due to the fact that in the Igneous Intrusion Modeling Case all WPs will be damaged and subjected to large percolating water fluxes, resulting in quick depletion of soluble radionuclides ^{99}Tc, ^{129}I, and ^{14}C and accumulation of a large quantity of ^{238}U and ^{234}U in both the UZ and SZ, which will give rise to a high dose contribution of ^{226} Ra (a daughter product of ^{238}U and ^{234}U). Compared to the TSPA-LA Model Figures C7-11(d) and C7-12(d), the total mean annual contributions from soluble radionuclides remain practically the same in the PMA, while the contributions from solubility-controlled radionuclides, such as plutonium, neptunium, and uranium, are slightly decreased in the PMA results. It is worth noting that the contribution from ^{239}Pu is reduced by a factor of approximately 10, partly due to reduction in waste-form colloid transport as a result of the implementation of the colloid diversity model in the SZ (C6.7).

C7.3 KEY FACTORS AFFECTING THE PERFORMANCE MARGIN

Mechanical Damage of Waste Packages—For the PMA, the Seismic GM Modeling Case contributes a much lower dose over the first 250,000 years compared with the TSPA-LA results, as can be seen on Figure C7-8 (c). For the TSPA-LA Model results, the predominate mechanism causing damage to the CDSP and CSNF WPs consisted of small cracks (SCC) that result in releases from the WPs by diffusion (Section 8.2.4.1). Diffusive transport of dissolved radionuclides through the cracks is sufficiently high that they contribute significantly to the mean annual dose. In the Seismic GM Modeling Case for the PMA, fewer WP are damaged by SCC. The PMA uses an increase for the lower bound of the range for the residual stress threshold, which is used to evaluate the SCC along the closure welds. In addition, the damaged area on WPs used in the PMA is generally smaller, resulting in fewer openings in a failed WP (Section C6.8). Seismic induced SCC failure of both of CDSP and transportation-, aging-, and disposal-bearing WPs are dependent upon the stress threshold for Alloy 22. At approximately 200,000 years after closure, the PMA Seismic GM Modeling Case begins to contribute to the PMA Total Dose. The timing is significant in that not until enough WPs begin to fail due to general corrosion effects, after approximately 100,000 years, will the GM damage begin to occur to the transportation, aging, and disposal WPs. The PMA Seismic GM Modeling Case dose continues to rise from 200,000 to approximately 600,000 years after closure, as a result of seismic ground motion damage to the WPs. The use of slower DS corrosion rates in the PMA (Section C6.3) increases the lifetime of a DS, which in turn will increase the damage area for

failed WPs under intact DSs. This damage mechanism, referred to as kinematic damage, is invoked when WPs are free to move beneath and intact DSs (SNL 2007 [DIRS 178851], Section 6.5.1 through Section 6.5.4 and Section 6.6.1 through 6.6.4). The Seismic Damage Submodel in the TSPA calculates the damage area WPs with degraded internals and intact DSs (Section 6.6.1.2.2.2). The increase in damage area that is calculated as a result of the longer DSs life time mitigates some of the margin gained by the longer WP life spans, as can be seen by the rise in the dose from approximately 200,000 years to its peak at approximately 600,000 years after closure. However, the dominant effect of increasing WP durability through the modified SCC threshold is significant for accounting for the margin in both the 10,000-year and 1,000,000-year time periods for PMA. The Seismic GM Modeling Case is reduced by two orders of magnitude below the Igneous Intrusion Modeling Case dose results over the 10,000-year time period (Figure C7-7(f)).

General Corrosion of Waste Packages—The PMA considers an ACM included in *General Corrosion and Localized Corrosion of Waste Package Outer Barrier* (SNL 2007 [DIRS 178519], Section 6.4.3.5.2), which uses the corrosion rates of weight-loss samples to derive the R_o distribution for use in the General Corrosion Model of the WP outer barrier (Section C6.3). This ACM does not involve the use of a conceptual model that differs from that used in the WP General Corrosion Model but does make use of a different distribution for Alloy 22 general corrosion rates. This evaluation of the effects of the exclusion of the weight-loss data from the TSPA-LA was conducted using two alternative PMA modeling cases that evaluated the affects on the Seismic GM and Nominal Modeling Cases. The baseline PMA results discussed above (Section C.7.1 and Section C.7.2) do not include the weight-loss data in the WP general corrosion submodel calculations. The Seismic GM Modeling Case was chosen since it is one of the dominant dose contributors to the total mean annual dose for both 10,000 years and 1,000,000 years postclosure. In addition, the Nominal Modeling Case was selected so that the general corrosion effects could be evaluated without any interference from other WP failure mechanisms.

Figure C7-13 shows a comparison of the total mean annual dose for the Seismic GM Modeling Cases for the TSPA-LA and the PMA with and without using weight-loss corrosion data. In the TSPA-LA Model results, the most likely failure mechanism from a seismic event was accelerated SCC in the damaged areas that exceed the residual stress threshold for Alloy 22 (the waste package outer barrier). The PMA increased the lower bound for the residual stress threshold (RST) for Alloy 22 and reduced the crack density for the damaged areas that exceed the RST (Section C6.3). The effect of these changes are seen between 0 and approximately 100,000 years postclosure as the PMA is two orders of magnitude below the TSPA-LA mean dose for the Seismic GM Modeling Case (Figure C7-13). In all three modeling cases shows on Figure C7-13, the ground motion enhanced SCC accounts for all the WP failures before 100,000 years and thus, the PMA with the weight-loss data shows a nearly identically dose history as the PMA Seismic GM Modeling Case with the TSPA-LA WP general corrosion model. After, approximately 120,000 years, the PMA Seismic GM Modeling Case shows the effects of the addition of the WPs failed from general corrosion as can be seen by a change in the slope of the mean annual dose curve shown on Figure C7-13. In contrast, the mean annual dose curve for the PMA Seismic GM Modeling Case using the alternative weight-loss general corrosion data does not change slope at approximately 140,000 years; rather, there is a more subtle change in the slope at approximately 220,000 years postclosure. The weight-loss general corrosion data yields a result that includes the first WP failure

at approximately 200,000 years postclosure while the TSPA-LA WP General Corrosion Submodel calculates the first WP failures to occur at approximately 100,000 years postclosure. This is demonstrated on Figure C7-14, which shows a comparison of the total mean annual dose for the Nominal Modeling Cases for the TSPA-LA and the PMA for a period of 1,000,000 years postclosure.

Advective Water Flux and Waste Form Degradation Rates—As discussed in Section C6.4, by incorporating additional hydrologic/chemical processes as well as water balance model parameters, the PMA predicts much lower advective water flux percolating through breached WPs than the TSPA-LA Model. In addition, the PMA reduces waste form degradation rates for both the CSNF and the HLW glass. The PMA calculations show that the combination of reduced water flux and waste form degradation rates has a notable effect on the predicted total annual dose over the first 10,000 years for the Drip Shield EF, Seismic GM, and Seismic FD Modeling Cases. This can be best seen for soluble radionuclides such as ^{99}Tc, ^{129}I, and ^{14}C, the release rates of which highly depend on the waste form degradation rate. As shown on Figure C7-9, the annual dose contributions from these three radionuclides for the first 10,000 years are systematically lower as compared to the TSPA-LA model results (Figure C7-11 and Figure C7-12) for the Drip Shield EF, Seismic GM, and Seismic FD Modeling Cases. As can be seen by comparison of the solubility controlled species (^{237}Np and ^{239}Pu), the lower water flux results in a lower dose in these cases, including during the late stage of WP failure, all of which involve advective water flows. Based on the discussion in Section C7.2, the performance margin gain from a the updated water balance model and waste degradation rates is estimated to be more than one order of magnitude for soluble radionuclides.

Note that the water balance model described in Section C6.4 was not applied to the Igneous Intrusion Modeling Case. In addition, it is likely that the reduced waste form degradation rates were not invoked in both the TSPA-LA and the PMA simulations for the Igneous Intrusion Modeling Case because the thermal pulse due to magmatic intrusion causes waste forms to degrade at a pre-specified maximum rate. Therefore, the dependence of dose contributions from soluble radionuclides on the newly implemented water balance model and the reduced waste form degradation rates is not observed for this modeling case.

Radionuclide Solubility—Solubility-controlled radionuclides such as ^{242}Pu, ^{239}Pu, ^{237}Np, and ^{233}U are expected to quickly reach their solubility limits after WP breaching, given the repository condition of high solid/water ratio as well as the relatively large inventories of these radionuclides. The release of these radionuclides, therefore, is mainly controlled by their solubility limits and the rate of water percolating through WPs. The release of these radionuclides is insensitive to the rates of waste form degradation. As discussed in Section C7.2, compared to the TSPA-LA Model, the total dose contributions from plutonium, neptunium, and uranium are reduced by one to two orders of magnitude for the time period of 1,000,000 years. By excluding the potential effect of reduced water flux as discussed above, the performance margin gain from using a narrower range of solubility uncertainties is estimated to be about one order of magnitude for radionuclides ^{242}Pu, ^{239}Pu, ^{237}Np, and ^{233}U.

It is important to note that the PMA only narrowed the uncertainty ranges of radionuclide solubility but did not change the solubilities themselves. The PMA results thus indicate that the dose contributions from ^{242}Pu, ^{239}Pu, ^{237}Np, and ^{233}U are sensitive to the upper limits of their

solubilities. This is reasonable based on the consideration that the solubility uncertainties are sampled on a logarithmic scale while the mean dose is calculated from radionuclide concentrations in a linear space. As a result, the mean dose calculated as such is expected to be influenced significantly by a few realizations with extremely high resultant radionuclide solubilities.

Irreversible Waste Form Colloids—It is important to mention that for the Igneous Intrusion Modeling Case only an early dose reduction is observed, which is primarily a function of a reduction in the amount of plutonium that reaches the accessible environment in the PMA. This effect can be seen by comparing Figure C7-9(e) and Figure C7-10(e) with Figure C7-11(e) and Figure C7-12(e). This early dose reduction is due to the colloid diversity model used for transport through the natural system (Section C6.6) as well as the reduction in the dissolved concentration limit uncertainty applied to plutonium isotopes (Section C6.5). The PMA calculations show that the dose contribution from ^{239}Pu-embedded waste form colloids is significantly reduced as compared to the TSPA-LA results. Both ^{239}Pu and ^{242}Pu are present mainly in waste form colloids for the first 10,000 years and then in dissolved forms over the rest of the 1,000,000-year time period.

Redox Conditions in SZ—As described in Section C6.7, the PMA includes the potential effect of reducing environments that may exist in the flow pathway in the SZ. These reducing environments can potentially affect the mobility of redox-sensitive radionuclides such as ^{99}Tc and ^{237}Np. In the PMA, this effect is captured by using appropriate sorption coefficients for ^{99}Tc and ^{237}Np in the SZ Radionuclide Transport Model. It is important to bear in mind that a sorption process generally delays the breakthrough time of sorbed radionuclides. Since no significant delay for ^{99}Tc and ^{237}Np in the SZ was observed in the PMA (Figure C7-3(b) and Figure C7-6(b)) as compared to the TSPA-LA Model (Figure C7-3(a) and Figure C7-6(a)), it appears that reducing environments in the SZ flow pathway have little effect on radionuclide doses.

C.8 SUMMARY

The objective of this PMA is to carefully and quantitatively evaluate the significance of the major explicit and implicit conservatisms embedded in the TSPA-LA model. This analysis was performed in two steps: (1) identifying the scenario classes and modeling cases that produce the most significant releases and dominate the projected doses, and (2) determining the sources of uncertainty and/or conservatisms that are most influential in producing the spread of the distribution of projected doses for these modeling cases. The PMA performed a separate set of TSPA calculations in parallel to those of the TSPA-LA for the modeling cases of Drip Shield EF, Waste Package EF, Seismic GM, Seismic FD, and Igneous Intrusion Modeling Cases. The performance margin of the TSPA-LA model was evaluated by comparing the mean values of the projected annual doses to the RMEI obtained from the PMA to those from TSPA-LA.

The PMA calculations have show that (1) the PMA mean annual doses are nearly an order of magnitude lower than the mean annual dose from the TSPA-LA Model for the first 250,000 years, (2) the largest PMA mean annual doses calculated over 10,000 years are lower by an order of magnitude than the largest mean annual dose from the TSPA-LA Model, and (3) the largest PMA mean annual doses calculated over 1,000,000 years are lower by a factor of two

than the largest mean annual dose from the TSPA-LA Model. Thus, the PMA calculations confirm that, when propagated individually through the TSPA-LA Model, the conservatisms introduced at submodel levels are conservative with respect to the total system performance measures (e.g., peak mean annual dose). In the PMA, the Igneous Intrusion Modeling Case contributes the most to the calculated mean annual doses for both 10,000 years and 1,000,000 years. The mean annual dose projected for the Seismic GM Modeling Case is on the order of 10^{-1} mrem or less and is the second largest contributor to the calculated total mean annual dose for 1,000,000 years after closure. The total dose contribution from other modeling cases is negligible over that time period. The major contributors to the peak mean dose in the PMA, ranked from highest to lowest, are: ^{99}Tc, ^{129}I, ^{14}C, ^{239}Pu, ^{240}Pu, ^{237}Np, and ^{234}U for the first 10,000 years and ^{226}Ra, ^{242}Pu, ^{237}Np, ^{129}I, ^{233}U, ^{135}Cs, ^{99}Tc, ^{229}Th, and ^{230}Th for the time period of 1,000,000 years, in the same order as the TSPA-LA Model predicts.

It is important to evaluate the performance margin of the TSPA-LA Model for each individual modeling case. Although the Igneous Intrusion Modeling Case dominates the calculated annual dose in the PMA and results in a relatively small performance margin, it is important to bear in mind that the mean annual frequency for a dike to intersect the repository is estimated to be 1.7×10^{-8} per year. This frequency is only slightly greater than the NRC frequency threshold for unlikely FEPs, which can be omitted by regulation. It is important to notice that the performance margins of the TSPA-LA Model for other modeling cases, especially the Drip Shield EF, Waste Package EF, and Seismic FD, are apparently much larger than that for the Igneous Intrusion Modeling Case. The factors that can significantly affect the performance margin include: mechanical damage of WPs by seismic ground motion, general corrosion rates of the WP outer barrier layer, in-package water balance, waste form degradation rates, radionuclide solubility uncertainties, and Colloidal Diversity Model for the SZ. Reducing environments in the SZ has little effect on radionuclide transport due to the already rapid transport in the SZ.

C.9 IMPACT ANALYSIS

After the PMA was completed and its feeds were frozen, several issues were identified in the TSPA-LA Model during post-model development checking activities that are related to errors in implementation and changes in parameter values. These issues are addressed in Appendix P as per the review criteria outlined in Sections 2.1.4 and 2.3.5.2.1 of the *Technical Work Plan for: Total System Performance Assessment FY 07-08 Activities* (SNL 2008 [DIRS 184920]). Since the PMA modifications were performed using a copy of the TSPA-LA Model, the issue descriptions and impact analyses in Appendix P apply equally to the PMA. In addition, PMA post-model development checking activities identified errors in implementation and changes in parameter values specific to the PMA. Table C9-1 summarizes the known PMA model errors and provides a qualitative assessment of the expected impact on the PMA. None of the issues evaluated on Table C9-1 or in Appendix P present a significant impact on the assessment of the performance margin or to the conclusions presented in Section C8. Thus, the confidence in the PMA results as an estimator of the performance margin in the mean dose to the reasonably RMEI can be maintained.

Table C3-1. Software Codes Specific to the PMA

Code	Version	Software Tracking Number	Operating System	DIRS Number
FEHM	2.25-00	STN: 10086-2.25-00	Windows 2000 Windows 2003 Windows XP	DIRS 182477
iTough	5.0	STN: 10003-5.0-00	SUN OS 5.5.1, OSF1 V5.1, RedHat V7.2 and V7.3	DIRS 160106

Table C3-2. TSPA-LA Model Software Codes used in the PMA

Code	Version	Software Tracking Number	Operating System	DIRS Number
CWD[a]	2.0	STN: 10363-2.0-00	Windows 2000	DIRS 162809
CWD[a]	2.0	STN: 10363-2.0-01	Windows 2003	DIRS 181037
EXDOC_LA[b]	2.0	STN: 11193-2.0-00	Windows 2000 Windows 2003 Windows XP	DIRS 182102
FEHM[a,c]	2.24-01	STN: 10086-2.24-00	Windows 2000 Windows 2003 Windows XP	DIRS 179419
GetThk_LA[a]	1.0	STN: 11229-1.0-00	Windows 2000 Windows 2003	DIRS 181040
GoldSim[a]	9.60.100	STN: 10344-9.60-01	Windows 2000 Windows 2003 Windows XP	DIRS 181903
InterpZdll_LA[a]	1.0	STN: 11107-1.0-00	Windows 2000	DIRS 167885
InterpZdll_LA[a]	1.0	STN: 11107-1.0-01	Windows 2003	DIRS 181043
MFCP_LA[a]	1.0	STN: 11071-1.0-00	Windows 2000	DIRS 167884
MFCP_LA[a]	1.0	STN: 11071-1.0-01	Windows 2003	DIRS 181045
MkTable_LA[a]	1.0	STN: 11217-1.0-00	Windows 2000	DIRS 181047
MkTable_LA[a]	1.0	STN: 11217-1.0-01	Windows 2003	DIRS 181048
MView[b]	4.0	STN: 10072-4.0-01	Windows XP	DIRS 181049
PassTable1D_LA[a]	2.0	STN: 11142-2.0-00	Windows 2000 Windows 2003	DIRS 181051
PassTable3D_LA[a]	2.0	STN: 11143-2.0-00	Windows 2000 Windows 2003	DIRS 182556
PREWAP_LA[b]	1.1	STN: 10939-1.1-00	Windows 2000	DIRS 181053
SCCD[a]	2.01	STN: 10343-2.01-00	Windows 2000	DIRS 181157
SCCD[a]	2.01	STN: 10343-2.01-01	Windows 2003	DIRS 181054
SEEPAGEDLL_LA[a]	1.3	STN: 11076-1.3-00	Windows 2000	DIRS 180318

Table C3-2. TSPA-LA Model Software Codes use in the PMA (Continued)

Code	Version	Software Tracking Number	Operating System	DIRS Number
SEEPAGEDLL_LA[a]	1.3	STN: 11076-1.3-01	Windows 2003	DIRS 181058
SZ_Convolute[a]	3.10.01	STN: 10207-3.10.01-00	Windows 2000/ Windows 2003	DIRS 181060
TSPA_Input_DB[a]	2.2	STN: 10931-2.2-00	Windows 2000	DIRS 181061
TSPA_Input_DB[a]	2.2	STN: 10931-2.2-01	Windows 2003	DIRS 181062
WAPDEG[a]	4.07	STN: 10000-4.07-00	Windows 2000	DIRS 181774
WAPDEG[a]	4.07	STN: 10000-4.07-01	Windows 2003	DIRS 181064

[a] Codes used in the TSPA-LA Model that are used for TSPA-LA Model development and to develop results and conclusions in Section 8.

[b] Code is a pre- or post-processor that does not require GoldSim to run codes that are used for TSPA-LA Model development and to develop results and conclusions in Section 8.

[c] Codes used in the PMA Model that are not used in the TSPA-LA Model development and to develop results and conclusions in Section 8.

Table C3-3. Unqualified Software

Description	Status	Software Tracking Number
SZ_Post_NonQ	Unqualified	STN: LL2000
Reduce_Track_NonQ	Unqualified	STN LL2001

Unqualifed software used for corroborative PMA analyses per SCI-PRO-006, *Models*.

Table C3-4. FEHM Software Documents

Version 2.25 Windows 2000, XP, and 2003 (STN: 10086-2.25-00)			
Description	**Document ID**	**DIRS Number**	**Tracking Number**
Requirements Document (RD)	10086-RD-2.25-01	DIRS 182561	MOL.20070712.0361
Design Document (DD)	10086-DD-2.25-01	DIRS 182562	MOL.20070712.0363
User Information Document (UID)	10086-UID-2.25-00	DIRS 182565	MOL.20070712.0365
Software Validation Report (SVR)	10086-SVR-2.25-00 WIN2000	DIRS 182566	MOL.20070712.0371
Software Validation Report (SVR)	10086-SVR-2.25-00-WIN2003	DIRS 182567	MOL.20070712.0373
Software Validation Report (SVR)	10086-SVR-2.25-00-WINXP	DIRS 182568	MOL.20070712.0375

Table C3-5. TSPA_Input_DBv2.2 Software Documents

Version 2.2 Windows 2000 (STN:10931-2.2-00)*			
Description	**Document ID**	**DIRS Number**	**Tracking Number**
Requirements Document (RD)	10931-RD-2.0-00	DIRS 173449	MOL.20050131.0427
Design Document (DD)	10931-DD-2.0-00	DIRS 173450	MOL.20050131.0430
User Information Document (UID)	10931-UID-2.2-00	DIRS 181137	MOL.20060222.0419
Software Validation Report (SVR)	10931-SVR-2.2-00-WIN2000	DIRS 181139	MOL.20060222.0422
Version 2.2 Windows 2003 (STN:10931-2.2-01)*			
Requirements Document (RD)	Same as above	NA	NA
Design Document (DD)	Same as above	NA	NA
User Information Document (UID)	Same as above	NA	NA
Software Validation Report (SVR)	10931-SVR-2.2-01-WIN2003	DIRS 181140	MOL.20061011.0198

* The PMA uses the same software for the model input database as the TSPA-LA Model database (TSPA_Input_DBv2.2).

Table C3-6. iTough V5.0 Software Documents

Version 5.0 SUN OS 5.5.1, OSF1 V5.1, and RedHat V7.2 and V7.3 (STN:10003-5.0-00)			
Description	**Document ID**	**DIRS Number**	**Tracking Number**
Requirements Document (RD)	10003-RD-5.0-00	DIRS 161067	MOL.20020923.0143
Design Document (DD)	10003-DD-5.0-00	DIRS 161068	MOL.20020923.0144
Users Manual (UM)	10003-UM-5.0-00	DIRS 161066	MOL.20020923.0147
Validation Test Report (VTR)	10003-VTR-5.0-00	DIRS 160437	MOL.20020923.0148

Table C4-1. TSPA-LA Model Parameters Changed or Deleted for the PMA

Parameter Name in TSPA-LA Compliance Model	Description	Parameter Value for Compliance Model (including DTN)	Parameter Value for PMA Model (including DTN)	Rationale for Changes
Drift Scale UZ Flow				
SMPA_C.dat	An alternative extended range seepage lookup table that considers seepage into only a 5.5-m wide center section of a collapsed drift.	Lookup Table (DTN: LB0702PASEEP01.001_R0 [DIRS 179511])	Lookup Table (Corroborative DTN: LB0704PASEEP02.001_R1 [DIRS 181093])	This PMA option assumes that when the drift is in a collapsed state, water moves vertically downward and the waste package is affected only by seepage from directly above it.
Waste Form Degradation and Radionuclide Mobilization				
Np2O5_Eps_1_high_a	RN Solubility, Np, epsilon 1, high ionic strength (1-3 mol/kg).	Normal [0, 0.85], truncated at +/- 2σ, MO0702PADISCON.001_R0 [DIRS 179358]	Replaced by new PMA parameters	The PMA uses more realistic uncertainty ranges for radionuclide solubility limits.
Np2O5_Eps_1_low_a	RN Solubility, Np, epsilon 1, low ionic strength (<1 mol/kg).	Normal [0, 0.8], truncated at +/- 2σ, MO0702PADISCON.001_R0 [DIRS 179358]	Replaced by new PMA parameters	The PMA uses more realistic uncertainty ranges for radionuclide solubility limits.
Np2O5_Eps_2_CDSP_ High_a	RN Solubility, Np2O5, epsilon 2, CDSP, I >= 0.004m, Cell 1b.	Triangular [0, 0, 853], MO0702PAFLUORI.000_R1 [DIRS 181219]	Replaced by new PMA parameters	The PMA uses more realistic uncertainty ranges for radionuclide solubility limits.
Np2O5_Eps_2_CSNF_ High_a	RN Solubility, Np2O5, epsilon 2, CSNF, I >= 0.2m.	Triangular [0, 0, 197], MO0702PAFLUORI.000_R1 [DIRS 181219]	Replaced by new PMA parameters	The PMA uses more realistic uncertainty ranges for radionuclide solubility limits.
Np2O5_Eps_2_Glass_L ow_a	RN Solubility, Np2O5, epsilon 2, CDSP cell 1a, CDSP I < 0.004m Cell 1b, CSNF I < 0.2m.	Triangular [0, 0, 11], MO0702PAFLUORI.000_R1 [DIRS 181219]	Replaced by new PMA parameters	The PMA uses more realistic uncertainty ranges for radionuclide solubility limits.
NpO2_Eps_1_high_a	RN Solubility, Np, epsilon 1, high ionic strength (1-3 mol/kg).	Normal [0, 0.67], truncated at +/- 2σ, MO0702PADISCON.001_R0 [DIRS 179358]	Replaced by new PMA parameters	The PMA uses more realistic uncertainty ranges for radionuclide solubility limits.
NpO2_Eps_1_low_a	RN Solubility, Np, epsilon 1, low ionic strength (<1 mol/kg).	Normal [0, 0.6], truncated at +/- 2σ, MO0702PADISCON.001_R0 [DIRS 179358]	Replaced by new PMA parameters	The PMA uses more realistic uncertainty ranges for radionuclide solubility limits.

Table C4-1. TSPA-LA Model Parameters Changed or Deleted for the PMA (Continued)

Parameter Name	Description	Parameter Value for Compliance Model (including DTN)	Parameter Value for PMA Model (including DTN)	Rationale for Changes
Waste Form Degradation and Radionuclide Mobilization (Continued)				
NpO2_Eps_2_CDSP_High_a	RN Solubility, Np2O5, epsilon 2, CDSP, I >= 0.004m, Cell 1b, Invert.	Triangular [0, 0, 1,093.5], MO0702PAFLUORI.000_R1 [DIRS 181219]	Replaced by new PMA parameters	The PMA uses more realistic uncertainty ranges for radionuclide solubility limits.
NpO2_Eps_2_CSNF_High_a	RN Solubility, Np2O5, epsilon 2, CSNF, I >= 0.2m, Invert.	Triangular [0, 0, 255.8], MO0702PAFLUORI.000_R1 [DIRS 181219]	Replaced by new PMA parameters	The PMA uses more realistic uncertainty ranges for radionuclide solubility limits.
NpO2_Eps_2_Glass_Low_a	RN Solubility, Np2O5, epsilon 2, CDSP cell 1a, CDSP I < 0.004m Cell 1b, CSNF I < 0.2m.	Triangular [0, 0, 14.1], MO0702PAFLUORI.000_R1 [DIRS 181219]	Replaced by new PMA parameters	The PMA uses more realistic uncertainty ranges for radionuclide solubility limits.
Pu_Eps_1_high_a	RN Solubility, Pu, epsilon 1, high ionic strength (1-3 mol/kg).	Normal [0, 0.76], truncated at +/- 2σ, MO0702PADISCON.001_R0 [DIRS 179358]	Replaced by new PMA parameters	The PMA uses more realistic uncertainty ranges for radionuclide solubility limits.
Pu_Eps_1_low_a	RN Solubility, Pu, epsilon 1, low ionic strength (<1 mol/kg).	Normal [0, 0.7], truncated at +/- 2σ, MO0702PADISCON.001_R0 [DIRS 179358]	Replaced by new PMA parameters	The PMA uses more realistic uncertainty ranges for radionuclide solubility limits.
Pu_Eps_2_CSNF_High_a	RN Solubility, Pu, epsilon 2, CSNF, I > = 0.2m, Invert.	Triangular [0, 0, 1,374], MO0702PAFLUORI.000_R1 [DIRS 181219]	Replaced by new PMA parameters	The PMA uses more realistic uncertainty ranges for radionuclide solubility limits.
Pu_Eps_2_CDSP_High_a	RN Solubility, Pu, epsilon 2, CDSP, I > = 0.004m, Cell 1b, Invert.	Triangular [0, 0, 5,460], MO0702PAFLUORI.000_R1 [DIRS 181219]	Replaced by new PMA parameters	The PMA uses more realistic uncertainty ranges for radionuclide solubility limits.
Pu_Eps_2_Glass_Low_a	RN Solubility, Pu, epsilon 2, CDSP cell 1a, CDSP I < 0.004m Cell 1b, CSNF I < 0.2m.	Triangular [0, 0, 79], MO0702PAFLUORI.000_R1 [DIRS 181219]	Replaced by new PMA parameters	The PMA uses more realistic uncertainty ranges for radionuclide solubility limits.

Table C4-1. TSPA-LA Model Parameters Changed or Deleted for the PMA (Continued)

Parameter Name	Description	Parameter Value for Compliance Model (including DTN)	Parameter Value for PMA Model (including DTN)	Rationale for Changes
Waste Form Degradation and Radionuclide Mobilization (Continued)				
U_Eps_1_high_Other_a	RN Solubility, U, epsilon 1, high ionic strength (1-3 mol/kg).	Normal [0, 0.6], truncated at +/- 2σ, MO0702PADISCON.001_R0 [DIRS 179358]	Replaced by new PMA parameters	The PMA uses more realistic uncertainty ranges for radionuclide solubility limits.
U_Eps_1_low_Other_a	RN Solubility, U, epsilon 1, low ionic strength (<1 mol/kg).	Normal [0, 0.5], truncated at +/- 2σ, MO0702PADISCON.001_R0 [DIRS 179358]	Replaced by new PMA parameters	The PMA uses more realistic uncertainty ranges for radionuclide solubility limits.
U_Eps_2_Schoepite_CSNF_High_a	RN Solubility, U-Schoepite, epsilon 2, CSNF, I >= 0.2m, Invert.	Triangular [0, 0, 1,361], MO0702PAFLUORI.000_R1 [DIRS 181219]	Replaced by new PMA parameters	The PMA uses more realistic uncertainty ranges for radionuclide solubility limits.
U_Eps_2_Schoepite_CDSP_High_a	RN Solubility, U-Schoepite, epsilon 2, CDSP, I >= 0.004m, Cell 1b, Invert.	Triangular [0, 0, 5,385], MO0702PAFLUORI.000_R1 [DIRS 181219]	Replaced by new PMA parameters	The PMA uses more realistic uncertainty ranges for radionuclide solubility limits.
U_Eps_2_Boltwoodite_CSNF_Hig_a	RN Solubility, U-Na-Boltwoodite, epsilon 2, CSNF, I >= 0.2m, Invert.	Triangular [0, 0, 57.01], MO0702PAFLUORI.000_R1 [DIRS 181219]	Replaced by new PMA parameters	The PMA uses more realistic uncertainty ranges for radionuclide solubility limits.
U_Eps_2_Boltwoodite_CDSP_Hig_a	RN Solubility U-Na-Boltwoodite, epsilon 2, CDSP, I >= 0.004m, Cell 1b, Invert.	Triangular [0, 0, 272.3], MO0702PAFLUORI.000_R1 [DIRS 181219]	Replaced by new PMA parameters	The PMA uses more realistic uncertainty ranges for radionuclide solubility limits.
U_Eps_2_Schoepite_Glass_Low_a	RN Solubility, U-Schoepite, epsilon 2, CDSP cell 1a, CDSP I < 0.004m Cell 1b, CSNF I < 0.2m.	Triangular [0, 0, 78], MO0702PAFLUORI.000_R1 [DIRS 181219]	Replaced by new PMA parameters	The PMA uses more realistic uncertainty ranges for radionuclide solubility limits.
U_Eps_2_Boltwoodite_Glass_Lo_a	RN Solubility, U-Na-Boltwoodite, epsilon 2, CDSP cell 1a, CDSP I < 0.004m Cell 1b, CSNF I < 0.2m.	Triangular [0, 0, 6.13], MO0702PAFLUORI.000_R1 [DIRS 181219]	Replaced by new PMA parameters	The PMA uses more realistic uncertainty ranges for radionuclide solubility limits.

Table C4-1. TSPA-LA Model Parameters Changed or Deleted for the PMA (Continued)

Parameter Name	Description	Parameter Value for Compliance Model (including DTN)	Parameter Value for PMA Model (including DTN)	Rationale for Changes
Waste Form Degradation and Radionuclide Mobilization (Continued)				
U_Eps_1_high_Nominal_a	RN Solubility, U, epsilon 1, high ionic strength (1-3 mol/kg).	Normal [0, 0.6], truncated at +/- 2σ, MO0702PADISCON.001_R0 [DIRS 179358]	Replaced by new PMA parameters	The PMA uses more realistic uncertainty ranges for radionuclide solubility limits.
U_Eps_1_low_Nominal_a	RN Solubility, U, epsilon 1, low ionic strength (<1 mol/kg).	Normal [0, 0.5], truncated at +/- 2σ, MO0702PADISCON.001_R0 [DIRS 179358]	Replaced by new PMA parameters	The PMA uses more realistic uncertainty ranges for radionuclide solubility limits.
U_Eps_2_CSNF_Low_Nominal_a	RN Solubility, U, epsilon 2, CSNF, I < 0.2m, Invert, nominal seismic.	Triangular [0, 0, 78], MO0702PAFLUORI.000_R1 [DIRS 181219]	Replaced by new PMA parameters	The PMA uses more realistic uncertainty ranges for radionuclide solubility limits.
U_Eps_2_CSNF_High_Nominal_a	RN Solubility, U, epsilon 2, CSNF, I >= 0.2m, Invert, nominal seismic.	Triangular [0, 0, 1,361], MO0702PAFLUORI.000_R1 [DIRS 181219]	Replaced by new PMA parameters	The PMA uses more realistic uncertainty ranges for radionuclide solubility limits.
SZ Flow and Transport Parameters				
FPVO	Flowing interval porosity.	CDF (Log_{10} – transformed) with Probability (0, .05, .5, .8,1) and Value (-5, -4, -3, -2, -1) (SN0702PASZFTMA.002_R1 [DIRS 183471]).	CDF (Log_{10} – transformed) with Probability (0, .5, .8, 1) and Value (-4, -3, -2, -1) (Corroborative DTN: SN0704PMASZFTA.00_R1 [DIRS 184395])	The lower bound of the compliance model might be very low for bulk average parameter value (i.e., average value over the volcanic zone) that is being applied at the km scale (i.e., the model domain). Thus, the lower bound flowing interval porosity was set at 1e-4.
FPVO	Correlation coefficient between the flowing interval porosity and the groundwater specific discharge multiplier, GWSPD.	N/A (a value of 0 is used by default in the TSPA-LA model)	0.64 (Corroborative DTN: SN0704PMASZFTA.001_R1 [DIRS 184395])	In a fractured flow aquifer, there are theoretical and geometric arguments that suggest the two parameters are at least partially correlated. As fracture density and apertures increase, one would expect both flowing interval porosity and permeability to also increase. Thus, a correlation factor was obtained from literature survey.

Table C4-1. TSPA-LA Model Parameters Changed or Deleted for the PMA (Continued)

Parameter Name	Description	Parameter Value for Compliance Model (including DTN)	Parameter Value for PMA Model (including DTN)	Rationale for Changes
SZ Flow and Transport Parameters (Continued)				
SZ_01_01	SZ, Breakthrough Curves, C, I, Cl, SR1.	Table (SN0702PASZFTMA.001_R0 [DIRS 179504])	Table (Corroborative DTN: SN0704PMASZFTA.001_R1 [DIRS 184395])	New breakthrough curves that incorporated PMA changes.
SZ_01_02	SZ, Breakthrough Curves, C, I, Cl, SR2.	Table (SN0702PASZFTMA.001_R0 [DIRS 179504])	Table (Corroborative DTN: SN0704PMASZFTA.001_R1 [DIRS 184395])	New breakthrough curves that incorporated PMA changes.
SZ_01_03	SZ, Breakthrough Curves, C, I, Cl, SR3.	Table (SN0702PASZFTMA.001_R0 [DIRS 179504])	Table (Corroborative DTN: SN0704PMASZFTA.001_R1 [DIRS 184395])	New breakthrough curves that incorporated PMA changes.
SZ_01_04	SZ, Breakthrough Curves, C, I, Cl, SR4.	Table (SN0702PASZFTMA.001_R0 [DIRS 179504])	Table (Corroborative DTN: SN0704PMASZFTA.001_R1 [DIRS 184395])	New breakthrough curves that incorporated PMA changes.
SZ_02_01	SZ, Breakthrough Curves, Am, Th, Pa, SR1.	Table (SN0702PASZFTMA.001_R0 [DIRS 179504])	Table (Corroborative DTN: SN0704PMASZFTA.001_R1 [DIRS 184395])	New breakthrough curves that incorporated PMA changes.
SZ_02_02	SZ, Breakthrough Curves, Am, Th, Pa, SR2.	Table (SN0702PASZFTMA.001_R0 [DIRS 179504])	Table (Corroborative DTN: SN0704PMASZFTA.001_R1 [DIRS 184395])	New breakthrough curves that incorporated PMA changes.
SZ_02_03	SZ, Breakthrough Curves, Am, Th, Pa, SR3.	Table (SN0702PASZFTMA.001_R0 [DIRS 179504])	Table (Corroborative DTN: SN0704PMASZFTA.001_R1 [DIRS 184395])	New breakthrough curves that incorporated PMA changes.
SZ_02_04	SZ, Breakthrough Curves, Am, Th, Pa, SR4.	Table (SN0702PASZFTMA.001_R0 [DIRS 179504])	Table (Corroborative DTN: SN0704PMASZFTA.001_R1 [DIRS 184395])	New breakthrough curves that incorporated PMA changes.
SZ_03_01	SZ, Breakthrough Curves, Cs, SR1.	Table (SN0702PASZFTMA.001_R0 [DIRS 179504])	Table (Corroborative DTN: SN0704PMASZFTA.001_R1 [DIRS 184395])	New breakthrough curves that incorporated PMA changes.
SZ_03_02	SZ, Breakthrough Curves, Cs, SR2.	Table (SN0702PASZFTMA.001_R0 [DIRS 179504])	Table (Corroborative DTN: SN0704PMASZFTA.001_R1 [DIRS 184395])	New breakthrough curves that incorporated PMA changes.

Table C4-1. TSPA-LA Model Parameters Changed or Deleted for the PMA (Continued)

Parameter Name	Description	Parameter Value for Compliance Model (including DTN)	Parameter Value for PMA Model (including DTN)	Rationale for Changes
SZ_03_03	SZ, Breakthrough Curves, Cs, SR3.	Table (SN0702PASZFTMA.001_R0 [DIRS 179504])	Table (Corroborative DTN: SN0704PMASZFTA.001_R1 [DIRS 184395])	New breakthrough curves that incorporated PMA changes.
SZ Flow and Transport Parameters (Continued)				
SZ_03_04	SZ, Breakthrough Curves, Cs, SR4.	Table (SN0702PASZFTMA.001_R0 [DIRS 179504])	Table (Corroborative DTN: SN0704PMASZFTA.001_R1 [DIRS 184395])	New breakthrough curves that incorporated PMA changes.
SZ_04_01	SZ, Breakthrough Curves, Pu, SR1.	Table (SN0702PASZFTMA.001_R0 [DIRS 179504])	Table (Corroborative DTN: SN0704PMASZFTA.001_R1 [DIRS 184395])	New breakthrough curves that incorporated PMA changes.
SZ_04_02	SZ, Breakthrough Curves, Pu, SR2.	Table (SN0702PASZFTMA.001_R0 [DIRS 179504])	Table (Corroborative DTN: SN0704PMASZFTA.001_R1 [DIRS 184395])	New breakthrough curves that incorporated PMA changes.
SZ_04_03	SZ, Breakthrough Curves, Pu, SR3.	Table (SN0702PASZFTMA.001_R0 [DIRS 179504])	Table (Corroborative DTN: SN0704PMASZFTA.001_R1 [DIRS 184395])	New breakthrough curves that incorporated PMA changes.
SZ_04_04	SZ, Breakthrough Curves, Pu, SR4.	Table (SN0702PASZFTMA.001_R0 [DIRS 179504])	Table (Corroborative DTN: SN0704PMASZFTA.001_R1 [DIRS 184395])	New breakthrough curves that incorporated PMA changes.
SZ_05_01	SZ, Breakthrough Curves, Np, SR1.	Table (SN0702PASZFTMA.001_R0 [DIRS 179504])	Table (Corroborative DTN: SN0704PMASZFTA.001_R1 [DIRS 184395])	New breakthrough curves that incorporated PMA changes.
SZ_05_02	SZ, Breakthrough Curves, Np, SR2.	Table (SN0702PASZFTMA.001_R0 [DIRS 179504])	Table (Corroborative DTN: SN0704PMASZFTA.001_R1 [DIRS 184395])	New breakthrough curves that incorporated PMA changes.
SZ_05_03	SZ, Breakthrough Curves, Np, SR3.	Table (SN0702PASZFTMA.001_R0 [DIRS 179504])	Table (Corroborative DTN: SN0704PMASZFTA.001_R1 [DIRS 184395])	New breakthrough curves that incorporated PMA changes.
SZ_05_04	SZ, Breakthrough Curves, Np, SR4.	Table (SN0702PASZFTMA.001_R0 [DIRS 179504])	Table (Corroborative DTN: SN0704PMASZFTA.001_R1 [DIRS 184395])	New breakthrough curves that incorporated PMA changes.

Table C4-1. TSPA-LA Model Parameters Changed or Deleted for the PMA (Continued)

Parameter Name	Description	Parameter Value for Compliance Model (including DTN)	Parameter Value for PMA Model (including DTN)	Rationale for Changes
SZ_06_01	SZ, Breakthrough Curves, IcPu, IcAm, IcTh, SR1.	Table (SN0702PASZFTMA.001_R0 [DIRS 179504])	Table (Corroborative DTN: SN0704PMASZFTA.001_R1 [DIRS 184395])	New breakthrough curves that incorporated PMA changes.
SZ_06_02	SZ, Breakthrough Curves, IcPu, IcAm, IcTh, SR2.	Table (SN0702PASZFTMA.001_R0 [DIRS 179504])	Table (Corroborative DTN: SN0704PMASZFTA.001_R1 [DIRS 184395])	New breakthrough curves that incorporated PMA changes.
SZ Flow and Transport Parameters (Continued)				
SZ_06_03	SZ, Breakthrough Curves, IcPu, IcAm, IcTh, SR3.	Table (SN0702PASZFTMA.001_R0 [DIRS 179504])	Table (Corroborative DTN: SN0704PMASZFTA.001_R1 [DIRS 184395])	New breakthrough curves that incorporated PMA changes.
SZ_06_04	SZ, Breakthrough Curves, IcPu, IcAm, IcTh, SR4.	Table (SN0702PASZFTMA.001_R0 [DIRS 179504])	Table (Corroborative DTN: SN0704PMASZFTA.001_R1 [DIRS 184395])	New breakthrough curves that incorporated PMA changes.
SZ_07_01	SZ, Breakthrough Curves, Ra, SR1.	Table (SN0702PASZFTMA.001_R0 [DIRS 179504])	Table (Corroborative DTN: SN0704PMASZFTA.001_R1 [DIRS 184395])	New breakthrough curves that incorporated PMA changes.
SZ_07_02	SZ, Breakthrough Curves, Ra, SR2.	Table (SN0702PASZFTMA.001_R0 [DIRS 179504])	Table (Corroborative DTN: SN0704PMASZFTA.001_R1 [DIRS 184395])	New breakthrough curves that incorporated PMA changes.
SZ_07_03	SZ, Breakthrough Curves, Ra, SR3.	Table (SN0702PASZFTMA.001_R0 [DIRS 179504])	Table (Corroborative DTN: SN0704PMASZFTA.001_R1 [DIRS 184395])	New breakthrough curves that incorporated PMA changes.
SZ_07_04	SZ, Breakthrough Curves, Ra, SR4.	Table (SN0702PASZFTMA.001_R0 [DIRS 179504])	Table (Corroborative DTN: SN0704PMASZFTA.001_R1 [DIRS 184395])	New breakthrough curves that incorporated PMA changes.
SZ_08_01	SZ, Breakthrough Curves, Sr, SR1.	Table (SN0702PASZFTMA.001_R0 [DIRS 179504])	Table (Corroborative DTN: SN0704PMASZFTA.001_R1 [DIRS 184395])	New breakthrough curves that incorporated PMA changes.
SZ_08_02	SZ, Breakthrough Curves, Sr, SR2.	Table (SN0702PASZFTMA.001_R0 [DIRS 179504])	Table (Corroborative DTN: SN0704PMASZFTA.001_R1 [DIRS 184395])	New breakthrough curves that incorporated PMA changes.

Table C4-1. TSPA-LA Model Parameters Changed or Deleted for the PMA (Continued)

Parameter Name	Description	Parameter Value for Compliance Model (including DTN)	Parameter Value for PMA Model (including DTN)	Rationale for Changes
SZ_08_03	SZ, Breakthrough Curves, Sr, SR3.	Table (SN0702PASZFTMA.001_R0 [DIRS 179504])	Table (Corroborative DTN: SN0704PMASZFTA.001_R1 [DIRS 184395])	New breakthrough curves that incorporated PMA changes.
SZ_08_04	SZ, Breakthrough Curves, Sr, SR4.	Table (SN0702PASZFTMA.001_R0 [DIRS 179504])	Table (Corroborative DTN: SN0704PMASZFTA.001_R1 [DIRS 184395])	New breakthrough curves that incorporated PMA changes.
SZ_09_01	SZ, Breakthrough Curves, U, SR1.	Table (SN0702PASZFTMA.001_R0 [DIRS 179504])	Table (Corroborative DTN: SN0704PMASZFTA.001_R1 [DIRS 184395])	New breakthrough curves that incorporated PMA changes.
SZ Flow and Transport Parameters (Continued)				
SZ_09_02	SZ, Breakthrough Curves, U, SR2.	Table (SN0702PASZFTMA.001_R0 [DIRS 179504])	Table (Corroborative DTN: SN0704PMASZFTA.001_R1 [DIRS 184395])	New breakthrough curves that incorporated PMA changes.
SZ_09_03	SZ, Breakthrough Curves, U, SR3.	Table (SN0702PASZFTMA.001_R0 [DIRS 179504])	Table (Corroborative DTN: SN0704PMASZFTA.001_R1 [DIRS 184395])	New breakthrough curves that incorporated PMA changes.
SZ_09_04	SZ, Breakthrough Curves, U, SR4.	Table (SN0702PASZFTMA.001_R0 [DIRS 179504])	Table (Corroborative DTN: SN0704PMASZFTA.001_R1 [DIRS 184395])	New breakthrough curves that incorporated PMA changes.
SZ_10_01	SZ, Breakthrough Curves, IfPu, IfAm, IfTh, SR1.	Table (SN0702PASZFTMA.001_R0 [DIRS 179504])	Table (Corroborative DTN: SN0704PMASZFTA.001_R1 [DIRS 184395])	New breakthrough curves that incorporated PMA changes.
SZ_10_02	SZ, Breakthrough Curves, IfPu, IfAm, IfTh, SR2.	Table (SN0702PASZFTMA.001_R0 [DIRS 179504])	Table (Corroborative DTN: SN0704PMASZFTA.001_R1 [DIRS 184395])	New breakthrough curves that incorporated PMA changes.
SZ_10_03	SZ, Breakthrough Curves, IfPu, IfAm, IfTh, SR3.	Table (SN0702PASZFTMA.001_R0 [DIRS 179504])	Table (Corroborative DTN: SN0704PMASZFTA.001_R1 [DIRS 184395])	New breakthrough curves that incorporated PMA changes.
SZ_10_04	SZ, Breakthrough Curves, IfPu, IfAm, IfTh, SR4.	Table (SN0702PASZFTMA.001_R0 [DIRS 179504])	Table (Corroborative DTN: SN0704PMASZFTA.001_R1 [DIRS 184395])	New breakthrough curves that incorporated PMA changes.

Table C4-1. TSPA-LA Model Parameters Changed or Deleted for the PMA (Continued)

Parameter Name	Description	Parameter Value for Compliance Model (including DTN)	Parameter Value for PMA Model (including DTN)	Rationale for Changes
SZ_11_01	SZ, Breakthrough Curves, Se, SR1.	Table (SN0702PASZFTMA.001_R0 [DIRS 179504])	Table (Corroborative DTN: SN0704PMASZFTA.001_R1 [DIRS 184395])	New breakthrough curves that incorporated PMA changes.
SZ_11_02	SZ, Breakthrough Curves, Se, SR2.	Table (SN0702PASZFTMA.001_R0 [DIRS 179504])	Table (Corroborative DTN: SN0704PMASZFTA.001_R1 [DIRS 184395])	New breakthrough curves that incorporated PMA changes.
SZ_11_03	SZ, Breakthrough Curves, Se, SR3.	Table (SN0702PASZFTMA.001_R0 [DIRS 179504])	Table (Corroborative DTN: SN0704PMASZFTA.001_R1 [DIRS 184395])	New breakthrough curves that incorporated PMA changes.
SZ_11_04	SZ, Breakthrough Curves, Se, SR4.	Table (SN0702PASZFTMA.001_R0 [DIRS 179504])	Table (Corroborative DTN: SN0704PMASZFTA.001_R1 [DIRS 184395])	New breakthrough curves that incorporated PMA changes.
SZ Flow and Transport Parameters (Continued)				
SZ_12_01	SZ, Breakthrough Curves, Sn, SR1.	Table (SN0702PASZFTMA.001_R0 [DIRS 179504])	Table (Corroborative DTN: SN0704PMASZFTA.001_R1 [DIRS 184395])	New breakthrough curves that incorporated PMA changes.
SZ_12_02	SZ, Breakthrough Curves, Sn, SR2.	Table (SN0702PASZFTMA.001_R0 [DIRS 179504])	Table (Corroborative DTN: SN0704PMASZFTA.001_R1 [DIRS 184395])	New breakthrough curves that incorporated PMA changes.
SZ_12_03	SZ, Breakthrough Curves, Sn, SR3.	Table (SN0702PASZFTMA.001_R0 [DIRS 179504])	Table (Corroborative DTN: SN0704PMASZFTA.001_R1 [DIRS 184395])	New breakthrough curves that incorporated PMA changes.
SZ_12_04	SZ, Breakthrough Curves, Sn, SR4.	Table (SN0702PASZFTMA.001_R0 [DIRS 179504])	Table (Corroborative DTN: SN0704PMASZFTA.001_R1 [DIRS 184395])	New breakthrough curves that incorporated PMA changes.

NOTE: SZ = saturated zone; Ic = irreversible colloids; If = fast fraction of irreversible colloids; SR = source region; C = carbon; I = iodine; Cl = chlorine; Am = americium; Th = thorium; Pa = protactinium; Cs = cesium; Pu = plutonium; Np = neptunium; Ra = radium; Sr = strontium; U = uranium; Se = selenium; Sn = tin; FPVO = fracture porosity in volcanic units; and GWSPD = ground water specific discharge multiplier.

Table C4-2. Input Parameters Added for the PMA

Parameter Name	Description	Parameter Distribution	Rationale for Inclusion	Data Source
EBS Thermal-Hydrology Parameters				
B1_CSNF_REP_P10_PMA.ou	PREWAP output file for representative TH (DS T and RH)	File	Files re-generated to include the DS RH values used in the DS corrosion rate model for PMA.	LL0703PA011MST.006_R0 [DIRS 179853]
B1_CSNF_REP_P10H_PMA.ou	PREWAP output file for representative TH (DS T and RH)	File	Same as above.	LL0703PA017MST.012_R0 [DIRS 179859]
B1_CSNF_REP_P10L_PMA.ou	PREWAP output file for representative TH (DS T and RH)	File	Same as above.	LL0703PA015MST.010_R0 [DIRS 179857]
B1_CSNF_REP_P30_PMA.ou	PREWAP output file for representative TH (DS T and RH)	File	Same as above.	LL0703PA012MST.007_R0 [DIRS 179854]
B1_CSNF_REP_P30H_PMA.ou	PREWAP output file for representative TH (DS T and RH)	File	Same as above.	LL0703PA035MST.017_R0 [DIRS 179985]
B1_CSNF_REP_P30L_PMA.ou	PREWAP output file for representative TH (DS T and RH)	File	Same as above.	LL0703PA034MST.016_R0 [DIRS 179982]
B1_CSNF_REP_P50_PMA.ou	PREWAP output file for representative TH (DS T and RH)	File	Same as above.	LL0703PA013MST.008_R0 [DIRS 179855]
B1_CSNF_REP_P50H_PMA.ou	PREWAP output file for representative TH (DS T and RH)	File	Same as above.	LL0703PA037MST.019_R0 [DIRS 179989]
B1_CSNF_REP_P50L_PMA.ou	PREWAP output file for representative TH (DS T and RH)	File	Same as above.	LL0703PA036MST.018_R0 [DIRS 179986]
B1_CSNF_REP_P90_PMA.ou	PREWAP output file for representative TH (DS T and RH)	File	Same as above.	LL0703PA014MST.009_R0 [DIRS 179856]
B1_CSNF_REP_P90H_PMA.ou	PREWAP output file for representative TH (DS T and RH)	File	Same as above.	LL0703PA016MST.011_R0 [DIRS 179858]
B1_CSNF_REP_P90L_PMA.ou	PREWAP output file for representative TH (DS T and RH)	File	Same as above.	LL0703PA038MST.020_R0 [DIRS 179992]
B1_DHLW_REP_P10_PMA.ou	PREWAP output file for representative TH (DS T and RH)	File	Same as above.	LL0703PA011MST.006_R0 [DIRS 179853]
B1_DHLW_REP_P10H_PMA.ou	PREWAP output file for representative TH (DS T and RH)	File	Same as above.	LL0703PA017MST.012_R0 [DIRS 179859]
B1_DHLW_REP_P10L_PMA.ou	PREWAP output file for representative TH (DS T and RH)	File	Same as above.	LL0703PA015MST.010_R0 [DIRS 179857]

Table C4-2. Input Parameters Added for the PMA (Continued)

Parameter Name	Description	Parameter Distribution	Rationale for Inclusion	Data Source
EBS Thermal-Hydrology Parameters (Continued)				
B1_DHLW_REP_P30_PMA.ou	PREWAP output file for representative TH (DS T and RH)	File	Same as above.	LL0703PA012MST.007_R0 [DIRS 179854]
B1_DHLW_REP_P30H_PMA.ou	PREWAP output file for representative TH (DS T and RH)	File	Same as above.	LL0703PA035MST.017_R0 [DIRS 179985]
B1_DHLW_REP_P30L_PMA.ou	PREWAP output file for representative TH (DS T and RH)	File	Same as above.	LL0703PA034MST.016_R0 [DIRS 179982]
B1_DHLW_REP_P50_PMA.ou	PREWAP output file for representative TH (DS T and RH)	File	Same as above.	LL0703PA013MST.008_R0 [DIRS 179855]
B1_DHLW_REP_P50H_PMA.ou	PREWAP output file for representative TH (DS T and RH)	File	Same as above.	LL0703PA037MST.019_R0 [DIRS 179989]
B1_DHLW_REP_P50L_PMA.ou	PREWAP output file for representative TH (DS T and RH)	File	Same as above.	LL0703PA036MST.018_R0 [DIRS 179986]
B1_DHLW_REP_P90_PMA.ou	PREWAP output file for representative TH (DS T and RH)	File	Same as above.	LL0703PA014MST.009_R0 [DIRS 179856]
B1_DHLW_REP_P90H_PMA.ou	PREWAP output file for representative TH (DS T and RH)	File	Same as above.	LL0703PA016MST.011_R0 [DIRS 179858]
B1_DHLW_REP_P90L_PMA.ou	PREWAP output file for representative TH (DS T and RH)	File	Same as above.	LL0703PA038MST.020_R0 [DIRS 179992]
B2_CSNF_REP_P10_PMA.ou	PREWAP output file for representative TH (DS T and RH)	File	Same as above.	LL0703PA011MST.006_R0 [DIRS 179853]
B2_CSNF_REP_P10H_PMA.ou	PREWAP output file for representative TH (DS T and RH)	File	Same as above.	LL0703PA017MST.012_R0 [DIRS 179859]
B2_CSNF_REP_P10L_PMA.ou	PREWAP output file for representative TH (DS T and RH)	File	Same as above.	LL0703PA015MST.010_R0 [DIRS 179857]
B2_CSNF_REP_P30_PMA.ou;	PREWAP output file for representative TH (DS T and RH)	File	Same as above.	LL0703PA012MST.007_R0 [DIRS 179854]
B2_CSNF_REP_P30H_PMA.ou	PREWAP output file for representative TH (DS T and RH)	File	Same as above.	LL0703PA035MST.017_R0 [DIRS 179985]
B2_CSNF_REP_P30L_PMA.ou	PREWAP output file for representative TH (DS T and RH)	File	Same as above.	LL0703PA034MST.016_R0 [DIRS 179982]
B2_CSNF_REP_P50_PMA.ou;	PREWAP output file for representative TH (DS T and RH)	File	Same as above.	LL0703PA013MST.008_R0 [DIRS 179855]

Table C4-2. Input Parameters Added for the PMA (Continued)

Parameter Name	Description	Parameter Distribution	Rationale for Inclusion	Data Source
EBS Thermal-Hydrology Parameters (Continued)				
B2_CSNF_REP_P50H_PMA.ou	PREWAP output file for representative TH (DS T and RH)	File	Same as above.	LL0703PA037MST.019_R0 [DIRS 179989]
B2_CSNF_REP_P50L_PMA.ou	PREWAP output file for representative TH (DS T and RH)	File	Same as above.	LL0703PA036MST.018_R0 [DIRS 179986]
B2_CSNF_REP_P90_PMA.ou	PREWAP output file for representative TH (DS T and RH)	File	Same as above.	LL0703PA014MST.009_R0 [DIRS 179856]
B2_CSNF_REP_P90H_PMA.ou	PREWAP output file for representative TH (DS T and RH)	File	Same as above.	LL0703PA016MST.011_R0 [DIRS 179858]
B2_CSNF_REP_P90L_PMA.ou	PREWAP output file for representative TH (DS T and RH)	File	Same as above.	LL0703PA038MST.020_R0 [DIRS 179992]
B2_DHLW_REP_P10_PMA.ou	PREWAP output file for representative TH (DS T and RH)	File	Same as above.	LL0703PA011MST.006_R0 [DIRS 179853]
B2_DHLW_REP_P10H_PMA.ou	PREWAP output file for representative TH (DS T and RH)	File	Same as above.	LL0703PA017MST.012_R0 [DIRS 179859]
B2_DHLW_REP_P10L_PMA.ou	PREWAP output file for representative TH (DS T and RH)	File	Same as above.	LL0703PA015MST.010_R0 [DIRS 179857]
B2_DHLW_REP_P30_PMA.ou	PREWAP output file for representative TH (DS T and RH)	File	Same as above.	LL0703PA012MST.007_R0 [DIRS 179854]
B2_DHLW_REP_P30H_PMA.ou	PREWAP output file for representative TH (DS T and RH)	File	Same as above.	LL0703PA035MST.017_R0 [DIRS 179985]
B2_DHLW_REP_P30L_PMA.ou	PREWAP output file for representative TH (DS T and RH)	File	Same as above.	LL0703PA034MST.016_R0 [DIRS 179982]
B2_DHLW_REP_P50_PMA.ou	PREWAP output file for representative TH (DS T and RH)	File	Same as above.	LL0703PA013MST.008_R0 [DIRS 179855]
B2_DHLW_REP_P50H_PMA.ou	PREWAP output file for representative TH (DS T and RH)	File	Same as above.	LL0703PA037MST.019_R0 [DIRS 179989]
B2_DHLW_REP_P50L_PMA.ou	PREWAP output file for representative TH (DS T and RH)	File	Same as above.	LL0703PA036MST.018_R0 [DIRS 179986]
B2_DHLW_REP_P90_PMA.ou	PREWAP output file for representative TH (DS T and RH)	File	Same as above.	LL0703PA014MST.009_R0 [DIRS 179856]
B2_DHLW_REP_P90H_PMA.ou	PREWAP output file for representative TH (DS T and RH)	File	Same as above.	LL0703PA016MST.011_R0 [DIRS 179858]

Table C4-2. Input Parameters Added for the PMA (Continued)

Parameter Name	Description	Parameter Distribution	Rationale for Inclusion	Data Source
EBS Thermal-Hydrology Parameters (Continued)				
B2_DHLW_REP_P90L_PMA.ou	PREWAP output file for representative TH (DS T and RH)	File	Same as above.	LL0703PA038MST.020_R0 [DIRS 179992]
B3_CSNF_REP_P10_PMA.ou	PREWAP output file for representative TH (DS T and RH)	File	Same as above.	LL0703PA011MST.006_R0 [DIRS 179853]
B3_CSNF_REP_P10H_PMA.ou	PREWAP output file for representative TH (DS T and RH)	File	Same as above.	LL0703PA017MST.012_R0 [DIRS 179859]
B3_CSNF_REP_P10L_PMA.ou	PREWAP output file for representative TH (DS T and RH)	File	Same as above.	LL0703PA015MST.010_R0 [DIRS 179857]
B3_CSNF_REP_P30_PMA.ou	PREWAP output file for representative TH (DS T and RH)	File	Same as above.	LL0703PA012MST.007_R0 [DIRS 179854]
B3_CSNF_REP_P30H_PMA.ou	PREWAP output file for representative TH (DS T and RH)	File	Same as above.	LL0703PA035MST.017_R0 [DIRS 179985]
B3_CSNF_REP_P30L_PMA.ou	PREWAP output file for representative TH (DS T and RH)	File	Same as above.	LL0703PA034MST.016_R0 [DIRS 179982]
B3_CSNF_REP_P50_PMA.ou	PREWAP output file for representative TH (DS T and RH)	File	Same as above.	LL0703PA013MST.008_R0 [DIRS 179855]
B3_CSNF_REP_P50H_PMA.ou	PREWAP output file for representative TH (DS T and RH)	File	Same as above.	LL0703PA037MST.019_R0 [DIRS 179989]
B3_CSNF_REP_P50L_PMA.ou	PREWAP output file for representative TH (DS T and RH)	File	Same as above.	LL0703PA036MST.018_R0 [DIRS 179986]
B3_CSNF_REP_P90_PMA.ou	PREWAP output file for representative TH (DS T and RH)	File	Same as above.	LL0703PA014MST.009_R0 [DIRS 179856]
B3_CSNF_REP_P90H_PMA.ou	PREWAP output file for representative TH (DS T and RH)	File	Same as above.	LL0703PA016MST.011_R0 [DIRS 179858]
B3_CSNF_REP_P90L_PMA.ou	PREWAP output file for representative TH (DS T and RH)	File	Same as above.	LL0703PA038MST.020_R0 [DIRS 179992]
B3_DHLW_REP_P10_PMA.ou	PREWAP output file for representative TH (DS T and RH)	File	Same as above.	LL0703PA011MST.006_R0 [DIRS 179853]
B3_DHLW_REP_P10H_PMA.ou	PREWAP output file for representative TH (DS T and RH)	File	Same as above.	LL0703PA017MST.012_R0 [DIRS 179859]
B3_DHLW_REP_P10L_PMA.ou	PREWAP output file for representative TH (DS T and RH)	File	Same as above.	LL0703PA015MST.010_R0 [DIRS 179857]

Table C4-2. Input Parameters Added for the PMA (Continued)

Parameter Name	Description	Parameter Distribution	Rationale for Inclusion	Data Source
EBS Thermal-Hydrology Parameters (Continued)				
B3_DHLW_REP_P30_PMA .ou;	PREWAP output file for representative TH (DS T and RH)	File	Same as above.	LL0703PA012MST.007_R0 [DIRS 179854]
B3_DHLW_REP_P30H_P MA.ou	PREWAP output file for representative TH (DS T and RH)	File	Same as above.	LL0703PA035MST.017_R0 [DIRS 179985]
B3_DHLW_REP_P30L_PM A.ou	PREWAP output file for representative TH (DS T and RH)	File	Same as above.	LL0703PA034MST.016_R0 [DIRS 179982]
B3_DHLW_REP_P50_PMA .ou	PREWAP output file for representative TH (DS T and RH)	File	Same as above.	LL0703PA013MST.008_R0 [DIRS 179855]
B3_DHLW_REP_P50H_P MA.ou	PREWAP output file for representative TH (DS T and RH)	File	Same as above.	LL0703PA037MST.019_R0 [DIRS 179989]
B3_DHLW_REP_P50L_PM A.ou	PREWAP output file for representative TH (DS T and RH)	File	Same as above.	LL0703PA036MST.018_R0 [DIRS 179986]
B3_DHLW_REP_P90_PMA .ou	PREWAP output file for representative TH (DS T and RH)	File	Same as above.	LL0703PA014MST.009_R0 [DIRS 179856]
B3_DHLW_REP_P90H_P MA.ou	PREWAP output file for representative TH (DS T and RH)	File	Same as above.	LL0703PA016MST.011_R0 [DIRS 179858]
B3_DHLW_REP_P90L_PM A.ou	PREWAP output file for representative TH (DS T and RH)	File	Same as above.	LL0703PA038MST.020_R0 [DIRS 179992]
B4_CSNF_REP_P10_PMA .ou	PREWAP output file for representative TH (DS T and RH)	File	Same as above.	LL0703PA011MST.006_R0 [DIRS 179853]
B4_CSNF_REP_P10H_PM A.ou	PREWAP output file for representative TH (DS T and RH)	File	Same as above.	LL0703PA017MST.012_R0 [DIRS 179859]
B4_CSNF_REP_P10L_PM A.ou	PREWAP output file for representative TH (DS T and RH)	File	Same as above.	LL0703PA015MST.010_R0 [DIRS 179857]
B4_CSNF_REP_P30_PMA .ou	PREWAP output file for representative TH (DS T and RH)	File	Same as above.	LL0703PA012MST.007_R0 [DIRS 179854]
B4_CSNF_REP_P30H_PM A.ou	PREWAP output file for representative TH (DS T and RH)	File	Same as above.	LL0703PA035MST.017_R0 [DIRS 179985]
B4_CSNF_REP_P30L_PM A.ou	PREWAP output file for representative TH (DS T and RH)	File	Same as above.	LL0703PA034MST.016_R0 [DIRS 179982]
B4_CSNF_REP_P50_PMA .ou	PREWAP output file for representative TH (DS T and RH)	File	Same as above.	LL0703PA013MST.008_R0 [DIRS 179855]

Table C4-2. Input Parameters Added for the PMA (Continued)

Parameter Name	Description	Parameter Distribution	Rationale for Inclusion	Data Source
EBS Thermal-Hydrology Parameters (Continued)				
B4_CSNF_REP_P50H_PMA.ou	PREWAP output file for representative TH (DS T and RH)	File	Same as above.	LL0703PA037MST.019_R0 [DIRS 179989]
B4_CSNF_REP_P50L_PMA.ou	PREWAP output file for representative TH (DS T and RH)	File	Same as above.	LL0703PA036MST.018_R0 [DIRS 179986]
B4_CSNF_REP_P90_PMA.ou	PREWAP output file for representative TH (DS T and RH)	File	Same as above.	LL0703PA014MST.009_R0 [DIRS 179856]
B4_CSNF_REP_P90H_PMA.ou	PREWAP output file for representative TH (DS T and RH)	File	Same as above.	LL0703PA016MST.011_R0 [DIRS 179858]
B4_CSNF_REP_P90L_PMA.ou	PREWAP output file for representative TH (DS T and RH)	File	Same as above.	LL0703PA038MST.020_R0 [DIRS 179992]
B4_DHLW_REP_P10_PMA.ou	PREWAP output file for representative TH (DS T and RH)	File	Same as above.	LL0703PA011MST.006_R0 [DIRS 179853]
B4_DHLW_REP_P10H_PMA.ou	PREWAP output file for representative TH (DS T and RH)	File	Same as above.	LL0703PA017MST.012_R0 [DIRS 179859]
B4_DHLW_REP_P10L_PMA.ou	PREWAP output file for representative TH (DS T and RH)	File	Same as above.	LL0703PA015MST.010_R0 [DIRS 179857]
B4_DHLW_REP_P30_PMA.ou	PREWAP output file for representative TH (DS T and RH)	File	Same as above.	LL0703PA012MST.007_R0 [DIRS 179854]
B4_DHLW_REP_P30H_PMA.ou	PREWAP output file for representative TH (DS T and RH)	File	Same as above.	LL0703PA035MST.017_R0 [DIRS 179985]
B4_DHLW_REP_P30L_PMA.ou	PREWAP output file for representative TH (DS T and RH)	File	Same as above.	LL0703PA034MST.016_R0 [DIRS 179982]
B4_DHLW_REP_P50_PMA.ou	PREWAP output file for representative TH (DS T and RH)	File	Same as above.	LL0703PA013MST.008_R0 [DIRS 179855]
B4_DHLW_REP_P50H_PMA.ou	PREWAP output file for representative TH (DS T and RH)	File	Same as above.	LL0703PA037MST.019_R0 [DIRS 179989]
B4_DHLW_REP_P50L_PMA.ou	PREWAP output file for representative TH (DS T and RH)	File	Same as above.	LL0703PA036MST.018_R0 [DIRS 179986]
B4_DHLW_REP_P90_PMA.ou	PREWAP output file for representative TH (DS T and RH)	File	Same as above.	LL0703PA014MST.009_R0 [DIRS 179856]
B4_DHLW_REP_P90H_PMA.ou	PREWAP output file for representative TH (DS T and RH)	File	Same as above.	LL0703PA016MST.011_R0 [DIRS 179858]

Table C4-2. Input Parameters Added for the PMA (Continued)

Parameter Name	Description	Parameter Distribution	Rationale for Inclusion	Data Source
EBS Thermal-Hydrology Parameters (Continued)				
B4_DHLW_REP_P90L_PMA.ou	PREWAP output file for representative TH (DS T and RH)	File	Same as above.	LL0703PA038MST.020_R0 [DIRS 179992]
B5_CSNF_REP_P10_PMA.ou	PREWAP output file for representative TH (DS T and RH)	File	Same as above.	LL0703PA011MST.006_R0 [DIRS 179853]
B5_CSNF_REP_P10H_PMA.ou	PREWAP output file for representative TH (DS T and RH)	File	Same as above.	LL0703PA017MST.012_R0 [DIRS 179859]
B5_CSNF_REP_P10L_PMA.ou	PREWAP output file for representative TH (DS T and RH)	File	Same as above.	LL0703PA015MST.010_R0 [DIRS 179857]
B5_CSNF_REP_P30_PMA.ou	PREWAP output file for representative TH (DS T and RH)	File	Same as above.	LL0703PA012MST.007_R0 [DIRS 179854]
B5_CSNF_REP_P30H_PMA.ou	PREWAP output file for representative TH (DS T and RH)	File	Same as above.	LL0703PA035MST.017_R0 [DIRS 179985]
B5_CSNF_REP_P30L_PMA.ou	PREWAP output file for representative TH (DS T and RH)	File	Same as above.	LL0703PA034MST.016_R0 [DIRS 179982]
B5_CSNF_REP_P50_PMA.ou;	PREWAP output file for representative TH (DS T and RH)	File	Same as above.	LL0703PA013MST.008_R0 [DIRS 179855]
B5_CSNF_REP_P50H_PMA.ou	PREWAP output file for representative TH (DS T and RH)	File	Same as above.	LL0703PA037MST.019_R0 [DIRS 179989]
B5_CSNF_REP_P50L_PMA.ou	PREWAP output file for representative TH (DS T and RH)	File	Same as above.	LL0703PA036MST.018_R0 [DIRS 179986]
B5_CSNF_REP_P90_PMA.ou	PREWAP output file for representative TH (DS T and RH)	File	Same as above.	LL0703PA014MST.009_R0 [DIRS 179856]
B5_CSNF_REP_P90H_PMA.ou	PREWAP output file for representative TH (DS T and RH)	File	Same as above.	LL0703PA016MST.011_R0 [DIRS 179858]
B5_CSNF_REP_P90L_PMA.ou	PREWAP output file for representative TH (DS T and RH)	File	Same as above.	LL0703PA038MST.020_R0 [DIRS 179992]
B5_DHLW_REP_P10_PMA.ou	PREWAP output file for representative TH (DS T and RH)	File	Same as above.	LL0703PA011MST.006_R0 [DIRS 179853]
B5_DHLW_REP_P10H_PMA.ou	PREWAP output file for representative TH (DS T and RH)	File	Same as above.	LL0703PA017MST.012_R0 [DIRS 179859]
B5_DHLW_REP_P10L_PMA.ou	PREWAP output file for representative TH (DS T and RH)	File	Same as above.	LL0703PA015MST.010_R0 [DIRS 179857]

Table C4-2. Input Parameters Added for the PMA (Continued)

Parameter Name	Description	Parameter Distribution	Rationale for Inclusion	Data Source
EBS Thermal-Hydrology Parameters (Continued)				
B5_DHLW_REP_P30_PMA.ou	PREWAP output file for representative TH (DS T and RH)	File	Same as above.	LL0703PA012MST.007_R0 [DIRS 179854]
B5_DHLW_REP_P30H_PMA.ou	PREWAP output file for representative TH (DS T and RH)	File	Same as above.	LL0703PA035MST.017_R0 [DIRS 179985]
B5_DHLW_REP_P30L_PMA.ou	PREWAP output file for representative TH (DS T and RH)	File	Same as above.	LL0703PA034MST.016_R0 [DIRS 179982]
B5_DHLW_REP_P50_PMA.ou	PREWAP output file for representative TH (DS T and RH)	File	Same as above.	LL0703PA013MST.008_R0 [DIRS 179855]
B5_DHLW_REP_P50H_PMA.ou	PREWAP output file for representative TH (DS T and RH)	File	Same as above.	LL0703PA037MST.019_R0 [DIRS 179989]
B5_DHLW_REP_P50L_PMA.ou	PREWAP output file for representative TH (DS T and RH)	File	Same as above.	LL0703PA036MST.018_R0 [DIRS 179986]
B5_DHLW_REP_P90_PMA.ou	PREWAP output file for representative TH (DS T and RH)	File	Same as above.	LL0703PA014MST.009_R0 [DIRS 179856]
B5_DHLW_REP_P90H_PMA.ou	PREWAP output file for representative TH (DS T and RH)	File	Same as above.	LL0703PA016MST.011_R0 [DIRS 179858]
B5_DHLW_REP_P90H_PMA.ou	PREWAP output file for representative TH (DS T and RH)	File	Same as above.	LL0703PA038MST.020_R0 [DIRS 179992]
MFCP_LA_Input.txt	Simulation Settings: Master File Control Program support file.	File	Same as above.	Corroborative DTN: MO0708TSPAPROC.000_R0 [DIRS 182979]
pass_table_master_PMA.in	List of TH files for DS temperature and RH.	File	Same as above.	Corroborative DTN: MO0708TSPAPROC.000_R0 [DIRS 182979]
Drift Scale UZ Flow Parameters				
SMPA_C_PMA.dat	Seepage model input for performance assessment used for PMA collapsed-drift look-up table.	File	Necessary to implement the PMA seepage model.	Corroborative DTN: LB0704PASEEP02.001_R1 [DIRS 181093]

Table C4-2. Input Parameters Added for the PMA (Continued)

Parameter Name	Description	Parameter Distribution	Rationale for Inclusion	Data Source
EBS Flow and Transport Parameters				
WB_Campbell_b_a	Campbell parameter.	Uniform [3.5, 5]	Necessary for developing a more realistic water balance model.	Corroborative DTN: SN0704PMAWBCAL.001_R 2 [DIRS 182335]
WB_Ionic_strength_seep_a	Ionic strength of seepage water.	Uniform [0.001 mol/kg, 0.02 mol/kg]	Necessary for developing a more realistic water balance model.	Corroborative DTN: SN0704PMAWBCAL.001_R 2 [DIRS 182335]
WB_Mean_Particle_Diam_a	Mean particle diameter for water balance model.	Log-uniform [0.001 mm, 1 mm]	Necessary for developing a more realistic water balance model.	Corroborative DTN: SN0704PMAWBCAL.001_R 2 [DIRS 182335]
WB_Permeability_CP_a	Corrosion product permeability.	Log-uniform [1E-014 m^2, 1E-010 m^2]	Necessary for developing a more realistic water balance model.	Corroborative DTN: SN0704PMAWBCAL.001_R 2 [DIRS 182335]
WB_Porosity_Deg_Prod_a	Porosity of the degradation product.	Uniform [0.35, 0.5]	Necessary for developing a more realistic water balance model.	Corroborative DTN: SN0704PMAWBCAL.001_R 2 [DIRS 182335]
WB_Salt_CDSP_a	Moles of salt released from 1 kg HLW degraded.	Uniform [0.062 mol/kg, 1.078 mol/kg]	Necessary for developing a more realistic water balance model.	Corroborative DTN: SN0704PMAWBCAL.001_R 2 [DIRS 182335]
WB_Salt_SS_a	Moles of salt released from 1 kg SS degraded.	Uniform [0.062 mol/kg, 0.133 mol/kg]	Necessary for developing a more realistic water balance model.	Corroborative DTN: SN0704PMAWBCAL.001_R 2 [DIRS 182335]
WB_Water_Film_Thickness_a	Water film thickness.	Uniform [0.1 mm, 3 mm]	Necessary for developing a more realistic water balance model.	Corroborative DTN: SN0704PMAWBCAL.001_R 2 [DIRS 182335]
WB_Alpha_Potential	Alpha potential.	0.002332021	Necessary for developing a more realistic water balance model.	Corroborative DTN: SN0704PMAWBCAL.001_R 2 [DIRS 182335]
WB_Beta_Potential	Beta potential.	0.023762087	Necessary for developing a more realistic water balance model.	Corroborative DTN: SN0704PMAWBCAL.001_R 2 [DIRS 182335]
WB_Bulk_Volume_DSNF	Initial bulk volume of the DSNF waste form.	0.749727 m^3	Necessary for developing a more realistic water balance model.	Corroborative DTN: SN0704PMAWBCAL.001_R 2 [DIRS.182335]

Table C4-2. Input Parameters Added for the PMA (Continued)

Parameter Name	Description	Parameter Distribution	Rationale for Inclusion	Data Source
EBS Flow and Transport Parameters (Continued)				
WB_Density_CDSP	Density of CDSP.	3.34 g/cm^3	Necessary for developing a more realistic water balance model.	Corroborative DTN: SN0704PMAWBCAL.001_R 2 [DIRS.182335]
WB_Density_CSNF	Density of CSNF.	10.08 g/cm^3	Necessary for developing a more realistic water balance model.	Corroborative DTN: SN0704PMAWBCAL.001_R 2 [DIRS.182335]
WB_Density_Steel	Density of steel.	7.98 g/cm^3	Necessary for developing a more realistic water balance model.	Corroborative DTN: SN0704PMAWBCAL.001_R 2 [DIRS.182335]
WB_Density_water	Density of liquid water.	0.99707 g/cm^3	Necessary for developing a more realistic water balance model.	Corroborative DTN: SN0704PMAWBCAL.001_R 2 [DIRS.182335]
WB_Initial_Void_Vol_CDSP_WP	Initial void volume in CDSP waste package.	8.49117 m^3	Necessary for developing a more realistic water balance model.	Corroborative DTN: SN0704PMAWBCAL.001_R 2 [DIRS.182335]
WB_Initial_Void_Vol_CSNF_WP	Initial void volume in CSNF waste package.	6.723077 m^3	Necessary for developing a more realistic water balance model.	Corroborative DTN: SN0704PMAWBCAL.001_R 2 [DIRS.182335]
WB_Mol_Wt_Water	Molecular weight of water.	18.01534 g/mol	Necessary for developing a more realistic water balance model.	Corroborative DTN: SN0704PMAWBCAL.001_R 2 [DIRS.182335]
WB_Molar_Vol_Water	Molar volume of water.	1.80683e-005 m^3/mol	Necessary for developing a more realistic water balance model.	Corroborative DTN: SN0704PMAWBCAL.001_R 2 [DIRS.182335]
WB_Num_Active_Species	Number of osmotically active species.	2	Necessary for developing a more realistic water balance model.	Corroborative DTN: SN0704PMAWBCAL.001_R 2 [DIRS.182335]
WB_Radius_WP_CDSP	CDSP waste package radius.	1.06 m	Necessary for developing a more realistic water balance model.	Corroborative DTN: SN0704PMAWBCAL.001_R 2 [DIRS.182335]
WB_Radius_WP_CSNF	CSNF waste package radius.	0.9408 m	Necessary for developing a more realistic water balance model.	Corroborative DTN: SN0704PMAWBCAL.001_R 2 [DIRS 182335]

Table C4-2. Input Parameters Added for the PMA (Continued)

Parameter Name	Description	Parameter Distribution	Rationale for Inclusion	Data Source
EBS Flow and Transport Parameters (Continued)				
WB_Ref_Temp	Waste package reference temperature.	25 C	Necessary for developing a more realistic water balance model.	Corroborative DTN: SN0704PMAWBCAL.001_R 2 [DIRS 182335]
WB_Residual_water_conte nt	Residual water content in degradation products.	0.05	Necessary for developing a more realistic water balance model.	Corroborative DTN: SN0704PMAWBCAL.001_R 2 [DIRS 182335]
WB_Salt_CSNF	Moles of salt released from 1 kg CSNF.	0.034 mol/kg	Necessary for developing a more realistic water balance model.	Corroborative DTN: SN0704PMAWBCAL.001_R 2 [DIRS 182335]
WB_Vol_CP_Per_Kg_SS	Volume of corrosion products from 1 kg stainless steel.	0.00033 m^3/kg	Necessary for developing a more realistic water balance model.	Corroborative DTN: SN0704PMAWBCAL.001_R 2 [DIRS 182335]
WB_Vol_Degrad_prod_Per _Kg_CDSP	Solid volume produced from 1 kg of CDSP degraded.	0.00059 m^3/kg	Necessary for developing a more realistic water balance model.	Corroborative DTN: SN0704PMAWBCAL.001_R 2 [DIRS 182335]
WB_Vol_Degrad_prod_Per _Kg_CSNF	Solid volume produced from 1 kg of CSNF degraded.	0.000239 m^3/kg	Necessary for developing a more realistic water balance model.	Corroborative DTN: SN0704PMAWBCAL.001_R 2 [DIRS 182335]
WB_Water_Consum_Per_ Kg_CDSP	Moles of water consumed per kg CDSP degraded.	10.52 mol/kg	Necessary for developing a more realistic water balance model	Corroborative DTN: SN0704PMAWBCAL.001_R 2 [DIRS 182335]
WB_Water_Consum_Per_ Kg_CSNF	Moles of water consumed per kg CSNF degraded.	7.23 mol/kg	Necessary for developing a more realistic water balance model.	Corroborative DTN: SN0704PMAWBCAL.001_R 2 [DIRS182335]
WB_Water_Consum_Per_ Kg_SS	Moles of water consumed per kg stainless steel degraded.	14.15 mol/kg	Necessary for developing a more realistic water balance model.	Corroborative DTN: SN0704PMAWBCAL.001_R 2 [DIRS 182335]

Table C4-2. Input Parameters Added for the PMA (Continued)

Parameter Name	Description	Parameter Distribution	Rationale for Inclusion	Data Source
Waste Package and Drip Shield Degradation Parameters				
Gp1_RH_Threshold_table	RH threshold for fluoride activity.	Lookup Table (1D)	DS corrosion is a function of F ion concentration which was correlated to RH for use in selecting the DS corrosion rates.	Corroborative DTN: MO0708TSPAPROC.000_R0 [DIRS 182979]
Gp2_RH_Threshold_table	RH threshold for fluoride activity.	Lookup Table (1D)	Same as above.	Corroborative DTN: MO0708TSPAPROC.000_R0 [DIRS 182979]
Gp3_RH_Threshold_table	RH threshold for fluoride activity.	Lookup Table (1D)	Same as above.	Corroborative DTN: MO0708TSPAPROC.000_R0 [DIRS 182979]
Gp4_RH_Threshold_table	RH threshold for fluoride activity. f_WP_failed_area_EF_DS_PMA_a	Lookup Table (1D)	Same as above.	Corroborative DTN: MO0708TSPAPROC.000_R0 [DIRS 182979]
f_WP_failed_area_EF_DS_PMA_a	Fraction of waste package area failed by localized corrosion in the early failed drip shield modeling case.	Log-Uniform [0.0005, 1]	Used ACM for localized corrosion failure area provided in *General Corrosion and Localized Corrosion of Waste Package Outer Barrier*, ANL-EBS-MD-000003 REV 03 [DIRS 178519].	ANL-EBS-MD-000003 REV 03 [DIRS 178519]
WAP_file	List of filenames for GoldSim-WAPDEG file transfer.	File	Necessary to for Weight Loss data based corrosion model.	Corroborative DTN: MO0708TSPAPROC.000_R0 [DIRS 182979]
WDlnR_ASC_WL_cdf	CDF for the natural logarithm of the GC rate for Alloy 22 (average patch) using the weight-loss data.	File	Same as above.	Corroborative DTN: MO0708TSPAPROC.000_R0 [DIRS 182979]
WDlnR_ESC_WL_cdf	CDF for the natural logarithm of the GC rate for Alloy 22 (extreme patch) using the weight-loss data.	File	Same as above.	Corroborative DTN: MO0708TSPAPROC.000_R0 [DIRS 182979]
Stress_Thresh_SCC_PMA_a	Distribution for residual stress threshold.	Uniform [351, 368.55]	Necessary to implement less conservative threshold for stress corrosion cracking.	ANL-EBS-MD-000005 Rev 04 [DIRS 181953]

Table C4-2. Input Parameters Added for the PMA (Continued)

Parameter Name	Description	Parameter Distribution	Rationale for Inclusion	Data Source
Waste Package and Drip Shield Degradation Parameters (Continued)				
Initial_Rod_Failures_PMA_a	Fraction of CSNF Zircaloy-clad fuel rods that are failed upon receipt to the repository (PMA model).	Log-Uniform [0.0001, 0.01]	Necessary to implement cladding credit.	MO0411SPACLDDG.003_R1 [DIRS 180755]
Inven_SS	Fraction of CSNF fuel rods that are SS-Clad.	Constant Value [0.01]	Necessary to implement cladding credit.	MO0411SPACLDDG.003_R1 [DIRS 180755]
Frac_CSNF_Pkgs_SS_a	Fraction of CSNF Waste Packages that contain SS-Clad fuel.	Log-Uniform [0.01, 0.02]	Necessary to implement cladding credit.	MO0702PAFRACSS.000_R1 [DIRS 181588]
HLW_Fast_Fraction_a	Fraction of glass waste form that dissolves at the forward reaction rate.	Triangular [0.0033, 0.011, 0.033]	Necessary for developing a more realistic water balance model	Corroborative DTN: SN0704PMAGDEGM.001_R2 [DIRS 183955]
HLW_RA_final_a	Final reaction affinity.	Log-triangular [1E-005, 0.0005, 0.01]	Necessary for developing a more realistic water balance model	Corroborative DTN: SN0704PMAGDEGM.001_R2 [DIRS 183955]
HLW_k0	Intrinsic glass dissolution rate.	10,000,000 $g/m^2/d$	Necessary for developing a more realistic water balance model	Corroborative DTN: SN0704PMAGDEGM.001_R2 [DIRS 183955]
Log_Specific_SA_CSNF_PMA_a	Log of the specific surface area for CSNF.	Triangular [-7.3, -7.3, -6.7]	Necessary for developing a more realistic water balance model	Corroborative DTN: SN0707PMACSNFD.001_R0 [DIRS 183045]
Scaling_Fact_Long_Term_Diss_a	Scaling factor for long-term dissolution.	Uniform [3, 10]	Necessary for developing a more realistic water balance model	Corroborative DTN: SN0707PMACSNFD.001_R0 [DIRS 183045]
Scaling_Fact_Radiolysis_a	Scaling factor for changes in Radiolysis.	Uniform [5, 10]	Necessary for developing a more realistic water balance model	Corroborative DTN: SN0707PMACSNFD.001_R0 [DIRS 183045]
Np2O5_PMA_Eps	Uncertainty of Np_2O_5 solubility for PMA.	Triangular [-1, 0, 1]	New uncertainty ranges derived by comparison of model prediction with experimental data	Corroborative DTN: SN0704PMASOLUB.001_R1[DIRS 182787]
Np_Carbonate_PMA_Eps	Uncertainty of $NaNpO_2CO_3$ for PMA.	Normal [0, 0.25] truncated at +/- 2σ	New uncertainty ranges derived by comparison of model prediction with experimental data	Corroborative DTN: SN0704PMASOLUB.001_R1[DIRS 182787]

Table C4-2. Input Parameters Added for the PMA (Continued)

Parameter Name	Description	Parameter Distribution	Rationale for Inclusion	Data Source
Waste Package and Drip Shield Degradation Parameters (Continued)				
NpO2_PMA_Eps	Uncertainty of NpO_2 solubility for PMA.	Triangular [-1.07, 0, 1.07]	New uncertainty ranges derived by comparison of model prediction with experimental data.	Corroborative DTN: SN0704PMASOLUB.001_R1[DIRS 182787]
Pu_PMA_Eps_a	Uncertainty of Pu solubility model for PMA.	Normal [0, 0.79] truncated at +/- 1σ	New uncertainty ranges derived by comparison of model prediction with experimental data.	Corroborative DTN: SN0704PMASOLUB.001_R1[DIRS 182787]
U_schoepite_PMA_Eps	Uncertainty of schoepite solubility for PMA.	Triangular [-0.4, 0, 0.4]	New uncertainty ranges derived by comparison of model prediction with experimental data.	Corroborative DTN: SN0704PMASOLUB.001_R1[DIRS 182787]
U_Boltwoodite_PMA_Eps	Uncertainty of Na-boltwoodite solubility for PMA.	Triangular [-0.5, 0, 0.3]	New uncertainty ranges derived by comparison of model prediction with experimental data.	Corroborative DTN: SN0704PMASOLUB.001_R[DIRS 182787]
U_Carbonate_PMA_Eps	Uncertainty of $Na_4UO_2(CO_3)_3$ solubility for PMA.	Triangular [-0.3, 0, 0.3]	New uncertainty ranges derived by comparison of model prediction with experimental data.	Corroborative DTN: SN0704PMASOLUB.001_R1[DIRS 182787]
IPC_PMA_pH_2DHLW_HS_Choice	Record which random number to use for the dual triangular distribution of CDSP Cell 1a pH high-dripping.	Discrete [0.5, 1, 0.5,2]	Necessary for calculating more realistic in-package pH values.	Corroborative DTN: SN0704PMAIPCAB.001_R1 [DIRS 182602]
IPC_PMA_pH_2DHLW_HS_Rand_1_a	Sampling for the dual triangular distribution, 2DHLW, High-seepage.	Uniform [0,1]	Necessary for calculating more realistic in-package pH values.	Corroborative DTN: SN0704PMAIPCAB.001_R1 [DIRS 182602]
IPC_PMA_pH_2DHLW_HS_Rand_2_a	Sampling for the dual triangular distribution, 2DHLW, High-seepage.	Uniform [0,1]	Necessary for calculating more realistic in-package pH values.	Corroborative DTN: SN0704PMAIPCAB.001_R1 [DIRS 182602]

Table C4-2. Input Parameters Added for the PMA (Continued)

Parameter Name	Description	Parameter Distribution	Rationale for Inclusion	Data Source
Waste Form Degradation and Radionuclide Mobilization Parameter (Continued)				
IPC_PMA_pH_2DHLW_NS_Choice	Record which random number to use for the dual triangular distribution of CDSP Cell 1a pH no-dripping	Discrete [0.5, 1, 0.5,2]	Necessary for calculating more realistic in-package pH values	Corroborative DTN: SN0704PMAIPCAB.001_R1 [DIRS 182602]
IPC_PMA_pH_2DHLW_NS_Rand_1_a	Sampling for the dual triangular distribution, 2DHLW, Non-seepage	Uniform [0,1]	Necessary for calculating more realistic in-package pH values	Corroborative DTN: SN0704PMAIPCAB.001_R1 [DIRS 182602]
IPC_PMA_pH_2DHLW_NS_Rand_2_a	Sampling for the dual triangular distribution, 2DHLW, Non-seepage	Uniform [0,1]	Necessary for calculating more realistic in-package pH values	Corroborative DTN: SN0704PMAIPCAB.001_R1 [DIRS 182602]
IPC_PMA_pH_2MCO_HS_Choice	Record which random number to use for the dual triangular distribution of CDSP Cell 1b pH high-dripping	Discrete [0.5, 1, 0.5,2]	Necessary for calculating more realistic in-package pH values	Corroborative DTN: SN0704PMAIPCAB.001_R1 [DIRS 182602]
IPC_PMA_pH_2MCO_HS_Rand_1_a	Sampling for the dual triangular distribution, 2MCO, High-seepage	Uniform [0,1]	Necessary for calculating more realistic in-package pH values	Corroborative DTN: SN0704PMAIPCAB.001_R1 [DIRS 182602]
IPC_PMA_pH_2MCO_HS_Rand_2_a	Sampling for the dual triangular distribution, 2MCO, High-seepage	Uniform [0,1]	Necessary for calculating more realistic in-package pH values	Corroborative DTN: SN0704PMAIPCAB.001_R1 [DIRS 182602]
IPC_PMA_pH_2MCO_NS_Choice	Record which random number to use for the dual triangular distribution of CDSP Cell 1b pH no-dripping	Discrete [0.5, 1, 0.5,2]	Necessary for calculating more realistic in-package pH values	Corroborative DTN: SN0704PMAIPCAB.001_R1 [DIRS 182602]
IPC_PMA_pH_2MCO_NS_Rand_1_a	Sampling for the dual triangular distribution, 2MCO, Non-seepage	Uniform [0,1]	Necessary for calculating more realistic in-package pH values	Corroborative DTN: SN0704PMAIPCAB.001_R1 [DIRS 182602]
IPC_PMA_pH_2MCO_NS_Rand_2_a	Sampling for the dual triangular distribution, 2MCO, Non-seepage	Uniform [0,1]	Necessary for calculating more realistic in-package pH values	Corroborative DTN: SN0704PMAIPCAB.001_R1 [DIRS 182602]
IPC_PMA_pH_CSNF_HS_Choice	Record which random number to use for the dual triangular distribution of CSNF Cell 1 pH high-dripping	Discrete [0.5, 1, 0.5,2]	Necessary for calculating more realistic in-package pH values	Corroborative DTN: SN0704PMAIPCAB.001_R1 [DIRS 182602]
IPC_PMA_pH_CSNF_HS_Rand_1_a	Sampling for the dual triangular distribution, CSNF High-seepage	Uniform [0,1]	Necessary for calculating more realistic in-package pH values	Corroborative DTN: SN0704PMAIPCAB.001_R1 [DIRS 182602]

Table C4-2. Input Parameters Added for the PMA (Continued)

Parameter Name	Description	Parameter Distribution	Rationale for Inclusion	Data Source
Waste Form Degradation and Mobilization (Continued)				
IPC_PMA_pH_CSNF_HS_Rand_2_a	Sampling for the dual triangular distribution, CSNF, High-seepage	Uniform [0,1]	Necessary for calculating more realistic in-package pH values	Corroborative DTN: SN0704PMAIPCAB.001_R1 [DIRS 182602]
IPC_PMA_pH_CSNF_NS_Choice	Record which random number to use for the dual triangular distribution of CSNF Cell 1 pH no-dripping	Discrete [0.5, 1, 0.5,2]	Necessary for calculating more realistic in-package pH values	Corroborative DTN: SN0704PMAIPCAB.001_R1 [DIRS 182602]
IPC_PMA_pH_CSNF_NS_Rand_1_a	Sampling for the dual triangular distribution, CSNF, Non-seepage	Uniform [0,1]	Necessary for calculating more realistic in-package pH values	Corroborative DTN: SN0704PMAIPCAB.001_R1 [DIRS 182602]
IPC_PMA_pH_CSNF_NS_Rand_2_a	Sampling for the dual triangular distribution, CSNF, Non-seepage	Uniform [0,1]	Necessary for calculating more realistic in-package pH values	Corroborative DTN: SN0704PMAIPCAB.001_R1 [DIRS 182602]
Density_2DHLW_SS304L	Density of Stainless Steel 304L in CDSP Cell 1a	Single Value, 7.94 g/cm^3	Necessary for calculating more realistic pH values inside a waste package	SN0702PAIPC1CA.001_R2 [DIRS 180451]
Density_2MCO_SS304L	Density of Stainless Steel 304L in CDSP Cell 1b	Single Value, 7.94 g/cm^3	Necessary for calculating more realistic pH values inside a waste package	SN0702PAIPC1CA.001_R2 [DIRS 180451]
Density_CSNF_SS304B	Density of 304B SS, CSNF	Single Value, 7.81 g/cm^3	Necessary for calculating more realistic pH values inside a waste package	SN0702PAIPC1CA.001_R2 [DIRS 180451]
Density_CSNF	Density of CSNF	Single Value, 10080 kg/m^3	Necessary for calculating more realistic pH values inside a waste package	SN0702PAIPC1CA.001_R2 [DIRS 180451]
Density_HLW	Density of HLW*	Single Value, 3340 kg/m^3	Necessary for calculating more realistic pH values inside a waste package	SN0702PAIPC1CA.001_R2 [DIRS 180451]
Density_DSNF	Density of DSNF*	Single Value, 2300 kg/m^3	Necessary for calculating more realistic pH values inside a waste package	SN0702PAIPC1CA.001_R2 [DIRS 180451]
Initial_Mass_2DHLW_SS304	Initial mass of 304L SS, 2DHLW	Single Value, 1490 kg	Necessary for calculating more realistic pH values inside a waste package	SN0702PAIPC1CA.001_R2 [DIRS 180451]

Table C4-2. Input Parameters Added for the PMA (Continued)

Parameter Name	Description	Parameter Distribution	Rationale for Inclusion	Data Source
Waste Form Degradation and Mobilization (Continued)				
Initial_Mass_2MCO_SS304	Initial mass of 304L SS, 2MCO	Single Value, 4720 kg	Necessary for calculating more realistic pH values inside a waste package	SN0702PAIPC1CA.001_R2 [DIRS 180451]
Initial_Mass_CSNF_SS304	Initial mass of 304B4 SS, CSNF	Single Value, 38200 mol	Necessary for calculating more realistic pH values inside a waste package	SN0702PAIPC1CA.001_R2 [DIRS 180451]
Initial_Mass_CSNF_SS316	Initial mass of 316 SS, CSNF	Single Value, 61800 mol	Necessary for calculating more realistic pH values inside a waste package	SN0702PAIPC1CA.001_R2 [DIRS 180451]
Initial_Mass_CSNF	Initial mass of CSNF	Single Value, 110000 mol	Necessary for calculating more realistic pH values inside a waste package	SN0702PAIPC1CA.001_R2 [DIRS 180451]
Initial_Mass_DHLW	Initial mass of HLW	Single Value, 6910 kg	Necessary for calculating more realistic pH values inside a waste package	SN0702PAIPC1CA.001_R2 [DIRS 180451]
Initial_Mass_DSNF	Initial mass of DSNF	Single Value, 13700 kg	Necessary for calculating more realistic pH values inside a waste package	SN0702PAIPC1CA.001_R2 [DIRS 180451]
MW_304B_SS_CSNF	Molecular weight of 304B SS, CSNF	Single Value, 100 g/mol	Necessary for calculating more realistic pH values inside a waste package	ANL-EBS-MD-000037 Rev 04 AD 01, [DIRS 180506],Table 6.5[a]
MW_304L_SS_2DHLW	Molecular weight of 304L SS, 2DHLW	Single Value, 100 g/mol	Necessary for calculating more realistic pH values inside a waste package	ANL-EBS-MD-000037 Rev 04 AD 01, [DIRS 180506],Table 6.5[a]
MW_304L_SS_2MCO	Molecular weight of 304L SS, 2MCO	Single Value, 100 g/mol	Necessary for calculating more realistic pH values inside a waste package	ANL-EBS-MD-000037 Rev 04 AD 01, [DIRS 180506],Table 6.5[a]
MW_316_SS_CSNF	Molecular weight of 316 SS, CSNF	Single Value, 100 g/mol	Necessary for calculating more realistic pH values inside a waste package	ANL-EBS-MD-000037 Rev 04 AD 01, [DIRS 180506],Table 6.5[a]
MW_CSNF_WF	Molecular weight of CSNF	Single Value, 100 g/mol	Necessary for calculating more realistic pH values inside a waste package	ANL-EBS-MD-000037 Rev 04 AD 01, [DIRS 180506],Table 6.5[a]

Table C4-2. Input Parameters Added for the PMA (Continued)

Parameter Name	Description	Parameter Distribution	Rationale for Inclusion	Data Source
Waste Form Degradation and Mobilization (Continued)				
MW_DSNF_WF	Molecular weight of DSNF	Single Value, 100 g/mol	Necessary for calculating more realistic pH values inside a waste package	ANL-EBS-MD-000037 Rev 04 AD 01 , [DIRS 180506], Table 6.5[a]
MW_HLW_WF	Molecular weight HLW	Single Value, 100 g/mol	Necessary for calculating more realistic pH values inside a waste package	ANL-EBS-MD-000037 Rev 04 AD 01 , [DIRS 180506],Table 6.5[a]
Surface_Area_2DHLW	Surface area of DHLW	Single Value, 680000 cm^2	Necessary for calculating more realistic pH values inside a waste package	SN0702PAIPC1CA.001_R2 [DIRS 180451]
Surface_Area_2DHLW_SS304	Surface area of 304 SS, 2DHLW	Single Value, 357000 cm^2	Necessary for calculating more realistic pH values inside a waste package	SN0702PAIPC1CA.001_R2 [DIRS 180451]
Surface_Area_2MCO_SS304	Surface area of 304 SS, 2MCO	Single Value, 271000 cm^2	Necessary for calculating more realistic pH values inside a waste package	SN0702PAIPC1CA.001_R2 [DIRS 180451]
Surface_Area_CSNF	Surface area of CSNF	Single Value, 5030000 cm^2	Necessary for calculating more realistic pH values inside a waste package	SN0702PAIPC1CA.001_R2 [DIRS 180451]
Surface_Area_CSNF_SS304	Surface area of 304 SS, CSNF	Single Value, 881000 cm^2	Necessary for calculating more realistic pH values inside a waste package	SN0702PAIPC1CA.001_R2 [DIRS 180451]
Surface_Area_CSNF_SS316	Surface area of 316 SS, CSNF	Single Value, 1950000 cm^2	Necessary for calculating more realistic pH values inside a waste package	SN0702PAIPC1CA.001_R2 [DIRS 180451]
Surface_Area_2MCO	Surface area of DSNF	Single Value, 9580000 cm^2	Necessary for calculating more realistic pH values inside a waste package	SN0702PAIPC1CA.001_R2 [DIRS 180451]
Da_HF_log	Log Damkohler ratio of high-dripping conditions	Single value, -1 log mole	Necessary for calculating more realistic pH values inside a waste package	Corroborative DTN: SN0702PAIPCAB.001_R1 [DIRS 182602]
Da_NS_log	Log Damkohler ratio of no-dripping	Single value, 2 log mole	Necessary for calculating more realistic pH values inside a waste package	Corroborative DTN: SN0704PMAIPCAB.001_R1 [DIRS 182602]

Table C4-2. Input Parameters Added for the PMA (Continued)

Parameter Name	Description	Parameter Distribution	Rationale for Inclusion	Data Source
Waste Form Degradation and Mobilization (Continued)				
IPC_2DHLW_HiFlo_pH_Cond	pH look-up table under high flow conditions, condensated water, for CDSP Cell 1a	Lookup Table (2D)	Necessary for calculating more realistic pH values inside a waste package	Corroborative DTN: SN0704PMAIPCAB.001_R1 [DIRS 182602]
IPC_2DHLW_pCO2_Thresh_15	pCO_2 (=-log P $_{CO2}$) threshold value provides input to the DHLW pH routine.	Single Value, 1.5	Necessary for calculating more realistic pH values inside a waste package	Corroborative DTN: SN0704PMAIPCAB.001_R1 [DIRS 182602]
IPC_2DHLW_pCO2_Thresh_2	pCO_2 threshold value provides input to the DHLW pH routine.	Single Value, 2.0	Necessary for calculating more realistic pH values inside a waste package	Corroborative DTN: SN0704PMAIPCAB.001_R1 [DIRS 182602]
IPC_2DHLW_pCO2_Thresh_3	pCO_2 threshold value provides input to the DHLW pH routine.	Single Value, 3.0	Necessary for calculating more realistic pH values inside a waste package	Corroborative DTN: SN0704PMAIPCAB.001_R1 [DIRS 182602]
IPC_2DHLW_pCO2_Thresh_4	pCO_2 threshold value provides input to the DHLW pH routine.	Single Value, 4.0	Necessary for calculating more realistic pH values inside a waste package	Corroborative DTN: SN0704PMAIPCAB.001_R1 [DIRS 182602]
IPC_2MCO_HiFlo_pH_Cond	pH look-up table under high flow conditions, condensated water, for CDSP Cell 1b	Lookup Table (2D)	Necessary for calculating more realistic pH values inside a waste package	Corroborative DTN: SN0704PMAIPCAB.001_R1 [DIRS 182602]
IPC_2MCO_pCO2_Thresh_15	pCO_2 threshold value provides input to the MCO pH routine.	Single Value, 1.5	Necessary for calculating more realistic pH values inside a waste package	Corroborative DTN: SN0704PMAIPCAB.001_R1 [DIRS 182602]
IPC_2MCO_pCO2_Thresh_2	pCO_2 threshold value provides input to the MCO pH routine.	Single Value, 2.0	Necessary for calculating more realistic pH values inside a waste package	Corroborative DTN: SN0704PMAIPCAB.001_R1 [DIRS 182602]
IPC_2MCO_pCO2_Thresh_3	pCO_2 threshold value provides input to the MCO pH routine.	Single Value, 3.0	Necessary for calculating more realistic pH values inside a waste package	Corroborative DTN: SN0704PMAIPCAB.001_R1 [DIRS 182602]
IPC_2MCO_pCO2_Thresh_4	pCO_2 threshold value provides input to the MCO pH routine.	Single Value, 4.0	Necessary for calculating more realistic pH values inside a waste package	Corroborative DTN: SN0704PMAIPCAB.001_R1 [DIRS 182602]
IPC_CSNF_HiFlo_pH_Cond	pH look-up table under high flow conditions, condensated water, for CSNF Cell 1	Lookup Table (2D)	Necessary for calculating more realistic pH values inside a waste package	Corroborative DTN: SN0704PMAIPCAB.001_R1 [DIRS 182602]

Table C4-2. Input Parameters Added for the PMA (Continued)

Parameter Name	Description	Parameter Distribution	Rationale for Inclusion	Data Source
Waste Form Degradation and Mobilization (Continued)				
IPC_CSNF_pCO2_Thresh_15	pCO_2 threshold value provides input to the CSNF pH routine.	Single Value, 1.5	Necessary for calculating more realistic pH values inside a waste package	Corroborative DTN: SN0704PMAIPCAB.001_R1 [DIRS 182602]
IPC_CSNF_pCO2_Thresh_2	pCO_2 threshold value provides input to the CSNF pH routine.	Single Value, 2.0	Necessary for calculating more realistic pH values inside a waste package	Corroborative DTN: SN0704PMAIPCAB.001_R1 [DIRS 182602]
IPC_CSNF_pCO2_Thresh_3	pCO_2 threshold value provides input to the CSNF pH routine.	Single Value, 3.0	Necessary for calculating more realistic pH values inside a waste package	Corroborative DTN: SN0704PMAIPCAB.001_R1 [DIRS 182602]
IPC_CSNF_pCO2_Thresh_4	pCO_2 threshold value provides input to the CSNF pH routine.	Single Value, 4.0	Necessary for calculating more realistic pH values inside a waste package	Corroborative DTN: SN0704PMAIPCAB.001_R1 [DIRS 182602]
IPC_CSNF_Rsw_Thresh_A	Log Rsw (solid/water ratio) threshold value provides input to the CSNF pH routine.	Single Value, -2.0	Necessary for calculating more realistic pH values inside a waste package	Corroborative DTN: SN0704PMAIPCAB.001_R1 [DIRS 182602]
IPC_CSNF_Rsw_Thresh_B	Log Rsw threshold value provides input to the CSNF pH routine.	Single Value, -1.0	Necessary for calculating more realistic pH values inside a waste package	Corroborative DTN: SN0704PMAIPCAB.001_R1 [DIRS 182602]
IPC_CSNF_Rsw_Thresh_C	Log Rsw threshold value provides input to the CSNF pH routine.	Single Value, -0.522878745	Necessary for calculating more realistic pH values inside a waste package	Corroborative DTN: SN0704PMAIPCAB.001_R1 [DIRS 182602]
IPC_CSNF_Rsw_Thresh_D	Log Rsw threshold value provides input to the CSNF pH routine.	Single Value, 0	Necessary for calculating more realistic pH values inside a waste package	Corroborative DTN: SN0704PMAIPCAB.001_R1 [DIRS 182602]
IPC_CSNF_Rsw_Thresh_E	Log Rsw threshold value provides input to the CSNF pH routine.	Single Value, 0.1760912591	Necessary for calculating more realistic pH values inside a waste package	Corroborative DTN: SN0704PMAIPCAB.001_R1 [DIRS 182602]
IPC_CSNF_Rsw_Thresh_F	Log Rsw threshold value provides input to the CSNF pH routine.	Single Value, 0.3010299957	Necessary for calculating more realistic pH values inside a waste package	Corroborative DTN: SN0704PMAIPCAB.001_R1 [DIRS 182602]
IPC_CSNF_Rsw_Thresh_G	Log Rsw threshold value provides input to the CSNF pH routine.	Single Value, 0.4771212547	Necessary for calculating more realistic pH values inside a waste package	Corroborative DTN: SN0704PMAIPCAB.001_R1 [DIRS 182602]

Table C4-2. Input Parameters Added for the PMA (Continued)

Parameter Name	Description	Parameter Distribution	Rationale for Inclusion	Data Source
Waste Form Degradation and Mobilization (Continued)				
IPC_CSNF_Rsw_Thresh_H	Log Rsw hreshold value provides input to the CSNF pH routine.	Single Value, 1	Necessary for calculating more realistic pH values inside a waste package	Corroborative DTN: SN0704PMAIPCAB.001_R1 [DIRS 182602]
IPC_CSNF_Rsw_Thresh_I	Log Rsw hreshold value provides input to the CSNF pH routine.	Single Value, 2	Necessary for calculating more realistic pH values inside a waste package	Corroborative DTN: SN0704PMAIPCAB.001_R1 [DIRS 182602]
IPC_CSNF_pH_Rsw_15_A_LUT	LUT for CSNF pH.	Lookup Table (2D)	Necessary for calculating more realistic pH values inside a waste package	Corroborative DTN: SN0704PMAIPCAB.001_R1 [DIRS 182602]
IPC_CSNF_pH_Rsw_15_B_LUT	Same as above	Lookup Table (2D)	Necessary for calculating more realistic pH values inside a waste package	Corroborative DTN: SN0704PMAIPCAB.001_R1 [DIRS 182602]
IPC_CSNF_pH_Rsw_15_C_LUT	Same as above	Lookup Table (2D)	Necessary for calculating more realistic pH values inside a waste package	Corroborative DTN: SN0704PMAIPCAB.001_R1 [DIRS 182602]
IPC_CSNF_pH_Rsw_15_D_LUT	Same as above	Lookup Table (2D)	Necessary for calculating more realistic pH values inside a waste package	Corroborative DTN: SN0704PMAIPCAB.001_R1 [DIRS 182602]
IPC_CSNF_pH_Rsw_15_E_LUT	Same as above	Lookup Table (2D)	Necessary for calculating more realistic pH values inside a waste package	Corroborative DTN: SN0704PMAIPCAB.001_R1 [DIRS 182602]
IPC_CSNF_pH_Rsw_15_F_LUT	Same as above	Lookup Table (2D)	Necessary for calculating more realistic pH values inside a waste package	Corroborative DTN: SN0704PMAIPCAB.001_R1 [DIRS 182602]
IPC_CSNF_pH_Rsw_15_G_LUT	Same as above	Lookup Table (2D)	Necessary for calculating more realistic pH values inside a waste package	Corroborative DTN: SN0704PMAIPCAB.001_R1 [DIRS 182602]
IPC_CSNF_pH_Rsw_15_H_LUT	Same as above	Lookup Table (2D)	Necessary for calculating more realistic pH values inside a waste package	Corroborative DTN: SN0704PMAIPCAB.001_R1 [DIRS 182602]
IPC_CSNF_pH_Rsw_15_I_LUT	Same as above	Lookup Table (2D)	Necessary for calculating more realistic pH values inside a waste package	Corroborative DTN: SN0704PMAIPCAB.001_R1 [DIRS 182602]

Table C4-2. Input Parameters Added for the PMA (Continued)

Parameter Name	Description	Parameter Distribution	Rationale for Inclusion	Data Source
Waste Form Degradation and Mobilization (Continued)				
IPC_CSNF_pH_Rsw_2_A_LUT	Same as above	Lookup Table (2D)	Necessary for calculating more realistic pH values inside a waste package	Corroborative DTN: SN0704PMAIPCAB.001_R1 [DIRS 182602]
IPC_CSNF_pH_Rsw_2_B_LUT	Same as above	Lookup Table (2D)	Necessary for calculating more realistic pH values inside a waste package	Corroborative DTN: SN0704PMAIPCAB.001_R1 [DIRS 182602]
IPC_CSNF_pH_Rsw_2_C_LUT	Same as above	Lookup Table (2D)	Necessary for calculating more realistic pH values inside a waste package	Corroborative DTN: SN0704PMAIPCAB.001_R1 [DIRS 182602]
IPC_CSNF_pH_Rsw_2_D_LUT	Same as above	Lookup Table (2D)	Necessary for calculating more realistic pH values inside a waste package	Corroborative DTN: SN0704PMAIPCAB.001_R1 [DIRS 182602]
IPC_CSNF_pH_Rsw_2_E_LUT	Same as above	Lookup Table (2D)	Necessary for calculating more realistic pH values inside a waste package	Corroborative DTN: SN0704PMAIPCAB.001_R1 [DIRS 182602]
IPC_CSNF_pH_Rsw_2_F_LUT	Same as above	Lookup Table (2D)	Necessary for calculating more realistic pH values inside a waste package	Corroborative DTN: SN0704PMAIPCAB.001_R1 [DIRS 182602]
IPC_CSNF_pH_Rsw_2_G_LUT	Same as above	Lookup Table (2D)	Necessary for calculating more realistic pH values inside a waste package	Corroborative DTN: SN0704PMAIPCAB.001_R1 [DIRS 182602]
IPC_CSNF_pH_Rsw_2_H_LUT	Same as above	Lookup Table (2D)	Necessary for calculating more realistic pH values inside a waste package	Corroborative DTN: SN0704PMAIPCAB.001_R1 [DIRS 182602]
IPC_CSNF_pH_Rsw_2_I_LUT	Same as above	Lookup Table (2D)	Necessary for calculating more realistic pH values inside a waste package	Corroborative DTN: SN0704PMAIPCAB.001_R1 [DIRS 182602]
IPC_CSNF_pH_Rsw_3_A_LUT	Same as above	Lookup Table (2D)	Necessary for calculating more realistic pH values inside a waste package	Corroborative DTN: SN0704PMAIPCAB.001_R1 [DIRS 182602]
IPC_CSNF_pH_Rsw_3_B_LUT	Same as above	Lookup Table (2D)	Necessary for calculating more realistic pH values inside a waste package	Corroborative DTN: SN0704PMAIPCAB.001_R1 [DIRS 182602]

Table C4-2. Input Parameters Added for the PMA (Continued)

Parameter Name	Description	Parameter Distribution	Rationale for Inclusion	Data Source
Waste Form Degradation and Mobilization (Continued)				
IPC_CSNF_pH_Rsw_3_C_LUT	Same as above	Lookup Table (2D)	Necessary for calculating more realistic pH values inside a waste package	Corroborative DTN: SN0704PMAIPCAB.001_R1 [DIRS 182602]
IPC_CSNF_pH_Rsw_3_D_LUT	Same as above	Lookup Table (2D)	Necessary for calculating more realistic pH values inside a waste package	Corroborative DTN: SN0704PMAIPCAB.001_R1 [DIRS 182602]
IPC_CSNF_pH_Rsw_3_E_LUT	Same as above	Lookup Table (2D)	Necessary for calculating more realistic pH values inside a waste package	Corroborative DTN: SN0704PMAIPCAB.001_R1 [DIRS 182602]
IPC_CSNF_pH_Rsw_3_F_LUT	Same as above	Lookup Table (2D)	Necessary for calculating more realistic pH values inside a waste package	Corroborative DTN: SN0704PMAIPCAB.001_R1 [DIRS 182602]
IPC_CSNF_pH_Rsw_3_G_LUT	Same as above	Lookup Table (2D)	Necessary for calculating more realistic pH values inside a waste package	Corroborative DTN: SN0704PMAIPCAB.001_R1 [DIRS 182602]
IPC_CSNF_pH_Rsw_3_H_LUT	Same as above	Lookup Table (2D)	Necessary for calculating more realistic pH values inside a waste package	Corroborative DTN: SN0704PMAIPCAB.001_R1 [DIRS 182602]
IPC_CSNF_pH_Rsw_3_I_LUT	Same as above	Lookup Table (2D)	Necessary for calculating more realistic pH values inside a waste package	Corroborative DTN: SN0704PMAIPCAB.001_R1 [DIRS 182602]
IPC_CSNF_pH_Rsw_4_A_LUT	Same as above	Lookup Table (2D)	Necessary for calculating more realistic pH values inside a waste package	Corroborative DTN: SN0704PMAIPCAB.001_R1 [DIRS 182602]
IPC_CSNF_pH_Rsw_4_B_LUT	Same as above	Lookup Table (2D)	Necessary for calculating more realistic pH values inside a waste package	Corroborative DTN: SN0704PMAIPCAB.001_R1 [DIRS 182602]
IPC_CSNF_pH_Rsw_4_C_LUT	Same as above	Lookup Table (2D)	Necessary for calculating more realistic pH values inside a waste package	Corroborative DTN: SN0704PMAIPCAB.001_R1 [DIRS 182602]
IPC_CSNF_pH_Rsw_4_D_LUT	Same as above	Lookup Table (2D)	Necessary for calculating more realistic pH values inside a waste package	Corroborative DTN: SN0704PMAIPCAB.001_R1 [DIRS 182602]

Table C4-2. Input Parameters Added for the PMA (Continued)

Parameter Name	Description	Parameter Distribution	Rationale for Inclusion	Data Source
Waste Form Degradation and Mobilization (Continued)				
IPC_CSNF_pH_Rsw_4_E_LUT	Same as above	Lookup Table (2D)	Necessary for calculating more realistic pH values inside a waste package	Corroborative DTN: SN0704PMAIPCAB.001_R1 [DIRS 182602]
IPC_CSNF_pH_Rsw_4_F_LUT	Same as above	Lookup Table (2D)	Necessary for calculating more realistic pH values inside a waste package	Corroborative DTN: SN0704PMAIPCAB.001_R1 [DIRS 182602]
IPC_CSNF_pH_Rsw_4_G_LUT	Same as above	Lookup Table (2D)	Necessary for calculating more realistic pH values inside a waste package	Corroborative DTN: SN0704PMAIPCAB.001_R1 [DIRS 182602]
IPC_CSNF_pH_Rsw_4_H_LUT	Same as above	Lookup Table (2D)	Necessary for calculating more realistic pH values inside a waste package	Corroborative DTN: SN0704PMAIPCAB.001_R1 [DIRS 182602]
IPC_CSNF_pH_Rsw_4_I_LUT	Same as above	Lookup Table (2D)	Necessary for calculating more realistic pH values inside a waste package	Corroborative DTN: SN0704PMAIPCAB.001_R1 [DIRS 182602]
IPC_DHLW_Rsw_Thresh_A	Log Rsw threshold value provides input to the DHLW pH routine.	Single Value, -2.0	Necessary for calculating more realistic pH values inside a waste package	Corroborative DTN: SN0704PMAIPCAB.001_R1 [DIRS 182602]
IPC_DHLW_Rsw_Thresh_B	Log Rsw threshold value provides input to the DHLW pH routine.	Single Value, -1.0	Necessary for calculating more realistic pH values inside a waste package	Corroborative DTN: SN0704PMAIPCAB.001_R1 [DIRS 182602]
IPC_DHLW_Rsw_Thresh_C	Log Rsw threshold value provides input to the DHLW pH routine.	Single Value, 0	Necessary for calculating more realistic pH values inside a waste package	Corroborative DTN: SN0704PMAIPCAB.001_R1 [DIRS 182602]
IPC_DHLW_Rsw_Thresh_D	Log Rsw threshold value provides input to the DHLW pH routine.	Single Value, 1	Necessary for calculating more realistic pH values inside a waste package	Corroborative DTN: SN0704PMAIPCAB.001_R1 [DIRS 182602]
IPC_DHLW_Rsw_Thresh_E	Log Rsw threshold value provides input to the DHLW pH routine.	Single Value, 1.39794000867204	Necessary for calculating more realistic pH values inside a waste package	Corroborative DTN: SN0704PMAIPCAB.001_R1 [DIRS 182602]
IPC_DHLW_Rsw_Thresh_F	Log Rsw threshold value provides input to the DHLW pH routine.	Single Value, 1.6989700043	Necessary for calculating more realistic pH values inside a waste package	Corroborative DTN: SN0704PMAIPCAB.001_R1 [DIRS 182602]

Table C4-2. Input Parameters Added for the PMA (Continued)

Parameter Name	Description	Parameter Distribution	Rationale for Inclusion	Data Source
Waste Form Degradation and Mobilization (Continued)				
IPC_DHLW _Rsw_Thresh_G	Log Rsw threshold value provides input to the DHLW pH routine.	Single Value, 1.8750612634	Necessary for calculating more realistic pH values inside a waste package	Corroborative DTN: SN0704PMAIPCAB.001_R1 [DIRS 182602]
IPC_DHLW _Rsw_Thresh_H	Log Rsw threshold value provides input to the DHLW pH routine.	Single Value, 2	Necessary for calculating more realistic pH values inside a waste package	Corroborative DTN: SN0704PMAIPCAB.001_R1 [DIRS 182602]
IPC_DHLW _Rsw_Thresh_I	Log Rsw threshold value provides input to the DHLW pH routine.	Single Value, 3	Necessary for calculating more realistic pH values inside a waste package	Corroborative DTN: SN0704PMAIPCAB.001_R1 [DIRS 182602]
IPC_DHLW_pH_Rsw_15_A _LUT	LUT for 2DHLW pH	Lookup Table (2D)	Necessary for calculating more realistic pH values inside a waste package	Corroborative DTN: SN0704PMAIPCAB.001_R1 [DIRS 182602]
IPC_DHLW_pH_Rsw_15_B _LUT	Same as above	Lookup Table (2D)	Necessary for calculating more realistic pH values inside a waste package	Corroborative DTN: SN0704PMAIPCAB.001_R1 [DIRS 182602]
IPC_DHLW_pH_Rsw_15_ C_LUT	Same as above	Lookup Table (2D)	Necessary for calculating more realistic pH values inside a waste package	Corroborative DTN: SN0704PMAIPCAB.001_R1 [DIRS 182602]
IPC_DHLW_pH_Rsw_15_ D_LUT	Same as above	Lookup Table (2D)	Necessary for calculating more realistic pH values inside a waste package	Corroborative DTN: SN0704PMAIPCAB.001_R1 [DIRS 182602]
IPC_DHLW_pH_Rsw_15_E _LUT	Same as above	Lookup Table (2D)	Necessary for calculating more realistic pH values inside a waste package	Corroborative DTN: SN0704PMAIPCAB.001_R1 [DIRS 182602]
IPC_DHLW_pH_Rsw_15_F _LUT	Same as above	Lookup Table (2D)	Necessary for calculating more realistic pH values inside a waste package	Corroborative DTN: SN0704PMAIPCAB.001_R1 [DIRS 182602]
IPC_DHLW_pH_Rsw_15_ G_LUT	Same as above	Lookup Table (2D)	Necessary for calculating more realistic pH values inside a waste package	Corroborative DTN: SN0704PMAIPCAB.001_R1 [DIRS 182602]
IPC_DHLW_pH_Rsw_15_ H_LUT	Same as above	Lookup Table (2D)	Necessary for calculating more realistic pH values inside a waste package	Corroborative DTN: SN0704PMAIPCAB.001_R1 [DIRS 182602]

Table C4-2. Input Parameters Added for the PMA (Continued)

Parameter Name	Description	Parameter Distribution	Rationale for Inclusion	Data Source
Waste Form Degradation and Mobilization (Continued)				
IPC_DHLW_pH_Rsw_15_I_LUT	Same as above	Lookup Table (2D)	Necessary for calculating more realistic pH values inside a waste package	Corroborative DTN: SN0704PMAIPCAB.001_R1 [DIRS 182602]
IPC_DHLW_pH_Rsw_2_A_LUT	Same as above	Lookup Table (2D)	Necessary for calculating more realistic pH values inside a waste package	Corroborative DTN: SN0704PMAIPCAB.001_R1 [DIRS 182602]
IPC_DHLW_pH_Rsw_2_B_LUT	Same as above	Lookup Table (2D)	Necessary for calculating more realistic pH values inside a waste package	Corroborative DTN: SN0704PMAIPCAB.001_R1 [DIRS 182602]
IPC_DHLW_pH_Rsw_2_C_LUT	Same as above	Lookup Table (2D)	Necessary for calculating more realistic pH values inside a waste package	Corroborative DTN: SN0704PMAIPCAB.001_R1 [DIRS 182602]
IPC_DHLW_pH_Rsw_2_D_LUT	Same as above	Lookup Table (2D)	Necessary for calculating more realistic pH values inside a waste package	Corroborative DTN: SN0704PMAIPCAB.001_R1 [DIRS 182602]
IPC_DHLW_pH_Rsw_2_E_LUT	Same as above	Lookup Table (2D)	Necessary for calculating more realistic pH values inside a waste package	Corroborative DTN: SN0704PMAIPCAB.001_R1 [DIRS 182602]
IPC_DHLW_pH_Rsw_2_F_LUT	Same as above	Lookup Table (2D)	Necessary for calculating more realistic pH values inside a waste package	Corroborative DTN: SN0704PMAIPCAB.001_R1 [DIRS 182602]
IPC_DHLW_pH_Rsw_2_G_LUT	Same as above	Lookup Table (2D)	Necessary for calculating more realistic pH values inside a waste package	Corroborative DTN: SN0704PMAIPCAB.001_R1 [DIRS 182602]
IPC_DHLW_pH_Rsw_2_H_LUT	Same as above	Lookup Table (2D)	Necessary for calculating more realistic pH values inside a waste package	Corroborative DTN: SN0704PMAIPCAB.001_R1 [DIRS 182602]
IPC_DHLW_pH_Rsw_2_I_LUT	Same as above	Lookup Table (2D)	Necessary for calculating more realistic pH values inside a waste package	Corroborative DTN: SN0704PMAIPCAB.001_R1 [DIRS 182602]
IPC_DHLW_pH_Rsw_3_A_LUT	Same as above	Lookup Table (2D)	Necessary for calculating more realistic pH values inside a waste package	Corroborative DTN: SN0704PMAIPCAB.001_R1 [DIRS 182602]

Table C4-2. Input Parameters Added for the PMA (Continued)

Parameter Name	Description	Parameter Distribution	Rationale for Inclusion	Data Source
Waste Form Degradation and Mobilization (Continued)				
IPC_DHLW_pH_Rsw_3_B_LUT	Same as above	Lookup Table (2D)	Necessary for calculating more realistic pH values inside a waste package	Corroborative DTN: SN0704PMAIPCAB.001_R1 [DIRS 182602]
IPC_DHLW_pH_Rsw_3_C_LUT	Same as above	Lookup Table (2D)	Necessary for calculating more realistic pH values inside a waste package	Corroborative DTN: SN0704PMAIPCAB.001_R1 [DIRS 182602]
IPC_DHLW_pH_Rsw_3_D_LUT	Same as above	Lookup Table (2D)	Necessary for calculating more realistic pH values inside a waste package	Corroborative DTN: SN0704PMAIPCAB.001_R1 [DIRS 182602]
IPC_DHLW_pH_Rsw_3_E_LUT	Same as above	Lookup Table (2D)	Necessary for calculating more realistic pH values inside a waste package	Corroborative DTN: SN0704PMAIPCAB.001_R1 [DIRS 182602]
IPC_DHLW_pH_Rsw_3_F_LUT	Same as above	Lookup Table (2D)	Necessary for calculating more realistic pH values inside a waste package	Corroborative DTN: SN0704PMAIPCAB.001_R1 [DIRS 182602]
IPC_DHLW_pH_Rsw_3_G_LUT	Same as above	Lookup Table (2D)	Necessary for calculating more realistic pH values inside a waste package	Corroborative DTN: SN0704PMAIPCAB.001_R1 [DIRS 182602]
IPC_DHLW_pH_Rsw_3_H_LUT	Same as above	Lookup Table (2D)	Necessary for calculating more realistic pH values inside a waste package	Corroborative DTN: SN0704PMAIPCAB.001_R1 [DIRS 182602]
IPC_DHLW_pH_Rsw_3_I_LUT	Same as above	Lookup Table (2D)	Necessary for calculating more realistic pH values inside a waste package	Corroborative DTN: SN0704PMAIPCAB.001_R1 [DIRS 182602]
IPC_DHLW_pH_Rsw_4_A_LUT	Same as above	Lookup Table (2D)	Necessary for calculating more realistic pH values inside a waste package	Corroborative DTN: SN0704PMAIPCAB.001_R1 [DIRS 182602]
IPC_DHLW_pH_Rsw_4_B_LUT	Same as above	Lookup Table (2D)	Necessary for calculating more realistic pH values inside a waste package	Corroborative DTN: SN0704PMAIPCAB.001_R1 [DIRS 182602]
IPC_DHLW_pH_Rsw_4_C_LUT	Same as above	Lookup Table (2D)	Necessary for calculating more realistic pH values inside a waste package	Corroborative DTN: SN0704PMAIPCAB.001_R1 [DIRS 182602]

Table C4-2. Input Parameters Added for the PMA (Continued)

Parameter Name	Description	Parameter Distribution	Rationale for Inclusion	Data Source
Waste Form Degradation and Mobilization (Continued)				
IPC_DHLW_pH_Rsw_4_D_LUT	Same as above	Lookup Table (2D)	Necessary for calculating more realistic pH values inside a waste package	Corroborative DTN: SN0704PMAIPCAB.001_R1 [DIRS 182602]
IPC_DHLW_pH_Rsw_4_E_LUT	Same as above	Lookup Table (2D)	Necessary for calculating more realistic pH values inside a waste package	Corroborative DTN: SN0704PMAIPCAB.001_R1 [DIRS 182602]
IPC_DHLW_pH_Rsw_4_F_LUT	Same as above	Lookup Table (2D)	Necessary for calculating more realistic pH values inside a waste package	Corroborative DTN: SN0704PMAIPCAB.001_R1 [DIRS 182602]
IPC_DHLW_pH_Rsw_4_G_LUT	Same as above	Lookup Table (2D)	Necessary for calculating more realistic pH values inside a waste package	Corroborative DTN: SN0704PMAIPCAB.001_R1 [DIRS 182602]
IPC_DHLW_pH_Rsw_4_H_LUT	Same as above	Lookup Table (2D)	Necessary for calculating more realistic pH values inside a waste package	Corroborative DTN: SN0704PMAIPCAB.001_R1 [DIRS 182602]
IPC_DHLW_pH_Rsw_4_I_LUT	Same as above	Lookup Table (2D)	Necessary for calculating more realistic pH values inside a waste package	Corroborative DTN: SN0704PMAIPCAB.001_R1 [DIRS 182602]
IPC_MCO_Rsw_Thresh_A	Log Rsw threshold value provides input to the MCO pH routine.	Single Value, -7.0	Necessary for calculating more realistic pH values inside a waste package	Corroborative DTN: SN0704PMAIPCAB.001_R1 [DIRS 182602]
IPC_MCO _Rsw_Thresh_B	Log Rsw threshold value provides input to the MCO pH routine.	Single Value, -6.0	Necessary for calculating more realistic pH values inside a waste package	Corroborative DTN: SN0704PMAIPCAB.001_R1 [DIRS 182602]
IPC_MCO _Rsw_Thresh_C	Log Rsw threshold value provides input to the MCO pH routine.	Single Value, -4.0	Necessary for calculating more realistic pH values inside a waste package	Corroborative DTN: SN0704PMAIPCAB.001_R1 [DIRS 182602]
IPC_MCO _Rsw_Thresh_D	Log Rsw threshold value provides input to the MCO pH routine.	Single Value, -2.0	Necessary for calculating more realistic pH values inside a waste package	Corroborative DTN: SN0704PMAIPCAB.001_R1 [DIRS 182602]
IPC_MCO_pH_Rsw_15_A_LUT	LUT for 2MCO pH	Lookup Table (2D)	Necessary for calculating more realistic pH values inside a waste package	Corroborative DTN: SN0704PMAIPCAB.001_R1 [DIRS 182602]

Table C4-2. Input Parameters Added for the PMA (Continued)

Parameter Name	Description	Parameter Distribution	Rationale for Inclusion	Data Source
Waste Form Degradation and Mobilization (Continued)				
IPC_MCO_pH_Rsw_15_B_LUT	Same as above	Lookup Table (2D)	Necessary for calculating more realistic pH values inside a waste package	Corroborative DTN: SN0704PMAIPCAB.001_R1 [DIRS 182602]
IPC_MCO_pH_Rsw_15_C_LUT	Same as above	Lookup Table (2D)	Necessary for calculating more realistic pH values inside a waste package	Corroborative DTN: SN0704PMAIPCAB.001_R1 [DIRS 182602]
IPC_MCO_pH_Rsw_15_D_LUT	Same as above	Lookup Table (2D)	Necessary for calculating more realistic pH values inside a waste package	Corroborative DTN: SN0704PMAIPCAB.001_R1 [DIRS 182602]
IPC_MCO_pH_Rsw_2_A_LUT	Same as above	Lookup Table (2D)	Necessary for calculating more realistic pH values inside a waste package	Corroborative DTN: SN0704PMAIPCAB.001_R1 [DIRS 182602]
IPC_MCO_pH_Rsw_2_B_LUT	Same as above	Lookup Table (2D)	Necessary for calculating more realistic pH values inside a waste package	Corroborative DTN: SN0704PMAIPCAB.001_R1 [DIRS 182602]
IPC_MCO_pH_Rsw_2_C_LUT	Same as above	Lookup Table (2D)	Necessary for calculating more realistic pH values inside a waste package	Corroborative DTN: SN0704PMAIPCAB.001_R1 [DIRS 182602]
IPC_MCO_pH_Rsw_2_D_LUT	Same as above	Lookup Table (2D)	Necessary for calculating more realistic pH values inside a waste package	Corroborative DTN: SN0704PMAIPCAB.001_R1 [DIRS 182602]
IPC_MCO_pH_Rsw_3_A_LUT	Same as above	Lookup Table (2D)	Necessary for calculating more realistic pH values inside a waste package	Corroborative DTN: SN0704PMAIPCAB.001_R1 [DIRS 182602]
IPC_MCO_pH_Rsw_3_B_LUT	Same as above	Lookup Table (2D)	Necessary for calculating more realistic pH values inside a waste package	Corroborative DTN: SN0704PMAIPCAB.001_R1 [DIRS 182602]
IPC_MCO_pH_Rsw_3_C_LUT	Same as above	Lookup Table (2D)	Necessary for calculating more realistic pH values inside a waste package	Corroborative DTN: SN0704PMAIPCAB.001_R1 [DIRS 182602]
IPC_MCO_pH_Rsw_3_D_LUT	Same as above	Lookup Table (2D)	Necessary for calculating more realistic pH values inside a waste package	Corroborative DTN: SN0704PMAIPCAB.001_R1 [DIRS 182602]

Table C4-2. Input Parameters Added for the PMA (Continued)

Parameter Name	Description	Parameter Distribution	Rationale for Inclusion	Data Source
Waste Form Degradation and Mobilization (Continued)				
IPC_MCO_pH_Rsw_4_A_LUT	Same as above	Lookup Table (2D)	Necessary for calculating more realistic pH values inside a waste package	Corroborative DTN: SN0704PMAIPCAB.001_R1 [DIRS 182602]
IPC_MCO_pH_Rsw_4_B_LUT	Same as above	Lookup Table (2D)	Necessary for calculating more realistic pH values inside a waste package	Corroborative DTN: SN0704PMAIPCAB.001_R1 [DIRS 182602]
IPC_MCO_pH_Rsw_4_C_LUT	Same as above	Lookup Table (2D)	Necessary for calculating more realistic pH values inside a waste package	Corroborative DTN: SN0704PMAIPCAB.001_R1 [DIRS 182602]
IPC_MCO_pH_Rsw_4_D_LUT	Same as above	Lookup Table (2D)	Necessary for calculating more realistic pH values inside a waste package	Corroborative DTN: SN0704PMAIPCAB.001_R1 [DIRS 182602]
IPC_Read_pH_Column_2DHLW	Input value to direct GoldSim to read the pH column of the IPC pH lookup tables	Single Value, 2.0	Necessary for calculating more realistic pH values inside a waste package	Corroborative DTN: SN0704PMAIPCAB.001_R1 [DIRS 182602]
IPC_Read_pH_Column_2MCO	Input value to direct GoldSim to read the pH column of the IPC pH lookup tables	Single Value, 2.0	Necessary for calculating more realistic pH values inside a waste package	Corroborative DTN: SN0704PMAIPCAB.001_R1 [DIRS 182602]
IPC_Read_pH_Column_CSNF	Input value to direct GoldSim to read the pH column of the IPC pH lookup tables	Single Value, 2.0	Necessary for calculating more realistic pH values inside a waste package	Corroborative DTN: SN0704PMAIPCAB.001_R1 [DIRS 182602]
Unsaturated Zone Transport				
kdet	Detachment rate constant used for Colloid Diversity Model. The median travel time τ is obtained from the Pu fast breakthrough curves. (Used in both the UZ and SZ transport models)	Log10 transformed triangular distribution defined by: $\log10(0.01/\tau)$, $\log10(0.1/\tau)$, $\log10(1/\tau)$]. τ is in hours.	The colloid retardation factor is a function of the detachment rate constant. The distribution is based on experimental data reported in DTN: LA0705PR150304.001 [DIRS 181744].	Corroborative DTN: SN0704PMASZFTA.001_R1 [DIRS 184395]
R_Min	Lower limit of the distribution used for the retardation coefficient	Constant - 2.0	Provides a more realistic distribution for colloid retardation factors in fractures	Corroborative DTN: MO0704PAUZFEHM.000_R0 [DIRS 182790]

Table C4-2. Input Parameters Added for the PMA (Continued)

Parameter Name	Description	Parameter Distribution	Rationale for Inclusion	Data Source
Unsaturated Zone Transport (Continued)				
Slope_m	Slope of the equation approximating the CDF of the filtration rate constant (Used in both the UZ and SZ transport models)	Lookup Table (1D): based on SZ PMA sampling of a triangular distribution with values [0.17, 0.31 51, and 0.85]	Provides a more realistic distribution for colloid retardation factors in fractures	Corroborative DTN: SN0704PMASZFTA.001_R1 [DIRS 184395]
Intercept_b	y-intercept of the equation approximating the CDF of the filtration rate constant	Constant – 0.2	Provides a more realistic distribution for colloid retardation factors in fractures	Corroborative DTN: MO0704PAUZFEHM.000_R 0 [DIRS 182790]
Water_Table_a	Water table elevation after change the Present Day climate ends	Cumulative Distribution: 0 750 0.05 755 0.1 760 0.25 770 0.5 780 0.7 790 0.9 830 0.95 840 1 850	Provides uncertainty to the degree of water table rise associated with climate changes	Section 6.6.1.2 Corroborative DTN: MO0704PAUZFEHM.000_R 0 [DIRS 182790]
ff2100.ini	FEHM external file containing the flow field data for the monsoonal climate 10th percentile infiltration case without water-table adjustment.	External File	Necessary for FEHM code to accurately track the RN species.	DTN: LB0701MOFEHMFF.001_R 0. [DIRS 179297]
ff2200.ini	FEHM external file containing the flow field data for the monsoonal climate 30th percentile infiltration case without water-table adjustment.	External File	Necessary for FEHM code to accurately track the RN species.	DTN: LB0701MOFEHMFF.001_R 0 [DIRS 179297]
ff2300.ini	FEHM external file containing the flow field data for the monsoonal climate 50th percentile infiltration case without water-table adjustment.	External File	Necessary for FEHM code to accurately track the RN species.	DTN: LB0701MOFEHMFF.001_R 0 [DIRS 179297]
ff2400.ini	FEHM external file containing the flow field data for the monsoonal climate 90th percentile infiltration case without	External File	Necessary for FEHM code to accurately track the RN species.	DTN: LB0701MOFEHMFF.001_R 0 [DIRS 179297]

Table C4-2. Input Parameters Added for the PMA (Continued)

Parameter Name	Description	Parameter Distribution	Rationale for Inclusion	Data Source
	water-table adjustment.			
Unsaturated Zone Transport (Continued)				
ff3100.ini	FEHM external file containing the flow field data for the glacial climate 10th percentile infiltration case without water-table adjustment.	External File	Necessary for FEHM code to accurately track the RN species.	DTN: LB0701GTFEHMFF.001_R0 [DIRS 179160]
ff3200.ini	FEHM external file containing the flow field data for the glacial climate 30th percentile infiltration case without water-table adjustment.	External File	Necessary for FEHM code to accurately track the RN species.	DTN: LB0701GTFEHMFF.001_R0 [DIRS 179160]
ff3300.ini	FEHM external file containing the flow field data for the glacial climate 50th percentile infiltration case without water-table adjustment.	External File	Necessary for FEHM code to accurately track the RN species.	DTN: LB0701GTFEHMFF.001_R0 [DIRS 179160]
ff3400.ini	FEHM external file containing the flow field data for the glacial climate 90th percentile infiltration case without water-table adjustment.	External File	Necessary for FEHM code to accurately track the RN species.	DTN: LB0701GTFEHMFF.001_R0 [DIRS 179160]
ff4100.ini	FEHM external file containing the flow field data for the 4th climate 10th percentile infiltration case without water-table adjustment.	External File	Necessary for FEHM code to accurately track the RN species.	DTN: LB0701PAFEM10K.002_R0 [DIRS 179507]
ff4200.ini	FEHM external file containing the flow field data for the 4th climate 30th percentile infiltration case without water-table adjustment.	External File	Necessary for FEHM code to accurately track the RN species.	DTN: LB0701PAFEM10K.002_R0 [DIRS 179507]
ff4300.ini	FEHM external file containing the flow field data for the 4th climate 50th percentile infiltration case without water-table adjustment.	External File	Necessary for FEHM code to accurately track the RN species.	DTN: LB0701PAFEM10K.002_R0 [DIRS 179507]
ff4400.ini	FEHM external file containing the flow field data for the 4th climate 90th percentile infiltration case without water-table adjustment.	External File	Necessary for FEHM code to accurately track the RN species.	DTN: LB0701PAFEM10K.002_R0 [DIRS 179507]
fehmn.gold	GoldSim/FEHM external interface control file containing length of input array used to pass data from GoldSim	External File	Necessary for FEHM code to accurately track the RN species.	Corroborative DTN: MO0708TSPAPROC.000_R0 [DIRS 182979]

Table C4-2. Input Parameters Added for the PMA (Continued)

Parameter Name	Description	Parameter Distribution	Rationale for Inclusion	Data Source
	to FEHM.			
Unsaturated Zone Transport (Continued)				
UZ_Params_Multi_PMA_21_300rlz	FEHM stochastic external file for PMA. 300 rlzs, random seed 1, Colloid Diversity model 2, Interface Area 1.	External File	Necessary for FEHM code to accurately track the RN species.	Corroborative DTN: MO0708TSPAPROC.000_R0 [DIRS 182979]
fehm_PMA_10kyr.mptr	FEHM external file containing the control data, physical params., and chemical params. for multiple-species ingrowth particle tracking in 10,000 yr. non-igneous simulations. The file contains pointer indices for sampled params.	External File	Necessary for FEHM code to accurately track the RN species.	Corroborative DTN: MO0708TSPAPROC.000_R0 [DIRS 182979]
fehm_PMA_10kyr_ef_cdsp.mptr	FEHM external file containing the control data, physical params., and chemical params. for multiple-species ingrowth particle tracking in 10 kyr. non-igneous simulations. The file contains pointer indices for sampled params.	External File	Necessary for FEHM code to accurately track the RN species.	Corroborative DTN: MO0708TSPAPROC.000_R0 [DIRS 182979]
fehm_PMA_10kyr_ef_csnf.mptr	FEHM external file containing the control data, physical params., and chemical params. for multiple-species ingrowth particle tracking in 10 kyr. non-igneous simulations. The file contains pointer indices for sampled params.	External File	Necessary for FEHM code to accurately track the RN species.	Corroborative DTN: MO0708TSPAPROC.000_R0 [DIRS 182979]
fehm_PMA_10kyr_lgn.mptr	FEHM external file containing the control data, physical params., and chemical params. for multiple-species ingrowth particle tracking in 10,000 yr. igneous simulations. The file contains pointer indices for sampled params.	External File	Necessary for FEHM code to accurately track the RN species.	Corroborative DTN: MO0708TSPAPROC.000_R0 [DIRS 182979]
fehm_PMA_10kyr_lgn_ni.mptr	FEHM ext. file containing the control data, physical params., and chemical params. for multiple-species ingrowth particle tracking in 10,000 yr. igneous simulations. The file contains ptr indices for sampled params (no irreversibles).	External File	Necessary for FEHM code to accurately track the RN species.	Corroborative DTN: MO0708TSPAPROC.000_R0 [DIRS 182979]

Table C4-2. Input Parameters Added for the PMA (Continued)

Parameter Name	Description	Parameter Distribution	Rationale for Inclusion	Data Source
Unsaturated Zone Transport (Continued)				
fehm_PMA_10kyr_ni.mptr	FEHM ext. file containing the control data, physical params., and chemical params. for multiple-species ingrowth particle tracking in 10,000 yr. simulations. The file contains ptr indices for sampled params (no irreversibles).	External File	Necessary for FEHM code to accurately track the RN species.	Corroborative DTN: MO0708TSPAPROC.000_R 0 [DIRS 182979]
fehm_PMA_1Myr.mptr	FEHM external file containing the control data, physical params., and chemical params. for multiple-species ingrowth particle tracking in one million yr. non-igneous simulations. The file contains pointer indices for sampled params.	External File	Necessary for FEHM code to accurately track the RN species.	Corroborative DTN: MO0708TSPAPROC.000_R 0 [DIRS 182979]
fehm_PMA_1Myr_ef_cdsp. mptr	FEHM external file containing the control data, physical params., and chemical params. for multiple-species ingrowth particle tracking in one million yr. non-igneous simulations. The file contains pointer indices for sampled params.	External File	Necessary for FEHM code to accurately track the RN species.	Corroborative DTN: MO0708TSPAPROC.000_R 0 [DIRS 182979]
fehm_PMA_1Myr_ef_csnf. mptr	FEHM external file containing the control data, physical params., and chemical params. for multiple-species ingrowth particle tracking in one million yr. non-igneous simulations. The file contains pointer indices for sampled params.	External File	Necessary for FEHM code to accurately track the RN species.	Corroborative DTN: MO0708TSPAPROC.000_R 0 [DIRS 182979]
fehm_PMA_1Myr_lgn.mptr	FEHM external file containing the control data, physical params., and chemical params. for multiple-species ingrowth particle tracking in one million yr. igneous simulations. The file contains pointer indices for sampled params.	External File	Necessary for FEHM code to accurately track the RN species.	Corroborative DTN: MO0708TSPAPROC.000_R 0 [DIRS 182979]

Table C4-2. Input Parameters Added for the PMA (Continued)

Parameter Name	Description	Parameter Distribution	Rationale for Inclusion	Data Source
Unsaturated Zone Transport (Continued)				
fehm_PMA_1Myr_Ign_ni.mptr	FEHM ext. file containing the control data, physical params., and chemical params. for multiple-species ingrowth particle tracking in 1M yr. igneous simulations. The file contains ptr indices for sampled params (no irreversibles).	External File	Necessary for FEHM code to accurately track the RN species.	Corroborative DTN: MO0708TSPAPROC.000_R0 [DIRS 182979]
fehm_PMA_1Myr_ni.mptr	FEHM ext. file containing the control data, physical params., and chemical params. for multiple-species ingrowth particle tracking in 1M yr. simulations. The file contains ptr indices for sampled params (no irreversibles).	External File	Necessary for FEHM code to accurately track the RN species.	Corroborative DTN: MO0708TSPAPROC.000_R0 [DIRS 182979]
fehm_PMA_gs_1Myr.dat	UZ Transport: FEHM external file containing the general control data needed for the one million yr. simulations.	External File	Necessary for FEHM code to accurately track the RN species.	Corroborative DTN: MO0708TSPAPROC.000_R0 [DIRS 182979]
fehm_PMA_gs_20kyr.dat	FEHM external file containing the general control data needed for the 10,000/20,000 yr. simulations.	External File	Necessary for FEHM code to accurately track the RN species.	Corroborative DTN: MO0708TSPAPROC.000_R0 [DIRS 182979]
fehmn.files	FEHM external file containing names of major input and output files used in a simulation.	External File	Necessary for FEHM code to accurately track the RN species.	Corroborative DTN: MO0708TSPAPROC.000_R0 [DIRS 182979]
fehm_TSPA_10kyr.mptr	FEHM external file containing the control data, physical params., and chemical params. for multiple-species ingrowth particle tracking in 10,000 yr. non-igneous simulations. The file contains pointer indices for sampled params.	External File	Slight adjustment from the TSPA-LA compliance file to include reference the expanded file list used for PMA	Corroborative DTN: MO0708TSPAPROC.000_R0 [DIRS 182979]
fehm_TSPA_1Myr.mptr	Same as above for 1,000,000 year simulations.	External File	Same as above	Corroborative DTN: MO0708TSPAPROC.000_R0 [DIRS 182979]
fehm_TSPA_10kyr_ign.mptr	Same as fehm_TSPA_10kyr.mptr adjusted for the igneous simulations	External File	Same as above	Corroborative DTN: MO0708TSPAPROC.000_R0 [DIRS 182979]

Table C4-2. Input Parameters Added for the PMA (Continued)

Parameter Name	Description	Parameter Distribution	Rationale for Inclusion	Data Source
Unsaturated Zone Transport (Continued)				
fehm_TSPA_1Myr_ign.mptr	Same as fehm_TSPA_1Myr.mptr adjusted for the igneous simulations	External File	Same as above	Corroborative DTN: MO0708TSPAPROC.000_R0 [DIRS 182979]
fehm_TSPA_10kyr_ef_cdsp.mptr	FEHM external file containing the control data, physical params., and chemical params. for multiple-species ingrowth particle tracking in 10 kyr.early failure simulations. The file contains pointer indices for sampled params.	External File	Same as above	Corroborative DTN: MO0708TSPAPROC.000_R0 [DIRS 182979]
fehm_TSPA_10kyr_ef_csnf.mptr	Same as above for CSNF WPs.	External File	Same as above	Corroborative DTN: MO0708TSPAPROC.000_R0 [DIRS 182979]
fehm_TSPA_1Myr_ef_cdsp.mptr	Same as above for 1 million year simulations and CDSP WPs.	External File	Same as above	Corroborative DTN: MO0708TSPAPROC.000_R0 [DIRS 182979]
fehm_TSPA_1Myr_ef_csnf.mptr	Same as above for CSNF WPs.	External File	Same as above	Corroborative DTN: MO0708TSPAPROC.000_R0 [DIRS 182979]
SZ Flow and Transport Parameters				
SZ_Block_Length	Block length for matrix diffusion from UZ to SZ	250 m (constant)	The parameter value is the horizontal grid dimension of the saturated zone flow and transport model.	Corroborative DTN: SN0704PMASZFTA.001_R1 [DIRS 184395]
SZ_Block_Thickness	Block thickness for matrix diffusion from UZ to SZ	10 m (constant)	The parameter value reflects the thickness of the top most layer in the SZ below the water table.	Corroborative DTN: SN0704PMASZFTA.001_R1 [DIRS 184395]
kdet	Detachment rate constant used for Colloid Diversity Model. The median travel time τ is obtained from the Pu fast breakthrough curves. (Used in both the UZ and SZ transport models)	Log10 transformed triangular distribution defined by: $\log10(0.01/\tau)$, $\log10(0.1/\tau)$, $\log10(1/\tau)$]. τ is in hours.	The colloid retardation factor is a function of the detachment rate constant. The distribution is based on experimental data reported in DTN: LA0705PR150304.001 [DIRS 181744].	Corroborative DTN: SN0704PMASZFTA.001_R1 [DIRS 184395]

Table C4-2. Input Parameters Added for the PMA (Continued)

Parameter Name	Description	Parameter Distribution	Rationale for Inclusion	Data Source
SZ Flow and Transport Parameters (Continued)				
Slope_m	Slope of filtration rate constant vs. travel time plot used for the Colloid Diversity Model. (Used in both the UZ and SZ transport models)	Lookup Table (1D)	The colloid retardation factor is a function of the slope of filtration rate constant vs. travel time plot. The distribution is based on experimental data reported in DTN: LA0705PR150304.001 [DIRS 181744].	Corroborative DTN: SN0704PMASZFTA.001_R1 [DIRS 184395]
Intercept_b	Y-intercept of filtration rate constant vs. travel time plot used for the Colloid Diversity Model.	0.2 (constant)	The colloid retardation factor is a function of the intercept of filtration rate constant vs. travel time plot. The distribution is based on experimental data reported in DTN: LA0705PR150304.001 [DIRS 181744].	Corroborative DTN: SN0704PMASZFTA.001_R1 [DIRS 184395]
Rf1 to Rf10	Colloid retardation factors for the Colloid Diversity Model	Table	The parameter values are computed based on the Colloid Diversity Model.	Corroborative DTN: SN0704PMASZFTA.001_R1 [DIRS 184395]
Rl	Lower bound retardation factor used to calculate the minimum probability value for the Colloid Diversity Model.	2.0 (constant)	The lower bound retardation factor was set based on observations of experimental data.	Corroborative DTN: SN0704PMASZFTA.001 [DIRS 184395]
Kd_Tc_RZ	Sorption coefficient for technetium in the reducing zone	Lookup Table (1D)	Technetium sorption coefficient representing areas with reducing conditions. Sorption distribution based on Lieser and Bauscher (1988 [DIRS 172722]).	Corroborative DTN: SN0704PMASZFTA.001_R1 [DIRS 184395]

Table C4-2. Input Parameters Added for the PMA (Continued)

Parameter Name	Description	Parameter Distribution	Rationale for Inclusion	Data Source
SZ Flow and Transport Parameters (Continued)				
KD_Np_RZ	Sorption coefficient for neptunium in the reducing zone	Lookup Table (1D)	Technetium sorption coefficient representing areas with reducing conditions. Sorption distribution based on Lieser and Muhlenweg (1988 [DIRS 106684]).	Corroborative DTN: SN0704PMASZFTA.001_R1 [DIRS 184395]
FPLRZN	Factor for Northern reducing zone boundary	Lookup Table (1D)	Parameter used as a multiplying factor to the ranges given in meters in defining the northern boundaries of the reducing zone for each realization. Dimensions based on BSC (2006 [DIRS 178672]).	Corroborative DTN: SN0704PMASZFTA.001_R1 [DIRS 184395]
FPLRZS	Factor for Southern reducing zone boundary	Lookup Table (1D)	Parameter used as a multiplying factor to the ranges given in meters in defining the southern boundaries of the reducing zone for each realization (BSC 2006 [DIRS 178672]).	Corroborative DTN: SN0704PMASZFTA.001_R1 [DIRS 184395]
FPLRZE	Factor for Eastern reducing zone boundary	Lookup Table (1D)	Parameter used as a multiplying factor to the ranges given in meters in defining the eastern boundaries of the reducing zone for each realization (BSC 2006 [DIRS 178672]).	Corroborative DTN: SN0704PMASZFTA.001_R1 [DIRS 184395]
FPVO_PMA	Flowing interval porosity A	Table	Parameter used for the flowing interval porosity in the Saturated Zone transport model	Corroborative DTN: SN0704PMASZFTA.001_R1 [DIRS 184395]

Table C4-2. Input Parameters Added for the PMA (Continued)

Parameter Name	Description	Parameter Distribution	Rationale for Inclusion	Data Source
SZ Flow and Transport Parameters (Continued)				
RZ_Pipe_Length_Data	Pipe length data for the SZ 1-D transport	Table	Estimation of the reducing zone length for the 1-D SZ transport model based on particle tracking data analysis and the rectangular dimensions of the reducing zone.	Corroborative DTN: SN0704PMASZFTA.001_R1 [DIRS 184395]
SZ_13_01 to SZ_13_04	SZ, Breakthrough Curves, C,Tc, I, SR1, SR2, SR3, and SR4	File	Breakthrough curves for the SZ PMA model	Corroborative DTN: SN0704PMASZFTA.001_R1 [DIRS 184395]
SZ_14_01 to SZ_14_04	SZ, Breakthrough Curves, Am, Th, Pa SR1, SR2, SR3, and SR4	File	Breakthrough curves for the SZ PMA model	Corroborative DTN: SN0704PMASZFTA.001_R1 [DIRS 184395]
SZ_15_01 to SZ_15_04	SZ, Breakthrough Curves, Cs, SR1, SR2, SR3, and SR4	File	Breakthrough curves for the SZ PMA model	Corroborative DTN: SN0704PMASZFTA.001_R1 [DIRS 184395]
SZ_16_01 to SZ_16_04	SZ, Breakthrough Curves, Pu, SR1, SR2, SR3, and SR4	File	Breakthrough curves for the SZ PMA model	Corroborative DTN: SN0704PMASZFTA.001_R1 [DIRS 184395]
SZ_17_01 to SZ_17_04	SZ, Breakthrough Curves, Np, SR1, SR2, SR3, and SR4	File	Breakthrough curves for the SZ PMA model	Corroborative DTN: SN0704PMASZFTA.001_R1 [DIRS 184395]
SZ_18_01 to SZ_18_04	SZ, Breakthrough Curves, IcPu, IcAm SR1, SR2, SR3, and SR4	File	Breakthrough curves for the SZ PMA model	Corroborative DTN: SN0704PMASZFTA.001_R1 [DIRS 184395]
SZ_19_01 to SZ_19_04	SZ, Breakthrough Curves, Ra, SR1, SR2, SR3, and SR4	File	Breakthrough curves for the SZ PMA model	Corroborative DTN: SN0704PMASZFTA.001_R1 [DIRS 184395]
SZ_20_01 to SZ_20_04	SZ, Breakthrough Curves, Sr, SR1, SR2, SR3, and SR4	File	Breakthrough curves for the SZ PMA model	Corroborative DTN: SN0704PMASZFTA.001_R1 [DIRS 184395]
SZ_21_01 to SZ_21_04	SZ, Breakthrough Curves, U, SR1, SR2, SR3, and SR4	File	Breakthrough curves for the SZ PMA model	Corroborative DTN: SN0704PMASZFTA.001_R1 [DIRS 184395]

Table C4-2. Input Parameters Added for the PMA (Continued)

Parameter Name	Description	Parameter Distribution	Rationale for Inclusion	Data Source
SZ Flow and Transport Parameters (Continued)				
SZ_22_01 to SZ_22_04	SZ, Breakthrough Curves, IfPu, IfAm, SR1, SR2, SR3, and SR4	File	Breakthrough curves for the SZ PMA model	Corroborative DTN: SN0704PMASZFTA.001_R1 [DIRS 184395]
SZ_23_01 to SZ_23_04	SZ, Breakthrough Curves, Se, SR1, SR2, SR3, and SR4	File	Breakthrough curves for the SZ PMA model	Corroborative DTN: SN0704PMASZFTA.001_R1 [DIRS 184395]
SZ_24_01 to SZ_24_04	SZ, Breakthrough Curves, Sn, SR1, SR2, SR3, and SR4	File	Breakthrough curves for the SZ PMA model	Corroborative DTN: SN0704PMASZFTA.001_R1 [DIRS 184395]
SZ_25_01 to SZ_25_04	SZ, Breakthrough Curves, Tc, SR1, SR2, SR3, and SR4	File	Breakthrough curves for the SZ PMA model	Corroborative DTN: SN0704PMASZFTA.001_R1 [DIRS 184395]
sz_convolute2_1Myr_pma.dat	SZ, Control file, 1,000,000 yr duration for PMA model	File	Input file for the SZ PMA model	Corroborative DTN: SN0704PMASZFTA.001_R1 [DIRS 184395]
sz_convolute2_20kyr_pma.dat	SZ, Control file, 20,000 yr duration for PMA model	File	Input file for the SZ PMA model	Corroborative DTN: SN0704PMASZFTA.001_R1 [DIRS 184395]
Seismic Scenario Parameters				
Stress_Thresh_A22_PMA_a	Distribution for residual stress threshold factor.	Uniform [100, 105]	Necessary to implement less conservative threshold for stress corrosion cracking	ANL-EBS-MD-000005 Rev 04 [DIRS 181953]
WP_Crack_Area_Density_PMA	Modified WP SCC crack density.	Constant Value [0.00327]	Value needed to implement alternative crack density model	ANL-EBS-MD-000005 Rev 04 [DIRS 181953]

* It is acknowledged that different density values may have been used for both HLW and DSNF. These values were derived from different assumptions or choices of representative waste components. The use of different values is expected to have little effect on the PMA results.

Table C4-3. Sources and Parameter Entry Form Numbers for the PMA-Specific Direct Inputs

Line #	Document_ID	Reference_Document	Document DIRS	DTN	DTN DIRS	PEF
1	ANL-EBS-MD-000003 REV 03	General Corrosion and Localized Corrosion of Waste Package Outer Barrier	178519	NA	NA	520
2	ANL-EBS-MD-000033 REV06	Engineered Barrier System: Physical and Chemical Environment	177412	SN0701PAEBSPCE.001_R1	180523	513
3	ANL-EBS-MD-000037 REV04 AD01	In-Package Chemistry Abstraction	180506	SN0702PAIPC1CA.001_R2	180451	506
4	ANL-EBS-MD-000049 REV03 AD01	Multiscale Thermohydrologic Model	181383	LL0703PA011MST.006_R0	179853	508
5	ANL-EBS-MD-000049 REV03 AD01	Multiscale Thermohydrologic Model	181383	LL0703PA012MST.007_R0	179854	527
6	ANL-EBS-MD-000049 REV03 AD01	Multiscale Thermohydrologic Model	181383	LL0703PA013MST.008_R0	179855	528
7	ANL-EBS-MD-000049 REV03 AD01	Multiscale Thermohydrologic Model	181383	LL0703PA014MST.009_R0	179856	529
8	ANL-EBS-MD-000049 REV03 AD01	Multiscale Thermohydrologic Model	181383	LL0703PA015MST.010_R0	179857	530
9	ANL-EBS-MD-000005 Rev 04	Stress Corrosion Cracking of Waste Package Outer Barrier and Drip Shield Materials	181953	NA	NA	539
10	ANL-EBS-MD-000049 REV03 AD01	Multiscale Thermohydrologic Model	181383	LL0703PA016MST.011_R0	179858	531
11	ANL-EBS-MD-000049 REV03 AD01	Multiscale Thermohydrologic Model	181383	LL0703PA017MST.012_R0	179859	532
12	ANL-EBS-MD-000049 REV03 AD01	Multiscale Thermohydrologic Model	181383	LL0703PA034MST.016_R0	179982	533

Table C4-3. Sources and Parameter Entry Form Numbers for the PMA-Specific Direct Inputs (Continued)

Line #	Document_ID	Reference_Document	Document DIRS	DTN	DTN DIRS	PEF
13	ANL-EBS-MD-000049 REV03 AD01	Multiscale Thermohydrologic Model	181383	LL0703PA035MST.017_R0	179985	534
14	ANL-EBS-MD-000049 REV03 AD01	Multiscale Thermohydrologic Model	181383	LL0703PA036MST.018_R0	179986	535
15	ANL-EBS-MD-000049 REV03 AD01	Multiscale Thermohydrologic Model	181383	LL0703PA037MST.019_R0	179989	536
16	ANL-EBS-MD-000049 REV03 AD01	Multiscale Thermohydrologic Model	181383	LL0703PA038MST.020_R0	179992	537
17	ANL-WIS-MD-000021 REV03 AD01	Cladding Degradation Summary for LA	180616	MO0411SPACLDDG.003_R1	180755	515
18	ANL-WIS-MD-000021 REV03 AD01	Cladding Degradation Summary for LA	180616	MO0702PAFRACSS.000_R1	181588	522
19	MDL-MGR-GS-000007	Supplemental Earthquake Ground Motion Input for a Geologic Repository at Yucca Mountain	NA	MO0801HCUHSREB.001_R0	184803	538
20	MDL-WIS-PA-000005	Total System Performance Assessment Model/Analysis for the License Application	NA	SN0704PMAIPCAB.001_R1	182602	523
21	MDL-NBS-HS-000006 REV03	UZ Flow Models and Submodels	184614	LB0701GTFEHMFF.001_R0	179160	525
22	MDL-NBS-HS-000006 REV03	UZ Flow Models and Submodels	184614	LB0701MOFEHMFF.001_R0	179297	510
23	MDL-NBS-HS-000006 REV03	UZ Flow Models and Submodels	184614	LB0702PAFEM10K.002_R0	179507	526
24	MDL-NBS-HS-000019 REV01 AD01	Abstraction of Drift Seepage	181244	LB0702PASEEP01.001_R0	179511	514
25	MDL-NBS-HS-000020 REV 02 AD02	Particle Tracking Model and Abstraction of Transport Processes	184748	MO0704PAFEHMBR.001_R3	184647	512
26	MDL-NBS-HS-000021 REV03 AD02	Saturated Zone Flow and Transport Model Abstraction	183750	Corroborative DTN: SN0704PMASZFTA.001_R1	184395	519

Table C4-3. Sources and Parameter Entry Form Numbers for the PMA-Specific Direct Inputs (Continued)

Line #	Document_ID	Reference_Document	Document DIRS	DTN	DTN DIRS	PEF
27	MDL-WIS-PA-000005	Total System Performance Assessment Model/Analysis for the License Application	NA	Corroborative DTN: LB0704PASEEP02.001_R1	181093	516
28	MDL-WIS-PA-000005	Total System Performance Assessment Model/Analysis for the License Application	NA	Corroborative DTN: MO0704PAUZFEHM.000_R0	182790	507, 509, 524
29	MDL-WIS-PA-000005	Total System Performance Assessment Model/Analysis for the License Application	NA	Corroborative DTN: MO0708TSPAPROC.000_R0	182979	507, 508, 509, 512, 513, 517, 518, 519, 521, 527, 528, 529, 530, 531, 532, 533, 534, 535, 536, 537, 538, 541, 542, 543
30	MDL-WIS-PA-000005	Total System Performance Assessment Model/Analysis for the License Application	NA	Corroborative DTN: SN0704PMAGDEGM.001_R2	183955	503

Table C4-3. Sources and Parameter Entry Form Numbers for the PMA-Specific Direct Inputs (Continued)

Line #	Document_ID	Reference_Document	Document DIRS	DTN	DTN DIRS	PEF
31	MDL-WIS-PA-000005	Total System Performance Assessment Model/Analysis for the License Application	NA	Corroborative DTN: SN0704PMAIPCAB.001_R1	182602	500
32	MDL-WIS-PA-000005	Total System Performance Assessment Model/Analysis for the License Application	NA	Corroborative DTN: SN0704PMASOLUB.001_R1	182787	505
33	MDL-WIS-PA-000005	Total System Performance Assessment Model/Analysis for the License Application	NA	Corroborative DTN: SN0704PMASZFTA.001_R1_R0	184395	501
34	MDL-WIS-PA-000005	Total System Performance Assessment Model/Analysis for the License Application	NA	Corroborative DTN: SN0704PMAWBCAL.001_R2	182335	502
35	MDL-WIS-PA-000005	Total System Performance Assessment Model/Analysis for the License Application	NA	Corroborative DTN: SN0707PMACSNFD.001_R0	183045	504
36	MDL-WIS-PA-000005	Total System Performance Assessment Model/Analysis for License Application	NA	NA	NA	511
37	MDL-WIS-PA-000005	In-Package Chemistry Abstraction, ANL-EBS-MD-000037 Rev 04 AD 01	180506	NA	NA	540
38	MDL-NBS-HS-000008, REV 02 ADD 01	Radionuclide Transport Models Under Ambient Conditions	177396	LA0408AM831341.001_R0	171584	509
39	MDL-NBS-HS-000008, REV 02 ADD 01	Radionuclide Transport Models Under Ambient Conditions	177396	LB0701PAKDSESN.001_R0	179299	509
40	MDL-NBS-HS-000020 REV 02 AD02	Particle Tracking Model and Abstraction of Transport Processes	184748	LA0701PANS02BR.003_R2	180497	509

Table C4-3. Sources and Parameter Entry Form Numbers for the PMA-Specific Direct Inputs (Continued)

Line #	Document_ID	Reference_Document	Document DIRS	DTN	DTN DIRS	PEF
41	MDL-NBS-HS-000008, REV 02 ADD 01	Radionuclide Transport Models Under Ambient Conditions	177396	LB0702PAUZMTDF.001_R1	180776	509
42	MDL-WIS-PA-000005	Total System Performance Assessment Model/Analysis for License Application	NA	MO0707UZKDCORR.000_R0	183003	509

Table C5-1. Assumptions Identified as Potentially Conservative and Significant to Annual Dose Rate

Submodel	TSPA-LA Assumption	PMA Treatment	Basis for Change
Drift Seepage	Seepage abstraction collapsed-drift look-up table was generated from seepage simulations conducted with the seepage model for performance assessment (SMPA) (BSC 2004 [DIRS 181244], Section 6.1[a]), assuming a rubble-filled circular opening with 11 m diameter as the final state after collapse.	The PMA model includes this analysis for collapsed drifts using an alternative seepage look-up table developed from revised SMPA simulations. The alternative look-up table gives seepage only when the seepage location at the ceiling is within the 5.5-m wide center section of the rubble-filled opening.	In the TSPA seepage component, the total flow of liquid water from the fractured formation into the rubble-filled opening is considered seepage, independent of the actual seepage location, and subsequent TSPA components, such as those for radionuclide mobilization and transport, use this total seepage rate. This is a conservative treatment of seepage, since the mostly gravity-driven flow in the rubble-filled opening would effectively prohibit contact of water with the waste packages or waste forms for off-center seepage locations. Such conservative treatment was chosen in the TSPA compliance model to account for possible uncertainties in the seepage modeling approach for collapsed drifts.
WF Degradation and Radionuclide Mobilization	All of the CSNF (Zircaloy and Stainless Steel) cladding is assumed to be failed at time of WP failure (Section 5.1.3).	For 10,000 year EF WP and EF DS cases, spent-fuel, zirconium-based (Zircaloy) cladding is assumed to split instantly along the length of a fuel rod only if the cladding is perforated at the time of WP failure based upon the initial failed fraction. No credit is taken for stainless-steel cladding because it is assumed to be failed upon receipt.	It is expected that unfailed (not breached or perforated) Zircaloy cladding will remain intact for at least 10,000 years, in absence of rock fall induced damage (SNL 2007 [DIRS 180616], Section 1.0). The groups of waste packages represented in the TSPA-LA model have an initial percentage of failed rods defined by the log uniform distribution with a range 0.01% to 1%. This fuel rod failure rate is based on historical data on reactor operation and includes uncertainty. It also includes failure from wet and dry storage at the reactor site, and handling (SNL 2007 [DIRS 180616], Section 7.1.1).

Table C5-1. Assumptions Identified as Potentially Conservative and Significant to Annual Dose Rate (Continued)

Submodel	TSPA-LA Assumption	PMA Treatment	Basis for Change
WF Degradation and Radionuclide Mobilization (Continued)	CSNF WF Degradation The commercial SNF waste-form degradation rate is calculated as a function of temperature, oxygen fugacity, total carbonate concentration, and pH (BSC 2004 [DIRS 169987]), based on a set of conservative assumptions that may overestimate the rate and extent of waste degradation.	The functional dependence on water chemistry remains the same as in the compliance model. However, the distribution range of the effective surface area of commercial SNF is modified based on fractional release rate measurements in fuel rod segment tests (BSC 2004 [DIRS 169987]), and two additional scaling factors are included to capture the effect of long-term dissolution and the decrease in radiolysis.	CSNF WF Degradation • The fractional release rate is a parameter that is directly measured in leaching experiments. The effective surface area should be chosen to reflect these measurements. In addition, the rod segment tests may most accurately mimic the likely state of spent fuels in a breached waste package. • The linear dependence of dissolution rate on water saturation has been used in modeling mineral dissolution in soils. • Experimental data show that the degradation rates decrease with time and with a decrease in radiation field.
	HLW WF Degradation Key parameters used by the compliance model for glass degradation are based on short-term experimental dissolution rate data for a variety of HLW glasses.	The PMA model accounts for the long-term effect by including a chemical affinity term and the effect of rind thickness.	Because laboratory dissolution rates tend to be many times faster than long-term field rates reported for natural glasses, the TSPA-LA model for glass degradation may be overly conservative, especially at long times (e.g., greater than several hundred years) following breach of a waste package.
	Np, Pu, U DCL Uncertainty (Section 5.1.3) The uncertainty assessments are mainly based on many potential sources of uncertainty effecting solubility and/or solubility calculations. These include uncertainties due to: (1) thermodynamic data in the solubility calculations, (2) variations in solution chemistry, (3) temperature effects, and (4) calculations of activity coefficients at different ionic strengths.	The uncertainties for the solubilities of solids controlling the concentrations of the radionuclides U(VI), Pu(IV), Np(IV), and Np(V) have been assessed by comparisons between the EQ3/6 code predictions using the thermodynamic database *data0.ymp.R5* and solubility data available in the peer-review scientific literature. The uncertainties estimated as such are considered as total uncertainties.	The TSPA dissolved concentration limits submodel captures the extent of various uncertainties in thermodynamic data by combining them additively (in log-space) to generate an uncertainty envelope. However, because these uncertainties may not simply be additive, this method may overestimate the uncertainty in any single result.

Table C5-1. Assumptions Identified as Potentially Conservative and Significant to Annual Dose Rate (Continued)

Submodel	TSPA-LA Assumption	PMA Treatment	Basis for Change
WF Degradation and Radionuclide Mobilization (Continued)	The IPC model is a batch reactor model that assumes the bulk in-package chemistry and calculates the result of mixing the components within the waste-form cells of the waste package with water and atmospheric gases to predict equilibrium solution compositions. The effect of water/rock ratio is not included.	The PMA calculations for in-package chemistry consist of two parts: The first part is used to construct the functional dependence of pH on waste degradation kinetics for the cases where vapor diffusion is a dominant mechanism for water transport through a breached waste package. The second part is to establish the relationship between the water chemistry and the flux of liquid water that percolates the waste package.	The modified in-package chemistry abstraction was necessary to support the in-package water balance abstraction, the liquid water is assumed to be restricted to the pores of the available degradation products. Rather than using the bulk chemistry based in-package chemistry abstraction to predict pH in the pore water of waste-form degradation products exposed to liquid or vapor influx.
WP and DS Degradation	The TSPA-LA Model uses a Stress Threshold value for SCC based upon a temperature of 125°C and a stress safety factor of 2.0 (SNL 2007 [DIRS 181953] Section 6.2.2[a]). The SCC stress threshold is conservatively applied with an uncertainty, a range from 0.9 to 1.05 yield strength with a uniform distribution between these values is selected for use in TSPA (SNL 2007 [DIRS 181953], Table 6-3[a], Section 6.2.2[a]).	The PMA model uses a SCC damage threshold range for Alloy 22 of 100-105% of the yield strength.	The narrower range of uncertainty is justified for use in the performance margin analysis since the stress corrosion cracking threshold stress initiation criterion for Alloy 22 was already conservatively defined at 105% by including a safety factor of 2.0 (SNL 2007 [DIRS 181953], Section 6.2.2[a])
	Stress Corrosion Cracking of Waste Package outer Barrier and Drip Shield Materials (SNL 2007 [DIRS 181953], Section 6.7.3.3) provide estimates of the crack area through analysis of networks of cracks arranged in hexagonal and circular geometries, respectively, circumscribed by a single through-wall crack. The TSPA-LA Model crack density ranges from 3.27×10^{-3} to 1.31×10^{-2} .	In the PMA model the crack area density was changed to a constant value equal to the lower bound used in the TSPA-LA model, 3.27×10^{-3}.	Because the hexagonal array represents a high effective density (close spacing) of individual cracks, this hexagonal case, with crack center spacing is considered a conservative representation (SNL 2007 [DIRS 181953], Sections 8.4.2). An alternative model for the crack area density yields a value at room temperature of 7.22×10^{-3} (SNL 2007 [DIRS 181953], Section 6.7.4). This is considered a limiting case (SNL 2007 [DIRS 181953], Section 6.7.2). This lower bound (3.27×10^{-3}) used in the PMA represents a less conservative value and more closely resembles the results of the alternative model.

Table C5-1. Assumptions Identified as Potentially Conservative and Significant to Annual Dose Rate (Continued)

Submodel	TSPA-LA Assumption	PMA Treatment	Basis for Change
WP and DS Degradation (Continued)	It is assumed that using only the crevice specimen data is sufficient for the GC model for TSPA-LA. Differences in surface-polishing treatments between weight-loss and crevice samples are not evaluated and the conservative crevice data (i.e., higher) corrosion rates are used (SNL 2007 [DIRS 178519], Section 6.4.3.2).	The PMA includes an alternative model using the corrosion rates of weight-loss samples to derive the Ro distribution for use in the general corrosion model of WP outer barrier (Alloy 22). These rates are documented in *General Corrosion and Localized Corrosion of Waste Package Outer Barrier* (SNL 2007 [DIRS 178519], Section 6.4.3.5.2).	The observed general corrosion rates of the crevice specimens are higher than those of the plain weight-loss specimens (SNL 2007 [DIRS 178519], Section 6.4.3.2). The use of only higher general corrosion rates of the crevice specimens in the TSPA-LA is conservative and an evaluation of the weight-loss data is justified.
	The TSPA-LA Model applies the "aggressive-environment" drip shield general corrosion rate to the topside surface of the drip shields when they are exposed to seepage dripping, regardless of the changes in water chemistry due to the thermal evolution of the repository (SNL 2007 [DIRS 180778], Section 6.1.2[a]).	PMA model explicitly evaluates the chemical environment for on the drip shield surface and only applies the aggressive DS corrosion rates to the topside of the DS when the seepage chemistry exceeds the critical (or minimum) fluoride ion concentration of 0.5 millimolar (mM) (SNL 2007 [DIRS 180778], Section 6.1.2[a]).	Application of aggressive conditions to all topside surfaces, with benign conditions only applied to the underside surfaces applies the higher corrosion rate from aggressive conditions to more of the drip shield surfaces is conservative, i.e., it results in an earlier failure of a portion of the drip shields (SNL 2007 [DIRS 180778], Section 6.1.2[a]). The fluoride ion concentrations of the ambient water at the repository horizon have a range of 0.02 to 0.17 mM (SNL 2007 [DIRS 177412], Table 4.1-3). The repository is expected to return to near ambient conditions are after 10,000 years post-closure. Applying the aggressive DS GC rates to for 1e6 year modeling cases is conservative.

Table C5-1. Assumptions Identified as Potentially Conservative and Significant to Annual Dose Rate (Continued)

Submodel	TSPA-LA Assumption	PMA Treatment	Basis for Change
EBS Flow and Transport	The TSPA-LA Model assumes that (Section 5.1.4): 1) Evaporation of water from the surface or interior of a WP does not occur; 2) Water consumption by chemical reactions is negligible; 3) Water vapor is in equilibrium between the inside and the outside of a waste package; 4) Rind saturation is controlled by surface adsorption; and 5)There is no resistance to water percolation over WP failures.	The PMA water balance: (1) accounts for water consumption by reactions; and (2) fully couples hydrologic effects (e.g., the sheet flow on the waste package surface and capillarity effect of porous corrosion products) and chemical processes (e.g., water consumption and salt release by reactions; the depression of water activity with increasing dissolved salt concentration).	Water availability and water flux are two important parameters for predicting the extents of chemical reactions and the transport of radionuclides inside a breached waste package. The objective of this performance margin analysis submodel is to obtain a more detailed estimate of the quantity of water available inside a breached waste package for waste degradation and radionuclide transport in order to evaluate the potential conservatism in the TSPA-LA Model water balance assumptions.

Table C5-1. Assumptions Identified as Potentially Conservative and Significant to Annual Dose Rate (Continued)

Submodel	TSPA-LA Assumption	PMA Treatment	Basis for Change
UZ Transport	In the TSPA-LA model, the diffusive tortuosity differs for each of the three UZ rock units, but is independent of radioelement, whereas the free-water diffusion coefficient is a property of the radioelement (SNL 2008 [DIRS 184748], Section 6.5.5). In the TSPA-LA model, laboratory based values of matrix diffusion coefficients, which are derived as the product of tortuosity and free-water diffusion coefficient, are utilized. Added effects of small scale fractures are not considered.	For the PMA model, the effect of a presumed increase in the effective diffusion coefficient due to small-scale fractures (BSC 2006 [DIRS 178275], Section 6.4.1) is modeled by applying an alternate conceptual model and enhancement factor for matrix diffusion.	In Section 7.6 of *UZ Flow Models and Submodels* (SNL 2007 [DIRS 184614]), a flow and transport field test and model is presented for a percolation and tracer test conducted along a fault in Alcove 8/Niche 3. A Multiple Interacting Continua (MINC) discrete fracture model was developed for simulating flow and transport during the test. The fault was explicitly included, along with finely discretized grid spacings in the matrix adjacent to the fault. An analysis is presented regarding the influence of matrix diffusion and the parameter ranges required to match the breakthrough curves of two conservative, diffusing tracers with different diffusion coefficients in free water. Figure 7.8-9 of SNL (2007 [DIRS 184614]) shows that in order to obtain a good match to the tracer tests, the interface area had to be increased by a factor of 45 above that of the original data. Likewise, in Section 7.3 of SNL (2007 [DIRS 177396]), the same analysis is provided; in both reports, a discussion of the reasons for the need to adjust the interface area is provided. In Liu et al. (2004 [DIRS 169948]), this scale effect is described in the form of an increase in the matrix diffusion coefficient, but the description in the paper postulates that the increase could be due to the increase in available surface area for diffusion as a solute encounters a greater number of fractures during its transit through a fractured medium.

Table C5-1. Assumptions Identified as Potentially Conservative and Significant to Annual Dose Rate (Continued)

Submodel	TSPA-LA Assumption	PMA Treatment	Basis for Change
UZ Transport (Continued)	In the compliance model (SNL 2008 [DIRS 184748], Section 6.4.5), radionuclides assumed to be affected by colloid-facilitated transport are handled using a composite of three individual components: 1) the reversibly sorbed species, 2) a fraction that is governed by irreversible attachment to colloids that undergo retardation due to colloid attachment/detachment processes, and 3) a 'fast fraction' of colloids that were assumed to transport conservatively (without any filtration or retardation).	Colloid-facilitated contaminant transport in the PMA treats the variability of mobility of individual colloids as a process that is inherent to the colloid population, rather than as observations that lead to uncertainty in the transport properties within a conventional, single-valued parameter. The process of retardation via attachment and detachment of colloids on immobile surfaces is modeled assuming a diverse population of transport properties that account for the inherent variability of colloid size, surface charge and chemical properties, mineralogy, and their concomitant impact on colloid mobility.	This approach is modified in the PMA to address technical issues that could lead to overly conservative performance of the natural barriers for colloid-facilitated radionuclides. Principally, the TSPA-LA model is considered to be conservative because it does not account, except in a coarse way, for the inherent variability of transport properties of individual colloids in a colloid population.
	The water table in the UZ Transport Model under the future climate states is assumed to rise to a level of 850 m for all realizations, a nominal rise of 120 m from the present-day value. In the compliance model, the rise of 120 m was adopted without uncertainty (SNL 2008 [DIRS 184748], Section 6.6.2.1).	In the PMA model, the water table elevation is taken as an uncertain parameter with a distribution that results in most realizations being conducted with a water table elevation that is less than 850 m.	This approach for the TSPA-LA Model was considered to be conservative with respect to the UZ transport times, because 850 m was considered to be an upper bound, and the higher water table shortens the travel distance and travel times through the UZ. This change for PMA creates a model analysis that is more realistic with respect to UZ transport times than the compliance model, and one in which the uncertainty in water table elevation is more faithfully represented.
SZ Flow and Transport	The change in groundwater flow in the SZ from one climatic state to another occurs rapidly and is approximated by a shift from one steady-state flow condition to another steady-state flow condition over one timestep (Section 5.1.5).	In the PMA model, the water table elevation is taken as an uncertain parameter with a distribution that results in most realizations being conducted with a water table elevation that is less than 850 m.	This approach for the TSPA-LA Model was considered to be conservative with respect to the SZ transport times, because the entire RN mass between the lower and the higher water table elevations was put in the SZ in one timestep which shortens the travel distance and travel times (SNL 2008 [DIRS 183750], Section 6.5, p. 6-18).

Table C5-1. Assumptions Identified as Potentially Conservative and Significant to Annual Dose Rate (Continued)

Submodel	TSPA-LA Assumption	PMA Treatment	Basis for Change
SZ Flow and Transport (Continued)	The radionuclide mass reaching the water table in both the matrix and fractures of the UZ released from the UZ Transport Model is transferred to flow through the fractures in the SZ Radionuclide Transport Model (SNL 2008 [DIRS 183750], Sections 6.3.3 and 6.5.2.13).	The PMA model channels the radionuclide mass release from the UZ to the SZ three-dimensional and one-dimensional transport models and accounts for transport in the matrix.	The model assumption in the TSPA-LA Model is equivalent to assuming that the radionuclide mass instantly diffuses out of the UZ matrix and into the SZ fractures at the interface between the UZ and SZ. This approximation is conservative as it reduces the transport time (SNL 2008 [DIRS 183750], Sections 6.3.3 and 6.5.2.13).
	A large fraction of the colloids are retarded by sorption while a small fraction, known as fast-fraction, are transported unretarded. In the TSPA-LA Model (SNL 2008 [DIRS 183750], Section 6.5.2.11), transport of irreversible colloids for the retarded fraction in both the volcanic units and alluvium is calculated using single retardation factors per realization	Using a Colloid Diversity Model, colloids are assigned a wide range of retardation factors within a given TSPA realization in recognition of their diverse sizes, shapes, compositions, and surface properties.	There is significant variability (diversity) in the attachment/detachment rate constants resulting from differences in water chemistry, colloid size, colloid mineralogy, colloid surface charge, and characteristics of sorption sites on the aquifer media (Robinson et al. 2007 [DIRS 180698]). Implementation of a single retardation factor for all nonfast-fraction colloids in the volcanic rocks and alluvium is conservative.
	The base-case conceptual model of SZ transport developed for the TSPA-LA model is implicitly taken to be oxidizing conditions in the SZ, based on the uncertainty distributions for sorption coefficients of technetium and neptunium (SNL 2008 [DIRS 183750]).	The PMA model adapts the SZ Flow and Transport Abstraction Model to simulate the transport of technetium and neptunium with enhanced sorption in zones of potentially reducing geochemical conditions. Uncertainty in the transport of these redox-sensitive species is evaluated with regard to the location and size of a potential reducing zone in the SZ and uncertainty in the sorption coefficients within the reducing zone.	Potential variations in redox conditions in the SZ could have significant impacts on the migration of redox-sensitive radionuclide species released from the repository at Yucca Mountain (BSC 2006 [DIRS 178672]). Under reducing geochemical conditions, the solubility limit can be much lower and the sorption coefficient can be much higher for radioelements such as technetium and neptunium. Ignoring the effects of encountering potential reducing zones in the SZ such as precipitation from lower solubility limits and retardation from enhanced sorption would lead to conservative transport times in the SZ before reaching the boundary of the accessible environment.

Table C5-1. Assumptions Identified as Potentially Conservative and Significant to Annual Dose Rate (Continued)

Submodel	TSPA-LA Assumption	PMA Treatment	Basis for Change
SZ Flow and Transport (Continued)	The flowing interval porosity (FPVO) is defined as the volume of the pore space through which significant groundwater flow occurs. To define the lower bound value, estimates of fracture porosity of intact cores of volcanic rock were used. More details can be found in *Saturated Zone Flow and Transport Model Abstraction* (SNL 2008 [DIRS 183750], Section 6.5.2.5).	For the PMA, the lower bound will be raised from 10^{-5} to 10^{-4}, which increases the lower bound by an order of magnitude.	A study of the cumulative distribution function plot for parameter FPVO (SNL 2008 [DIRS 183750], Figure 6-13) shows that less weight is given to the bottom of the distribution (i.e. very low FPVO) than the rest of the distribution. This is based on data from the Experimental Studies Facility (ESF) as well as data from other sources (i.e. theoretical models, pumping tests and tracer tests). The 0.5 probability value of 10^{-3} is considered to be representative of the smallest values of fracture porosity estimated from the ESF data and field tests (SNL 2008 [DIRS 183750], Section 6.5.2.5).
	In the TSPA-LA Model, the ground water specific discharge (which is the function of permeability) and flowing interval porosity are uncorrelated variables (SNL 2008 [DIRS 183750], Sections 6.5.2.1 and 6.5.2.5).	For the PMA value of 0.64 was used as the correlation factor for the parameters FPVO and GWSPD during parameter sampling This affects the SZ breakthrough curves as well as sampled data used in the SZ one-dimensional pipe model.	In a fractured flow aquifer, as fracture density and apertures increase, both flowing interval porosity and permeability to also increase. An uncorrelated model could generate parameter combinations (large specific discharge and small flowing interval porosity) that are not physically consistent. An uncorrelated model could generate parameter combinations (large specific discharge and small flowing interval porosity) that are not physically consistent.

Table C6-1. Relative Humidity Threshold for 0.5mM Fluoride Concentration

Look-up tables* for water 1		RH Threshold	Look-up tables for water 2		RH Threshold	Look-up tables for water 3		RH Threshold	Look-up tables for water 4		RH Threshold
1	1bp2t1.xls	0.99155	1	2bp2t1.xls	0.459231	1	3bp2t1.xls	0.38266	1	4bp2t1.xls	0.559223
2	1bp2t30.xls	0.990971	2	2bp2t30.xls	0.459281	2	3bp2t30.xls	0.44001	2	4bp2t30.xls	0.556413
3	1bp2t70.xls	0.991264	3	2bp2t70.xls	0.427894	3	3bp2t70.xls	0.417156	3	4bp2t70.xls	0.517622
4	1bp3t1.xls	0.991775	4	2bp3t1.xls	0.459335	4	3bp3t1.xls	0.382874	4	4bp3t1.xls	0.559247
5	1bp3t30.xls	0.991533	5	2bp3t30.xls	0.457475	5	3bp3t30.xls	0.440007	5	4bp3t30.xls	0.556864
6	1bp3t70.xls	0.991761	6	2bp3t70.xls	0.425404	6	3bp3t70.xls	0.401144	6	4bp3t70.xls	0.517596
7	1bp4t1.xls	0.991368	7	2bp4t1.xls	0.45937	7	3bp4t1.xls	0.382895	7	4bp4t1.xls	0.559253
8	1bp4t30.xls	0.991944	8	2bp4t30.xls	0.426394	8	3bp4t30.xls	0.388749	8	4bp4t30.xls	0.55688
9	1bp4t70.xls	0.991744	9	2bp4t70.xls	0.425895	9	3bp4t70.xls	0.401212	9	4bp4t70.xls	0.517528
10	1cp2t1.xls	0.991357	10	2cp2t1.xls	0.476173	10	3cp2t1.xls	0.380135	10	4cp2t1.xls	0.558955
11	1cp2t30.xls	0.990736	11	2cp2t30.xls	0.462071	11	3cp2t30.xls	0.440003	11	4cp2t30.xls	0.556412
12	1cp2t70.xls	0.991053	12	2cp2t70.xls	0.428376	12	3cp2t70.xls	0.420008	12	4cp2t70.xls	0.517607
13	1cp3t1.xls	0.991593	13	2cp3t1.xls	0.475998	13	3cp3t1.xls	0.380356	13	4cp3t1.xls	0.558975
14	1cp3t30.xls	0.991333	14	2cp3t30.xls	0.450614	14	3cp3t30.xls	0.440009	14	4cp3t30.xls	0.556865
15	1cp3t70.xls	0.991575	15	2cp3t70.xls	0.426551	15	3cp3t70.xls	0.407961	15	4cp3t70.xls	0.517692
16	1cp4t1.xls	0.991164	16	2cp4t1.xls	0.47617	16	3cp4t1.xls	0.380376	16	4cp4t1.xls	0.558998
17	1cp4t30.xls	0.991761	17	2cp4t30.xls	0.418463	17	3cp4t30.xls	0.425837	17	4cp4t30.xls	0.55688
18	1cp4t70.xls	0.991557	18	2cp4t70.xls	0.426235	18	3cp4t70.xls	0.408021	18	4cp4t70.xls	0.517699
19	1dp2t1.xls	0.990947	19	2dp2t1.xls	0.517331	19	3dp2t1.xls	0.33659	19	4dp2t1.xls	0.558053
20	1dp2t30.xls	0.990234	20	2dp2t30.xls	0.5568	20	3dp2t30.xls	0.477803	20	4dp2t30.xls	0.556413
21	1dp2t70.xls	0.990604	21	2dp2t70.xls	0.442767	21	3dp2t70.xls	0.416811	21	4dp2t70.xls	0.517951
22	1dp3t1.xls	0.991206	22	2dp3t1.xls	0.517304	22	3dp3t1.xls	0.336916	22	4dp3t1.xls	0.55809
23	1dp3t30.xls	0.990909	23	2dp3t30.xls	0.556865	23	3dp3t30.xls	0.449625	23	4dp3t30.xls	0.556865
24	1dp3t70.xls	0.991178	24	2dp3t70.xls	0.442582	24	3dp3t70.xls	0.422049	24	4dp3t70.xls	0.518003
25	1dp4t1.xls	0.99073	25	2dp4t1.xls	0.517284	25	3dp4t1.xls	0.460022	25	4dp4t1.xls	0.558092
26	1dp4t30.xls	0.991369	26	2dp4t30.xls	0.55688	26	3dp4t30.xls	0.481359	26	4dp4t30.xls	0.55688
27	1dp4t70.xls	0.991159	27	2dp4t70.xls	0.442424	27	3dp4t70.xls	0.422094	27	4dp4t70.xls	0.518015
28	1ep2t1.xls	0.990592	28	2ep2t1.xls	0.529443	28	3ep2t1.xls	0.336589	28	4ep2t1.xls	0.561883
29	1ep2t30.xls	0.99527	29	2ep2t30.xls	0.5568	29	3ep2t30.xls	0.505668	29	4ep2t30.xls	0.556412
30	1ep2t70.xls	0.990215	30	2ep2t70.xls	0.524391	30	3ep2t70.xls	0.414621	30	4ep2t70.xls	0.518674
31	1ep3t1.xls	0.99087	31	2ep3t1.xls	0.528825	31	3ep3t1.xls	0.33688	31	4ep3t1.xls	0.561791
32	1ep3t30.xls	0.990539	32	2ep3t30.xls	0.556865	32	3ep3t30.xls	0.453249	32	4ep3t30.xls	0.556864
33	1ep3t70.xls	0.990833	33	2ep3t70.xls	0.524333	33	3ep3t70.xls	0.415086	33	4ep3t70.xls	0.518671
34	1ep4t1.xls	0.990354	34	2ep4t1.xls	0.528903	34	3ep4t1.xls	0.336896	34	4ep4t1.xls	0.561779
35	1ep4t30.xls	0.991028	35	2ep4t30.xls	0.556877	35	3ep4t30.xls	0.428995	35	4ep4t30.xls	0.55688
36	1ep4t70.xls	0.990812	36	2ep4t70.xls	0.52425	36	3ep4t70.xls	0.415105	36	4ep4t70.xls	0.518693
37	1fp2t1.xls	0.990079	37	2fp2t1.xls	0.565735	37	3fp2t1.xls	0.384397	37	4fp2t1.xls	0.567246
38	1fp2t30.xls	0.991139	38	2fp2t30.xls	0.556799	38	3fp2t30.xls	0.505668	38	4fp2t30.xls	0.550692
39	1fp2t70.xls	0.989651	39	2fp2t70.xls	0.530004	39	3fp2t70.xls	0.500638	39	4fp2t70.xls	0.52025
40	1fp3t1.xls	0.990384	40	2fp3t1.xls	0.565712	40	3fp3t1.xls	0.383386	40	4fp3t1.xls	0.567252
41	1fp3t30.xls	0.990384	41	2fp3t30.xls	0.565712	41	3fp3t30.xls	0.383386	41	4fp3t30.xls	0.567252
42	1fp3t70.xls	0.990384	42	2fp3t70.xls	0.565712	42	3fp3t70.xls	0.383386	42	4fp3t70.xls	0.567252

Table C6-1. Relative Humidity Threshold for 0.5mM Fluoride Concentration (Continued)

Look-up tables for water 1		RH Threshold	Look-up tables for water 2		RH Threshold	Look-up tables for water 3		RH Threshold	Look-up tables for water 4		RH Threshold
43	1fp4t1.xls	0.990384	43	2fp4t1.xls	0.565712	43	3fp4t1.xls	0.383386	43	4fp4t1.xls	0.567252
44	1fp4t30.xls	0.990384	44	2fp4t30.xls	0.565712	44	3fp4t30.xls	0.383386	44	4fp4t30.xls	0.567252
45	1fp4t70.xls	0.990384	45	2fp4t70.xls	0.565712	45	3fp4t70.xls	0.383386	45	4fp4t70.xls	0.567252
46	1gp2t1.xls	0.990384	46	2gp2t1.xls	0.565712	46	3gp2t1.xls	0.383386	46	4gp2t1.xls	0.567252
47	1gp2t30.xls	0.990384	47	2gp2t30.xls	0.565712	47	3gp2t30.xls	0.383386	47	4gp2t30.xls	0.567252
48	1gp2t70.xls	0.990384	48	2gp2t70.xls	0.565712	48	3gp2t70.xls	0.383386	48	4gp2t70.xls	0.567252
49	1gp3t1.xls	0.990384	49	2gp3t1.xls	0.565712	49	3gp3t1.xls	0.383386	49	4gp3t1.xls	0.567252
50	1gp3t30.xls	0.990384	50	2gp3t30.xls	0.565712	50	3gp3t30.xls	0.383386	50	4gp3t30.xls	0.567252
51	1gp3t70.xls	0.989604	51	2gp3t70.xls	0.522893	51	3gp3t70.xls	0.497909	51	4gp3t70.xls	0.51394
52	1gp4t1.xls	0.989046	52	2gp4t1.xls	0.565013	52	3gp4t1.xls	0.53999	52	4gp4t1.xls	0.556558
53	1gp4t30.xls	0.989804	53	2gp4t30.xls	0.638204	53	3gp4t30.xls	0.648868	53	4gp4t30.xls	0.541255
54	1gp4t70.xls	0.989578	54	2gp4t70.xls	0.522839	54	3gp4t70.xls	0.49796	54	4gp4t70.xls	0.5131
55	1hp2t1.xls	0.988313	55	2hp2t1.xls	0.555012	55	3hp2t1.xls	0.539994	55	4hp2t1.xls	0.608822
56	1hp2t30.xls	0.986973	56	2hp2t30.xls	0.603528	56	3hp2t30.xls	0.652043	56	4hp2t30.xls	0.603527
57	1hp2t70.xls	0.9877	57	2hp2t70.xls	0.541019	57	3hp2t70.xls	0.555884	57	4hp2t70.xls	0.582732
58	1hp3t1.xls	0.988703	58	2hp3t1.xls	0.555023	58	3hp3t1.xls	0.540003	58	4hp3t1.xls	0.608848
59	1hp3t30.xls	0.988136	59	2hp3t30.xls	0.603691	59	3hp3t30.xls	0.652386	59	4hp3t30.xls	0.603689
60	1hp3t70.xls	0.98858	60	2hp3t70.xls	0.54102	60	3hp3t70.xls	0.555924	60	4hp3t70.xls	0.582756
61	1hp4t1.xls	0.987944	61	2hp4t1.xls	0.555025	61	3hp4t1.xls	0.540005	61	4hp4t1.xls	0.608838
62	1hp4t30.xls	0.988787	62	2hp4t30.xls	0.603733	62	3hp4t30.xls	0.652438	62	4hp4t30.xls	0.60372
63	1hp4t70.xls	0.98855	63	2hp4t70.xls	0.541013	63	3hp4t70.xls	0.600666	63	4hp4t70.xls	0.582745
64	1ip2t1.xls	0.986787	64	2ip2t1.xls	0.720004	64	3ip2t1.xls	0.586237	64	4ip2t1.xls	0.608062
65	1ip2t30.xls	0.990796	65	2ip2t30.xls	0.607439	65	3ip2t30.xls	0.604172	65	4ip2t30.xls	0.579992
66	1ip2t70.xls	0.986018	66	2ip2t70.xls	0.620008	66	3ip2t70.xls	0.570486	66	4ip2t70.xls	0.586302
67	1ip3t1.xls	0.987243	67	2ip3t1.xls	0.720006	67	3ip3t1.xls	0.586285	67	4ip3t1.xls	0.608067
68	1ip3t30.xls	0.98651	68	2ip3t30.xls	0.899994	68	3ip3t30.xls	0.603691	68	4ip3t30.xls	0.579993
69	1ip3t70.xls	0.987056	69	2ip3t70.xls	0.617002	69	3ip3t70.xls	0.570494	69	4ip3t70.xls	0.586242
70	1ip4t1.xls	0.986337	70	2ip4t1.xls	0.71999	70	3ip4t1.xls	0.586279	70	4ip4t1.xls	0.60807
71	1ip4t30.xls	0.987257	71	2ip4t30.xls	0.939993	71	3ip4t30.xls	0.603738	71	4ip4t30.xls	0.58
72	1ip4t70.xls	0.987019	72	2ip4t70.xls	0.617094	72	3ip4t70.xls	0.570497	72	4ip4t70.xls	0.586259
73	1jp2t1.xls	0.984584	73	2jp2t1.xls	0.984522	73	3jp2t1.xls	0.613285	73	4jp2t1.xls	0.980003
74	1jp2t30.xls	0.982339	74	2jp2t30.xls	0.98398	74	3jp2t30.xls	0.610202	74	4jp2t30.xls	0.960001
75	1jp2t70.xls	0.983577	75	2jp2t70.xls	0.984197	75	3jp2t70.xls	0.610609	75	4jp2t70.xls	0.980001
76	1jp3t1.xls	0.985126	76	2jp3t1.xls	0.984658	76	3jp3t1.xls	0.613262	76	4jp3t1.xls	0.980003
77	1jp3t30.xls	0.989258	77	2jp3t30.xls	0.9843	77	3jp3t30.xls	0.610389	77	4jp3t30.xls	0.980003
78	1jp3t70.xls	0.984822	78	2jp3t70.xls	0.984495	78	3jp3t70.xls	0.61066	78	4jp3t70.xls	0.980002
79	1jp4t1.xls	0.984024	79	2jp4t1.xls	0.984438	79	3jp4t1.xls	0.613248	79	4jp4t1.xls	0.980003
80	1jp4t30.xls	0.985008	80	2jp4t30.xls	0.984575	80	3jp4t30.xls	0.610447	80	4jp4t30.xls	0.980002
81	1jp4t70.xls	0.984778	81	2jp4t70.xls	0.984778	81	3jp4t70.xls	0.610732	81	4jp4t70.xls	0.980002
82	1Lp2t1.xls	0.980009	82	2Lp2t1.xls	0.96	82	3Lp2t1.xls	0.940004	82	4Lp2t1.xls	0.960004
83	1Lp2t30.xls	0.98	83	2Lp2t30.xls	0.960094	83	3Lp2t30.xls	0.939998	83	4Lp2t30.xls	0.960006
84	1Lp2t70.xls	0.979998	84	2Lp2t70.xls	0.960006	84	3Lp2t70.xls	0.940001	84	4Lp2t70.xls	0.960003

Table C6-1. Relative Humidity Threshold for 0.5mM Fluoride Concentration (Continued)

Look-up tables for water 1		RH Threshold	Look-up tables for water 2		RH Threshold	Look-up tables for water 3		RH Threshold	Look-up tables for water 4		RH Threshold
85	1Lp3t1.xls	0.98001	85	2Lp3t1.xls	0.973538	85	3Lp3t1.xls	0.940001	85	4Lp3t1.xls	0.959994
86	1Lp3t30.xls	0.98	86	2Lp3t30.xls	0.963402	86	3Lp3t30.xls	0.939999	86	4Lp3t30.xls	0.960005
87	1Lp3t70.xls	0.980008	87	2Lp3t70.xls	0.960001	87	3Lp3t70.xls	0.940002	87	4Lp3t70.xls	0.960003
88	1Lp4t1.xls	0.979995	88	2Lp4t1.xls	0.960003	88	3Lp4t1.xls	0.94	88	4Lp4t1.xls	0.960002
89	1Lp4t30.xls	0.980006	89	2Lp4t30.xls	0.964723	89	3Lp4t30.xls	0.94611	89	4Lp4t30.xls	0.959999
90	1Lp4t70.xls	0.980425	90	2Lp4t70.xls	0.960001	90	3Lp4t70.xls	0.940003	90	4Lp4t70.xls	0.959997
91	10p2t1.xls	0.980425	91	20p2t1.xls	0.960001	91	30p2t1.xls	0.940003	91	40p2t1.xls	0.959997
92	10p2t30.xls	0.980425	92	20p2t30.xls	0.960001	92	30p2t30.xls	0.940003	92	40p2t30.xls	0.959997
93	10p2t70.xls	0.980425	93	20p2t70.xls	0.960001	93	30p2t70.xls	0.940003	93	40p2t70.xls	0.959997
94	10p3t1.xls	0.980425	94	20p3t1.xls	0.960001	94	30p3t1.xls	0.940003	94	40p3t1.xls	0.959997
95	10p3t30.xls	0.980425	95	20p3t30.xls	0.960001	95	30p3t30.xls	0.940003	95	40p3t30.xls	0.959997
96	10p3t70.xls	0.980425	96	20p3t70.xls	0.960001	96	30p3t70.xls	0.940003	96	40p3t70.xls	0.959997
97	10p4t1.xls	0.980425	97	20p4t1.xls	0.960001	97	30p4t1.xls	0.940003	97	40p4t1.xls	0.959997
98	10p4t30.xls	0.980425	98	20p4t30.xls	0.960001	98	30p4t30.xls	0.940003	98	40p4t30.xls	0.959997
99	10p4t70.xls	0.980425	99	20p4t70.xls	0.960001	99	30p4t70.xls	0.940003	99	40p4t70.xls	0.959997

Source: DTN: SN0701PAEBSPCE.001_R1 [DIRS 180523]

Table C6-2. Stoichiometries of Waste Degradation Reactions

Waste/WP Component	Water Consumed (mole)	Volume of Corrosion Products Produced (m^3)	Hygroscopic Salt Released (Mole NaCl Equivalent)
1 kg CSNF reacted	7.23	2.39×10^{-4}	0.034
1 kg N-reactor reacted	8.40	2.78×10^{-4}	0
1 kg HLW reacted	10.52	5.9×10^{-4}	0.062-1.078
1 kg SS316 reacted	14.15	3.3×10^{-4}	0.062-0.133

Source: Corroborative DTN: SN0704PMAWBCAL.001_R2 [DIRS 182335]

Table C6-3. Parameter Values Used in Diffusion-Dominated Simulations

Variable	Units	CSNF	2DHLW	2MCO
pCO_2	Negative log bar	1.5, 2, 3, and 4	1.5, 2, 3, and 4	1.5, 2, 3, and 4
q	L/yr	0	0	0
k_{ss}/k_{wf}	Nondimensional	0.01, 0.1, 0.3, 1, 1.5, 2, 3, 10, and 100	0.01, 0.1, 1, 10, 25, 50, 75, 100, and 1,000	1×10^{-2}, 1×10^{-4}, 1×10^{-6}, and 1×10^{-7}
V_s/V_w	Nondimensional	≥ 1.5 (continuous)	≥ 1.5 (continuous)	≥ 1.5 (continuous)

Source: Corroborative DTN: SN0704PMAIPCPM.001 [DIRS 180745]

Table C6-4. Parameter Values Used in Liquid Influx Simulations

Parameter	Units	CSNF	2DHLW	2MCO
pCO2	Log bar	1.5, 3, and 4	1.5, 3, and 4	1.5, 3, and 4
q	L/yr	0.1, 1, 10, 100, and 1,000	0.01, 0.1, 1, 10, and 100	1, 10, 100, and 1,000
kss/kwf	nondimensional	0.1, 1.5, and 10	10 and 100	$1x10^{-2}$, $1x10^{-4}$, and $1x10^{-7}$
Vs/Vw	nondimensional	1.5	1.5	1.5

Source: Corroborative DTN: SN0704PMAIPCPM.001 [DIRS 180745]

Table C6-5. Controlling Factors for CSNF Dissolution

Process/Parameter	Impact on Dissolution	Treatment in Compliance Model	Treatment in PMA
Water chemistry (e.g., oxygen fugacity, total carbonate molar concentration, and pH)	The rate of CSNF dissolution depends on temperature, oxygen fugacity, total carbonate molar concentration, and pH (BSC 2004 [DIRS 169987]).	Explicitly included in a0 through a4.	Use the same functional dependence as in the compliance model.
Water chemistry (e.g., dissolved Ca, Si)	Dissolved Ca and Si tend to inhibit CSNF dissolution (Wilson and Gray 1990 [DIRS 115085]).	At least partly included in a0 through a4 since simulated groundwater is used in leaching tests.	The same as the compliance model.
Fuel chemistry–Non-uranium cation effect	Non-uranium cations such as Pu, Zr, and Mo are known to inhibit CSNF dissolution (Grandstaff 1976 [DIRS 113255]).	At least partly included in a0 through a4 since actual fuels are used in leaching tests.	The same as the compliance model.
Chemical affinity	The overall dissolution rate decreases as the dissolved uranium concentration approaches saturation with respect to secondary reaction products (Pierce et al. 2005 [DIRS 182055]).	Not included	Not included
Effective surface areas	The dissolution rate is directly proportional to the effective surface area of the fuel (BSC 2004 [DIRS 169987]).	The distribution of effective surface area is conservatively derived from fractional release measurements, geometrical calculations, and particle size distributions.	Constrained from fractional release measurements from rod segment tests. Included in As.
Water saturation	Dissolution takes place at the water-solid interface. As water saturation decreases, the effective surface area also decreases (Kuechler and Noack 2007 [DIRS 182054]; Sverdrup and Warfvinge 1988 [DIRS 182056]).	Not included	Included in Eq. C6.5-2. The effective surface area is set to be proportional to water saturation.

Table C6-5. Controlling Factors for CSNF Dissolution (Continued)

Process/Parameter	Impact on Dissolution	Treatment in Compliance Model	Treatment in PMA
Long-term effect	The rate of CSNF dissolution decreases with time (Hanson et al. 2004 [DIRS 182008]).	Not include	Included in a scaling factor (f1).
Changes in radiolysis	Both gamma and beta radiations enhance fuel dissolution (Shoesmith and Sunder 1992 [DIRS 113368]; Shoesmith 2000 [DIRS 114445]). As a result, the actual rates of CSNF dissolution will be lower than those measured in the lab.	Not included	Included in a scaling factor (f2)
Diffusion limit	Diffusion through the layer of degradation products could potentially limit dissolution reactions as the corrosion layer builds up.	Not included	Partly included as a long-term effect (f1).

Table C6-6. Controlling Parameter Distributions for CSNF Degradation

Parameter	Distribution
Log (A_s m^2/mg)	Triangular Low: -7.3 Apex: -7.3 High: -6.7
f_1	Uniform Low: 3 High: 10
f_2	Uniform Low: 5 High: 10

Source: Corroborative DTN: SN0704PMAGDEGM.001_R2 [DIRS 183955]

Table C6-7. Distribution of T_{RC} Used in the Glass Degradation Model for PMA

T_{RC} (mm)	T_{RC} (m)	M_D/M_0 (Fast Fraction)	Distribution (triangular)	Corresponding Slow Fraction
0.03	0.00003	0.0033 (0.33 %)	Minimum	99.67 %
0.1	0.0001	0.011 (1.10 %)	Most probable	98.90 %
0.3	0.0003	0.033 (3.3 %)	Maximum	96.70 %

Source: Corroborative DTN: SN0704PMAGDEGM.001_R2 [DIRS 183955]

Table C6-8. Recommended Uncertainties for Radionuclide Solubilities

Solid	Distribution
PuO_2(aged,hyd)	Log normal, truncated at ±1σ Mean (μ): 0 Standard deviation (σ): 0.79
NpO_2	Triangular a: -1.07 b: 0 c: 1.07
Np_2O_5	Triangular a: -1 b: 0 c: 1
$NaNpO_2CO_3$	Log normal, truncated at ±1σ Mean (μ): 0 Standard deviation (σ): 0.25
Schoepite	Triangular a: -0.4 b: 0 c: 0.4
Na-Boltwoodite	Triangular a: -0.5 b: 0 c: 0.3
$NaNpO_2CO_3$	Triangular a: -0.3 b: 0 c: 0.3

Source: Corroborative DTN: SN0704PMASOLUB.001 [DIRS 182787]

Table C6-9. Uncertain Parameters for the Impacts of Reducing Zones in the PMA

Parameter Name	Input Description	Values	Units
FPLRZN	Northern boundary of the reducing zone used for the 3-D model	Uniform: Minimum: 0.0 Maximum: 1.0	NA
FPLRZS	Southern boundary of the reducing zone used for the 3-D model	Uniform: Minimum: 0.0 Maximum: 1.0	NA
FPLRZE	Eastern boundary of the reducing zone used for the 3-D model	Uniform: Minimum: 0.0 Maximum: 1.0	NA
KD_TC_RZ	Sorption coefficient for technetium in the reducing zone	Normal: Mean: 1,000 Standard Deviation: 150	mL/g
KD_NP_RZ	Sorption coefficient for neptunium in the reducing zone	Normal: Mean: 1.000 Standard Deviation: 150	mL/g

Source: Corroborative DTN: SN0704PMASZFTA.001_R1 [DIRS 184395]

Table C6-10. Cumulative Distribution for FPVO for Use in the PMA (log_{10}-transformed)

Probability	Value
0.0	-4.0
0.50	-3.0
0.80	-2.0
1.0	-1.0

Source: Corroborative DTN: SN0704PMASZFTA.001_R1 [DIRS 184395]

Table C9-1. Impact Assessment Summary Table

	ISSUE DESCRIPTION	IMPACT ASSESSMENT
1	Fifteen of the sixteen UZ_Params_Multi_PMA tables, input files to FEHM DLL (version 2.25), need to be populated at run time according to the model simulation specific settings.	This issue does not impact the TSPA-LA PMA dose calculation which uses the appropriate updated UZ_Params file for 300 epistemic realizations. The UZ_Params_Multi files, tables of sampled values of epistemically uncertain parameters, are only used when the PMA model is run with the compliance implementation of the UZ.
2	The 4 external FEHM .mptr input files for the EF 10k and 1Myr cases need to be updated to point to the correct UZ_Params_Multi_PMA file to use.	This modification only impacts EF EXDOC PMA simulations that turn the PMA UZ implementation off (i.e compliance UZ implementation is used). This feature was not used for the PMA dose calculations, but was intended for future sensitivity analyses. This change needs to occur in conjunction with populating the UZ_Params_Mult files identified in issue #1. This issue does not have any impact on dose results.
3	The selector containing the logic for the determination of the CDSP WP Seismic first damage time is incorrectly set.	The first switch in the selector element, Seismic_1st_Dam_Time_CDSP is incorrectly set to suppress any seismic events. The correct setting should select the EXDOC table, Seismic_Time_A1_Spec, which specifies the sampling configuration for the Seismic GM 10,000-year simulation. This issue, which only applies to the 10,000-year Seismic GM simulation, was corrected prior to running the model, and therefore has no impact on dose.
4	UZ tortuosity parameters, UZ_Tortuosity_RG2_a and UZ_Tortuosity_RG3_a were incorrectly set (v10.002) (err#-case# 001-10.002 needs to change to 002-10.002)	The UZ tortuosity parameters should Correct settings: min(1.0,(10^(UZDC_Mean_RG2+UZDC_STN_RG2*UZDC_SD_RG2))) The expression for UZ_Tortuosity_RG3_a should be min(1.0,(10^(UZDC_Mean_RG3+UZDC_STN_RG3*UZDC_SD_RG3))) This error should have negligible or no impact in all modeling cases.
5	The IWPD submodel selector elements for the timing of the first Igneous or Seismic event are incorrectly set to supress events until 400,000 years. To correct this, the first two switches in the selector elements, Event_Time_Feed_IWPD_CDSP and Event_Time_Feed_IWPD_CSNF need to be deleted. (err#-case# 002-10.016)	This issue is scenario specific to the Igneous, Seismic-FD, and Seismic-GM 10,000-year simulations, as well as the Seismic-FD 1, 000,000 year simulations. The model file for each of the affected cases was corrected prior to running the file, and therefore does not impact the dose calculations.

Table C9-1. Impact Assessment Summary Table (Continued)

	ISSUE DESCRIPTION	IMPACT ASSESSMENT
6	ExDoc type runs for both 1Myr EF cases are run with the PMA cladding failure submodel calculations turned on. (err#-case# 003-10.016)	This is not an error and is not applicable to the impact evaluation.
7	The RH threshold for the fluoride ion calculation is incorrect in nineteen of the tables.	Most of these incorrect values were not used in the actual simulations because these values, both the incorrect and the corrected ones, are low (<0.65). At such low RH, the temperatures in the drift will be still high (> 96 ^{o} C) and there will be no seepage water dripping. For the other incorrect values, the differences between the incorrect and the correct ones are small (<0.012). Therefore, the impact on dose is expected to be negligible.
8	The PMA early failure scenarios distribute the EBS mass released to the UZ nodes unevenly within a given percolation subregion.	Although the EBS mass released to the UZ nodes is distributed unevenly within a given percolation subregion in each realization, the even distribution is captured by calculating the annual mean dose from 300 realizations sampling uncertainty uniformly. Therefore no dose impact is expected.
9	Certain parameters within the model were not connected to the PMA database.	The PMA simulations use the correct values for the parameters listed below, and therefore this issue does not affect the dose calculations. The parameters that need to be linked to the PMA database include, FPLRZN, FPLRZS, FPLRZE, FPVO_PMA, Rf1-Rf10, Kd_Np_RZ, Kd_Np_RZ, SZ_Block_Length, SZ_Block_Thickness, Viscosity_water_T, Sat_Vap_Density_Outside_WP, Water_Vap_Diff_Coeff, Water_Vap_Diff_Cond, Air_Entry_Potential, Sat_Vap_Density_Inside_WP, Osmotic_Coeff, pH_eq
10	Certain parameters within the model were not locked on to the PMA database. GoldSim allows you to “lock onto” the file that is being referenced by a file element. When you lock onto a file (by checking the Lock onto this file option in the File element dialog), the following additional information regarding the referenced file is saved with the element: File and path name; Date the file was created; Date the file was last modified; File size; and CRC signature. Once you have locked onto a file, this information is displayed in a tool-tip when you hold your cursor over the filename in the dialog.	The PMA simulations used the correct files because they were downloaded from the controlled PMA database when the model was run, and therefore this issue does not affect the dose calculations.

Table C9-1. Impact Assessment Summary Table (Continued)

	ISSUE DESCRIPTION	IMPACT ASSESSMENT
11	The pH regression equation contains incorrect coefficients.	The coefficients in the regression for pH_eq need to be corrected. The value of 7.2625 should be rounded to 7.3. The value of 0.00185 has an extra zero and should also be rounded to 0.02. pH_eq is the pH where the acid and the alkaline dissolution rates cross over, and this pH weakly depends on temperature. For the most part of repository time period, the resulting difference in pH_eq due to the error is less than one unit, which is within the uncertainty range of predicted in-package pH values. Therefore, the impact on annual dose is expected to be negligible.
12	There are incorrect values in some of the tables used in the in-package chemistry calculations.	Some of the inputs in the PMA database for the lookup tables named: IPC_XXX_pH_Rsw_YY_Z_LUT (where XXX = CSNF, DHLW, or MCO; YY = 15, 2, 3, or 4; and Z = A-I) has some rows with erroneous data. The DTN that supplied the tables had some independent variables that were duplicated in multiple rows. GoldSim could not read tables with these duplicate independent variables. The DTN supplier indicated that it was acceptable to average these rows together. The error occurred because the analyst who averaged these rows failed to expand out each cell to display the maximum number of significant figures. Therefore some rows were rounded together that did not need to be. No impacts to the dose results are expected. More information is provided in PEF 500. The PEF has a Roadmap to the TSPA-produced DTN that holds the modified lookup tables. This DTN now has two file sets: Uncorrected and Corrected. To correct this error, replace the PMA database entries with the tables in the Corrected folder.
13	The parameter specifying the value of Np Carbonate Eps is incorrect.	The input in the PMA database for parameter “Np_Carbonate_PMA_Eps” is not correct. It should be a triangular distribution with a=-0.5 and b=0 and c=0.5 rather than a truncated normal distribution. The truncated normal distribution is equally well justified. No impacts to the dose results are expected.
14	In determining whether the drift chemical environment is benign or aggressive for drip shield general corrosion, 5 mM dissolved fluoride concentration is used instead of 0.5 mM as suggested in C6.3.1.	The value of 5 mM is justifiable because this value is close to the middle point of the fluoride concentration interval within which the corrosion rate starts to increase at the lower bound (0.5 mM) and then levels off at the upper bound (5 mM). Furthermore, this error only affects one out four initial seepage waters used in the model and this effect will diminish as the seepage water composition returns to the ambient conditions after the thermal event. Therefore, the impact of this error is negligible.

INTENTIONALLY LEFT BLANK

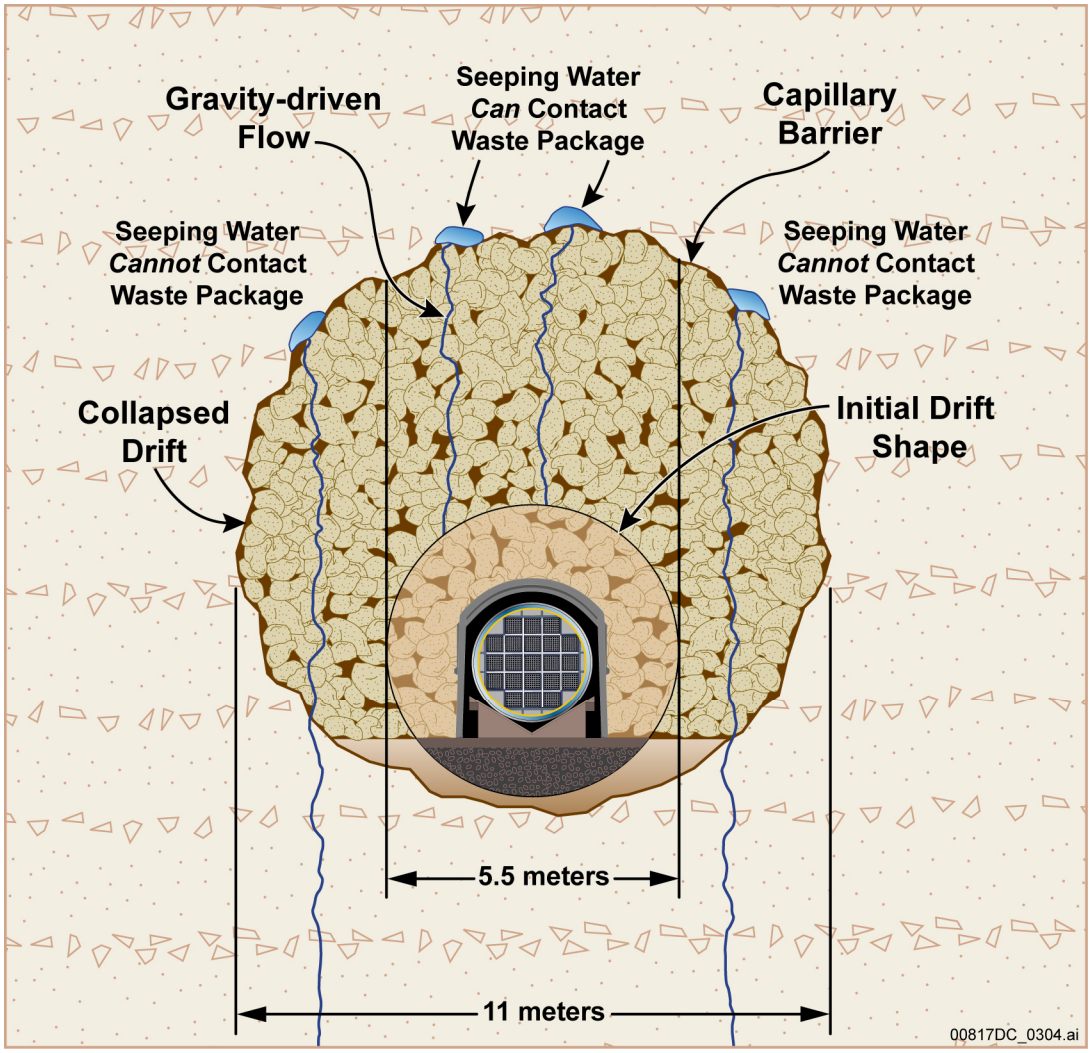

Figure C6-1. Schematic Illustration of Expected Flow Behavior of Seepage in a Rubble-Filled Collapsed Drift

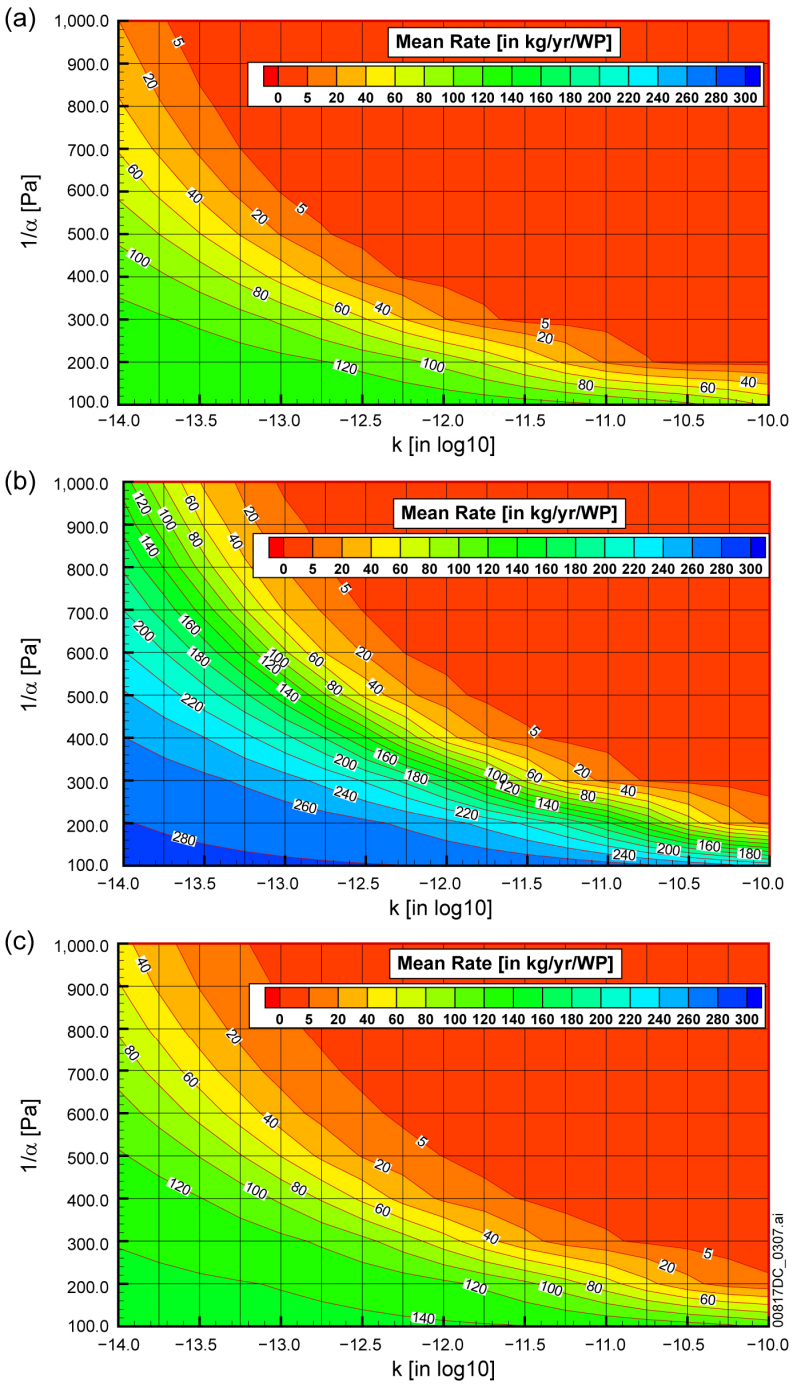

Source: (a) DTN: LB0304SMDCREV2.002 [DIRS 163687], file: Fig6-3to6-8.dat, (b) DTN: LB0307SEEPDRCL.002 [DIRS 180511], file: ResponsSurfaceSMPACollapsedDrift.dat, (c) Corroborative DTN: LB0704PASEEP01.001 [DIRS 181223], file: LookupTableSeepageCollapsedDriftCenter.xls.

NOTES: Seepage Rate Shown as a Function of Capillary-Strength Parameter and Mean Permeability for a Percolation Flux of 5 mm/year. Plots conducted with Tecplot V9.0 graphical software. Horizontal and vertical lines indicate simulated SMPA parameter combinations. Permeability values in log10 of unit m^2.

Figure C6-2. Mean Seepage Rate for (a) Intact Drift, (b) Collapsed Drift with Seepage Collected over 11-Meter Wide Drift, and (c) Collapsed Drift with Seepage Collected over 5.5-Meter Wide Center Section of Drift

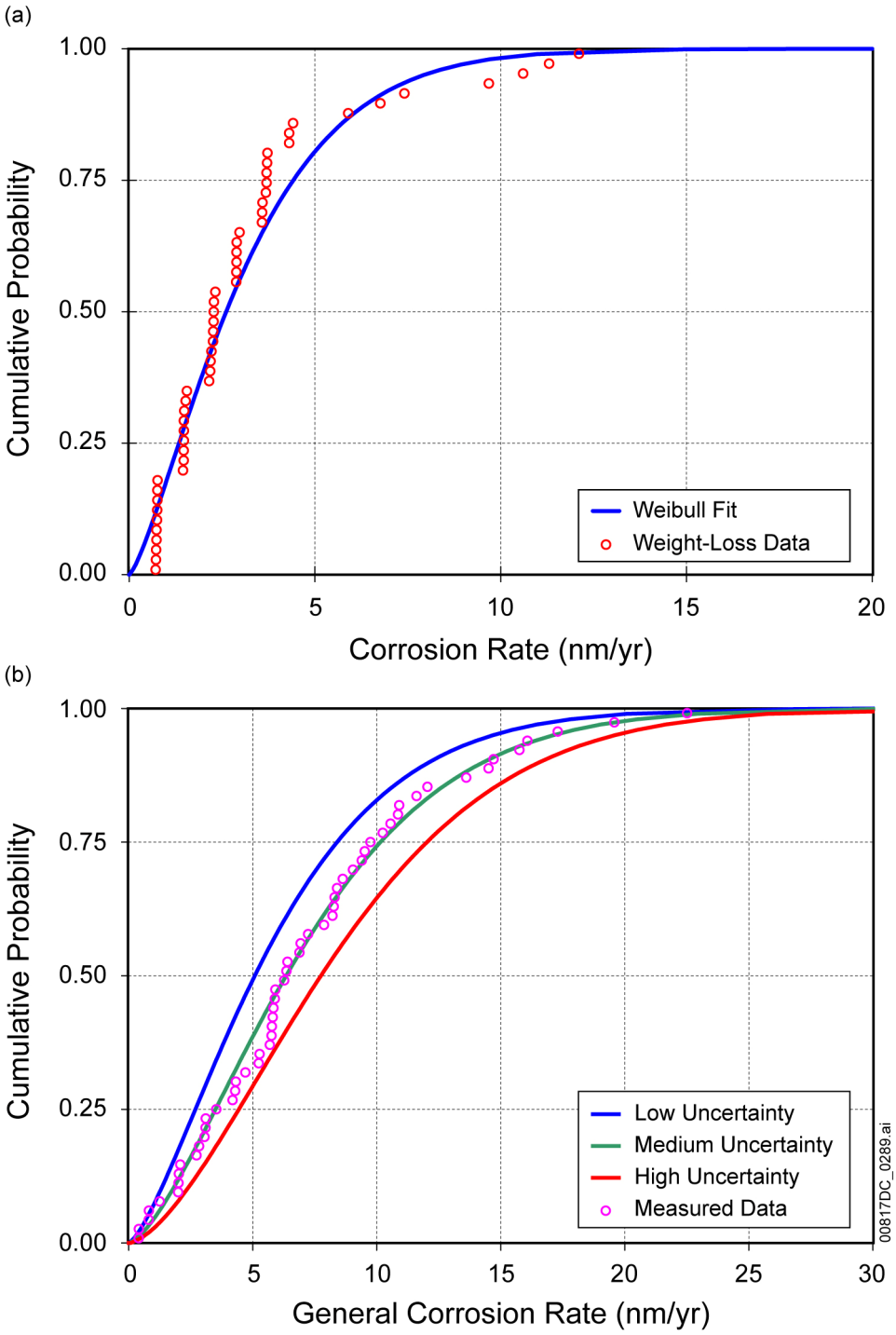

Sources: DTN: LL03041251251.057 [DIRS 163712], *C22 5 Year Coupon Corrosion Rates 4-14-03.xls*;
DTN: MO0612WPOUTERB.000, [DIRS 182035], *ACM GC Rate CDF.xls*.

Figure C6-3. General Corrosion Rate Distribution Resulting from Fitting of Five-year Exposed Weight-Loss Sample Data

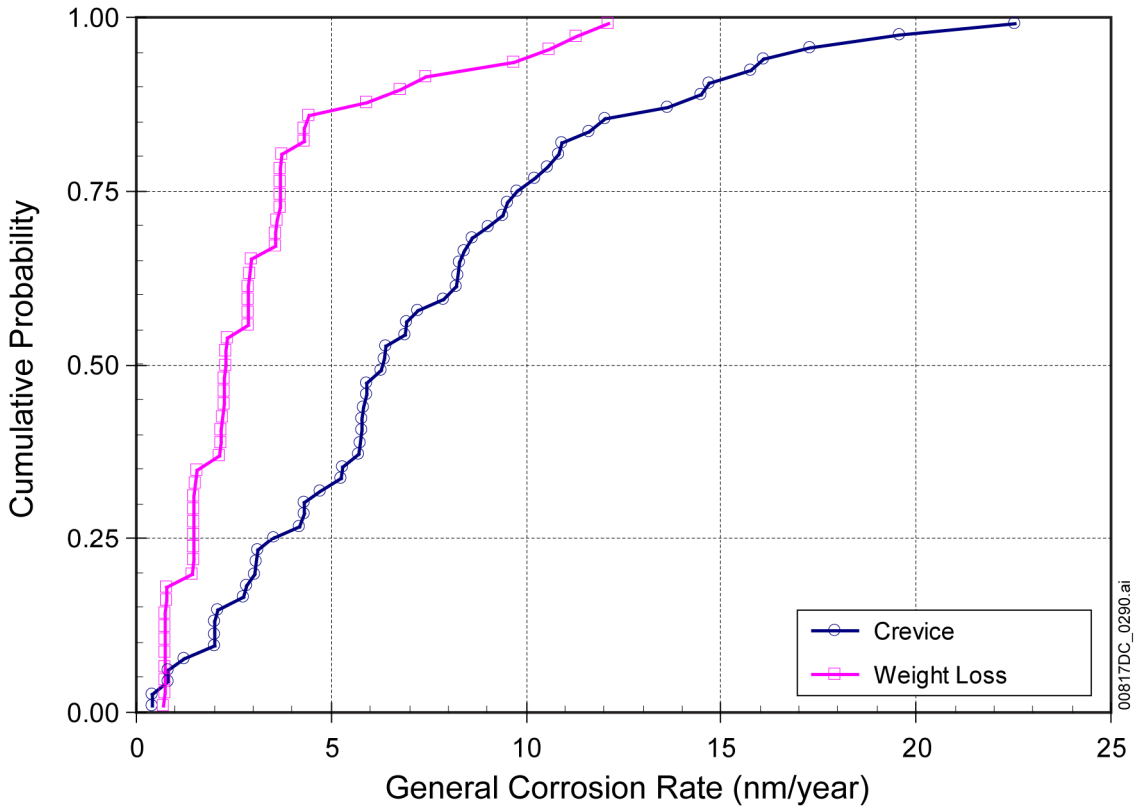

Sources: DTN: MO0612WPOUTERB.000 [DIRS 182035], *Alloy22_5yr_CreviceAnalysis.xls*.

Figure C6-4. Empirical Cumulative Distribution for General Corrosion Rate of Alloy 22 Weight-Loss and Crevice Samples after Five-Year Exposure in Long-Term Corrosion Test Facility

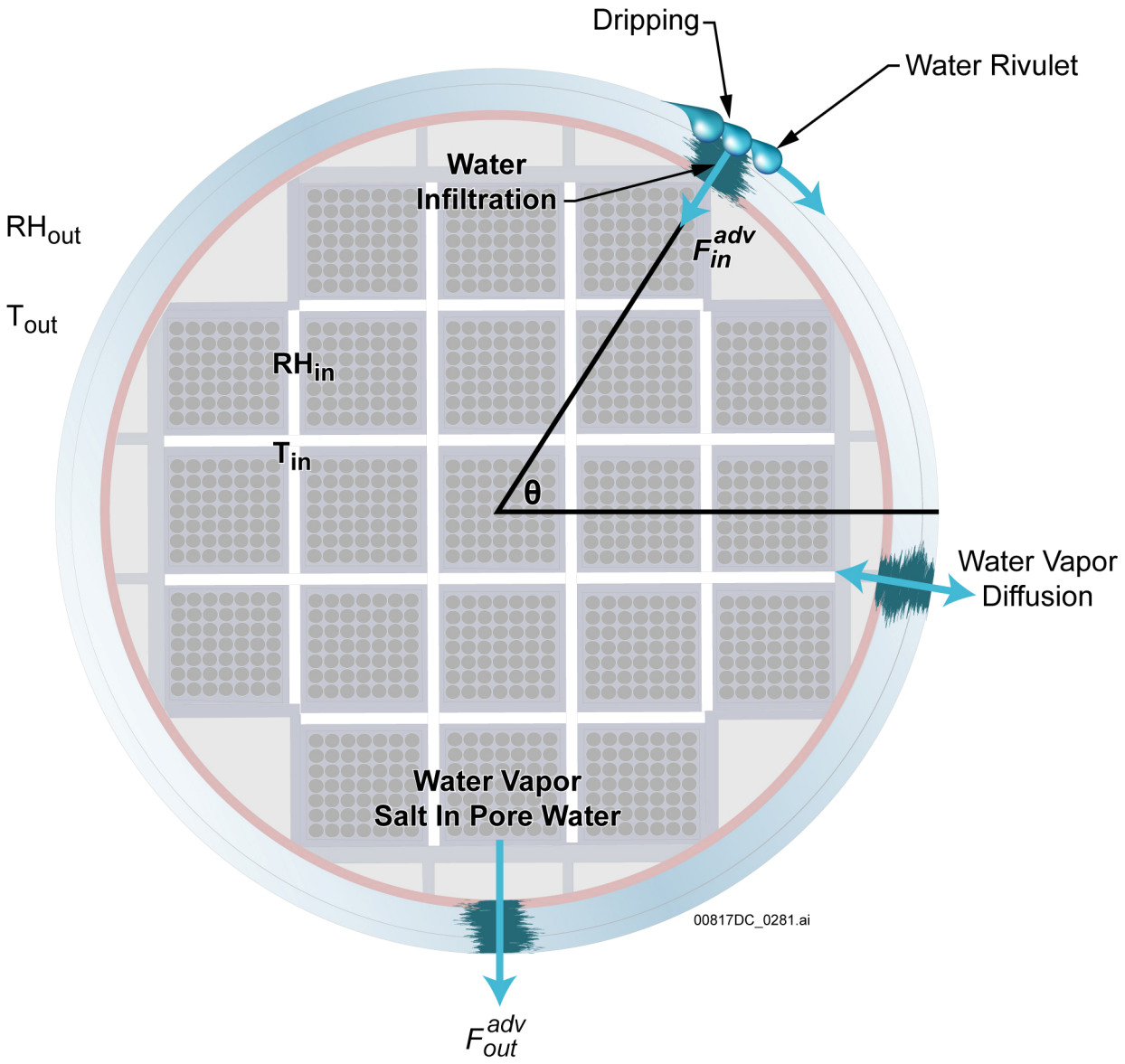

Figure C6-5. Schematic Diagram of Modeling System for In-Package Water Balance

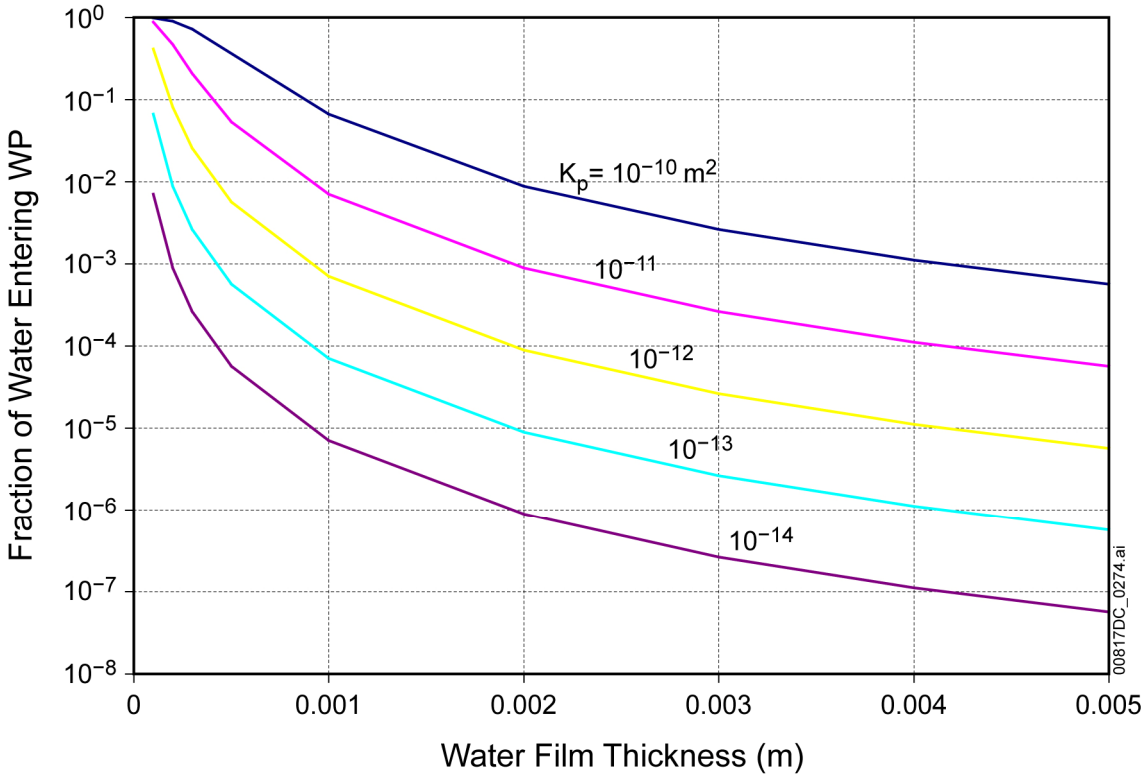

Source: Corroborative DTN: SN0704PMAWBCAL.001_R1 [DIRS 182335], file: *inputs_to_water_balance model.xls, worksheet "water-flux"*.

NOTES: f = 0.1 and ϕ = 0.4

Figure C6-6. Fraction of Water Entering Waste Package Estimated from the Sheet-Flow Model

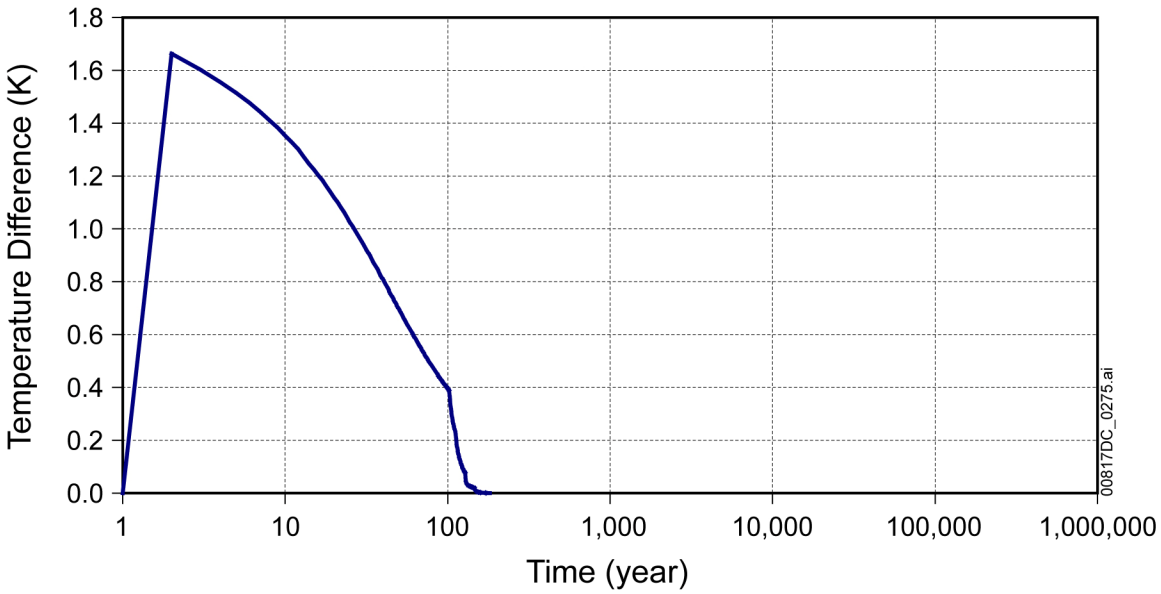

Source: Corroborative DTN: SN0704PMAWBCAL.001 [DIRS 182335], file: *inputs_to_water_balance model.xls, worksheet "Thermal Evolution"*.

Figure C6-7. Temperature Difference between the Inside and Outside of a Waste Package

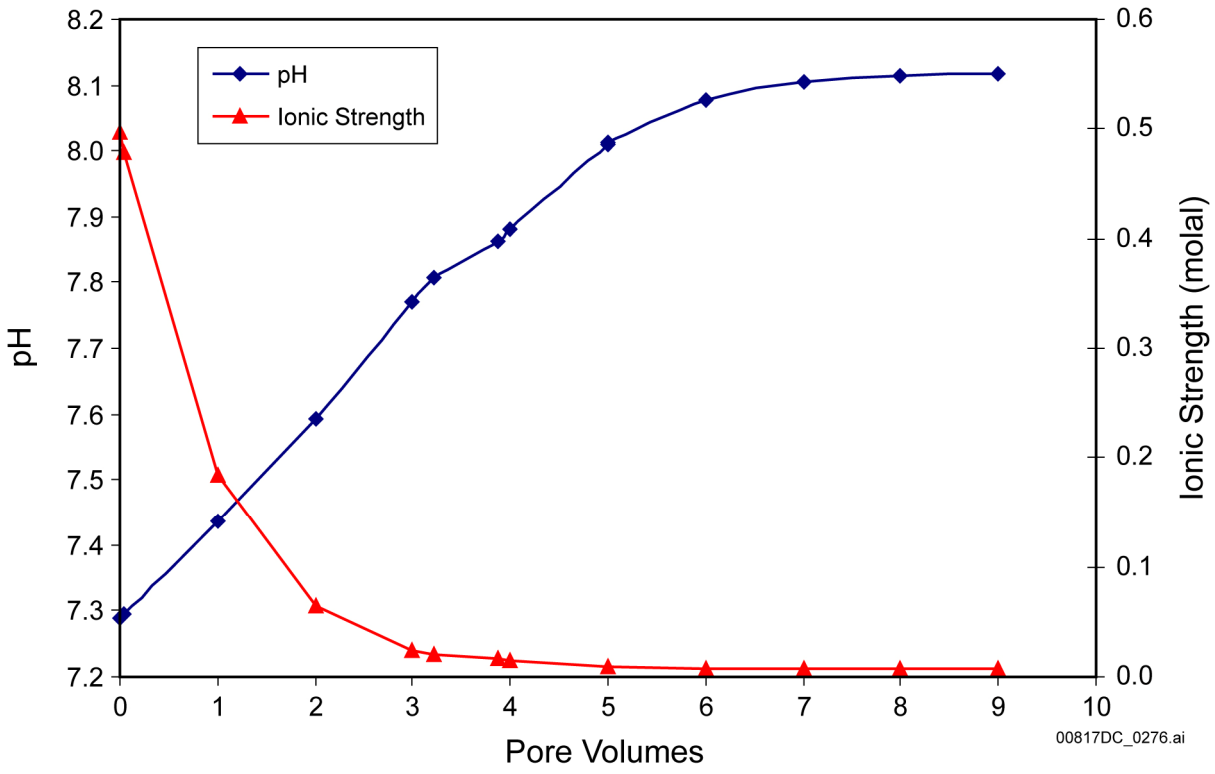

Source: Corroborative DTNs: SN0704PMAIPCPM.001_R0 [DIRS 180745], file: *p0c3fp0s.elem_aqu.xls*; MO0709MARGANAL.000_R0 [DIRS 182978].

Figure C6-8. Illustration of the Approach to Steady State pH and Ionic Strength as a Function of Pore Volumes Flushed

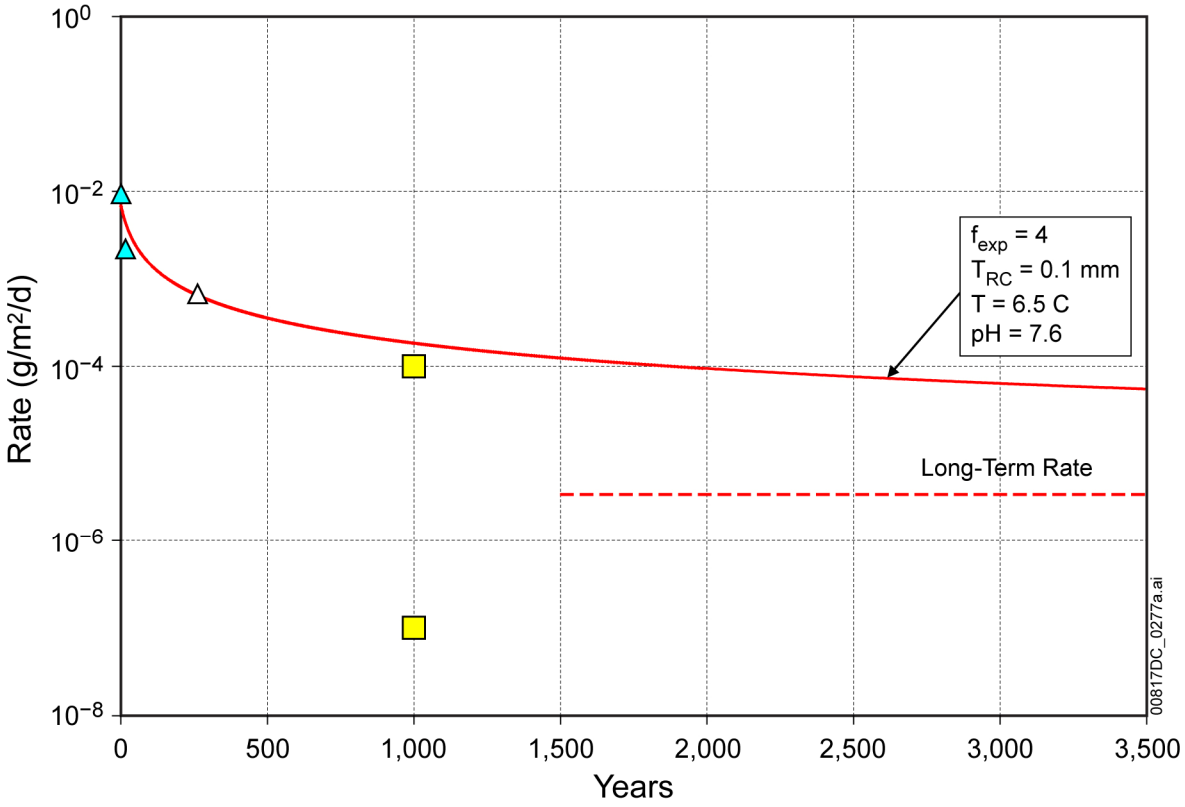

Sources: Triangles from Ojovan et al. (2005 [DIRS 180494]); squares from Gordon and Brady (2003 [DIRS 176673], Table 4); Corroborative DTN: SN0704PMAGDEGM.001_R2 [DIRS 183955], file: *PMA model_revised.xls, worksheet "rate(PMA)"*.

Figure C6-9. Comparison of Performance Margin Analysis Model for High-Level Waste Glass Dissolution

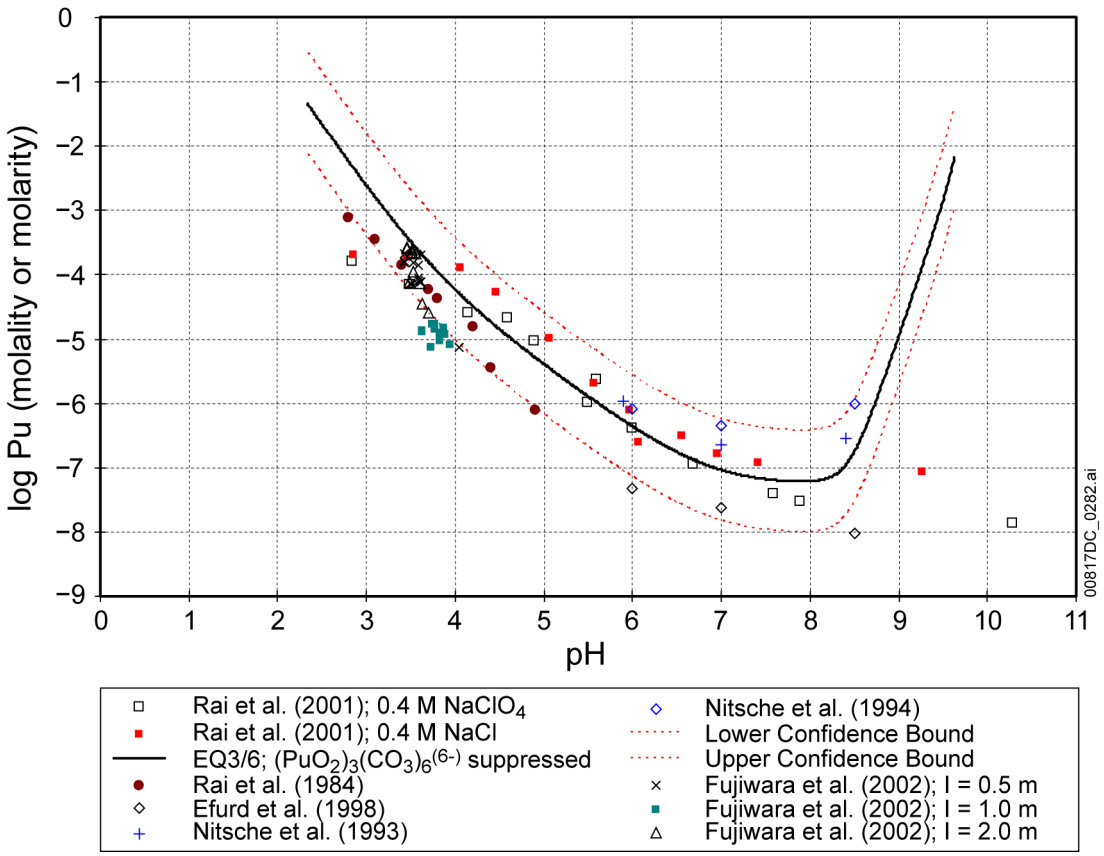

Source: Corroborative DTN: SN0704PMASOLUB.001_R1 [DIRS 182787], file: *Recommended_Uncertainties_Pu_Np_U_Rev01.xls, worksheet "PuO2(hyd,aged)_Summary"*.

NOTE: Computed solubility curve is in molality units (logfO_2(aq)=-7; logPCO_2=-3.5 bars).

Figure C6-10. Plot of Log Transformed PuO_2(am) Solubility vs. pH

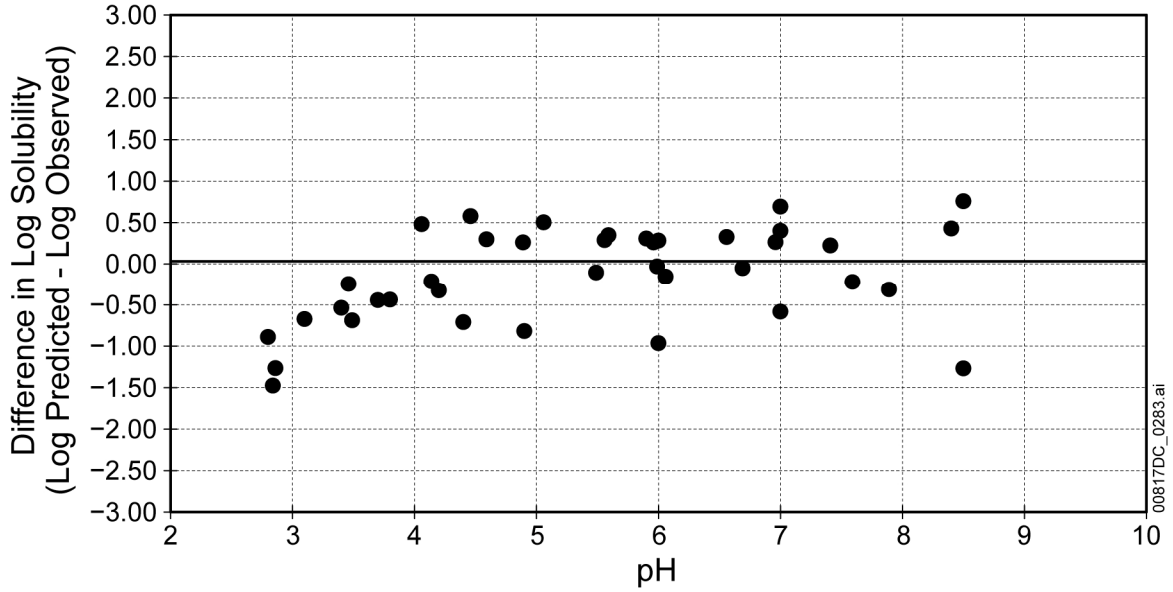

Source: Corroborative DTN: SN0704PMASOLUB.001_R1 [DIRS 182787], file: *Recommended_Uncertainties_Pu_Np_U_Rev01.xls, worksheet "PuO2(hyd,aged)_Summary".*

NOTE: Log predicted stands for solubility values obtained by EQ3/6 simulations. Log observed is the reported solubilities by various sources.

Figure C6-11. Plot of Log Transformed Differences (Log Predicted−Log Observed) for PuO_2(am) Solubility

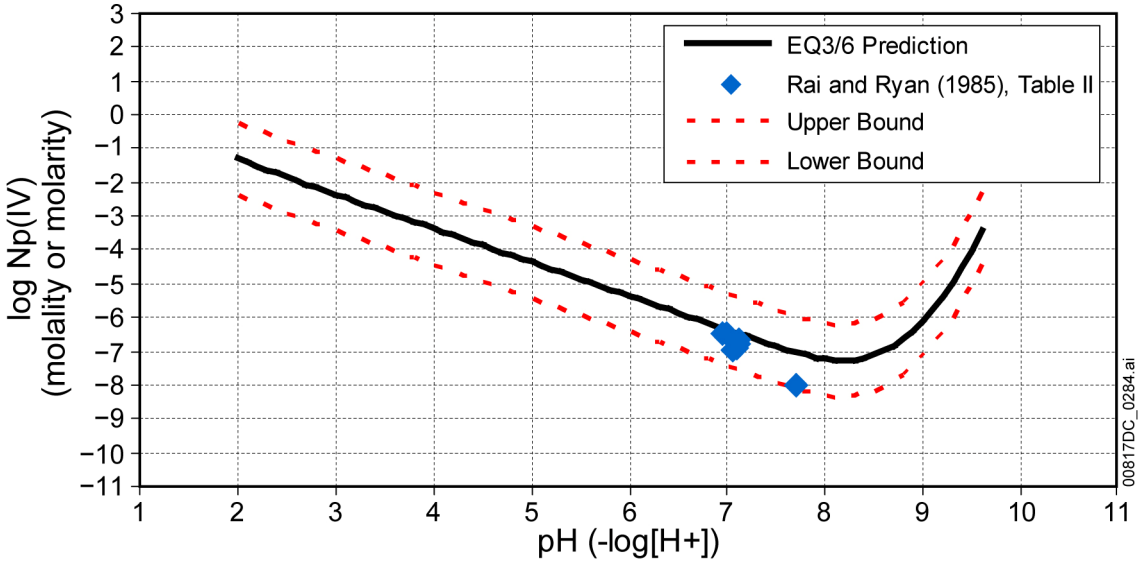

Source: DTN: SN0612T0502404.014 [DIRS 178850]; Corroborative DTN: SN0704PMASOLUB.001_R1 [DIRS 182787], file: *Recommended_Uncertainties_Pu_Np_U_Rev01.xls, worksheet "Np_summary*".

NOTE: The predicted solubility by EQ3/6 is calculated using the thermodynamic database *data0.ymp.R5* (DTN: SN0612T0502404.014 [DIRS 178850]). The summary of calculations is given in Corroborative DTN: SN0704PMASOLUB.001_R1 [DIRS 182787].

Figure C6-12. Comparison of Predicted (EQ3/6) and Observed Values for NpO_2 Solubility along with Uncertainty Bounds

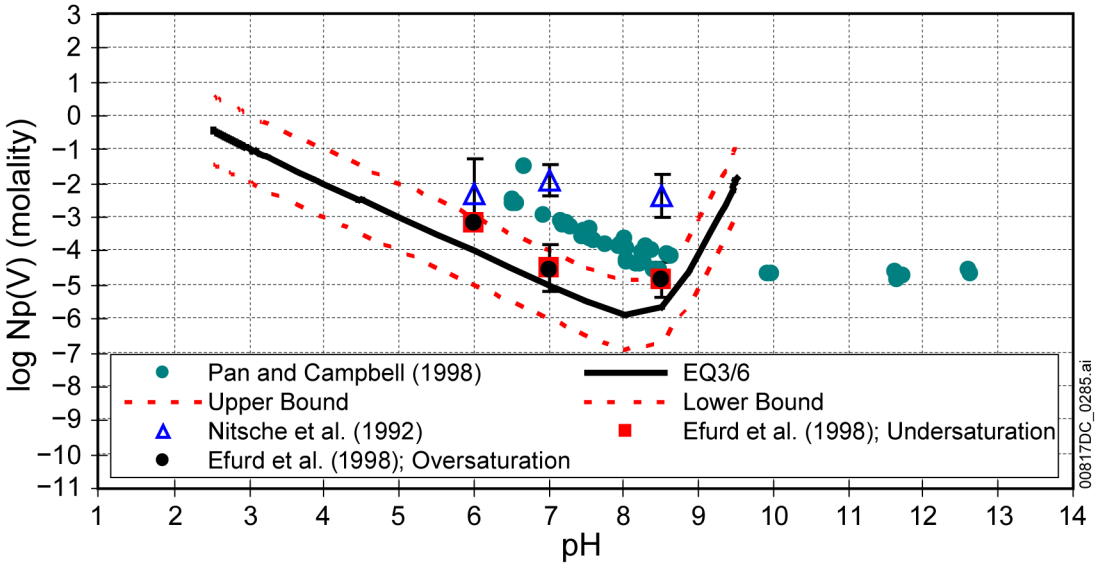

Source: DTN: SN0612T0502404.014 [DIRS 178850]; Corroborative DTN: SN0704PMASOLUB.001_R1 [DIRS 182787], file: *Recommended_Uncertainties_Pu_Np_U_Rev01.xls, worksheet* "*Np_summary*".

NOTE: The predicted solubility by EQ3/6 is calculated using the thermodynamic database *data0.ymp.R5* (DTN: SN0612T0502404.014 [DIRS 178850]). Vertical error bars represent one standard deviation. The summary of calculations is given in Corroborative DTN: SN0704PMASOLUB.001_R1 [DIRS 182787].

Figure C6-13. Comparison of Predicted (EQ3/6) and Observed Values for Np_2O_5 Solubility along with Uncertainty Bounds

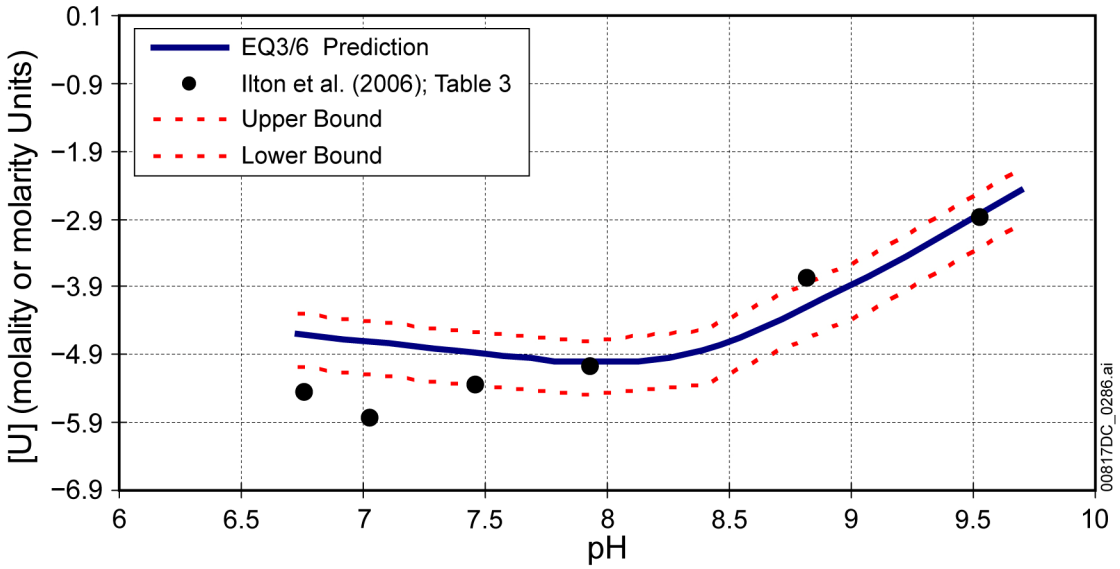

Source: DTN: SN0612T0502404.014 [DIRS 178850]; Corroborative DTN: SN0704PMASOLUB.001_R1 [DIRS 182787], file: *Recommended_Uncertainties_Pu_Np_U_Rev01.xls, worksheet* "U(VI)*_summary*".

NOTE: The predicted solubility by EQ3/6 is calculated using the thermodynamic database *data0.ymp.R5* (DTN: SN0612T0502404.014 [DIRS 178850]). The summary of calculations is given in Corroborative DTN: SN0704PMASOLUB.001_R1 [DIRS 182787].

Figure C6-14. Comparison of Predicted (EQ3/6) and Observed Values for Na-Boltwoodite Solubility along with Uncertainty Bounds

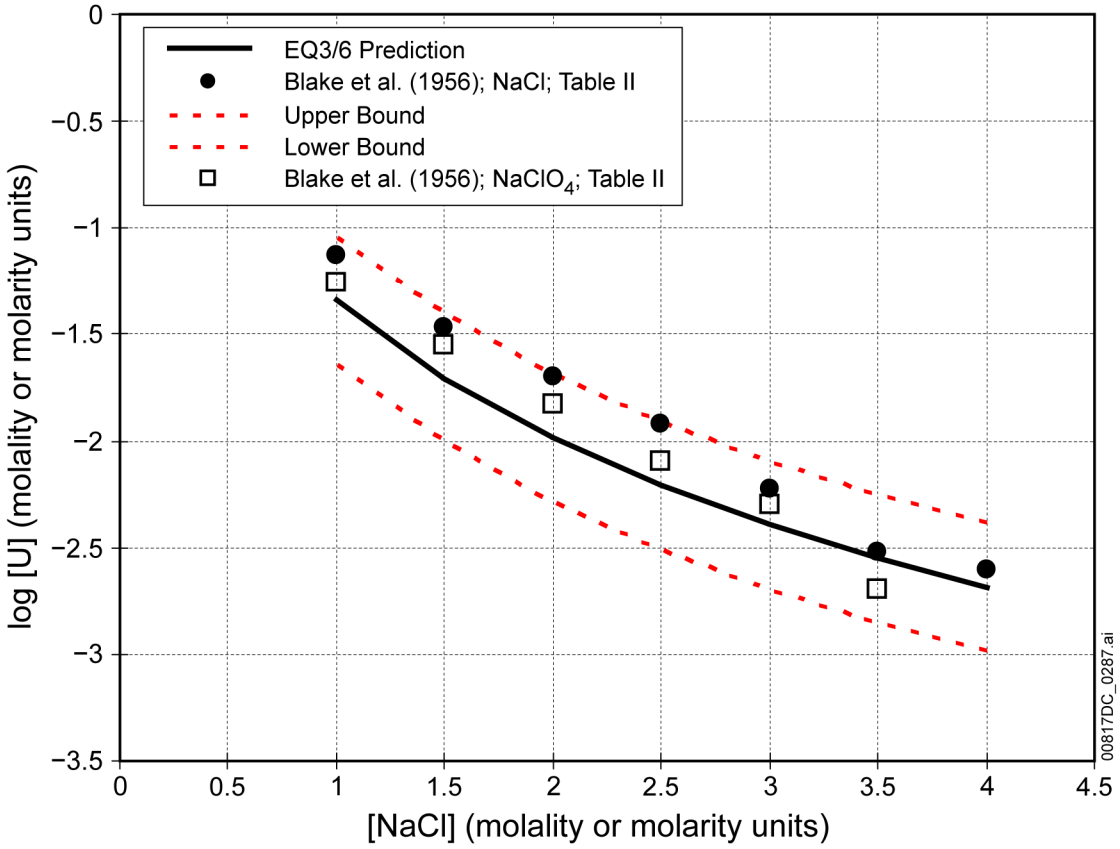

Source: DTN: SN0612T0502404.014 [DIRS 178850]; Corroborative DTN: SN0704PMASOLUB.001_R1 [DIRS 182787], file: *Recommended_Uncertainties_Pu_Np_U_Rev01.xls, worksheet* "U(VI)*_summary*".

NOTE: The predicted solubility by EQ3/6 is calculated using the thermodynamic database *data0.ymp.R5* (DTN: SN0612T0502404.014 [DIRS 178850]). The summary of calculations is given in Corroborative DTN: SN0704PMASOLUB.001_R1 [DIRS 182787].

Figure C6-15. Comparison of Predicted (EQ3/6) and Observed Values for $Na_4UO_2(CO_3)_3$ Solubility along with Uncertainty Bounds

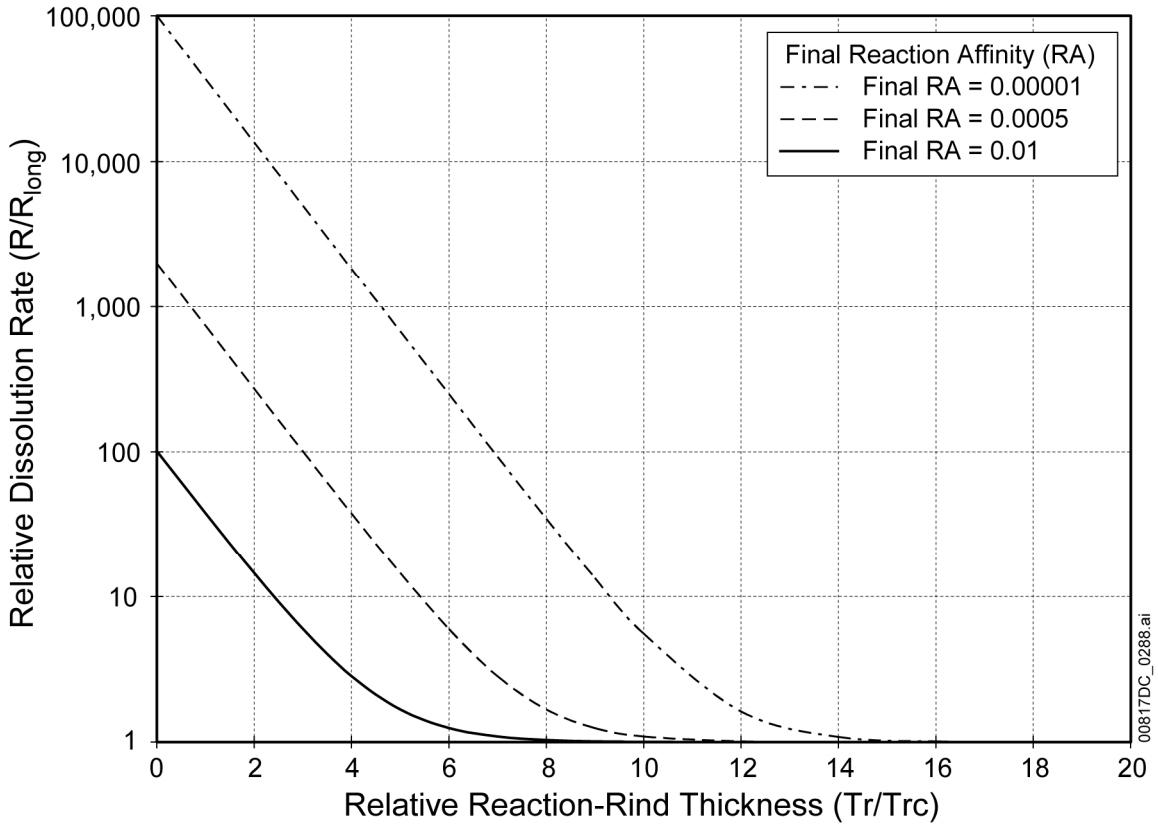

Source: Corroborative DTNs: SN0704PMAGDEGM.001_R2 [DIRS 183955], file: *PMA Model_revised.xls, worksheet "L-T rate"*; MO0709MARGANAL.000 [DIRS 182978].

Figure C6-16. Decrease in Relative Dissolution Rate as a Function of Critical Reaction-Rind Thickness for Each of Three Values for the Final Reaction Affinity

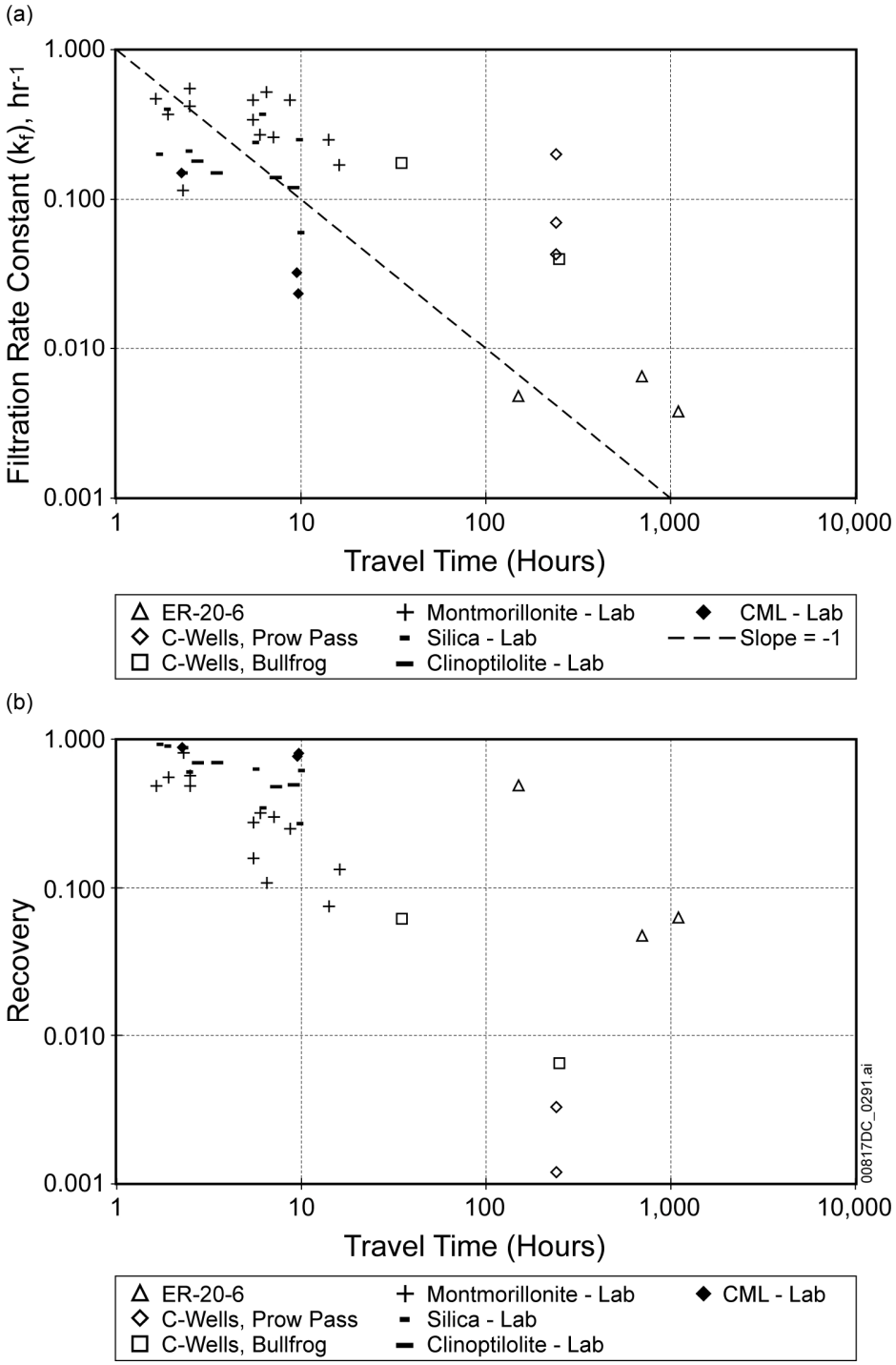

Source: Output DTN: LA0705PR150304.001 [DIRS 181744], file: *Colloid_Diversity_Parameters.xls, worksheet "Volcanics Data*; and Corroborative DTN: MO0709MARGANAL.000 [DIRS 182978].

NOTE: Travel times in field tests are peak conservative tracer travel times.

Figure C6-17. Colloid Filtration Rate Constants and Fractional Recoveries vs. Unretarded Groundwater Travel Times (Determined from Conservative Solute Tracers) from Tracer Experiments in Saturated Fractured Volcanics

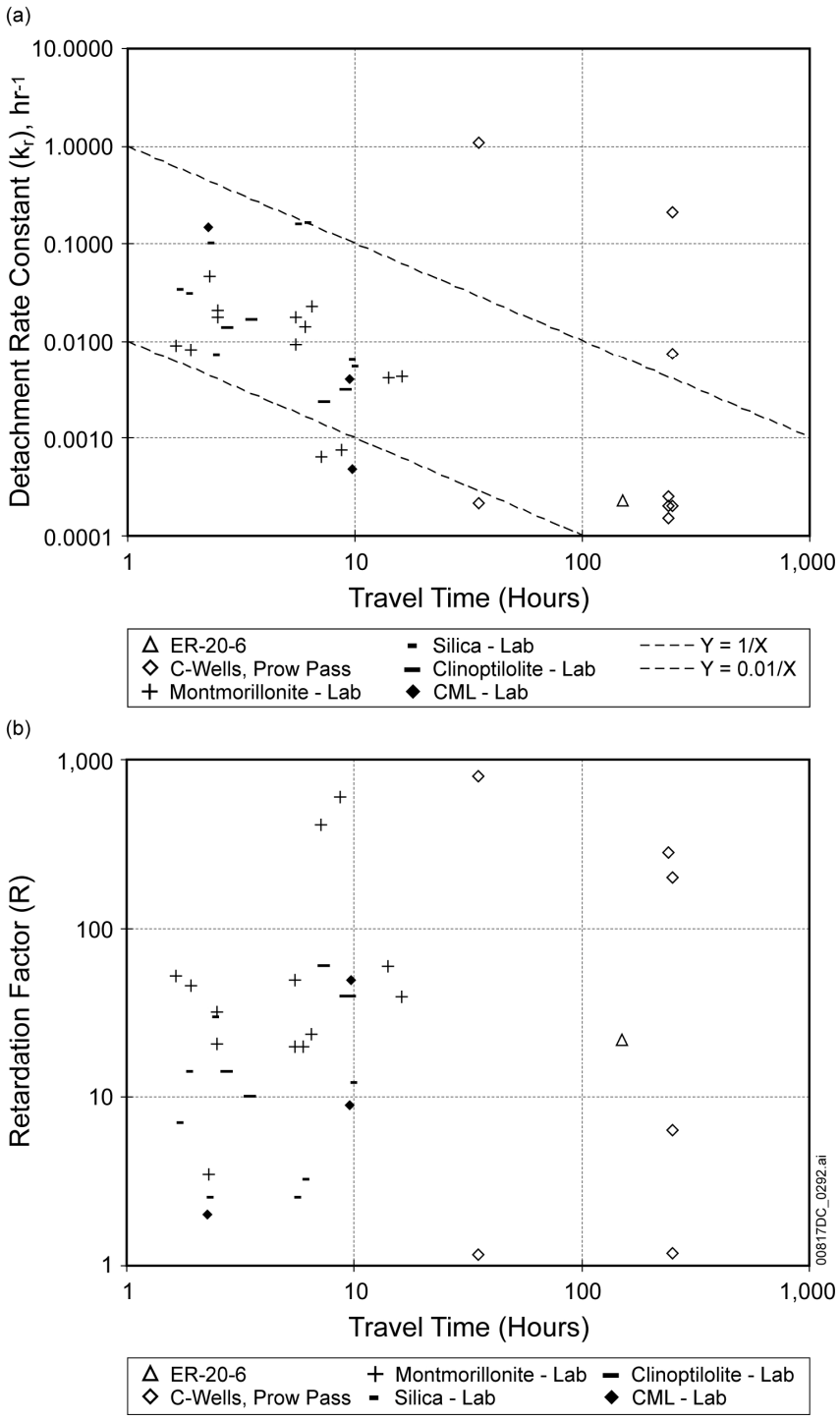

Source: Output DTN: LA0705PR150304.001 [DIRS 181744], file: *Colloid_Diversity_Parameters.xls, worksheet "Volcanics Data"*; and Corroborative DTN: MO0709MARGANAL.000 [DIRS 182978].

NOTE: Travel times in field tests are peak conservative tracer travel times.

Figure C6-18. Colloid Detachment Rate Constants and Retardation Factors vs. Unretarded Groundwater Travel Times (Determined from Conservative Solute Tracers) from Tracer Experiments in Saturated Fractured Volcanics

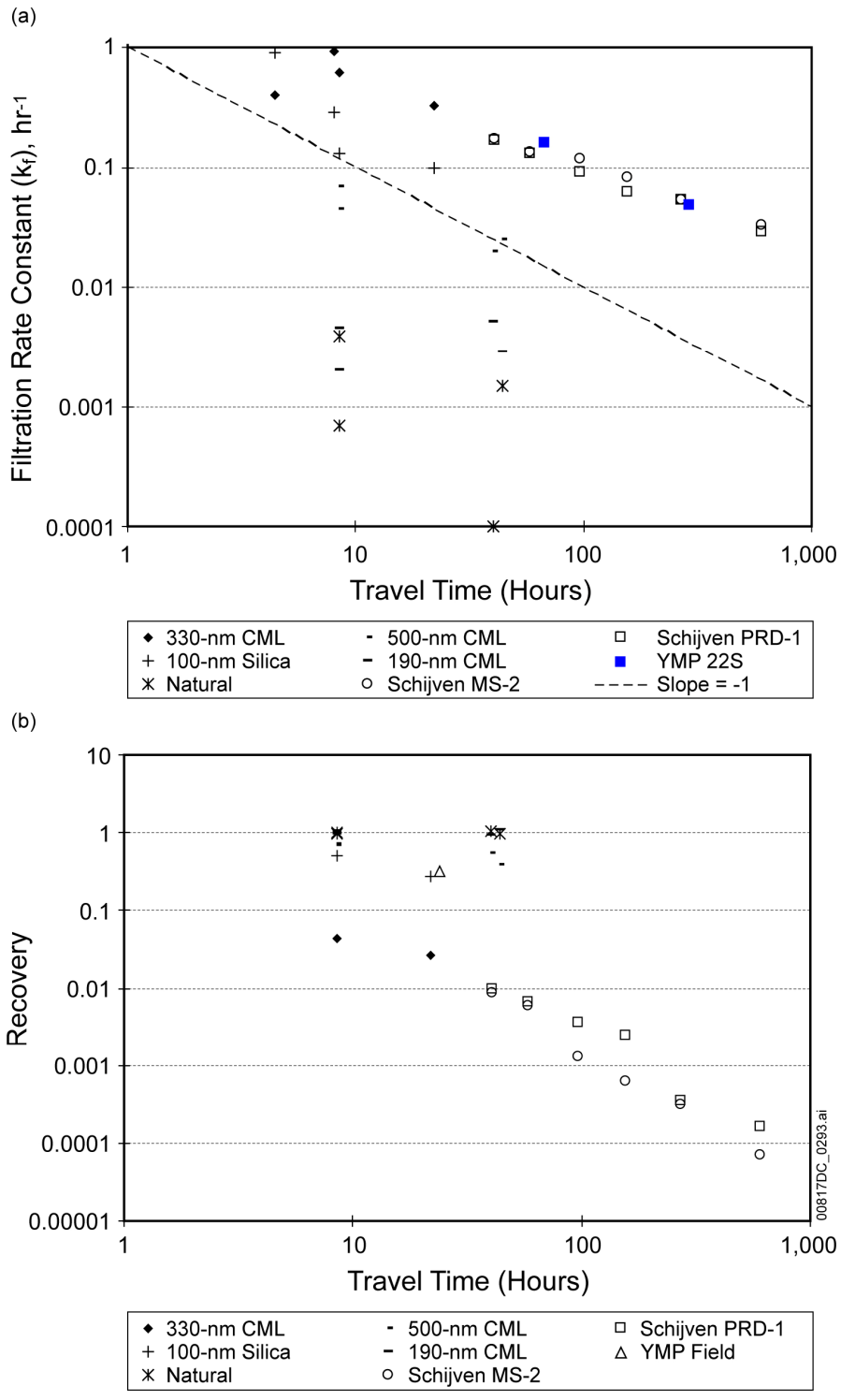

Source: Output DTN: LA0705PR150304.001 [DIRS 181744], file: *Colloid_Diversity_Parameters.xls, worksheet "Alluvium Data"*; and Corroborative DTN: MO0709MARGANAL.000 [DIRS 182978].

Figure C6-19. Colloid Filtration Rate Constants and Fractional Recoveries vs. Unretarded Groundwater Travel Times (Determined from Conservative Solute Tracers) from Tracer Experiments in Saturated Alluvium

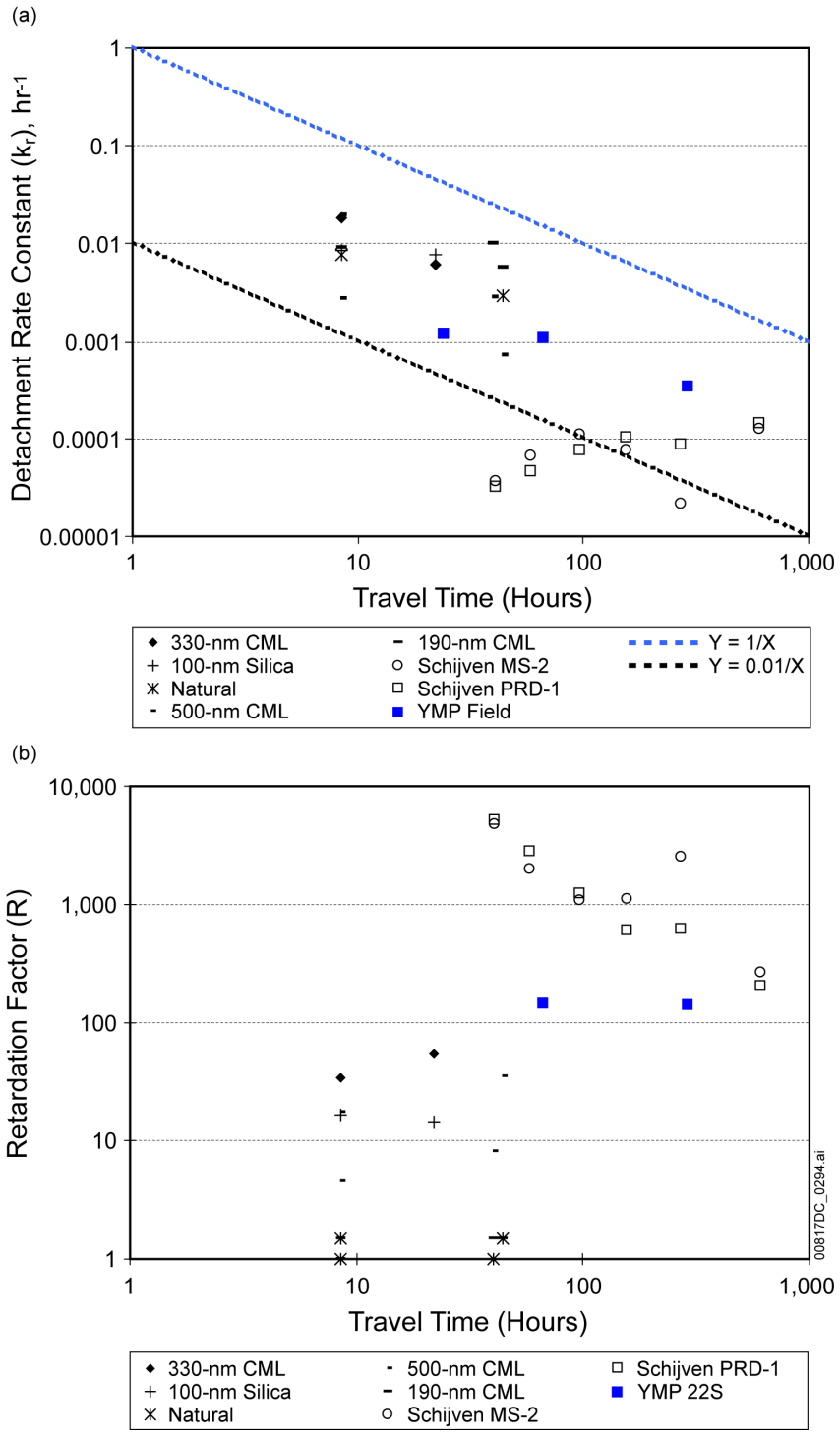

Source: DTN: LA0705PR150304.001 [DIRS 181744], file: *Colloid_Diversity_Parameters.xls, worksheet "Alluvium Data"*; and Corroborative DTN: MO0709MARGANAL.000 [DIRS 182978].

NOTE: Travel times in field tests are peak conservative tracer travel times.

Figure C6-20. Colloid Detachment Rate Constants and Retardation Factors vs. Unretarded Groundwater Travel Times (Determined from Conservative Solute Tracers) from Tracer Experiments in Saturated Alluvium

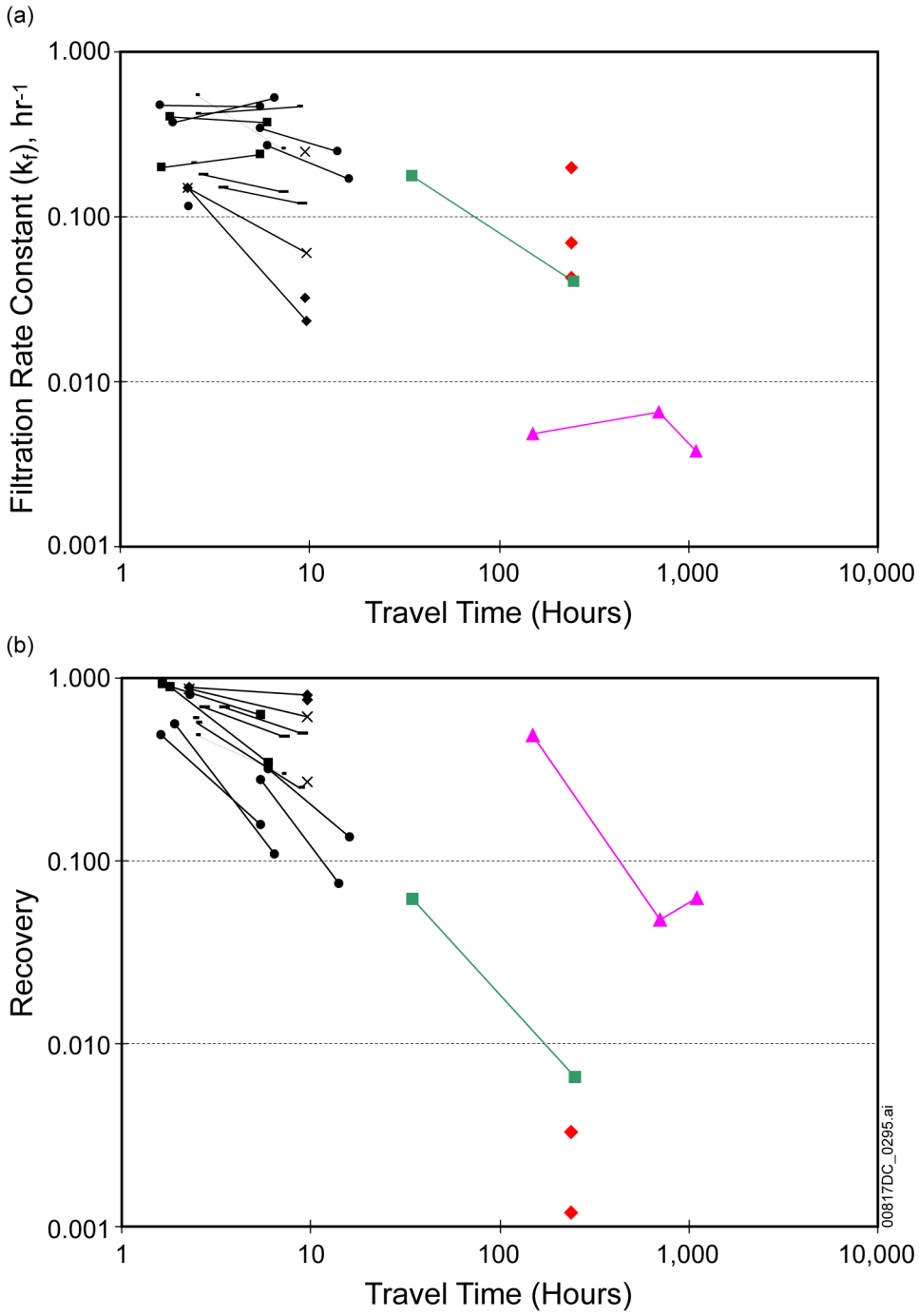

Source: Output DTN: LA0705PR150304.001 [DIRS 181744], file: *Colloid_Diversity_Parameters.xls, worksheet "Volcanics Data"*; and Corroborative DTN: MO0709MARGANAL.000 [DIRS 182978].

NOTE: Lines have been drawn to connect experiments conducted with the same colloids in the same flow system. Colored data are for field tests.

Figure C6-21. Colloid Filtration Rate Constants and Fractional Recoveries Unretarded Groundwater Travel Times for Saturated Fractured Volcanics (Data Replotted from Figure C6-17)

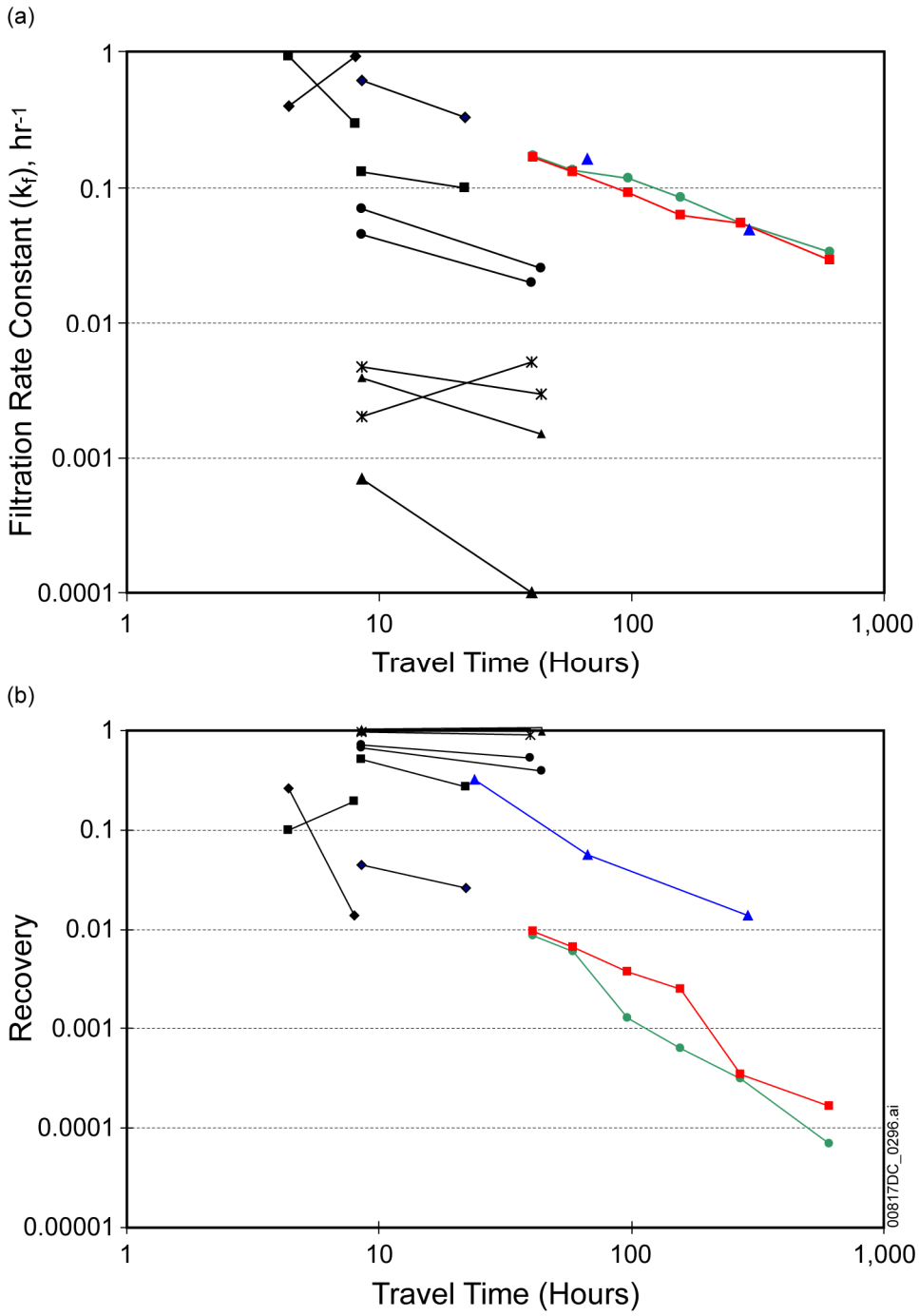

Source: Output DTN: LA0705PR150304.001 [DIRS 181744], file: *Colloid_Diversity_Parameters.xls, worksheet "Alluvium Data"*; and Corroborative DTN: MO0709MARGANAL.000 [DIRS 182978].

NOTE: Lines have been drawn to connect experiments conducted with the same colloids in the same flow system. Colored data are for field tests.

Figure C6-22. Colloid Filtration Rate Constants and Fractional Recoveries Unretarded Groundwater Travel Times for Saturated Alluvium (Data Replotted from Figure C6-19)

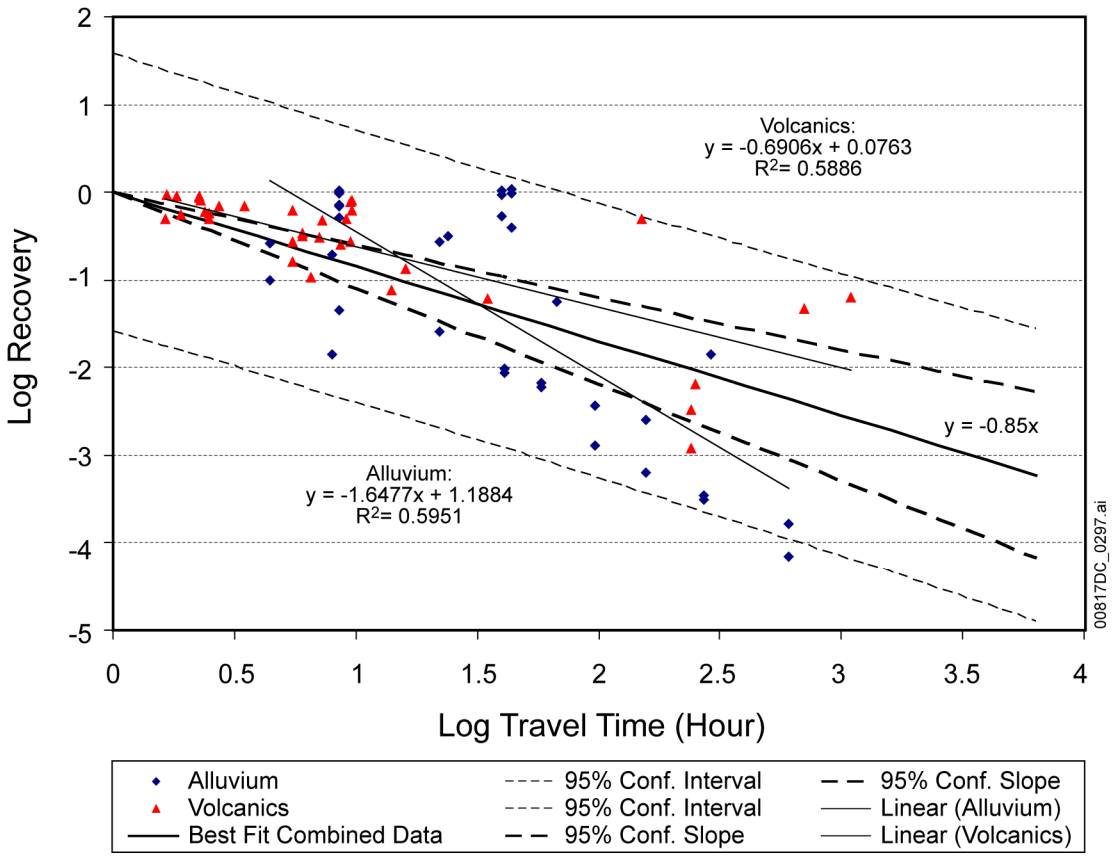

Source: Output DTN: LA0705PR150304.001 [DIRS 181744], file: *Colloid_Diversity_Parameters.xls, worksheet "Alluvium&Volcanics"*; and Corroborative DTN: MO0709MARGANAL.000 [DIRS 182978].

NOTE: The combined fit is forced to go through the origin. The light dashed lines are the 95 percent confidence intervals for the combined fit, and the dark dashed lines are plotted using the 95 percent confidence intervals for the slope of the combined fit.

Figure C6-23. Volcanic and Alluvium Log Fractional Recoveries vs. Log Groundwater Travel Time Plotted Together and Fitted by Linear Regression Separately and Together

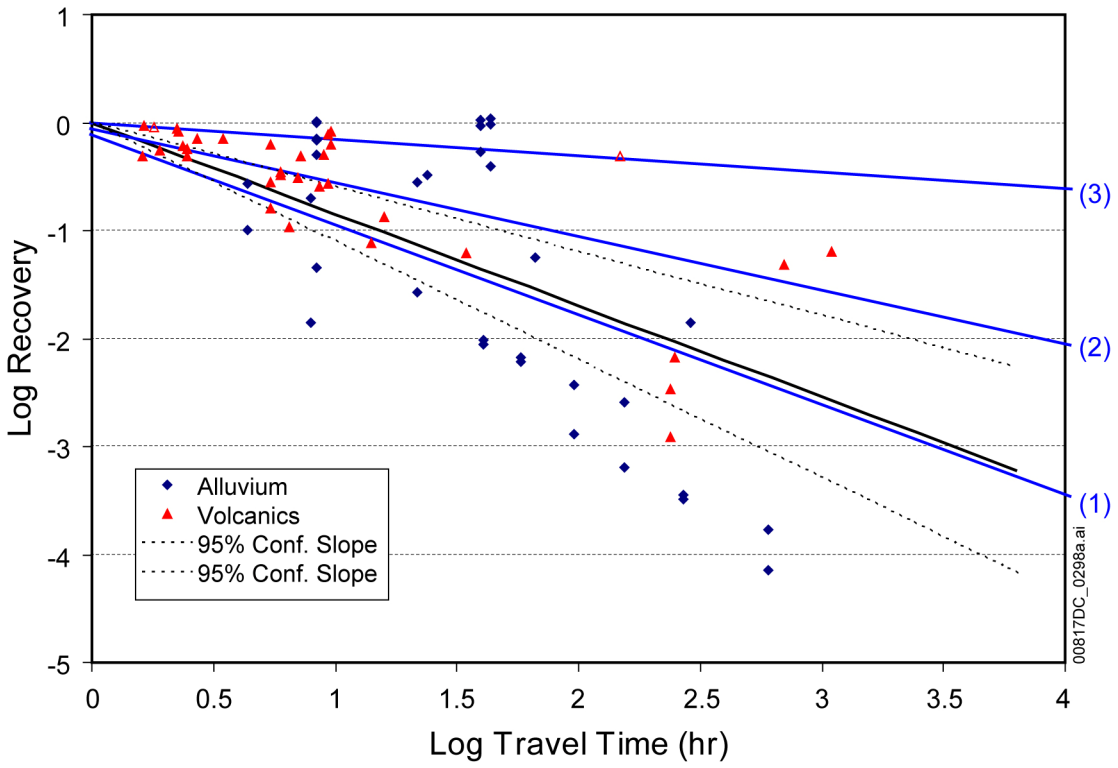

Source: Output DTN: LA0705PR150304.001 [DIRS 181744], file: *Colloid_Diversity_Parameters.xls, worksheet "Alluvium&Volcanics"*; and Corroborative DTN: MO0709MARGANAL.000 [DIRS 182978].

NOTES: Log Fractional Recoveries vs. Log Ground Travel Time for Filtration Rate Constant CDFs Associated with (1) Best Linear Fit (passing through the origin) to the combined alluvium and volcanic data (slope of approximately 0.85), (2) CDF of all rate constants (with twice the weight given to field data; slope of approximately 0.51), and (3) Best fit to the two highest recovery data points associated with the filed tracer test in the fractured volcanics at the ER-20-6 site (open triangles), which had the highest recoveries of any of the field tests (Slope of Approximately 0.17).

Figure C6-24. Log Fractional Recoveries versus Log Ground Travel Time

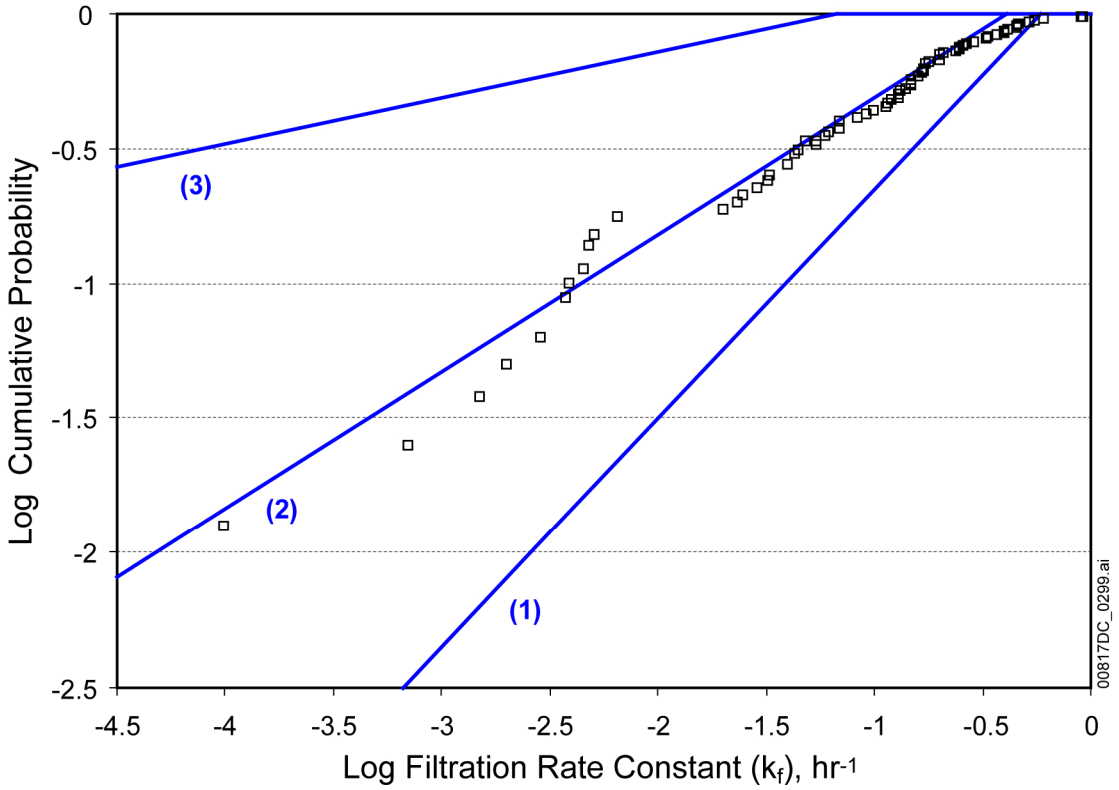

Source: Output DTN: LA0705PR150304.001 [DIRS 181744], file: *Colloid_Diversity_Parameters.xls, worksheet "kfCDF"*; and Corroborative DTN: MO0709MARGANAL.000 [DIRS 182978].

NOTE: The data CDF was generated by assigning twice the probabilistic weight to field data relative to laboratory data. The slopes of the lines are the negative of the slopes of the corresponding lines in the previous figure (0.85, 0.51, and 0.17).

Figure C6-25. Colloid Filtration Rate Constant Cumulative Distribution Functions Associated with (1), (2), and (3) from Figure C6-24 Plotted along with the Actual Cumulative Distribution Function of the Filtration Rate Constants (Data Points)

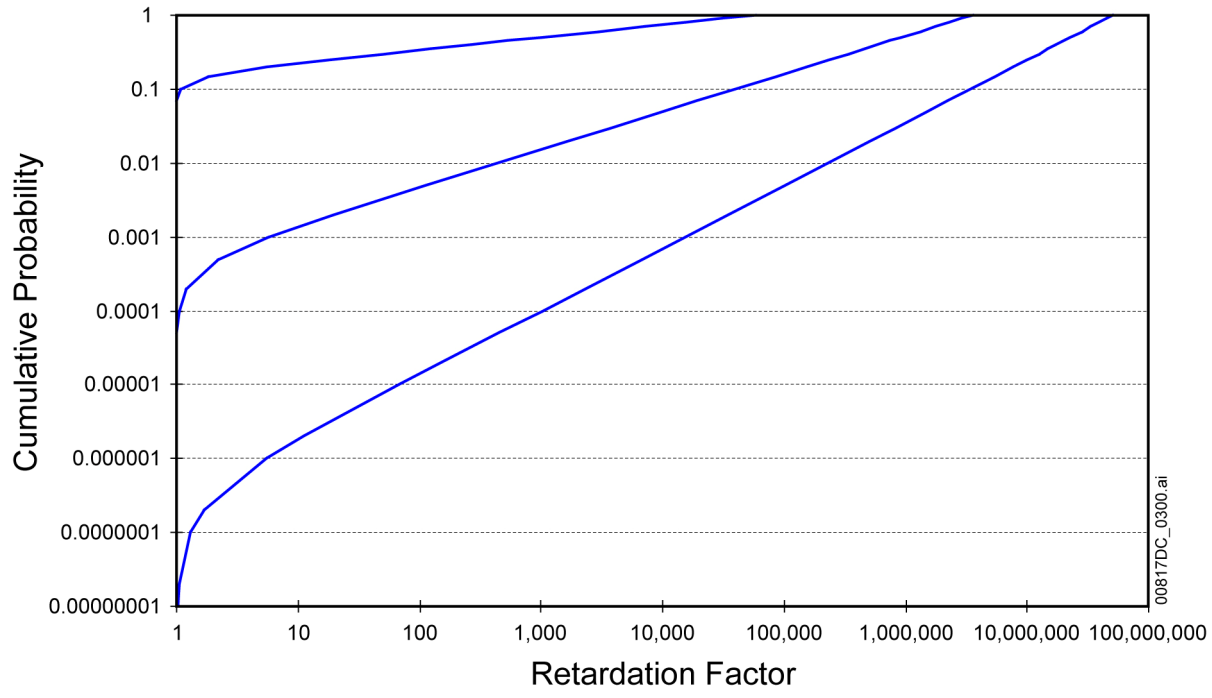

Source: Output DTN: LA0705PR150304.001 [DIRS 181744], file: *Colloid_Diversity_Parameters.xls, worksheet "Alluvium&Volcanics"*; and Corroborative DTN: MO0709MARGANAL.000 [DIRS 182978].

Figure C6-26. Minimum, Central, and Maximum Cumulative Distribution Functions of Colloid Retardation Factors Associated with a 100-Year Groundwater Travel Times

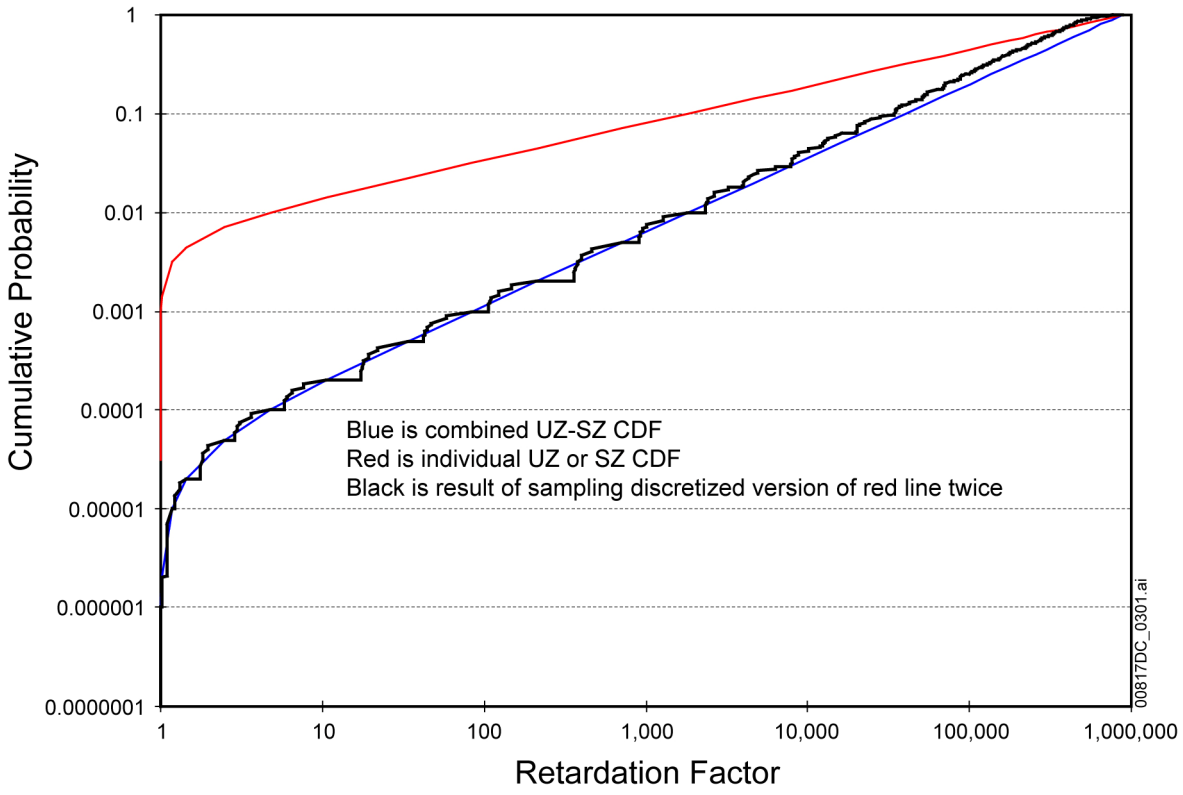

Source: Output DTN: LA0705PR150304.001 [DIRS 181744], file: *Colloid_Diversity_Parameters.xls, worksheet "Alluvium&Volcanics"*; and Corroborative DTN: MO0709MARGANAL.000 [DIRS 182978].

NOTE: The black line is the discretized combined CDF obtained numerically, and the blue line is the original combined unsaturated zone-saturated zone CDF from the approach developed herein.

Figure C6-27. Results of Sampling a Discretized Version of the Retardation Factor CDF Two Times to Obtain an Effective Retardation Distribution in the Combined Unsaturated Zone and Saturated Zone

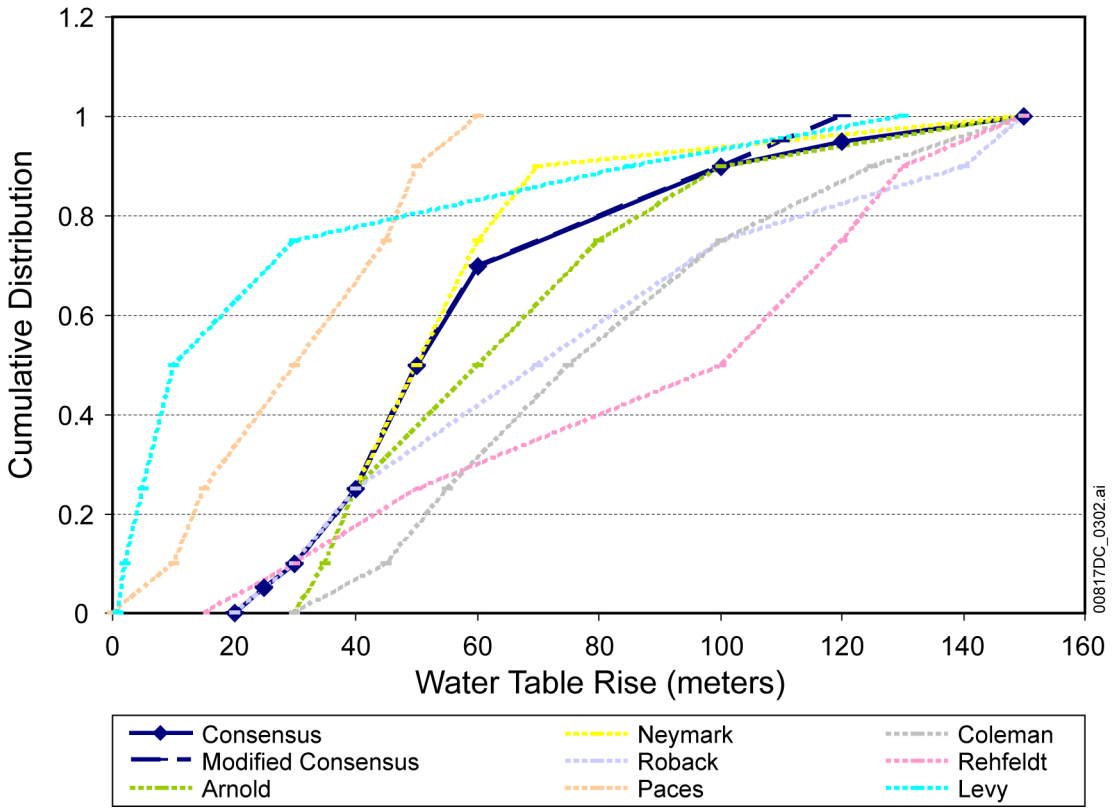

Source: Corroborative DTN: MO0704PAUZFEHM.000 [DIRS 182790], file: *water_table_rise_uncert_summaryDTN.xls, worksheet "sheet1"*.

Figure C6-28. Cumulative Distribution Functions of Uncertainty in Water Table Rise for Individual Workshop Participants

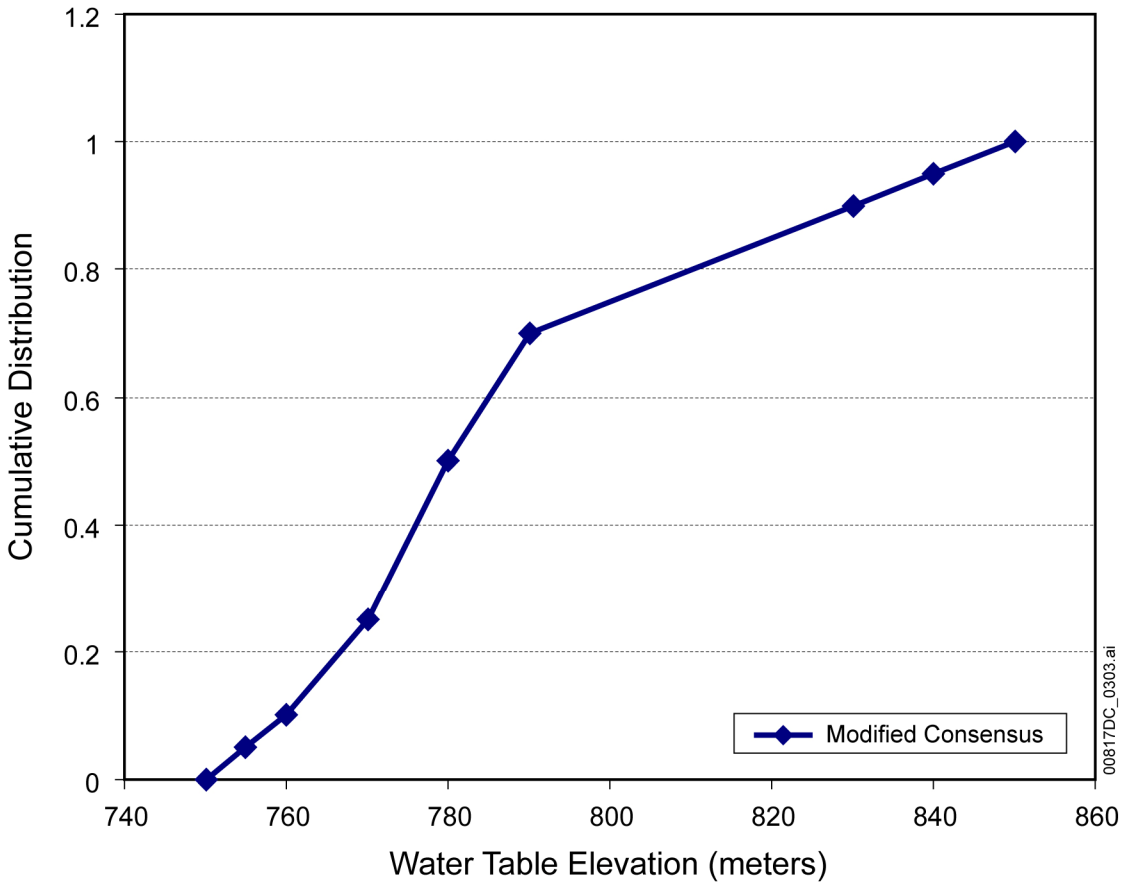

Source: Corroborative DTN: MO0704PAUZFEHM.000 [DIRS 182790], file: *water_table_rise_uncert_summaryDTN.xls, worksheet "sheet1"*.

Figure C6-29. Cumulative Distribution Functions of Uncertainty in Water Table Rise by Consensus

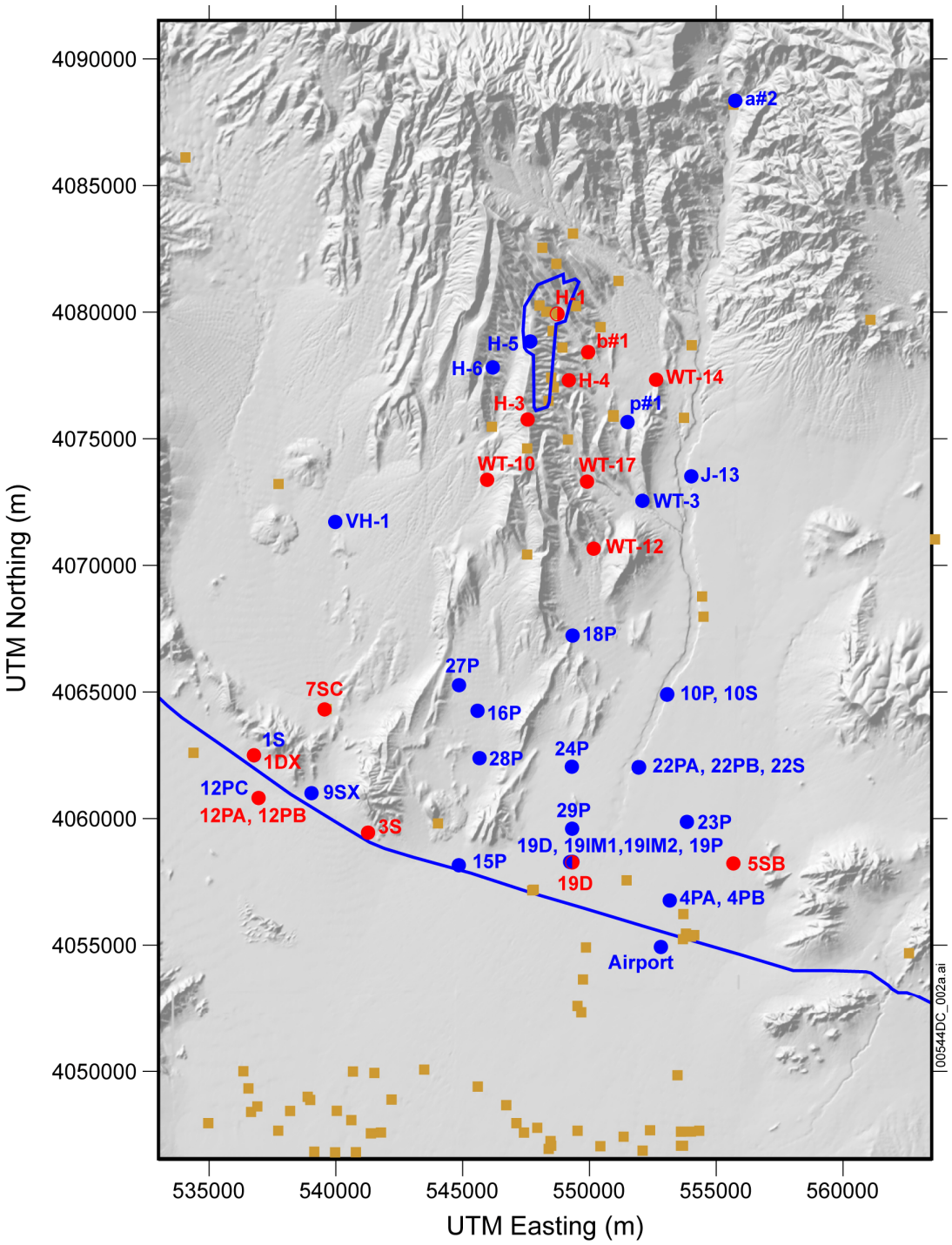

Source: BSC 2006 [DIRS 178672], Figure 2.1-2, p. F-2.

NOTES: Wells with oxidizing groundwater are shown with blue filled circles, wells with reducing groundwater are shown with red filled circles, and wells in which redox conditions have not been measured are shown with brown filled squares. Wells with both oxidizing and reducing conditions (H-1 and 19-D) are shown with half-filled circles. The repository is outlined in blue in the north-central part of the map, and Highway 95 is shown as the blue line in the southern part of the map.

Figure C6-30. Map Showing Locations of Wells with Oxidizing and Reducing Groundwaters

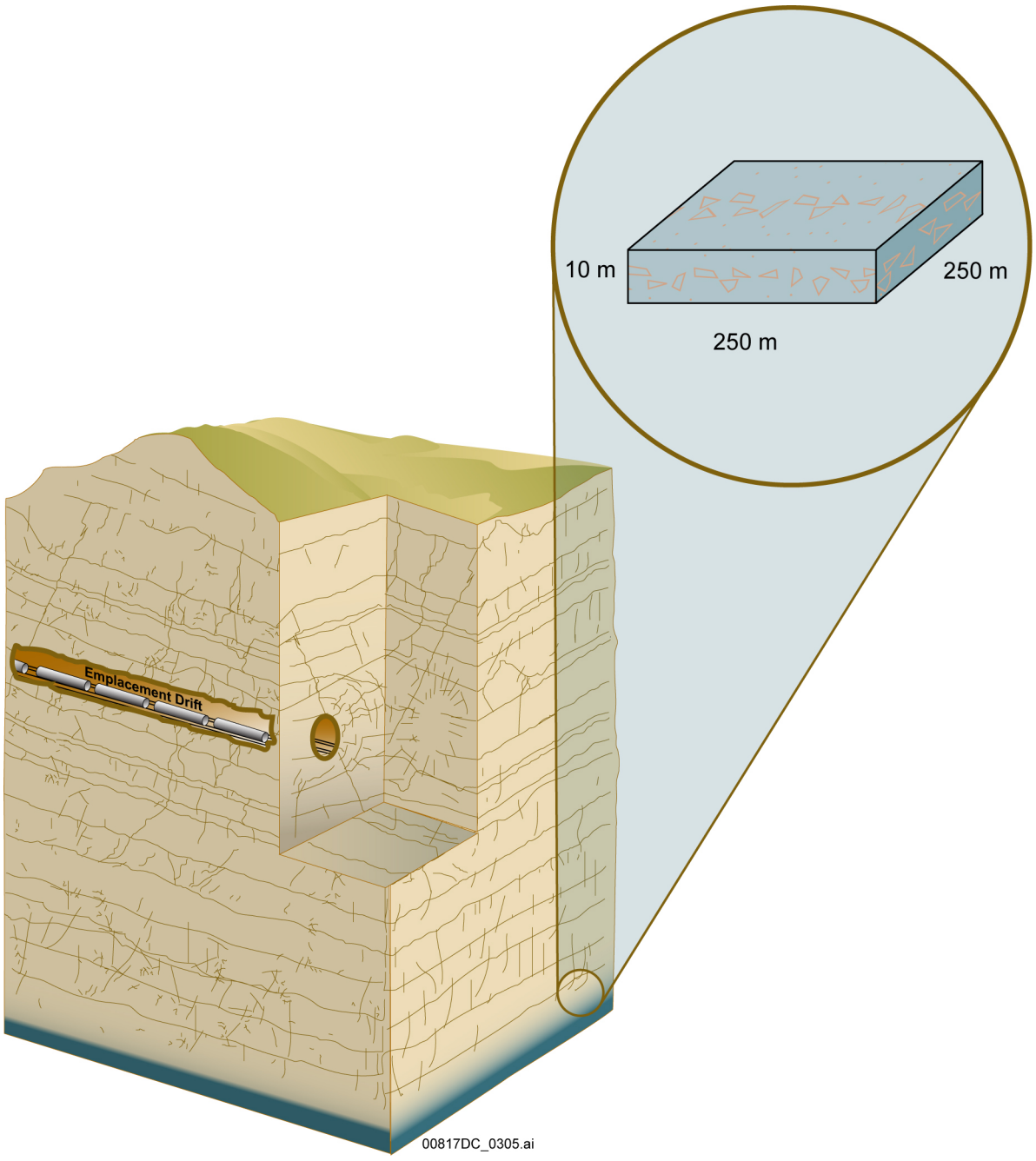

Figure C6-31. Saturated Zone Matrix Block Used as a Conduit for Unsaturated Matrix Mass Flux to the Saturated Zone

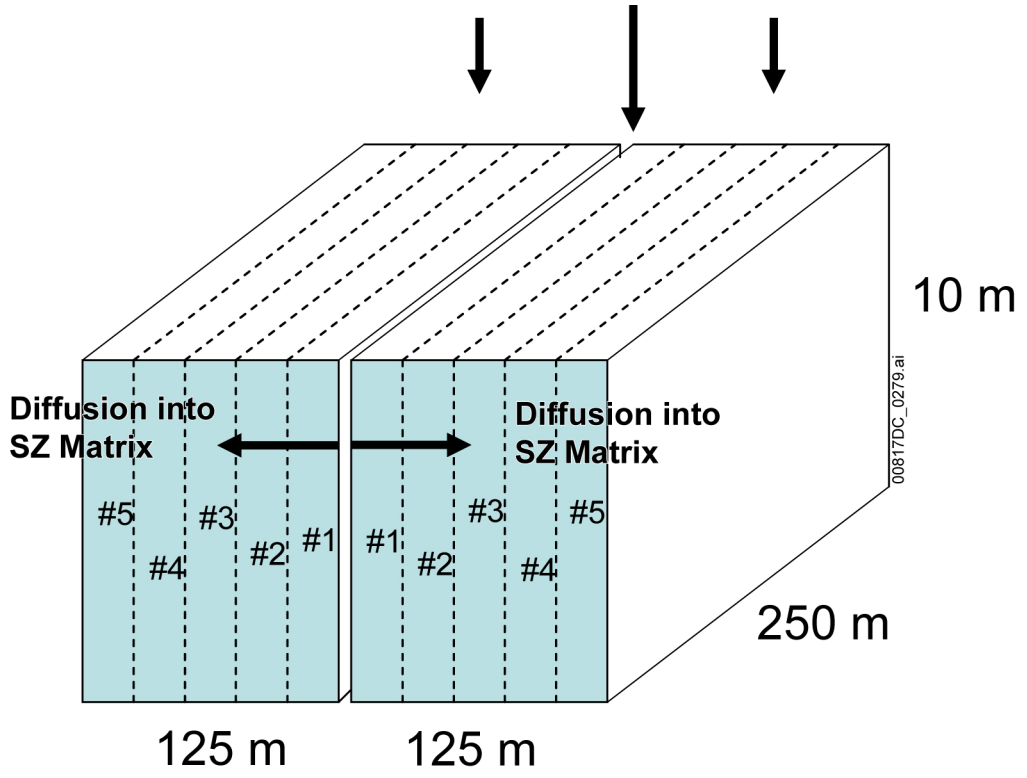

NOTE: The 125 m length represents half of the total block length. In this example, FISVO, which is the total length between fractures, is 250 m.

Figure C6-32. Schematic Diagram Showing Conceptual Dual-Porosity Model for the Unsaturated Zone to Saturated Zone Mass Flux

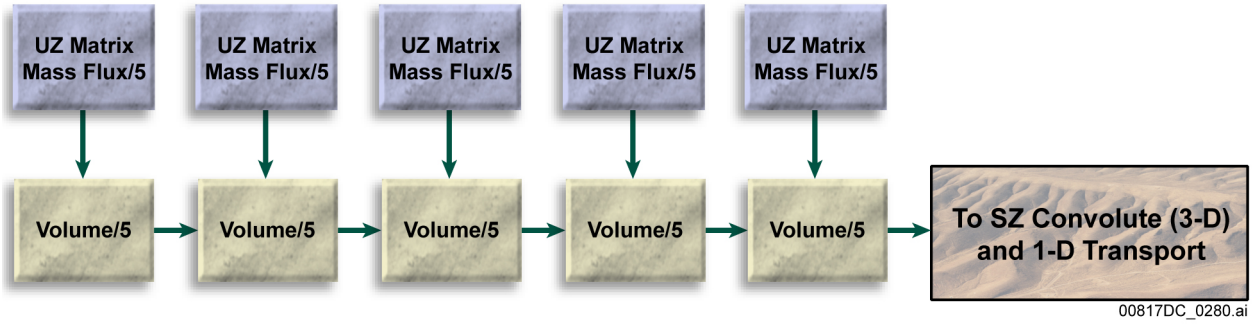

Figure C6-33. Configuration of Unsaturated Zone to Saturated Zone Matrix Diffusion

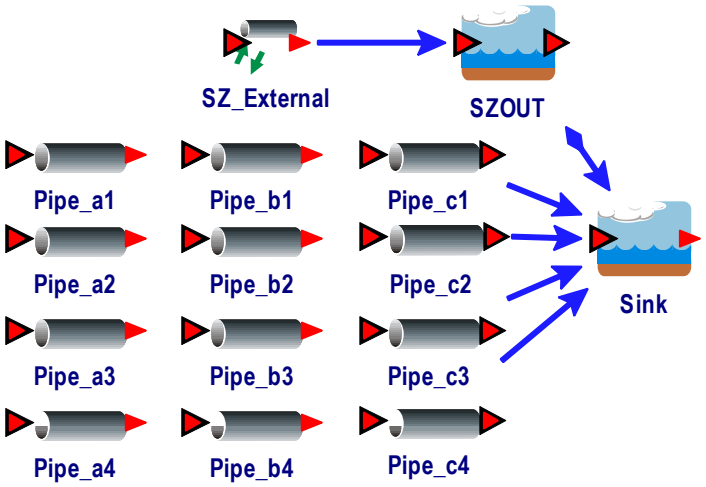

Figure C6-34. Structure of the GoldSim Saturated Zone1-D Transport Model Setup for the Compliance Model

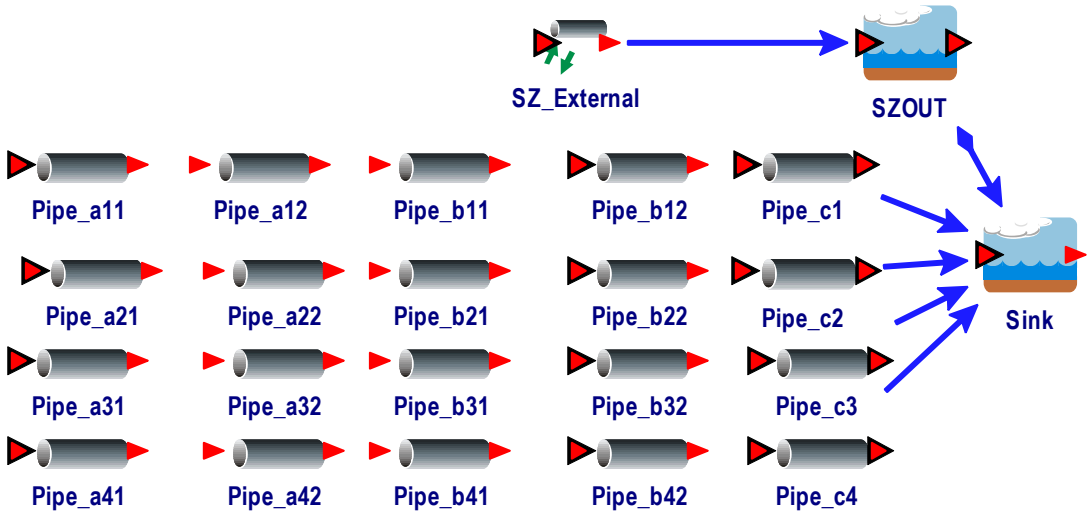

Figure C6-35. Structure of the GoldSim Saturated Zone1-D Transport Model with Modifications for the Reducing Zones Model

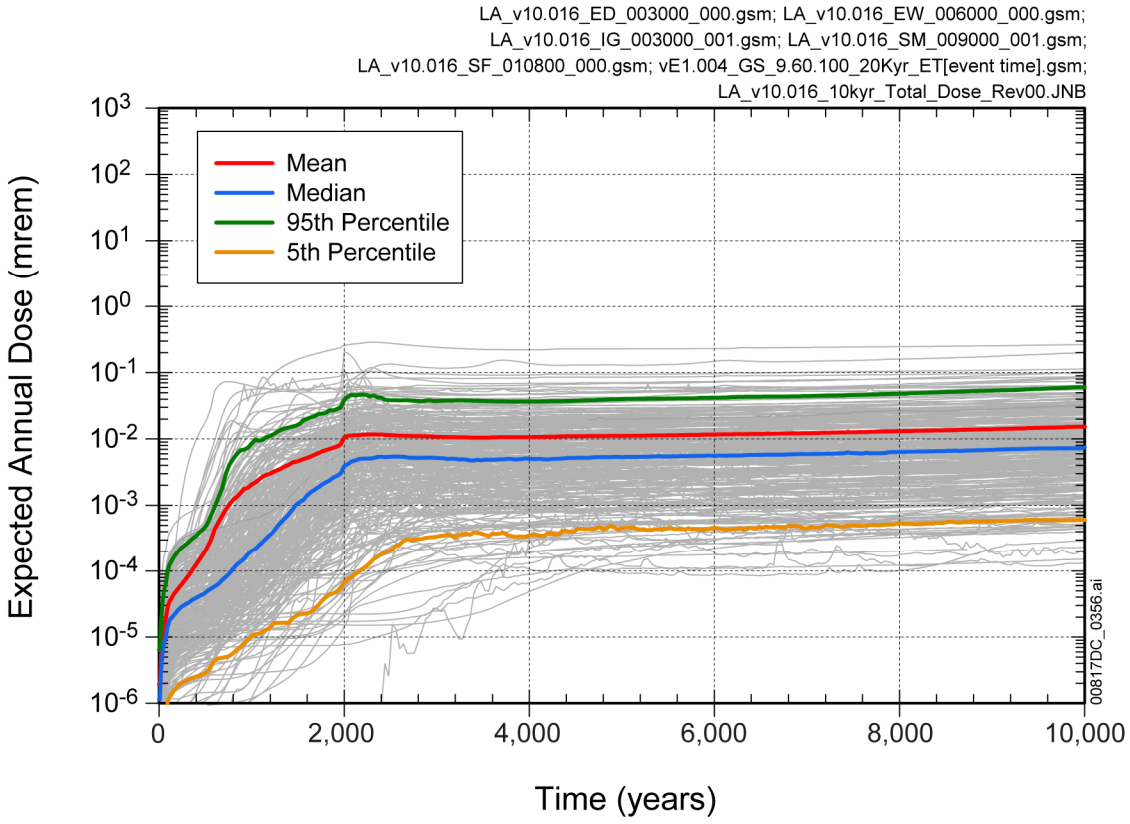

Source: Corroborative DTN: MO0709MARGANAL.000 [DIRS 182978]; and Output DTN: MO0709TSPAREGS.000 [DIRS 182976].

Figure C7-1. Probabilistic Projections of the Performance Margin Analysis Total Dose for 10,000 Years after Repository Closure

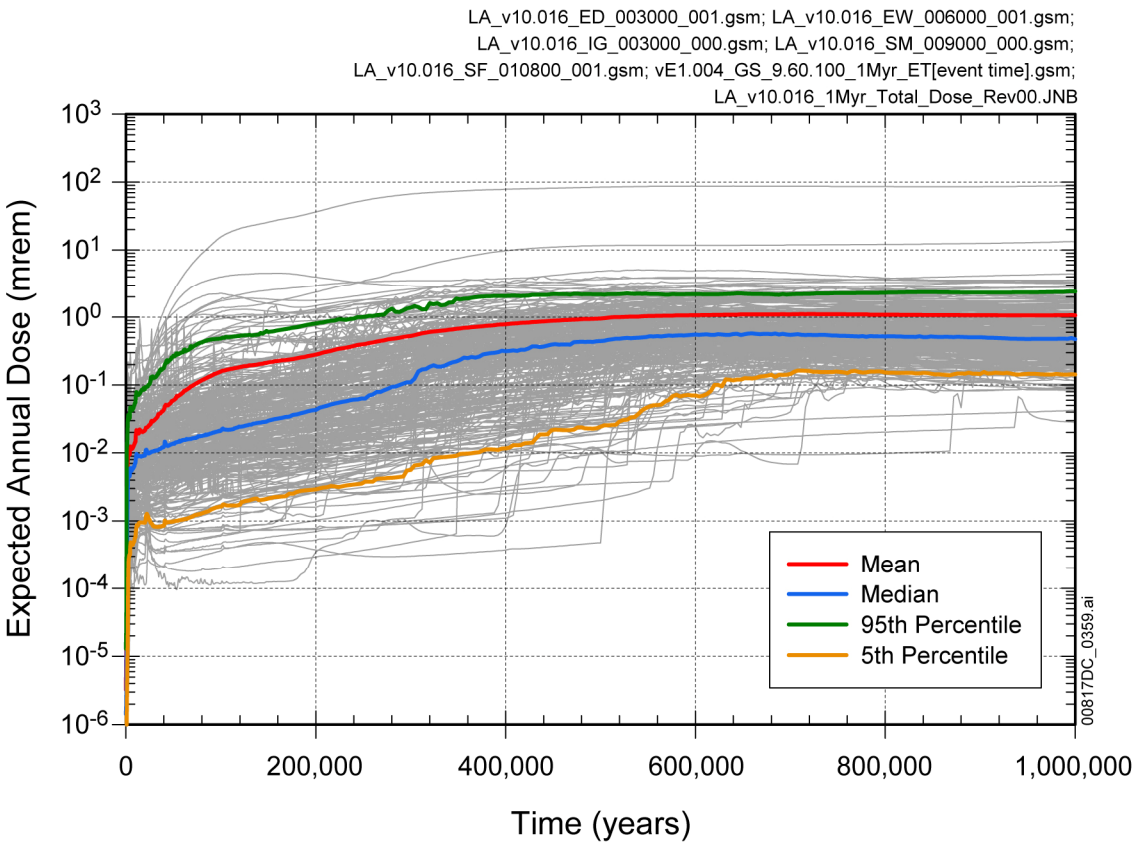

Source: Corroborative DTN: MO0709MARGANAL.000 [DIRS 182978]; and Output DTN: MO0709TSPAREGS.000 [DIRS 182976].

Figure C7-2. Probabilistic Projections of Performance Margin Analysis Total Dose for 1,000,000 Years after Repository Closure

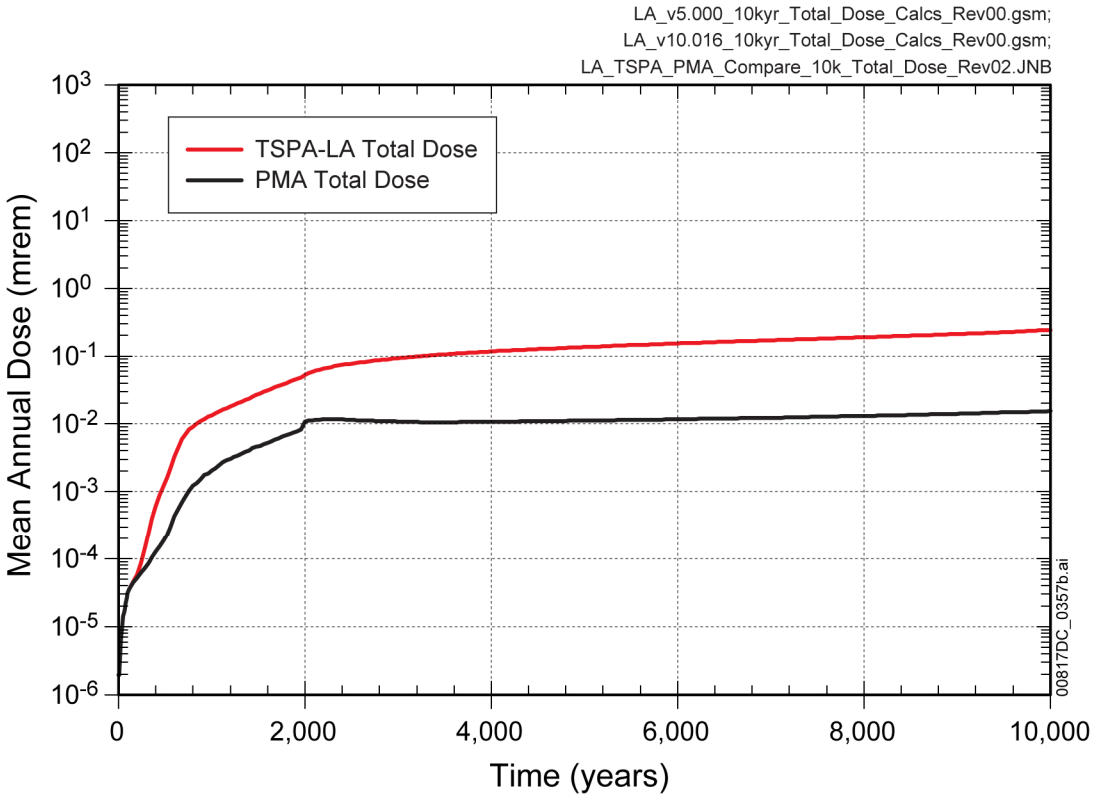

Source: Output DTN: MO0709TSPAPLOT.000 [DIRS 183010].

Figure C7-3. Comparison of the Projected Total Mean Annual Dose for the TSPA-LA Model Relative to the Performance Margin Analysis for 10,000 Years after Repository Closure

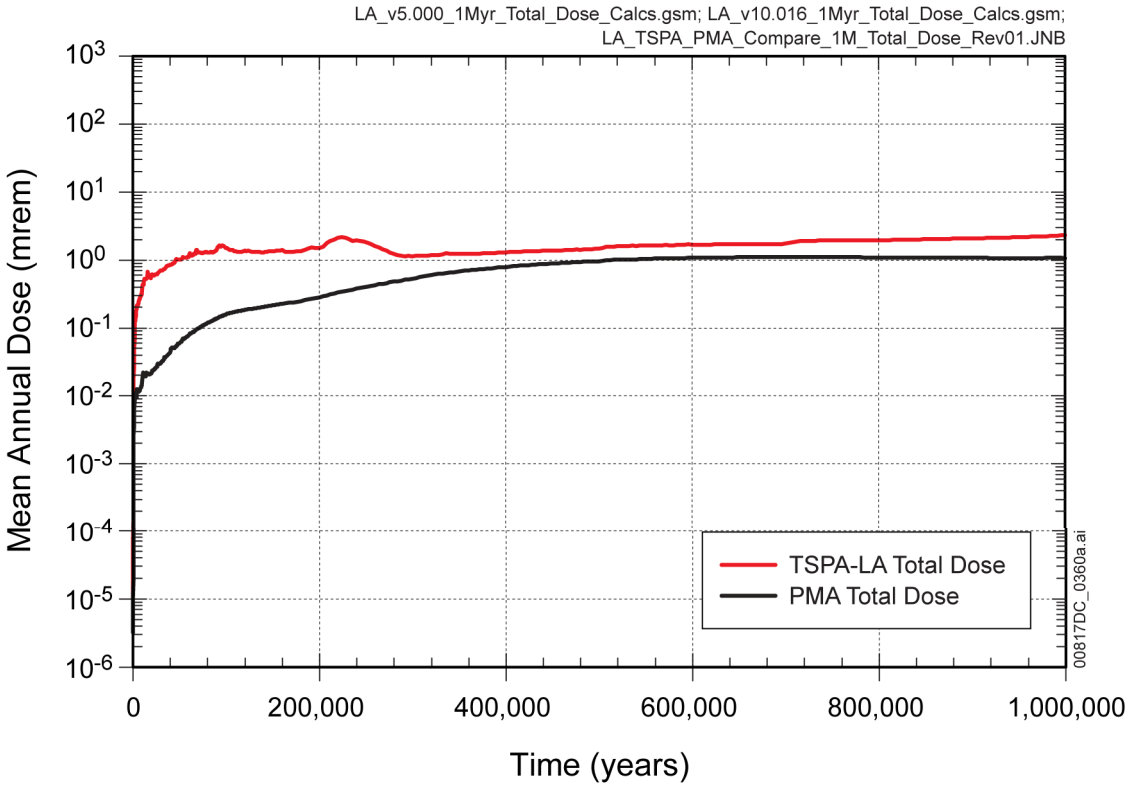

Source: Output DTN: MO0709TSPAPLOT.000 [DIRS 183010].

Figure C7-4. Comparison of the Projected Total Mean Annual Dose for the TSPA-LA Relative to the Performance Margin Analysis for 1,000,000 Years after Repository Closure

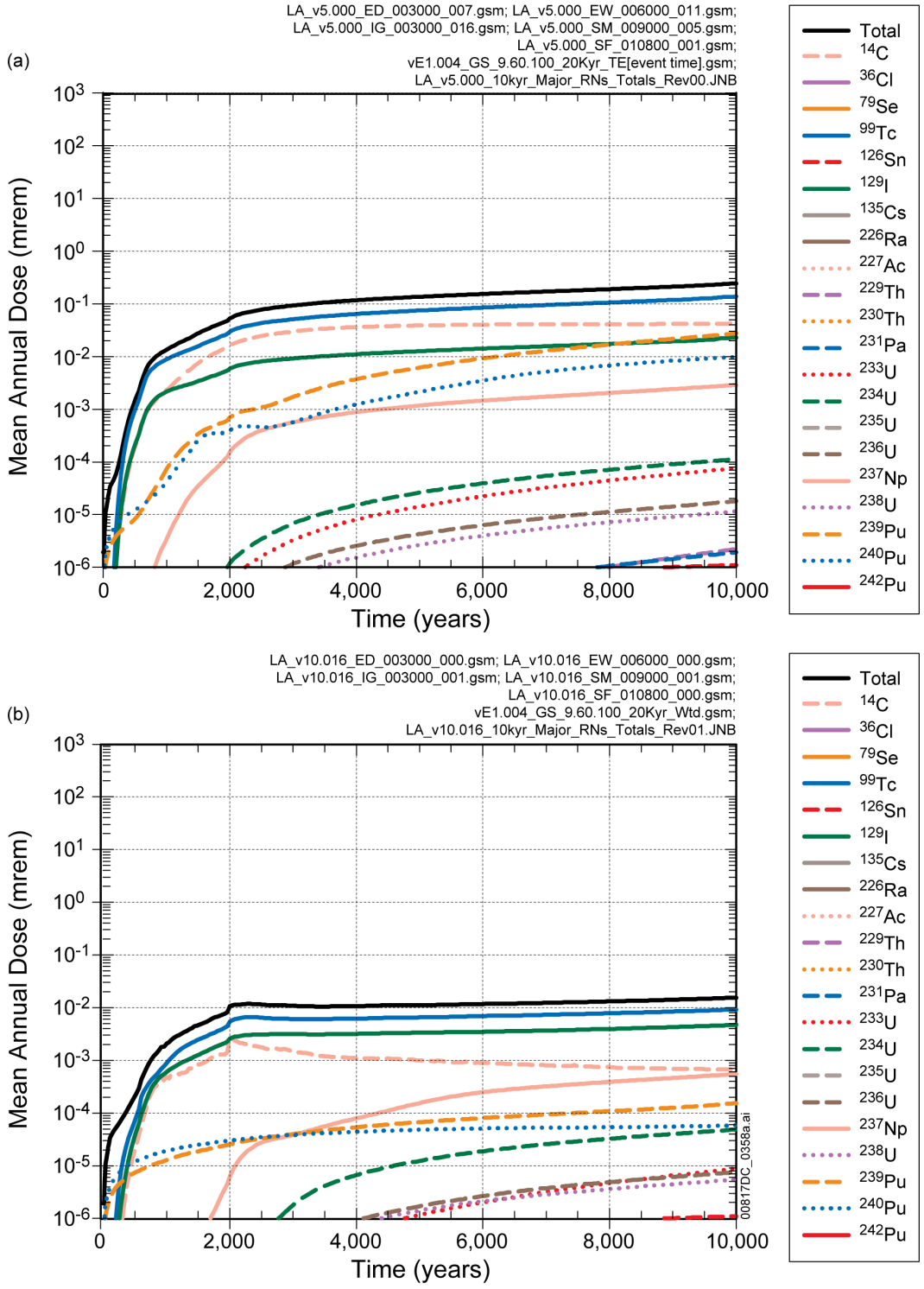

Source: Corroborative DTN: MO0709MARGANAL.000 [DIRS 182978]; and Output DTN: MO0709TSPAREGS.000 [DIRS 182976].

Figure C7-5. Contributions of Individual Radionuclides to Total Mean Annual Dose for (a) the TSPA-LA and (b) the Performance Margin Analysis 10,000 Years after Repository Closure

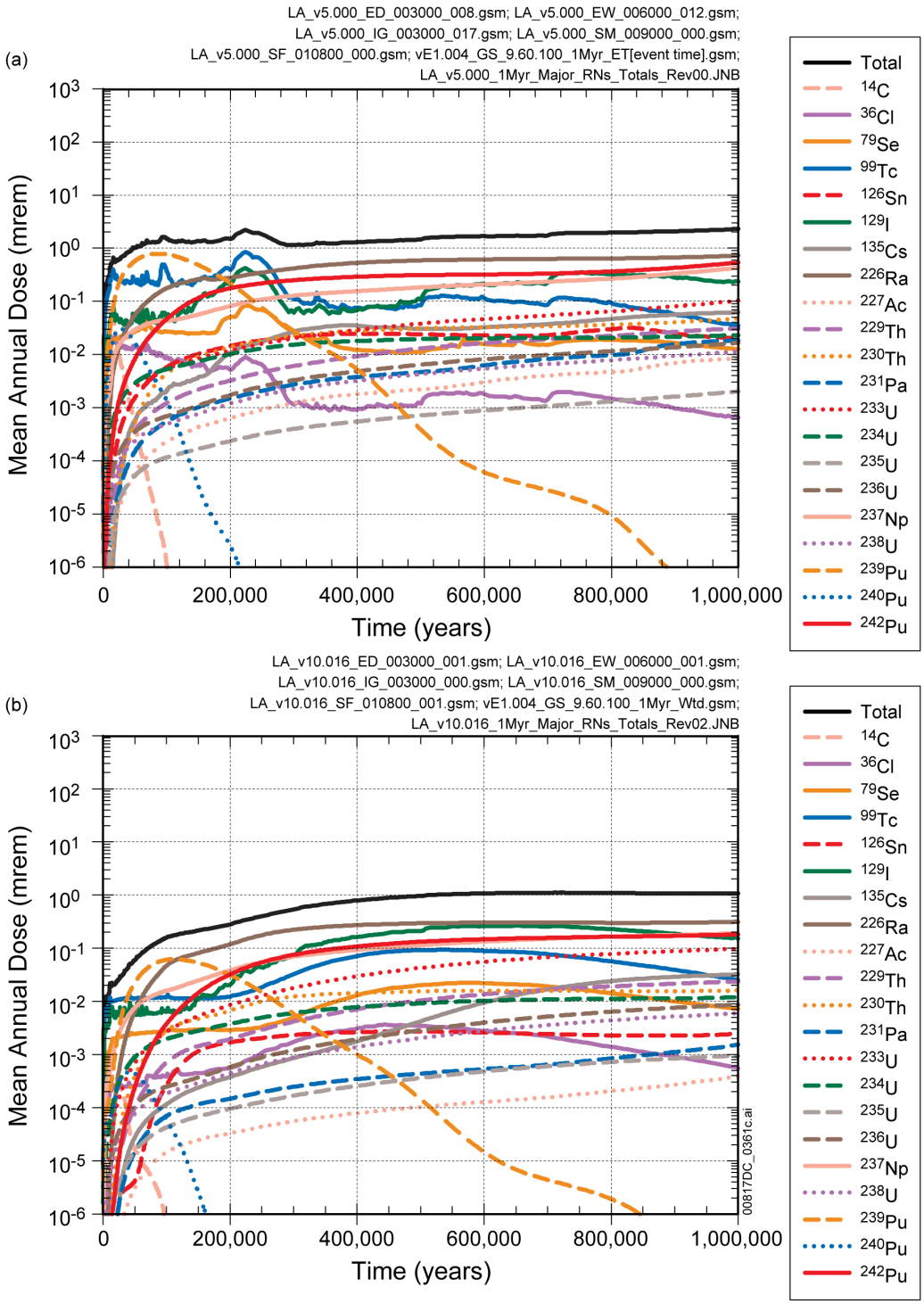

Source: Corroborative DTN: MO0709MARGANAL.000 [DIRS 182978]; and Output DTN: MO0709TSPAREGS.000 [DIRS 182976].

Figure C7-6. Contributions of Individual Radionuclides to Total Mean Annual Dose History for (a) the TSPA-LA and (b) the Performance Margin Analysis for 1,000,000 Years after Repository Closure

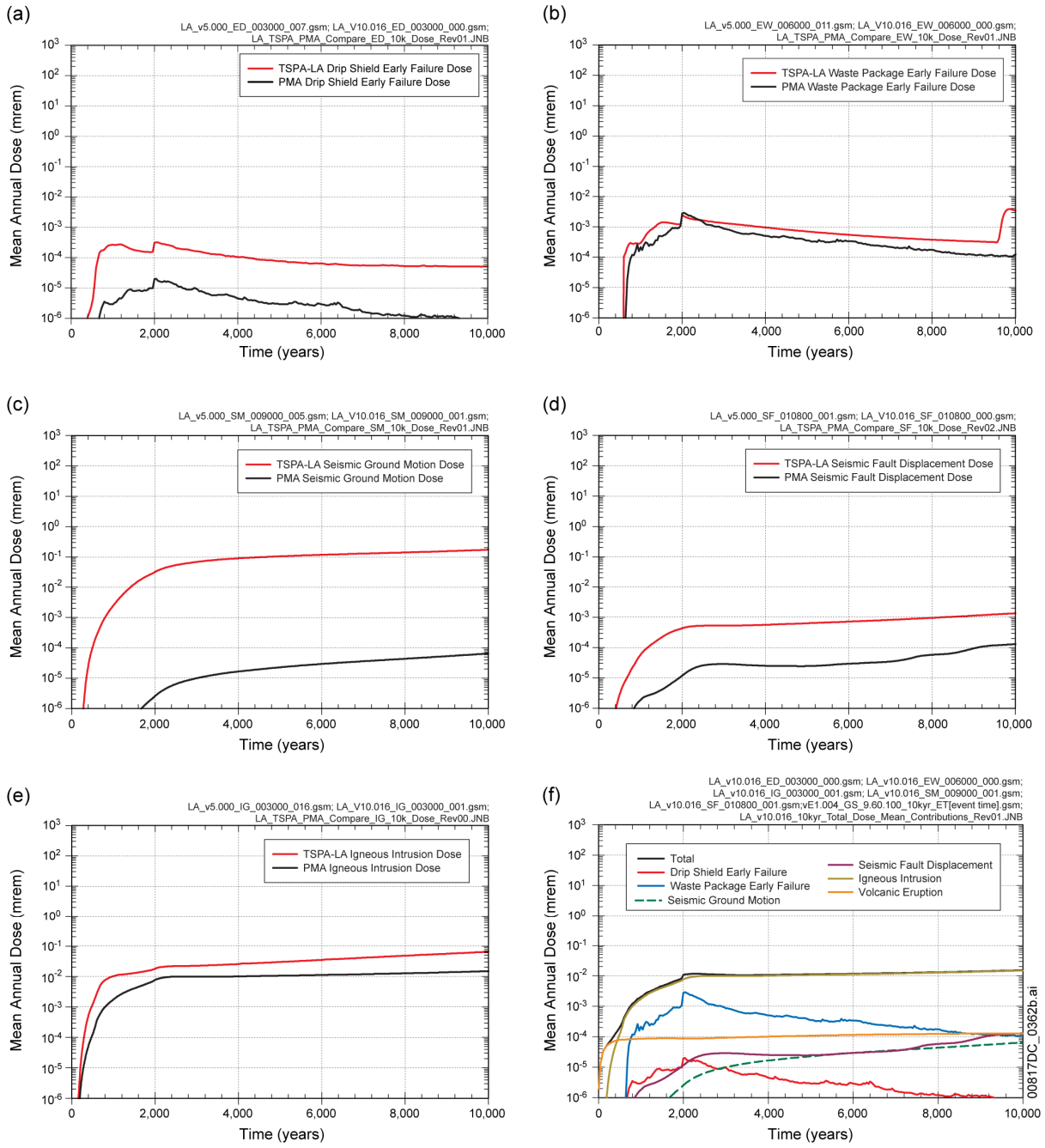

Source: Output DTN: MO0709TSPAREGS.000 [DIRS 182976]; and Corroborative DTN: MO0709MARGANAL.000 [DIRS 182978].

Figure C7-7. Comparison of Scenario Modeling Cases to Projected Total Mean Annual Dose 10,000 Years after Repository Closure for (a) Drip Shield Early Failure, (b) Waste Package Early Failure, (c) Seismic Ground Motion, (d) Seismic Fault Displacement, (e) Igneous Intrusion, and (f) Relative Contributions of Scenario Modeling Cases to the Projected Mean Annual Dose for the Performance Margin Analysis.

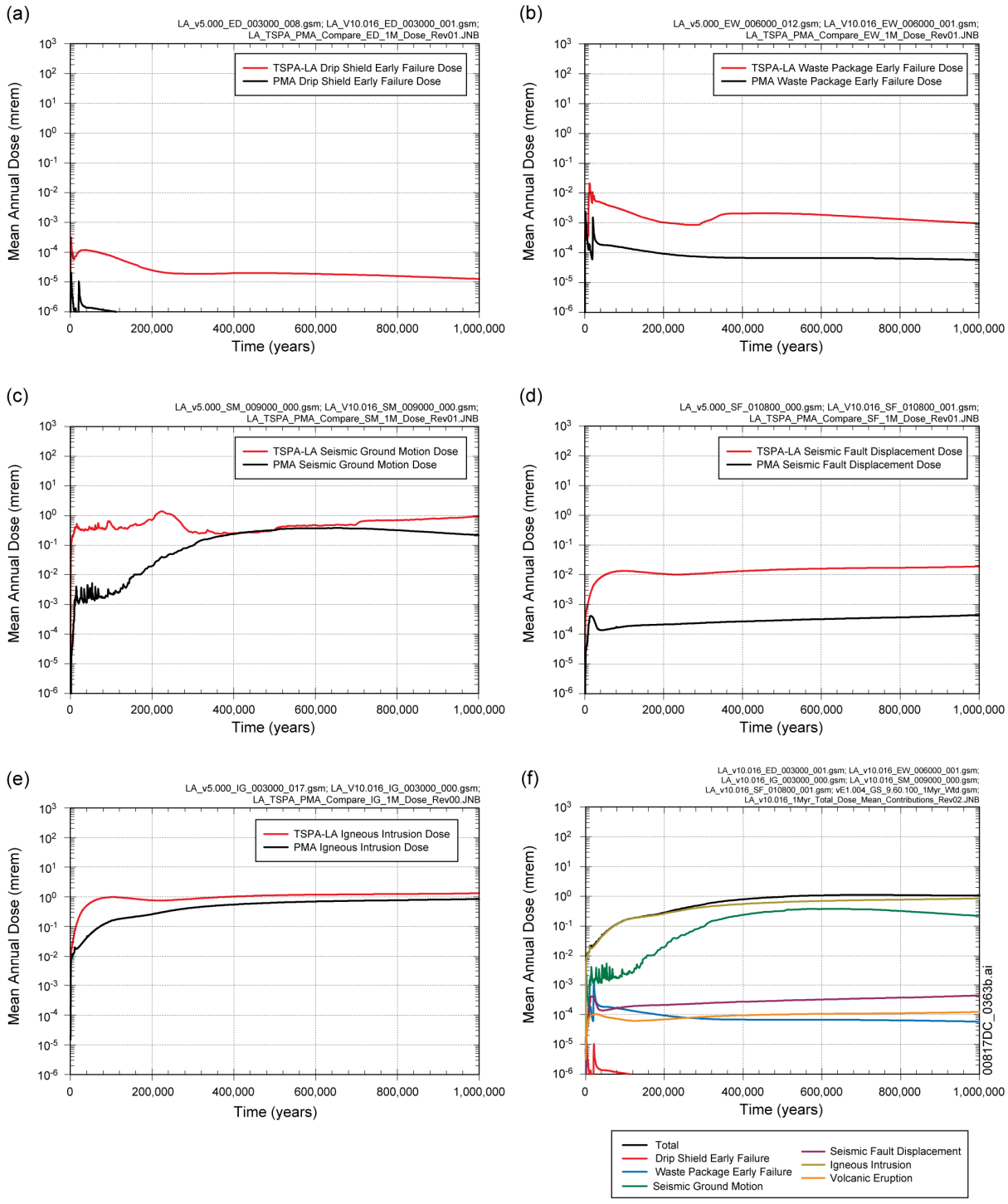

Source: Output DTN: MO0709TSPAREGS.000 [DIRS 182976] and Corroborative DTN: MO0709MARGANAL.000 [DIRS 182978].

Figure C7-8. Comparison of Scenario Modeling Cases to Projected Total Mean Annual Dose 1,000,000 Years after Repository Closure for (a) Drip Shield Early Failure, (b) Waste Package Early Failure, (c) Seismic Ground Motion, (d) Seismic Fault Displacement, (e) Igneous Intrusion, and (f) Relative Contributions of Scenario Modeling Cases to the Projected Mean Annual Dose for the Performance Margin Analysis

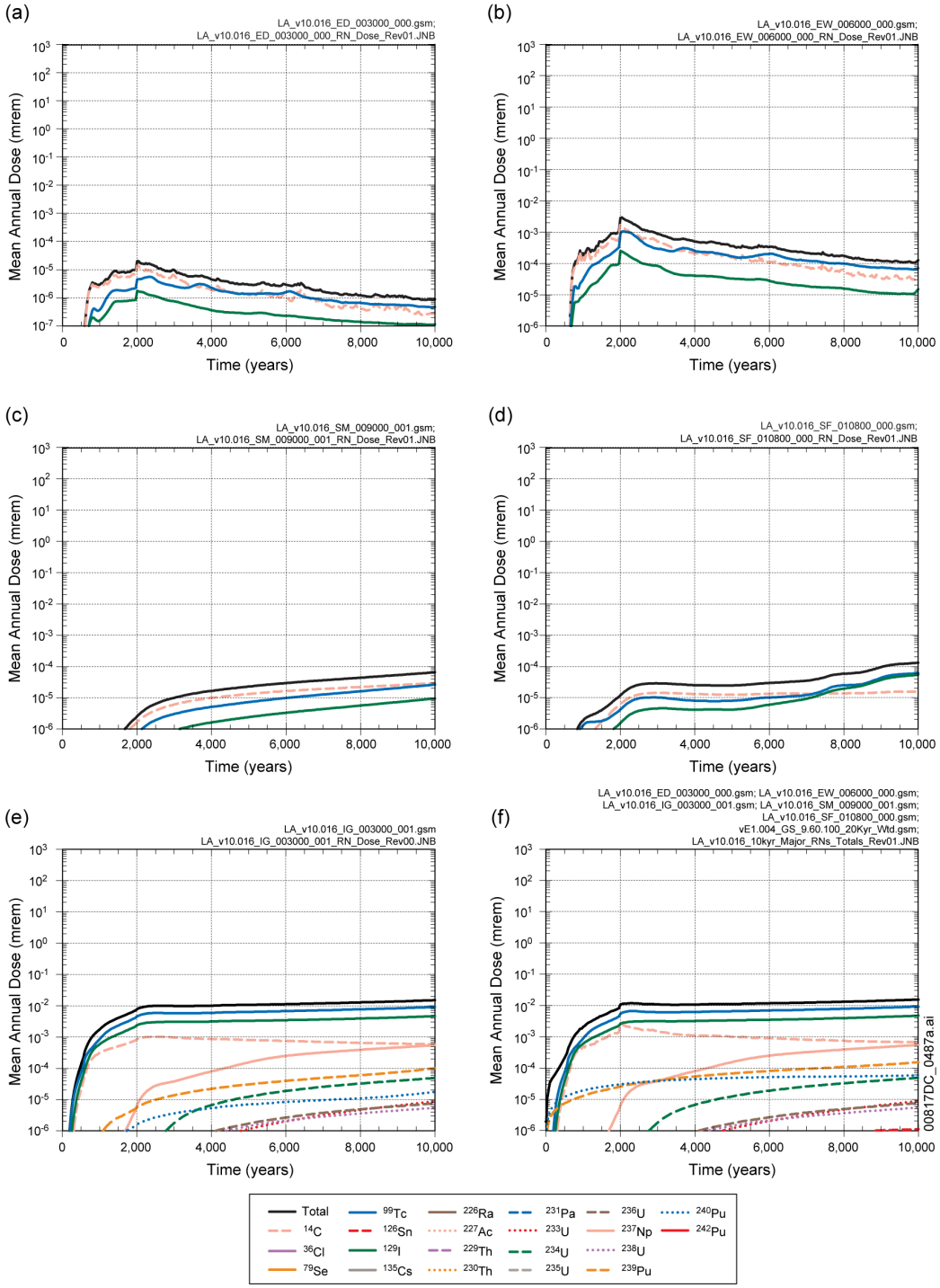

Source: Corroborative DTN: MO0709MARGANAL.000 [DIRS 182978]; and Output DTN: MO0709TSPAREGS.000 [DIRS 182976].

Figure C7-9. PMA Scenario Modeling Cases to Radionuclide Contributions to Projected Total Mean Annual Dose 10,000 Years after Repository Closure for (a) Drip Shield Early Failure, (b) Waste Package Early Failure, (c) Seismic Ground Motion, (d) Seismic Fault Displacement, (e) Igneous Intrusion, and (f) Total Mean Annual Dose for the Performance Margin Analysis

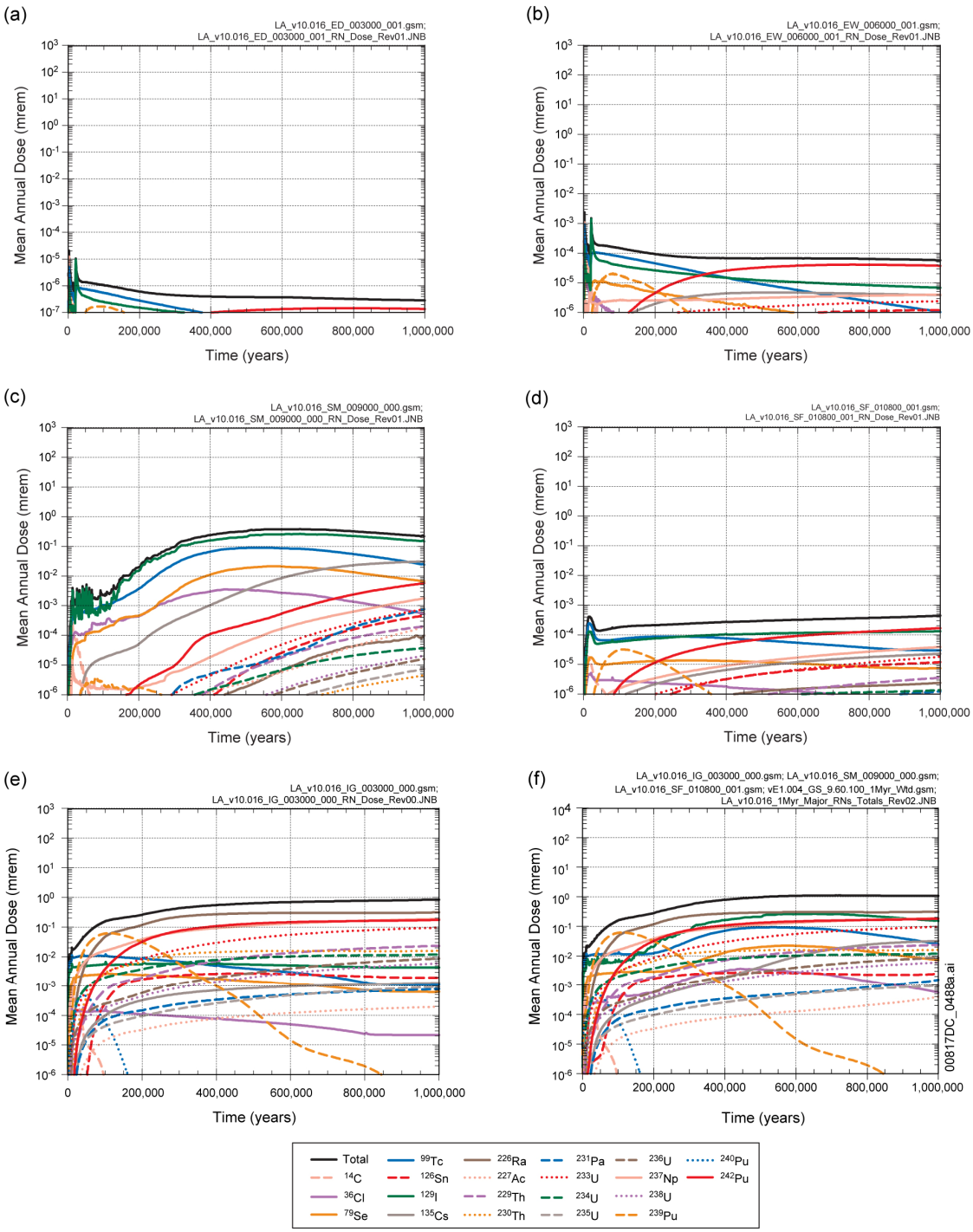

Source: Corroborative DTN: MO0709MARGANAL.000 [DIRS 182978]; and Output DTN: MO0709TSPAREGS.000 [DIRS 182976].

Figure C7-10. PMA Scenario Modeling Cases to Radionuclide Contributions to Projected Total Mean Annual Dose 1,000,000 Years after Repository Closure for (a) Drip Shield Early Failure, (b) Waste Package Early Failure, (c) Seismic Ground Motion, (d) Seismic Fault Displacement, (e) Igneous Intrusion, and (f) Total Mean Annual Dose for the Performance Margin Analysis

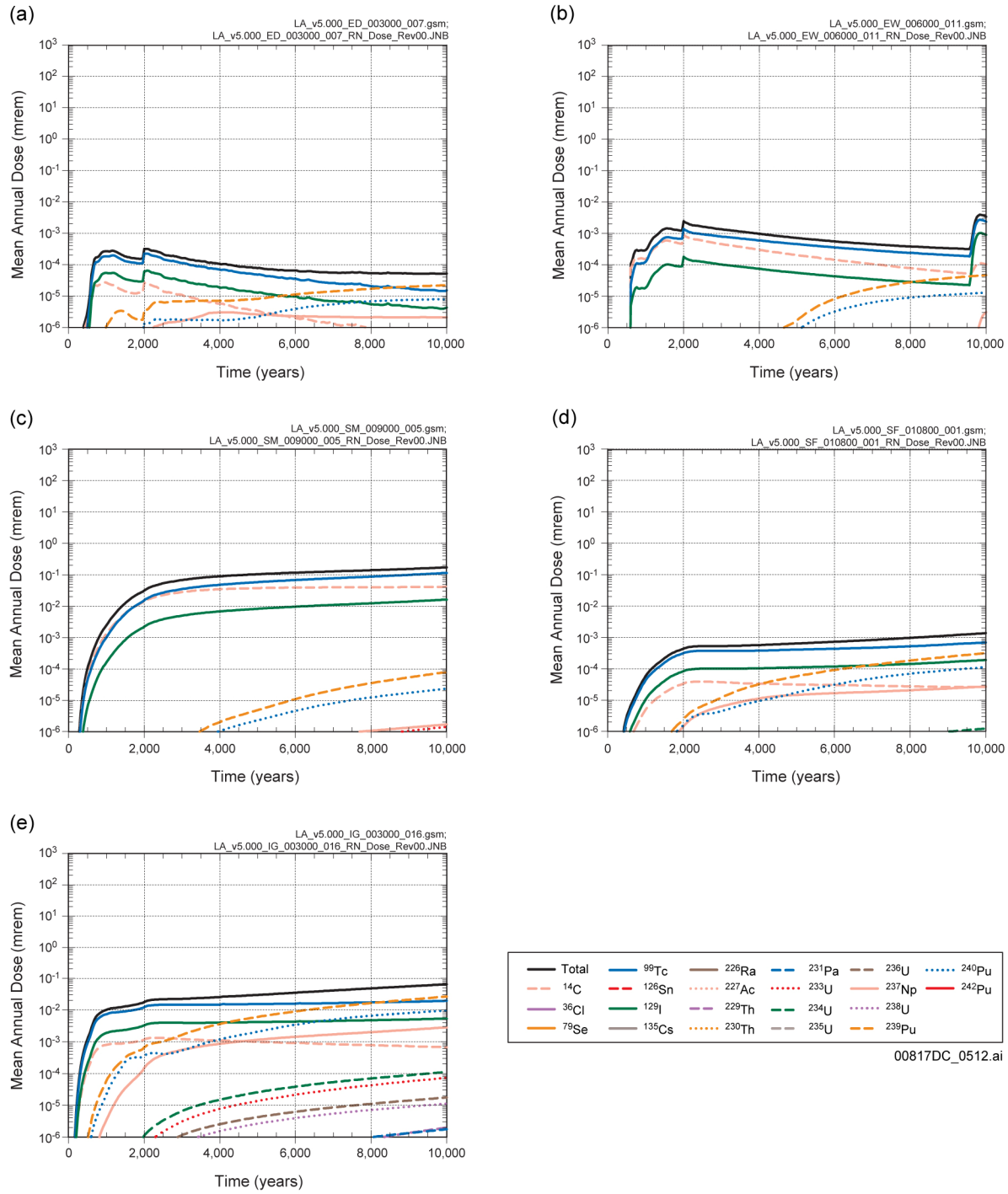

Source: Output DTN: MO0709TSPAREGS.000 [DIRS 182976].

Figure C7-11. TSPA-LA Scenario Modeling Cases Radionuclide Contributions to Projected Total Mean Annual Dose 10,000 Years after Repository Closure for (a) Drip Shield Early Failure, (b) Waste Package Early Failure, (c) Seismic Ground Motion, (d) Seismic Fault Displacement, and (e) Igneous Intrusion

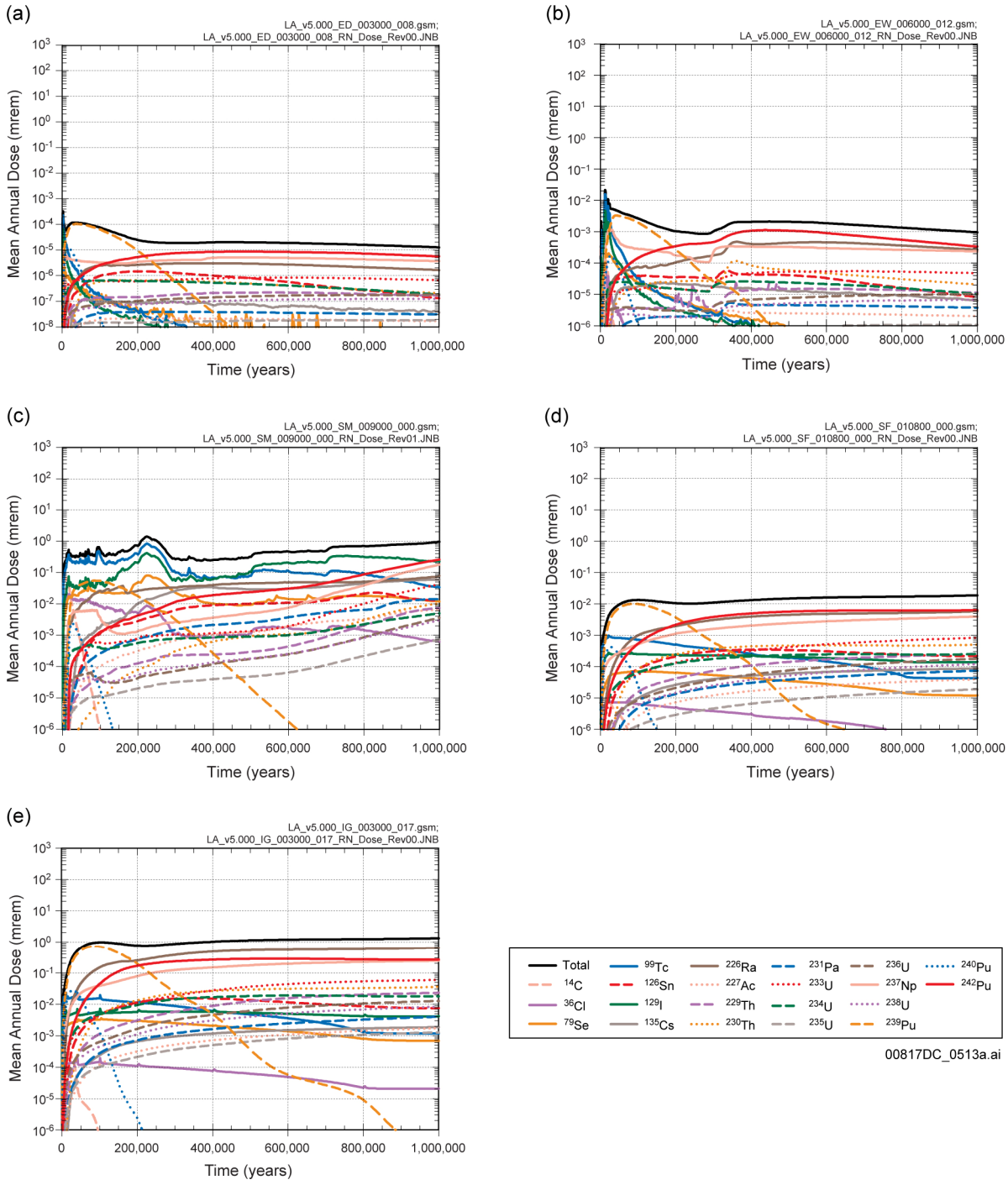

Source: Output DTN: MO0709TSPAREGS.000 [DIRS 182976].

Figure C7-12. TSPA-LA Scenario Modeling Cases Radionuclide Contributions to Projected Total Mean Annual Dose 1,000,000 Years after Repository Closure for (a) Drip Shield Early Failure, (b) Waste Package Early Failure, (c) Seismic Ground Motion, (d) Seismic Fault Displacement, and (e) Igneous Intrusion

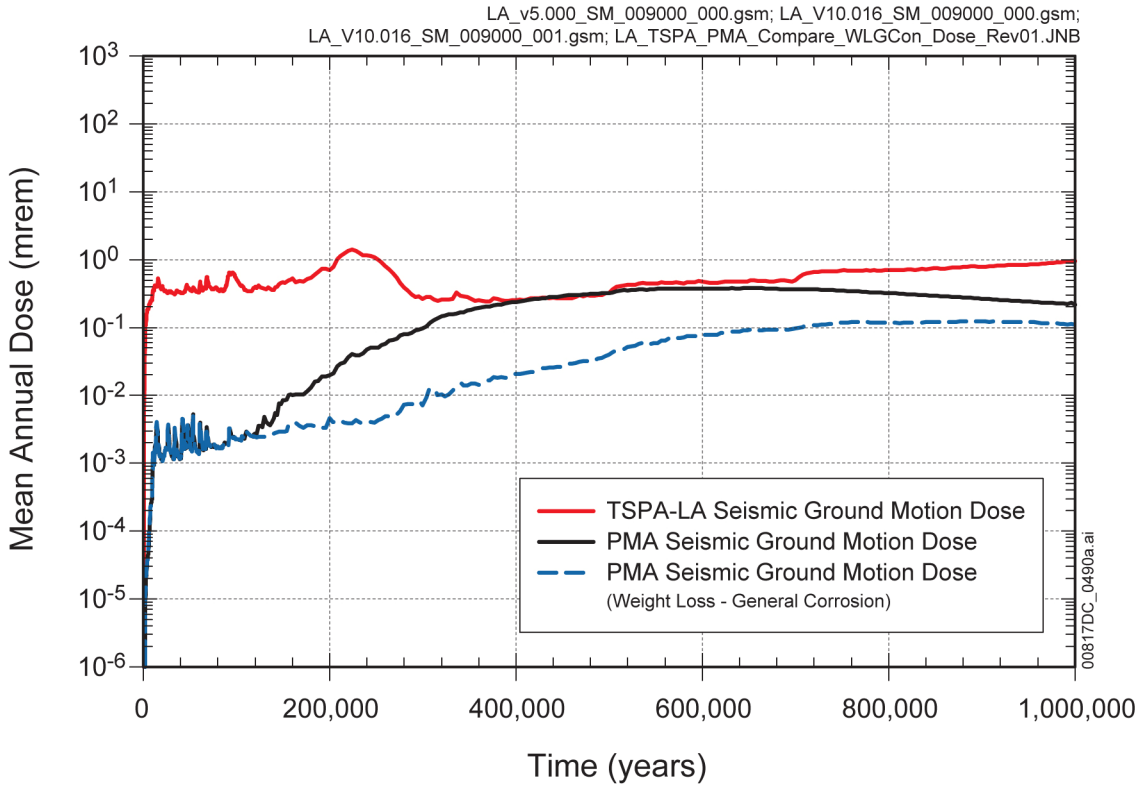

Source: Output DTN: MO0709TSPAREGS.000 [DIRS 182976] and Corroborative DTN: MO0709MARGANAL.000 [DIRS 182978].

Figure C7-13. Comparison of Seismic Ground Motion Modeling Cases to Projected Total Mean Annual Dose 1,000,000 Years after Repository Closure for TSPA-LA, Performance Margin Analysis, and the Performance Margin Analysis, including General Corrosion Weight-Loss Data

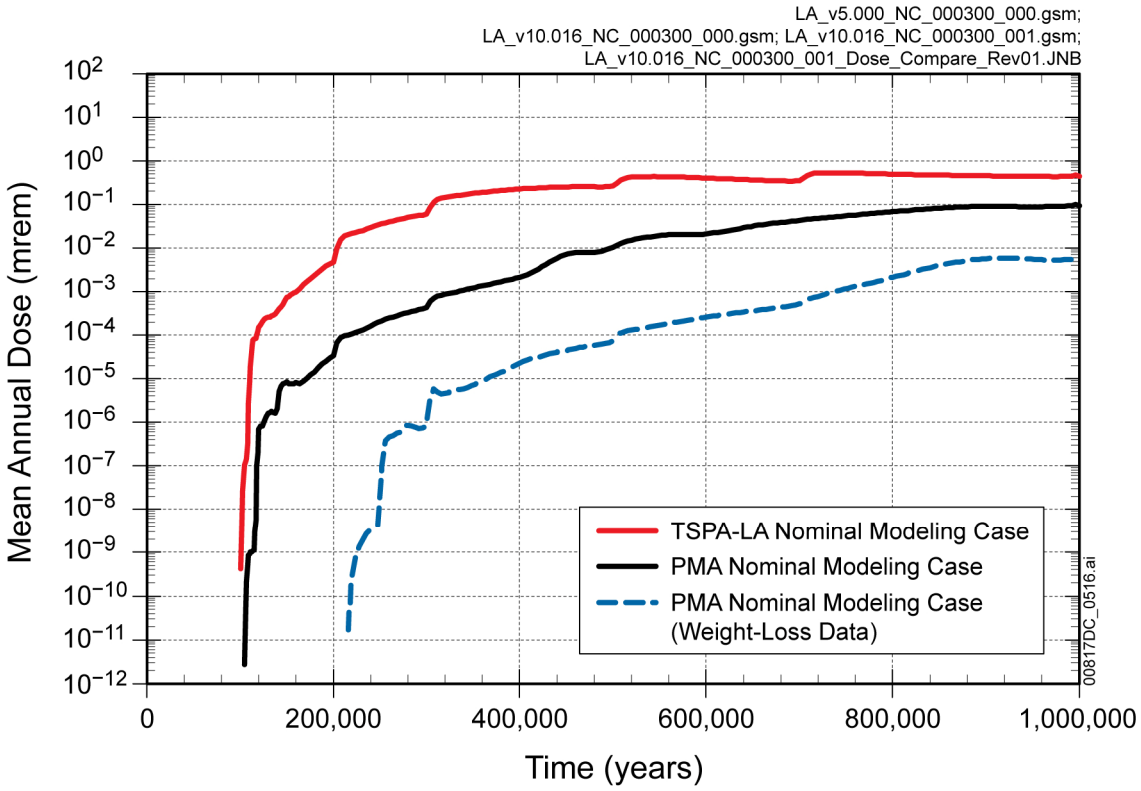

Source: Output DTN: MO0709TSPAREGS.000 [DIRS 182976] and Corroborative DTN: MO0709MARGANAL.000 [DIRS 182978].

Figure C7-14. Comparison of Nominal Modeling Cases to Projected Total Mean Annual Dose History 1,000,000 Years after Repository Closure for TSPA-LA, Performance Margin Analysis, and the Performance Margin Analysis, including General Corrosion Weight-Loss Data

INTENTIONALLY LEFT BLANK

APPENDIX D
PARAMETER LISTING

D1. INTRODUCTION

The Total System Performance Assessment (TSPA) Input Database contains the list of parameters used in the TSPA-LA Model. The details of this database are described in Section 4. Additionally, Appendix K contains two tables that describe the significant uncertain parameters (Tables K.3-1 and K.3-2.).

INTENTIONALLY LEFT BLANK

APPENDIX E
RESPONSE TO REVIEW COMMENTS FROM THE INTERNATIONAL REVIEW TEAM

E1. INTRODUCTION

The Total System Performance Assessment for the License Application (TSPA-LA) Model has evolved from the numerous TSPA models that were completed during the past decade (Sections ES2 and 1.1). In the summer of 2001, an International Review Team (IRT) jointly organized by the Nuclear Energy Agency of the Organization for Economic Cooperation and Development, and the International Atomic Energy Agency of the United Nations, met in Paris, France, and conducted an evaluation of the most recent performance assessment of the Yucca Mountain Repository, the Total System Performance Assessment for the Site Recommendation (TSPA-SR), and the accompanying TSPA-SR performance-assessment model. The IRT's evaluation is documented in: *An International Peer Review of the Yucca Mountain Project TSPA-SR* (OECD/IAEA 2002 [DIRS 158098]). The conclusions of the summary document support the TSPA methodology used for the Yucca Mountain Repository, and also provide a number of recommendations for future TSPA analyses and models related to the repository (OECD/IAEA 2002 [DIRS 158098], pp. 63 to 66). This appendix provides a summary of the recommendations provided by the IRT, and also identifies actions undertaken in response to those recommendations.

The Yucca Mountain Project conducted numerous analyses, evaluations, and impact analyses in response to many of the IRT recommendations. The recommendations from IRT were used, along with improvements in the understanding of the processes and engineered systems related to Yucca Mountain, to develop the TSPA-LA Model and its supporting submodels and analyses.

Table E-1 summarizes the status of the additional work conducted in response to the recommendations provided by the IRT.

INTENTIONALLY LEFT BLANK

Table E-1. Summary of Responses to International Review Team Summary Review Comments

IRT Recommendation Number	IRT Comment	Additional DOE Work Conducted since Review	Documentation
General	In particular, the IRT recommends that the inclusion of a diffusion pathway, in the absence of any advective flow onto or into the WP or the presence of any liquid water, should be independently reviewed to determine if it is credible and whether the complexity serves a valid purpose. If this over conservatism is removed, the calculated repository performance beyond 10,000 years could improve substantially.	The TSPA-LA Model is a modification of the TSPA-SR Model but is still conservative. The inclusion of a diffusion pathway in the absence of advective flow has not yet been independently reviewed. The current diffusion model is a key component of the *EBS Radionuclide Transport Abstraction* and is described in Section 7.2.1 and Appendix L of that report. Some aspects of the diffusion model that the IRT found to be very conservative were retained, including: (1) diffusion through thin water films that cover all EBS surfaces (SNL 2007 [DIRS 177407], Sections 6.3.1.2 and 6.3.4); (2) the presence of an emplacement pallet that was ignored in the EBS Radionuclide Transport assessment (SNL 2007 [DIRS 177407], Sections 6.1.1 and 6.3.1.2); (3) placing the WPs on the surface of invert (SNL 2007 [DIRS 177407], Sections 6.3.2.2 and 6.3.1.2); and (4) not allowing evaporation from DSs or WPs (SNL 2007 [DIRS 177407], Sections 6.3.2.4 and 6.3.3.2). Although conservative, the approach is appropriate for bounding analyses of repository performance for 10,000 years after repository closure and until the period of geologic stability per NRC Proposed Rule at 10 CFR 63.302 [DIRS 178394].	*EBS Radionuclide Transport Abstraction* (SNL 2007 [DIRS 177407], Sections 6.1, 6.3, 7.2.1, and Appendix L)
General	One aspect that has not been given sufficient attention is the possibility for any liquid water to exist on and within WPs over long periods of time. The probability of extraordinarily high seepage should be investigated in more depth. Design fixes, such as capillary barrier backfill, could be considered for the areas where seepage could be too high.	The *Multiscale Thermohydrologic Model* (SNL 2007 [DIRS 181383], Sections 6.1.3 and 6.3.16[a]) summarizes the relationship between percolation flux and seepage that contributes to Section 6.3.1. High percolation flux scenarios were not found to cause or encourage extraordinarily high seepage into repository drifts (Section 6.3.1.1). In addition, Section 6.3.1.2 shows that heat does not enhance seepage. Further, high percolation causes boiling duration to be shorter at the drift walls. Conversely, a low flux may encourage boiling for a longer period of time. In addition, thermal conductivity greatly affects how heat is dissipated in rock. Design fixes, such as capillary barrier backfill, were not included. Although a range of design alternatives may be evaluated by DOE, the basis for the License Application design of the repository is limited by the approved conceptual design found in *Total System Performance Assessment Data Input Package for Requirements Analysis for EBS In-Drift Configuration* (SNL 2007 [DIRS 179354], which serves as a source for the relevant model abstractions.	Engineered Barrier System: Physical and Chemical Environment Model: *Engineered Barrier System: Physical and Chemical Environment* (SNL 2007 [DIRS 177412], Sections 6.6, 6.9, and 6.15.1) Engineered Barrier System: *Multiscale Thermohydrologic Model* (SNL 2007 [DIRS 181383], Sections 6.1.3 and 6.3.16[a])

Table E-1. Summary of Responses to International Review Team Summary Review Comments (Continued)

IRT Recommendation Number	IRT Comment	Additional DOE Work Conducted since Review	Documentation
1	Include more disaggregation of TSPA-LA Model results and a more realistic assessment of the likely performance of the repository.	The evaluation of postclosure performance provided in this document includes a detailed presentation of subsystem results and other disaggregation of system-level results. Sections 7.1 to 7.4 and 7.7 and Appendix K provide information regarding assessments of the subsystems of the TSPA-LA Model. Because of the nature of the information provided to the TSPA and the overall approach required for an LA, the analysis includes some conservatisms. These conservatisms are noted as appropriate in subsections of Section 6.3, and their effect is qualitatively discussed.	Sections 6.3, 7.1 to 7.4 and 7.7 and Appendix K
2	Take steps to enhance the use of prior project information.	The project approach is to use available, quality information to conduct the performance assessment for the LA.	NA
3	Develop a safety case similar to the Nuclear Energy Agency approach.	This is a strategic project issue. No TSPA action is necessary.	NA

Table E-1. Summary of Responses to International Review Team Summary Review Comments (Continued)

IRT Recommendation Number	IRT Comment	Additional DOE Work Conducted since Review	Documentation
4	Develop and implement a comprehensive and systematic method for identification and treatment of uncertainty.	The approach developed in part, in response to the IRT recommendation, resulted in *Guidelines for Developing and Documenting Alternative Conceptual Models, Model Abstractions, and Parameter Uncertainty in the Total System Performance Assessment for the License Application*, and further specified for the TSPA in the *Technical Work Plan for: Total System Performance Assessment FY 07 to 08 Activities*. Uncertainty was incorporated in the development and implementation of the supporting models and abstractions and in the TSPA-LA Model. As part of this implementation, TSPA analysts reviewed relevant model abstractions and evaluated each input. When introducing uncertain parameters, the guidelines provided in the aforementioned documentation were followed. Section 6.1.2 discusses how uncertainty is incorporated in the calculation of mean annual dose using the TSPA-LA Model, and subsections to Section 6.3 contain discussions of the implementation of uncertainty with respect to the process models and submodels. Section 7.3 considers variability in terms of uncertainty and statistical stability (Section 7.3.1), variable numbers of Latin Hypercube samples with respect to the numerical accuracy of the calculation of mean annual dose (7.3.2), and temporal and spatial variability (Sections 7.3.3 and 7.3.4, respectively). Section 7.4 describes how uncertainty is incorporated into the modeling cases that are used to analyze the TSPA-LA Model scenario classes.	Sections 6.1.2, 7.3.1, 7.3.2, 7.3.3, 7.3.4, and 7.4 *Guidelines for Developing and Documenting Alternative Conceptual Models, Model Abstractions, and Parameter Uncertainty in the Total System Performance Assessment for the License Application* (BSC 2002 [DIRS 158794], Section 4) *Technical Work Plan for: Total System Performance Assessment FY 07 to 08 Activities* (SNL 2008 [DIRS 184920])

Table E-1. Summary of Responses to International Review Team Summary Review Comments (Continued)

IRT Recommendation Number	IRT Comment	Additional DOE Work Conducted since Review	Documentation
5	Quantitatively evaluate the importance of risk dilution.	The potential for risk dilution was minimized in the TSPA-LA process by evaluating and propagating realistic uncertainty in the distributions and ranges of the parameter values used in the TSPA-LA Model. One of the objectives of the Appendix C Performance Margin Analysis (PMA) as described in Section 7.7.4 was to ensure that the removal of the evaluated conservatisms did not introduce any inappropriate risk dilution in the TSPA-LA Model results as demonstrated by the absence of higher peak mean annual doses in the PMA results for both the probabilistic projections of the total dose histories and the comparison of the projected total mean dose history for the PMA relative to the TSPA-LA. The inclusion of uncertainty was significantly enhanced from previous TSPA models and follows the guidelines in *Guidelines for Developing and Documenting Alternative Conceptual Models, Model Abstractions, and Parameter Uncertainty in the Total System Performance Assessment for the License Application.* Section 6.1.2 describes the calculation of total mean annual dose and total median annual dose for the defined scenario classes for the TSPA-LA Model. In Section 7.7.4, the PMA also examines the sensitivity of the TSPA-LA Model with respect to conservatisms, parameter values, and model integration. These analyses provide comparisons between the base-case TSPA-LA Model and models that quantify the impact of various modeling issues. Furthermore, uncertainty within the TSPA-LA Model is quantitatively analyzed in Appendix K. Appendix K provides sensitivity analyses and discussions of parameters that were assessed to be important to the uncertainty of the model results. The TSPA-LA Model results include analyses of the impact of these parameters on the dose calculations.	Sections 6.1.2 and 7.7.4 and Appendix K *Guidelines for Developing and Documenting Alternative Conceptual Models, Model Abstractions, and Parameter Uncertainty in the Total System Performance Assessment for the License Application* (BSC 2002 [DIRS 158794])
6	Establish a program-wide focus on the reduction of uncertainty where it has the greatest effect.	Uncertainty in the TSPA-LA Model is addressed and described in Sections 6.1.2, 7.3.1, 7.3.2, 7.3.3, 7.3.4, and 7.4. Performance Confirmation testing and monitoring will assess the adequacy of the information used in the LA. Performance Confirmation test plans identify importance and/or relevance to the safety case and quantify parameters and condition limits for each test activity. If information obtained during Performance Confirmation challenges the information used in the licensing basis, the impact on repository performance will be evaluated and the regulator will be notified.	Sections 6.1.2, 7.3.1, 7.3.2, 7.3.3, 7.3.4, and 7.4 *Performance Confirmation Plan*, BSC 2004 [DIRS 172452]

Table E-1. Summary of Responses to International Review Team Summary Review Comments (Continued)

IRT Recommendation Number	IRT Comment	Additional DOE Work Conducted since Review	Documentation
7	Review and improve the EBS Transport Submodel.	Transport modeling through the EBS has been enhanced, including an Invert Diffusion Submodel, a section on retardation in the EBS, an In-Package Diffusion Submodel for Commercial Spent Nuclear Fuel Waste Packages, and sections discussing colloidal transport, transport through stress corrosion cracks, and transport through the waste-form rind. Supporting analyses and discussions are presented in *EBS Radionuclide Transport Abstraction* (SNL 2007 [DIRS 177407].	*EBS Radionuclide Transport Abstraction* (SNL 2007 [DIRS 177407], Section 6.3.4)
8	Improve the SZ regional model and the site-scale flow model. Run the model for in-spatial variability analysis, not just with a large uncertainty factor.	Although the SZ Regional and Site-Scale Models were developed outside the scope of the TSPA, the reference document supports the SZ Flow and Transport Model, the SZ Transport Model Component, and the SZ Flow and Transport Model Component. The SZ Regional and Site-Scale Models were updated with a number of modifications to: (1) reflect the current understanding of the SZ flow; (2) enhance model validation and uncertainty analyses; and (3) incorporate new data collected since the TSPA-SR. Changes introduced since the TSPA-SR Model report include the following: • Use of field and laboratory tests (hydraulic and tracer data collected since the TSPA-SR Model report) to establish and confirm the conceptual model for flow, constrain model parameter calibration, and provide data for model validation. • For validation purposes, use of recently collected hydraulic and geologic data that were obtained from the Nye County Early Warning Drilling Program. Despite these improvements, there remains uncertainty concerning the SZ flow component of the SZ flow model. This uncertainty represents a current lack of knowledge regarding the geophysical and hydrologic properties of the SZ. This uncertainty is represented in the assumptions in the reference document and in this TSPA-LA Model document, along with the bases and rationales for these assumptions.	*Saturated Zone Site-Scale Flow Model* (SNL 2007 [DIRS 177391], Sections 5, 6.4.3, 6.5, 6.7, and 7.2.2)

Table E-1. Summary of Responses to International Review Team Summary Review Comments (Continued)

IRT Recommendation Number	IRT Comment	Additional DOE Work Conducted since Review	Documentation
9	Develop a realistic understanding of radionuclide transport in a closed basin utilizing natural analogues.	Work is continuing on the evaluation of natural analogues and on the overall hydrogeologic system. In particular, the Peña Blanca Natural Analogue ongoing investigations include water sampling, rock and water analyses, and plans for PA modeling to assess groundwater flow and transport as part of studies under the DOE Office of Science and Technology (Goldstein et al. 2006 [DIRS 181364], p. 217). Section 7.8 contains a discussion of relevant natural analogues.	Section 7.8 Goldstein et al. 2006 ([DIRS 181364], p. 217) *Natural Analogue Synthesis Report* (BSC 2004 [DIRS 169218], Section 10)
10	Develop various levels of documentation, including a summary document.	The TSPA-LA Model documentation is supported by individual submodels and subordinate analysis and/or model reports. Section 6 of this report describes the essence of the main features of the TSPA-LA Model Section 1 and the Executive Summary provide summary descriptions of the TSPA-LA Model and its components as well as descriptions of the TSPA methodology.	Executive Summary and Section 6 .
11	Discuss design improvements and their role in the safety strategy in future documents.	The design of the repository is beyond the scope of this document. Quality Assurance processes are in place to ensure proper updating of controlled design inputs to the TSPA Model based on modifications to repository design. The scope of the documentation regarding design improvements is developed by the TSPA department and coordinated with DOE through mechanisms such as the Technical Management Review Board.	CC-PRO-1001, Rev. 2, *Technical Management Review Board Operations*
12	Long-term corrosion tests should be carried out on WP and DS materials, and the scientific understanding of corrosion mechanisms should be improved.	Long-term corrosion testing was conducted for both general corrosion and localized corrosion and more testing is scheduled in the Performance Confirmation Plan. There are about 5 years of corrosion data for WP and DS materials and about 10 years of data relating to stress corrosion cracking. The results of the corrosion testing are incorporated in the WP and DS models used in the TSPA-LA Model.	*Analysis of Dust Deliquescence for FEP Screening* (SNL 2007 [DIRS 181267]) *General Corrosion and Localized Corrosion of the Drip Shield* (SNL 2007 [DIRS 180778]) *General Corrosion and Localized Corrosion of Waste Package Outer Barrier* (SNL 2007 [DIRS 178519]) *Performance Confirmation Plan* (BSC 2004 [DIRS 172452])

Table E-1. Summary of Responses to International Review Team Summary Review Comments (Continued)

IRT Recommendation Number	IRT Comment	Additional DOE Work Conducted since Review	Documentation
13	The inventory screening procedure should be reviewed and amended, as appropriate, so that all potentially important radionuclides are included in the analysis.	The radionuclide screening procedure was reviewed, resulting in revised starting inventories for screening and a revised list of screened-in radionuclides. The revised list includes 32 nuclides (DTN: SN0310T0505503.004_R0 [DIRS 168761]. Thus, radionuclide screening analysis included (screen in) or removed radionuclides from further consideration (screen out) as contributors to radiation dose to the public from a nuclear waste repository at Yucca Mountain. The radionuclide screening analysis separately considered two different postclosure time periods: the 10,000-year period and the period from 10,000 years up to 1 million years after emplacement. Four release scenarios were considered: (1) the nominal scenario, (2) the human-intrusion scenario, (3) an intrusive igneous event, and (4) an eruptive igneous event. A radionuclide is screened out for a particular screening set, a grouping of radionuclides for a given waste form according to transport characteristics of each radionuclide, and waste form at a particular time. For comparison of results, the screening for the groundwater scenarios was used as the reference case to compare results. Of the 20 radionuclides collectively identified by the 10 studies, 13 were screened in for groundwater scenarios during the 10,000-year regulatory compliance period: ^{227}Ac, ^{243}Am, ^{14}C, ^{135}Cs, ^{129}I, ^{237}Np, ^{231}Pa, ^{239}Pu, ^{240}Pu, ^{226}Ra, ^{99}Tc, ^{229}Th, and ^{233}U. Four more were screened in for times up to 1,000,000 years: ^{36}Cl, ^{242}Pu, ^{79}Se, and ^{236}U. A fine-screen test, using a 99% cutoff level (contributes less than 1% of the dose), indicated that ^{36}Cl is potentially of marginal importance in the groundwater scenarios during the 10,000-year regulatory compliance period. OECD (Organization for Economic Co-operation and Development) 1997 ([DIRS 103445], Section 2.11) identified the radionuclides that contributed most to dose rate in “reference” studies of 10 repository performance assessments. Only one of the 10 studies found ^{94}Nb to be a major contributor to dose. *Radionuclide Screenin*g (SNL 2007 [DIRS 177424] developed the following results.	*Initial Radionuclide Inventories* (SNL 2007 [DIRS 180472], Table 6-2[a]) *Radionuclide Screenin*g (SNL 2007 [DIRS 177424], Sections 6.2.1, 6.7.2, and 7)

Table E-1. Summary of Responses to International Review Team Summary Review Comments (Continued)

IRT Recommendation Number	IRT Comment	Additional DOE Work Conducted since Review	Documentation
13 (Continued)		• ^{94}Nb is screened out for all scenarios and times. However, ^{94}Nb is found to be potentially of marginal importance for the groundwater scenarios after the 10,000-year regulatory compliance period. • ^{107}Pd is screened out for all scenarios and all times, and is not identified as marginally important by the fine-screen test. • ^{223}Ra has a half-life less than 10 years, and it is accounted for in the groundwater scenario only as a decay daughter from parents, such as ^{227}Ac. • For the waste forms considered and the physical processes employed in making the screening decision, ^{223}Ra is excluded as a primary radionuclide. • ^{245}Cm, ^{246}Cm, or ^{59}Ni are not important contributors to dose. • In addition to the radionuclides identified by the screening analysis, ^{241}Pu, ^{245}Cm, ^{228}Ra, and ^{235}U, were included in the radionuclide inventory to account for screened-in daughter products or due to augmentation from a screened-in precursor radionuclide. Also, ^{228}Ra was included because it is included in the groundwater protection standard.	
14	Further work should be carried out to strengthen confidence in the role of the cladding as a long-term containment barrier.	The cladding degradation analysis for the TSPA-LA Model starts with a discussion of cladding as a barrier and discusses the various parts of the cladding degradation abstraction analysis. The analysis document includes discussions of alternative scientific approaches, a summary of included FEPs, and a discussion of uncertainty. The document relies on 25 cladding-related documents for the sources of information used to develop and corroborate the analysis of cladding performance for the TSPA-LA Model. However, Cladding Degradation Summary for LA [DIRS 180616] conservatively concludes that, “For the no-cladding-credit compliance case, all fuel is taken to be failed upon receipt at the repository and the cladding is split when the waste package fails.” Thus, the TSPA-LA Model does not take credit for spent fuel cladding.	*Cladding Degradation Summary for LA* (SNL 2007 [DIRS 180616])

Table E-1. Summary of Responses to International Review Team Summary Review Comments (Continued)

IRT Recommendation Number	IRT Comment	Additional DOE Work Conducted since Review	Documentation
15	More experimental data should be obtained to validate thermodynamic modeling, especially with regard to the complex interactions between the waste form and components of the WP.	Work to improve validation of thermodynamic modeling has continued, including thermal testing in the Exploratory Studies Facility (ESF). However, the need to increase knowledge of in-package interactions between the waste form and the components of the WP persists. To satisfy this need, the Performance Confirmation program includes plans for continued laboratory waste-form testing, including WP coupled effects (see Performance Confirmation Plan Activity ID #226).	*Multiscale Thermohydrologic Model* (SNL 2007 [DIRS 181383], Section 6.2.3.1, 6.3.3, 7.1, and 8.4.2[a]) *In-Package Chemistry Abstraction* (SNL 2007 [DIRS 180506], Sections 6.3.2.1.1, 6.3.1.1[a], and 7.2[a]) *Performance Confirmation Plan* (BSC 2004 [DIRS 172452])
16 and 17	Additional experiments should be performed to enhance confidence in the model of flow and transport in the UZ. Head measurements in the rock matrix and water extraction by the ventilation system should be used to test the 3-D UZ Flow and Transport Model.	The validation activities for the UZ Flow Model Component include corroboration with experimental data and modeling studies using the following: 1. Observational data from the transverse cross drift above the repository horizon, the Enhanced Characterization Repository Block (ECRB) drift, conducted within the validation activities for the UZ Flow Model Component, which includes corroboration within the ESF; 2. Perched-water data from borehole WT-24; 3. Gas-flow data from boreholes SD-12 and UZ-7a; 4. Measured ^{14}C borehole data. In addition, validation efforts were also performed for the calcite model, and strontium model. The following demonstrations met the validation criteria: 1. Simulated water potential values are within the range of measurements along the ECRB drift (*Technical Work Plan for: Performance Assessment Unsaturated Zone*, Attachment I-1-2-1).	Unsaturated Zone Transport: *UZ Flow Models and Submodels* (SNL2007 [DIRS 184614], Section 7) *Radionuclide Transport Models Under Ambient Conditions* (SNL 2007 [DIRS 177396], Section 7) *Technical Work Plan for: Performance Assessment Unsaturated Zone* (BSC 2004 [DIRS 167969])

Table E-1. Summary of Responses to International Review Team Summary Review Comments (Continued)

IRT Recommendation Number	IRT Comment	Additional DOE Work Conducted since Review	Documentation
16 and 17 (Continued)		2. Simulated perched water elevation matches the observed value within 10 m (*Technical Work Plan for: Performance Assessment Unsaturated Zone*, Attachment I-1-2-1). 3. Simulated gas pressures and their patterns of variations consistently compare closely with observed values. Simulations consistently reproduce increases and decreases resulting from changes in barometric pressure at the ground surface (*Technical Work Plan for: Performance Assessment Unsaturated Zone*, Attachment I-1-2-1). 4. The comparison between simulated matrix pore-water age and observed ^{14}C ages indicates that with active fracture parameter, ã = 0.4 (for UZ Model layers TSw32 to TSw38), the simulated tracer transport time can reasonably represent the measured ^{14}C ages of boreholes UZ-1 and SD-12. In addition, the simulated matrix pore-water age is sensitive to ã. Water potential data were collected from heat dissipation probes installed in the tunnel wall along the ECRB drift inside the ESF. Water potential data were collected from heat dissipation sensors that were calibrated for matrix potential. The validation activities of the conservative UZ Transport Model component demonstrated adequate reproduction of field transport test results relative to the Busted Butte test series, and Alcove 8-Niche 3 tests as described in *Radionuclide Transport Models Under Ambient Conditions*. As part of the 3-D flow and transport modeling validation process, modeled results of water potentials were compared to field observation data collected from the tunnel wall to check the accuracy of the modeling predictions. Even though the data available for comparison at the ECRB drift are limited, results indicated that the UZ Flow and Transport Model Component predicted the observed range of the water potential data collected in field studies.	

Table E-1. Summary of Responses to International Review Team Summary Review Comments (Continued)

IRT Recommendation Number	IRT Comment	Additional DOE Work Conducted since Review	Documentation
18	The probability of bimodal basaltic-rhyolitic volcanism should be estimated and, if relevant, analyzed.	The Yucca Mountain Project does not agree with this peer review recommendation because, "It is inferred that a volcano that might form at Yucca Mountain … will exhibit similar eruptive processes to those recorded in the deposits at Lathrop Wells volcano" (SNL 2007 [DIRS 174260] Section 6.3), which is a distinctly basaltic volcano. Therefore, DOE did not estimate or analyze the probability of bimodal basaltic-rhyolitic volcanism. More discussion on the magmatic sequence at Yucca Mountain is included in NRC 2007 [DIRS 182132], Section 3.2.1.	Disruptive Events-Igneous: *Characterize Framework for Igneous Activity at Yucca Mountain*, *Nevada* (BSC 2004 [DIRS 169989], Section 6.1.1) Disruptive Events-Igneous: *Characterize Eruptive Processes at Yucca Mountain*, *Nevada* (SNL 2007 [DIRS 174260], Appendix F.2.6) *Igneous Activity at Yucca Mountain: Technical Basis for Decision Making* (NRC 2007 [DIRS 182132], Section 3.2.1)
19	Direct flow of surface water into a human-intrusion borehole should be considered in future assessments.	The conditions for analyzing the Human Intrusion Scenario are specified in NRC Proposed Rule 10 CFR 63.322 [DIRS 180319]. The specifications do not include surface water down the borehole. Therefore, this circumstance was not included in the TSPA-LA Model analysis of the Human Intrusion Scenario. Further, this condition would not occur under "the common techniques and practices that are currently employed in exploratory drilling for groundwater in the region surrounding Yucca Mountain" (10 CFR 63.322(c) [DIRS 180319]) because current practice would call for a surface seal, which would prevent water from falling into the borehole.	Section 6.7 FEPs DTN: MO0706SPAFEPLA.001; FEP Numbers 1.4.04.01.0A and 1.1.11.00.0A [DIRS 181613] NRC Proposed Rule 10 CFR 63.322 [DIRS 180319]
20	Conduct additional work at Peña Blanca.	Section 7.8.2 provides a summary of completed work at Peña Blanca, which provides confidence in the PA of the Yucca Mountain Repository using the TSPA-LA Model. Additional field data are being collected at the Peña Blanca natural analogue site as described in Goldstein et al. 2006 ([DIRS 181364], p. 217). The additional investigations will continue to support the Yucca Mountain project.	Section 7.8.2 *Natural Analogue Synthesis Report* (BSC 2004 [DIRS 169218], Section 10) Goldstein et al., 2006 ([DIRS 181364], p. 217)

Table E-1. Summary of Responses to International Review Team Summary Review Comments (Continued)

IRT Recommendation Number	IRT Comment	Additional DOE Work Conducted since Review	Documentation
21	Continue the investigation of naturally occurring uranium and its progeny in Yucca Mountain tuffs.	In addition to the work already conducted and presented in Paces and Neymark 2004 [DIRS 174513], and Neymark et al. 2005 [DIRS 180924], USGS researchers are collecting and analyzing additional field data.	Paces, J.B. and Neymark, L.A. 2004. "U-Series Evidence of Water-Rock Interaction at Yucca Mountain, Nevada, USA" [DIRS 174513] Neymark, L.A.; Paces, J.B.; Marshall, B.D.; Peterman, Z.E.; and Whelan, J.F. 2005. "Geochemical and C, O, Sr, and U-series Isotopic Evidence for the Meteoric Origin of Calcrete at Solitario Wash, Crater Flat, Nevada, USA." [DIRS180924]
22	Screen FEPs in two stages: (1) all FEPs required for understanding, and (2) regulatory considerations.	The Yucca Mountain Project FEP database was reviewed in accordance with the recommended two-stage process as part of the development of the TSPA-LA. FEP screening decisions were reviewed and documented. The results are incorporated in DTN: MO0706SPAFEPLA.001 [DIRS 181613].	FEPS descriptions, screening arguments, and dispositions are consolidated in DTN: MO0706SPAFEPLA.001 [DIRS 181613]
23	Present a best estimate or most probable dose range, plus the upper limit value at an appropriate percentile, as a measure of maximum reasonably expected value.	NRC Proposed Rule 10 CFR Part 63 ([DIRS 178394] and [DIRS 180319]) require that the results of the PA analyses present annual dose to the RMEI in terms of the mean annual dose for the first 10,000 years postclosure, and as the median annual dose for the period from 10,000 years to the period of geologic stability (10 CFR 63.303 [DIRS 178394]). In addition, the TSPA-LA Model calculates at the 5^{th} and 95^{th} percentiles of dose to the RMEI.	NRC Proposed Rule 10 CFR Part 63 [DIRS 178394] and [DIRS 180319]

Table E-1. Summary of Responses to International Review Team Summary Review Comments (Continued)

IRT Recommendation Number	IRT Comment	Additional DOE Work Conducted since Review	Documentation
24	Base the probabilistic analysis on realistic rather than conservative representation.	The realistic analysis is not required by current regulations (10 CFR 63.114(b) [DIRS 178394]). However, the general approach for the TSPA-LA Model is to improve realism by reducing the number of conservative assumptions. Regardless of this general approach, it should be noted that "simplifications and assumptions are involved out of necessity..." (40 CFR Part 197 [DIRS 173176]). This results in the TSPA-LA Model being a hybrid "conservative/probabilistic" Model in which reasonable incorporation of conservatism is used when necessary. Further, Appendix C presents the results of a Performance Margin Analysis, summarized in Section 7.7.4, which uses less conservative, i.e., more "realistic," values of some TSPA-LA Model parameters to estimate the range of performance with respect to choices of parameter values, thus indicating the potential performance margin embedded in the TSPA-LA Model's dose calculations.	10 CFR Part 63 [DIRS 178394] and [DIRS 180319] 40 CFR Part 197 [DIRS 173176]
25	Use a more formal approach to determine convergence of probabilistic results. Consider using alternative sampling schemes and larger numbers of realizations.	The approach to be utilized is described, and the results of the statistical stability analysis are presented in Section 7.3.1. Larger numbers of realizations and alternative sampling schemes were utilized. Section 7.3.2 considers variable numbers of Latin hypercube sample, and TSPA-LA Model realizations with respect to the numerical accuracy of the calculation of mean annual dose. In addition, temporal and spatial variability are addressed in Sections 7.3 and 7.4, respectively. After establishing the stability of the calculation methodology, the TSPA-LA Model utilizes enough realizations to provide statistically stable results.	Sections 7.3.1, 7.3.2, 7.3.3, and 7.3.4

Table E-1. Summary of Responses to International Review Team Summary Review Comments (Continued)

IRT Recommendation Number	IRT Comment	Additional DOE Work Conducted since Review	Documentation
26	Present probability density function of calculated doses.	The complete array of annual doses used in calculating the mean annual dose for each modeling case is provided in Section 8.2 and Appendix K. These plots present the same relevant data that could alternatively be displayed as probability density function curves, although these data are not presented in that form in Section 8 or Appendix K. In addition, the distribution of calculated annual doses at 10,000 and 1,000,000 years after repository closure is provided for each modeling case in Sections 8.2 and Appendix K.	Section 8.2 and Appendix K
27	Use sensitivity analysis to assist in building an integrated and comprehensive understanding of the relative importance and role of different barriers and processes.	Such analyses were conducted and are described in Section 8.3 and Appendix K.	Section 8.3 and Appendix K

APPENDIX F

DYNAMICALLY LINKED LIBRARIES DESCRIPTION AND FEEDS

F1. INTRODUCTION

Appendix F provides a summary of the dynamically linked libraries (DLLs) used in the Total System Performance Assessment for the License Application (TSPA-LA) Model and their associated input files. Each DLL is identified by software name and version, software tracking number (STN), and Document Input Reference System (DIRS) number. Some DLL names differ slightly from their corresponding software names. Appendix F also includes tables that list the input file(s) used by each DLL. Since only input files are described, the DLLs that do not use input files are briefly identified for completeness.

Table F-1 provides a brief description of each DLL and identifies the subsequent table that contains the input files for the DLL. Tables F-2 through F-13 contain a list of the input files used by each DLL, a description of the files, the Data Tracking Number (DTN) containing the files, and a list of the control information and data within the input files. For TSPA-LA Model V5.000, the DLLs are identified as DLL Set 35 and their input files are identified as Input File Set 62. Some TSPA-LA Model V5.000 groundwater transport simulations used DLL Set 34 and Input File Set 61. These DLLs and associated input files are the same for the groundwater transport analyses as in DLL Set 35 and Input File Set 62. The only differences between these sets are with respect to the Volcanic Eruption Modeling case.

The TSPA-LA Model V5.000 simulations were processed using GoldSim V9.60.100 (STN: 10344-9.60-01 [DIRS 181903]) as described in Section 3.1.2. During a TSPA-LA Model multi-realization simulation, the DLLs and their associated input files are automatically downloaded from a controlled computer network area into the primary run directory on the master processor. The file-transfer process utilizes the GoldSim model file elements to ensure that the external supporting files to GoldSim, including both the DLL executable files and their associated input files used in a simulation, are directly accessed from a controlled environment. These files are in turn passed from the master processor to slaves when the GoldSim *Distributed Process Module* is utilized. This automated file transfer process allows GoldSim to provide an 'audit trail' of the DLL executable files and associated input files used in any simulation. In addition, the TSPA-LA Model utilizes the file-locking option of the GoldSim file elements, which permits the simulation to proceed only if the file being used for the simulation is exactly the same as the file that the element was initially locked onto. The names of the DLL executable files and their associated input files are parameters in the TSPA-LA Model Input Database (Section 4.7), which are directly accessed by the GoldSim file elements.

F2. INPUT FILES BY DYNAMICALLY LINKED LIBRARY

F2.1 FEHMN_V2_24-01.DLL

The DLL fehmn_v2_24-01.dll (FEHM V 2.24-01, STN: 10086-2.24-01-00 [DIRS 179419]) is designed to perform radionuclide transport calculations. Transport through the unsaturated zone (UZ) is simulated in the TSPA-LA Model using a residence-time, transfer-function particle-tracking technique as described in *Particle Tracking Model and Abstraction of Transport Processes* (SNL 2008 [DIRS 184748]). A complete description of fehmn_v2_24-01.dll and the input files is documented in *Software Users Manual (UM) for the*

FEHM Application Version 2.21 (LANL 2003 [DIRS 167579]) and *User Information for: FEHM V2.24-01* (DOE 2007 [DIRS 181096]).

In TSPA-LA Model simulations, GoldSim and fehmn_v2_24-01.dll (also generally abbreviated as FEHM for Finite Element, Heat and Mass Model) are coupled through a predefined interface. Data passed from GoldSim directly through the interface for each timestep includes: (1) the simulation time; (2) a flow-field index (instructing FEHM which flow-field file to read for the present timestep and infiltration scenario; (3) two random seeds, one used to initiate sampling for particle-tracking logic and one used to initialize logic for determining the source release location; (4) the number of source bins; (5) the number of waste packages (WPs) contributing mass to the engineered barrier system (EBS) release to the UZ for each percolation subregion; (6) the fraction of mass in each source bin for each species entering the UZ that is applied to the fractures; and (7) the EBS mass release rates. Additional control data for the number of WP early failures are also passed, but the option is not used in the TSPA-LA Model as indicated by the passed control index. For efficiency, FEHM does not simulate the flow fields. Instead, FEHM reads pre-existing flow fields at the start of each realization and at times of climate changes. These flow fields were generated in advance using TOUGH2 V1.6 (LBNL 2003 [DIRS 161491]). At the end of each simulation timestep, FEHM passes the radionuclide mass fluxes generated at the water table back to GoldSim through the interface.

The fehmn_v2_24-01.dll input stream is controlled by two main files. The input file fehmn.files contains a list of the main input and output files used by FEHM. The input file fehm_TSPA_template.dat is a generic file that contains both FEHM input parameters and input file names, where additional parameters are found. For the TSPA-LA Model, either fehm_TSPA_gs_20kyr.dat for 10,000/20,000-year simulations or fehm_TSPA_gs_1Myr.dat for one-million-year simulations is automatically copied into fehm_TSPA_template.dat.

The following subsections describe the input files used by fehmn_v24_2.-01.dll. The file names used refer to actual UZ Transport Submodel files. A complete list of these files and their contents is presented in Table F-2.

F2.1.1 Control Data File for Primary Inputs and Outputs

As described in Table F-2, the input file fehmn.files is the default fehmn_v2_24-01.dll control file read at the start of a run. It contains names of the main input data file, grid file, initial zone file, output file, flow-field (or restart) file, updated restart file, simulation history file, stiffness matrix file, Solute history output file, and check file; contour files (if used); a screen output indicator and information on supplementary subroutines. See the user's manual (LANL 2003 [DIRS 167579], Section 6.2.1) for a description of the file.

F2.1.2 Control Data Files for Input Parameters

As described in Table F-2, the two input files fehm_TSPA_gs_20kyr.dat and fehm_TSPA_gs_1Myr.dat contain control information and data for 10,000/20,000-year and one-million year simulations. The two files are based on the template file fehm_TSPA_template.dat obtained from DTN: MO0704PAFEHMBR.001_R3 [DIRS 184647], which is an output DTN from *Particle Tracking Model and Abstraction of Transport Processes*

(SNL 2008 [DIRS 184748]). Minor modifications were made to the template file to create the two input files that allow the TSPA-LA Model to control the time stepping. At the start of each TSPA-LA Model simulation, the appropriate file for the chosen simulation time length is copied into a generic file named in the control file fehmn.files (described in Section F2.1.1). Both of the input files contain simulation control information and names of parameter files containing data for rock properties, a dual permeability option, a colloid interface-filtration model, a spatial zonation of properties, and a generic multiple-species particle tracking transport model. See the user's manual (LANL 2003 [DIRS 167579], Section 6.0) for a description of the file.

To enhance the input process, FEHM contains a macro control structure for data input. The macro command structure is based on a set of control statements that is recognized by the program. When a macro control statement (or keyword) is encountered in an input file, the input control module reads in a specific set of data in a prescribed order. This allows the user to set up an input file or set of files using structured blocks of data assembled in any order. Except for macro control statements, data within each block are read in by free format. This adds to the flexibility of the model, but dictates that values be added for all input variables. In addition, because the model allows the user to assign data by node, groups of nodes, or for the entire system, data lists are generally followed by blank lines indicating to the model that no more data of that specific type follows. Within blocks of data, the user can include the keyword 'file', followed by a file name, indicating that the next data expected by the input module are contained in the file noted.

Basic macros controlled by parameters listed in the above data control files include: (1) *perm*, which assigns default permeabilities to all zones; (2) *rlp*, the relative permeability and capillary pressure model; (3) *time*, the which sets up the timesteps for and ending time of the simulation; (4) *itfc*, which controls colloid filtration at matrix interfaces; (5) *ctrl*, which lists the general run parameters needed for equation solver and matrix solver routines; (6) *sol*, which defines the solution type and element integration method; (7) *rflo*, which signifies that the flow field will be read in; (8) *airwater,* which signifies that the problem is two-phased; and (9) *node*, which can be used to assign specific nodes for output. Note that many of the parameters associated with the above macros are not used in the coupled GoldSim/FEHM simulations.

F2.1.3 Nodal-Coordinate Data File

As described in Table F-2, the input file fehmn.grid contains a list of the grid node numbers and their associated location coordinates and elevations. The nodal-coordinates are based on the Nevada State Plane eastings (m), northings (m), and elevations (meters above mean sea level). Note that only the node numbers for the fracture media are listed. The node number for the spatially equivalent matrix node is found by adding 120,711 to the fracture medium node number. Although the element connectivities are defined in this file, they are not used in the particle-tracking model. See the user's manual (LANL 2003 [DIRS 167579], Section 6.2.12) for a complete description.

F2.1.4 Zone Data File – Initial

As described in Table F-2, the input file fehmn.zone is the initial material zone file. See the user's manual (LANL 2003 [DIRS 167579], Section 6.2.74) for a description of the input parameters.

The zones defined below are used for all zone-based property assignments until superseded by another zone file listed in the main input file. All zone-based property assignments following a new zone-file assignment will be based upon the new file until a new zone file occurs in the input stream. The data are in the form of a list of nodes for each zone. As listed below, there are 96 material zones in the model. The first 46 represent rock matrix, the second 46 represent the corresponding fractures overlaying the same space, and zones 93 through 96 represent fault zones.

1. tcwM1-Tiva Canyon Layer 1 welded tuff rock matrix
2. tcwM2-Tiva Canyon Layer 2 welded tuff rock matrix
3. tcwM3-Tiva Canyon Layer 3 welded tuff rock matrix
4. ptnM1-Paintbrush Layer 1 nonwelded tuff rock matrix
5. ptnM2-Paintbrush Layer 2 nonwelded tuff rock matrix
6. ptnM3-Paintbrush Layer 3 nonwelded tuff rock matrix
7. ptnM4-Paintbrush Layer 4 nonwelded tuff rock matrix
8. ptnM5-Paintbrush Layer 5 nonwelded tuff rock matrix
9. ptnM6-Paintbrush Layer 6 nonwelded tuff rock matrix
10. tswM1-Topopah Springs Layer 1 welded tuff rock matrix
11. tswM2-Topopah Springs Layer 2 welded tuff rock matrix
12. tswM3-Topopah Springs Layer 3 welded tuff rock matrix
13. tswM4-Topopah Springs Layer 4 welded tuff rock matrix
14. tswM5-Topopah Springs Layer 5 welded tuff rock matrix
15. tswM6-Topopah Springs Layer 6 welded tuff rock matrix
16. tswM7-Topopah Springs Layer 7 welded tuff rock matrix
17. tswM8-Topopah Springs Layer 8 welded tuff rock matrix
18. tswMz-Topopah Springs Layer 9 zeolitized tuff rock matrix
19. tswMz-Topopah Springs Layer 9 vitric tuff rock matrix
20. ch1Mz-Calico Hills Layer 1 zeolitized tuff rock matrix
21. ch1Mv-Calico Hills Layer 1 vitric tuff rock matrix
22. ch2Mv-Calico Hills Layer 2 vitric tuff rock matrix
23. ch3Mv-Calico Hills Layer 3 vitric tuff rock matrix
24. ch4Mv-Calico Hills Layer 4 vitric tuff rock matrix
25. ch5Mv-Calico Hills Layer 5 vitric tuff rock matrix
26. ch2Mz-Calico Hills Layer 2 zeolitized tuff rock matrix
27. ch3Mz-Calico Hills Layer 3 zeolitized tuff rock matrix

28. ch4Mz-Calico Hills Layer 4 zeolitized tuff rock matrix
29. ch5Mz-Calico Hills Layer 5 zeolitized tuff rock matrix
30. ch6Mz-Calico Hills Layer 6 zeolitized tuff rock matrix
31. ch6Mv-Calico Hills Layer 6 vitric tuff rock matrix
32. pp4Mz-Prow Pass Layer 4 zeolitized tuff rock matrix
33. pp3Md-Prow Pass Layer 3 differentiated tuff rock matrix
34. pp2Md-Prow Pass Layer 2 differentiated tuff rock matrix
35. pp1Mz-Prow Pass Layer 1 zeolitized tuff rock matrix
36. bf3Md-Bull Frog Layer 3 differentiated tuff rock matrix
37. bf2Mz-Bull Frog Layer 2 zeolitized tuff rock matrix
38. tr3Md-Tram Layer 3 differentiated tuff rock matrix
39. tr2Mz-Tram Layer 2 zeolitic tuff rock matrix
40. pcM38-Perched water layer corresponding to Topopah Springs Layer 8 rock matrix
41. pcM39-Perched water layer corresponding to Topopah Springs Layer 9 rock matrix
42. pcM1z-Perched water layer corresponding to Calico Hills zeolitic Layer 1 matrix
43. pcM2z-Perched water layer corresponding to Calico Hills zeolitic Layer 2 matrix
44. pcM5z-Perched water layer corresponding to Calico Hills zeolitic Layer 5 matrix
45. pcM6z-Perched water layer corresponding to Calico Hills zeolitic Layer 6 matrix
46. pcM4p-Perched water layer corresponding to Prow Pass zeolitic Layer 4 matrix
47. tcwF1-Tiva Canyon Layer 1 welded tuff fractures
48. tcwF2-Tiva Canyon Layer 2 welded tuff fractures
49. tcwF3-Tiva Canyon Layer 3 welded tuff fractures
50. ptnF1-Paintbrush Layer 1 nonwelded tuff fractures
51. ptnF2-Paintbrush Layer 2 nonwelded tuff fractures
52. ptnF3-Paintbrush Layer 3 nonwelded tuff fractures
53. ptnF4-Paintbrush Layer 4 nonwelded tuff fractures
54. ptnF5-Paintbrush Layer 5 nonwelded tuff fractures
55. ptnF6-Paintbrush Layer 6 nonwelded tuff fractures
56. tswF1-Topopah Springs Layer 1 welded tuff fractures
57. tswF2-Topopah Springs Layer 2 welded tuff fractures
58. tswF3-Topopah Springs Layer 3 welded tuff fractures
59. tswF4-Topopah Springs Layer 4 welded tuff fractures
60. tswF5-Topopah Springs Layer 5 welded tuff fractures
61. tswF6-Topopah Springs Layer 6 welded tuff fractures
62. tswF7-Topopah Springs Layer 7 welded tuff fractures
63. tswF8-Topopah Springs Layer 8 welded tuff fractures
64. tswFz-Topopah Springs Layer 9 zeolitized tuff fractures
65. tswFv-Topopah Springs Layer 9 vitric tuff fractures

66. ch1Fz-Calico Hills Layer 1 zeolitized tuff fractures
67. ch1Fv-Calico Hills Layer 1 vitric tuff fractures
68. ch2Fv-Calico Hills Layer 2 vitric tuff fractures
69. ch3Fv-Calico Hills Layer 3 vitric tuff fractures
70. ch4Fv-Calico Hills Layer 4 vitric tuff fractures
71. ch5Fv-Calico Hills Layer 5 vitric tuff fractures
72. ch2Fz-Calico Hills Layer 2 zeolitized tuff fractures
73. ch3Fz-Calico Hills Layer 3 zeolitized tuff fractures
74. ch4Fz-Calico Hills Layer 4 zeolitized tuff fractures
75. ch5Fz-Calico Hills Layer 5 zeolitized tuff fractures
76. ch6Fz-Calico Hills Layer 6 zeolitized tuff fractures
77. ch6Fv-Calico Hills Layer 6 vitric tuff fractures
78. pp4Fz-Prow Pass Layer 4 zeolitized tuff fractures
79. pp3Fd-Prow Pass Layer 3 differentiated tuff fractures
80. pp2Fd-Prow Pass Layer 2 differentiated tuff fractures
81. pp1Fz-Prow Pass Layer 1 zeolitized tuff fractures
82. bf3Fd-Bull Frog Layer 3 differentiated tuff fractures
83. bf2Fz-Bull Frog Layer 2 zeolitized tuff fractures
84. tr3Fd-Tram Layer 3 differentiated tuff fractures
85. tr2Fz-Tram Layer 2 zeolitized tuff fractures
86. pcF38-Perched water layer corresponding to Topopah Springs Layer 8 fractures
87. pcF39-Perched water layer corresponding to Topopah Springs Layer 9 fractures
88. pcF1z-Perched water layer corresponding to Calico Hills Layer 1 zeolitic fractures
89. pcF2z-Perched water layer corresponding to Calico Hills zeolitic Layer 2 fractures
90. pcF5z-Perched water layer corresponding to Calico Hills zeolitic Layer 5 fractures
91. pcF6z-Perched water layer corresponding to Calico Hills zeolitic Layer 6 fractures
92. pcF4p-Perched water layer corresponding to Prow Pass zeolitic Layer 4 fractures
93. tcwFf–Faults in Tiva Canyon welded hydrologic units
94. ptnFf-Faults in Paintbrush nonwelded hydrologic units
95. tswFf-Faults in Topopah Spring welded hydrologic units
96. chnFf-Faults in Calico Hills nonwelded hydrologic units.

F2.1.5 Initialization Files

As described in Table F-2, the 16 input files ffij00.ini are restart/initialization files that contain nodal pressure and saturation data for each node and flux data for each pair of adjacent nodes. These data are used to describe the flow field for different climates and infiltration scenarios. The data initializes at the beginning of each model realization and at each timestep when the climate changes. For this analysis, the initialization files contain the flow fields generated by TOUGH2 in FEHM format that are read by FEHM at run time. Although pressure data is

required, it is not used in the particle-tracking analysis. The structure of the flow-field files is consistent with the structure of restart records written by FEHM. Particle tracking records written to the restart files are not part of the flow-field files used in the coupled GoldSim/FEHM runs. See the user's manual (LANL 2003 [DIRS 167579], Section 7.2) for a description of the file.

The naming convention, ffij00.ini, is used for the coupled GoldSim/FEHM analyses. The saturation and flux data are used to describe the flow field as follows:

i = 1 (present-day climate)
i = 2 (monsoon climate)
i = 3 (glacial-transition climate)
i = 4 (post-10,000 years)
j = 1 (10th percentile infiltration scenario)
j = 2 (30th percentile infiltration scenario)
j = 3 (50th percentile infiltration scenario)
j = 4 (90th percentile infiltration scenario).

Note that the classification of 10^{th}, 30^{th}, 50^{th}, and 90^{th} percentile infiltration scenarios is based on the infiltration maps used to develop the flow fields for the first three climates. For the post-10,000-year climate, the four equivalent flow fields are generated using the scaled 90th percentile present-day, 50th percentile Glacial Transition, 90th percentile glacial transition, and the 90th percentile monsoon infiltration maps, respectively (see Section 6.3.1). The flow-field index, ij00, is passed from GoldSim to FEHM at each timestep. When the index changes from its original value to ij00, FEHM will reinitialize the flow field with the contents of ffij00.ini. The flow field input files are renamed from the original file names and are found in the output DTN: MO0708TSPAGENT.000 [DIRS 183000]. The files are grouped as follows:

Present-day files ff1100.ini, ff1200.ini, ff1300.ini, and ff1400.ini are equivalent to the original files pd10.ini, pd30.ini, pd50.ini, and pd90.ini (DTN: LB0612PDFEHMFF.001_R0 [DIRS 179296]), respectively.

Monsoon-climate files ff2100.ini, f2200.ini, ff2300.ini, and ff2400.ini are equivalent to the original files mo10wtrise.ini, mo30wtrise.ini, mo50wtrise.ini, and mo90wtrise.ini (DTN: LB0701MOFEHMFF.001_R0 [DIRS 179297]), respectively.

Glacial-transition climate flow field files, ff3100.ini, ff3200.ini, ff3300.ini, and ff3400.ini are equivalent to the original files gt10wtrise.ini, gt30wtrise.ini, gt50wtrise.ini, and gt90wtrise.ini (gt10wtrise.ini, gt30wtrise.ini, gt50wtrise.ini, gt90wtrise.ini (DTN: LB0701GTFEHMFF.001_R0 [DIRS 179160]), respectively.

Post-10,000 year flow fields, ff4100.ini, ff4200.ini, ff4300.ini, and ff4400.ini are equivalent to the original files post10kWTRISEpkdq1.ini, post10kWTRISEpkdq2.ini, post10kWTRISEpkdq3.ini, and post10kWTRISEpkdq4.ini (DTN: LB0702PAFEM10K.002_R0 [DIRS 179507]), respectively.

F2.1.6 Stiffness Matrix Data File

As described in Table F-2, the input file fehmn.stor contains the pre-calculated stiffness matrix data associated with the grid file used in the UZ transport calculation. This input file contains finite element coefficients designed to speed-up the execution of the software. Note that dummy area coefficients are also included in this file. See the user's manual (LANL 2003 [DIRS 167579], Section 7.7) for a description of the file.

The stiffness matrix file contains two required text lines describing information about the file and the following data:

1. Number of storage locations needed to store geometric input types (974,283).
2. Number of fracture (or matrix) nodes (120,711).
3. Number of positions for which information needs to be stored (1,094,995).
4. Volume associated with each node.
5. Nodal connectivity information including array positions followed by the node numbers grouped by connectivity.
6. Finite element geometric coefficients along with their starting positions for each node and the position of the primary nodes in the connectivity array. Note that the geometric coefficients are all set to -1.0 for the multiple-species particle tracking model.

F2.1.7 Double Porosity/Double Permeability Data File

As described in Table F-2, the input file fehm_TSPA.dpdp contains dual porosity/dual permeability geometric data for each fracture zone identified in Section F2.1.4 (zones 47 through 96). The first set of data defines the volume fraction (unitless) of the effective nodal volume taken up by the fracture. The volume fraction is used to define the accumulation (storage) terms. The second set of data defines the length scale of matrix nodes. See the user's manual (LANL 2003 [DIRS 167579], Section 6.2.14) for a description of the file.

F2.1.8 Rock Data File

As described in Table F-2, the input file fehm_TSPA.rock contains rock bulk density, specific heat, and porosity data for each zone defined in fehmn.zone (described in Section F.2.1.4). See the user's manual (LANL 2003 [DIRS 167579], Section 6.2.58) for a description of the file.

F2.1.9 Pore Size Data Files

As described in Table F-2, the 16 input files contain pore-size (filtration) cumulative probability data for the various rock matrix zones used to determine which size of colloidal particles will be filtered out during the rock layer contact filtration analysis. The pore-size distribution data are used to simulate the effect of colloid filtration at matrix interfaces on radionuclide transport. See the user's manual (LANL 2003 [DIRS 167579], Section 6.2.40) for a description of the file.

F2.1.10 Zone Data File – Updated

As described in Table F-2, the input file fehm.zone2 is an updated zone file that contains the same zone data as fehmn.zone described in Section F2.1.4*)*, plus two supplemental sets of zones at the end of the file. See the user's manual (LANL 2003 [DIRS 167579], Section 6.2.74) for a description of the file.

The first supplemental set of zones defines fracture zones (Zones 501 through 505) and matrix radionuclide release zones (Zones 601 through 605) for mass entering the UZ from the EBS. Note that for the TSPA-LA Model analysis, only the fracture zones 501 through 505 are used. The nodal numbering convention indicates the number of the matrix node that is spatially equivalent to a specified fracture node, which can be derived as $node\#_{matrix} = node\#_{fracture} + 120{,}711$, where 120,711 is the number of fault or matrix nodes.

The second supplemental set of zones (Zones 701 through 704) contains the nodes from which the radionuclide mass flux is summed for each zone to provide four source terms for the Saturated Zone (SZ) Flow and Transport Submodel. The nodes in these bins are found at or below the water table. The areal distribution of the four bins is as follows:

Bin #701–NSP Easting(m) < 171190 and NSP Northing(m) > 233460
Bin #702–NSP Easting(m) > 171190 and NSP Northing(m) > 233460
Bin #703–NSP Easting(m) < 171190 and NSP Northing(m) < 233460
Bin #704–NSP Easting(m) > 171190 and NSP Northing(m) < 233460.

F2.1.11 Multiple-Species Particle Tracking Data Files

As described in Table F-2, the 8 input files contain parameter values and names of parameter files containing data used for multiple-species particle tracking transport simulations. The input files are based on TSPA-LA Model modifications to the template file fehm_TSPA.mptr obtained from DTN: MO0704PAFEHMBR.001_R3 [DIRS 184647]. During a TSPA-LA Model simulation, the appropriate file based on simulation length and scenario type is automatically copied into a generic file by MFCP_LA.dll (MFCP_LA V1.0, STN: 11071-1.0-00 [DIRS 167884]), as described in Section F2.2. See the User Information Document (DOE 2007 [DIRS 181096], Section 2.5.1) for a description of the file.

The file fehm_TSPA_10kyr.mptr is identical to fehm_TSPA.mptr, except it has been updated from UNIX to PC format. The files with *ign* (for igneous simulations) and *ef* (for early failure simulations) in the filename contain updates associated with the assignment of particles by mass, as opposed to by timestep, for the radionuclides ^{99}Tc and ^{129}I. The difference between the igneous and early failure files, and the other files, is the manner with which particles are assigned for ^{129}I and ^{99}Tc. Because the igneous model generates short-duration spike-type source terms for ^{129}I and ^{99}Tc, the number of particles released for each timestep is based upon the mass released. As described in the User Information Document (DOE 2007 [181096] Section 2.5.1), the value for the input variable CONFACTOR is chosen to assign a specific number of particles per mole based on the maximum number of moles that could possibly be released from the repository.

In some of the early failure simulations, only a single WP is failed so that for ^{129}I and ^{99}Tc the maximum possible mass release for one package is used as the basis for determining the number of moles of radionuclides that each particle represents. The calculations used to determine CONFACTOR values for these early failure simulations are based on the maximum number of moles per WP that could be released. For all other species in the igneous and early failure simulations and all species in other simulations, the particles are assigned based upon a function of the size of the timestep, the number of years remaining in the simulation, and the number of particles left.

Other changes to the original files are associated with the need to increase the array allocation lengths for specific arrays that are dimensioned based on a function of the number of timesteps. These array sizes are increased for the 1,000,000-year simulations.

The multiple-species particle tracking files contain species-independent control and transport parameters and species-dependent control and transport parameters (or indices pointing to the transport parameters) for particle tracking simulations.

The species-independent control parameters include the number of species simulated, the maximum number of property zones, the maximum number of particles that can be released per species, an index indicating whether FEHM is being used in conjunction with GoldSim, the maximum allowable length for timestep dependent one-dimensional arrays, activation control of the active fracture model, output control parameters, and the names of input files for specific multiple-species particle tracking options. The output control parameters include basic file format instructions and as well as more specific controls indicating what zones are considered output (mass release zones). In the coupled FEHM/GoldSim simulations, species-specific mass releases for each defined zone are returned from FEHM to GoldSim at the end of each timestep.

Particle tracking files defined in the multiple-species particle tracking input file include the transfer function file and the sampled parameters used in the UZ particle tracking analysis as described in Section F2.1.13. The sampled parameters are in turn referenced by the multiple-species particle tracking files using column indices (as indicated by a negative sign) in lieu of deterministic values. The random seed for the particle tracking analysis is also found in the multiple-species particle tracking files, but this value is not used in a coupled GoldSim/FEHM simulation where sampled random-seed values are passed from GoldSim to fehmn_v2_24-01.dll. Additionally, data property zone assignments for repository and water-table collection zones are listed in the multiple-species particle tracking files.

Species-independent transport data found in the multiple-species particle tracking files include x-direction, y-direction, and z-direction dispersivities; values for fracture apertures; porosities within fractures; residual saturations; and active fracture model gammas. These transport parameters are assigned by rock property zones.

Inputs grouped by species alone include the fluid phase type, radionuclide half life, index of daughter product, ratio of particles per mole (for use with particle assignment by mass option), the radionuclide atomic weight, a factor for saving a percentage of species-based storage allocation for ingrowth products and the storage length for timestep dependent arrays. Additional species dependent input data include colloid size distributions.

Control and transport data grouped by both species and rock property zones include the transport conceptual model, matrix sorption coefficients, fracture retardation coefficients, matrix diffusion coefficients, colloid distribution parameters, colloid retardation coefficients, and colloid fracture-matrix filtration parameters.

F2.1.12 Transfer Function Curve Data Files

As described in Table F-2, the input files uz_tfcurves_nn_dualk_4680.in and uz_tfcurves_nn_4680.in are used for the dual k (dual permeability) and discrete fracture models, respectively. These files contain transfer function curve data to be read by fehmn_v2_24-01.dll at run time for matrix diffusion simulations. Although both files have the same file format, uz_tfcurves_nn_4680.in is not presently used in the TSPA-LA Model, but included here for completeness. The transfer function curves are comprised of time/concentration pairs for each set of three dimensionless parameter values used to generate the curves as described in Appendix C of *Particle Tracking Model and Abstraction of Transport Processes* (SNL 2008 [DIRS 184748]). See the user's manual (LANL 2003 [DIRS 167579], Section 6.2.3) for a description of the file.

F2.1.13 Sampled Parameter File

As described in Table F-2, the input files UZ_Pa_LA_300rlz_rs1_042307.txt and UZ_Pa_LA_1000rlz_rs1_042307.txt are sampled parameters for 300 and 1,000 realizations, respectively, to be used by the TSPA-LA Model. The sampled parameter file is an alternate transport parameter file containing sampled parameters for multiple realizations. *UZ_Params_Multi_LA_Compliance* is the generic file name that the TSPA-LA Model uses to copy a number of realizations-specific alternate transport parameter files to be read by FEHM and used as instructed in the multiple-species particle tracking file. A file of material properties is generated by GoldSim using uncertainty distributions. These properties consist of fracture apertures, active fracture-model gamma parameters, sorption coefficients, matrix diffusion coefficients, colloid distribution parameter, and colloid retardation factors. Sampling procedures and uncertainty distributions used in the sampling of parameters are described in Section 6.3.9. See the user's manual (LANL 2003 [DIRS 167579], Sections 6.2.44 and 6.2.54) for a description of the file.

F2.1.14 Interface Control File

As described in Table F-2, the input file fehmn.gold is a GoldSim/FEHM interface control file. The only active input in this file is the first line, which indicates the number of parameters that will be passed to fehmn_v2_24-01.dll in front of the mass releases from the EBS. The second input indicates whether added concentration average mass flux and peak concentration data are to be returned to GoldSim. See the user's manual (LANL 2003 [DIRS 167579], Section 6.1.1.4) for a complete description.

F2.2 MFCP_LA.DLL

The DLL MFCP_LA.dll (MFCP_LA Vl.0, STN: 11071-1.0-00 [DIRS 167884] and MFCP_LA Vl.0, STN: 11071-1.0-01 [DIRS 181045]) is designed to select the correct version of parameter-dependent input files for all TSPA-LA Model run types. This DLL uses GoldSim

modeling control parameters to select the correct (scenario and/or realization dependent) file from a suite of files and then copies its contents to a generic file name. A complete description of MFCP_LA.dll and the input file is documented in *Software Management Report, MFCP_LA, V1.0* (DOE 2003 [DIRS 167597]). As described in Table F-3, MFCP_LA.dll uses only one input file called MFCP_LA_input.txt.

F2.3 SEEPAGEDLL_LA.DLL

The DLL SEEPAGEDLL_LA.dll (SEEPAGEDLL_LA V1.3, STN: 11076-1.3-00 [DIRS 180318] for Windows 2000 and SEEPAGEDLL_LA V1.3, STN: 11076-1.3-01 [DIRS 181058] for Windows 2003) is designed to calculate the average seepage flux per WP for each fuel type in each percolation subregion, the fraction of WPs that have seepage for each fuel type in each percolation subregion, and the fraction of WPs emplaced in lithophysal units. A complete description of SEEPAGEDLL_LA.dll and the input files is documented in *User Information Document for: SEEPAGEDLL_LA V1.3* (DOE 2006 [DIRS 181133]).

As described in Table F-4, SEEPAGEDLL_LA.dll uses five input files. The first three files listed are control files that also contain a list of the PREWAP (PREWAP_LA V1.1, STN: 10939-1.1-00 [DIRS 181053]) output files (Appendix F2.8) to be read by the DLL. The realization dependent choice of the three files is then copied by *MFCP_LA.dll* into a generic file named *SEEPAGE_MASTER_INPUT.IN*. The last two files are the seepage look-up tables for nominal and collapsed drift conditions. SEEPAGEDLL_LA.dll interpolates seepage rates from the look-up tables based on percolation rates from the PREWAP output files and values of capillary strengths and log permeabilities passed from GoldSim.

F2.4 SZ_CONV_3.10.DLL

The DLL sz_conv_3.10.dll (SZ_CONVOLUTE V3.10.01, STN: 10207-3.10.01-00 [DIRS 181060]) is designed to calculate radionuclide mass flux rates in the SZ between the Yucca Mountain repository and specified locations downgradient from the repository. A complete description of sz_conv_3.10.dll and the input files is documented in *User Information Document for: SZ_Convolute V. 3.10* (DOE 2007 [DIRS 181288]).

As described in Table F-5, sz_conv_3.10.dll uses 50 input files in conjunction with the TSPA-LA Model. Of these files, two are control files for 10,000-year simulations (sz_convolute2_20kyr.dat) and one-million-year simulations (sz_convolute2_1Myr.dat). The simulation-length dependent choice of the files is then copied by MFCP_LA.dll into a generic file named SZ_CONVOLUTE2.DAT. The 10,000-year simulations are actually run for 20,000 years so that any changes in results immediately after the 10,000-year compliance timeframe can be assessed.

The remaining forty-eight files contain predefined static breakthrough curve data (e.g., SZ_03_04). Each of these files contains 200 sets each of three cumulative mass flux breakthrough curves generated using the streamlined particle tracking option in FEHM V2.24-01 [DIRS 179419]. The three curves are representative of mass fluxes in the SZ integrated over time at three distinct distances downgradient from the repository. The 200 sets of curves reflect 200 realizations of data sampling performed using GoldSim V.9.60.100 [DIRS 181903].

The 18 km compliance distance used in the TSPA-LA Model is represented by the second of the three sets of curves. The cumulative mass flux breakthrough curves are also used in conjunction with mass releases from the UZ Transport Submodel. This is done to derive time histories of radionuclide mass fluxes at the 18 km compliance distance using a convolution integral approach described in *Saturated Zone Flow and Transport Model Abstraction* (SNL 2008 [DIRS 183750], Sections 6 and 8).

F2.5 WAPDEG.DLL

The DLL wapdeg.dll (WAPDEG V4.07, STN: 10000-4.07-00 [DIRS 181774] and WAPDEG V4.07, STN: 10000-4.07-01 [DIRS 181064]) is designed to perform WP and drip shield (DS) degradation calculations. This DLL reads several input control files, cumulative distribution functions, and look-up table files. A complete description of *wapdeg.dll* and the input files is documented in *Users' Manual for WAPDEG 4.07* (BSC 2002 [DIRS 162606]).

As described in Table F-6, *wapdeg.dll* uses three input files. The initially empty file, WD4DLL.dbg, is used to record an echo of the run. Although this file is initially empty, it is populated by a DLL run and subsequently used to debug any problems with the run. The WD4DLL.wap file lists names of files that contain thermal-hydrologic (TH) exposure history data, cumulative distribution functions, probability density functions, or look-up tables. The initially empty file, WD4DLL.thk, is used to record WP thickness data at run time. Although this file is initially empty, it is populated by a DLL run.

F2.6 MKTABLE_LA.DLL

The DLL MkTable_LA.dll *(*MkTable_LA V. 1.0, STN: 11217-1.0-00 [DIRS 181047] and MkTable_LA V. 1.0, STN: 11217-1.0-01 [DIRS 181048]) is designed to randomly select a subset of files from an existing set of TH history files. A complete description of mktable_LA.dll and the input files is documented in *User Information Document for: MkTable_LA v1.0* (DOE 2006 [DIRS 181116]).

As described in Table F-7, MkTable_LA.dll uses 13 input files. The 12 TH history file names are obtained from rows 11 through 23 of the WD4DLL.wap file described in Section F2.5. These 12 files correspond to combinations of the 10th, 30th, 50th, and 90th percentile infiltration scenarios and the low, medium, and high thermal conductivities. The choice of which of these files to be used by MkTable_LA.dll is controlled by MFCP_LA.dll (Section F2.2). For example, WDhist.inp.P10 contains the list of PREWAP (described in Section F2.8) output files for the 10th percentile infiltration scenario and the mean thermal conductivity case.

The file THFiles.in is a text file containing a list of 16 file names. These 16 files contain the incremental temperatures and relative humidities that are added to the temperatures and relative humidities in the TH history files, after the drift fills with lithophysal rubble. The order of the file names in THFiles.in matches the order of the TH history data tables.

F2.7 SCCD.DLL

The DLL *SCCD.dll* (SCCD V2.01, STN: 10343-2.01-00 [DIRS 181157] and SCCD V2.01, STN: 10343-2.01-01 [DIRS 181054]) is designed to implement the stress and stress intensity

factor analysis for the Alloy 22 closure-lid welds on the WP outer surface. A complete description of SCCD.dll and the input files is documented in *SCCD Software Routine Report* (CRWMS M&O 2000 [DIRS 152499]). As described in Table F-8, *SCCD.dll* uses only one input file, WDKIinO.fil.

F2.8 PREWAP_LA.EXE

The executable file PREWAP_LA.exe (PREWAP_LA V1.1, STN: 10939-1.1-00 [DIRS 181053]) is designed to process and format the output files produced by the Multiscale Thermohydrologic Abstraction Code (MSTHAC V7.0, STN: 10419-7.0-00 [DIRS 164274]) to be read by other TSPA-LA Model DLLs. The resulting files are inputs to MkTable_LA.dll, SEEPAGEDLL_LA.dll, and PassTable1D_LAv2.dll (PassTable1D_LA V2.0, STN: 11142-2.0-00 [DIRS 181051]). These files contain TH histories for the repository and percolation rates. Although PREWAP_LA.exe is not a DLL used directly by the TSPA-LA Model, it is described here because of its relationship to several TSPA-LA Model DLLs. A complete description of PREWAP_LA.exe and the input and output files is documented in *User Information Document for:* PREWAP_LA v1.1 (DOE 2006 [DIRS 181129]).

As described in Table F-9, PREWAP_LA.exe generates 240 output files. These files are composed of the following: 12 percolation flux/host rock thermal conductivity scenarios (10th, 30th, 50th, and 90th percentile percolation flux with low, mean, and high thermal conductivity); two WP types (co-disposed [CDSP] and commercial spent nuclear fuel [CSNF]); five percolation subregions (1 through 5); and two types of TH data (representative TH and WP degradation TH). Two examples of these files are B1_DHLW_REP_P30L.ou (30th percentile percolation flux, low thermal conductivity, representative CDSP WP type, and percolation Subregion 1) and B3_CSNF_WAPDEG_P10H.ou (10th percentile percolation flux, high thermal conductivity, CSNF WP type used in WP degradation calculations, and percolation subregion 3).

The inputs to PREWAP_LA.exe are the output DTNs generated by the Multiscale Thermohydrologic Model (Sandia 2007 [DIRS 181383]) listed below and identified in the DTN shown on Table F-9.

LL0703PA011MST.006_R0 [DIRS 179853]
LL0703PA012MST.007_R0 [DIRS 179854]
LL0703PA013MST.008_R0 [DIRS 179855]
LL0703PA014MST.009_R0 [DIRS 179856]
LL0703PA015MST.010_R0 [DIRS 179857]
LL0703PA016MST.011_R0 [DIRS 179858]
LL0703PA017MST.012_R0 [DIRS 179859]
LL0703PA034MST.016_R0 [DIRS 179982]
LL0703PA035MST.017_R0 [DIRS 179985]
LL0703PA036MST.018_R0 [DIRS 179986]
LL0703PA037MST.019_R0 [DIRS 179989]
LL0703PA038MST.020_R0 [DIRS 179992]

F2.9 PASSTABLE1D_LAV2.DLL

The DLL PassTable1D_LAv2.dll (PassTable1D_LA V 2.0, STN: 11142-2.0-00 [DIRS 181051]) is designed to reformat one-dimensional tabular information from an input file and pass that information into GoldSim. The reformatted data is in the form of a one-dimensional look-up table element that conforms to the external interface method and function calls described in the *User's Guide, GoldSim Probabilistic Simulation Environment* (GoldSim Technology Group 2007 [DIRS 181727], Chapter 10 and Appendix C).

PassTable1D_LAv2.dll supports the evaluation of localized corrosion initiation on the WPs, the WP thickness calculations for the seismic calculations, the thermo hydrology parameters for the EBS environment calculations, and the volcanic eruption calculations. A complete description of PassTable1D_LAv2.dll and the input files is documented in *User Information Document for:* PassTable1D_LA Version 2.0 (DOE 2007 [DIRS 181123]).

As described in Table F-10, PassTable1D_LAv2.dll uses five input files. The pass_table_master.in input file contains a list of 240 PREWAP output file names that contain data for input to the TH model. These files are comprised of two data sets, one for all appropriate locations and the other for only representative locations. Each set contains 120 file names for cases defined by five percolation bins, two fuel types, three thermal conductivity scenarios, and four infiltration scenarios ($5 \times 2 \times 3 \times 4 = 120$). The pass_table_master1.in input file contains a list of 30 localized corrosion failure fraction files that are used to find the maximum WP failure fraction occurring at the simulation duration time. These files are defined by the five percolation bins, the two fuel types, and three modeling cases (Nominal, Seismic Ground Motion, and Seismic Fault Displacement). The pass_table_master2.in input file contains a list of 10 file names for files containing the WP thickness versus time for 5 percolation subregions and 2 fuel types.

For the Volcanic Eruption Modeling Case, the input file pass_table_master_eruptive.in contains data for a 20,000-year simulation and pass_table_master1_eruptive.in contains data for a one-million-year simulation. These files each identify the names of two files containing time-series data of concentration calculated for an eruptive event occurring at time zero. These data are used to calculate concentrations for later event times.

F2.10 PASSTABLE3DV2.DLL

The DLL PassTable3Dv2.dll (PassTable3D_LA V. 2.0, STN: 11143-2.0-00 [DIRS 182556]) is designed to reformat three-dimensional tabular information from an input file and pass that information into GoldSim. The reformatted information is in the form of a three-dimensional look-up table element that conforms to the external interface method and function calls described in the *User's Guide, GoldSim Probabilistic Simulation Environment* (GoldSim Technology Group 2007 [DIRS 181727], Chapter 10 and Appendix C).

PassTable3Dv2.dll is used only in the stand-alone Localized Corrosion Initiation Submodel file. This DLL supports the evaluation of localized corrosion on the WPs by reading the nominal and collapsed drift-seepage data files described in Section F2.3 and returning four three-dimensional look-up tables containing mean seepages and standard deviations for both the nominal and

collapsed drifts. A complete description of PassTable3Dv2.dll and the input file is documented in *User Information Document for: PassTable3D_LA Version 2.0* (DOE 2007 [DIRS 182918]).

As described in Table F-11, PassTable3Dv2.dll uses only one input file, pass_table_3d_master.in, that provides the file names of the external data files to be processed.

F2.11 GETTHK_LA.DLL

The DLL GetThk_LA.dll (GetThk_LA V. 1.0, STN: 11229-1.0-00 [DIRS 181040]) is designed to process the file WD4DLL.thk generated by the wapdeg.dll described in Section F2.5. This file contains sets of WP barrier thicknesses as a function of time. The output from GetThk_LA.dll includes barrier thickness data and thickness statistics as a function of time. Output also includes a single value for the number of timesteps per data set that is used for controlling the sequence of calling DLLs within GoldSim. A complete description of GetThk_LA.dll and the input file is documented in *User Information Document for: GetThk_LA v1.0* (DOE 2006 [DIRS 181102]). As described in Table F-12, GetThk_LA.dll uses only one input file.

F2.12 FAR_1-2.DLL

The DLL FAR_1-2.dll (FAR V1.2, STN: 11190-1.2-00 [DIRS 182225]) is designed to evaluate the redistribution of volcanic ash and associated radionuclides within the Fortymile Wash drainage area and the subsequent radionuclide migration in the soil at the location of the reasonably maximally exposed individual on the Fortymile Wash fan. A complete description of FAR_1-2.dll and the input file is documented in *User Information Document for: FAR Version 1.2* (DOE 2007 [DIRS 183116]).

As described in Table F-13, FAR_1-2.dll uses only one input file, farinputdem.txt, that contains a Digital Elevation Model (DEM) at a 30-meter-resolution. The DEM covers the Fortymile Wash drainage basin extending to the latitude of the Fortymile Wash fan apex. The DEM file contains topographical elevations at coordinates within the Fortymile Wash watershed and null values of -9999.0 at coordinates located outside of the watershed.

F2.13 ASHPLUME21_DLL_LA.DLL

The DLL Ashplume21_dll_la.dll (ASHPLUME_DLL_LA V2.1, STN: 11117-2.1-00 [DIRS 181035] and ASHPLUME_DLL_LA V2.1, STN: 11117-2.1-01 [DIRS 180147]) is designed to calculate the waste and ash areal depositional densities on the ground surface from a hypothetical volcanic eruption through the repository. The DLL is called from another program that conforms to the external interface method and function calls described in the *User's Guide, GoldSim Probabilistic Simulation Environment* (GoldSim Technology Group 2007 [DIRS 181727], Chapter 10 and Appendix C).

A complete description of Ashplume21_dll_la.dll and the inputs is documented in *User Information Document for: ASHPLUME_DLL_LA Version 2.1* (DOE 2006 [DIRS 181076]). As described in Table F-1, Ashplume21_dll_la.dll uses specific parameters as input instead of an input file.

F2.14 CWD.DLL

The DLL CWD.dll (CWD V2.0, STN: 10363-2.0-00 [DIRS 162809] and CWD V2.0, STN: 10363-2.0-01 [DIRS 181037]) is designed to implement the abstraction results of the probability of occurrence and size of manufacturing defects in the closure lid welds of the Alloy 22 WP outer surface. The DLL is called from GoldSim and conforms to the external interface method and function calls described in the *User's Guide, GoldSim Probabilistic Simulation Environment* (GoldSim Technology Group 2007 [DIRS 181727], Chapter 10 and Appendix C).

A complete description of CWD.dll and the inputs is documented in *Software Management Report: CWD Version Number 2.0* (DOE 2003 [DIRS 167564]). As described in Table F-1, CWD.dll uses specific parameters as input instead of an input file.

F2.15 INTERPZDLL_LA.DLL

The DLL InterpZdll_LA.dll (InterpZdll_LA V1.0, STN: 11107-1.0-00 [DIRS 167885] and InterpZdll_LA V1.0, STN: 11107-1.0-01 [DIRS 181043] is designed to provide interpolation capabilities for the EBS Chemical Environment Submodel of the TSPA-LA Model. The DLL is called from GoldSim and conforms to the external interface method and function calls described in the *User's Guide, GoldSim Probabilistic Simulation Environment* (GoldSim Technology Group 2007 [DIRS 181727], Chapter 10 and Appendix C).

A complete description of InterpZdll_LA.dll and the inputs is documented in *Software Management Report, INTERPZDLL_LA V1.0* (DOE 2004 [DIRS 168988]). As described in Table F-1, InterpZdll_LA.dll uses specific parameters as input instead of an input file.

INTENTIONALLY LEFT BLANK

Table F-1. Summary of the Dynamically Linked Libraries used in the TSPA-LA Model

DLL File Name	Description	Location
Ashplume21_dll_la.dll	Calculates fuel and ash deposition and areal concentrations from a volcanic eruption.	None [a]
CWD.dll	Performs closure weld defect probability calculations.	None [a]
FAR_1-2.dll	Evaluates redistribution of volcanic ash and associate radionuclides within the Fortymile Wash drainage area; models redistribution of radionuclides in soil at the location of a reasonably maximally exposed individual on the Fortymile Wash fan.	Table F-13
fehmn_v2_24-01.dll	Performs radionuclide transport calculations through the UZ using FEHM's multi-species, particle-tracking option.	Table F-2
GetThk_LA.dll	Processes the file WD4DLL.thk by extracting barrier thickness data, generating thickness statistics based on these data, and outputting tables containing these statistics. In addition, a single value for the number of timesteps per data set is generated to be used for controlling the sequence of calling DLLs within GoldSim.	Table F-12
InterpZdll_LA.dll	Performs a four point linear interpolation that can accommodate any single missing point in the data.	None [a]
MFCP_LA.dll	Conducts the selection and implementation of input files for DLLs that are part of the TSPA-LA Model.	Table F-3
MkTable_LA.dll	Performs sampling of the TH time history files used as input to WAPDEG for performing WP degradation calculations.	Table F-7
PassTable1D _LAv2.dll	Extracts columns from tabular input files and converts the data into the format required by a GoldSim for a one-dimensional look-up table element.	Table F-10
PassTable3Dv2.dll	Reformats a file containing tabular information into the format required by GoldSim for a three-dimensional look-up table element.	Table F-11
PREWAP_LA.exe [b]	Reformats TH data into files for input to MkTable_LA.dll, SEEPAGEDLL_LA.dll, and PassTable1D_LAv2.dll.	Table F-9
SCCD.dll	Applies the analysis of the Alloy 22 WP outer surface stress intensity factors to the TSPA-LA Model.	Table F-8
SEEPAGEDLL_LA.dll	Performs drift-seepage calculations.	Table F-4
sz_conv_3.10.dll	Performs radionuclide mass flux rate calculations in the SZ between the Yucca Mountain repository and specified locations downgradient from the repository.	Table F-5
wapdeg.dll	Performs WP degradation calculations.	Table F-6

NOTES: [a] Input is not in the form of files.
[b] Executable file used as a preprocessor for other DLLs and listed for completeness.

Table F-2. *fehmn_v2_24-01.dll* Input Files

File(s)	Description	Data Source	Inputs
fehmn.files	Control file specifying FEHM main input and output file names.	DTN: MO0704PAFEHMBR.001_R3 [DIRS 184647]	Controls: List of input and output files
fehm_TSPA_gs_20kyr.dat fehm_TSPA_gs_1Myr.dat	General control information and data for 10,000/20,000-year and one-million-year simulations.	Output DTN: MO0708TSPAGENT.000_R0 [DIRS 183000]	Data: Permeability data Residual liquid saturation Residual vapor saturation Maximum liquid saturation Maximum vapor saturation Capillary pressure at zero saturation Saturation that defines zero capillary pressure Equation solver control data Control data for FEHM linear equation solver Reference temperature and pressure Controls: Input file names Initial timestep Final simulation time Maximum number of timesteps allowed Printout interval for dependent variables Simulation start year Simulation start month Initial time of startup Species subject to filtration Files containing filtration or size exclusion data

Table F-2. *fehmn_v2_24-01.dll* Input Files (Continued)

File(s)	Description	Data Source	Inputs
fehmn.grid	Nodal coordinate and finite element connectivity data.	DTN: MO0704PAFEHMBR.001_R3 [DIRS 184647]	Data: Nodal-coordinate data: (NSP Easting, NSP Northing [m] and elevation) Finite element connectivity data
fehmn.zone	Defines material zones and nodes contained in each declared zone.	DTN: MO0704PAFEHMBR.001_R3 [DIRS 184647]	Controls: List of nodes for each material zone
ff1100.ini ff1200.ini ff1300.ini ff1400.ini ff2100.ini ff2200.ini ff2300.ini ff2400.ini ff3100.ini ff3200.ini ff3300.ini ff3400.ini ff4100.ini ff4200.ini ff4300.ini ff4400.ini	A restart/initialization file containing nodal pressure, saturation, and adjacent node flux data used to describe the flow field for the different climates and infiltration scenarios as derived from the TOUGH2 generated flow fields.	Output DTN: MO0708TSPAGENT.000 _R0 [DIRS 183000]	Data: Saturation values in the fracture nodes Saturation values in the rock-matrix nodes Total pressures in the fracture nodes Total pressures in the rock-matrix nodes Water flux data

Table F-2. *fehmn_v2_24-01.dll* Input Files (Continued)

File(s)	Description	Data Source	Inputs
fehmn.stor	Precalculated stiffness matrix associated with the grid file used during the UZ transport calculation.	DTN: MO0704PAFEHMBR.001_R3 [DIRS 184647]	Data: Volume data for each node Finite element geometric coefficients Finite element geometric coefficients for stress module Controls: Nodal connectivity data Starting position for each connection Position of element in connectivity array for each node
fehmn_TSPA.dpdp	Fracture geometry data for each defined fracture zone in the dual permeability model.	DTN: MO0704PAFEHMBR.001_R3 [DIRS 184647]	Data: Volume fraction of effective nodal volume taken up by the fractures Length scale of matrix nodes
fehm_TSPA.rock	Rock bulk density, specific heat, and porosity data for both matrix and fracture material zones defined in the file *fehmn.zone*.	DTN: MO0704PAFEHMBR.001_R3 [DIRS 184647]	Data: Rock bulk density Rock specific heat Porosity

Table F-2. *fehmn_v2_24-01.dll* Input Files (Continued)

File(s)	Description	Data Source	Inputs
ltfc_tsw4.txt ltfc_tsw5.txt ltfc_tsw6.txt ltfc_tsw7.txt ltfc_tsw8.txt ltfc_tsw9.txt ltfc_chv.txt ltfc_chz.txt ltfc_ch1.txt ltfc_ch6.txt ltfc_pp1.txt ltfc_pp2.txt ltfc_pp3.txt ltfc_pp4.txt ltfc_bf2.txt ltfc_bf3.txt	Pore-size cumulative probability data for the following rock units: Topopah Springs (tsw) layers 4 through 9 Calico Hills (ch*) layers vitric, zeolitic, 1, and 6 Prow Pass (pp) layers 1 through 4 Bull Frog (bf) layers 2 and 3.	DTN: MO0704PAFEHMBR.001_R3 [DIRS 184647]	Data: Pore-size Cumulative probability data
fehm.zone2	fehmn.zone data plus radionuclide source releases zones and water table collecting zones defined at the UZ-SZ interface.	DTN: LA0702PANS02BR.001_R1 [DIRS 180322]	Controls: List of node numbers for each material zone Fracture and matrix radionuclide EBS release zone data Node numbers within UZ collecting (mass exit) zones when found beneath the water table
fehm_TSPA_10kyr.mptr fehm_TSPA_10kyr_ign.mptr fehm_TSPA_1Myr.mptr fehm_TSPA_1Myr_ign.mptr fehm_TSPA_10kyr_ef_cdsp.mptr	Parameter values and files used for multiple species particle-tracking transport simulations for lower-bound infiltration rate simulations. Automatically assigns particles based upon timestep length, total time of analysis, ingrowth, and maximum number of particles. The '_ign_' and '_ef_' files assign particles for ^{99}Tc and ^{129}I by mass and timestep for the other. All other files assign particles by timestep.	Output DTN: MO0708TSPAGENT.000 [DIRS 183000]	Data: A 6-digit random seed Start/end times for particle tracking Start/end times for disabling the flow solution X-direction dispersivity

Table F-2. *fehmn_v2_24-01.dll* Input Files (Continued)

File(s)	Description	Data Source	Inputs
fehm_TSPA_1Myr_ef_cdsp.mptr fehm_TSPA_10kyr_ef_csnf.mptr fehm_TSPA_1Myr_ef_csnf.mptr			Y-direction dispersivity Z-direction dispersivity Mean fracture aperture Matrix porosity Residual saturation Exponent in active fracture model Zone to rock property link data Rock property to repository water table collecting zone assignments Species index Fluid-phase type Radionuclide half-life data Index of daughter products Conversion factors Atomic weights Decay-ingrowth particle release factors Species names Cumulative probability of colloid sizes Zone numbers Transport analysis flag Matrix sorption coefficients Fracture retardation factor Matrix diffusion coefficient Ratio of radionuclide colloid mass to aqueous mass Colloidal retardation factor Colloidal filtration factor Number of particles or moles

Table F-2. *fehmn_v2_24-01.dll* Input Files (Continued)

File(s)	Description	Data Source	Inputs
			to be input at each location Injection start and end times Controls: Input file names Number of species Maximum number of property zones Maximum number of particles that can be used Parameter to define transfer function curve Number of zones for breakthrough curve data List of zone numbers Array size declarations
uz_tfcurves_nn_dualk_4680.in uz_tfcurves_nn_4680.in	Dual permeability transfer function curve data used in matrix diffusion simulations. Note that the file for the discrete fracture model (*uz_tfcurves_nn_4680.in*) is currently not used.	DTN: MO0704PAPTTFBR.002_R0 [DIRS 180442]	Data: Transfer function time and data pairs Controls: Curve scaling factor Normalization control parameters Interpolation scheme
UZ_Pa_LA_300rlz_rs1_042307.txt UZ_Pa_LA_1000rlz_rs1_042307.txt Corresponding parameter names: UZ_Params_Multi_LA_300rlz UZ_Params_Multi_LA_1000rlz	Sampled parameters for 300 and 1,000 realizations using a random seed of 1.	Output DTN: MO0708TSPAGENT.000_R0 [DIRS 183000]	Data: Fracture apertures Matrix diffusion coefficients Active fracture gamma sorption coefficients K_d values Colloid distribution parameter (Ratio of radionuclide colloid mass to aqueous mass) Colloid retardation coefficient

Table F-2. *fehmn_v2_24-01.dll* Input Files (Continued)

File(s)	Description	Data Source	Inputs
fehmn.gold	Input and output control data for variables passed from GoldSim to FEHM and from FEHM to GoldSim.	Output DTN: MO0708TSPAGENT.000_R0 [DIRS 183000]	Controls: Index parameter indicating number of parameters passed to FEHM Output control parameter indicating only time vs. mass flux results

Table F-3. *MFCP_LA.dll* Input Files

File(s)	Description	Data Source	Inputs
MFCP_LA_input.txt	List of control parameter-dependent input files.	Output DTN: MO0708TSPAGENT.000_R0 [DIRS 183000]	Controls: Input file names Number of file sets Number of names per set

Table F-4. *SEEPAGEDLL_LA.dll* Input Files

File(s)	Description	Data Source	Inputs
Seepage_Master_Input_File_LKT.in Seepage_Master_Input_File_MKT.in Seepage_Master_Input_File_HKT.in	List of input files for low, medium, and high thermal k.	Output DTN: MO0708TSPAGENT.000_R0 [DIRS 183000]	Controls: Input file names Number of fuel types Number of bins per fuel type Number of climates Times when climates change Number of infiltration types
SMPA_N.dat SMPA_C.dat	Seepage model for performance assessment response surfaces for non-collapsed and collapsed drift conditions.	DTN: LB0702PASEEP01.001_R0 [DIRS 179511]	Data: Log permeability Capillary strength Percolation Mean seepage Standard deviation seepage

Table F-5. sz_conv_3.10.dll Input Files

File(s)	Description	Data Source	Inputs
sz_convolute2_20kyr.dat sz_convolute2_1Myr.dat	Climate, time, and radionuclide species data for 10,000-year and one-million-year simulations.	DTN: SN0702PASZFTMA.001_R0 [DIRS 179504]	Controls: Output file name Maximum number of climate states Maximum number of timesteps Maximum number of SZ points Smallest timestep Number of species Number of breakthrough curves Number of climate states Data: Climate multiplier values Climate concentration multiplier Total simulation time Initial timestep size Half-life data for each species

Table F-5. sz_conv_3.10.dll Input Files (Continued)

SZ_**xx_yy** Total of 48 files for 12 solute types in each of 4 regions	Breakthrough curve data for: Solute xx (below) and Region yy = 01 to 04 01 = solute C 02 = Kc_Am 03 = Kc_Cs 04 = Kc_Pu 05 = Np 06 = solute Pu 07 = solute Ra 08 = solute Sr 09 = solute U 10 = solute Pu_fast 11 = solute Se 12 = solute Sn.	DTN: SN0702PASZFTMA.001_R0 [DIRS 179504]	Controls: Region identifier and number Number of realizations in the file Data: Percent of solute transported at a given timestep

Table F-6. *wapdeg.dll* Input Files

File(s)	Description	Data Source	Inputs
WD4DLL.dbg	Initially empty debug file used to record an echo of a run.	Output DTN: MO0707WPDRIPSD.000_R0 [DIRS 183005]	None
WD4DLL.wap	List of all input and intermediate file names previously produced by *CWD.dll*, *SCCD.dll*, and *mktable_LA.dll*.	Output DTN: MO0707WPDRIPSD.000_R0 [DIRS 183005]	Controls: Input file names
WD4DLL.thk	Initially empty capture file used to record WP thicknesses generated by a run.	Output DTN: MO0707WPDRIPSD.000_R0 [DIRS 183005]	None

Table F-7. *MkTable_LA.dll* Input Files

File(s)	Description	Data Source	Inputs
THFiles.in	List of 16 file names that contain the incremental temperatures and relative humidities to be added to the temperatures and relative humidities in the TH history files after the drift fills with lithophysal rubble.	Output DTN: MO0707WPDRIPSD.000_R0 [DIRS 183005]	Controls: Input file names
WDhist.inp.P10L WDhist.inp.P10 WDhist.inp.P10H WDhist.inp.P30L WDhist.inp.P30 WDhist.inp.P30H WDhist.inp.P50L WDhist.inp.P50 WDhist.inp.P50H WDhist.inp.P90L WDhist.inp.P90 WDhist.inp.P90H	List of PREWAP output file names for TH history data sets associated with each of the 12 percolation flux/host rock thermal conductivity combinations (10th, 30th, 50^{t}h, and 90th percentile percolation flux with low, mean, and high thermal conductivity).	Output DTN: MO0707WPDRIPSD.000_R0 [DIRS 183005]	Controls: Maximum number of tables Bin parameters PREWAP file names

Table F-8. *SCCD.dll* Input Files

File(s)	Description	Data Source	Inputs
WDKlinO.fil	One-dimensional table containing stress intensity factors (KI) vs. depths for the WP outer lid. The corresponding parameter name is WDKlinO.	DTN: MO0702PASTRESS.002_R2 [DIRS 180514]	Data: Stress intensity factors Depths

Table F-9. PREWAP_LA.exe Output Files

File(s)	Description	Data Source	Inputs
B**x**_CSNF_WAPDEG_P**y**L.ou B**x**_CSNF_WAPDEG_P**y**.ou B**x**_CSNF_WAPDEG_P**y**H.ou B**x**_DHLW_WAPDEG_P**y**L.ou B**x**_DHLW_WAPDEG_P**y**.ou B**x**_DHLW_WAPDEG_P**y**H.ou	TH properties in percolation subregion **x** for each CSNF and CDSP WP modeled at each MSTHM location: where **x** = 1 to 5 and **y** = 10, 30, 50, or 90 for a total of 5 × 4 x 6 = 120 files.	Output DTN: MO0707PREWAPMS.000_R0 [DIRS 183002]	Controls: Time WP temperature WP relative humidity DS temperature DS relative humidity Drift-wall temperature Percolation rates
B**x**_CSNF_REP_P**y**L.ou B**x**_CSNF_REP_P**y**.ou B**x**_CSNF_REP_P**y**H.ou B**x**_DHLW_REP_P**y**L.ou B**x**_DHLW_REP_P**y**.ou B**x**_DHLW_REP_P**y**H.ou	TH properties in percolation subregion **x** for each CSNF and CDSP WP modeled at representative MSTHM location: where **x** = 1 to 5 and **y** = 10, 30, 50, or 90 for a total of 5 × 4 x 6 = 120 files.		

Table F-10. PassTable1D_LAv2.dll Input Files

File(s)	Description	Data Source	Inputs
pass_table_master.in *pass_table_master1.in* *pass_table_master2.in*	List of PREWAP output files containing TH data. Localized corrosion (LC) failure fraction histories. WP thickness versus time.	Output DTN: MO0708TSPAGENT.000_R0 [DIRS 183000]	Controls: PREWAP file names, LC failure fraction file names, WP thickness file names.
pass_table_master_eruptive.in *pass_table_master1_eruptive.in*	Time-series data of concentration for an eruptive event that occurs at time = 0 for 20,000-year and one-million-year simulations.	Output DTN: MO0708TSPAGENT.000_R0 [DIRS 183000]	Controls: Concentration file names

Table F-11. PassTable3Dv2.dll Input Files

File(s)	Description	Data Source	Inputs
pass_table_3d_master.in	Seepage data input file names for nominal and collapsed drifts.	Output DTN: MO0708TSPAGENT.000_R0 [DIRS 183000]	Controls: Input file names

Table F-12. GetThk_LA.dll Input Files

File(s)	Description	Data Source	Inputs
WD4DLL.thk	Generic file generated by *wapdeg.dll* during TSPA-LA Model simulations that contains multiple time-series of WP barrier thicknesses.	Output DTN: MO0707WPDRIPSD.000_R0 [DIRS 183005]	Data: Number of WP thickness data sets Time series of WP barrier thicknesses

Table F-13. FAR_1-2.dll Input Files

File(s)	Description	Data Source	Inputs
farinputdem.txt	DEM file covering the Fortymile Wash drainage basin at a 30-meter resolution.	DTN: MO0605SPAFORTY.000_R1 [DIRS 182281]	Data: Elevation data

INTENTIONALLY LEFT BLANK

APPENDIX G
WIRING DIAGRAMS FOR MODEL INFORMATION FEEDS

G1. INTRODUCTION

Appendix G provides a set of diagrams that illustrate in detail the information flow between model components and submodels within the Total System Performance Assessment for the License Application (TSPA-LA) Model.

Figure G-1 is an overall TSPA-LA Model information flow diagram and provides a schematic description of the model structure for the Nominal Scenario Class, with boxes representing model components and submodels, and arrows representing the flow of data. The Nominal Scenario Class represents the expected initial starting conditions for the repository system, and is, therefore, the primary focus of Appendix G. Information flow diagrams are also provided for the Early Failure Scenario Class (Figure G-2), Igneous Intrusion Modeling Case (Figure G-3), Seismic Scenario Class (Figure G-4), and the Human Intrusion Scenario (Figure G-5). Additionally, information flow diagrams showing only the flow of water (Figure G-6) and radionuclides (Figure G-7) are also presented.

Within the schematic diagrams, white boxes indicate models external to the TSPA-LA Model and grey boxes represent TSPA-LA Model components and submodels. The general philosophy used throughout the *Total System Performance Assessment Model/Analysis for the License Application* is that this TSPA-LA Model is comprised of eight principal model component areas that are combined to evaluate repository system performance for the Nominal, Early Failure, Igneous, and Seismic Scenario Classes, and the Human Intrusion Scenario. The colored areas shown on these figures are used to group the model components and submodels into these eight areas. The eight areas, as depicted in the legend, are as follows: unsaturated zone (UZ) flow, engineered barrier system (EBS), waste package (WP) and drip shield (DS) degradation, waste form degradation and mobilization, EBS flow and transport, UZ transport, saturated zone (SZ) flow and transport, and biosphere.

The colors of the arrows on the flow diagrams indicate the type of information passed between the model components and submodels. Water flux (blue) and radionuclide flux (red) are the main data types presented. EBS-related components include data flows representing thermal-hydrologic (TH) data, water chemistry, DS and/or WP failure, and other model information (e.g., number of failed WPs).

TSPA-LA Model components and submodels shown with a dashed line on the overall flow diagram for the Nominal Scenario Class are presented in further detail as separate information flow diagrams. The overall factors affecting flow through the EBS are shown on Figure G-8. The overall factors affecting the radionuclide transport through the EBS are shown on Figure G-9. The Waste Form Degradation and Mobilization Model Component has two associated submodel flow diagrams representing CSNF waste forms (Figure G-10) and CDSP waste forms (Figure G-11).

INTENTIONALLY LEFT BLANK

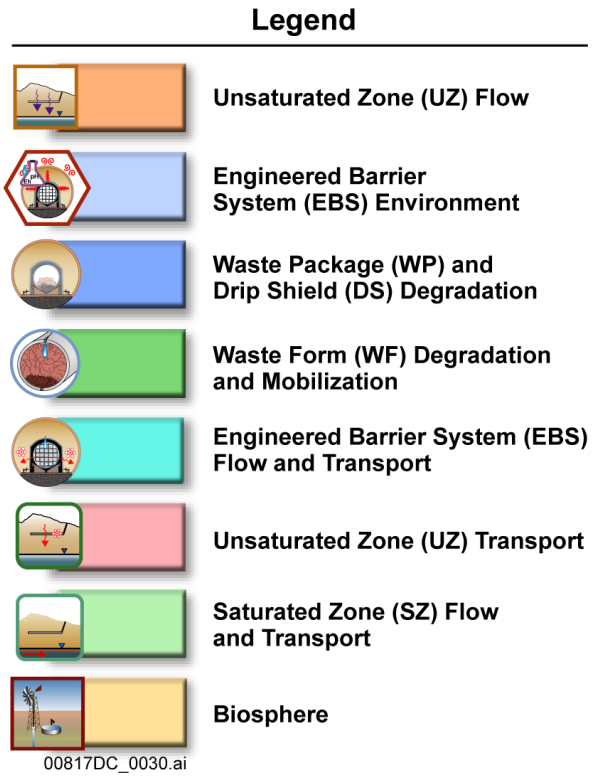

NOTE: This legend explains the colors and icons appearing in the following figures. The icons and colors are used throughout the document and are intended to provide consistency and to assist the reader with understanding how all the various components interact with each other.

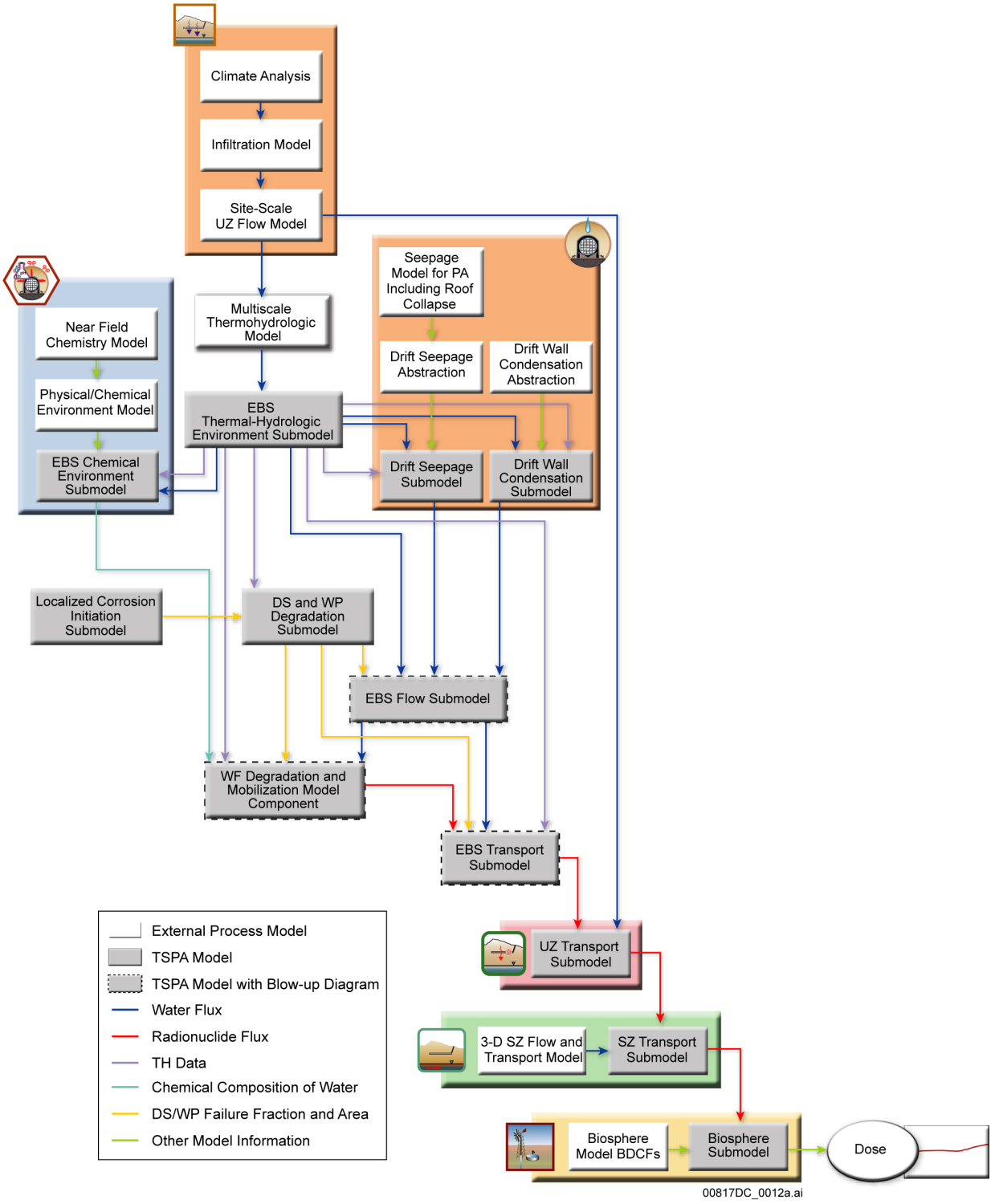

Figure G-1. Illustration of the Transfer of Information between Model Components and Submodels of the TSPA-LA Model for the Nominal Scenario Class

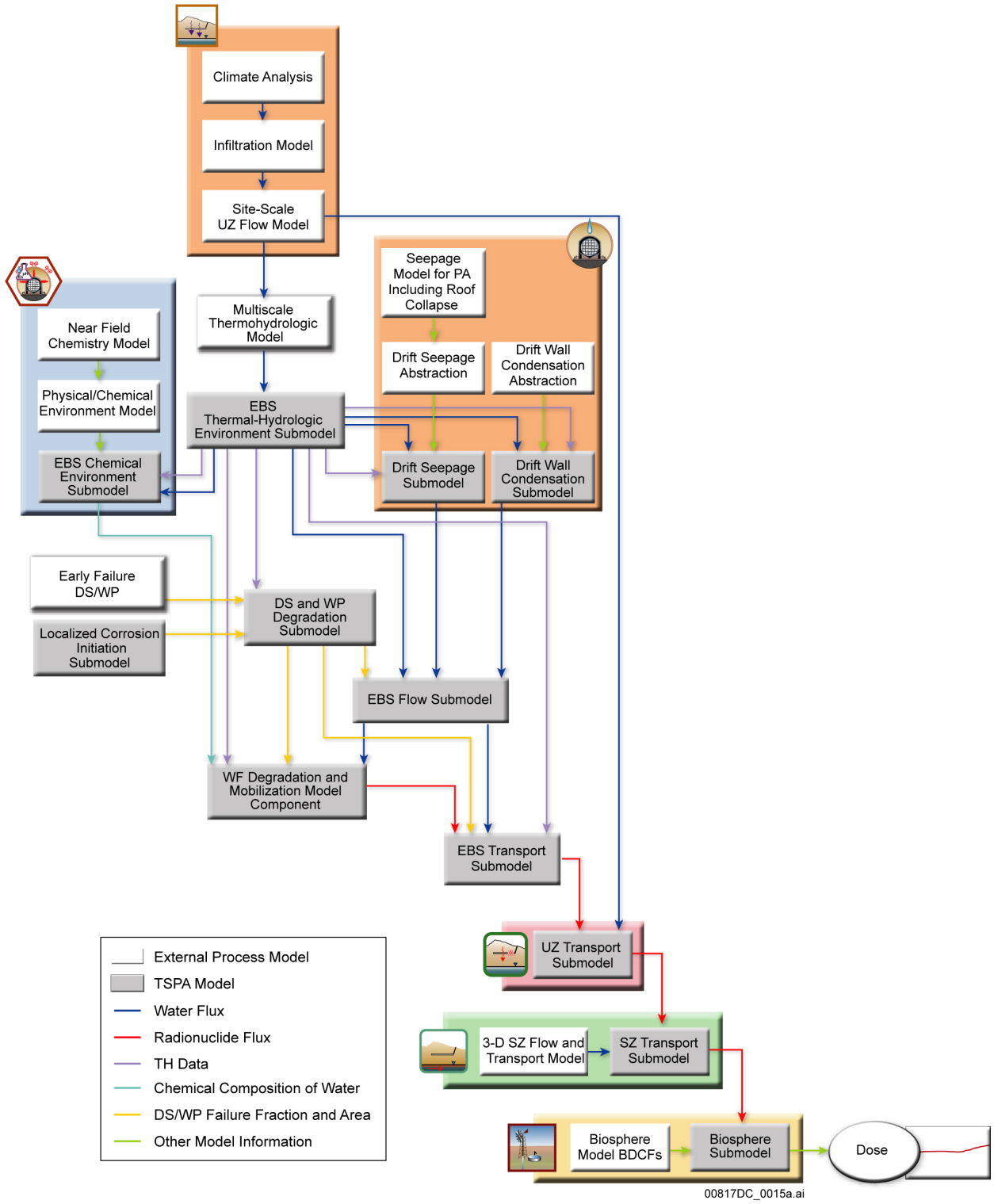

Figure G-2. Illustration of the Transfer of Information between Model Components and Submodels of the TSPA-LA Model for the Early Failure Scenario Class

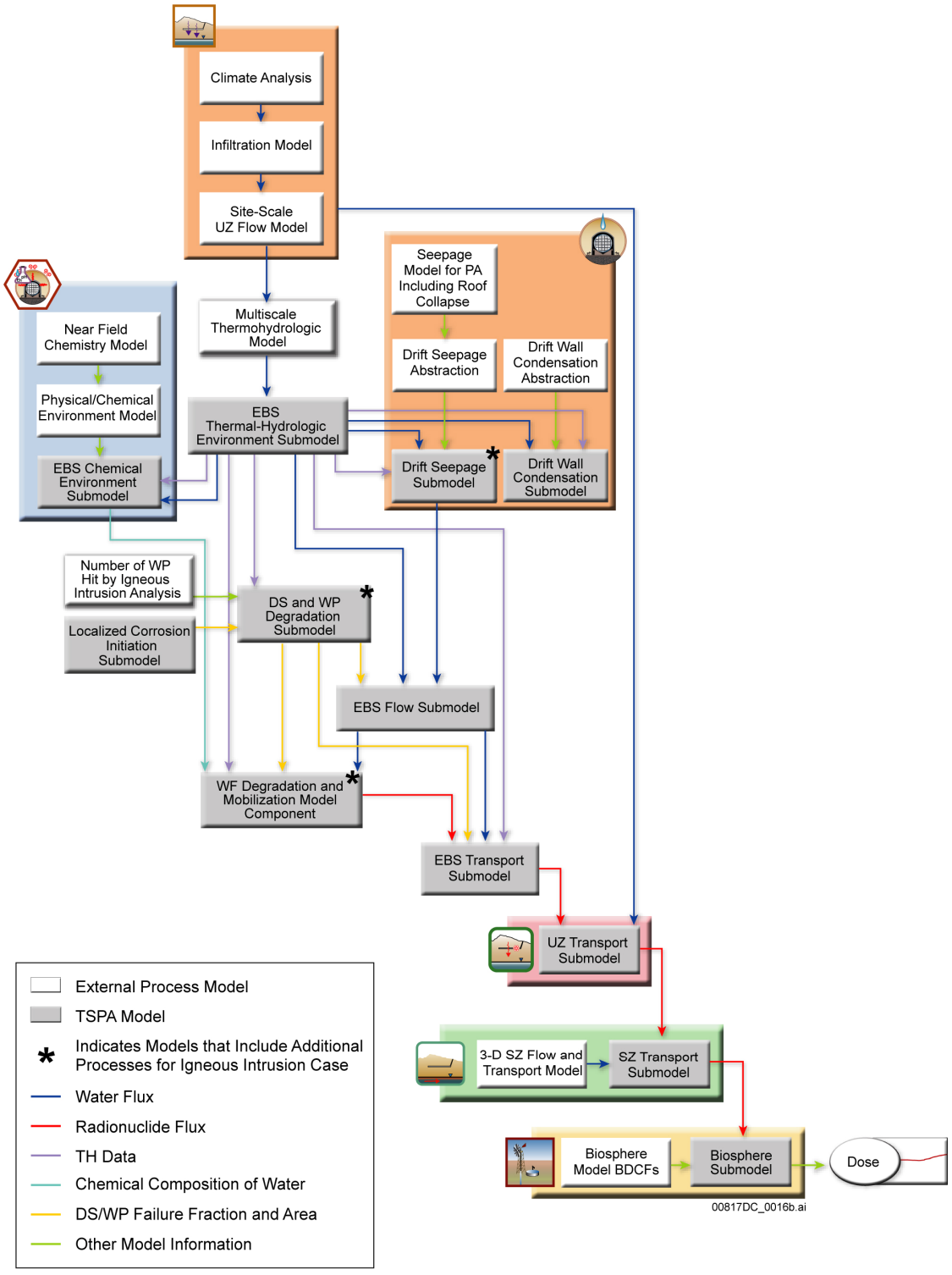

Figure G-3. Illustration of the Transfer of Information between Model Components and Submodels of the TSPA-LA Model for the Igneous Intrusion Modeling Case

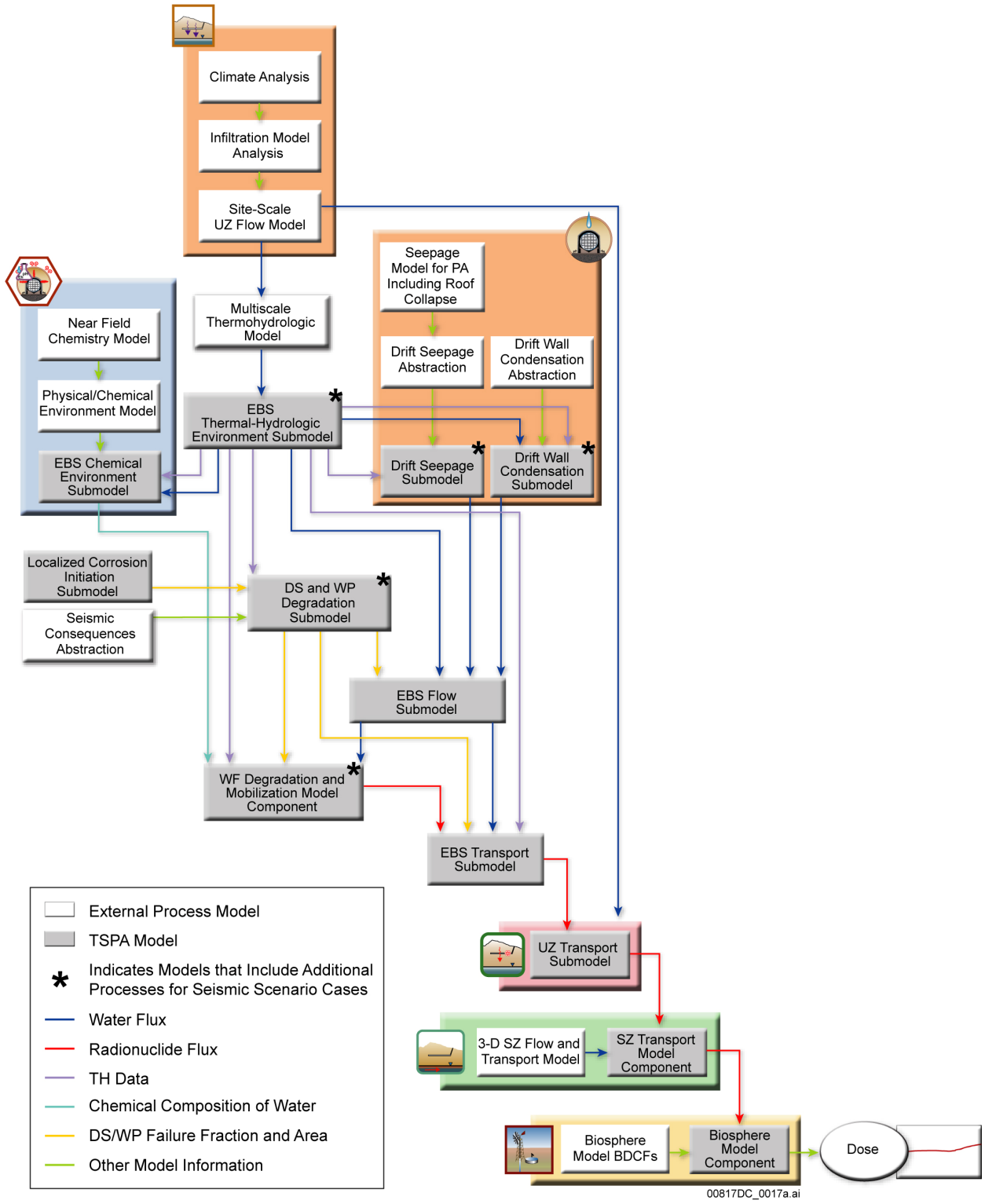

Figure G-4. Illustration of the Transfer of Information between Model Components and Submodels of the TSPA-LA Model for the Seismic Ground Motion and Fault Displacement Modeling Cases

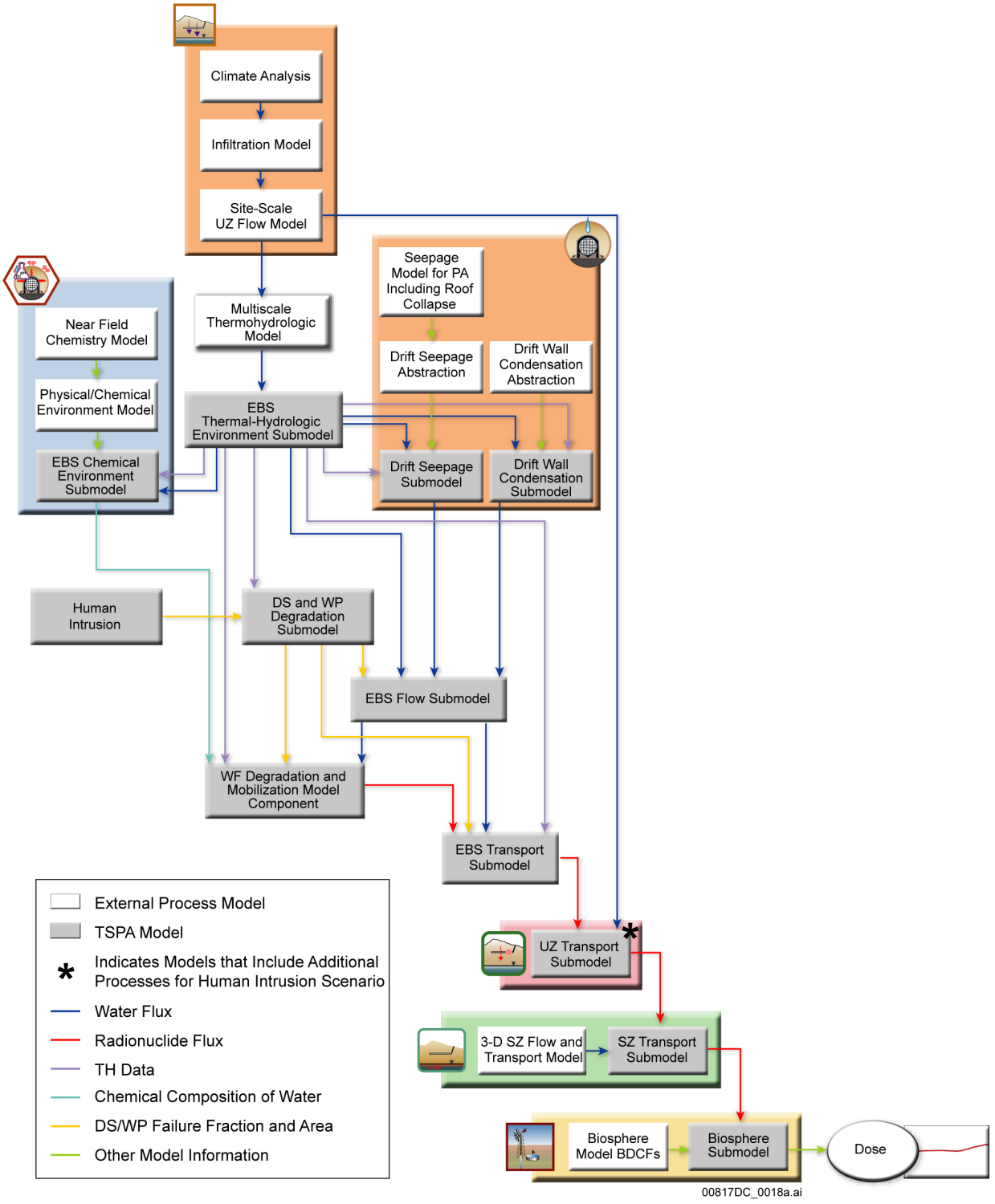

Figure G-5. Illustration of the Transfer of Information between Model Components and Submodels of the TSPA-LA Model for the Human Intrusion Scenario Class

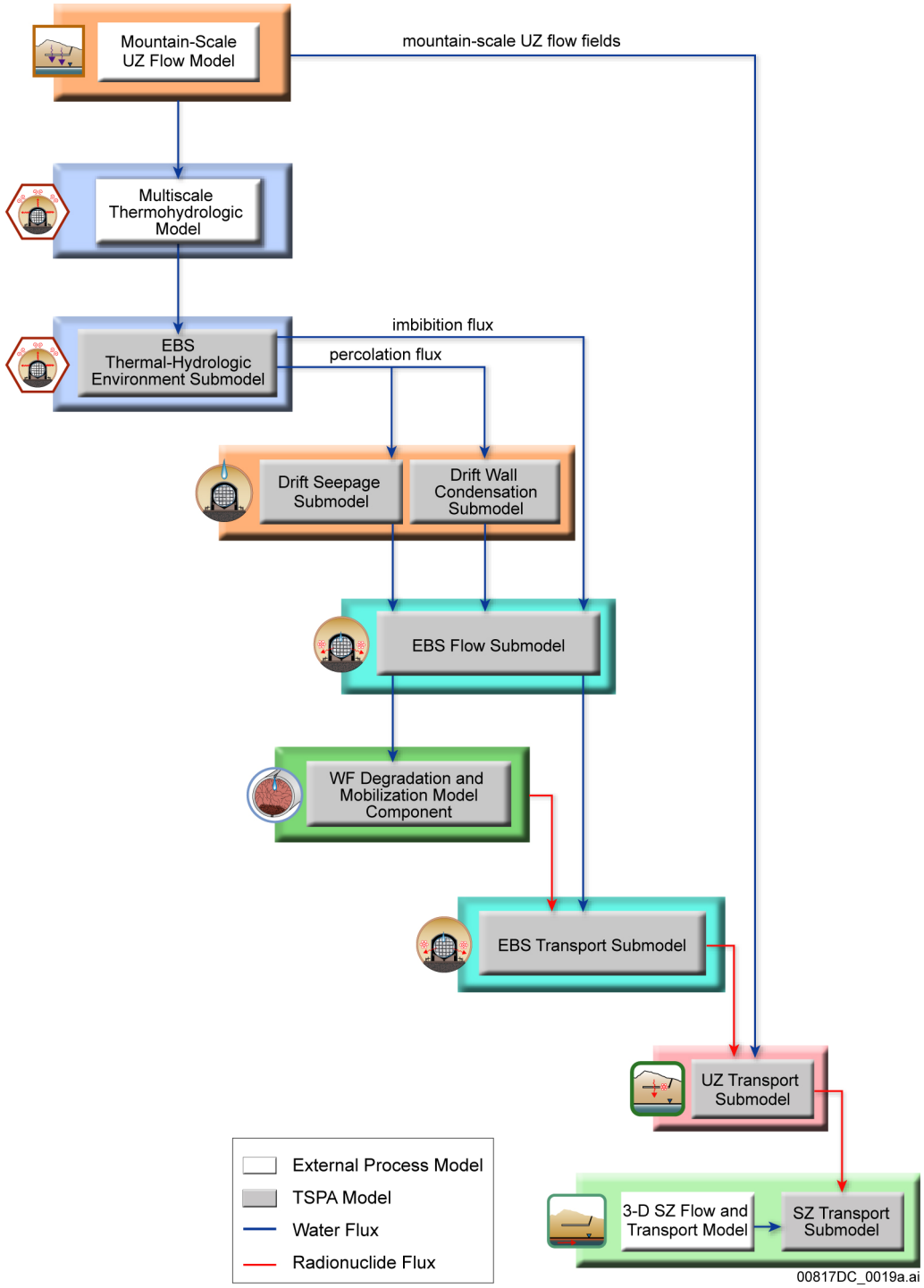

Figure G-6. Illustration of the Transfer of Information on Water Fluxes between Model Components and Submodels of the TSPA-LA Model

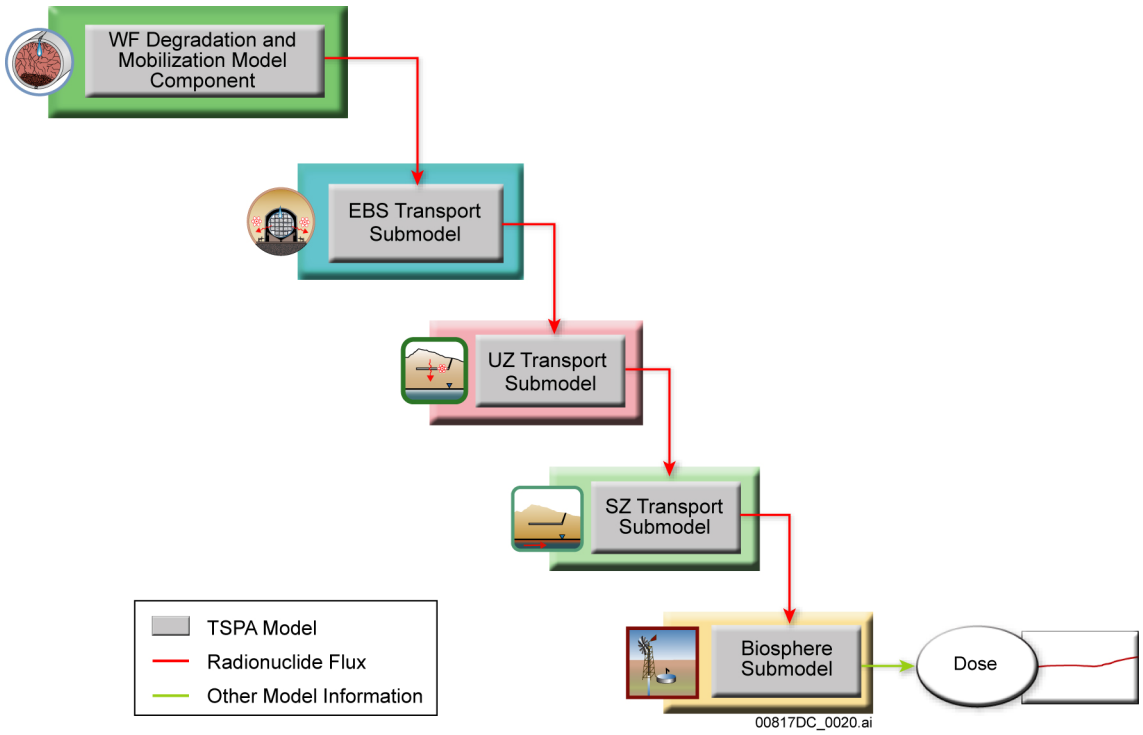

Figure G-7. Illustration of the Transfer of Information on Radionuclide Fluxes between Model Components and Submodels of the TSPA-LA Model

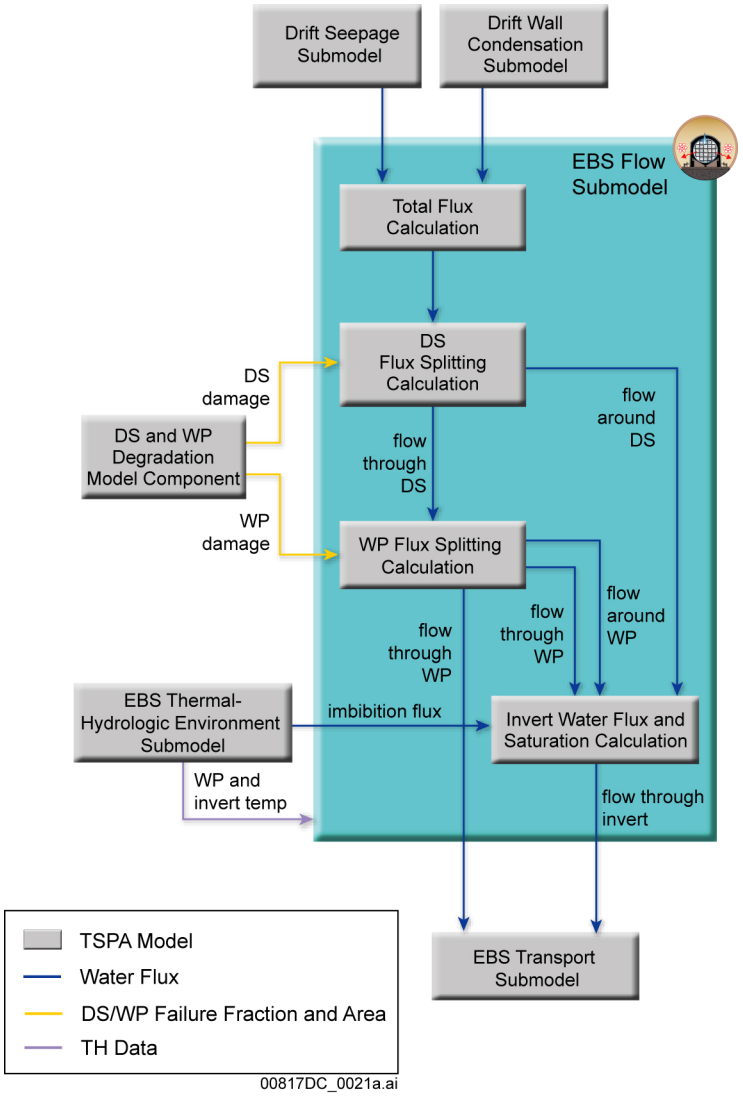

Figure G-8. Illustration of the Transfer of Information between Model Components and Submodels of the TSPA-LA Model for Factors that Affect Flow through the EBS

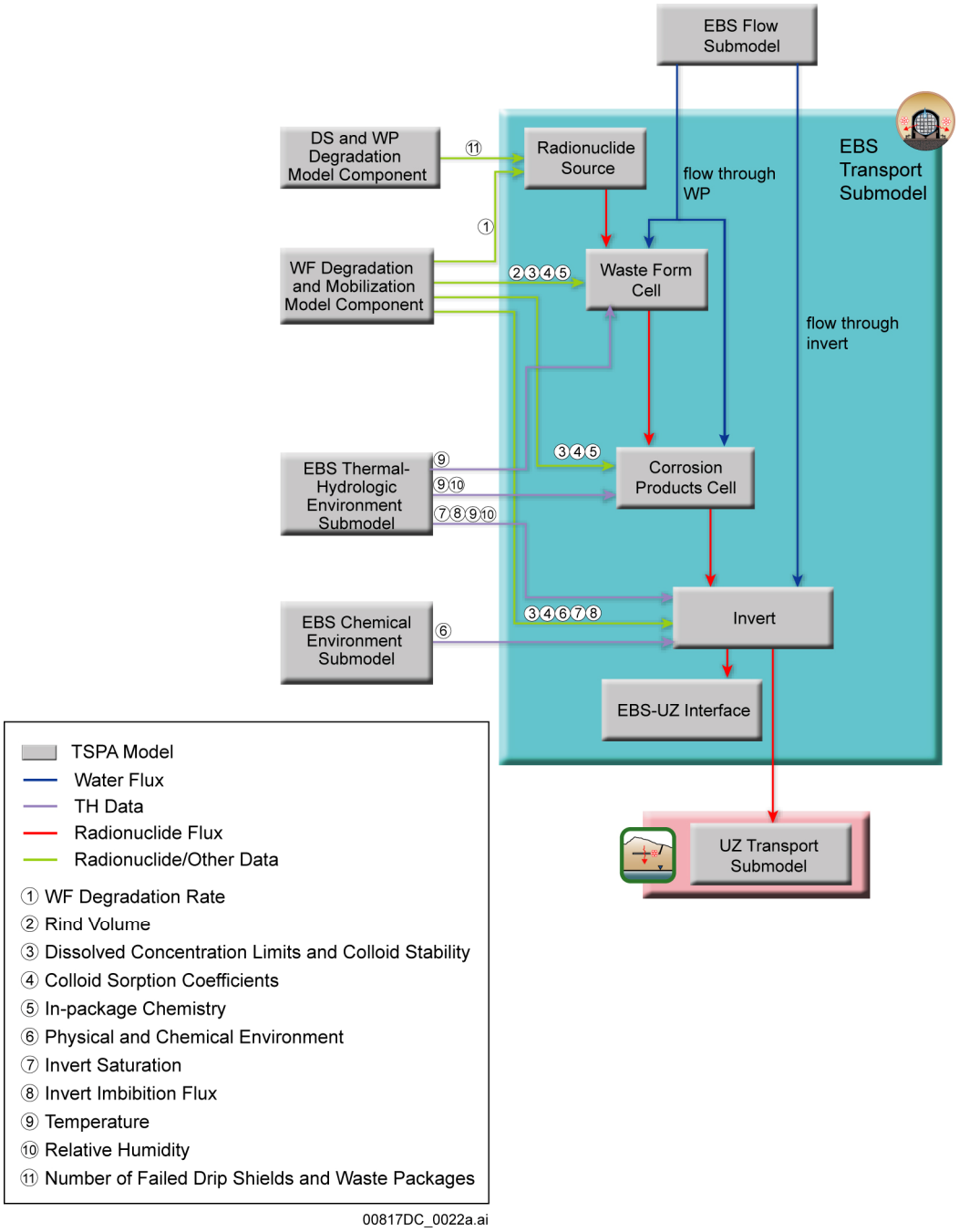

Figure G-9. Illustration of the Transfer of Information between Model Components and Submodels of the TSPA-LA Model that affect Radionuclide Transport through the EBS

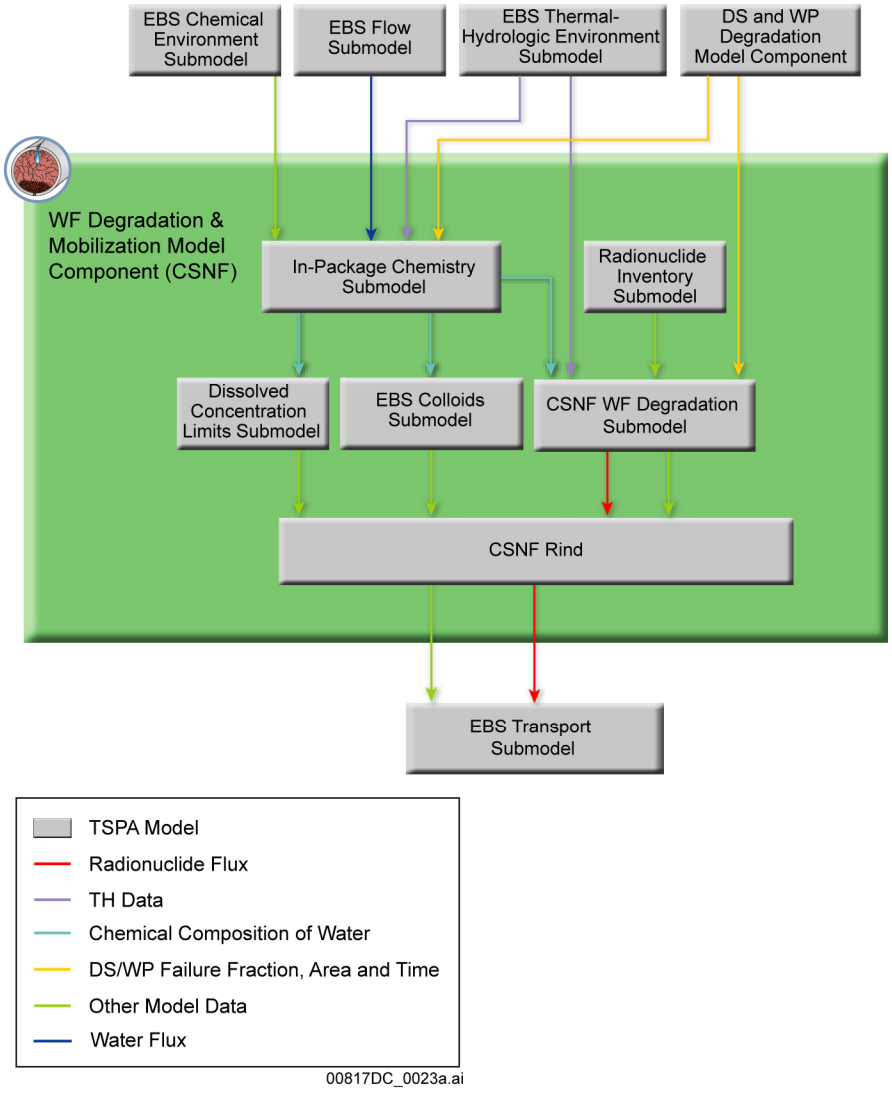

Figure G-10. Illustration of the Transfer of Information between Model Components and Submodels of the TSPA-LA Model, Nominal Scenario Class, for Factors that Affect Waste Form Degradation for CSNF WPs

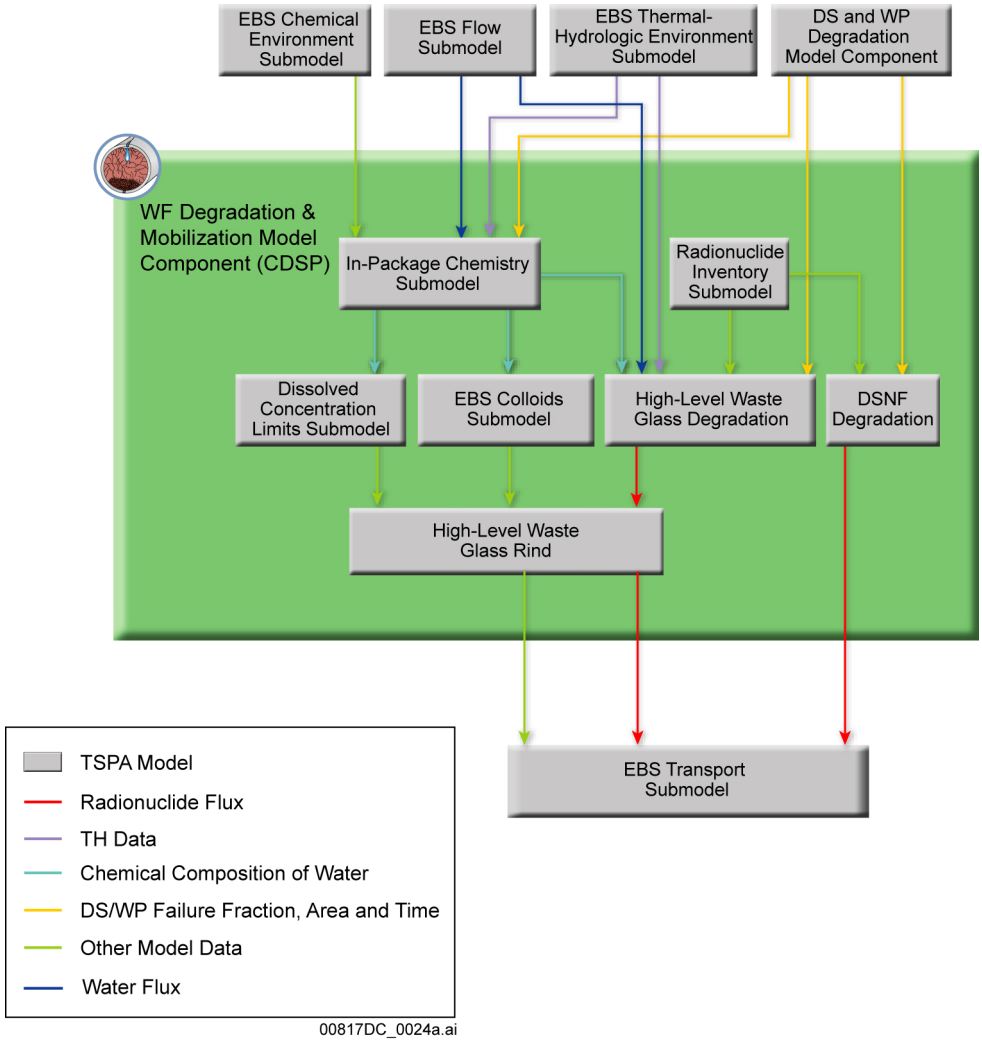

Figure G-11. Illustration of the Transfer of Information between Model Components and Submodels of the TSPA-LA Model, Nominal Scenario Class, for Factors that Affect Waste Form Degradation for CDSP WPs

APPENDIX H

YUCCA MOUNTAIN REVIEW PLAN ACCEPTANCE CRITERIA

H1. EVALUATION OF THE TOTAL SYSTEM PERFORMANCE ASSESSMENT FOR THE LICENSE APPLICATION MODEL DOCUMENT AGAINST REGULATORY REQUIREMENTS

Pursuant to the Technical Work Plan (SNL 2008 [DIRS 184920], Section 3.3 and Table 3.3-1), for the TSPA-LA Model, the *Total System Performance Assessment Model/Analysis for the License Application* is to be evaluated against sections of Subpart E—Technical Criteria of the U.S. Nuclear Regulatory Commission (NRC) Proposed Rule 10 CFR Part 63 ([DIRS 178394] and [DIRS 180319]). In particular, 10 CFR 63.113(a), (b), (c), and (d); and 10 CFR 63.115(a), and (b) [DIRS 180319] and to the acceptance criteria specified in the *Yucca Mountain Review Plan, Final Report* (NUREG-1804) (NRC 2003 [DIRS 163274]) that apply to these requirements. NUREG-1804 (NRC 2003 [DIRS 163274]) acceptance criteria addressed in the *Total System Performance Assessment Model/Analysis for the License Application* and their correlation with the sections of Subpart E of 10 CFR Part 63 ([DIRS 178394] and [DIRS 180319]) are summarized in Table H-1. The following sections provide pointers to the sections of the *Total System Performance Assessment Model/Analysis for the License Application* that address the specified sections of the NRC Rule and the associated acceptance criteria.

Section H1.1 points to the sections of the *Total System Performance Assessment Model/Analysis for the License Application* related to NRC Rule 10 CFR 63.113(a); and 10 CFR 63.115(a) and (b) [DIRS 180319]. The identified sections of this model report provide information that can be used in evaluating the multiple barriers against the NUREG-1804 (NRC 2003 [DIRS 163274]) acceptance criteria.

Section H1.2 points to the sections of the *Total System Performance Assessment Model/Analysis for the License Application* related to 10 CFR 63.113(b) [DIRS 180319]. The identified sections of this model report provide information that can be used in evaluating NUREG-1804 (NRC 2003 [DIRS 163274]) acceptance criteria regarding the postclosure performance objective associated with protection of the reasonably maximally exposed individual (RMEI).

Section H1.3 points to the sections of the *Total System Performance Assessment Model/Analysis for the License Application* related to 10 CFR 63.113(c) [DIRS 180319]. The identified sections of the *Total System Performance Assessment Model/Analysis for the License Application* provide information that can be used in evaluating NUREG-1804 (NRC 2003 [DIRS 163274]) acceptance criteria regarding the postclosure performance objective associated with protection of the groundwater.

Section H1.4 points to the sections of this model report related to 10 CFR 63.113(d) [DIRS 180319]. The identified sections of this model report provide information that can be used in evaluating NUREG-1804 (NRC 2003 [DIRS 163274]) acceptance criteria regarding the postclosure performance objective associated with protection of the RMEI if there is a human intrusion into the repository.

H1.1. EVALUATION AGAINST 10 CFR 63.113(A); 10 CFR 63.115(A); AND 10 CFR 63.115(B)

The requirements given in 10 CFR 63.113(a); and 10 CFR 63.115(a) and (b) [DIRS 180319] address the multiple barriers. The NRC's review of the information provided will focus on these requirements according to NUREG-1804 (NRC 2003 [DIRS 163274], Section 2.2.1.1) (see Table H-1). The following sections of this model report provide information relevant to the acceptance criteria specified in this section of NUREG-1804.

Acceptance Criterion 1–Identification of Barriers is Adequate—Section 8.3 identifies barriers important to waste isolation. These barriers are the Upper Natural Barrier, the Engineered Barrier System (EBS), and the Lower Natural Barrier. The discussion in Section 8.3 therefore, provides information for evaluating Acceptance Criterion 1.

Acceptance Criterion 2–Description of Barrier Capability to Isolate Waste is Acceptable—Section 8.3 discusses the capability of the barriers identified as important to waste isolation. This section summarizes the capabilities of the barriers that are important to waste isolation to prevent or substantially reduce the rate of radionuclide movement from the Yucca Mountain Repository to the accessible environment, or to prevent the release or substantially reduce the release rate of radionuclides from the waste. The discussion in Section 8.3 therefore, provides information useful for evaluating Acceptance Criterion 2.

Acceptance Criterion 3–Technical Basis for Barrier Capability is Adequately Presented—Section 6.3 summarizes the model components of the TSPA-LA Model, which include the submodels used to evaluate barrier capability. The technical basis for these models is provided in the analysis and model reports referenced in Section 6.3.

H1.2. EVALUATION AGAINST 10 CFR 63.113(B)

The requirements given in NRC Rule 10 CFR 63.113(b) [DIRS 180319], address the postclosure performance objectives associated with protection of the RMEI. The review by the NRC, of the information provided, will focus on the individual protection requirements according to NUREG-1804 (NRC 2003 [DIRS 163274], Section 2.2.1.4.1) (Table H-1). The following sections of this model report provide information relevant to the acceptance criteria specified in this section of NUREG-1804.

Acceptance Criterion 1–Scenarios Used in the Calculation of the Annual Dose as a Function of Time are Adequate—Section 8.1.1 describes the mean annual dose history calculated for the repository system. This mean annual dose history is a sum of the mean annual dose histories for all modeling cases that represent the scenario classes determined to be sufficiently probable or to have a sufficient effect on overall performance, and therefore, were included in the analyses. Section 6.1.2 discusses the summing of results for these modeling cases and shows that the contribution to mean annual dose properly accounts for the random time of occurrence of the disruptive events. Section 6.1.2 also summarizes the probabilities of all scenario classes and shows that the approach in the TSPA-LA Model provides an appropriate sum of these probabilities.

Acceptance Criterion 2–An Adequate Demonstration is Provided that the Annual Dose to the Reasonably Maximally Exposed Individual in Any Year During the Compliance Period Does Not Exceed the Exposure Standard—The analyses in Sections 7.3 and 8.1.1 show that mean annual dose is calculated with a sufficient number of realizations for each scenario class modeling case to ensure that the results of the calculations are statistically stable. The analyses in Section 8.1.1 also address the uncertainty in the estimate of mean annual dose and Sections 8.2.1 through 8.2.4 show the range of annual doses used to estimate mean annual dose in each of the TSPA-LA Model modeling cases. This range represents the full range of uncertainty in each estimate of mean annual dose. Subsystem analyses in Sections 8.3.1 through 8.3.4 show that the performances of individual components and subsystems are consistent and reasonable. The results in Section 8.1.1, Sections 8.2.1 through 8.2.4, and Sections 8.3.1 through 8.3.4, therefore provide information useful in evaluating this acceptance criterion.

Acceptance Criterion 3–The Total System Performance Assessment (TSPA) Code Provides a Credible Representation of Repository Performance—Section 5 discusses the general assumptions used in the TSPA-LA Model development and justification for these assumptions. Sections 6.3, 6.4, 6.5, 6.6, and 6.7, document the use of these assumptions and the parameter values that differ among components and submodels of the TSPA-LA Model. Section 6.1 provides an overview of the conceptual TSPA-LA Model. The subsections of Section 6.1 describe the transfer of information among the TSPA-LA Model components. Section 6.3 provides details of the components of the TSPA-LA Model for the Nominal Scenario Class. Section 6.4 presents the detail for the Early Failure Scenario Class, with Section 6.4.1 discussing the Drip Shield Early Failure Modeling Case, and Section 6.4.2 discussing the Waste Package Early Failure Modeling Case. Section 6.5 provides details for the Igneous Scenario Class and Section 6.6 presents the Seismic Scenario Class information. Section 6.7 discusses the details for the Human Intrusion Scenario, including the conceptual model in Section 6.7.1, and the TSPA-LA Model implementation in Section 6.7.2. Section 7.2 confirms that the TSPA-LA Model is properly verified and that information transfer between and among components and submodels, is conducted properly. Section 7.4 provides results of the uncertainty analyses, and corrective actions implemented when appropriate. Section 7.4 also shows that the estimate of the uncertainty in the performance assessment results is consistent with the model and the uncertainty in parameter values. Section 6.1.3 shows that a Latin hypercube sampling approach addresses all quantified uncertainties, and that this approach ensures that parameter values are sampled across their ranges of uncertainty. Section 7.10 summarizes the validation of the TSPA-LA Model and provides confidence that the TSPA-LA Model adequately represents the physical processes of the repository system. The overview of the TSPA-LA Model in Section 6 and the model validation and confidence building information in Section 7 therefore, provide information useful in evaluating this acceptance criterion.

H1.3. EVALUATION AGAINST 10 CFR 63.113(C)

The requirements at NRC Rule 10 CFR 63.113(c) [DIRS 180319] address the postclosure performance objective associated with protection of groundwater. 10 CFR 63.113(c) [DIRS 180319] points to the requirements of the NRC Rule 10 CFR 63.331 [DIRS 180319], which address the standards for groundwater protection, and the requirements at 10 CFR 63.332 [DIRS 180319], which define the representative volume. The review by the NRC of the

information that will be provided in the TSPA-LA Model and the *Total System Performance Assessment Model/Analysis for the License Application* will focus on these groundwater protection requirements according to NUREG-1804 (NRC 2003 [DIRS 163274], Section 2.2.1.4.3) (Table H-1). The following sections of the *Total System Performance Assessment Model/Analysis for the License Application* provide information relevant to the acceptance criteria specified in this section of NUREG-1804.

Acceptance Criterion 1–An Adequate Demonstration is Provided that the Expected Concentration of Combined ^{226}Ra and ^{228}Ra, Expected Concentration of Specified Alpha–Emitting Radionuclides, and Expected Whole Body or Organ–Specific Doses from any Photon– or Beta–Emitting Radionuclides at Any Year During the Compliance Period Do Not Exceed the Separate Groundwater Protection Standards—Section 8.1.2 presents the results of analyses addressing the groundwater protection standards. In particular, Section 8.1.2 shows the estimate of groundwater radioactivity for the representative volume of groundwater that includes combined ^{226}Ra and ^{228}Ra, gross alpha activity (including due to ^{226}Ra, but excluding that due to radon and uranium), and combined beta- and photon-emitting radionuclides. Sections 6.3 and 8.1.2 discuss the methods, assumptions, models, and data used in calculating these estimates. Sections 6.3 and 8.1.2 show that these estimates are consistent with the repository performance assessment calculations for likely processes and events that may occur after disposal, and that the calculations are supported by an adequate technical basis. Therefore, the material in Sections 6.3 and 8.1.2 provides information useful in evaluating Acceptance Criterion 1.

Acceptance Criterion 2–The Methods and Assumptions Used to Determine the Position of the Representative Volume of Groundwater are Credible and Consistent, and the Representative Volume of Groundwater Includes the Highest Concentration Level in the Plume of Contamination in the Accessible Environment—Section 6.3.10 discusses the methods and assumptions for determination of groundwater concentrations in the representative volume that is located along the radionuclide migration path from the repository at Yucca Mountain to the accessible environment. Section 8.1.2 provides results and a detailed evaluation of the concentrations in the context of the groundwater concentration standards. In the TSPA-LA Model, a conservative approach is used in which radionuclide concentrations are estimated by assuming the entire annual release from the repository system is discharged into the representative volume, located 18 km from the repository. Therefore, the estimated radionuclide concentrations provide an upper bound to the groundwater concentrations needed to assess the groundwater protection requirements. This approach eliminates the need to specify the dimensions of the representative volume or the water usage by the RMEI (Section 1.1.1). The information provided in Sections 6.3.10 and 8.1.2 therefore, supports evaluation of Acceptance Criterion 2 by the NRC.

Acceptance Criterion 3–The Methods and Assumptions Used to Calculate the Physical Dimensions of the Representative Volume of Groundwater are Credible and Consistent—The dose results presented in Section 8.1.2 are estimated by assuming that the entire annual release from the repository system is discharged into the representative volume. Therefore, the associated concentrations provide an upper bound to the groundwater concentrations needed to assess the groundwater protection requirements. This approach eliminates the need to specify the physical dimensions of the representative volume or the water

usage by the RMEI (Section 1.1.1). The information in Section 8.1.2 therefore, supports evaluation of this Acceptance Criterion 3.

H1.4. EVALUATION AGAINST 10 CFR 63.113(D)

The requirements given in NRC Rule 10 CFR 63.113(d) [DIRS 180319] address the postclosure performance objective associated with protection of the RMEI due to a human intrusion into the repository. Section 63.113(d) [DIRS 180319] points to the requirements: (1) in 10 CFR 63.321 [DIRS 178394], which address the selection of the time of occurrence of the human intrusion, (2) for conducting the TSPA for the human intrusion separately from the overall TSPA, and meets the requirements for performance assessments (PA) specified in NRC Proposed Rule 10 CFR 63.114 [DIRS 178394], which are the same as for the overall TSPA, and (3) in 10 CFR 63.322 [DIRS 180319], which specifies the Human Intrusion Scenario for the DOE to use in addressing the postclosure individual protection standard. The review by the NRC of the information that will be provided in the TSPA-LA Model and the *Total System Performance Assessment Model/Analysis for the License Application*, will focus on these requirements according to NUREG-1804 (NRC 2003 [DIRS 163274], Section 2.2.1.4.2) (Table H-1). The following sections of the TSPA-LA Model report provide information relevant to the acceptance criteria specified in Section 2.2.1.4.2 of NUREG-1804.

Acceptance Criterion 1–Evaluation of the Time of an Intrusion Event—Section 6.7.2 provides the technical basis and associated analyses in support of the selection of time of occurrence of the human intrusion, as specified in 10 CFR 63.321 [DIRS 178394]. Specifically, Section 6.7.2.1 describes the TSPA-LA analysis for drip shield (DS) and waste package (WP) degradation. Section 6.7.2.2 discusses the unlikely events-related damage mechanisms. Section 6.7.2.3 describes the potential for WP penetration during drilling. Section 6.7.2.4 provides the earliest time of WP penetration by a human intrusion. The information provided in Section 6.7.2 therefore supports evaluation of Acceptance Criterion 1.

Acceptance Criterion 2–Evaluation of an Intrusion Event Demonstrates That the Annual Dose to the Reasonably Maximally Exposed Individual in Any Year During the Compliance Period Is Acceptable—Sections 6.7 and 8.1.3 discuss how the TSPA-LA Model addresses the Human Intrusion Scenario, the implementation, and how the resultant RMEI dose complies with the requirement of this acceptance criterion. Section 6.7.3 specifically discusses implementation of the TSPA-LA Model for human intrusion separately from the overall TSPA, and is consistent with the requirements for PAs, as specified in 10 CFR 63.114 [DIRS 178394]. Sections 6.7.3 and 6.7.4 show that the TSPA for human intrusion is identical as applicable to the TSPA for individual protection, except that it assumes the occurrence of a postulated human intrusion event with characteristics as defined in 10 CFR 63.322 [DIRS 180319], and excludes the consideration of 10 CFR 63.342 [DIRS 178394] for unlikely natural features, events, or processes (6.7.2.2). Sections 7.3 and 8.1.1 provide information regarding the fact that a sufficient number of realizations have been run using the TSPA-LA Model, to ensure that the results of the calculations are statistically stable. Section 8.1.3 discusses the overall system performance analyses and presents the resulting annual dose curves for the Human Intrusion Scenario. The information provided in Sections 6.7 and 8.1 supports confirmation that the repository system meets performance objectives specified in 10 CFR 63.321 [DIRS 178394] for a human intrusion into the repository.

Acceptance Criterion 3—The Total System Performance Assessment Code Provides a Credible Representation of the Intrusion Event—Sections 5, 6.7.1 through 6.7.5, 7.2, 7.4, and 7.7, provide the information needed to evaluate this acceptance criterion as shown in Table H-1. Section 6.7.3 describes the implementation of the TSPA-LA Model for simulating the Human Intrusion Scenario. The parameter sampling for the TSPA-LA Model is discussed in Section 6.1.3. Section 6.7.4 provides information on the assessment of the impact due to the assumptions used, and model and parameter uncertainty on the dose calculated by the TSPA-LA Model, which are reflected in modeling the Human Intrusion Scenario. Section 6.7.4 discusses the consistency among model components and submodels, and identifies the conservative assumptions in abstractions, process models, and parameter sets supporting the modeling case for the Human Intrusion Scenario. Section 7.2 documents the TSPA-LA Model verification activities in order to ensure that the TSPA-LA Model inputs are properly verified providing confidence that the code was modeling the physical processes in the repository system in a manner that is consistent with the characteristics of the postulated human intrusion event. The information in Section 7.3 ensures that the individual dose curves do indeed represent the model and are not due to errors and lack of transfer of data (coupling) between the modules of the code. Section 6.1.3 discusses the treatment of uncertainty in the TSPA-LA Model input parameters. Section 7.4 presents an uncertainty characterization review and remedial actions implemented. Section 6.7.4 discusses the application of the uncertainty treatment, and characterization reviews to the Human Intrusion Scenario. The measures described above together provide the information needed to support evaluation of this Acceptance Criterion 3.

Table H-1. Applicable Regulatory Requirements of 10 CFR Part 63 and NUREG-1804 Acceptance Criteria Addressed in this Document

Applicable Sections of 10 CFR Part 63	Associated Section of NUREG-1804 Acceptance Criterion	NUREG-1804 Acceptance Criterion		Section of Report Addressing NUREG-1804 Acceptance Subcriterion
		Criterion	Subcriterion	
10 CFR 63.113(a), 10 CFR 63.115(a), and 10 CFR 63.115(b) [DIRS 180319]	2.2.1.1.3 System Description and Demonstration of Multiple Barriers	1. Identification of Barriers	1. Identification of barriers	8.3
		2. Description of Barrier Capability	1. Time period of applicable function	8.3
			2. Uncertainty in barrier capability	8.3
			3. Description consistent with the TSPA-LA Model	8.3
			4. Description consistent with barrier definition	8.3
		3. Technical Basis for Barrier Capability	1. Technical basis for barrier capability	6.3
10 CFR 63.113(b) [DIRS 180319]	2.2.1.4.1.3 Demonstration of Compliance with Postclosure Individual Protection Standard	1. Scenario Classes	1. Scenario class screening	6.1.2
			2. Combining mean annual dose from scenario classes	6.1.2 and 8.1.1.1
		2. Mean Annual Doses	1. Number of realizations	8.1.1.2, 7.3
			2. Uncertainty in mean annual dose	6.1.3 and 8.1.1.2
			3. Performance of components and subsystems	8.2 – 8.4
			4. Comparison with individual protection standard	8.1.1.2
		3. Credible TSPA-LA Model	1. Consistency of assumptions	5, 6.3 to 6.6
			2. Model verification	7.2
			3. Uncertainty analysis	6.1.3 and 7.4
			4. Parameter sampling	6.1.3
10 CFR 63.113(c) [DIRS 180319]	2.2.1.4.3.3 Demonstration of Compliance with Groundwater Protection Standards	1. Groundwater Protection Standards	1. Compliance with concentration and dose standards	8.1.2.1 to 8.1.2.2, and 8.1.2.3
			2. Methods and assumptions	8.1.2
			3. Comparison with groundwater protection standards	8.1.2
		2. Position of Representative Volume	1. Along radionuclide migration path	6.3.10
			2. Method of locating position	6.3.10
			3. Highest concentration	6.3.10
		3. Dimensions of Representative Volume	1. Specifications on representative volume	8.1.2
			2. Method to determine dimensions	6.3.10 and 8.1.2
			3. Consistency with water usage	8.1.2 and 6.3.11

Table H-1. Applicable Regulatory Requirements of 10 CFR Part 63 and NUREG-1804 Acceptance Criteria Addressed in this Document (Continued)

Applicable Sections of 10 CFR Part 63	Associated Section of NUREG-1804 Acceptance Criterion	NUREG-1804 Acceptance Criterion		Section of Report Addressing NUREG-1804 Acceptance Subcriterion
		Criterion	Subcriterion	
10 CFR 63.113(d) [DIRS 180319]	2.2.1.4.2 Demonstration of Compliance with the Human Intrusion Standard	1. Evaluation of the Time of a Human Intrusion Event	1. The technical basis and associated analyses adequately support the selection of the time of occurrence of a human intrusion, as specified in 10 CFR 63.321 [DIRS 178394].	6.7.2
		2. Evaluation of an Intrusion Event Demonstrates That the Annual Dose to the RMEI in Any Year During the Compliance Period Is Acceptable	1. The TSPA for the Human Intrusion Scenario is performed separately from the overall TSPA, and meets the requirements for performance assessments, specified in 10 CFR 63.114 [DIRS 178394].	6.7.3 and 6.7.4
			2. The TSPA for Human Intrusion Scenario is identical to the TSPA for individual protection, except that it assumes the occurrence of a postulated human intrusion event with characteristics, as defined in 10 CFR 63.322 [DIRS 180319] and excludes the consideration of unlikely natural features, events, or processes in 10 CFR 63.342 [DIRS 178394].	6.7.2.2, 6.7.3, and 6.7.4
			3. A sufficient number of realizations have been run using the TSPA code, to ensure that the results of the calculations are statistically stable.	8.1.1.2 and 7.3
			4. The estimated repository performance is reasonable and consistent with the analysis of overall repository performance, and with the characteristics of the postulated Human Intrusion Scenario.	8.1.3.2
			5. The annual dose curve for limited human intrusion confirms that the repository system meets performance objectives, specified in 10 CFR 63.321 [DIRS 178394], for limited human intrusion events.	8.1.3.2

Table H-1. Applicable Regulatory Requirements of 10 CFR Part 63 and NUREG-1804 Acceptance Criteria Addressed in this Document (Continued)

Applicable Sections of 10 CFR Part 63	Associated Section of NUREG-1804 Acceptance Criterion	NUREG-1804 Acceptance Criterion		Section of Report Addressing NUREG-1804 Acceptance Subcriterion
		Criterion	Subcriterion	
		3. The TSPA Code Provides a Credible Representation of a Human Intrusion Event.	1. Assumptions made on the method of transport from a breached WP within the TSPA for evaluating the postulated intrusion event are consistent among different modules of the code. The use of assumptions and parameter values that differ among modules of the code is adequately documented.	5, 6.7.1 to 6.7.5, and 7.7
			2. The TSPA code for evaluating human intrusion is properly verified, such that there is confidence that the code is modeling the physical processes in the repository system in a manner that is consistent with the characteristics of the postulated intrusion event. The transfer of data between modules of the code is conducted properly.	7.2
			3. The estimate of uncertainty in the performance assessment results is consistent with the uncertainties considered in the characteristics of the postulated intrusion event, and with model and parameter uncertainty.	8.1.3, 6.7.3 ,6.1.3, and 7.4
			4. The sampling method used in the TSPA ensures that sampled parameters of the postulated intrusion event have been sampled across their ranges of uncertainty.	6.1.3, 6.7, and 7.4

Sources: 10 CFR Part 63 [DIRS 178394 and DIRS 180319]; NUREG-1804 (NRC 2003 [DIRS 163274])

INTENTIONALLY LEFT BLANK

APPENDIX I

FEATURES, EVENTS, AND PROCESSES MAPPED TO TSPA-LA MODEL

I1. FEATURES, EVENTS, AND PROCESSES MAPPED TO TSPA-LA MODEL

I1.1. INTRODUCTION

This appendix provides summary information about how features, events, and processes (FEPs) are implemented in the Total System Performance Assessment for the License Application (TSPA-LA) Model. Section 6.1.1 discusses the process of FEP screening and development. Section 6.1.1 also lists the criteria used to determine whether or not individual FEPs are included in or excluded from the TSPA-LA Model. The FEPs that are included as a result of the FEPs screening process are implemented in the TSPA-LA Model in various ways (Figure I-1). A FEP may be included by direct incorporation into the GoldSim simulation software (STN: 10344-9.60-01[DIRS 181903]) model file, such as in a parameter in a functional relation. (Throughout Appendix I, all references to GoldSim and the GoldSim model file refer to V9.60.100 (STN: 10344-9.60-01[DIRS 181903]) unless otherwise noted.) A FEP may also be included in the TSPA-LA Model by incorporation into a dynamically linked library (DLL) that is called by the GoldSim model file. A FEP may also be included in the TSPA-LA Model by incorporation into an abstraction of a process model. The development process for the TSPA-LA Model utilizes the development of several process models, as discussed in Section 6.1.5 (TSPA-LA Model File Architecture), which are abstracted for inclusion into the GoldSim model file. For example, FEP 1.1.02.02.0A, Preclosure Ventilation, is included in the Multiscale Thermohydrologic Model (MSTHM) Process Model and analysis that is used to develop the thermal hydrologic (TH) abstraction for the TSPA. Preclosure ventilation is included in the MSTHM analysis by accounting for the removal of heat in the energy source term.

Complete documentation for the FEPs abstracted in this appendix can be found in *Features, Events, and Processes for the Total System Performance Assessment: Methods* (SNL 2008 [DIRS 179476]), and *Features, Events, and Processes for the Total System Performance Assessment: Analyses* (SNL 2008 [DIRS 183041]). These documents contain information on the FEP screening process, applicable criteria, pertinent regulations, and detailed discussions of all 374 FEPs, including screening decisions, screening justifications, and full text TSPA dispositions. The TSPA disposition contains information on how each included FEP is implemented in a particular submodel or submodels. This information is also consolidated in the FEP data set (DTN: MO0706SPAFEPLA.001 [DIRS 181613]), which can be viewed using the FEPS database software program (STN: 611664-1.0-00 [DIRS 181089]).

The FEPs included in the TSPA-LA Model, require inclusion in one or more performance assessments conducted to demonstrate compliance with the proposed individual protection standard (10 CFR 63.311 [DIRS 178394]), groundwater protection standard (10 CFR 63.331 [DIRS 180319]), and/or the proposed individual protection standard for human intrusion (10 CFR 63.321 [DIRS 178394]). The results of this evaluation are incorporated in this appendix. Section 6.1.1 further explains this process and the regulatory requirements.

Figure I-1 pictorially describes the incorporation of an included FEP in the TSPA-LA Model. Table I-2 contains a brief description of how each included FEP is implemented in the TSPA-LA Model. More detailed TSPA dispositions are provided in the FEP data set (DTN: MO0706SPAFEPLA.001 [DIRS 181613]), which is too lengthy to include in its entirety

in this appendix. Information in this appendix provides a path to a location within the GoldSim model file where a FEP is implemented. The details of implementation for specific submodels are best understood by direct review of the TSPA-LA Model implementation within GoldSim, also known as a GoldSim model file. The text within the GoldSim model files described in this report was updated after the models were run. The updated GoldSim models with the descriptive text are part of output DTN: MO0708GWEFINAL.000 [DIRS 182977].

Sections 6.3.1 through 6.3.11, and 6.4 through 6.7 of this report describe the submodels included in the TSPA-LA Model. Each subsection also discusses the implementation of the submodels in the TSPA-LA Model and provides a pathway to the appropriate location in the GoldSim model file, allowing a detailed review of the implementation. In addition, the GoldSim model file includes descriptions of the inputs and calculations being performed within each submodel. Table 6.1.5-1 provides the GoldSim model file locations containing submodel documentation.

Table I-1 explains the information contained in the table headings used in Table I-2, and Table I-2 gives the TSPA implementation information for each FEP included in the TSPA-LA Model. The GoldSim model path listed is provided to guide the reader to the submodel within the TSPA-LA Model file. Different types of information will be found at these path locations depending on how the individual FEP is implemented or how broad the FEP is in nature. Implementation of each FEP, whether directly in the GoldSim model file, indirectly by a process model abstraction, or through a DLL, results in variations in the GoldSim model file paths identified in Table I-2. The GoldSim model paths shown for each FEP provides a location of the submodel where the feature, event or process is included. FEPs are not listed specifically in the GoldSim model file.

FEPs can be implemented by more than one submodel, and therefore can appear more than once in Table I-2. Effort was made to indicate only those FEPs that are directly implemented in a particular submodel and not include all downstream implementation of the same FEP. Additionally, FEPs identified in the nominal scenario class are, in general, included in the disruptive scenario classes. See sections 6.4- 6.7 for more information.

The GoldSim model file has evolved during the development of the TSPA-LA Model and this evolution has resulted in some inconsistencies in the use of terminology. For instance, Section 6 describes percolation subregions and discusses how they are defined and used in the TSPA-LA Model. In the GoldSim model file, these are referred to as bins. There is also legacy coding in the GoldSim model file that is no longer being used but was retained to allow for future sensitivity analyses or other investigations. Text has been added to the GoldSim model file to identify these special situations.

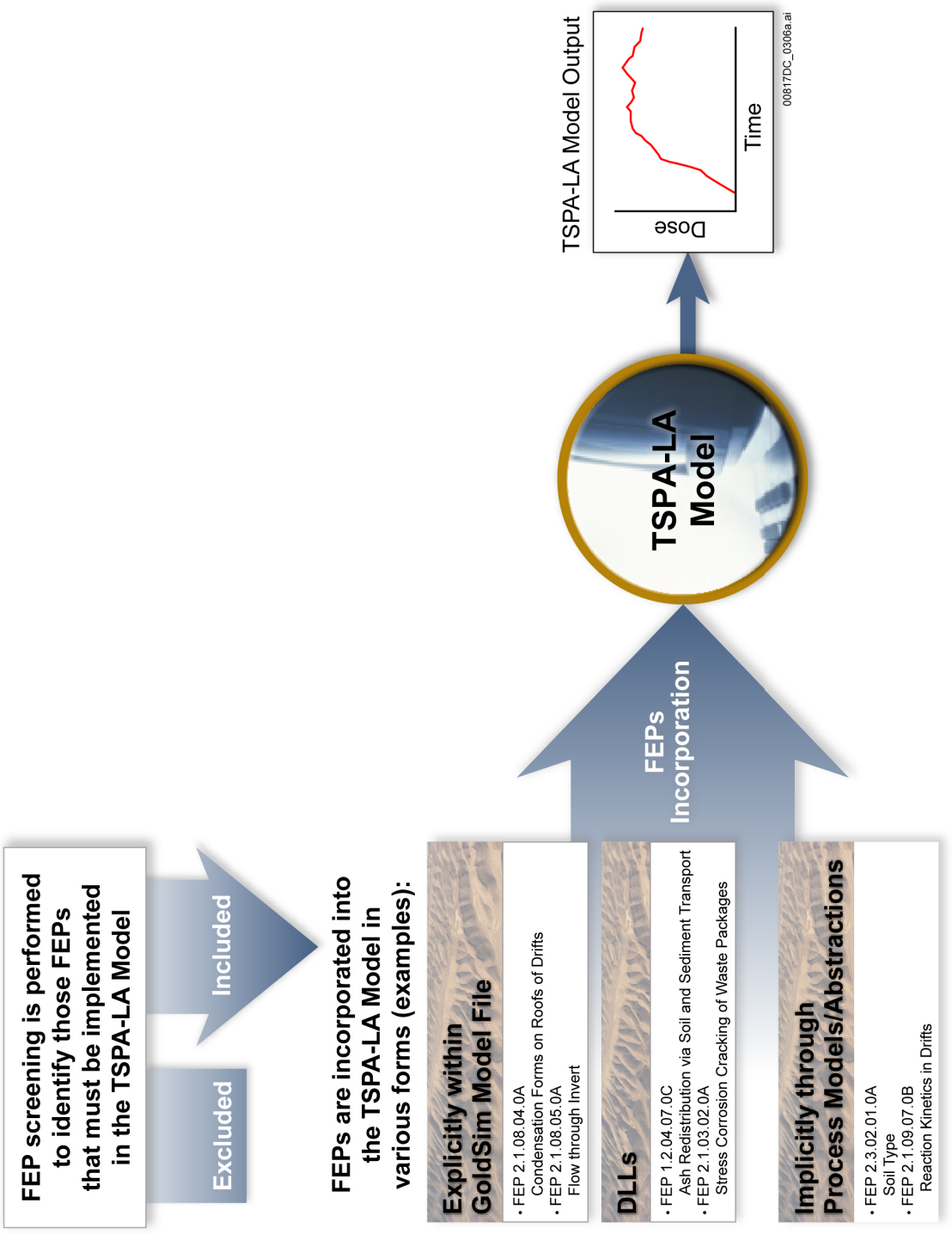

Figure I-1. Implementation of Features, Events, and Processes in the TSPA-LA Model

INTENTIONALLY LEFT BLANK

Table I-1. Explanation of the Column Headings in Table I-2

Column Heading	Explanation
Submodel implemented in the TSPA-LA Model and Section Number	This is the name of the submodel where the FEP is implemented. The number below the submodel name represents the section in this document where submodel information can be found.
Path in GoldSim Model File	The GoldSim path showing where the FEP is implemented in the GoldSim model. This is meant to provide a sampling of important paths. Other implementation paths may exist that are not shown in this column. Some FEP implementations are in multiple parallel locations in the GoldSim model because they contain multiple waste forms and multiple discrete repository regions.
FEPs included in the Submodel	The numbers and titles of the features, events and processes that are implemented in the TSPA-LA Model through the appropriate submodel.
TSPA Inclusion Explanation	A short description of how the FEP is implemented in the TSPA-LA Model.
Performance Assessment Standard	This column identifies the relevant regulatory standard the FEP is addressing: Groundwater Protection Standard (10 CFR 63.331 [DIRS 180319]), proposed Individual Protection Standard (10 CFR 63.311 [DIRS 178394]), or proposed Individual Protection Standard for Human Intrusion (10 CFR 63.321 [DIRS 178394]).
TSPA-LA Model Implementation	This column indicates how the FEP is implemented in the TSPA-LA Model; GSM = directly into the GoldSim model; MA = Process Model Abstraction; DLL= Dynamically Linked Library.

Table I-2. Model Implementation for Included Features, Events, and Processes

Submodel implemented in the TSPA-LA Model and Section Number	Path in GoldSim Model File	FEPs Included in the Submodel	TSPA Inclusion Explanation	Performance Assessment Standard[a]	TSPA-LA Model Implementation
UZ Flow Fields Abstraction 6.3.1	Epistemic: \Input_Params_Epistemic\Epistemic_Params_UZ_Flow EBS: \Time_Zero\EBS_PS_Loop\Static_Calcs_PS_Loop\Static_Calcs_UZ_Flow \Global_Inputs_and_Calcs\Global_UZ_Flow	1.3.01.00.0A Climate change	Climate change is addressed in the TSPA based on the record of climate changes in the past, which are used to predict the expected changes in climate for the future. Climate modeling is incorporated into TSPA through the site-scale unsaturated zone (UZ) flow fields which use different infiltration maps (water-flux boundary condition maps) corresponding to four different climates: present-day, monsoon, and glacial-transition, and the post-10,000-year climate.	10 CFR 63.311 10 CFR 63.331 10 CFR 63.321	GSM
UZ Flow Fields Abstraction for Human Intrusion assessment 6.7		1.3.07.02.0B Water table rise affects UZ	The water table will be higher in future climate states that have greater infiltration rates. To include this predicted water table rise in the TSPA calculations, the water table elevation is instantaneously increased up to 120m when the climate changes from present-day to monsoon climate, and the glacial-transition climate state. Water table changes are implemented in the TSPA by allowing the water table to change elevation instantaneously upon change in climate affecting the unsaturated flow and pathways in the UZ.	10 CFR 63.311 10 CFR 63.331 10 CFR 63.321	GSM
		1.4.01.01.0A Climate modification increases recharge	The Infiltration Model includes the effects of climate change. These effects are captured in the net infiltration map outputs that are used as upper boundary condition water-flux inputs for the Site-Scale UZ Flow Model. The Site-Scale UZ Flow Model is used to develop UZ flow fields corresponding to the four uncertainty cases for water flux at the upper boundary of the UZ Flow Model and four distinct climate states: present-day, monsoon, and glacial-transition, as well as the post-10,000-year period. These flow fields are used directly by the TSPA-LA Model.	10 CFR 63.311 10 CFR 63.331 10 CFR 63.321	GSM

Table I-2. Model Implementation for Included Features, Events, and Processes (Continued)

Submodel implemented in the TSPA-LA Model and Section Number	Path in GoldSim Model File	FEPs Included in the Submodel	TSPA Inclusion Explanation	Performance Assessment Standard[a]	TSPA-LA Model Implementation
UZ Flow Fields Abstraction 6.3.1 (Continued)	Epistemic: \Input_Params_Epistemic\Epistemic_Params_UZ_Flow EBS: \Time_Zero\EBS_PS_Loop\Static_Calcs_PS_Loop\Static_Calcs_UZ_Flow \Global_Inputs_and_Calcs\Global_UZ_Flow	1.2.02.01.0A Fractures	Fractures are included in the Site-Scale UZ Flow Model by using models based on the dual-permeability concept, with fractures represented by a distinct continuum. The fracture continuum models spatially averaged flow through discrete fractures. The fracture continuum interacts with the matrix continuum, which represents matrix blocks separated by the network of fractures. Fracture porosity, fracture spacing, and fracture volume fraction, measured in the field and within different stratigraphic units, determine geometrical parameters of fractures that are incorporated. The flow fields generated by the Site-Scale UZ Flow Model are used directly by the TSPA.	10 CFR 63.311 10 CFR 63.331 10 CFR 63.321	MA
		1.2.02.02.0A Faults	Stratigraphic displacement, dip-slip, strike-slip, and detachments due to faulting within the model domain are explicitly discretized in the Site-Scale UZ Flow Model. Specific hydrogeologic properties are assigned to the fault zones, supported by measurements within fault zones or across faults. The flow fields generated by the Site-Scale UZ Flow Model are used directly by the TSPA.	10 CFR 63.311 10 CFR 63.331 10 CFR 63.321	MA
		2.1.08.01.0A Water influx at the repository	Spatial and temporal changes in UZ flow are represented by the Site-Scale UZ Flow Model. The flow fields generated by the Site-Scale UZ Flow Model are used directly by the TSPA-LA Model. The local percolation flux at the repository for different climate states and different locations within the repository is provided by these flow fields. In the TSPA-LA Model these percolation fluxes are used by the Drift Seepage Submodel to calculate the influx of water into the repository.	10 CFR 63.311 10 CFR 63.331 10 CFR 63.321	MA

Table I-2. Model Implementation for Included Features, Events, and Processes (Continued)

Submodel implemented in the TSPA-LA Model and Section Number	Path in GoldSim Model File	FEPs Included in the Submodel	TSPA Inclusion Explanation	Performance Assessment Standard[a]	TSPA-LA Model Implementation
UZ Flow Fields Abstraction 6.3.1 (Continued)	Epistemic: \Input_Params_Epistemic\Epistemic_Params_UZ_Flow EBS: \Time_Zero\EBS_PS_Loop\Static_Calcs_PS_Loop\Static_Calcs_UZ_Flow \Global_Inputs_and_Calcs\Global_UZ_Flow	2.2.03.01.0A Stratigraphy	Stratigraphic units and layers provide the structural basis for the Site-Scale UZ Flow Model grid. Hydrologic properties corresponding to each unit and layer are also assigned to the flow model grid. The flow fields generated by the Site-Scale UZ Flow Model are used directly by the TSPA.	10 CFR 63.311 10 CFR 63.331 10 CFR 63.321	MA
		2.2.03.02.0A Rock properties of host rock and other units	Rock properties are defined for each of the stratigraphic units and layers and associated with the model grid for the Site-Scale UZ Flow Model. Heterogeneity is modeled in terms of the sequence of hydrogeologic units and discrete faults. The flow fields generated by the Site-Scale UZ Flow Model are used directly by the TSPA.	10 CFR 63.311 10 CFR 63.331 10 CFR 63.321	MA
		2.2.07.02.0A Unsaturated groundwater flow in the geosphere	The three-dimensional the Site-Scale UZ Flow Model represents flow in a heterogeneous dual-permeability system that includes fractures and discrete fault zones that allow for a realistic description of flow pathways in the UZ. The flow fields generated by the Site-Scale UZ Flow Model are used directly by the TSPA.	10 CFR 63.311 10 CFR 63.331 10 CFR 63.321	GSM

Table I-2. Model Implementation for Included Features, Events, and Processes (Continued)

Submodel implemented in the TSPA-LA Model and Section Number	Path in GoldSim Model File	FEPs Included in the Submodel	TSPA Inclusion Explanation	Performance Assessment Standard[a]	TSPA-LA Model Implementation
UZ Flow Fields Abstraction 6.3.1 (Continued)	Epistemic: \Input_Params_Epistemic\Epistemic_Params_UZ_Flow EBS: \Time_Zero\EBS_PS_Loop\Static_Calcs_PS_Loop\Static_Calcs_UZ_Flow \Global_Inputs_and_Calcs\Global_UZ_Flow	2.2.07.03.0A Capillary rise in the UZ	Capillary forces are included in the Site-Scale UZ Flow Model. These forces affect the distribution of water in the UZ through capillary effects on water flow, also known as capillary wicking. Parameters used for capillarity modeling are incorporated within the matrix properties and fracture properties. These parameters are used as direct input to the Site-Scale UZ Flow Model. The flow fields generated by the Site-Scale UZ Flow Model are used directly by the TSPA.	10 CFR 63.311 10 CFR 63.331 10 CFR 63.321	MA
		2.2.07.04.0A Focusing of unsaturated flow (fingers, weeps)	Large-scale flow focusing caused by flow in faults and fractures are represented in the Site-Scale UZ Flow Model. Faults are included in the Site-Scale UZ Flow Model as discrete features. Fractures are included by using the dual-permeability concept, with fractures represented by a distinct continuum. Flow focused model results indicate that, as flow moves downward through the UZ, the flow tends to focus into fractures and fault zones. Intermediate-scale focusing of flow from the site scale to the drift scale is accounted for in the seepage abstraction (Section 6.3.3 by using appropriate flow-focusing factors). The flow fields generated by the Site-Scale UZ Flow Model are used directly by the TSPA. Large scale focusing is included in human intrusion because percolation flux in the UZ above the repository at the base of the PTn is used to determine the flux downward through the borehole. Intermediate-scale focusing is not included in human intrusion because the seepage model is not implemented for this assessment.	10 CFR 63.311 10 CFR 63.331 10 CFR 63.321	MA

Table I-2. Model Implementation for Included Features, Events, and Processes (Continued)

Submodel implemented in the TSPA-LA Model and Section Number	Path in GoldSim Model File	FEPs Included in the Submodel	TSPA Inclusion Explanation	Performance Assessment Standard[a]	TSPA-LA Model Implementation
UZ Flow Fields Abstraction 6.3.1 (Continued)	Epistemic: \Input_Params_Epistemic\Epistemic_Params_UZ_Flow EBS: \Time_Zero\EBS_PS_Loop\Static_Calcs_PS_Loop\Static_Calcs_UZ_Flow \Global_Inputs_and_Calcs\Global_UZ_Flow	2.2.07.07.0A Perched water develops	Perched water bodies above the repository were not observed and are not included in the flow fields predicted by the Site-Scale UZ Flow Model. The effects of existing perched-water zones below the repository are included, as are potential changes in these perched-water zones caused by climate. Lateral diversion of flow is associated with low permeability zeolites immediately above and within the CHn unit. Because of low permeability, perched water may form at the contacts with CHn zeolitic (CHnz) tuffs, and a large portion of the percolating flux may be diverted laterally to the east. The low permeability zeolitic layers are represented by the Site-Scale UZ Flow Model grid. The flow fields generated by the Site-Scale UZ Flow Model are used directly by the TSPA. The effects of underlying low permeability layers are not included in human intrusion because flow and transport is down the borehole from the repository to the SZ.	10 CFR 63.311 10 CFR 63.331	MA
		2.2.07.08.0A Fracture flow in the UZ	Fracture flow in the UZ is included in the Site-Scale UZ Flow Model by using models based on the dual-permeability concept, with fractures represented by a distinct continuum. The fracture continuum, models spatially averaged flow through discrete fractures. The fracture continuum interacts with the matrix continuum, which represents matrix blocks separated by the network of fractures. Fracture porosity, fracture spacing, and fracture volume fraction measured in the field and within different stratigraphic units determine geometrical parameters of fractures that are incorporated in the model. The flow fields generated by the Site-Scale UZ Flow submodel are used directly by the TSPA-LA Model	10 CFR 63.311 10 CFR 63.331 10 CFR 63.321	GSM

Table I-2. Model Implementation for Included Features, Events, and Processes (Continued)

Submodel implemented in the TSPA-LA Model and Section Number	Path in GoldSim Model File	FEPs Included in the Submodel	TSPA Inclusion Explanation	Performance Assessment Standard[a]	TSPA-LA Model Implementation
UZ Flow Fields Abstraction 6.3.1 (Continued)	Epistemic: \Input_Params_Epistemic\Epistemic_Params_UZ_Flow EBS: \Time_Zero\EBS_PS_Loop\Static_Calcs_PS_Loop\Static_Calcs_UZ_Flow \Global_Inputs_and_Calcs\Global_UZ_Flow	2.2.07.09.0A Matrix imbibition in the UZ	Matrix imbibition is included in the Site-Scale UZ Flow Model. Matrix imbibition refers to the movement of water into the matrix as a result of capillary forces. Capillary forces are represented by characteristic curves for the fracture and matrix continua that are a function of saturation. This process affects the distribution of flow between fractures and matrix in a dual-permeability flow model for fractured rock. The flow fields generated by the Site-Scale UZ Flow Model are used directly by the TSPA.	10 CFR 63.311 10 CFR 63.331 10 CFR 63.321	MA
		2.2.07.19.0A Lateral flow from Solitario Canyon Fault enters drift	The Site-Scale UZ Flow Model contains potential hydrogeologic connections between the Solitario Canyon Fault and the waste emplacement horizon. The potential connection is captured using a property set of the PTn unit with calibrated fracture-matrix properties that favor lateral flow. Therefore, flow from this fault to waste emplacement locations is addressed. This water may seep into waste emplacement drifts if the flux is sufficient to overcome the capillary barrier represented in the drift seepage model. The lateral flow effect is incorporated in the output flow fields generated by the Site-Scale UZ Flow Model and used directly by the TSPA.	10 CFR 63.311 10 CFR 63.331 10 CFR 63.321	MA

Table I-2. Model Implementation for Included Features, Events, and Processes (Continued)

Submodel implemented in the TSPA-LA Model and Section Number	Path in GoldSim Model File	FEPs Included in the Submodel	TSPA Inclusion Explanation	Performance Assessment Standard[a]	TSPA-LA Model Implementation
UZ Flow Fields Abstraction 6.3.1 (Continued)	Epistemic: \Input_Params_Epistemic\Epistemic_Params_UZ_Flow EBS: \Time_Zero\EBS_PS_Loop\Static_Calcs_PS_Loop\Static_Calcs_UZ_Flow \Global_Inputs_and_Calcs\Global_UZ_Flow	2.2.10.03.0B Natural geothermal effects on flow in the UZ	Natural geothermal effects, observed as the natural temperature profile in the UZ, are included in the Site-Scale UZ Model calibration. The temperature profile is primarily determined by the ground surface temperature, the water table temperature, water flux through the UZ, and the thermal conductivity from layer to layer. The influence of water flux on temperature is utilized to calibrate the probabilities for different surface water flux boundary conditions for the UZ Flow Model. The calibration is based on the generalized likelihood uncertainty estimation (GLUE) methodology, utilizing temperature observations and model predictions as well as chloride observations and model predictions. The probabilities for surface water flux are applied as flow weighting factors for UZ flow fields in the TSPA, which are used for present-day, monsoon, and glacial-transition, and post-10,000-year climates.	10 CFR 63.311 10 CFR 63.331 10 CFR 63.321	MA
		2.3.01.00.0A Topography and morphology	Topographical features, precipitation, and surficial permeability distribution are incorporated into the Infiltration Model. Topographical features are captured in the net Infiltration Model using digital elevation data. The impacts of topography and morphology on preferential flow and percolation in the UZ are incorporated into the TSPA through the UZ flow fields that use the net Infiltration Model results as upper boundary conditions.	10 CFR 63.311 10 CFR 63.331 10 CFR 63.321	MA
		2.3.11.01.0A Precipitation	Precipitation affects the net infiltration. Precipitation is captured in the net infiltration map outputs used as boundary condition water-flux inputs for the Site-Scale UZ Flow Model. The flow fields generated by the Site-Scale UZ Flow Model include the affects of precipitation and are used directly by the TSPA.	10 CFR 63.311 10 CFR 63.331 10 CFR 63.321	MA

Table I-2. Model Implementation for Included Features, Events, and Processes (Continued)

Submodel implemented in the TSPA-LA Model and Section Number	Path in GoldSim Model File	FEPs Included in the Submodel	TSPA Inclusion Explanation	Performance Assessment Standard[a]	TSPA-LA Model Implementation
UZ Flow Fields Abstraction 6.3.1 (Continued)	Epistemic: \Input_Params_Epistemic\Epistemic_Params_UZ_Flow EBS: \Time_Zero\EBS_PS_Loop\Static_Calcs_PS_Loop\Static_Calcs_UZ_Flow \Global_Inputs_and_Calcs\Global_UZ_Flow	2.3.11.02.0A Surface runoff and evapotranspiration	Surface runoff and flooding affect the net infiltration. These effects are captured in the net infiltration map outputs used as inputs for the Site-Scale UZ Flow Model. The flow fields generated by the Site-Scale UZ Flow Model are used directly by the TSPA.	10 CFR 63.311 10 CFR 63.331 10 CFR 63.321	MA
		2.3.11.03.0A Infiltration and recharge	The hydrologic effects of infiltration and recharge are included in the Infiltration Model. The Infiltration Model includes the effects of seasonal and climate variations, climate change, surface-water runoff, and site topology, such as hill slopes and washes. The time dependence of infiltration results are linked to the timing of climate change. These effects are captured in the net infiltration map outputs used as upper boundary condition inputs for the Site-Scale UZ Flow Model. The flow fields generated by the Site-Scale UZ Flow Model are used directly by the TSPA.	10 CFR 63.311 10 CFR 63.331 10 CFR 63.321	MA

Table I-2. Model Implementation for Included Features, Events, and Processes (Continued)

Submodel implemented in the TSPA-LA Model and Section Number	Path in GoldSim Model File	FEPs Included in the Submodel	TSPA Inclusion Explanation	Performance Assessment Standard[a]	TSPA-LA Model Implementation
Infiltration Submodel 6.3.1	Epistemic: \Input_Params_Epistemic\Epistemic_Params_UZ_Flow\Uncertain_Params_Infiltration EBS: \Time_Zero\EBS_PS_Loop\Static_Calcs_PS_Loop\Static_Calcs_UZ_Flow\Infiltration \Global_Inputs_and_Calcs\Global_UZ_Flow\Infiltration	1.4.01.01.0A Climate modification increases recharge	The effects of climate changes on UZ flux through the repository are incorporated through the explicit simulations of UZ flow fields corresponding to the 10th, 30th, 50th, and 90th percentile infiltrations of four distinct climates: present-day, monsoon, and glacial-transition, in addition to the post-10,000-year climate. **Note**: Infiltration processes are included in the TSPA-LA Model through the UZ flow fields abstraction and that the Infiltration Submodel in the TSPA-LA Model implements epistemic uncertainty in the net infiltration rates by sampling the different UZ flow fields once per realization based on the probability weighting factors as described in Section 6.3.1.3	10 CFR 63.311 10 CFR 63.331 10 CFR 63.321	GSM
Climate Submodel 6.3.1	EBS: \Global_Inputs_and_Calcs\Global_UZ_Flow\Climate Other: \TSPA_Model\UZ_Flow\Climate	1.3.01.00.0A Climate change	Global climate change is addressed in the TSPA-LA Model using a climate analysis based on the record of climate changes in the past, which is used to forecast the expected changes in climate for the future. The climate analysis is incorporated into the TSPA-LA Model through UZ flow fields having different surface-water infiltration as a result of different climates that correspond to four distinct future climate states: present-day (from 0 to 600 years after present), monsoon (from 600 to 2,000 years after present), and glacial-transition (from 2,000 to 10,000 years after present and the post-10,000-year climate.	10 CFR 63.311 10 CFR 63.331 10 CFR 63.321	GSM

Table I-2. Model Implementation for Included Features, Events, and Processes (Continued)

Submodel implemented in the TSPA-LA Model and Section Number	Path in GoldSim Model File	FEPs Included in the Submodel	TSPA Inclusion Explanation	Performance Assessment Standard[a]	TSPA-LA Model Implementation
Drift Seepage Submodel 6.3.3.1 Note: This model is not implemented for human intrusion	Epistemic: \Input_Params_Epistemic\Epistemic_Params_UZ_Flow\Input_Params_Seepage_Uncert \Input_Params_Epistemic\Epistemic_Params_UZ_Flow\Uncertain_Params_Seepage EBS: \Time_Zero\EBS_PS_Loop\Static_Calcs_PS_Loop\Static_Calcs_UZ_Flow\Drift_Seepage \Global_Inputs_and_Calcs\Global_UZ_Flow\Drift_Seepage	1.1.02.02.0A Preclosure ventilation	Preclosure ventilation in drifts will remove a considerable amount of the heat output from the waste packages (WPs). The ventilation period following emplacement is 50 years, during which a large fraction of the heat energy supplied to the rock by the waste is removed from the drifts by ventilation. This heat removal effect of preclosure ventilation is explicitly simulated with the Thermal Seepage Model. Thus, the thermal seepage modeling results inherently include these effects. The abstraction of thermal seepage utilizes these modeling results to develop a simplified thermal-seepage abstraction for the TSPA. The thermal seepage abstraction is implemented in the TSPA by setting drift seepage to zero when drift-wall temperature is greater than 100°C. Initial rock drying in the drift vicinity as a result of evaporation effects due to ventilation is not explicitly addressed, which conservatively overestimates the quantity of water available for drift seepage early in the postclosure period.	10 CFR 63.311 10 CFR 63.331	MA

Table I-2. Model Implementation for Included Features, Events, and Processes (Continued)

Submodel implemented in the TSPA-LA Model and Section Number	Path in GoldSim Model File	FEPs Included in the Submodel	TSPA Inclusion Explanation	Performance Assessment Standard[a]	TSPA-LA Model Implementation
Drift Seepage Submodel 6.3.3.1 (Continued)	Epistemic: \Input_Params_Epistemic\Epistemic_Params_UZ_Flow\Input_Params_Seepage_Uncert \Input_Params_Epistemic\Epistemic_Params_UZ_Flow\Uncertain_Params_Seepage EBS: \Time_Zero\EBS_PS_Loop\Static_Calcs_PS_Loop\Static_Calcs_UZ_Flow\Drift_Seepage \Global_Inputs_and_Calcs\Global_UZ_Flow\Drift_Seepage	1.2.02.01.0A Fractures	The seepage calibration model and seepage model for performance assessment are stochastic fracture continuum models that include fracture properties. These models provide the basis for the Seepage Abstraction Model. Fracture properties and their effects on drift seepage are included in the Drift Seepage Abstraction Model implemented in the TSPA-LA Model.	10 CFR 63.311 10 CFR 63.331	MA
		1.3.01.00.0A Climate change	The effects of climate change on seepage are included explicitly in the TSPA through the UZ flow fields that are used to evaluate the local percolation fluxes. The local percolation flux is explicitly evaluated for different climate states and different locations within the repository. The local percolation flux is used to evaluate seepage into waste emplacement drifts as provided in lookup tables from the seepage abstraction model for performance assessment.	10 CFR 63.311 10 CFR 63.331 10 CFR 63.321	GSM

Table I-2. Model Implementation for Included Features, Events, and Processes (Continued)

Submodel implemented in the TSPA-LA Model and Section Number	Path in GoldSim Model File	FEPs Included in the Submodel	TSPA Inclusion Explanation	Performance Assessment Standard[a]	TSPA-LA Model Implementation
Drift Seepage Submodel 6.3.3.1 (Continued)	Epistemic: \Input_Params_Epistemic\Epistemic_Params_UZ_Flow\Input_Params_Seepage_Uncert \Input_Params_Epistemic\Epistemic_Params_UZ_Flow\Uncertain_Params_Seepage EBS: \Time_Zero\EBS_PS_Loop\Static_Calcs_PS_Loop\Static_Calcs_UZ_Flow\Drift_Seepage \Global_Inputs_and_Calcs\Global_UZ_Flow\Drift_Seepage	1.4.01.01.0A Climate modification increases recharge	The effects of climate changes on seepage are included explicitly in the TSPA through the UZ flow fields that are used to evaluate the local percolation fluxes. The local percolation flux is explicitly evaluated for different climate states and different locations within the repository. The local percolation flux is used to evaluate seepage into waste emplacement drifts as provided in lookup tables from the seepage abstraction model for performance assessment.	10 CFR 63.311 10 CFR 63.331 10 CFR 63.321	GSM
		2.1.08.01.0A Water influx at the repository	The local percolation flux is one of the key factors affecting drift seepage and a key input to the Drift Seepage Abstraction Model. Spatial and temporal changes in the local percolation flux are thus included in the TSPA-LA Model. The local percolation flux is explicitly evaluated for different climate states and different locations within the repository. Moreover, the local percolation flux is modified to account for random, intermediate-scale flow-focusing effects and the impact of small-scale heterogeneity. The local percolation flux is used to evaluate seepage into waste emplacement drifts as provided in lookup tables from the seepage abstraction model for performance assessment.	10 CFR 63.311 10 CFR 63.331	DLL
		2.1.08.02.0A Enhanced influx at the repository	The impact of an underground opening on the unsaturated flow field (including capillary barrier effect and the related flow diversion around the drifts) and its relevance for seepage is explicitly captured in the seepage calibration model and seepage model for performance assessment, which provide the basis for the drift seepage abstraction implementation in the TSPA-LA Model.	10 CFR 63.311 10 CFR 63.331	DLL

Table I-2. Model Implementation for Included Features, Events, and Processes (Continued)

Submodel implemented in the TSPA-LA Model and Section Number	Path in GoldSim Model File	FEPs Included in the Submodel	TSPA Inclusion Explanation	Performance Assessment Standard[a]	TSPA-LA Model Implementation
Drift Seepage Submodel 6.3.3.1 (Continued)	Epistemic: \Input_Params_Epistemic\Epistemic_Params_UZ_Flow\Input_Params_Seepage_Uncert \Input_Params_Epistemic\Epistemic_Params_UZ_Flow\Uncertain_Params_Seepage EBS: \Time_Zero\EBS_PS_Loop\Static_Calcs_PS_Loop\Static_Calcs_UZ_Flow\Drift_Seepage \Global_Inputs_and_Calcs\Global_UZ_Flow\Drift_Seepage	2.1.08.03.0A Repository dryout due to waste heat	The process of dryout due to waste heat is explicitly simulated with the thermal seepage model. Using this model, the impact of such coupled processes on seepage is assessed for various simulation cases. These simulations provide the basis for the simplified thermal seepage abstraction implemented in the TSPA-LA Model (i.e., no seepage when the drift-wall temperature is greater than 100°C, and ambient seepage when the drift wall temperature is less than 100°C. Thus, the thermal seepage modeling results inherently include these effects.	10 CFR 63.311 10 CFR 63.331	GSM
		2.1.08.11.0A Repository resaturation due to waste cooling	The Thermal Seepage Model includes dryout of the repository followed by resaturation as the WPs cool. The Thermal Seepage Model provides the technical basis for the thermal seepage abstraction implemented in the TSPA-LA Model. The thermal seepage abstraction is implemented by setting drift seepage to zero when drift-wall temperature is greater than 100°C and to ambient seepage when the drift wall temperature is less than 100°C.	10 CFR 63.311 10 CFR 63.331	MA

Table I-2. Model Implementation for Included Features, Events, and Processes (Continued)

Submodel implemented in the TSPA-LA Model and Section Number	Path in GoldSim Model File	FEPs Included in the Submodel	TSPA Inclusion Explanation	Performance Assessment Standard[a]	TSPA-LA Model Implementation
Drift Seepage Submodel 6.3.3.1 (Continued)	Epistemic: \Input_Params_Epistemic\Epistemic_Params_UZ_Flow\Input_Params_Seepage_Uncert \Input_Params_Epistemic\Epistemic_Params_UZ_Flow\Uncertain_Params_Seepage EBS: \Time_Zero\EBS_PS_Loop\Static_Calcs_PS_Loop\Static_Calcs_UZ_Flow\Drift_Seepage \Global_Inputs_and_Calcs\Global_UZ_Flow\Drift_Seepage	2.1.11.01.0A Heat generation in EBS	Heat generation is explicitly simulated in the Thermal Seepage Model that provides the technical basis for the thermal seepage abstraction implemented in the TSPA-LA Model. The thermal seepage abstraction is implemented by setting drift seepage to zero when drift wall temperature is greater than 100°C and to ambient seepage when the drift-wall temperature is less than 100°C.	10 CFR 63.311 10 CFR 63.331 10 CFR 63.321	MA
		2.2.01.01.0A Mechanical effects of excavation and construction in the near field	Excavation effects and their impacts on seepage are included in the thermal and ambient drift seepage process models for through the use of seepage-relevant parameters calibrated for the excavation-disturbed zone around niches and drifts. These models and properties are used to develop the Drift Seepage Abstraction for implementation in the TSPA-LA Model.	10 CFR 63.311 10 CFR 63.331	MA
		2.2.07.02.0A Unsaturated groundwater flow in the geosphere	The impact of unsaturated flow at the repository level on seepage is included in the TSPA-LA Model through the use of local percolation fluxes, which are derived from site-scale unsaturated flow fields, intermediate-scale flow-focusing factors, and small-scale flow simulations with a heterogeneous fracture permeability field.	10 CFR 63.311 10 CFR 63.331	DLL
		2.2.07.03.0A Capillary rise in the UZ	Capillary forces and their impact on seepage are explicitly included in the thermal and ambient Drift Seepage process models. These models are used to generate simulations of capillary- and gravity-driven water flow toward, around, and into waste emplacement drifts. These simulations are used as the basis for the Drift Seepage Abstraction for implementation in the TSPA-LA Model.	10 CFR 63.311 10 CFR 63.331	MA

Table I-2. Model Implementation for Included Features, Events, and Processes (Continued)

Submodel implemented in the TSPA-LA Model and Section Number	Path in GoldSim Model File	FEPs Included in the Submodel	TSPA Inclusion Explanation	Performance Assessment Standard[a]	TSPA-LA Model Implementation
Drift Seepage Submodel 6.3.3.1 (Continued)	Epistemic: \Input_Params_Epistemic\Epistemic_Params_UZ_Flow\Input_Params_Seepage_Uncert \Input_Params_Epistemic\Epistemic_Params_UZ_Flow\Uncertain_Params_Seepage EBS: \Time_Zero\EBS_PS_Loop\Static_Calcs_PS_Loop\Static_Calcs_UZ_Flow\Drift_Seepage \Global_Inputs_and_Calcs\Global_UZ_Flow\Drift_Seepage	2.2.07.04.0A Focusing of unsaturated flow (fingers, weeps)	The site-scale UZ flow fields represent the large-scale redistribution of infiltrating water as it percolates through hydrogeologic layers, with matrix, fractures, and faults explicitly taken into account. Intermediate-scale focusing of flow from the site scale to the drift scale is accounted for in the drift seepage abstraction by using a distribution of flow-focusing factors, which were determined from high-resolution simulations of flow in a heterogeneous fracture continuum. Preferential flow induced by small-scale heterogeneity is explicitly accounted for in the suite of seepage process models that feed the drift seepage abstraction and TSPA by using multiple, stochastic, heterogeneous fracture permeability fields. Thus, preferential flow is addressed in the seepage lookup tables and in the thermal component of the drift seepage abstraction.	10 CFR 63.311 10 CFR 63.331	DLL
		2.2.07.08.0A Fracture flow in the UZ	Fractures as potential conduits for fluid flow are explicitly accounted for in the Site-Scale UZ Flow Model providing the large-scale percolation flux distribution and the drift seepage process models used to evaluate seepage under ambient and thermal conditions. The fact that water may only flow through a portion of the fracture network is accounted for through the use of (1) the active fracture model (on the site-scale), (2) flow-focusing factors (on the intermediate scale), and (3) explicit simulation of preferential flow (on the drift scale). Thus, fracture flow and its spatial distribution are embedded in the lookup tables for seepage and propagated to TSPA.	10 CFR 63.311 10 CFR 63.331 10 CFR 63.321	DLL

Table I-2. Model Implementation for Included Features, Events, and Processes (Continued)

Submodel implemented in the TSPA-LA Model and Section Number	Path in GoldSim Model File	FEPs Included in the Submodel	TSPA Inclusion Explanation	Performance Assessment Standard[a]	TSPA-LA Model Implementation
Drift Seepage Submodel 6.3.3.1 (Continued)	Epistemic: \Input_Params_Epistemic\Epistemic_Params_UZ_Flow\Input_Params_Seepage_Uncert \Input_Params_Epistemic\Epistemic_Params_UZ_Flow\Uncertain_Params_Seepage EBS: \Time_Zero\EBS_PS_Loop\Static_Calcs_PS_Loop\Static_Calcs_UZ_Flow\Drift_Seepage \Global_Inputs_and_Calcs\Global_UZ_Flow\Drift_Seepage	2.2.07.09.0A Matrix imbibition in the UZ	Imbibition of water into the matrix is included in the UZ Flow Model which provides the percolation flux for the drift seepage process models, however, the ambient seepage models are stochastic fracture continuum models. The impact of the matrix on seepage during both the liquid-release tests used for model calibration and the calculation of steady-state ambient seepage into waste emplacement drifts is considered small enough that it can be lumped into seepage-relevant parameters applied to the fracture continuum. The Thermal Seepage Model, on the other hand, includes the rock matrix because the matrix impacts heat transfer and provides a source for water that evaporates during above-boiling temperature conditions. Thus, matrix imbibition is embedded in the lookup tables for the seepage abstraction implemented in the TSPA-LA Model.	10 CFR 63.311 10 CFR 63.331	MA
		2.2.07.10.0A Condensation zone forms around drifts	The coupled thermal-hydrologic processes of vapor condensation during the thermal period, which potentially leads to water accumulation above the drifts and shedding between drifts, is explicitly simulated with the Thermal Seepage Model that provides the basis for a simplified thermal drift seepage abstraction in the TSPA-LA Model. The Thermal seepage abstraction is implemented in the TSPA-LA Model by setting drift seepage to zero when drift wall temperature is greater than 100°C.	10 CFR 63.311 10 CFR 63.331	DLL

Table I-2. Model Implementation for Included Features, Events, and Processes (Continued)

Submodel implemented in the TSPA-LA Model and Section Number	Path in GoldSim Model File	FEPs Included in the Submodel	TSPA Inclusion Explanation	Performance Assessment Standard[a]	TSPA-LA Model Implementation
Drift Seepage Submodel 6.3.3.1 (Continued)	Epistemic: \Input_Params_Epistemic\Epistemic_Params_UZ_Flow\Input_Params_Seepage_Uncert \Input_Params_Epistemic\Epistemic_Params_UZ_Flow\Uncertain_Params_Seepage EBS: \Time_Zero\EBS_PS_Loop\Static_Calcs_PS_Loop\Static_Calcs_UZ_Flow\Drift_Seepage \Global_Inputs_and_Calcs\Global_UZ_Flow\Drift_Seepage	2.2.07.11.0A Resaturation of geosphere dry-out zone	Resaturation of the dryout zone around drifts and the potential of return flow from the condensation zone back to the drifts are explicitly simulated in the Thermal Seepage Model that feeds into the seepage abstraction implemented in the TSPA-LA Model. Thus, the thermal seepage modeling results inherently include these effects. The abstraction of thermal seepage utilizes these modeling results to develop an appropriate thermal seepage abstraction methodology. The thermal seepage abstraction is implemented in the TSPA-LA Model by setting drift seepage to zero when drift-wall temperature is greater than 100°C.	10 CFR 63.311 10 CFR 63.331	DLL
		2.2.07.18.0A Film flow into the repository	The impact of film flow through the fracture network leading to potential drop detachment at the drift wall is implicitly accounted for in the seepage-relevant parameters estimated by the seepage calibration model, which is calibrated against seepage-rate data from liquid-release tests. These seepage-rate data include film flow water appearing at and detaching from the drift wall. The seepage-relevant parameters thus include the effect of film flow; these parameters are propagated to the Drift Seepage Abstraction Model that is implemented in the TSPA-LA Model.	10 CFR 63.311 10 CFR 63.331	MA

Table I-2. Model Implementation for Included Features, Events, and Processes (Continued)

Submodel implemented in the TSPA-LA Model and Section Number	Path in GoldSim Model File	FEPs Included in the Submodel	TSPA Inclusion Explanation	Performance Assessment Standard[a]	TSPA-LA Model Implementation
Drift Seepage Submodel 6.3.3.1 (Continued)	Epistemic: \Input_Params_Epistemic\Epistemic_Params_UZ_Flow\Input_Params_Seepage_Uncert \Input_Params_Epistemic\Epistemic_Params_UZ_Flow\Uncertain_Params_Seepage EBS: \Time_Zero\EBS_PS_Loop\Static_Calcs_PS_Loop\Static_Calcs_UZ_Flow\Drift_Seepage \Global_Inputs_and_Calcs\Global_UZ_Flow\Drift_Seepage	2.2.07.20.0A Flow diversion around repository drifts	The impact of flow diversion around underground openings and its relevance for seepage are explicitly captured by the suite of seepage process models that provide the technical basis for the drift seepage abstraction implemented in the TSPA-LA Model. The seepage calibration model and seepage model for performance assessment simulate water flow driven by capillary forces and gravity, which are the main processes leading to flow diversion around and seepage into waste emplacement drifts. Site-specific, seepage-relevant parameters characterizing the capillary-barrier and flow-diversion effects are estimated from seepage-rate data and are used to develop the Drift Seepage Abstraction Model that is implemented in the TSPA-LA Model.	10 CFR 63.311 10 CFR 63.331	DLL
		2.2.10.03.0B Natural geothermal effects on flow in the UZ	The natural geothermal gradient in the UZ is explicitly included in boundary conditions for the Thermal Seepage Model in Drift-Scale Coupled Processes (DST and TH Seepage) Models (BSC 2005 [DIRS 172232], Section 6.5.2). Using this model, the impact of thermal and coupled processes on seepage is assessed for various simulation cases. These simulations provide the basis for the simplified thermal seepage abstraction implemented in the TSPA-LA Model (i.e., no seepage when the drift wall temperature is greater than 100°C, and ambient seepage when the drift wall temperature is less than 100°C). Thus, the seepage abstraction model implemented in the TSPA-LA Model inherently includes the effects of the natural thermal gradient in the UZ.	10 CFR 63.311 10 CFR 63.331	GSM

Table I-2. Model Implementation for Included Features, Events, and Processes (Continued)

Submodel implemented in the TSPA-LA Model and Section Number	Path in GoldSim Model File	FEPs Included in the Submodel	TSPA Inclusion Explanation	Performance Assessment Standard[a]	TSPA-LA Model Implementation
Drift Seepage Submodel 6.3.3.1 (Continued)	Epistemic: \Input_Params_Epistemic\Epistemic_Params_UZ_Flow\Input_Params_Seepage_Uncert \Input_Params_Epistemic\Epistemic_Params_UZ_Flow\Uncertain_Params_Seepage EBS: \Time_Zero\EBS_PS_Loop\Static_Calcs_PS_Loop\Static_Calcs_UZ_Flow\Drift_Seepage \Global_Inputs_and_Calcs\Global_UZ_Flow\Drift_Seepage	2.2.10.10.0A Two-phase buoyant flow/heat pipes	The coupled processes causing heat-pipe behavior are explicitly simulated with the thermal seepage model that provides the basis for the simplified thermal seepage abstraction implemented in the TSPA-LA Model (i.e., no seepage when the drift wall temperature is greater than 100°C and ambient seepage when the drift-wall temperature is less than 100°C).	10 CFR 63.311 10 CFR 63.331	GSM
		2.2.10.12.0A Geosphere dryout due to waste heat	The coupled processes of vaporization, dryout, and resaturation are explicitly simulated with the Thermal Seepage Model. Using this model, the impact of such coupled processes on seepage is assessed for various simulation cases. These simulations provide the basis for the simplified thermal seepage abstraction implemented in the TSPA-LA Model (i.e., no seepage when the drift-wall temperature is greater than 100°C and ambient seepage when the drift wall temperature is less than 100°C.).	10 CFR 63.311 10 CFR 63.331	GSM

Table I-2. Model Implementation for Included Features, Events, and Processes (Continued)

Submodel implemented in the TSPA-LA Model and Section Number	Path in GoldSim Model File	FEPs Included in the Submodel	TSPA Inclusion Explanation	Performance Assessment Standard[a]	TSPA-LA Model Implementation
Drift Seepage Submodel 6.3.3.1 (Continued)	Epistemic: \Input_Params_Epistemic\Epistemic_Params_UZ_Flow\Input_Params_Seepage_Uncert \Input_Params_Epistemic\Epistemic_Params_UZ_Flow\Uncertain_Params_Seepage EBS: \Time_Zero\EBS_PS_Loop\Static_Calcs_PS_Loop\Static_Calcs_UZ_Flow\Drift_Seepage \Global_Inputs_and_Calcs\Global_UZ_Flow\Drift_Seepage	2.2.03.01.0A Stratigraphy	Stratigraphic information is used in the TSPA-LA Model to evaluate seepage into waste emplacement drifts located in specific hydrogeologic units. Seepage-relevant parameters (permeability and capillary strength) are evaluated separately for lithophysal and nonlithophysal rock units, and the percolation flux used to determine seepage is taken from the UZ flow fields, which incorporate stratigraphic information. Seepage is evaluated for specific repository locations, capturing their respective host rock unit.	10 CFR 63.311 10 CFR 63.331	MA
		2.2.03.02.0A Rock properties of host rock and other units	Properties affecting seepage are defined for each of the repository rock units. The impact of intermediate-scale heterogeneity on flow and seepage is included through the use of flow-focusing factors; the impact of small-scale heterogeneity is explicitly modeled in the seepage calibration model and the seepage abstraction model for performance assessment, which provide the basis for the seepage evaluation in the TSPA-LA Model. The impact of potential changes in the physical properties as a result of coupled thermal, mechanical, and chemical processes has been evaluated and considered insignificant.	10 CFR 63.311 10 CFR 63.331	MA

Table I-2. Model Implementation for Included Features, Events, and Processes (Continued)

Submodel implemented in the TSPA-LA Model and Section Number	Path in GoldSim Model File	FEPs Included in the Submodel	TSPA Inclusion Explanation	Performance Assessment Standard[a]	TSPA-LA Model Implementation
Drift Seepage Submodel 6.3.3.1 (Continued)		2.3.11.03.0A Infiltration and recharge	The infiltration process is simulated by the net infiltration model MASSIF, which includes the effects of climate variations. The infiltration model output is in the form of infiltration maps that are used to provide input to the UZ flow model, which simulates the spatial distribution of percolation fluxes within the unsaturated zone. Percolation fluxes are used to calculate seepage fluxes into the repository by TSPA.	10 CFR 63.311 10 CFR 63.331	MA
Drift Wall Condensation Submodel 6.3.3.2 This model is not implemented in human intrusion	Epistemic: \Input_Params_Epistemic\Epistemic_Params_UZ_Flow\Uncertain_Params_DWC EBS: \Global_Inputs_and_Calcs\Global_UZ_Flow\Drift_Wall_Condensation	1.1.02.02.0A Preclosure ventilation	A 50-year preclosure period with ventilation, as abstracted in the Ventilation Model and Analysis Report is included at the beginning of the MSTHM analyses and is accounted for in the input to the TSPA model. The ventilation model and the MSTHM therefore address the effect of ventilation on the removal of waste package heat during the preclosure period. The TSPA model uses the abstraction results starting at the time of closure (at the end of the ventilation period).	10 CFR 63.311 10 CFR 63.331	GSM
		1.3.01.00.0A Climate Change	The effects of climate change on drift wall condensation are included in the TSPA through the UZ flow fields, which are used to evaluate the local percolation fluxes. The local percolation flux is explicitly evaluated for different climate states and different locations within the repository.	10 CFR 63.311 10 CFR 63.331	GSM
		1.4.01.01.0A Climate modification increases recharge	The effects of climate changes are included explicitly in the TSPA through the UZ flow fields developed by the Site-Scale UZ Flow Model. These flow fields are used to evaluate the t local percolation flux. The local percolation flux is an input to the drift-wall condensation model implemented in the TSPA-LA Model and is evaluated for different climate states and different locations within the repository.	10 CFR 63.311 10 CFR 63.331	GSM

Table I-2. Model Implementation for Included Features, Events, and Processes (Continued)

Submodel implemented in the TSPA-LA Model and Section Number	Path in GoldSim Model File	FEPs Included in the Submodel	TSPA Inclusion Explanation	Performance Assessment Standard[a]	TSPA-LA Model Implementation
Drift Wall Condensation Submodel 6.3.3.2 (Continued)	Epistemic: \Input_Params_Epistemic\Epistemic_Params_UZ_Flow\Uncertain_Params_DWC EBS: \Global_Inputs_and_Calcs\Global_UZ_Flow\Drift_Wall_Condensation	2.1.06.06.0A Effects of drip shield on flow	The role of the drip shield on flow processes in the in-drift environment is implemented in the TSPA-LA Model through the in-drift natural convection and condensation model, which develops a computational fluid dynamics model of natural convection during the postclosure period. The drift wall condensation rate is combined with the drift seepage rate in the EBS flow submodel to yield a total dripping rate onto the drip shield in the TSPA. The fraction of the total dripping rate that is diverted by the drip shield when breaches in the drip shield exist is also calculated in the TSPA using the EBS flow model.	10 CFR 63.311 10 CFR 63.331	MA
		2.1.08.01.0A Water influx at the repository	Water influx at the repository is included explicitly in the TSPA through the UZ flow fields developed by the Site-Scale UZ Flow Model. These flow fields are used to evaluate the local percolation flux. The local percolation flux is an input to the drift-wall condensation model implemented in the TSPA-LA Model and is evaluated for different climate states and different locations within the repository.	10 CFR 63.311 10 CFR 63.331	GSM
		2.1.08.04.0A Condensation forms on roofs of drifts (drift-scale cold traps)	The coupled processes of vapor condensation forming condensation and cold traps on the drift walls are simulated with the in-drift condensation process model. Using this model, the impact of condensation and its contributions to seepage are assessed for various simulation cases. These simulations are used to develop the drift-wall condensation abstraction model implemented in the TSPA-LA Model.	10 CFR 63.311 10 CFR 63.331	GSM

Table I-2. Model Implementation for Included Features, Events, and Processes (Continued)

Submodel implemented in the TSPA-LA Model and Section Number	Path in GoldSim Model File	FEPs Included in the Submodel	TSPA Inclusion Explanation	Performance Assessment Standard[a]	TSPA-LA Model Implementation
Drift Wall Condensation Submodel 6.3.3.2 (Continued)	Epistemic: \Input_Params_Epistemic\Epistemic_Params_UZ_Flow\Uncertain_Params_DWC EBS: \Global_Inputs_and_Calcs\Global_UZ_Flow\Drift_Wall_Condensation	2.1.08.04.0B Condensation forms at repository edges (repository-scale cold traps)	Condensation at the repository edges is included in the TSPA through application of the in-drift condensation model, which provides correlation functions representing the probability of condensation on the drift wall, and the magnitude of condensation where it occurs. This abstraction is used in conjunction with the abstracted output from the MSTHM, which describes the temperature evolution at WP locations. Condensation can occur only where the drift-wall temperature has cooled through the local boiling temperature (96°C), which happens first near the repository edges. The condensation rate is generally greater on cooler WPs, and the effect of repository edge cooling on drift-wall temperature is represented in the in-drift condensation model. The implementation in the TSPA uses repository-wide condensation frequency and magnitude distributions, which are not specific to WP location, applied to representative WPs based on correlation with percolation flux. The effect of repository-scale edge cooling on condensation is thus included in the TSPA-LA Model, in order to represent the potential effects on radionuclide transport in the invert and transport coupling to the UZ.	10 CFR 63.311 10 CFR 63.331	GSM
		2.1.11.01.0A Heat generation in EBS	The in-drift natural convection and condensation model uses an averaged line-load to calculate the wall temperatures through a heated drift and the individual heat generation rates for different packages to calculate the temperatures of the individual packages.	10 CFR 63.311 10 CFR 63.331	GSM

Table I-2. Model Implementation for Included Features, Events, and Processes (Continued)

Submodel implemented in the TSPA-LA Model and Section Number	Path in GoldSim Model File	FEPs Included in the Submodel	TSPA Inclusion Explanation	Performance Assessment Standard[a]	TSPA-LA Model Implementation
Drift Wall Condensation Submodel 6.3.3.2 (Continued)	Epistemic: \Input_Params_Epistemic\Epistemic_Params_UZ_Flow\Uncertain_Params_DWC EBS: \Global_Inputs_and_Calcs\Global_UZ_Flow\Drift_Wall_Condensation	2.1.11.02.0A Non-uniform heat distribution in EBS	Non-uniform heat distribution in EBS is included in the TSPA through application of the in-drift condensation model, which calculates a probability of condensate on the drift walls at any location and, if condensation occurs, the rate of condensation. The probability of occurrence of condensation and the condensation rate are abstracted as functions of the percolation flux.	10 CFR 63.311 10 CFR 63.331	GSM
		2.1.03.11.0A Physical form of waste package and drip shield	The effects of heat dissipation from the waste package and its impact on drift wall condensation are addressed in the in-drift natural convection and condensation process model implemented in the TSPA-LA Model.	10 CFR 63.311 10 CFR 63.331	MA
		2.1.11.09.0A Thermal effects on flow in the EBS	Thermal gradients in the repository could lead to localized accumulation of moisture within the cooler regions of the emplacement drifts. Such effects are represented in the TSPA by the condensation model. The abstraction of the condensation model defines the condensation rate and the likelihood of condensation on the drift wall, under the drip shield (DS), and on the WPs, and the rate of condensation should it occur. The condensation abstraction includes algorithms used in the TSPA for interpolating the condensation rates and probabilities, and specifies how parameters are used and where they are obtained.	10 CFR 63.311 10 CFR 63.331	GSM

Table I-2. Model Implementation for Included Features, Events, and Processes (Continued)

Submodel implemented in the TSPA-LA Model and Section Number	Path in GoldSim Model File	FEPs Included in the Submodel	TSPA Inclusion Explanation	Performance Assessment Standard[a]	TSPA-LA Model Implementation
Drift Wall Condensation Submodel 6.3.3.2 (Continued)	Epistemic: \Input_Params_Epistemic\Epistemic_Params_UZ_Flow\Uncertain_Params_DWC EBS: \Global_Inputs_and_Calcs\Global_UZ_Flow\Drift_Wall_Condensation	2.1.11.09.0C Thermally driven flow (convection) in drifts	The in-drift natural convection and condensation submodel includes explicit representation of two-dimensional and three-dimensional natural convection driven by temperature differences. Results from this model are used to develop an effective thermal conductivity for air that captures the heat transfer effects from natural convection, and is subsequently used in submodels of MSTHM. Temperature and relative humidity conditions derived from the MSTHM are used in the TSPA-LA Model calculations.	10 CFR 63.311 10 CFR 63.331	GSM
		2.3.11.03.0A Infiltration and recharge	Percolation fluxes are used to calculate seepage fluxes into the repository and condensation onto the drift walls. These processes are all affected by changes in infiltration, which are modeled in TSPA in the form of infiltration maps. The infiltration maps provide input to the UZ flow model, which calculates the spatial distribution of percolation fluxes within the unsaturated zone. The probability of occurrence and the rate of condensation on drift walls are abstracted in the TSPA-LA Model as functions of the percolation flux.	10 CFR 63.311 10 CFR 63.331	MA

Table I-2. Model Implementation for Included Features, Events, and Processes (Continued)

Submodel implemented in the TSPA-LA Model and Section Number	Path in GoldSim Model File	FEPs Included in the Submodel	TSPA Inclusion Explanation	Performance Assessment Standard[a]	TSPA-LA Model Implementation
EBS TH Environment Submodel 6.3.2	Epistemic: \Input_Params_Epistemic\Epistemic_Params_EBS_Environ\Uncertain_Params_TH EBS: \Global_Inputs_and_Calcs\Global_EBS_Environ\EBS_Environment\ThermoHydrology	1.1.02.02.0A Preclosure ventilation	Preclosure ventilation in drifts will remove a considerable amount of the heat output from the WPs. The ventilation period following emplacement is 50 years, during which a large fraction of the heat energy supplied to the rock by the waste is removed from the drifts by ventilation. This heat removal effect of preclosure ventilation is explicitly simulated with the MSTHM Process Model. Thus, the thermal-hydrologic modeling results inherently include these effects. The abstraction of thermal-hydrologic processes utilizes these modeling results to develop a simplified thermal-hydrologic abstraction that is implemented in the TSPA-LA Model.	10 CFR 63.311 10 CFR 63.331 10 CFR 63.321	MA
		1.2.02.01.0A Fractures	Fractures are included in MSTHM Process Model for predicting conditions in the EBS. The MSTHM Process Model is based on a dual-permeability concept, with fractures represented by a continuum. The fracture continuum represents the spatially averaged flow and heat transfer through discrete fractures. The fracture continuum interacts with the matrix continuum, which represents matrix blocks separated by fracture. Output results from the Multiscale Thermohydrologic process model are used to develop the TH abstraction implemented in the TSPA-LA Model.	10 CFR 63.311 10 CFR 63.331 10 CFR 63.321	MA
		1.3.01.00.0A Climate change	The effects of climate changes on TH conditions are included in the TSPA through the UZ flow fields, which are used to evaluate the local percolation fluxes. The local percolation flux is explicitly evaluated for different climate states and different locations within the repository. The local percolation flux is used to provide a flux boundary condition for the MSTHM process model. Output results from the MSTHM process model are used to develop the MSTHM abstraction that is implemented in the TSPA-LA Model.	10 CFR 63.311 10 CFR 63.331 10 CFR 63.321	GSM

Table I-2. Model Implementation for Included Features, Events, and Processes (Continued)

Submodel implemented in the TSPA-LA Model and Section Number	Path in GoldSim Model File	FEPs Included in the Submodel	TSPA Inclusion Explanation	Performance Assessment Standard[a]	TSPA-LA Model Implementation
EBS TH Environment Submodel 6.3.2 (Continued)	Epistemic: \Input_Params_Epistemic\Epistemic_Params_EBS_Environ\Uncertain_Params_TH EBS: \Global_Inputs_and_Calcs\Global_EBS_Environ\EBS_Environment\ThermoHydrology	1.4.01.01.0A Climate modification increases recharge	The effects of climate changes on UZ flux through the repository are incorporated through the explicit simulations of UZ flow fields using the Site-Scale UZ Flow Model corresponding to the 10th, 30th, 50th, and 90th percentile infiltration cases of four different climates: present-day, monsoon, and glacial-transition, and the post-10,000 year climate. MSTHM process model simulations are implemented for each of these infiltration cases using the UZ flow fields to prescribe boundary condition water fluxes at the top of the MSTHM process model domain. These simulations are used to develop the TH abstraction implemented in the TSPA-LA Model.	10 CFR 63.311 10 CFR 63.331 10 CFR 63.321	GSM
		2.1.03.11.0A Physical form of waste package and drip shield	Physical form of waste package and drip shield and its relevance for TH conditions in the EBS are explicitly captured in the MSTHM process model simulations. The MSTH process model captures repository thermal conditions during post-closure. These processes are reflected in model output variables of temperature in the near field host rock. Multiscale TH process simulations are used to develop the TH abstraction implemented in the TSPA-LA Model.	10 CFR 63.311 10 CFR 63.331 10 CFR 63.321	MA
		2.1.08.01.0A Water influx at the repository	Water influx at the repository is included explicitly in the TSPA through the UZ flow fields developed by the Site-Scale UZ Flow Model. These flow fields are used to evaluate the t local percolation flux. The local percolation flux is used to provide the upper water flux boundary condition for the MSTHM process model simulations. These simulations are used to develop the TH abstraction model implemented in the TSPA-LA Model.	10 CFR 63.311 10 CFR 63.331 10 CFR 63.321	GSM

Table I-2. Model Implementation for Included Features, Events, and Processes (Continued)

Submodel implemented in the TSPA-LA Model and Section Number	Path in GoldSim Model File	FEPs Included in the Submodel	TSPA Inclusion Explanation	Performance Assessment Standard[a]	TSPA-LA Model Implementation
EBS TH Environment Submodel 6.3.2 (Continued)	Epistemic: \Input_Params_Epistemic\Epistemic_Params_EBS_Environ\Uncertain_Params_TH EBS: \Global_Inputs_and_Calcs\Global_EBS_Environ\EBS_Environment\ThermoHydrology	2.1.08.03.0A Repository dryout due to waste heat	The impact of repository dryout due to waste heat and its relevance for TH conditions in the EBS are explicitly captured in the MSTHM process model simulations. The MSTH process model captures repository dryout during the heating phase and rewetting during the cooling phase. These processes are reflected in model output variables of temperature and liquid-phase flux in the near field host rock. Multiscale TH process simulations are used to develop the TH abstraction implemented in the TSPA-LA Model.	10 CFR 63.311 10 CFR 63.331 10 CFR 63.321	GSM
		2.1.08.05.0A Flow through Invert	Flow through the invert is included in the TSPA through the use of two models: the radionuclide transport abstraction and the MSTHM. The radionuclide transport abstraction is implemented directly within the TSPA to simulate the flow pathways through the EBS. Flow through the invert consists of flux diverted by the DS and by the WP and the flux through the WP, and is reduced by any evaporation from the invert. Water saturation and water flux through the invert, for the case of no drift seepage or condensation, is provided to TSPA by the MSTHM abstraction model, which includes capillary wicking from the host rock. In the human intrusion assessment flow and transport from the WP through the EBS is within the borehole, so the human intrusion assessment does not apply.	10 CFR 63.311 10 CFR 63.331	GSM

Table I-2. Model Implementation for Included Features, Events, and Processes (Continued)

Submodel implemented in the TSPA-LA Model and Section Number	Path in GoldSim Model File	FEPs Included in the Submodel	TSPA Inclusion Explanation	Performance Assessment Standard[a]	TSPA-LA Model Implementation
EBS TH Environment Submodel 6.3.2 (Continued)	Epistemic: \Input_Params_Epistemic\Epistemic_Params_EBS_Environ\Uncertain_Params_TH EBS: \Global_Inputs_and_Calcs\Global_EBS_Environ\EBS_Environment\ThermoHydrology	2.1.08.06.0A Capillary effects (wicking) in EBS	The MSTHM process model includes the processes that cause wicking from the host rock to the invert. The MSTHM process model results provide the basis for the MSTHM abstraction implemented in the TSPA. This abstraction also provides input to the radionuclide transport abstraction, which is implemented directly in the TSPA-LA Model to evaluate the fluxes through the invert. Capillary effects are included in all three assessments. However, capillary effects associated with the invert and water flux through the invert are not included in the human intrusion assessment. In the human intrusion assessment flow and transport from the WP through the EBS is within the borehole.	10 CFR 63.311 10 CFR 63.331	MA
		2.1.08.11.0A Repository resaturation due to waste cooling	The MSTHM process model includes processes controlling dryout of the repository followed by resaturation as the WPs cool. Dryout and resaturation effects are captured by running simulations for all climate states and infiltration cases. Results of these simulations are used to develop the MSTHM abstraction that is implemented in the TSPA-LA Model to predict relative humidity, temperature, and liquid saturations and fluxes, inside the emplacement drift.	10 CFR 63.311 10 CFR 63.331 10 CFR 63.321	GSM
		2.1.11.01.0A Heat generation in EBS	Heat generation and its thermal effects on TH environment in the EBS are calculated by the MSTHM process model. The thermal effects on TH are assessed by multiple MSTHM process model simulations. These simulations are used to develop the TH Abstraction implemented in the TSPA-LA Model.	10 CFR 63.311 10 CFR 63.331 10 CFR 63.321	GSM

Table I-2. Model Implementation for Included Features, Events, and Processes (Continued)

Submodel implemented in the TSPA-LA Model and Section Number	Path in GoldSim Model File	FEPs Included in the Submodel	TSPA Inclusion Explanation	Performance Assessment Standard[a]	TSPA-LA Model Implementation
EBS TH Environment Submodel 6.3.2 (Continued)	Epistemic: \Input_Params_Epistemic\Epistemic_Params_EBS_Environ\Uncertain_Params_TH EBS: \Global_Inputs_and_Calcs\Global_EBS_Environ\EBS_Environment\ThermoHydrology	2.1.11.02.0A Non-uniform heat distribution in EBS	The MSTHM process model predicts the repository thermal-hydrologic environment, including thermal gradients from the repository center to the edges and corners of the repository. Thus, the impact of uneven heating and cooling during both the thermal peak and the cool-down period is captured in the MSTHM process model outputs (e.g., temperature and relative humidity). These outputs are used to develop the MSTHM abstraction used by the TSPA.	10 CFR 63.311 10 CFR 63.331 10 CFR 63.321	GSM
		2.1.11.09.0A Thermal effects on flow in the EBS	Thermal effects on flow in the EBS are calculated by the MSTHM process model. Water flow within the drift is influenced by temperature and evaporation. Water fluxes in the invert are influenced by temperature and capillary pressure (wicking) processes. The thermal effects on flow are assessed by multiple MSTHM process model simulations. These simulations are used to develop the MSTHM Abstraction implemented in the TSPA-LA Model.	10 CFR 63.311 10 CFR 63.331 10 CFR 63.321	GSM
		2.1.11.09.0C Thermally driven flow (convection) in drifts	The MSTHM process model uses an average equivalent thermal conductivity correlation that is based on convection analyses. The effects of convection (in two-dimensional drift cross section) are assessed by multiple MSTHM process model simulations. These simulations are used to develop the MSTHM Abstraction implemented in the TSPA-LA Model.	10 CFR 63.311 10 CFR 63.331 10 CFR 63.321	GSM

Table I-2. Model Implementation for Included Features, Events, and Processes (Continued)

Submodel implemented in the TSPA-LA Model and Section Number	Path in GoldSim Model File	FEPs Included in the Submodel	TSPA Inclusion Explanation	Performance Assessment Standard[a]	TSPA-LA Model Implementation
EBS TH Environment Submodel 6.3.2 (Continued)	Epistemic: \Input_Params_Epistemic\Epistemic_Params_EBS_Environ\Uncertain_Params_TH EBS: \Global_Inputs_and_Calcs\Global_EBS_Environ\EBS_Environment\ThermoHydrology	2.2.03.01.0A Stratigraphy	This FEP is included in the UZ flow model by use of the grids developed with the information contained in the geologic framework model. The stratigraphic unit and layers are developed into the UZ flow model grid. Since the assignment of hydrologic properties is associated with the grid used for the UZ flow model, the stratigraphy information is embedded in the TSPA through the output flow fields. The Multiscale Thermohydrologic models Process Model uses the flow fields to define the upper flux boundary condition, as well as the grid layers from the UZ flow model. Output results from the MSTHM process model are used to develop the MSTHM abstraction that is implemented in the TSPA-LA Model.	10 CFR 63.311 10 CFR 63.331 10 CFR 63.321	MA
		2.2.03.02.0A Rock properties of host rock and other units	Rock properties used are defined for each of the stratigraphic units/layers classified in the geologic framework model, which is further developed into a model grid for the Site-Scale UZ Flow Model and the MSTHM process model. Heterogeneity is modeled in terms of the sequence of hydrogeologic units and discrete faults. Therefore, rock properties are embedded in the TSPA through the output flow fields, which are used to prescribe the upper boundary condition water fluxes for the MSTHM, with site-scale layering and faults explicitly taken into account and through the multiscale TH simulations. MSTHM process model simulations are used to develop the TH abstraction implemented in the TSPA-LA Model.	10 CFR 63.311 10 CFR 63.331 10 CFR 63.321	MA

Table I-2. Model Implementation for Included Features, Events, and Processes (Continued)

Submodel implemented in the TSPA-LA Model and Section Number	Path in GoldSim Model File	FEPs Included in the Submodel	TSPA Inclusion Explanation	Performance Assessment Standard[a]	TSPA-LA Model Implementation
EBS TH Environment Submodel 6.3.2 (Continued)	Epistemic: \Input_Params_Epistemic\Epistemic_Params_EBS_Environ\Uncertain_Params_TH EBS: \Global_Inputs_and_Calcs\Global_EBS_Environ\EBS_Environment\ThermoHydrology	2.2.07.02.0A Unsaturated groundwater flow in the geosphere	The Site-Scale UZ Flow Model uses a three-dimensional, steady flow in a heterogeneous dual-permeability system that includes discrete fault zones and allows for a realistic description of flow pathways in the UZ. The flow fields generated by the Site-Scale UZ Flow Model are used to prescribe the upper boundary condition water fluxes for the MSTHM process model. This process model also calculates processes of UZ flow and their effects on TH conditions in the EBS. MSTHM process model simulations are used to develop the MSTHM abstraction implemented in the TSPA-LA Model.	10 CFR 63.311 10 CFR 63.331 10 CFR 63.321	GSM
		2.2.07.08.0A Fracture flow in the UZ	The MSTHM process model is based on the dual-permeability concept, with the fractures represented by a continuum. The fracture continuum represents the spatially averaged flow through discrete fractures. The fracture continuum interacts with the matrix continuum, which represents matrix blocks separated by fractures. MSTHM process model simulations are used to develop the MSTHM abstraction implemented in the TSPA-LA Model.	10 CFR 63.311 10 CFR 63.331 10 CFR 63.321	GSM
		2.2.07.09.0A Matrix imbibition in the UZ	The impact of matrix imbibition in the UZ and in the invert due to capillary pressure differences and its relevance for thermal hydrologic conditions in the EBS are explicitly captured in the MSTHM process model simulations. These simulations are used to develop the MSTHM abstraction implemented in the TSPA-LA Model. Matrix imbibition is also captured explicitly in the Site-Scale UZ Flow Model and the UZ flow fields that are used to prescribe the upper boundary condition water fluxes to the MSTHM process model simulations.	10 CFR 63.311 10 CFR 63.331 10 CFR 63.321	MA

Table I-2. Model Implementation for Included Features, Events, and Processes (Continued)

Submodel implemented in the TSPA-LA Model and Section Number	Path in GoldSim Model File	FEPs Included in the Submodel	TSPA Inclusion Explanation	Performance Assessment Standard[a]	TSPA-LA Model Implementation
EBS TH Environment Submodel 6.3.2 (Continued)	Epistemic: \Input_Params_Epistemic\Epistemic_Params_EBS_Environ\Uncertain_Params_TH EBS: \Global_Inputs_and_Calcs\Global_EBS_Environ\EBS_Environment\ThermoHydrology	2.2.07.10.0A Condensation zone forms around drifts	The coupled processes of vapor condensation forming a condensation cap in the fractured rock above the drifts are explicitly simulated with the MSTHM process model. Using this model, the impact of condensation and shedding on TH conditions is assessed for various simulation cases. These modeling results are used to develop the MSTHM abstraction implemented in the TSPA-LA Model.	10 CFR 63.311 10 CFR 63.331 10 CFR 63.321	MA
		2.2.07.11.0A Resaturation of geosphere dry-out zone	Resaturation of the dryout zone around drifts and the potential for return flow from the condensation zone back to the drifts are explicitly represented in the MSTHM process model. This model is used to generate simulations of TH processes, including dryout. These simulations are used as the basis for the MSTHM Abstraction implemented in the TSPA-LA Model.	10 CFR 63.311 10 CFR 63.331 10 CFR 63.321	DLL
		2.2.07.20.0A Flow diversion around repository drifts	The impact of flow diversion around the drifts due to capillary pressure differences and its relevance for thermal-hydrologic conditions in the EBS are explicitly captured in the MSTHM process model simulations. These simulations are used to develop the MSTHM abstraction implemented in the TSPA-LA Model.	10 CFR 63.311 10 CFR 63.331 10 CFR 63.321	DLL
		2.2.10.03.0B Natural geothermal effects on flow in the UZ	Natural geothermal effects are included in the MSTHM process model used to describe the effects of waste heat in the repository. The MSTHM contains the natural geothermal gradient in its initialization. This gradient is primarily determined by the ground surface temperature, the water table temperature, water flux through the UZ, and the thermal conductivity from layer to layer. MSTHM process model simulations are used as the basis for the MSTHM abstraction implemented in the TSPA-LA Model.	10 CFR 63.311 10 CFR 63.331 10 CFR 63.321	MA

Table I-2. Model Implementation for Included Features, Events, and Processes (Continued)

Submodel implemented in the TSPA-LA Model and Section Number	Path in GoldSim Model File	FEPs Included in the Submodel	TSPA Inclusion Explanation	Performance Assessment Standard[a]	TSPA-LA Model Implementation
EBS TH Environment Submodel 6.3.2 (Continued)	Epistemic: \Input_Params_Epistemic\Epistemic_Params_EBS_Environ\Uncertain_Params_TH EBS: \Global_Inputs_and_Calcs\Global_EBS_Environ\EBS_Environment\ThermoHydrology	2.2.10.10.0A Two-phase buoyant flow/heat pipes	The coupled processes causing heat-pipe behavior are explicitly simulated with the MSTHM process model. This model is used to assess the impact of heat-pipe behavior on TH conditions in the drift for various simulation cases. These simulations are used to develop the MSTHM abstraction implemented in the TSPA-LA Model.	10 CFR 63.311 10 CFR 63.331 10 CFR 63.321	MA
		2.2.10.12.0A Geosphere dryout due to waste heat	The impact of geosphere dryout due to waste heat and the coupled processes of vaporization, dryout, and resaturation and their relevance for thermal hydrologic conditions in the EBS are explicitly captured in the MSTHM process model simulations. These processes are reflected in output variables of temperature and liquid-phase flux in the near field host rock. MSTHM process simulations are used to develop the MSTHM abstraction implemented in the TSPA-LA Model.	10 CFR 63.311 10 CFR 63.331 10 CFR 63.321	MA

Table I-2. Model Implementation for Included Features, Events, and Processes (Continued)

Submodel implemented in the TSPA-LA Model and Section Number	Path in GoldSim Model File	FEPs Included in the Submodel	TSPA Inclusion Explanation	Performance Assessment Standard[a]	TSPA-LA Model Implementation
EBS Chemical Environment Submodel 6.3.4	Epistemic: \Input_Params_Epistemic\Epistemic_Params_EBS_Environ\Uncertain_Params_EBS_CE Aleatory: \Input_Params_Aleatory\Input_Params_EBS_Environ\Input_Params_EBS_CE EBS: \Global_Inputs_and_Calcs\Global_EBS_Environ\EBS_Environment\EBS_Chemical_Environment	1.1.02.02.0A Preclosure ventilation	Preclosure ventilation in drifts will remove a considerable amount of the heat output from the WPs. Heat removal by ventilation during the ventilation period is modeled in the near field chemistry model by extracting vertical temperature profiles at various timesteps which are implemented directly into TSPA by the Physical and Chemical Environment submodel.	10 CFR 63.311 10 CFR 63.321 10 CFR 63.331	GSM
		1.3.01.00.0A Climate change	The near field chemistry submodel examines the water-rock interactions at 20 different sets of percolation fluxes each representing four climate states. This is computed at many different waste package locations throughout the repository and the abstractions are included in the Physical and Chemical Environment submodel in the TSPA-LA Model.	10 CFR 63.311 10 CFR 63.331 10 CFR 63.321	MA

Table I-2. Model Implementation for Included Features, Events, and Processes (Continued)

Submodel implemented in the TSPA-LA Model and Section Number	Path in GoldSim Model File	FEPs Included in the Submodel	TSPA Inclusion Explanation	Performance Assessment Standard[a]	TSPA-LA Model Implementation
EBS Chemical Environment Submodel 6.3.4	Epistemic: \Input_Params_Epistemic\Epistemic_Params_EBS_Environ\Uncertain_Params_EBS_CE Aleatory: \Input_Params_Aleatory\Input_Params_EBS_Environ\Input_Params_EBS_CE EBS: \Global_Inputs_and_Calcs\Global_EBS_Environ\EBS_Environment\EBS_Chemical_Environment	1.4.01.01.0A Climate modification increases recharge	The near field chemistry submodel examines the water-rock interactions at 20 different sets of percolation fluxes each representing four climate states. This is computed at many different waste package locations throughout the repository and the abstractions are included in the physical and chemical environment submodel in the TSPA-LA Model.	10 CFR 63.311 10 CFR 63.331 10 CFR 63.321	MA
		2.1.03.11.0A Physical form of waste package and drip shield	The physical form of waste packages and drip shields and their relevance to the chemical environment in the EBS are explicitly captured in the EBS Chemical environment model during post-closure. The radionuclide sorption characteristics of the corrosion products of waste package internal components are dependent on the CO_2 partial pressure provided by the EBS chemical environment submodel.	10 CFR 63.311 10 CFR 63.331 10 CFR 63.321	MA
		2.1.08.06.0A Capillary effects (wicking) in EBS	The invert chemistry abstraction includes evaluation of pore-water chemistry in the invert, which is affected by capillary condensation/wicking in the invert. This abstraction has two lookup tables: one for water entering the drift by crown seepage and the other for water entering the invert by capillary condensation and/or wicking. Flow and transport through the invert is not included in the human intrusion assessment.	10 CFR 63.311 10 CFR 63.331	GSM

Table I-2. Model Implementation for Included Features, Events, and Processes (Continued)

Submodel implemented in the TSPA-LA Model and Section Number	Path in GoldSim Model File	FEPs Included in the Submodel	TSPA Inclusion Explanation	Performance Assessment Standard[a]	TSPA-LA Model Implementation
EBS Chemical Environment Submodel 6.3.4 (Continued)	Epistemic: \Input_Params_Epistemic\Epistemic_Params_EBS_Environ\Uncertain_Params_EBS_CE Aleatory: \Input_Params_Aleatory\Input_Params_EBS_Environ\Input_Params_EBS_CE EBS: \Global_Inputs_and_Calcs\Global_EBS_Environ\EBS_Environment\EBS_Chemical_Environment	2.1.08.11.0A Repository resaturation due to waste cooling	The impact of repository resaturation due to waste cooling and the coupled processes of vaporization, dryout, and their relevance for thermal hydrologic conditions in the EBS are explicitly captured in the MSTHM process model simulations. These processes are reflected in output variables of temperature and liquid-phase flux in the near field host rock. MSTHM process simulations are used to develop the MSTHM abstraction implemented in the TSPA-LA Model.	10 CFR 63.311 10 CFR 63.331 10 CFR 63.321	GSM
		2.1.09.01.0A Chemical characteristics of water in drifts	The composition of water entering the drift by crown seepage, and subsequent evaporation, is determined in the TSPA through implementation of the seepage dilution/evaporation abstraction look-up tables provided by the Physical and Chemical Environment submodel. The composition of water entering within the invert is determined in the TSPA-LA Model through implementation of the invert chemistry abstraction look-up tables. Potential carrier plume effects are considered in the evaluation of seepage water interaction with stainless steel and carbon steel structural materials. Cementitious materials are not considered because they are not part of the repository design.	10 CFR 63.311 10 CFR 63.331 10 CFR 63.321	GSM

Table I-2. Model Implementation for Included Features, Events, and Processes (Continued)

Submodel implemented in the TSPA-LA Model and Section Number	Path in GoldSim Model File	FEPs Included in the Submodel	TSPA Inclusion Explanation	Performance Assessment Standard[a]	TSPA-LA Model Implementation
EBS Chemical Environment Submodel 6.3.4 (Continued)	Epistemic: \Input_Params_Epistemic\Epistemic_Params_EBS_Environ\Uncertain_Params_EBS_CE Aleatory: \Input_Params_Aleatory\Input_Params_EBS_Environ\Input_Params_EBS_CE EBS: \Global_Inputs_and_Calcs\Global_EBS_Environ\EBS_Environment\EBS_Chemical_Environment	2.1.09.06.0B Reduction-oxidation potential in drifts	The reduction-oxidation potential in the drifts is included in the Physical and Chemical Environment submodel abstractions, which are implemented directly in the TSPA. In particular, the gas abstraction accounts for redox potential in its oxygen mass balance. Oxidizing conditions are predicted to occur indefinitely in the in-drift environment, based on corrosion of carbon steel (which is rate-limited by oxygen supply) as the principal representative cause of oxygen consumption.	10 CFR 63.311 10 CFR 63.331 10 CFR 63.321	MA
		2.1.09.07.0B Reaction kinetics in drifts	The effects of reaction kinetics are implicitly included in each geochemical submodel developed in Engineered Barrier System: Physical and Chemical Environment submodel. In reaction path geochemical modeling calculations using an EQ3/6 equilibrium model of the water compositions resulting from seepage evaporation, reaction kinetics are implicitly included through suppression of individual mineral phases. Individual mineral phases were suppressed if those phases are kinetically inhibited from forming under repository conditions. The choice of mineral suppressions directly affects the modeled evolution of the in-drift waters, and hence the water compositions that are passed to the TSPA in the form of look-up tables. In addition, the kinetics of corrosion of committed materials was examined with respect to its effect on in-drift water and atmosphere compositions. Seepage water interactions with Stainless Steel Type 316L ground barrier components and low alloy invert steels were found to be of low consequence.	10 CFR 63.311 10 CFR 63.331 10 CFR 63.321	MA
		2.1.11.01.0A Heat generation in EBS	The Physical and Chemical Environment submodel uses vertical thermal profiles generated by the Near Field chemistry submodel. At each waste package location, the thermal profile is evaluated by summing the contribution of the heat generated by each of the 108 drifts within the repository lay-out, using an averaged line load of each drift.	10 CFR 63.311 10 CFR 63.331 10 CFR 63.321	MA

Table I-2. Model Implementation for Included Features, Events, and Processes (Continued)

Submodel implemented in the TSPA-LA Model and Section Number	Path in GoldSim Model File	FEPs Included in the Submodel	TSPA Inclusion Explanation	Performance Assessment Standard[a]	TSPA-LA Model Implementation
EBS Chemical Environment Submodel 6.3.4 (Continued)	Epistemic: \Input_Params_Epistemic\Epistemic_Params_EBS_Environ\Uncertain_Params_EBS_CE Aleatory: \Input_Params_Aleatory\Input_Params_EBS_Environ\Input_Params_EBS_CE EBS: \Global_Inputs_and_Calcs\Global_EBS_Environ\EBS_Environment\EBS_Chemical_Environment	2.1.11.08.0A Thermal effects on chemistry and microbial activity in the EBS	The Physical and Chemical Environment submodel abstractions capture the impact of temperature on the evolution of potential seepage chemistries within the EBS. The effects of temperature on mineral stabilities and chemical reaction rates are also included in the geochemical modeling used to create the seepage dilution/evaporation and invert chemistry abstractions. Temperature is one of the parameters required as input to implement these abstractions in the TSPA-LA Model.	10 CFR 63.311 10 CFR 63.331 10 CFR 63.321	GSM
		2.1.11.09.0C Thermally driven flow (convection) in drifts	Temperature and relative humidity conditions derived from the MSTHM are used to extract parameters of the in-drift chemical environment from the lookup-tables generated by the in-drift seepage dilution/evaporation model, developed in the Physical and Chemical Environment submodel and implemented by TSPA.	10 CFR 63.311 10 CFR 63.331 10 CFR 63.321	GSM

Table I-2. Model Implementation for Included Features, Events, and Processes (Continued)

Submodel implemented in the TSPA-LA Model and Section Number	Path in GoldSim Model File	FEPs Included in the Submodel	TSPA Inclusion Explanation	Performance Assessment Standard[a]	TSPA-LA Model Implementation
EBS Chemical Environment Submodel 6.3.4 (Continued)	Epistemic: \Input_Params_Epistemic\Epistemic_Params_EBS_Environ\Uncertain_Params_EBS_CE Aleatory: \Input_Params_Aleatory\Input_Params_EBS_Environ\Input_Params_EBS_CE EBS: \Global_Inputs_and_Calcs\Global_EBS_Environ\EBS_Environment\EBS_Chemical_Environment	2.2.07.02.0A Unsaturated groundwater flow in the geosphere	The effects of unsaturated groundwater flow are included in the submodel for seepage water chemistry. The approach used is a plug flow model that has a transport velocity equal to the percolation flux divided by the product of the average porosity and the average water saturation. The effects of flow on the water chemistry are evaluated in terms of the amount of feldspar dissolution that occurs during flow through the TSw. The amount of feldspar dissolution is passed to TSPA in a lookup table, as the water-rock interaction parameter, or WRIP.	10 CFR 63.311 10 CFR 63.331 10 CFR 63.321	GSM
		2.2.07.08.0A Fracture flow in the unsaturated zone	Flow processes in fractures or other channels and their effects on the water chemistry are evaluated by the thermal-hydrologic-chemical seepage process model. Thermal-hydrologic-chemical effects on fracture flow processes are evaluated in terms of the amount of feldspar dissolution that occurs during flow through the TSw. The starting point for evaluating potential water compositions in the near field is the composition of ambient pore waters in the TSw. The amount of feldspar dissolution is passed to TSPA in a lookup table, as the water-rock interaction parameter (WRIP).	10 CFR 63.311 10 CFR 63.331 10 CFR 63.321	GSM

Table I-2. Model Implementation for Included Features, Events, and Processes (Continued)

Submodel implemented in the TSPA-LA Model and Section Number	Path in GoldSim Model File	FEPs Included in the Submodel	TSPA Inclusion Explanation	Performance Assessment Standard[a]	TSPA-LA Model Implementation
EBS Chemical Environment Submodel 6.3.4 (Continued)	Epistemic: \Input_Params_Epistemic\Epistemic_Params_EBS_Environ\Uncertain_Params_EBS_CE Aleatory: \Input_Params_Aleatory\Input_Params_EBS_Environ\Input_Params_EBS_CE EBS: \Global_Inputs_and_Calcs\Global_EBS_Environ\EBS_Environment\EBS_Chemical_Environment	2.2.07.11.0A Resaturation of geosphere dry-out zone	The MSTHM model provides in-drift temperature and relative humidity inputs used by TSPA to extract water composition data from lookup tables generated by the seepage dilution/evaporation model. This submodel, in turn, evaluates in-drift processes and provides lookup tables for in-drift aqueous chemistry to TSPA.	10 CFR 63.311 10 CFR 63.331 10 CFR 63.321	GSM
		2.2.08.01.0B Chemical characteristics of groundwater in the UZ	The seepage dilution/evaporation abstraction model provided by the Physical and Chemical Environment submodel was developed using four different input water compositions spanning the range of compositions in the repository units. The variability of pore-water compositions reflects the spatial variations in rock mineralogy, temperature, and infiltration rates. The four input water compositions capture that variability as well as uncertainty, which are propagated to the TSPA through the seepage dilution/evaporation abstraction look-up tables created using results from the Physical and Chemical Environment submodel.	10 CFR 63.311 10 CFR 63.331 10 CFR 63.321	GSM

Table I-2. Model Implementation for Included Features, Events, and Processes (Continued)

Submodel implemented in the TSPA-LA Model and Section Number	Path in GoldSim Model File	FEPs Included in the Submodel	TSPA Inclusion Explanation	Performance Assessment Standard[a]	TSPA-LA Model Implementation
EBS Chemical Environment Submodel 6.3.4 (Continued)	Epistemic: \Input_Params_Epistemic\Epistemic_Params_EBS_Environ\Uncertain_Params_EBS_CE Aleatory: \Input_Params_Aleatory\Input_Params_EBS_Environ\Input_Params_EBS_CE EBS: \Global_Inputs_and_Calcs\Global_EBS_Environ\EBS_Environment\EBS_Chemical_Environment	2.2.08.12.0A Chemistry of water flowing into the drift	The near field chemistry submodel in the Physical and Chemical Environment model component evaluates the effects of the thermal-hydrologic-chemical processes in the rock on the chemistry of potential seepage water entering the drift. The seepage dilution/evaporation abstraction uses these waters to generate lookup tables of in-drift water chemistry couple TH processes and chemical processes for the TSPA-LA Model.	10 CFR 63.311 10 CFR 63.331 10 CFR 63.321	DLL
		2.2.10.12.0A Geosphere dryout due to waste heat	In the near-field chemistry submodel, the effect of dryout is implemented by adjusting the length of the flow pathway considered for water-rock interactions; however, the seepage compositions that are predicted during the boiling period are not used, because the abstraction of drift seepage does not predict seepage when the drift-wall temperature exceeds the boiling point.	10 CFR 63.311 10 CFR 63.331 10 CFR 63.321	DLL

Table I-2. Model Implementation for Included Features, Events, and Processes (Continued)

Submodel implemented in the TSPA-LA Model and Section Number	Path in GoldSim Model File	FEPs Included in the Submodel	TSPA Inclusion Explanation	Performance Assessment Standard[a]	TSPA-LA Model Implementation
EBS Chemical Environment Submodel 6.3.4 (Continued)	Epistemic: \Input_Params_Epistemic\Epistemic_Params_EBS_Environ\Uncertain_Params_EBS_CE Aleatory: \Input_Params_Aleatory\Input_Params_EBS_Environ\Input_Params_EBS_CE EBS: \Global_Inputs_and_Calcs\Global_EBS_Environ\EBS_Environment\EBS_Chemical_Environment	2.3.11.03.0A Infiltration and recharge	Changes in infiltration rate in the UZ could affect the composition of groundwater passing through the repository. The seepage dilution/evaporation abstraction model provided by the Physical and Chemical Environment submodel was developed using four different input water compositions spanning the range of compositions in the repository units. The variability of pore-water compositions reflects the spatial variations in rock mineralogy, temperature, and infiltration rates. The four input water compositions capture that variability as well as uncertainty, which are propagated to the TSPA through the seepage dilution/evaporation abstraction look-up tables created using results from the Physical and Chemical Environment submodel.	10 CFR 63.311 10 CFR 63.331 10 CFR 63.321	DLL

Table I-2. Model Implementation for Included Features, Events, and Processes (Continued)

Submodel implemented in the TSPA-LA Model and Section Number	Path in GoldSim Model File	FEPs Included in the Submodel	TSPA Inclusion Explanation	Performance Assessment Standard[a]	TSPA-LA Model Implementation
WP and DS Degradation Submodel 6.3.5	Epistemic: \Input_Params_Epistemic\Epistemic_Params_WP_DS_Deg\ Aleatory: \Model_Calcs_Aleatory\Aleatory_Calcs_WP_DS_Deg EBS: \Time_Zero\EBS_PS_Loop\Static_Calcs_PS_Loop\Static_Calcs_WP_DS_Deg \Global_Inputs_and_Calcs\Global_WP_DS_Deg\Global_IWPD	2.1.03.01.0A General corrosion of waste packages	General corrosion of WPs is modeled as uniform thinning of the WP outer barrier. The general corrosion model is constructed around crevice-corrosion geometry weight-loss corrosion data with a temperature-dependent term. The general corrosion rate is represented as constant versus time under a given temperature. General corrosion is modeled by dividing the WP surface into subareas (patches) that are used to simulate variability across the barrier surfaces.	10 CFR 63.311 10 CFR 63.331	DLL
		2.1.03.01.0B General corrosion of drip shields	General corrosion of the DS is modeled as uniform thinning of the DS. The general corrosion rate is modeled as constant with time and temperature and constructed around weight-loss data determined from long term corrosion tests. The general corrosion of the DS is modeled separately for the inner surface and the outer surfaces to reflect the less corrosive environment that will be present on the underside of the DS. Each DS is modeled as a single entity with no spatial variability. General corrosion of the DS is included implicitly in the assessment of the earliest time at which a WP could be penetrated without being detected by the driller.	10 CFR 63.311 10 CFR 63.331 10 CFR 63.321	DLL

Table I-2. Model Implementation for Included Features, Events, and Processes (Continued)

Submodel implemented in the TSPA-LA Model and Section Number	Path in GoldSim Model File	FEPs Included in the Submodel	TSPA Inclusion Explanation	Performance Assessment Standard[a]	TSPA-LA Model Implementation
WP and DS Degradation Submodel 6.3.5 (Continued)	Epistemic: \Input_Params_Epistemic\Epistemic_Params_WP_DS_Deg\ Aleatory: \Model_Calcs_Aleatory\Aleatory_Calcs_WP_DS_Deg EBS: \Time_Zero\EBS_PS_Loop\Static_Calcs_PS_Loop\Static_Calcs_WP_DS_Deg \Global_Inputs_and_Calcs\Global_WP_DS_Deg\Global_IWPD	2.1.03.02.0A Stress corrosion cracking of the waste packages	Stress corrosion cracking (SCC) of WPs is modeled as the initiation and propagation of cracks due to a sustainable tensile stress. The threshold stress, threshold stress intensity factor, and parameters associated with the slip dissolution/film rupture crack growth model are inputs to the TSPA SCC abstraction in WAPDEG, which is implemented by TSPA. SCC of the WP outer barrier closure weld region is modeled to initiate at incipient flaws or weld flaws in the closure weld region. Each WP closure lid is represented as a collection of approximately 40 patches. It is conservatively modeled that, when the first crack on a given patch penetrates through-wall, all possible through-wall cracks on that patch are considered to penetrate through-wall. SCC is excluded from the human intrusion assessment because SCC does not significantly alter the yield strength of the WP, and therefore, a driller would recognize penetration by the drill bit.	10 CFR 63.311 10 CFR 63.331	DLL
		2.1.03.05.0A Microbially induced corrosion of waste packages	Microbially influenced corrosion is modeled in the TSPA-LA Model as an enhancement factor uniformly distributed between 1 and 2 due to uncertainty. The factor is applied to the entire WP outer barrier general corrosion rate when the relative humidity at the WP outer corrosion barrier surface is equal to a threshold value represented by, and sampled from, a uniform distribution ranging from 75 percent to 90 percent. Microbially induced corrosion of the WP is not implemented directly in the assessment of human intrusion, however, it is included implicitly as part of general corrosion in the assessment of the earliest time at which a WP could be penetrated.	10 CFR 63.311 10 CFR 63.331	DLL

Table I-2. Model Implementation for Included Features, Events, and Processes (Continued)

Submodel implemented in the TSPA-LA Model and Section Number	Path in GoldSim Model File	FEPs Included in the Submodel	TSPA Inclusion Explanation	Performance Assessment Standard[a]	TSPA-LA Model Implementation
WP and DS Degradation Submodel 6.3.5(Continued)	Epistemic: \Input_Params_Epistemic\Epistemic_Params_WP_DS_Deg\ Aleatory: \Model_Calcs_Aleatory\Aleatory_Calcs_WP_DS_Deg EBS: \Time_Zero\EBS_PS_Loop\Static_Calcs_PS_Loop\Static_Calcs_WP_DS_Deg \Global_Inputs_and_Calcs\Global_WP_DS_Deg\Global_IWPD	2.1.03.11.0A Physical form of waste package and drip shield	General corrosion of WPs and DS are modeled as uniform thinning of the WP outer barrier, and uniform thinning of the DS. The WP general corrosion model is constructed around crevice-corrosion geometry weight-loss corrosion data with a temperature-dependent term. The general corrosion rate is represented as constant versus time under a given temperature. General corrosion of the WP is modeled by dividing the WP surface into subareas (patches) that are used to simulate variability across the barrier surfaces. The general corrosion rate of the DS is modeled as constant with time and temperature and constructed around weight-loss data determined from long term corrosion tests. The general corrosion of the DS is modeled separately for the inner surface and the outer surfaces to reflect the less corrosive environment that will be present on the underside of the DS. Each DS is modeled as a single entity with no spatial variability.	10 CFR 63.311 10 CFR 63.331 10 CFR 63.321	GSM

Table I-2. Model Implementation for Included Features, Events, and Processes (Continued)

Submodel implemented in the TSPA-LA Model and Section Number	Path in GoldSim Model File	FEPs Included in the Submodel	TSPA Inclusion Explanation	Performance Assessment Standard[a]	TSPA-LA Model Implementation
LC Initiation Submodel 6.3.5.2	Epistemic: \Input_Params_Epistemic\Epistemic_Params_WP_DS_Deg\ EBS: \Time_Zero\EBS_PS_Loop\Static_Calcs_PS_Loop\Static_Calcs_WP_DS_Deg \Global_Inputs_and_Calcs\Global_WP_DS_Deg\Global_LC	2.1.03.03.0A Localized corrosion of waste packages	Localized corrosion of WPs is implemented in the TSPA-LA Model using an initiation model and a propagation model. Localized corrosion can only be initiated when seepage contacts a WP during the thermal period, thus requiring a failed DS prior to 10,000 years. DSs potentially fail within 10,000 years in the Seismic Scenario Class and Early Failure Scenario Class only. The initiation model is a regression model that involves the following dependent variables: nitrate concentration, chloride concentration, temperature, pH, and nitrate to chloride ratio. Values for these time-dependent quantities are provided by the seepage dilution/evaporation abstraction model. Upon initiation of localized corrosion, the propagation depth is modeled using a constant rate and a distribution function to address uncertainty ranges found in the literature. The area affected by localized corrosion resulting from seepage brines is modeled as the entire WP surface area. In the case of an early-failed DS it is assumed that the underlying WP fails immediately due to localized corrosion.	10 CFR 63.311 10 CFR 63.331	GSM
Radionuclide Inventory Submodel 6.3.7.1	Epistemic: \Input_Params_Epistemic\Epistemic_Params_WF_Deg_Mob\Uncertain_Params_RN_Inventory EBS: \Global_Inputs_and_Calcs\Global_WF_Deg_Mob\RN_Inventory	2.1.01.01.0A Waste inventory	The TSPA models three representative waste form inventories: CSNF, DSNF, and HLW. Naval SNF is conservatively treated as CSNF. More than 100 radionuclides (e.g., fission products, actinides, and activation products) are screened for importance to expected dose. The abstraction is treated with uncertainty ranges for each waste form.	10 CFR 63.311 10 CFR 63.331 10 CFR 63.321	GSM

Table I-2. Model Implementation for Included Features, Events, and Processes (Continued)

Submodel implemented in the TSPA-LA Model and Section Number	Path in GoldSim Model File	FEPs Included in the Submodel	TSPA Inclusion Explanation	Performance Assessment Standard[a]	TSPA-LA Model Implementation
Radionuclide Inventory Submodel 6.3.7.1 (Continued)	Epistemic: \Input_Params_Epistemic\Epistemic_Params_WF_Deg_Mob\Uncertain_Params_RN_Inventory EBS: \Global_Inputs_and_Calcs\Global_WF_Deg_Mob\RN_Inventory	2.1.01.03.0A Heterogeneity of waste inventory	TSPA considers the gross heterogeneity between the waste form types: CSNF, DSNF, and HLW. Radionuclide inventory and degradation rates are provided for each waste form type. Heterogeneity is acknowledged in uncertainty parameters in each of these models.	10 CFR 63.311 10 CFR 63.331 10 CFR 63.321	GSM
		2.1.03.11.0A Physical form of waste package and drip shield	The effect of the physical form of the waste package is considered in the TSPA in representing all waste packages by two types—TADs for CSNF and 5-DHLW/DOE SNF – Long for codisposal. By using the most common CSNF waste package and the largest (as well as most common) codisposal waste package, the full radionuclide inventory is reasonably represented in the TSPA.	10 CFR 63.311 10 CFR 63.331 10 CFR 63.321	GSM
		3.1.01.01.0A Radioactive decay and ingrowth	Radioactive decay and ingrowth were considered in screening which radionuclides to include in the TSPA. The TSPA accounts for decay and ingrowth in the EBS using built-in functions of GoldSim. During execution, the GoldSim model automatically calculates decay and ingrowth of the included isotopes.	10 CFR 63.311 10 CFR 63.331 10 CFR 63.321	GSM

Table I-2. Model Implementation for Included Features, Events, and Processes (Continued)

Submodel implemented in the TSPA-LA Model and Section Number	Path in GoldSim Model File	FEPs Included in the Submodel	TSPA Inclusion Explanation	Performance Assessment Standard[a]	TSPA-LA Model Implementation
In Package Chemistry Submodel 6.3.7.2	Epistemic: \Input_Params_Epistemic\Epistemic_Params_WF_Deg_Mob\Uncertain_Params_InPkg_Chem Aleatory: NA EBS: \Global_Inputs_and_Calcs\Global_WF_Deg_Mob\In_Package_Chemistry	2.1.01.02.0B Interactions between co-disposed waste	The In-Package Chemistry Process Model provides the interactions between co-disposed wastes. These interactions and their relevance to in-package chemistry are assessed in multiple simulations. These simulations are used to develop the in-package chemistry abstraction implemented in the TSPA-LA Model. The DSNF degradation is modeled as insensitive to in-package chemistry and is modeled as instantaneous. The degradation rate of HLW depends on pH, which in turn is dependent on all materials within the package. Degradation of HLW tends to raise the in-package pH while degradation of disposal canisters and other in-package metals tends to lower the pH. Degradation of DSNF and surface complexation on corrosion products tends to bring the pH back toward neutral.	10 CFR 63.311 10 CFR 63.331 10 CFR 63.321	GSM
		2.1.03.11.0A Physical form of waste	The effect of waste package and drip shield materials on the chemical behavior of the disposal area is included in the in-package chemistry abstraction implemented in the TSPA-LA Model.	10 CFR 63.311 10 CFR 63.331 10 CFR 63.321	MA
		2.1.09.06.0A Reduction-oxidation potential in waste package	As long as there are reduced fuels and metals within the breached WP, there will be strong redox gradients between them and the atmosphere, providing the driving force for the reactions calculated in the In-Package Chemistry Process Model simulations. The In-Package Chemistry Process Model uses the bounding approximation that the bulk water within the package is in equilibrium with the atmosphere. In-Package Chemistry Process Model simulations are used to develop the In-Package Chemistry Abstraction implemented in TSPA.	10 CFR 63.311 10 CFR 63.331 10 CFR 63.321	MA

Table I-2. Model Implementation for Included Features, Events, and Processes (Continued)

Submodel implemented in the TSPA-LA Model and Section Number	Path in GoldSim Model File	FEPs Included in the Submodel	TSPA Inclusion Explanation	Performance Assessment Standard[a]	TSPA-LA Model Implementation
In Package Chemistry Submodel 6.3.7.2 (Continued)	Epistemic: \Input_Params_Epistemic\Epistemic_Params_WF_Deg_Mob\Uncertain_Params_InPkg_Chem Aleatory: NA EBS: \Global_Inputs_and_Calcs\Global_WF_Deg_Mob\In_Package_Chemistry	2.1.02.09.0A Chemical effects of void space in waste packages	Upon WP breach, the inert gas escapes and is replaced with humid air. The reaction of this air with WP internals and the resulting changes in water chemistry are modeled with the In-Package Chemistry Process Model. In-Package Chemistry Process Model simulations are used to develop the In-Package Chemistry Abstraction implemented in the TSPA-LA Model.	10 CFR 63.311 10 CFR 63.331 10 CFR 63.321	MA
		2.1.09.01.0B Chemical characteristics of water in waste package	The In-Package Chemistry Process Model accounts for the reaction of incoming water and air with the waste forms and metals within the WP. In-Package Chemistry Process Model simulations are used to develop the In-Package Chemistry Abstraction implemented in the TSPA-LA Model.	10 CFR 63.311 10 CFR 63.331 10 CFR 63.321	GSM
		2.1.09.07.0A Reaction kinetics in waste package	The In-Package Chemistry Process Model accounts for the impact of reaction kinetics on the resulting pH and ionic strength from the reaction of metals and waste forms with air and water within the package. . In-Package Chemistry Process Model simulations are used to develop the In-Package Chemistry Abstraction implemented in the TSPA-LA Model.	10 CFR 63.311 10 CFR 63.331 10 CFR 63.321	MA
		2.1.09.02.0A Chemical interaction with corrosion products	The chemical influence of corrosion products inside the package is modeled in the In-Package Chemistry Process Model. . In-Package Chemistry Process Model simulations are used to develop the In-Package Chemistry Abstraction implemented in the TSPA-LA Model.	10 CFR 63.311 10 CFR 63.331 10 CFR 63.321	GSM

Table I-2. Model Implementation for Included Features, Events, and Processes (Continued)

Submodel implemented in the TSPA-LA Model and Section Number	Path in GoldSim Model File	FEPs Included in the Submodel	TSPA Inclusion Explanation	Performance Assessment Standard[a]	TSPA-LA Model Implementation
In Package Chemistry Submodel 6.3.7.2 (Continued)	Epistemic: \Input_Params_Epistemic\Epistemic_Params_WF_Deg_Mob\Uncertain_Params_InPkg_Chem Aleatory: NA EBS: \Global_Inputs_and_Calcs\Global_WF_Deg_Mob\In_Package_Chemistry	2.2.08.12.0B Chemistry of water flowing into the waste package	Different representative initial water compositions were used to represent the chemistry of the water flowing into the WP. In-package chemistry simulations were used to asses the impact of these water compositions on chemistry of the evolving water in the WP. Results of these simulations verified that in-package chemistry was not significantly affected by starting water composition. Thus the In-Package Chemistry Abstraction implemented in the TSPA-LA Model does not require initial water composition as an input.	10 CFR 63.311 10 CFR 63.331 10 CFR 63.321	GSM
Waste Form Degradation Submodel 6.3.7.4	Epistemic: \Input_Params_Epistemic\Epistemic_Params_WF_Deg_Mob\Uncertain_Params_HLW_WF EBS: \Global_Inputs_and_Calcs\Global_WF_Deg_Mob\WF_Degradation\Input_Params_HLW_WF	2.1.01.02.0B Interactions between co-disposed waste	The In-Package Chemistry Process Model assesses the interaction between co-disposed wastes and its impact on in-package chemistry. The In-Package Chemistry Abstraction is used to represent these interactions in the TSPA-LA Model and provide inputs to the waste form degradation models. The DSNF degradation is modeled as insensitive to in-package chemistry and is modeled as instantaneous. The degradation rate of HLW depends on pH, which in turn is dependent on all materials within the package. Degradation of HLW tends to raise the in-package pH while degradation of disposal canisters and other in-package metals tends to lower the pH. Degradation of DSNF and surface complexation on corrosion products tends to bring the pH back toward neutral.	10 CFR 63.311 10 CFR 63.331 10 CFR 63.321	GSM

Table I-2. Model Implementation for Included Features, Events, and Processes (Continued)

Submodel implemented in the TSPA-LA Model and Section Number	Path in GoldSim Model File	FEPs Included in the Submodel	TSPA Inclusion Explanation	Performance Assessment Standard[a]	TSPA-LA Model Implementation
Waste Form Degradation Submodel 6.3.7.4 (Continued)	Epistemic: \Input_Params_Epistemic\Epistemic_Params_WF_Deg_Mob\Uncertain_Params_CSNF_WF	2.1.01.03.0A Heterogeneity of waste inventory	TSPA considers the gross heterogeneity between the waste form types: CSNF, DSNF, and HLW. Radionuclide inventory and degradation rates are provided for each waste form type. In-package chemistries and radionuclide solubilities are defined for each WP type: CSNF and CDSP.	10 CFR 63.311 10 CFR 63.331 10 CFR 63.321	GSM
	EBS: \Global_Inputs_and_Calcs\Global_WF_Deg_Mob\WF_Degradation\CSNF_WF_Dissolution	2.1.02.01.0A DSNF degradation (alteration, dissolution, and radionuclide release)	Naval SNF is conservatively treated as CSNF in the TSPA-LA Model calculations. The degradation rate of all DSNF except naval is bounded in the TSPA-LA Model as instantaneous. With the exception of naval SNF, no credit is given for DSNF cladding in the TSPA-LA Model. In addition, no credit is taken for any disposal canisters, including high-integrity canisters.	10 CFR 63.311 10 CFR 63.331 10 CFR 63.321	GSM
	EBS: \Global_Inputs_and_Calcs\Global_WF_Deg_Mob\WF_Degradation\Input_Params_DSNF_WF	2.1.02.02.0A CSNF degradation (alteration, dissolution, and radionuclide release)	TSPA uses an empirical CSNF degradation rate model that is a function of surface area, temperature, oxygen, carbonate concentration, and pH. Data for the empirical model are taken from several test programs.	10 CFR 63.311 10 CFR 63.331 10 CFR 63.321	GSM
	Epistemic: \Input_Params_Epistemic\Epistemic_Params_WF_Deg_Mob\Uncertain_Params_HLW_WF	2.1.02.03.0A HLW glass degradation (alteration, dissolution, and radionuclide release)	TSPA uses an empirical glass degradation rate model that is a function of surface area, temperature, and pH. Data used to develop the degradation model was collected under conditions similar to those expected for the repository.	10 CFR 63.311 10 CFR 63.331 10 CFR 63.321	GSM
	EBS: \Global_Inputs_and_Calcs\Global_WF_Deg_Mob\WF_Degradation\Input_Params_HLW_WF	2.1.02.05.0A HLW glass cracking	The increase in surface area due to cracking is included in the exposure factor, fexposure. A range of values is applied to account for experimental evidence.	10 CFR 63.311 10 CFR 63.331 10 CFR 63.321	GSM

Table I-2. Model Implementation for Included Features, Events, and Processes (Continued)

Submodel implemented in the TSPA-LA Model and Section Number	Path in GoldSim Model File	FEPs Included in the Submodel	TSPA Inclusion Explanation	Performance Assessment Standard[a]	TSPA-LA Model Implementation
Waste Form Degradation Submodel 6.3.7.4 (Continued)	Epistemic: \Input_Params_Epistemic\Epistemic_Params_WF_Deg_Mob\Uncertain_Params_CSNF_WF	2.1.02.07.0A Radionuclide release from gap and grain boundaries	The fraction of cesium, iodine, technetium, and strontium that resides in the gap and grain boundaries is represented in the TSPA-LA Model by the instantaneous release fractions. The fraction of CSNF that comprises this instantaneous release inventory is specified by four triangular distributions. The computed uncertain fraction is released instantly upon breach of the WP.	10 CFR 63.311 10 CFR 63.331 10 CFR 63.321	GSM
	\Global_Inputs_and_Calcs\Global_WF_Deg_Mob\WF_Degradation\CSNF_WF_Dissolution	2.1.02.12.0A Degradation of cladding prior to disposal	These cladding FEPs are included in the TSPA in a bounding way by assuming they provide no capability to prevent of reduce the flow of water or release of radionuclides. The cladding of all CSNF and DSNF is assumed to be failed upon arrival at the repository.	10 CFR 63.311 10 CFR 63.331 10 CFR 63.321	No barrier capability credit taken for cladding
EBS:	\Global_Inputs_and_Calcs\Global_WF_Deg_Mob\WF_Degradation\Input_Params_DSNF_WF	2.1.02.23.0A Cladding unzipping	These cladding FEPs are included in the TSPA in a bounding way by assuming they provide no capability to prevent of reduce the flow of water or release of radionuclides. The cladding of all CSNF and DSNF is assumed to be failed upon arrival at the repository.	10 CFR 63.311 10 CFR 63.331 10 CFR 63.321	No barrier capability credit taken for cladding

EBS:

Table I-2. Model Implementation for Included Features, Events, and Processes (Continued)

Submodel implemented in the TSPA-LA Model and Section Number	Path in GoldSim Model File	FEPs Included in the Submodel	TSPA Inclusion Explanation	Performance Assessment Standard[a]	TSPA-LA Model Implementation
Waste Form Degradation Submodel 6.3.7.4 (Continued)	Epistemic: \Input_Params_Epistemic\Epistemic_Params_WF_Deg_Mob\Uncertain_Params_HLW_WF EBS: \Global_Inputs_and_Calcs\Global_WF_Deg_Mob\WF_Degradation\Input_Params_HLW_WF	2.1.02.25.0B Naval cladding	This FEP is included in the TSPA in a bounding way by assuming cladding provides no capability to prevent of reduce the flow of water or release of radionuclides. The cladding of all CSNF and DSNF is assumed to be failed upon arrival at the repository.	10 CFR 63.311 10 CFR 63.331 10 CFR 63.321	No barrier capability credit taken for cladding
Epistemic:	\Input_Params_Epistemic\Epistemic_Params_WF_Deg_Mob\Uncertain_Params_CSNF_WF	2.1.02.28.0A Grouping of DSNF waste types into categories	DSNF is composed of a variety of fuel types and the quantities of each fuel type are considered when compiling the nominal radionuclide inventory in grams per package and uncertainty distributions for radionuclides important to dose calculations for the TSPA. For degradation rate determination, the various DSNF types have been classified into eleven groups for TSPA analyses	10 CFR 63.311 10 CFR 63.331 10 CFR 63.321	MA
		2.1.03.11.0A Physical form of waste package and drip shield	The physical form of waste package internal waste containers and their degradation is modeled in the TSPA by two representative waste package types (TADs and the 5-DHLW/DOE SNF – Long), which are the most common waste packages. The two types of waste packages also account for the predominant waste forms (CSNF, DSNF, and DHLW).	10 CFR 63.311 10 CFR 63.331 10 CFR 63.321	MA
		2.1.09.02.0A Chemical interaction with corrosion products	Chemical interaction with corrosion products is implemented in the waste form degradation submodel by using the results of tests from the defense HLW glass degradation abstraction when determining model parameter values for pH dependence in acidic and alkaline solutions.	10 CFR 63.311 10 CFR 63.331 10 CFR 63.321	MA

Table I-2. Model Implementation for Included Features, Events, and Processes (Continued)

Submodel implemented in the TSPA-LA Model and Section Number	Path in GoldSim Model File	FEPs Included in the Submodel	TSPA Inclusion Explanation	Performance Assessment Standard[a]	TSPA-LA Model Implementation
Waste Form Degradation Submodel 6.3.7.4 (Continued)	EBS: \Global_Inputs_and_Calcs\Global_WF_Deg_Mob\WF_Degradation\CSNF_WF_Dissolution EBS: \Global_Inputs_and_Calcs\Global_WF_Deg_Mob\WF_Degradation\Input_Params_DSNF_WF	2.1.11.08.0A Thermal effects on chemistry and microbial activity in the EBS	Test data show that the reaction rates for CSNF and HLW glass degradation are temperature dependent. Temperature dependence was included in degradation abstraction models implemented in the TSPA-LA Model for both waste forms. Total carbonate concentration, which is an input for CSNF degradation, is also temperature dependent.	10 CFR 63.311 10 CFR 63.331 10 CFR 63.321	GSM
Dissolved Concentration Limits Submodel 6.3.7.5	Epistemic: \Input_Params_Epistemic\Epistemic_Params_WF_Deg_Mob\Uncertain_Params_Solubility EBS: \Global_Inputs_and_Calcs\Global_WF_Deg_Mob\Global_Solubility	2.1.09.04.0A Radionuclide solubility, solubility limits, and speciation in the waste form and EBS	In the TSPA-LA Model, inventory concentrations of radioactive elements released from the waste forms (CSNF, DSNF, and HLW glass) are calculated according to the dissolution or degradation rates of waste forms and the volume of water within the (breached) WP and radionuclide inventory. Then the radioelement concentrations are compared against their solubility limits. If the concentration is greater than its solubility limit, then the amount of that radioactive element in excess of the solubility limit will precipitate, potentially available for transport at a later time. In the TSPA-LA Model, solubility limits are enforced in the WP and in the invert. This FEP is included in the human intrusion assessment for the WP. However, radionuclide solubility and flow and transport through the invert (EBS) are not included in the human intrusion assessment.	10 CFR 63.311 10 CFR 63.331 10 CFR 63.321	GSM

Table I-2. Model Implementation for Included Features, Events, and Processes (Continued)

Submodel implemented in the TSPA-LA Model and Section Number	Path in GoldSim Model File	FEPs Included in the Submodel	TSPA Inclusion Explanation	Performance Assessment Standard[a]	TSPA-LA Model Implementation
Dissolved Concentration Limits Submodel 6.3.7.5	Epistemic: \Input_Params_Epistemic\Epistemic_Params_WF_Deg_Mob\Uncertain_Params_Solubility EBS: \Global_Inputs_and_Calcs\Global_WF_Deg_Mob\Global_Solubility	2.1.09.06.0A Reduction-Oxidation potential in waste packages	Reduction-oxidation potential in WPs FEP is implemented in the Dissolved Concentration Limits Submodel by examining redox potential as it pertains to repository conditions, and develops an adjusted Eh model based on experimental data and natural analog information. This adjusted Eh model is used for the solubility calculations in the TSPA-LA Model.	10 CFR 63.311 10 CFR 63.331 10 CFR 63.321	GSM
		2.1.09.07.0A Reaction kinetics in waste package	Dissolution kinetics is included in the TSPA in-package chemistry submodel abstraction. The in-package chemistry submodel uses kinetic expressions – linear or transition state theory rate laws - to describe SNF degradation, DHLW glass degradation, and steel degradation. Kinetics is taken into account in the dissolved concentrations model when secondary phases that are kinetically inhibited from forming under repository conditions are suppressed in the calculations. The adjusted Eh model takes account of kinetic controls over Pu speciation.	10 CFR 63.311 10 CFR 63.331 10 CFR 63.321	GSM
		2.2.08.12.0B Chemistry of water flowing into the waste package	Four different initial water compositions were used to represent the chemistry of the water flowing into the waste package in the in-package chemistry abstraction The variability of the incoming water composition is included in the in-package chemistry abstraction passed to the TSPA, which then feeds these results to the solubility, colloid, CSNF, and HLW glass submodels.	10 CFR 63.311 10 CFR 63.331 10 CFR 63.321	GSM

Table I-2. Model Implementation for Included Features, Events, and Processes (Continued)

Submodel implemented in the TSPA-LA Model and Section Number	Path in GoldSim Model File	FEPs Included in the Submodel	TSPA Inclusion Explanation	Performance Assessment Standard[a]	TSPA-LA Model Implementation
Engineered Barrier System Colloids Submodel 6.3.7.6	Epistemic: \Input_Params_Epistemic\Epistemic_Params_EBS_F_and_T\Uncertain_Params_Colloids EBS: \Global_Inputs_and_Calcs\Global_EBS_F_and_T\Model_Input_EBS_Transport\Input_Params_Colloids	2.1.09.02.0A Chemical interaction with corrosion products	Corrosion products provide sorption sites along the transport pathway for radionuclide release from the waste form to the invert. In the TSPA-LA Model, sorption of radionuclides onto corrosion products retards radionuclide migration, while sorption onto mobile corrosion product colloids facilitates migration.	10 CFR 63.311 10 CFR 63.331 10 CFR 63.321	GSM
		2.1.09.16.0A Formation of pseudo-colloids (natural) in EBS	In the TSPA-LA Model, seepage water colloids included in the Colloid Model are modeled with reversible radionuclide attachment using linear sorption coefficients Kd.	10 CFR 63.311 10 CFR 63.331 10 CFR 63.321	GSM
		2.1.09.17.0A Formation of pseudo-colloids (corrosion product) in EBS	In the TSPA-LA Model, corrosion product colloids included in the Colloid Model are modeled with both reversible and irreversible radionuclide attachments.	10 CFR 63.311 10 CFR 63.331 10 CFR 63.321	GSM
		2.1.09.23.0A Stability of colloids in EBS	In the TSPA-LA Model, the stability of smectite colloids, which is applicable for the repository groundwater colloids and waste form colloids, is determined primarily by ionic strength but also to an extent by pH. The stability of iron-(hydr)oxide colloids, which is applicable to corrosion-product colloids, is determined by both ionic strength and pH.	10 CFR 63.311 10 CFR 63.331 10 CFR 63.321	GSM
		2.1.09.25.0A Formation of colloids (waste form) by co-precipitation in EBS	Colloids formed from the corrosion of HLW glass and the degradation of CSNF were found to contain embedded radionuclide-carrying phases. In the TSPA-LA Model, these radionuclides are modeled as irreversibly attached to the colloids.	10 CFR 63.311 10 CFR 63.331 10 CFR 63.321	GSM

Table I-2. Model Implementation for Included Features, Events, and Processes (Continued)

Submodel implemented in the TSPA-LA Model and Section Number	Path in GoldSim Model File	FEPs Included in the Submodel	TSPA Inclusion Explanation	Performance Assessment Standard[a]	TSPA-LA Model Implementation
EBS Flow Submodel 6.3.6	Epistemic: \Input_Params_Epistemic\Epistemic_Params_EBS_F_and_T\Uncertain_Params_Flux_Split EBS: \Time_Zero\EBS_PS_Loop\Static_Calcs_PS_Loop\Static_Calcs_EBS_F_and_T\EBS_Flow \Global_Inputs_and_Calcs\Global_EBS_F_and_T\Model_Feeds_EBS_Flow	2.1.06.06.0A Effects of drip shield on flow	The EBS Flow Abstraction Model implemented in the TSPA-LA Model accounts for the flow of water through and around the DS. An algorithm referred to as the DS flux-splitting submodel is developed for calculating the fraction of flow diverted by the DS when breaches in the DS exist, and is directly included in the TSPA-LA Model.	10 CFR 63.311 10 CFR 63.331	GSM
		2.1.08.04.0A Condensation forms on roofs of drifts (drift-scale cold traps)	Condensation represents one source of input into the dripping flux presented by the EBS radionuclide transport abstraction. The EBS RTA is used to quantify the release of radionuclides from the EBS to the UZ. Dripping flux comprises a major source of liquid flow into the EBS. The EBS flow model is implemented directly in TSPA.	10 CFR 63.311 10 CFR 63.331	GSM
		2.1.08.04.0B Condensation forms at repository edges (repository-scale cold traps)	Condensation represents one source of input into the dripping flux presented by the EBS radionuclide transport abstraction. The EBS RTA is used to quantify the release of radionuclides from the EBS to the UZ. Dripping flux comprises a major source of liquid flow into the EBS. The EBS flow model is implemented directly in TSPA.	10 CFR 63.311 10 CFR 63.331	GSM

Table I-2. Model Implementation for Included Features, Events, and Processes (Continued)

Submodel implemented in the TSPA-LA Model and Section Number	Path in GoldSim Model File	FEPs Included in the Submodel	TSPA Inclusion Explanation	Performance Assessment Standard[a]	TSPA-LA Model Implementation
EBS Flow Submodel 6.3.6	Epistemic: \Input_Params_Epistemic\Epistemic_Params_EBS_F_and_T\Uncertain_Params_Flux_Split EBS: \Time_Zero\EBS_PS_Loop\Static_Calcs_PS_Loop\Static_Calcs_EBS_F_and_T\EBS_Flow \Global_Inputs_and_Calcs\Global_EBS_F_and_T\Model_Feeds_EBS_Flow	2.1.08.05.0A Flow through invert	The EBS Flow Model explicitly models flow through the invert and the advective transport of radionuclides. Flow through the invert consists of the fluxes diverted by the DS and WP, the flux through the WP, and the imbibition flux from the UZ. Each of these terms is accounted for in the EBS Flow Abstraction Model, which is implemented in the TSPA-LA Model.	10 CFR 63.311 10 CFR 63.331	GSM
		2.1.08.06.0A Capillary effects (wicking) in EBS	The MSTHM process model includes wicking from the host rock to the invert. The MSTHM results are used to develop the TH abstraction implemented in the TSPA-LA Model. Wicking of water from the host rock to the invert is accounted for in the EBS Flow Model through the prediction of the matrix saturation of the invert provided by the TH abstraction. Matrix saturation is directly applied in the calculation of diffusion coefficient in both the WP and the invert.	10 CFR 63.311 10 CFR 63.331	GSM

Table I-2. Model Implementation for Included Features, Events, and Processes (Continued)

Submodel implemented in the TSPA-LA Model and Section Number	Path in GoldSim Model File	FEPs Included in the Submodel	TSPA Inclusion Explanation	Performance Assessment Standard[a]	TSPA-LA Model Implementation
EBS Flow Submodel (continued) 6.3.6	Epistemic: \Input_Params_Epistemic\Epistemic_Params_EBS_F_and_T\Uncertain_Params_Flux_Split EBS: \Time_Zero\EBS_PS_Loop\Static_Calcs_PS_Loop\Static_Calcs_EBS_F_and_T\EBS_Flow \Global_Inputs_and_Calcs\Global_EBS_F_and_T\Model_Feeds_EBS_Flow	2.1.08.07.0A Unsaturated flow in the EBS	Unsaturated flow is included in the TSPA through the flow component of the EBS radionuclide flow and transport abstraction. In the flow model, no explicit distinction between saturated and unsaturated flow is made. However, water saturations along the flow pathway, in the WP and in the invert, are typically less than one (fully saturated conditions). Invert and EBS/UZ interface aspects of this FEP are not implemented in the human intrusion assessment.	10 CFR 63.311 10 CFR 63.331	GSM
		2.1.11.09.0A Thermal effects on flow in the EBS	In the TSPA-LA Model, the temperature history in the EBS is calculated by the TH abstraction model. When drift wall temperatures exceed 100°C, seepage is not allowed to enter the drift, and flow in the EBS is assumed not to occur.	10 CFR 63.311 10 CFR 63.331	GSM
EBS Transport Submodel 6.3.8	Epistemic: \Input_Params_Epistemic\Epistemic_Params_EBS_F_and_T EBS: \Global_Inputs_and_Calcs\Global_EBS_F_and_T\Model_Input_EBS_Transport	2.1.03.11.0A Physical form of waste package and drip shield	The effect of the physical form of waste package is accounted for in the EBS transport submodel, in which different diffusive path lengths are used for each of the two representative waste packages (TADs for CSNF and 5-DHLW/DOE SNF – Long for codisposal). Radionuclide transport is impacted by the materials used in the waste package by means of material-specific degradation rates, diffusive properties, and radionuclide sorption characteristics implemented in the TSPA.	10 CFR 63.311 10 CFR 63.331 10 CFR 63.321	GSM

Table I-2. Model Implementation for Included Features, Events, and Processes (Continued)

Submodel implemented in the TSPA-LA Model and Section Number	Path in GoldSim Model File	FEPs Included in the Submodel	TSPA Inclusion Explanation	Performance Assessment Standard[a]	TSPA-LA Model Implementation
EBS Transport Submodel 6.3.8 (Continued)	Epistemic: \Input_Params_Epistemic\Epistemic_Params_EBS_F_and_T EBS: \Global_Inputs_and_Calcs\Global_EBS_F_and_T\Model_Input_EBS_Transport	2.1.08.07.0A Unsaturated flow in the EB	Unsaturated flow is included in the TSPA through the flow component of the EBS radionuclide flow and transport abstraction. In the flow model, no explicit distinction between saturated and unsaturated flow is made. However, water saturations along the flow pathway, in the WP and in the invert, are typically less than one (fully saturated conditions). This water flow is used by the EBS Transport abstraction model to advect radionuclides along the transport pathway from the waste form to the EBS/UZ interface. Invert and EBS-UZ interface aspects of this FEP are not implemented in the human intrusion assessment.	10 CFR 63.311 10 CFR 63.331 10 CFR 63.321	GSM
		2.1.09.01.0B Chemical characteristics of water in waste package	Chemical characteristics of water in waste package are implemented in the TSPA model through the in-package chemistry abstraction, which estimates pH in the waste form. In the EBS radionuclide transport abstraction, a range of waste form effluents is numerically equilibrated with waste package corrosion products to parameterize pH as a function of ambient carbon dioxide levels and corrosion product surface properties to estimate the distribution of radionuclides among colloids, stationary corrosion products, and the solution	10 CFR 63.311 10 CFR 63.331 10 CFR 63.321	MA
		2.1.09.02.0A Chemical interaction with corrosion products	The effect of corrosion products on the transport of radionuclides internal to the waste package is included in the TSPA-LA Model through the EBS radionuclide transport abstraction. No radionuclide sorption is modeled to occur on corrosion products in the invert. The EBS radionuclide transport abstraction models retardation of radionuclides in the waste package corrosion products using site-limited, competitive sorption coefficients for radionuclides on corrosion products.	10 CFR 63.311 10 CFR 63.331 10 CFR 63.321	MA

Table I-2. Model Implementation for Included Features, Events, and Processes (Continued)

Submodel implemented in the TSPA-LA Model and Section Number	Path in GoldSim Model File	FEPs Included in the Submodel	TSPA Inclusion Explanation	Performance Assessment Standard[a]	TSPA-LA Model Implementation
EBS Transport Submodel 6.3.8 (Continued)	Epistemic: \Input_Params_Epistemic\Epistemic_Params_EBS_F_and_T EBS: \Global_Inputs_and_Calcs\Global_EBS_F_and_T\Model_Input_EBS_Transport	2.1.09.08.0A Diffusion of dissolved radionuclides in EBS	Diffusive transport of dissolved radionuclides in the EBS is a major component of the EBS Transport model. Uncertainty in diffusive transport is incorporated via parameters for invert diffusion coefficient uncertainty, stainless steel and carbon steel corrosion rates, diffusive path length through corrosion products inside a WP, and the specific surface area of steel corrosion products. These parameters are sampled in TSPA-LA Model, and the model for diffusive transport of radionuclides is implemented directly in TSPA-LA Model Invert and EBS/UZ interface aspects of this FEP are not implemented in the human intrusion assessment.	10 CFR 63.311 10 CFR 63.331 10 CFR 63.321	GSM
		2.1.09.19.0B Advection of colloids in EBS	Advective transport of radionuclide-bearing colloids in the EBS is determined in the EBS Transport Model. The advective transport moves colloids (and the associated radionuclides) at about the same velocity as the liquid flux through the EBS. The concentration of colloids in EBS components, together with the water flow rates through each component, determines the rate of advective releases of colloids from the EBS. In the assessment of human intrusion, advection of colloids is included in the transport of colloids down the borehole from the WP to the UZ	10 CFR 63.311 10 CFR 63.331 10 CFR 63.321	GSM
		2.1.09.08.0B Advection of dissolved radionuclides in EBS	Advective transport, which depends on the fluxes through breaches in the DS and WP, is directly included in TSPA. The flux splitting submodel determines the fraction of the seepage flux that flows through the WP. Flux splitting submodel is not included in the human intrusion assessment	10 CFR 63.311 10 CFR 63.331 10 CFR 63.321	GSM

Table I-2. Model Implementation for Included Features, Events, and Processes (Continued)

Submodel implemented in the TSPA-LA Model and Section Number	Path in GoldSim Model File	FEPs Included in the Submodel	TSPA Inclusion Explanation	Performance Assessment Standard[a]	TSPA-LA Model Implementation
EBS Transport Submodel 6.3.8 (Continued)	Epistemic: \Input_Params_Epistemic\Epistemic_Params_EBS_F_and_T EBS: \Global_Inputs_and_Calcs\Global_EBS_F_and_T\Model_Input_EBS_Transport	2.1.09.05.0A Sorption of dissolved radionuclides in EBS	Sorption of dissolved radionuclides in the EBS is captured by two sorption models. In the WP, a complexation-based sorption submodel relates the mass concentration of a radionuclide component in a solid phase to the dissolved concentration of the same component in a contacting phase as a function of aqueous phase chemistry. This submodel accounts for sorption of radionuclides onto corrosion products in the WP. A linear sorption model accounts for sorption on crushed tuff in the invert. The proportionality constant in this submodel is the distribution coefficient (Kd). The Kds are uncertain parameters sampled in the TSPA-LA Model and used as input to the radionuclide transport calculation in TSPA. Sorption retards the transport of radionuclides through the EBS and thus has a direct impact on estimated releases of radionuclides from the EBS. Sorption to invert not included in the human intrusion assessment; however, sorption to corrosoion products inside the waste package in included for the human intrusion assessment	10 CFR 63.311 10 CFR 63.331 10 CFR 63.321	GSM

Table I-2. Model Implementation for Included Features, Events, and Processes (Continued)

Submodel implemented in the TSPA-LA Model and Section Number	Path in GoldSim Model File	FEPs Included in the Submodel	TSPA Inclusion Explanation	Performance Assessment Standard[a]	TSPA-LA Model Implementation
EBS Transport Submodel 6.3.8 (Continued)	Epistemic: \Input_Params_Epistemic\Epistemic_Params_EBS_F_and_T EBS: \Global_Inputs_and_Calcs\Global_EBS_F_and_T\Model_Input_EBS_Transport	2.1.09.24.0A Diffusion of Colloids in EBS	Diffusion of colloids in the EBS is determined by the EBS Transport model and implemented directly in TSPA. Three types of colloids are anticipated to exist in the EBS: (a) waste form colloids from degradation of HLW glass and CSNF, (b) iron oxyhydroxide colloids due to products from the corrosion of steel WPs, and (c) groundwater or seepage water colloids. On all three types of colloids, radionuclides may undergo reversible, or equilibrium, sorption. The waste form colloids may also contain embedded radionuclides that are not removable. General colloid-facilitated diffusive transport model is implemented in TSPA. In the assessment of human intrusion, diffusion of colloids is included in the transport of colloids down the borehole from the WP to the UZ	10 CFR 63.311 10 CFR 63.331 10 CFR 63.321	GSM
		2.2.07.06.0B Long-term release of radionuclides from the repository	The EBS radionuclide transport abstraction (RTA) is used to quantify the time-dependent radionuclide releases from a failed waste package and their subsequent transport through the EBS to the emplacement drift wall/UZ interface. The RTA model, which is implemented directly into the TSPA GoldSim model, allows quantification of radionuclide releases from a failed waste package over the entire compliance period.	10 CFR 63.311 10 CFR 63.331 10 CFR 63.321	GSM

Table I-2. Model Implementation for Included Features, Events, and Processes (Continued)

Submodel implemented in the TSPA-LA Model and Section Number	Path in GoldSim Model File	FEPs Included in the Submodel	TSPA Inclusion Explanation	Performance Assessment Standard[a]	TSPA-LA Model Implementation
EBS-UZ Interface Submodel 6.3.8 This submodel is not implemented in human intrusion assessment	Epistemic: \Input_Params_Epistemic\Epistemic_Params_EBS_F_and_T\Uncertain_Params_EBS_UZ_Trans EBS: \Global_Inputs_and_Calcs\Global_EBS_F_and_T\EBS_UZ_Transport_Inputs	1.2.02.01.0A Fractures	In TSPA, the EBS-UZ interface domain is included beneath the invert domain to establish a boundary condition for calculating the diffusive flux from the invert to the UZ and to compute the radionuclide mass flux fraction going into each of the UZ fracture and matrix continua.	10 CFR 63.311 10 CFR 63.331	GSM
		2.1.09.08.0A Diffusion of dissolved radionuclides in EBS	Diffusive transport of dissolved radionuclides from EBS to the UZ is determined by the EBS-UZ Interface Submodel. Uncertainty in diffusive transport is incorporated via parameters for invert diffusion coefficient uncertainty and UZ invert diffusion coefficient uncertainty. These parameters are sampled in TSPA, and the model for diffusive transport of radionuclides to the UZ is implemented directly in the TSPA-LA Model	10 CFR 63.311 10 CFR 63.331	GSM
		2.1.09.08.0B Advection of dissolved radionuclides in EBS	The EBS radionuclide transport abstraction is used to quantify the time-dependent radionuclide releases from a failed waste package and their subsequent transport through the EBS to the emplacement drift wall/UZ interface. The basic inputs to the RTA model consist of the drift seepage and drift-wall condensation flux, the environmental conditions in the drift (temperature, relative humidity, and water chemistry), and the degradation state of the EBS components. Outputs from the RTA are used in the TSPA to calculate the rates of radionuclide releases to the UZ. The RTA model is implemented directly into the TSPA GoldSim model to compute the radionuclide release rates from the EBS.	10 CFR 63.311 10 CFR 63.331	GSM

Table I-2. Model Implementation for Included Features, Events, and Processes (Continued)

Submodel implemented in the TSPA-LA Model and Section Number	Path in GoldSim Model File	FEPs Included in the Submodel	TSPA Inclusion Explanation	Performance Assessment Standard[a]	TSPA-LA Model Implementation
EBS-UZ Interface Submodel 6.3.8 (Continued) Model not implemented in human intrusion assessment	Epistemic: \Input_Params_Epistemic\Epistemic_Params_EBS_F_and_T\Uncertain_Params_EBS_UZ_Trans EBS: \Global_Inputs_and_Calcs\Global_EBS_F_and_T\EBS_UZ_Transport_Inputs	2.1.09.19.0B Advection of colloids in EBS	Advective transport of radionuclide-bearing colloids from the EBS to the UZ is determined EBS-UZ Interface Submodel. The advective transport moves colloids (and the associated radionuclides) from the EBS to the UZ at about the same velocity as the liquid flux through the invert.	10 CFR 63.311 10 CFR 63.331	GSM
		2.1.09.24.0A Diffusion of Colloids in EBS	Diffusive transport of dissolved colloids from EBS to the UZ is determined by the EBS-UZ Interface Submodel. The diffusion coefficient for colloidal particles is estimated to be a factor of 100 less than the diffusion coefficient for dissolved radionuclides. Uncertainty in diffusive transport is incorporated via parameters for invert diffusion coefficient uncertainty and UZ invert diffusion coefficient uncertainty. These parameters are sampled in TSPA, and the model for diffusive transport of radionuclides to the UZ is implemented directly in the TSPA-LA Model	10 CFR 63.311 10 CFR 63.331	GSM
UZ Transport Submodel (groundwater protection and individual protection assessment) 6.3.9	Epistemic: \Input_Params_Epistemic\Epistemic_Params_UZ_Transport Other: \TSPA_Model\UZ_Transport	1.2.02.01.0A Fractures	The influence of fractures on radionuclide transport is included in the UZ Transport Particle Tracking Transport Abstraction Model through the dual- permeability model for UZ flow and transport. Fracture aperture, porosity, and frequency are treated directly in the UZ radionuclide particle tracking transport abstraction model.	10 CFR 63.311 10 CFR 63.331	DLL

Table I-2. Model Implementation for Included Features, Events, and Processes (Continued)

Submodel implemented in the TSPA-LA Model and Section Number	Path in GoldSim Model File	FEPs Included in the Submodel	TSPA Inclusion Explanation	Performance Assessment Standard[a]	TSPA-LA Model Implementation
UZ Transport submodel for Human Intrusion Assessment 6.3.9 In the human intrusion assessment UZ transport is implemented using a 1D pipe model in GoldSim	Epistemic: \Input_Params_Epistemic\Epistemic_Params_UZ_Transport Other: \TSPA_Model\UZ_Transport	1.2.02.01.0A Fractures	The influence of fractures in the UZ on transport down the borehole is included in the 1D pipe model for human intrusion.	10 CFR 63.321	GSM

Table I-2. Model Implementation for Included Features, Events, and Processes (Continued)

Submodel implemented in the TSPA-LA Model and Section Number	Path in GoldSim Model File	FEPs Included in the Submodel	TSPA Inclusion Explanation	Performance Assessment Standard[a]	TSPA-LA Model Implementation
UZ Transport Submodel 6.3.9 (continued)	Epistemic: \Input_Params_Epistemic\Epistemic_Params_UZ_Transport Other: \TSPA_Model\UZ_Transport	1.2.02.02.0A Faults	The influence of faults on radionuclide transport is included in the UZ Transport Particle Tracking Transport Abstraction Model through the use of the dual-permeability flow model that directly represents the effects of faults on UZ flow. Fracture aperture, porosity, and frequency within faults are treated directly in the UZ radionuclide particle tracking transport abstraction model.	10 CFR 63.311 10 CFR 63.331	DLL
		1.3.01.00.0A Climate change	The effect of climate change on radionuclide transport in the UZ is included in the UZ Transport Particle Tracking Transport Abstraction Model by using pre-generated flow fields for different climates. Shorter term climate changes are incorporated in the range of uncertainty for all climate states.	10 CFR 63.311 10 CFR 63.331	DLL
		1.3.01.00.0A Climate change	In the human intrusion assessment the effect of climate change is included in the calculation of water flux through the borehole. Water flux through the borehole is determined from the percolation flux at the base of the PTn. See the UZ Flow Field Abstraction Submodel.	10 CFR 63.321	GSM
		1.3.07.02.0B Water table rise affects unsaturated zone	The effect of water table rise on transport in the UZ is included by shortening the length of the transport pathway between the EBS and UZ by the amount of water table rise. Also, all radionuclides that are contained in the UZ region captured by the water table rise are assumed to be released instantaneously into the SZ. Water table changes are implemented in the TSPA by allowing the water table to change elevation instantaneously upon change in climate, concurrent with changes in infiltration.	10 CFR 63.311 10 CFR 63.331	DLL

Table I-2. Model Implementation for Included Features, Events, and Processes (Continued)

Submodel implemented in the TSPA-LA Model and Section Number	Path in GoldSim Model File	FEPs Included in the Submodel	TSPA Inclusion Explanation	Performance Assessment Standard[a]	TSPA-LA Model Implementation
UZ Transport Submodel 6.3.9 (Continued)	Epistemic: \Input_Params_Epistemic\Epistemic_Params_UZ_Transport Other: \TSPA_Model\UZ_Transport		Water table rise affects the UZ as it impacts the water level in the borehole and is included in the human intrusion assessment. See the UZ Flow Field Abstraction Submodel.	10 CFR 63.321	
		1.4.01.01.0A Climate modification increases recharge	The effect of climate changes is included in the UZ Transport Particle Tracking Transport Abstraction Model in the form of increased recharge and is included in the UZ radionuclide transport abstraction model for TSPA through the use of pre-generated flow fields.	10 CFR 63.311 10 CFR 63.331	DLL
			The effect of climate modification and its impact on water flux down the borehole is included in the human intrusion assessment. See the UZ Flow Field Abstraction Submodel.	10 CFR 63.321	
		2.1.08.01.0A Water influx at the repository	The influence of water influx at the repository on radionuclide transport is included in the UZ Transport Particle Tracking Transport Abstraction Model through the use of pregenerated flow fields under different climates in the UZ Radionuclide Transport Abstraction Model.	10 CFR 63.311 10 CFR 63.331	DLL
			The effect of percolation flux above the repository and its impact on water flux down the borehole is included in the human intrusion assessment. See the UZ Flow Field Abstraction Submodel.	10 CFR 63.321	
		2.2.03.01.0A Stratigraphy	Stratigraphy is included in the UZ radionuclide transport abstraction model through the use of pre-generated flow fields.	10 CFR 63.311 10 CFR 63.331	MA

Table I-2. Model Implementation for Included Features, Events, and Processes (Continued)

Submodel implemented in the TSPA-LA Model and Section Number	Path in GoldSim Model File	FEPs Included in the Submodel	TSPA Inclusion Explanation	Performance Assessment Standard[a]	TSPA-LA Model Implementation
UZ Transport Submodel 6.3.9 (Continued)	Epistemic: \Input_Params_Epistemic\Epistemic_Params_UZ_Transport Other: \TSPA_Model\UZ_Transport	2.2.03.02.0A Rock properties of host rock and other units	Rock properties of host rock and other units are included and used in the TSPA simulations of radionuclide transport through the UZ. Matrix porosity, rock density, fracture porosity, fracture spacing, and aperture data are incorporated into the transport simulations.	10 CFR 63.311 10 CFR 63.331	MA
			In the human intrusion assessment the borehole is conceptualized to be filled with the rubble of collapsed matrix blocks that have preferential pathways such as fractures similar to the fractures in the undisturbed host rock near the drift. Fracture properties such as fracture aperture, porosity, and frequency are assumed to be the same as that for the rock type near the drift (such as the TSw unit).	10 CFR 63.321	
		2.2.07.02.0A Unsaturated groundwater flow in the geosphere	Water flow is the driving force for radionuclide transport through the UZ. This process is included through the use of pregenerated flow fields for transport. The effect of percolation flux above the repository and its impact on water flux down the borehole is included in the human intrusion assessment. See the UZ Flow Field Abstraction Submodel.	10 CFR 63.311 10 CFR 63.331 10 CFR 63.321	DLL
		2.2.07.04.0A Focusing of unsaturated flow (fingers, weeps)	The effect of focusing unsaturated flow is included through the use of pregenerated flow fields in the TSPA UZ transport simulations. Large scale focusing is included in human intrusion because percolation flux in the UZ above the repository at the base of the PTn is used to determine the flux downward through the borehole. Intermediate-scale focusing is not included in human intrusion because the seepage model is not implemented for this assessment	10 CFR 63.311 10 CFR 63.331 10 CFR 63.321	DLL

Table I-2. Model Implementation for Included Features, Events, and Processes (Continued)

Submodel implemented in the TSPA-LA Model and Section Number	Path in GoldSim Model File	FEPs Included in the Submodel	TSPA Inclusion Explanation	Performance Assessment Standard[a]	TSPA-LA Model Implementation
UZ Transport Submodel 6.3.9 (Continued)	Epistemic: \Input_Params_Epistemic\Epistemic_Params_UZ_Transport Other: \TSPA_Model\UZ_Transport	2.2.07.06.0B Long-term release of radionuclides from the repository	The effects of WP breaches over a long period of time are included in the source term model for TSPA, which affects the source term of radionuclide mass for the UZ radionuclide transport abstraction model implemented in TSPA.	10 CFR 63.311 10 CFR 63.331	DLL
		2.2.07.07.0A Perched water develops	Perched water is included through the use of pre-generated flow fields in the TSPA UZ transport simulations.	10 CFR 63.311 10 CFR 63.331	DLL
		2.2.07.08.0A Fracture flow in the unsaturated zone	The effects of fracture flow on radionuclide transport (advection) is included in the UZ radionuclide transport abstraction model implemented in the TSPA-LA Modelthrough the use of pre-generated unsaturated flow fields that include the occurrence of perched water.	10 CFR 63.311 10 CFR 63.331 10 CFR 63.321	DLL
		2.2.07.09.0A Matrix imbibition in the unsaturated zone	Matrix imbibition in the UZ is included through the use of pre-generated flow fields in the TSPA UZ transport simulations.	10 CFR 63.311 10 CFR 63.331	DLL
		2.2.07.15.0B Advection and dispersion in the unsaturated zone	Dispersion is incorporated in the UZ radionuclide transport abstraction model implemented in the TSPA-LA Model through the use of a transfer function based on an analytical solution to the advection-dispersion equation.	10 CFR 63.311 10 CFR 63.331 10 CFR 63.321	DLL
		2.2.08.01.0B Chemical characteristics of groundwater in the unsaturated zone	The effects of groundwater composition are incorporated into the probability distributions for radionuclide sorption in the UZ sampled in TSPA.	10 CFR 63.311 10 CFR 63.331 10 CFR 63.321	GSM
		2.2.08.06.0B Complexation in the unsaturated zone	The effects of complexation are included in the experimental data used to derive radionuclide sorption coefficients sampled in the TSPA-LA Model for sorption in the UZ.	10 CFR 63.311 10 CFR 63.331 10 CFR 63.321	DLL

Table I-2. Model Implementation for Included Features, Events, and Processes (Continued)

Submodel implemented in the TSPA-LA Model and Section Number	Path in GoldSim Model File	FEPs Included in the Submodel	TSPA Inclusion Explanation	Performance Assessment Standard[a]	TSPA-LA Model Implementation
UZ Transport Submodel 6.3.9 (Continued)	Epistemic: \Input_Params_Epistemic\Epistemic_Params_UZ_Transport Other: \TSPA_Model\UZ_Transport	2.2.08.08.0B Matrix diffusion in the UZ	Transfer functions that are used in the UZ radionuclide transport abstraction model for TSPA include the mechanism of matrix diffusion.	10 CFR 63.311 10 CFR 63.331 10 CFR 63.321	DLL
		2.2.08.09.0B Sorption in the unsaturated zone	Linear, equilibrium sorption is accounted for in the rock matrix continuum, with no sorption conservatively used in the fractures. Sorption coefficients are implemented in the TSPA-LA Model in terms of probability distributions for the sorption coefficient of each element of interest among the three major rock types (devitrified, zeolitic, and vitric) found in the UZ. The probability distributions account for uncertainties in water chemistry, mineralogy, and sorption mechanisms. In the human intrusion assessment, sorption of radionuclides in the UZ is modeled using the devitrified UZ Kd values as representative for the entire pathway. Sorption occurs on the matrix only.	10 CFR 63.311 10 CFR 63.331 10 CFR 63.321	DLL
		2.2.08.10.0B Colloid transport in the UZ	Colloid-facilitated radionuclide transport included in the TSPA-LA Model treats both radionuclides permanently attached to colloids and radionuclides that partition between colloids, the aqueous phase, and the rock matrix. Diffusion of colloids into the rock matrix is not included, which leads to greater facilitation of radionuclide transport by colloids. Colloid transport down the borehole through the UZ is included in the human intrusion assessment.	10 CFR 63.311 10 CFR 63.331 10 CFR 63.321	DLL

Table I-2. Model Implementation for Included Features, Events, and Processes (Continued)

Submodel implemented in the TSPA-LA Model and Section Number	Path in GoldSim Model File	FEPs Included in the Submodel	TSPA Inclusion Explanation	Performance Assessment Standard[a]	TSPA-LA Model Implementation
UZ Transport Submodel 6.3.9 (Continued)	Epistemic: \Input_Params_Epistemic\Epistemic_Params_UZ_Transport Other: \TSPA_Model\UZ_Transport	2.3.11.03.0A Infiltration and recharge	The hydrologic effects of infiltration and recharge are included in the Infiltration Model which includes the effects of seasonal and climate variations, climate change, surface-water runoff, and site topology, such as hill slopes and washes. The effects of climate change included in the TSPA through the UZ flow fields that are used to evaluate the local percolation fluxes. Percolation fluxes are used to calculate radionuclide transport from the repository to the SZ.	10 CFR 63.311 10 CFR 63.331 10 CFR 63.321	DLL
		3.1.01.01.0A Radioactive decay and ingrowth	Both simple decay and radionuclide chain-decay are directly included in the UZ Transport Model implemented in TSPA. Although the UZ Transport Submodel Is not implemented in the human intrusion assessment, radioactive decay and ingrowth down the borehole through the UZ is included in the human intrusion assessment.	10 CFR 63.311 10 CFR 63.331 10 CFR 63.321	DLL
SZ Flow and Transport Submodel 6.3.10	Epistemic: \Input_Params_Epistemic\Epistemic_Params_SZ_Transport Other: \TSPA_Model\SZ_Transport	1.2.02.01.0A Fractures	Groundwater flow through fractures in the volcanic units is included in the SZ flow and transport model which is implemented directly into the TSPA-LA model through an effective continuum flow model. Observations at Yucca Mountain indicate that flow is primarily through the fracture network instead of the matrix. The characteristics of the fracture properties, such as fracture orientation, aperture size, degree of infilling, and tortuosity are modeled through probabilistically modeled parameters.	10 CFR 63.311 10 CFR 63.331 10 CFR 63.321	GSM

Table I-2. Model Implementation for Included Features, Events, and Processes (Continued)

Submodel implemented in the TSPA-LA Model and Section Number	Path in GoldSim Model File	FEPs Included in the Submodel	TSPA Inclusion Explanation	Performance Assessment Standard[a]	TSPA-LA Model Implementation
SZ Flow and Transport Submodel (continued) 6.3.10	Epistemic: \Input_Params_Epistemic\Epistemic_Params_SZ_Transport Other: \TSPA_Model\SZ_Transport	1.2.02.02.0A Faults	In general, large-scale hydraulic features (e.g., major faults, fault zones, zones of chemical alteration) have been incorporated into the Site-Scale Saturated Zone (SZ) Flow Model as zones of enhanced or reduced permeability. The faults were generally modeled as anisotropic features with high conductivity along the fault (strike) and low conductivity in the direction across the fault. These features are reflected in the flow fields used in the SZ flow model abstraction implemented in TSPA.	10 CFR 63.311 10 CFR 63.331 10 CFR 63.321	GSM
		1.3.01.00.0A Climate Change	The effects of climate change are incorporated into the SZ flow and transport abstraction model and the SZ one-dimensional transport model as implemented in the TSPA by assuming instantaneous change from one steady-state flow condition to another steady-state condition in the SZ. Changes in climate state are assumed to affect the magnitude of groundwater flux through the SZ system but have a negligible impact on flow paths. The effect of changes in groundwater flux is incorporated into the SZ flow and transport abstraction model by scaling the timing of radionuclide mass breakthrough curves proportionally to the change in SZ-specific discharge	10 CFR 63.311 10 CFR 63.331 10 CFR 63.321	GSM
		1.3.07.02.0A Water table rise affects SZ	Water table rise and the effect of increased flow (due to wetter future climate conditions) on the SZ breakthrough curves are modeled using scaling factors representing the future climate states. The scaling factors used in this approach are the ratio of average SZ groundwater flow under the future climatic conditions to the flow under present conditions. The scaling factors are a direct input to TSPA.	10 CFR 63.311 10 CFR 63.331 10 CFR 63.321	GSM

Table I-2. Model Implementation for Included Features, Events, and Processes (Continued)

Submodel implemented in the TSPA-LA Model and Section Number	Path in GoldSim Model File	FEPs Included in the Submodel	TSPA Inclusion Explanation	Performance Assessment Standard[a]	TSPA-LA Model Implementation
SZ Flow and Transport Submodel (continued) 6.3.10	Epistemic: \Input_Params_Epistemic\Epistemic_Params_SZ_Transport Other: \TSPA_Model\SZ_Transport	1.4.01.01.0A Climate modification increases recharge	Climate modification is expected to lead to an increase in precipitation and net infiltration Increased net infiltration will become increased recharge to the saturated zone, and as more recharge enters the saturated zone, the water table may rise increasing the volumetric flow of groundwater. The larger flow in the saturated zone is simulated by a groundwater specific discharge scaling factor that increases the flow of water in the saturated zone corresponding to future climate conditions without changing the position of the water table. These scaling factors are a direct input to the TSPA.	10 CFR 63.311 10 CFR 63.331 10 CFR 63.321	GSM
		1.4.07.02.0A Wells	Dilution of radionuclide concentrations in groundwater used by the reasonable maximally exposed individual (RMEI) occurs both during transport in the SZ because of dispersion and in the process of extracting groundwater from wells. The Site-Scale SZ Flow Model domain was made sufficiently large to include wells in the Amargosa Valley at the southern end of the modeled area. At the accessible environment, located about 18 km south of Yucca Mountain, the RMEI is postulated to use well water that is extracted from the aquifer. In the TSPA, all radionuclide mass reaching the downgradient accessible environment is captured by the wells of the receptor group.	10 CFR 63.311 10 CFR 63.331 10 CFR 63.321	GSM
		2.2.03.01.0A Stratigraphy	The site-scale HFM is a representation of the hydrogeologic units and major structural features within the SZ flow system, encompassed by the domain of the Site-Scale SZ Flow Model. To represent the geologic heterogeneity introduced by stratigraphy in a groundwater model, geologic units were simplified into hydrogeologic units on the basis of similar hydrogeologic properties. The stratigraphy is reflected in the flow fields used in the SZ Flow Model abstraction implemented in TSPA.	10 CFR 63.311 10 CFR 63.331 10 CFR 63.321	MA

Table I-2. Model Implementation for Included Features, Events, and Processes (Continued)

Submodel implemented in the TSPA-LA Model and Section Number	Path in GoldSim Model File	FEPs Included in the Submodel	TSPA Inclusion Explanation	Performance Assessment Standard[a]	TSPA-LA Model Implementation
SZ Flow and Transport Submodel 6.3.10 (Continued)	Epistemic: \Input_Params_Epistemic\Epistemic_Params_SZ_Transport Other: \TSPA_Model\SZ_Transport	2.2.03.02.0A Rock properties of host rock and other units	Geologic features and heterogeneous hydrostratigraphic units are included in the SZ flow and transport abstraction model as cells with specific hydrologic parameter values in a configuration based on the hydrogeologic framework. Available geologic information of rock properties that affect saturated zone flow and transport in the Yucca Mountain region is used to determine the 23 hydrostratigraphic units modeled in the site-scale saturated zone flow domain. Rock properties are reflected in the flow fields used in the SZ Flow Model abstraction implemented in TSPA.	10 CFR 63.311 10 CFR 63.331 10 CFR 63.321	MA
		2.2.07.12.0A Saturated groundwater flow in the geosphere	Steady-state, saturated, three-dimensional groundwater flow within the Yucca Mountain vicinity is modeled through the Site-Scale SZ Flow Model. Flow through fractures is modeled through an effective continuum flow model. The continuum approach allows the use of widely accepted mathematical equations describing groundwater flow through porous medium as the mathematical basis for the Site-Scale SZ Flow Model.	10 CFR 63.311 10 CFR 63.331 10 CFR 63.321	GSM
		2.2.07.13.0A Water-conducting features in the SZ	To represent discrete features and regions having distinct hydrologic properties within the Site-Scale SZ Flow Model domain, a set of 17 hydrogeologic features complementary to the HFM were identified and incorporated into the Site-Scale SZ Flow Model. These features are reflected in the flow abstraction model implemented in TSPA. The SZ Flow and Transport Abstraction Model is implemented by the 1-D SZ Flow and Transport Model Component that is implemented in GoldSim and the 3-D SZ Flow and Transport Model component implemented by the SZ convolute DLL.	10 CFR 63.311 10 CFR 63.331 10 CFR 63.321	GSM/DLL

Table I-2. Model Implementation for Included Features, Events, and Processes (Continued)

Submodel implemented in the TSPA-LA Model and Section Number	Path in GoldSim Model File	FEPs Included in the Submodel	TSPA Inclusion Explanation	Performance Assessment Standard[a]	TSPA-LA Model Implementation
SZ Flow and Transport Submodel 6.3.10 (Continued	Epistemic: \Input_Params_Epistemic\Epistemic_Params_SZ_Transport Other: \TSPA_Model\SZ_Transport	2.2.07.15.0A Advection and dispersion in the SZ	The processes of advection and dispersion are modeled in the SZ transport models using the advective-dispersive transport equations and reflected in the SZ breakthrough curves implemented in the TSPA-LA Model. The processes are implemented using the FEHM code. Parameters used in the models related to dispersion are longitudinal dispersivity, horizontal transverse dispersivity, and vertical transverse dispersivity.	10 CFR 63.311 10 CFR 63.331 10 CFR 63.321	DLL
		2.2.07.16.0A Dilution of radionuclides in groundwater	In TSPA, dilution of radionuclide concentrations in groundwater used by the RMEI occurs both during transport in the SZ because of dispersion and in the process of extracting groundwater from wells.	10 CFR 63.311 10 CFR 63.331 10 CFR 63.321	GSM
		2.2.07.17.0A Diffusion in the SZ	The molecular diffusion coefficient is included as a component of the dispersion coefficient in SZ radionuclide transport simulations used to develop the 3D breakthrough curves implemented in the TSPA-LA Model via the convolution integral method and in the 1D SZ pipe model abstraction implemented by GoldSim. In both cases, the dispersion coefficient is dominated by the hydrodynamic dispersion component for most groundwater flow rates.	10 CFR 63.311 10 CFR 63.331 10 CFR 63.321	GSM
		2.2.08.01.0A Chemical characteristics of groundwater in the SZ	Hydrochemical data and chemical data on rock types in the flow system are used to corroborate groundwater flow patterns and flow rates, and to provide input to determine the sorption coefficient distributions. The effect of chemical characteristics of groundwater in the SZ on sorption coefficients is reflected in the uncertainty distributions used in the SZ transport abstraction model implemented in TSPA.	10 CFR 63.311 10 CFR 63.331 10 CFR 63.321	GSM

Table I-2. Model Implementation for Included Features, Events, and Processes (Continued)

Submodel implemented in the TSPA-LA Model and Section Number	Path in GoldSim Model File	FEPs Included in the Submodel	TSPA Inclusion Explanation	Performance Assessment Standard[a]	TSPA-LA Model Implementation
SZ Flow and Transport Submodel 6.3.10 (Continued	Epistemic: \Input_Params_Epistemic\Epistemic_Params_SZ_Transport Other: \TSPA_Model\SZ_Transport	2.2.08.06.0A Complexation in the SZ	Variations in groundwater chemistry may influence complexation of radionuclides with other aqueous species. Complexation can impact the sorption of radionuclides onto the aquifer material. In particular, the sorption behavior of uranium, neptunium, and plutonium is sensitive to bicarbonate and carbonate concentrations in groundwater. The influence of these variations is incorporated into the uncertainty distributions developed for SZ sorption coefficients implemented in TSPA.	10 CFR 63.311 10 CFR 63.331 10 CFR 63.321	GSM
		2.2.08.08.0A Matrix diffusion in the SZ	Diffusion in the SZ is implemented through a dual porosity effective continuum approach. The SZ Transport Model includes matrix diffusion in the volcanic rock matrix and is parameterized by the effective diffusion coefficient to distinguish it from the free water diffusion coefficient. Matrix diffusion is captured by the breakthrough curves generated by the SZ Transport Model and implemented in TSPA. Parameters used in the transport models related to matrix diffusion are flowing interval spacing, effective diffusion coefficient, and matrix porosity.	10 CFR 63.311 10 CFR 63.331 10 CFR 63.321	DLL
		2.2.08.09.0A Sorption in the SZ	Sorption is modeled in the SZ transport models using the linear sorption isotherm with sorption coefficient parameters that appear in the equations being treated as effective variables appropriate for the model scale. In TSPA, sorption is modeled to occur in the matrix of fractured volcanic rocks and in the porous medium of the alluvium. Sorption coefficients are primarily based on laboratory measurements using samples from the Yucca Mountain site. These data are combined with information on the variability and uncertainty in hydrochemical and mineralogical composition to assess the uncertainty in sorption coefficients.	10 CFR 63.311 10 CFR 63.331 10 CFR 63.321	GSM

Table I-2. Model Implementation for Included Features, Events, and Processes (Continued)

Submodel implemented in the TSPA-LA Model and Section Number	Path in GoldSim Model File	FEPs Included in the Submodel	TSPA Inclusion Explanation	Performance Assessment Standard[a]	TSPA-LA Model Implementation
SZ Flow and Transport Submodel 6.3.10 (Continued	Epistemic: \Input_Params_Epistemic\Epistemic_Params_SZ_Transport Other: \TSPA_Model\SZ_Transport	2.2.08.10.0A Colloid transport in the SZ	The impact of colloid filtration in the SZ is incorporated in transport simulations of radionuclides irreversibly attached to colloids with the colloid retardation factor parameter. Radionuclides that are reversibly sorbed onto colloids are modeled as temporarily attached to the surface of colloids. Colloid-facilitated transport of radionuclides reversibly attached to colloids is a function of two parameters: the concentration of colloids in the groundwater and the sorption coefficient for that radionuclide onto colloids. The SZ transport models use a semi-analytical method to include retardation due to diffusion and sorption and colloid-facilitated transport in a random-walk model.	10 CFR 63.311 10 CFR 63.331 10 CFR 63.321	GSM
		2.2.10.03.0A Natural geothermal effects on flow in the SZ	Representative hydrologic properties were assigned to each node in the SZ computational grid. For flow modeling, these properties include permeability, porosity, and viscosity. Because the viscosity of groundwater depends on temperature, the nodal values for viscosity were assigned based on the expected temperature distribution in the subsurface.	10 CFR 63.311 10 CFR 63.331 10 CFR 63.321	MA
		2.2.12.00.0B Undetected features in the SZ	The HFM contains an inherent level of uncertainty that is a function of data distribution and geologic complexity. Uncertainty in the HFM is addressed in the Site-Scale Flow Model. Through the definition and assemblage of the hydrogeologic units integral to its construction, the HFM provides an internally consistent, volume-filling representation of the spatial distribution of block-averaged hydrologic properties within the Site-Scale SZ Flow Model domain. In general, large-scale hydraulic features (e.g., major faults, fault zones, zones of chemical alteration) have been incorporated into the Site-Scale Model as zones of enhanced or reduced permeability.	10 CFR 63.311 10 CFR 63.331 10 CFR 63.321	MA

Table I-2. Model Implementation for Included Features, Events, and Processes (Continued)

Submodel implemented in the TSPA-LA Model and Section Number	Path in GoldSim Model File	FEPs Included in the Submodel	TSPA Inclusion Explanation	Performance Assessment Standard[a]	TSPA-LA Model Implementation
SZ Flow and Transport Submodel 6.3.10 (Continued	Epistemic: \Input_Params_Epistemic\Epistemic_Params_SZ_Transport Other: \TSPA_Model\SZ_Transport	2.3.11.03.0A Infiltration and recharge	The effect of increased flow in the SZ due to increased recharge (caused by climate change) from the UZ is modeled using scaling factors to increase specific discharge in the SZ. The scaling factors used in this approach are the ratio of average SZ groundwater flow under the future climatic conditions to the flow under present conditions. The scaling factors are a direct input from the SZ Flow and Transport Abstraction Model to TSPA.	10 CFR 63.311 10 CFR 63.331 10 CFR 63.321	MA
		3.1.01.01.0A Radioactive decay and ingrowth	The 1-D SZ Transport Model is used to calculate the mass of daughter products from the radioactive decay of several radionuclides. The one-dimensional model, which is implemented directly in the TSPA simulations, simulates the radioactive decay and in-growth of radionuclides in four decay chains. Radioactive decay is also applied to radionuclide mass flux calculated with the convolution integral method in the SZ Flow and Transport Abstraction Model.	10 CFR 63.311 10 CFR 63.331 10 CFR 63.321	GSM
Biosphere Submodel 6.3.11	Epistemic: \Input_Params_Epistemic\Epistemic_Params_Biosphere Other: \TSPA_Model\Biosphere	1.2.04.07.0A Ashfall	This FEP is dispositioned in the biosphere component of the TSPA-LA Model through the use of Biosphere Dose Conversion factors (BDCFs) that are direct inputs to the TSPA. Volcanic ash is the initial source of contamination for the eruption case of the volcanic scenario. Ash characteristics and depth were considered in development of the input parameters for the surface soil and air submodels.	10 CFR 63.311	GSM

Table I-2. Model Implementation for Included Features, Events, and Processes (Continued)

Submodel implemented in the TSPA-LA Model and Section Number	Path in GoldSim Model File	FEPs Included in the Submodel	TSPA Inclusion Explanation	Performance Assessment Standard[a]	TSPA-LA Model Implementation
Biosphere Submodel 6.3.11 (Continued)	Epistemic: \Input_Params_Epistemic\Epistemic_Params_Biosphere Other: \TSPA_Model\Biosphere	1.3.07.02.0A Water table rise affects SZ	The water table will likely be higher in future climate states that have greater infiltration rates. To include water table rise in the TSPA calculations, the water table elevation is instantaneously increased up to 120m when the climate changes from present-day to monsoon climate. This rise reduces the transport length in the UZ. This treatment is consistent with the instantaneous change of UZ flow fields. Water table rise also captures the radionuclides present in the UZ below the new water table elevation. The captured radionuclides are input as a source term to the SZ transport simulation.	10 CFR 63.311 10 CFR 63.331 10 CFR 63.321	GSM
		1.4.07.01.0A Water management activities	Water management activities conducted in the Yucca Mountain region (e.g., irrigation and fish farming) were incorporated throughout the conceptual and mathematical model and considered in the development of parameter values for the plant uptake and fish uptake submodels. All FEPs considered in the biosphere model and its input parameters are collectively included in BDCFs	10 CFR 63.311 10 CFR 63.321	GSM
		1.4.07.02.0A Wells	A well is the source of groundwater for domestic and agricultural uses in the groundwater exposure scenario. All FEPs considered in the Biosphere Model and its input parameters are collectively included in BDCFs	10 CFR 63.311 10 CFR 63.331 10 CFR 63.321	GSM
		2.2.08.01.0A Chemical characteristics of the groundwater in the SZ	The source of radionuclides in the biosphere groundwater scenario is the groundwater pumped from wells. The model addresses radionuclide accumulation and transport within and between biosphere compartments culminating in an annual dose to a defined receptor. All FEPs considered in the Biosphere Model and its input parameters are collectively included in BDCFs that are implemented in TSPA.	10 CFR 63.311 10 CFR 63.331 10 CFR 63.321	MA

Table I-2. Model Implementation for Included Features, Events, and Processes (Continued)

Submodel implemented in the TSPA-LA Model and Section Number	Path in GoldSim Model File	FEPs Included in the Submodel	TSPA Inclusion Explanation	Performance Assessment Standard[a]	TSPA-LA Model Implementation
Biosphere Submodel 6.3.11 (Continued)	Epistemic: \Input_Params_Epistemic\Epistemic_Params_Biosphere Other: \TSPA_Model\Biosphere	2.3.02.03.0A Soil and sediment transport in the biosphere	Soil and sediment transport via erosion were included in the surface soil and air submodels. All FEPs considered in the Biosphere Model and its input parameters are collectively included in BDCFs that are implemented in TSPA.	10 CFR 63.311 10 CFR 63.321	MA
		2.3.02.01.0A Soil type	This feature was included through the consideration of the soil characteristics in the reference biosphere in the development of parameter values for the surface soil, plant uptake, and ^{14}C submodels. All FEPs considered in the Biosphere Model and its input parameters are collectively included in BDCFs that are implemented in TSPA.	10 CFR 63.311 10 CFR 63.321	MA
		2.3.02.02.0A Radionuclide accumulation in soils	Accumulation of radionuclides in soil from deposition of irrigation water and volcanic ash was modeled in the surface soil submodel. All FEPs considered in the Biosphere Model and its input parameters are collectively included in BDCFs that are implemented in TSPA.	10 CFR 63.311 10 CFR 63.321	MA
		2.3.04.01.0A Surface water transport and mixing	The groundwater scenario implicitly included water transport because the model applied to the use of any water containing radionuclides, regardless of the origin, if the reference biosphere, water-use practices, and characteristics of the RMEI remain unchanged. The model did not consider mixing of contaminated and uncontaminated water. All FEPs considered in the Biosphere Model and its input parameters are collectively included in BDCFs	10 CFR 63.311 10 CFR 63.321	MA

Table I-2. Model Implementation for Included Features, Events, and Processes (Continued)

Submodel implemented in the TSPA-LA Model and Section Number	Path in GoldSim Model File	FEPs Included in the Submodel	TSPA Inclusion Explanation	Performance Assessment Standard[a]	TSPA-LA Model Implementation
Biosphere Submodel 6.3.11 (Continued)	Epistemic: \Input_Params_Epistemic\Epistemic_Params_Biosphere Other: \TSPA_Model\Biosphere	2.3.11.01.0A Precipitation	Levels of precipitation consistent with current knowledge of the reference biosphere were considered in the development of input parameter distributions for the surface soil, plant uptake, and ^{14}C submodels. All FEPs considered in the Biosphere Model and its input parameters are collectively included in BDCFs that are implemented in TSPA.	10 CFR 63.311 10 CFR 63.321	MA
		2.3.13.01.0A Biosphere characteristics	The principal components, conditions, and characteristics of the reference biosphere that influence radionuclide transport were represented in the conceptual and mathematical models. Current knowledge of the conditions in the reference biosphere was considered in the development of parameter distributions for all submodels. All FEPs considered in the Biosphere Model and its input parameters are collectively included in BDCFs that are implemented in TSPA.	10 CFR 63.311 10 CFR 63.321	MA
		2.3.13.02.0A Radionuclide alteration during biosphere transport	Changes in the physical and chemical form of radionuclides during transfer among biosphere components were incorporated throughout the conceptual and mathematical models. This FEP was also implicitly incorporated through the use of radionuclide-specific transfer factors in the plant uptake and animal uptake submodels. All FEPs considered in the Biosphere Model and its input parameters are collectively included in BDCFs that are implemented in TSPA.	10 CFR 63.311 10 CFR 63.321	MA
		2.4.01.00.0A Human characteristics (physiology, metabolism)	Metabolic and physiologic considerations consistent with present knowledge of adults, as per 10 CFR 63.312(e) [DIRS 180319], were used in the development of parameter distributions for the external exposure, inhalation, and ingestion submodels. The characteristics in these parameters are propagated to the BDCFs which are direct inputs to the TSPA for the scenario classes involving radionuclide release to the groundwater.	10 CFR 63.311 10 CFR 63.331 10 CFR 63.321	MA

Table I-2. Model Implementation for Included Features, Events, and Processes (Continued)

Submodel implemented in the TSPA-LA Model and Section Number	Path in GoldSim Model File	FEPs Included in the Submodel	TSPA Inclusion Explanation	Performance Assessment Standard[a]	TSPA-LA Model Implementation
Biosphere Submodel 6.3.11 (Continued)	Epistemic: \Input_Params_Epistemic\Epistemic_Params_Biosphere Other: \TSPA_Model\Biosphere	2.4.04.01.0A Human lifestyle	Activities representative of the living style of the residents of the Town of Amargosa Valley were incorporated throughout the conceptual and mathematical model. The living style of Amargosa Valley residents was considered in the development of parameter distributions for the air, external exposure, inhalation, and ingestion submodels. The characteristics in these parameters are propagated to the BDCFs which are direct inputs to the TSPA for the scenario classes involving radionuclide release to the groundwater.	10 CFR 63.311 10 CFR 63.321	MA
		2.4.07.00.0A Dwellings	Characteristics of dwellings representative of the living style of the residents of the Town of Amargosa Valley were considered in the development of input parameters for the air, external exposure, and inhalation submodels. The characteristics in these parameters are propagated to the BDCFs which are direct inputs to the TSPA for the scenario classes involving radionuclide release to the groundwater.	10 CFR 63.311 10 CFR 63.321	MA
		2.4.08.00.0A Wild and natural land and water use	Wild and natural land and water use (e.g., use of natural lands, ingestion of game animals) by the residents of the Town of Amargosa Valley was incorporated into the air, external exposure, and ingestion submodels. These lifestyle characteristics were considered in the development of parameters for those submodels. The characteristics in these parameters are propagated to the BDCFs which are direct inputs to the TSPA for the scenario classes involving radionuclide release to the groundwater.	10 CFR 63.311 10 CFR 63.321	MA

Table I-2. Model Implementation for Included Features, Events, and Processes (Continued)

Submodel implemented in the TSPA-LA Model and Section Number	Path in GoldSim Model File	FEPs Included in the Submodel	TSPA Inclusion Explanation	Performance Assessment Standard[a]	TSPA-LA Model Implementation
Biosphere Submodel 6.3.11 (Continued)	Epistemic: \Input_Params_Epistemic\Epistemic_Params_Biosphere Other: \TSPA_Model\Biosphere	2.4.09.01.0B Agricultural land use and irrigation	Agricultural land use and irrigation practices of the residents of the Town of Amargosa Valley were incorporated into the soil, air, plant uptake, animal uptake, ^{14}C, and fish uptake submodels. These practices were considered in the development of parameters for those submodels. All FEPs considered in the Biosphere Model and its input parameters are collectively included in BDCFs that are implemented in TSPA.	10 CFR 63.311 10 CFR 63.321	MA
		2.4.09.02.0A Animal farms and fisheries	Animal farm and fishery practices of the residents of the Town of Amargosa Valley were incorporated into the animal uptake and fish uptake submodels. These practices were considered in the development of parameters for those submodels. All FEPs considered in the Biosphere Model and its input parameters are collectively included in BDCFs	10 CFR 63.311 10 CFR 63.321	MA
		2.4.10.00.0A Urban and industrial land and water use	Land and water use in urban and industrial settings of the residents of the Town of Amargosa Valley were incorporated into the soil, air, ^{14}C, external exposure, inhalation, and ingestion submodels. These lifestyle characteristics were considered in the development of parameters for those submodels. All FEPs considered in the Biosphere Model and its input parameters are collectively included in BDCFs that are implemented in TSPA.	10 CFR 63.311 10 CFR 63.321	MA

Table I-2. Model Implementation for Included Features, Events, and Processes (Continued)

Submodel implemented in the TSPA-LA Model and Section Number	Path in GoldSim Model File	FEPs Included in the Submodel	TSPA Inclusion Explanation	Performance Assessment Standard[a]	TSPA-LA Model Implementation
Biosphere Submodel 6.3.11 (Continued)	Epistemic: \Input_Params_Epistemic\Epistemic_Params_Biosphere Other: \TSPA_Model\Biosphere	3.1.01.01.0A Radioactive decay and ingrowth	This FEP is dispositioned in the biosphere component of the TSPA-LA Model through the use of groundwater exposure scenario BDCFs that are direct inputs to the TSPA for the scenario classes involving radionuclide release to the groundwater. Annual doses are calculated as the product of radionuclide concentration in groundwater and BDCFs. The present-day climate BDCFs are used for the assessment of doses to the RMEI for the entire period of geologic stability. Radioactive decay and ingrowth is also included in the TSPA through the use of the conversion factors for evaluating compliance with the groundwater protection standards.	10 CFR 63.311 10 CFR 63.331 10 CFR 63.321	GSM
		3.2.10.00.0A Atmospheric transport of contaminants	The processes of atmospheric transport of radionuclides from resuspension of soil and ash particles, gaseous emission of radionuclides from soil, and generation of aerosols from evaporative coolers were included in the air and ^{14}C submodels. All FEPs considered in the Biosphere Model and its input parameters are collectively included in BDCFs that are implemented in TSPA.	10 CFR 63.311 10 CFR 63.321	GSM
		3.3.01.00.0A Contaminated drinking water, foodstuffs, and drugs	Consumption of contaminated water and soil and consumption of locally produced crops, animal products, and fish were included in the ingestion submodel. Consumption rates were based on the diet of the residents of the Town of Amargosa Valley and the requirements of 10 CFR 63.312 [DIRS 180319]. All FEPs considered in the Biosphere Model and its input parameters are collectively included in BDCFs that are implemented in TSPA.	10 CFR 63.311 10 CFR 63.331 10 CFR 63.321	MA
		3.3.02.01.0A Plant uptake	The process of plant uptake of radionuclides was included in the plant uptake and ^{14}C submodels. All FEPs considered in the Biosphere Model and its input parameters are collectively included in BDCFs that are implemented in TSPA.	10 CFR 63.311 10 CFR 63.321	MA

Table I-2. Model Implementation for Included Features, Events, and Processes (Continued)

Submodel implemented in the TSPA-LA Model and Section Number	Path in GoldSim Model File	FEPs Included in the Submodel	TSPA Inclusion Explanation	Performance Assessment Standard[a]	TSPA-LA Model Implementation
Biosphere Submodel 6.3.11 (Continued)	Epistemic: \Input_Params_Epistemic\Epistemic_Params_Biosphere Other: \TSPA_Model\Biosphere	3.3.02.02.0A Animal uptake	The animal uptake submodel included the process of radionuclide uptake by farm animals. All FEPs considered in the Biosphere Model and its input parameters are collectively included in BDCFs	10 CFR 63.311 10 CFR 63.321	MA
		3.3.02.03.0A Fish uptake	The fish uptake submodel included the bioaccumulation of radionuclides in fish. All FEPs considered in the Biosphere Model and its input parameters are collectively included in BDCFs that are implemented in TSPA.	10 CFR 63.311 10 CFR 63.321	MA
		3.3.03.01.0A Contaminated non-food products and exposure	The external exposure submodel bounded exposure to the few nonfood products produced in Amargosa Valley that may contain radionuclides by assuming that the RMEI would be exposed to contaminated soil at all times while in the biosphere. All FEPs considered in the Biosphere Model and its input parameters are collectively included in BDCFs	10 CFR 63.311 10 CFR 63.321	MA
		3.3.04.01.0A Ingestion	The ingestion submodel included ingestion of contaminated food, drinking water, and soil. All FEPs considered in the Biosphere Model and its input parameters are collectively included in BDCFs that are implemented in TSPA.	10 CFR 63.311 10 CFR 63.331 10 CFR 63.321	MA
		3.3.04.02.0A Inhalation	The inhalation submodel includes inhalation of gaseous ^{14}C and radon decay products from radon exhalation from the ground, contaminated resuspended particles, and contaminated aerosols from evaporative coolers. All FEPs considered in the Biosphere Model and its input parameters are collectively included in BDCFs that are implemented in TSPA.	10 CFR 63.311 10 CFR 63.321	MA

Table I-2. Model Implementation for Included Features, Events, and Processes (Continued)

Submodel implemented in the TSPA-LA Model and Section Number	Path in GoldSim Model File	FEPs Included in the Submodel	TSPA Inclusion Explanation	Performance Assessment Standard[a]	TSPA-LA Model Implementation
Biosphere Submodel 6.3.11 (continued)	Epistemic: \Input_Params_Epistemic\Epistemic_Params_Biosphere Other: \TSPA_Model\Biosphere	3.3.04.03.0A External exposure	The external exposure submodel included external exposure to contaminated materials. The characteristics in these parameters are propagated to the BDCFs which are direct inputs to the TSPA for the scenario classes involving radionuclide release to the groundwater.	10 CFR 63.311 10 CFR 63.321	MA
		3.3.05.01.0A Radiation doses	Calculation of the predicted annual dose for a unit activity concentration of a radionuclide (i.e., BDCF) was conducted in the external exposure, inhalation, and ingestion submodels. All FEPs considered in the Biosphere Model and its input parameters are collectively included in BDCFs that are implemented in TSPA.	10 CFR 63.311 10 CFR 63.331 10 CFR 63.321	GSM
		3.3.08.00.0A Radon and radon decay product exposure	Exposure to radon (^{222}Rn) and radon decay products is included in the air and inhalation submodels of the groundwater and volcanic ash exposure scenarios. Concentrations of radon and radon decay products are calculated in the air submodels for the groundwater and volcanic ash exposure scenarios. This FEP is included in the biosphere component of the TSPA model through the use of groundwater exposure scenario BDCFs that are direct inputs to the TSPA for the scenario classes involving radionuclide release to the groundwater	10 CFR 63.311 10 CFR 63.331 10 CFR 63.321	GSM

Table I-2. Model Implementation for Included Features, Events, and Processes (Continued)

Submodel implemented in the TSPA-LA Model and Section Number	Path in GoldSim Model File	FEPs Included in the Submodel	TSPA Inclusion Explanation	Performance Assessment Standard[a]	TSPA-LA Model Implementation
WP Early Failure Submodel 6.4.2 Note: FEPS included here for the Early failure scenario class are in addition to the FEPS described above in sections 6.3.x	Epistemic: \Input_Params_Epistemic\Epistemic_Params_Events\Epistemic_Parameters_EF Aleatory: \Input_Params_Aleatory\Aleatory_Params_Events\Aleatory_Params_EF EBS: \Time_Zero\EBS_PS_Loop\Static_Calcs_PS_Loop\Static_Calcs_Events\Static_Calcs_EF \Global_Inputs_and_Calcs\Global_Events\Global_EF	2.1.03.08.0A Early failure of the waste package	Early failure of WPs due to manufacturing or handling-induced defects is modeled based on possible defects identified from literature and human error probability data. The resultant probability of early failure is evaluated by a log normal distribution with a median of 4.14×10^{-5} and an error factor of 8.17. These inputs are adjusted to conform to implementation requirements of GoldSim for log-normal distributions, which require geometric mean and geometric standard deviation as parameters. For WP early failure, the WPs are divided into two fuel-type groups denoted by CSNF early-failed WPs and CDSP early-failed WPs.	10 CFR 63.311 10 CFR 63.331	GSM
		2.1.03.11.0A Physical form of waste package and drip shield	The physical form of waste packages is represented in the TSPA by two nominal waste package configurations. For waste package early failure, the waste packages are divided into two fuel-type groups denoted by CSNF early-failed waste packages and CDSP early-failed waste packages.	10 CFR 63.311 10 CFR 63.331	GSM

Table I-2. Model Implementation for Included Features, Events, and Processes (Continued)

Submodel implemented in the TSPA-LA Model and Section Number	Path in GoldSim Model File	FEPs Included in the Submodel	TSPA Inclusion Explanation	Performance Assessment Standard[a]	TSPA-LA Model Implementation
DS Early Failure Submodel 6.4.1 Note: FEPS included here for the Early failure scenario class are in addition to the FEPS described above in sections 6.3.x	Epistemic: \Input_Params_Epistemic\Epistemic_Params_Events\Epistemic_Parameters_EF Aleatory: \Input_Params_Aleatory\Aleatory_Params_Events\Aleatory_Params_EF EBS: \Time_Zero\EBS_PS_Loop\Static_Calcs_PS_Loop\Static_Calcs_Events\Static_Calcs_EF \Global_Inputs_and_Calcs\Global_Events\Global_EF	2.1.03.08.0B Early failure of drip shields	Early failure of DSs due to manufacturing or handling-induced defects or errors in emplacement is modeled based on possible defects identified from literature and human error probability data. The resultant probability of early failure is evaluated by a log normal distribution with a median of 4.3×10^{-7} and an error factor of 14. These inputs are adjusted to conform to implementation requirements of GoldSim for log-normal distributions, which require geometric mean and geometric standard deviation as parameters. The rate of DS early failure is sampled in the TSPA-LA Model from this log-normal distribution. Early failed DSs are randomly placed in the repository. Early failure is assumed to occur at time zero and allows the full volume of seepage to contact the underlying WP. The underlying WP is also assumed to fail at time zero.	10 CFR 63.311 10 CFR 63.331	GSM
		2.1.03.11.0A Physical form of waste package and drip shield	Early failure of drip shields due to manufacturing or handling-induced defects or errors in emplacement, as identified from literature and human error probability data, is dependent on the specific form of the drip shield.	10 CFR 63.311 10 CFR 63.331	GSM

Table I-2. Model Implementation for Included Features, Events, and Processes (Continued)

Submodel implemented in the TSPA-LA Model and Section Number	Path in GoldSim Model File	FEPs Included in the Submodel	TSPA Inclusion Explanation	Performance Assessment Standard[a]	TSPA-LA Model Implementation
Igneous Intrusion Submodel 6.5.1 FEPS included here for the Igneous scenario class are in addition to the FEPS described above in sections 6.3.x	Epistemic: \Input_Params_Epistemic\Epistemic_Params_Events\Epistemic_Params_Igneous_Intr Aleatory: \Input_Params_Aleatory\Aleatory_Params_Events\Aleatory_Params_Igneous_Intr EBS: \Time_Zero\EBS_PS_Loop\Static_Calcs_PS_Loop\Static_Calcs_Events\Igneous_Intrusion\Global_Inputs_and_Calcs\Global_Events\Igneous_Scenario	1.2.04.03.0A Igneous intrusion into repository	The Igneous intrusion submodel includes the in-drift conditions that would accompany the intersection of one or more emplacement drifts by an ascending basaltic dike and subsequent cooling and solidification of the basaltic intrusion. This section also addresses estimating the number of WPs damaged in the intersected drifts.	10 CFR 63.311	GSM
Igneous Event Time and Probability Submodel 6.5.1 FEPS included here for the Igneous scenario class are in addition to the FEPS described above in sections 6.3.x		1.2.04.04.0A Igneous intrusion interacts with EBS components	In-drift conditions that would accompany intersection of one or more emplacement drifts by an ascending basaltic dike are described. The expected behavior of WPs exposed to magma is described. This supports the TSPA assumption that WPs, DSs, and cladding in intersected drifts provide no protection for the waste.	10 CFR 63.311	GSM
		1.2.04.06.0A Eruptive conduit to surface intersects repository	The modeling of eruption, dispersal, and transport of radionuclides is described, as well as the estimation of the number of WPs intersected by eruptive conduits. The descriptions provide the primary inputs for ASHPLUME to model the eruption case in TSPA.	10 CFR 63.311	GSM

Table I-2. Model Implementation for Included Features, Events, and Processes (Continued)

Submodel implemented in the TSPA-LA Model and Section Number	Path in GoldSim Model File	FEPs Included in the Submodel	TSPA Inclusion Explanation	Performance Assessment Standard[a]	TSPA-LA Model Implementation
Igneous Intrusion EBS Damage Submodel 6.5.1 Note: FEPS included here for the Igneous scenario class are in addition to the FEPS described above in sections 6.3.x	Epistemic: \Input_Params_Epistemic\Epistemic_Params_Events\Epistemic_Params_Igneous_Intr The five Volcanic eruption submodels from the Igneous Scenario Class are contained in a separate GoldSim model file:Aleatory: \Input_Params_Aleatory\Aleatory_Params_Events\Aleatory_Params_Igneous_Intr EBS: \Time_Zero\EBS_PS_Loop\Static_Calcs_PS_Loop\Static_Calcs_Events\Igneous_Intrusion\Global_Inputs_and_Calcs\Global_Events\Igneous_Scenario	1.2.04.03.0A Igneous intrusion into repository	The in-drift temperature conditions that would accompany the intersection of one or more emplacement drifts are represented in the TSPA-LA Model by the igneous intrusion thermal condition abstraction model.	10 CFR 63.311	GSM
		1.2.04.04.0A Igneous intrusion interacts with EBS components	TSPA implements the assumption that WPs and DSs in intersected drifts provide no protection for the waste immediately upon intrusion.	10 CFR 63.311	GSM
		2.1.03.11.0A Physical form of waste package and drip shield	In the igneous intrusion modeling case, magma from dikes is assumed to engulf all drip shields and waste packages in the repository, rendering them incapable of protecting their contents. Conceptually, the codisposal waste packages and CSNF waste packages no longer act to prevent or slow the rate of advective transport, leaving radionuclides available for transport by groundwater downward through the unsaturated zone to the water table. Both the geometry of the waste form (which is important for diffusive transport) and the formation of corrosion products from degradation of the waste package internal components (which impacts both diffusive transport and retardation due to sorption of radionuclides) are assumed to be the same as in the nominal scenario class.	10 CFR 63.311	GSM

Table I-2. Model Implementation for Included Features, Events, and Processes (Continued)

Submodel implemented in the TSPA-LA Model and Section Number	Path in GoldSim Model File	FEPs Included in the Submodel	TSPA Inclusion Explanation	Performance Assessment Standard[a]	TSPA-LA Model Implementation
EBS Chemical Environment Submodel Modifications for Igneous Intrusion 6.5.1 Note: FEPS included here for the Igneous scenario class are in addition to the FEPS described above in sections 6.3.x	Epistemic: \Input_Params_Epistemic\Epistemic_Params_Events\Epistemic_Params_Igneous_Intr The five Volcanic eruption submodels from the Igneous Scenario Class are contained in a separate GoldSim model file:Aleatory: \Input_Params_Aleatory\Aleatory_Params_Events\Aleatory_Params_Igneous_Intr EBS: \Time_Zero\EBS_PS_Loop\Static_Calcs_PS_Loop\Static_Calcs_Events\Igneous_Intrusion\Global_Inputs_and_Calcs\Global_Events\Igneous_Scenario	1.2.04.04.0B Chemical effects of magma and magmatic volatiles	Chemistry of water percolating into drifts that have cooled after an igneous intrusion could be affected by basalt-water interactions. Analogue data on basalt-water chemistry is included to support the abstraction of basalt-water chemistry used in the TSPA.	10 CFR 63.311	GSM

Table I-2. Model Implementation for Included Features, Events, and Processes (Continued)

Submodel implemented in the TSPA-LA Model and Section Number	Path in GoldSim Model File	FEPs Included in the Submodel	TSPA Inclusion Explanation	Performance Assessment Standard[a]	TSPA-LA Model Implementation
Volcanic Interaction with the Repository Submodel 6.5.2.1.1 FEPS included here for the Volcanic scenario class are in addition to the FEPS described above in sections 6.3.x	The Volcanic Eruption model is a separate GoldSim file: vE1.004_GS_9.60.100.gsm Epistemic: \Model_Uncertainties\EU\Inventory_Uncertainty and \Model_Uncertainties\EU\Eruptive_Case_Uncertainty Aleatory: \Model_Uncertainties\AU Other: \Eruptive_Model\Igneous_Erupt_Input and \Eruptive_Model\Igneous_Erupt_Calcs	1.2.04.04.0A Igneous intrusion interacts with EBS components	In the TSPA-LA Model the number of WPs intersected by magmatic conduits is a function of conduit area, the number of conduits, and the conduit location within the repository. Only WPs located partially or entirely within a magmatic conduit are assumed to be destroyed, making all of the waste in these WPs available for entrainment in the erupting pyroclastic material.	10 CFR 63.311	DLL
		1.2.04.06.0A Eruptive conduit to surface intersects repository	The consequences of an igneous intrusion through the repository and an associated eruptive event are explicitly included in the TSPA-LA Model through modeling of aerial dispersion followed by deposition and redistribution of potentially contaminated pyroclastic materials; the consequences are appropriately weighted by the probability of occurrence of the event.	10 CFR 63.311	DLL
Atmospheric Transport Submodel 6.5.2.1.2		1.2.04.07.0A Ashfall	The eruption model case that includes entrainment of waste in an ascending tephra plume and deposition of contaminated tephra on the land surface is described. The result is the areal concentration of contaminated tephra on the ground surface at the RMEI location.	10 CFR 63.311	DLL
Tephra Redistribution Submodel 6.5.2.1.3		1.2.04.07.0A Ashfall	Atmospheric transport of the tephra-waste mixture is modeled directly in the TSPA-LA Model using ASHPLUME, the atmospheric tephra dispersal model as it evaluates downwind transport of contaminated tephra and radioactive waste and their deposition on the ground surface.	10 CFR 63.311	DLL
		1.2.04.07.0C Ash redistribution via soil and sediment transport	The ash redistribution model is described, as are the results of surficial processes acting on primary tephra deposited on the two primary landforms near the RMEI location: distributary channels and interchannel divides. The model evaluates the effects of surficial processes on concentrations of waste as contaminated tephra is transported to the RMEI location.	10 CFR 63.311	DLL

Table I-2. Model Implementation for Included Features, Events, and Processes (Continued)

Submodel implemented in the TSPA-LA Model and Section Number	Path in GoldSim Model File	FEPs Included in the Submodel	TSPA Inclusion Explanation	Performance Assessment Standard[a]	TSPA-LA Model Implementation
Volcanic Ash Exposure Submodel 6.5.2.1.4	The Volcanic Eruption model is a separate GoldSim file: vE1.004_GS_9.60.100.gsm Epistemic: \Model_Uncertainties\EU\Biosphere_Uncertainty Aleatory: \Model_Uncertainties\AU Biosphere: \Eruptive_Model\Igneous_Erupt_Input\ST_Components and \Dose	1.2.04.07.0A Ashfall	Volcanic ash is the initial source of contamination for the eruption case of the volcanic scenario. Ash characteristics and depth were considered in development of the input parameters for the surface soil and air submodels.	10 CFR 63.311	DLL
		2.3.02.01.0A Soil Type	This FEP is dispositioned in the TSPA volcanic eruption modeling case through BDCFs for the volcanic ash exposure scenarios. Annual doses are calculated in the TSPA as the product of radionuclide concentration in soil contaminated by radionuclides volcanic tephra and the BDCF components. For the volcanic ash exposure scenario, three BDCF components are provided to the TSPA-LA Model that account for various RMEI exposure pathways.	10 CFR 63.311	DLL
		2.3.02.02.0A Radionuclide accumulation in soils	This FEP is dispositioned in the TSPA volcanic eruption modeling case through BDCFs for the volcanic ash exposure scenarios. Annual doses are calculated in the TSPA as the product of radionuclide concentration in soil contaminated by radionuclides volcanic tephra and the BDCF components. For the volcanic ash exposure scenario, three BDCF components are provided to the TSPA-LA Model that account for various RMEI exposure pathways.	10 CFR 63.311	DLL
		2.3.02.03.0A Soil and sediment transport in the biosphere	This FEP is dispositioned in the TSPA volcanic eruption modeling case through BDCFs for the volcanic ash exposure scenarios. Annual doses are calculated in the TSPA as the product of radionuclide concentration in soil contaminated by radionuclides volcanic tephra and the BDCF components. For the volcanic ash exposure scenario, three BDCF components are provided to the TSPA-LA Model that account for various RMEI exposure pathways.	10 CFR 63.311	DLL

Table I-2. Model Implementation for Included Features, Events, and Processes (Continued)

Submodel implemented in the TSPA-LA Model and Section Number	Path in GoldSim Model File	FEPs Included in the Submodel	TSPA Inclusion Explanation	Performance Assessment Standard[a]	TSPA-LA Model Implementation
Volcanic Ash Exposure Submodel 6.5.2.1.4 (Continued)	The Volcanic Eruption model is a separate GoldSim file: vE1.004_GS_9.60.100.gsm Epistemic: \Model_Uncertainties\EU\Biosphere_Uncertainty Aleatory: \Model_Uncertainties\AU Biosphere: \Eruptive_Model\Igneous_Erupt_Input\ST_Components and \Dose	2.3.11.01.0A Precipitation	This FEP is dispositioned in the TSPA Volcanic Eruption Modeling Case through BDCFs for the volcanic ash exposure scenario (because the mass loading levels and some agricultural parameters may depend on precipitation) and the radioactive waste concentration in the soil calculated by the Tephra Redistribution Model. Annual doses are calculated in the TSPA as the product of radionuclide concentration in the soil contaminated by radionuclides in volcanic tephra, the BDCF components, and the mass loading time decrease function. For the volcanic ash exposure scenario, three BDCF components are provided to the TSPA-LA Model that account for various RMEI exposure pathways.	10 CFR 63.311	DLL

Table I-2. Model Implementation for Included Features, Events, and Processes (Continued)

Submodel implemented in the TSPA-LA Model and Section Number	Path in GoldSim Model File	FEPs Included in the Submodel	TSPA Inclusion Explanation	Performance Assessment Standard[a]	TSPA-LA Model Implementation
Volcanic Ash Exposure Submodel 6.5.2.1.4 (Continued)	The Volcanic Eruption model is a separate GoldSim file: vE1.004_GS_9.60.100.gsm Epistemic: \Model_Uncertainties\EU\Biosphere_Uncertainty Aleatory: \Model_Uncertainties\AU Biosphere: \Eruptive_Model\Igneous_Erupt_Input\ST_Components and \Dose	2.3.13.01.0A Biosphere characteristics	The TSPA-LA Model calculates radiation dose as a product of the time-dependent source terms, the source-independent BDCFs, and the mass loading time decay function. For the volcanic ash exposure scenario, three BDCF components are provided to the TSPA-LA Model. The first is for exposure to sources external to the body, and the second and third BDCF components (the short-term and the long-term inhalation components) account for inhaling airborne particulates.	10 CFR 63.311	DLL
		2.3.13.02.0A Radionuclide alteration during biosphere transport	This FEP is dispositioned in the TSPA Volcanic Eruption Modeling Case through BDCFs for the volcanic ash exposure scenario. Annual doses are calculated in the TSPA as the product of radionuclide concentration in soil contaminated by radionuclides in volcanic tephra, the BDCF components, and the mass loading time decrease function. For the volcanic ash exposure scenario, three BDCF components are provided to the TSPA-LA Model that account for various RMEI exposure pathways.	10 CFR 63.311	DLL

Table I-2. Model Implementation for Included Features, Events, and Processes (Continued)

Submodel implemented in the TSPA-LA Model and Section Number	Path in GoldSim Model File	FEPs Included in the Submodel	TSPA Inclusion Explanation	Performance Assessment Standard[a]	TSPA-LA Model Implementation
Volcanic Ash Exposure Submodel 6.5.2.1.4 (Continued)	The Volcanic Eruption model is a separate GoldSim file: vE1.004_GS_9.60.100.gsm Epistemic: \Model_Uncertainties\EU\Biosphere_Uncertainty Aleatory: \Model_Uncertainties\AU Biosphere: \Eruptive_Model\Igneous_Erupt_Input\ST_Components and \Dose	2.4.01.00.0A Human characteristics (physiology, metabolism)	This FEP is dispositioned in the TSPA Volcanic Eruption Modeling Case through BDCFs for the volcanic ash exposure scenario. Annual doses are calculated in the TSPA as the product of radionuclide concentration in soil contaminated by radionuclides in volcanic tephra, the BDCF components, and the mass loading time decrease function. For the volcanic ash exposure scenario, three BDCF components are provided to the TSPA-LA Model that account for various RMEI exposure pathways: exposure to sources external to the body, (ingestion, and inhalation of radon decay products); and the short-term and long-term inhalation components.	10 CFR 63.311	DLL
		2.4.04.01.0A Human Lifestyle	This FEP is dispositioned in the TSPA Volcanic Eruption Modeling Case through BDCFs for the volcanic ash exposure scenario. Annual doses are calculated in the TSPA as the product of radionuclide concentration in soil contaminated by radionuclides in volcanic tephra, the BDCF components, and the mass loading time decrease function. For the volcanic ash exposure scenario, three BDCF components are provided to the TSPA-LA Model that account for various RMEI exposure pathways.	10 CFR 63.311	DLL

Table I-2. Model Implementation for Included Features, Events, and Processes (Continued)

Submodel implemented in the TSPA-LA Model and Section Number	Path in GoldSim Model File	FEPs Included in the Submodel	TSPA Inclusion Explanation	Performance Assessment Standard[a]	TSPA-LA Model Implementation
Volcanic Ash Exposure Submodel 6.5.2.1.4 (Continued)	The Volcanic Eruption model is a separate GoldSim file: vE1.004_GS_9.60.100.gsm Epistemic: \Model_Uncertainties\EU\Biosphere_Uncertainty Aleatory: \Model_Uncertainties\AU Biosphere: \Eruptive_Model\Igneous_Erupt_Input\ST_Components and \Dose	2.4.07.00.0A Dwellings	This FEP is dispositioned in the TSPA Volcanic Eruption Modeling Case through BDCFs for the volcanic ash exposure scenarios. Annual doses are calculated in the TSPA as the product of radionuclide concentration in soil contaminated by radionuclides volcanic tephra and the BDCF components. For the volcanic ash exposure scenario, three BDCF components are provided to the TSPA-LA Model that account for various RMEI exposure pathways	10 CFR 63.311	DLL
		2.4.08.00.0A Wild and natural land and water use	This FEP is dispositioned in the TSPA Volcanic Eruption Modeling Case through BDCFs for the volcanic ash exposure scenarios. Annual doses are calculated in the TSPA as the product of radionuclide concentration in soil contaminated by radionuclides volcanic tephra and the BDCF components. For the volcanic ash exposure scenario, three BDCF components are provided to the TSPA-LA Model that account for various RMEI exposure pathways	10 CFR 63.311	DLL
		2.4.09.01.0B Agricultural land use and irrigation	This FEP is dispositioned in the TSPA Volcanic Eruption Modeling Case through BDCFs for the volcanic ash exposure scenarios. Annual doses are calculated in the TSPA as the product of radionuclide concentration in soil contaminated by radionuclides volcanic tephra and the BDCF components. For the volcanic ash exposure scenario, three BDCF components are provided to the TSPA-LA Model that account for various RMEI exposure pathways	10 CFR 63.311	DLL

Table I-2. Model Implementation for Included Features, Events, and Processes (Continued)

Submodel implemented in the TSPA-LA Model and Section Number	Path in GoldSim Model File	FEPs Included in the Submodel	TSPA Inclusion Explanation	Performance Assessment Standard[a]	TSPA-LA Model Implementation
Volcanic Ash Exposure Submodel 6.5.2.1.4 (Continued)	The Volcanic Eruption model is a separate GoldSim file: vE1.004_GS_9.60.100.gsm Epistemic: \Model_Uncertainties\EU\Biosphere_Uncertainty Aleatory: \Model_Uncertainties\AU Biosphere: \Eruptive_Model\Igneous_Erupt_Input\ST_Components and \Dose	2.4.09.02.0A Animal farms and fisheries	This FEP is dispositioned in the TSPA Volcanic Eruption Modeling Case through BDCFs for the volcanic ash exposure scenarios. For the volcanic ash scenario, a fish consumption pathway is not included. Annual doses are calculated in the TSPA as the product of radionuclide concentration in soil contaminated by radionuclides in volcanic tephra, the BDCF components, and the mass loading time decrease function. For the volcanic ash exposure scenario, three BDCF components are provided to the TSPA-LA Model that account for various RMEI exposure pathways.	10 CFR 63.311	DLL
		2.4.10.00.0A Urban and industrial land and water use	This FEP is dispositioned in the TSPA Volcanic Eruption Modeling Case through BDCFs for the volcanic ash exposure scenarios. Annual doses are calculated in the TSPA as the product of radionuclide concentration in soil contaminated by radionuclides volcanic tephra and the BDCF components. For the volcanic ash exposure scenario, three BDCF components are provided to the TSPA-LA Model that account for various RMEI exposure pathways	10 CFR 63.311	DLL

Table I-2. Model Implementation for Included Features, Events, and Processes (Continued)

Submodel implemented in the TSPA-LA Model and Section Number	Path in GoldSim Model File	FEPs Included in the Submodel	TSPA Inclusion Explanation	Performance Assessment Standard[a]	TSPA-LA Model Implementation
Volcanic Ash Exposure Submodel 6.5.2.1.4 (Continued)	The Volcanic Eruption model is a separate GoldSim file: vE1.004_GS_9.60.100.gsm Epistemic: \Model_Uncertainties\EU\Biosphere_Uncertainty Aleatory: \Model_Uncertainties\AU Biosphere: \Eruptive_Model\Igneous_Erupt_Input\ST_Components and \Dose	3.2.10.00.0A Atmospheric transport of contaminants	This FEP is dispositioned in the TSPA Volcanic Eruption Modeling Case through BDCFs for the volcanic ash exposure scenario. Annual doses are calculated in the TSPA as the product of radionuclide concentration in soil contaminated by radionuclides in volcanic tephra, the BDCF components, and the mass loading time decrease function. For the volcanic ash exposure scenario, three BDCF components are provided to the TSPA-LA Model that account for various RMEI exposure pathways: exposure to sources external to the body, (ingestion, and inhalation of radon decay products); and the short-term and long-term inhalation components	10 CFR 63.311	DLL
		3.3.01.00.0A Contaminated drinking water, foodstuffs and drugs	This FEP is dispositioned in the TSPA Volcanic Eruption Modeling Case through BDCFs for the volcanic ash exposure scenario. Annual doses are calculated in the TSPA as the product of radionuclide concentration in soil contaminated by radionuclides in volcanic tephra, the BDCF components, and the mass loading time decrease function. For the volcanic ash exposure scenario, three BDCF components are provided to the TSPA-LA Model that account for various RMEI exposure pathways.	10 CFR 63.311	DLL

Table I-2. Model Implementation for Included Features, Events, and Processes (Continued)

Submodel implemented in the TSPA-LA Model and Section Number	Path in GoldSim Model File	FEPs Included in the Submodel	TSPA Inclusion Explanation	Performance Assessment Standard[a]	TSPA-LA Model Implementation
Volcanic Ash Exposure Submodel 6.5.2.1.4 (Continued)	The Volcanic Eruption model is a separate GoldSim file: vE1.004_GS_9.60.100.gsm Epistemic: \Model_Uncertainties\EU\Biosphere_Uncertainty Aleatory: \Model_Uncertainties\AU Biosphere: \Eruptive_Model\Igneous_Erupt_Input\ST_Components and \Dose	3.3.02.01.0A Plant uptake	This FEP is dispositioned in the TSPA Volcanic Eruption Modeling Case through BDCFs for the volcanic ash exposure scenario. Annual doses are calculated in the TSPA as the product of radionuclide concentration in soil contaminated by radionuclides in volcanic tephra, the BDCF components, and the mass loading time decrease function. For the volcanic ash exposure scenario, three BDCF components are provided to the TSPA-LA Model that account for various RMEI exposure pathways.	10 CFR 63.311	DLL
		3.3.02.02.0A Animal uptake	This FEP is dispositioned in the TSPA Volcanic Eruption Modeling Case through BDCFs for the volcanic ash exposure scenarios. Annual doses are calculated in the TSPA as the product of radionuclide concentration in soil contaminated by radionuclides in volcanic tephra, the BDCF components, and the mass loading time decrease function. For the volcanic ash exposure scenario, three BDCF components are provided to the TSPA-LA Model that account for various RMEI exposure pathways: short term and long term inhalation, and exposure to sources external to the body.	10 CFR 63.311	DLL

Table I-2. Model Implementation for Included Features, Events, and Processes (Continued)

Submodel implemented in the TSPA-LA Model and Section Number	Path in GoldSim Model File	FEPs Included in the Submodel	TSPA Inclusion Explanation	Performance Assessment Standard[a]	TSPA-LA Model Implementation
Volcanic Ash Exposure Submodel 6.5.2.1.4 (Continued)	The Volcanic Eruption model is a separate GoldSim file: vE1.004_GS_9.60.100.gsm Epistemic: \Model_Uncertainties\EU\Biosphere_Uncertainty Aleatory: \Model_Uncertainties\AU Biosphere: \Eruptive_Model\Igneous_Erupt_Input\ST_Components and \Dose	3.3.03.01.0A Contaminated non-food products and exposure	This FEP is dispositioned in the TSPA Volcanic Eruption Modeling Case through BDCFs for the volcanic ash exposure scenarios. Annual doses are calculated in the TSPA as the product of radionuclide concentration in soil contaminated by radionuclides in volcanic tephra, the BDCF components, and the mass loading time decrease function. For the volcanic ash exposure scenario, three BDCF components are provided to the TSPA-LA Model that account for various RMEI exposure pathways	10 CFR 63.311	DLL
		3.3.04.01.0A Ingestion	This FEP is also dispositioned in the TSPA Volcanic Eruption Modeling Case through BDCFs for the volcanic ash exposure scenario. Annual doses are calculated in the TSPA as the product of radionuclide concentration in soil contaminated by radionuclides in volcanic tephra, the BDCF components, and the mass loading time decrease function. For the volcanic ash exposure scenario, three BDCF components are provided to the TSPA-LA Model that account for various RMEI exposure pathways: exposure to sources external to the body, and short-term and long-term inhalation.	10 CFR 63.311	DLL

Table I-2. Model Implementation for Included Features, Events, and Processes (Continued)

Submodel implemented in the TSPA-LA Model and Section Number	Path in GoldSim Model File	FEPs Included in the Submodel	TSPA Inclusion Explanation	Performance Assessment Standard[a]	TSPA-LA Model Implementation
Volcanic Ash Exposure Submodel 6.5.2.1.4 (Continued)	The Volcanic Eruption model is a separate GoldSim file: vE1.004_GS_9.60.100.gsm Epistemic: \Model_Uncertainties\EU\Biosphere_Uncertainty Aleatory: \Model_Uncertainties\AU Biosphere: \Eruptive_Model\Igneous_Erupt_Input\ST_Components and \Dose	3.3.04.02.0A Inhalation	This FEP is dispositioned in the TSPA Volcanic Eruption Modeling Case through BDCFs for the volcanic ash exposure scenario. Annual doses are calculated in the TSPA as the product of radionuclide concentration in soil contaminated by radionuclides in volcanic tephra, the BDCF components, and the mass loading time decrease function. For the volcanic ash exposure scenario, three BDCF components are provided to the TSPA-LA Model that account for various RMEI exposure pathways: exposure to sources external to the body, ingestion, and inhalation of radon decay products; and the short-term and long-term inhalation components account for the remaining two.	10 CFR 63.311	DLL
		3.3.04.03.0A External exposure	This FEP is dispositioned in the TSPA Volcanic Eruption Modeling Case through BDCFs for the volcanic ash exposure scenarios. Annual doses are calculated in the TSPA as the product of radionuclide concentration in soil contaminated by radionuclides in volcanic tephra, the BDCF components, and the mass loading time decrease function. For the volcanic ash exposure scenario, three BDCF components are provided to the TSPA-LA Model that account for various RMEI exposure pathways, including external exposure.	10 CFR 63.311	DLL

Table I-2. Model Implementation for Included Features, Events, and Processes (Continued)

Submodel implemented in the TSPA-LA Model and Section Number	Path in GoldSim Model File	FEPs Included in the Submodel	TSPA Inclusion Explanation	Performance Assessment Standard[a]	TSPA-LA Model Implementation
Volcanic Ash Exposure Submodel 6.5.2.1.4 (Continued)	The Volcanic Eruption model is a separate GoldSim file: vE1.004_GS_9.60.100.gsm Epistemic: \Model_Uncertainties\EU\Biosphere_Uncertainty Aleatory: \Model_Uncertainties\AU Biosphere: \Eruptive_Model\Igneous_Erupt_Input\ST_Components and \Dose	3.3.05.01.0A Radiation doses	This FEP is dispositioned in the TSPA Volcanic Eruption Modeling Case through BDCFs for the volcanic ash exposure scenario. Because variation in radionuclide concentrations in deposited and redistributed volcanic tephra is not part of the biosphere model, BDCFs are calculated based on a unit radionuclide concentration in the soil, depending on the exposure pathway. The TSPA-LA Model calculates annual radiation dose as a product of the time-dependent source terms, the source-independent BDCFs, and the mass loading time decay function. For the volcanic ash exposure scenario, three BDCF components are provided to the TSPA-LA Model: exposure to sources external to the body, (ingestion, and inhalation of radon decay products) and the short-term and long-term inhalation of airborne particulates.	10 CFR 63.311	DLL
		3.3.08.00.0A Radon and radon decay product exposure	Radon (^{222}Rn) is a decay product of one of the primary radionuclides considered in the TSPA. Human exposure to radon and radon decay products occurs through inhalation. Concentrations of radon and radon decay products are calculated in the air submodels for the volcanic ash exposure scenario. For the volcanic ash exposure scenario, three BDCF components are provided to the TSPA model that account for various RMEI exposure pathways, including inhalation of radon and its decay products	10 CFR 63.311	DLL

Table I-2. Model Implementation for Included Features, Events, and Processes (Continued)

Submodel implemented in the TSPA-LA Model and Section Number	Path in GoldSim Model File	FEPs Included in the Submodel	TSPA Inclusion Explanation	Performance Assessment Standard[a]	TSPA-LA Model Implementation
Ground Motion Damage Submodel 6.6.1.1.1	Epistemic: \Input_Params_Epistemic\Epistemic_Params_Events\Epistemic_Params_Seismic Aleatory: \Input_Params_Aleatory\Aleatory_Params_Events\Input_Params_Seismic_Uncert \Input_Params_Aleatory\Aleatory_Params_Events\Input_Params_Seismic_FD_Uncert EBS: \Time_Zero\EBS_PS_Loop\Static_Calcs_PS_Loop\Static_Calcs_Events\Seismic_Fault_Displacement \Global_Inputs_and_Calcs\Global_Events\Seismic_Scenario	1.2.03.02.0A Seismic ground motion damages EBS components	Structural calculations were used to simulate the response of the DS and WP to vibratory ground motion. These calculations utilize a three-dimensional, dynamic structural analysis model that incorporates the details of the EBS design. Ground motion time histories input into the calculations represent postclosure hazard levels at the emplacement depth. The potential for structural damage and for separation of the DSs is examined. The potential damage to the WP due to ground motion-induced interactions of the WPs, the pallet, and the DS are examined. Surface area damage is determined for input to the abstraction of seismic consequence. Acceleration and potential structural failure of fuel cladding induced by the ground motions is also determined. Results of these studies are used in creating abstractions for TSPA	10 CFR 63.311 10 CFR 63.331	GSM

Table I-2. Model Implementation for Included Features, Events, and Processes (Continued)

Submodel implemented in the TSPA-LA Model and Section Number	Path in GoldSim Model File	FEPs Included in the Submodel	TSPA Inclusion Explanation	Performance Assessment Standard[a]	TSPA-LA Model Implementation
Ground Motion Damage Submodel 6.6.1.1.1 (Continued)	Epistemic: \Input_Params_Epistemic\Epistemic_Params_Events\Epistemic_Params_Seismic Aleatory: \Input_Params_Aleatory\Aleatory_Params_Events\Input_Params_Seismic_Uncert \Input_Params_Aleatory\Aleatory_Params_Events\Input_Params_Seismic_FD_Uncert EBS: \Time_Zero\EBS_PS_Loop\Static_Calcs_PS_Loop\Static_Calcs_Events\Seismic_Fault_Displacement \Global_Inputs_and_Calcs\Global_Events\Seismic_Scenario	1.2.03.02.0C Seismic-induced drift collapse damages EBS components	Drift collapse as a function of seismic shaking is the only mechanism in the TSPA-LA Model for rockfall and DS loading. Abstraction damage models for rock loading of DSs and WPs are provided by the Seismic Consequence Abstraction Model. The loading of the DS and its response to time-dependent drift degradation is represented in the TSPA-LA Model by a DS damage abstraction submodel. If the DS has corroded or collapsed rockfall may also load the WP. The loading of the DS and its response to time-dependent drift degradation is represented in the TSPA-LA Model by a WP damage abstraction submodel.	10 CFR 63.311 10 CFR 63.331	GSM

Table I-2. Model Implementation for Included Features, Events, and Processes (Continued)

Submodel implemented in the TSPA-LA Model and Section Number	Path in GoldSim Model File	FEPs Included in the Submodel	TSPA Inclusion Explanation	Performance Assessment Standard[a]	TSPA-LA Model Implementation
Ground Motion Damage Submodel 6.6.1.1.1 (Continued)	Epistemic: \Input_Params_Epistemic\Epistemic_Params_Events\Epistemic_Params_Seismic Aleatory: \Input_Params_Aleatory\Aleatory_Params_Events\Input_Params_Seismic_Uncert \Input_Params_Aleatory\Aleatory_Params_Events\Input_Params_Seismic_FD_Uncert EBS: \Time_Zero\EBS_PS_Loop\Static_Calcs_PS_Loop\Static_Calcs_Events\Seismic_Fault_Displacement \Global_Inputs_and_Calcs\Global_Events\Seismic_Scenario	1.2.03.03.0A Seismicity associated with igneous activity	Seismicity associated with igneous activity was considered as part of the probabilistic seismic hazard analysis for Yucca Mountain. The seismic source characterization expert teams either included specific seismic sources for seismicity associated with igneous activity or determined that such seismicity was included in their areal source zones representing background seismicity not associated with specific faults. Thus, seismicity associated with igneous activity is included in the ground motion hazard results that form the basis for developing seismic inputs for postclosure analyses.	10 CFR 63.311 10 CFR 63.331	MA
		2.1.06.05.0C Chemical degradation of emplacement pallet	A thickness reduction equal to the WP outer barrier thickness reduction is also applied to the Alloy 22 plates of the emplacement pallet for each analysis in the Seismic Consequence Abstraction. While no parameter was directly sent to TSPA, the seismic damage abstraction has an implicit treatment of chemical degradation of the pallet, that in effect reduces the pallet thickness and hence stiffness at a rate equal to the WP thinning. The thinning of the WP emplacement pallet due to chemical degradation is included in seismic analyses, however, the affect of the emplacement pallet on radionuclide release is not considered.	10 CFR 63.311 10 CFR 63.331	MA
		2.1.03.11.0A Physical form of waste package and drip shield	The seismic consequence abstraction takes into account that when a ground motion event occurs, the drip shield above the affected waste packages is assumed to be ruptured. The releases of radionuclides are mainly due to the failure of the drip shield and the open breach area in the waste package.	10 CFR 63.311 10 CFR 63.331	GSM
Fault Displacement Damage Submodel 6.6.1.1.3		1.2.02.03.0A Fault displacement damages EBS components	An analysis is performed that examines how fault displacement may contribute to mechanical disruption of the EBS. In this analysis, estimates of very low probability fault displacement are compared with the dimensions of the EBS features. Potential damage to the EBS is estimated, and the results are used to create an abstraction for TSPA.	10 CFR 63.311 10 CFR 63.331	GSM

Table I-2. Model Implementation for Included Features, Events, and Processes (Continued)

Submodel implemented in the TSPA-LA Model and Section Number	Path in GoldSim Model File	FEPs Included in the Submodel	TSPA Inclusion Explanation	Performance Assessment Standard[a]	TSPA-LA Model Implementation
Fault Displacement Damage Submodel 6.6.1.1.3		2.1.03.11.0A Physical form of waste package and drip shield	The seismic consequence abstraction takes into account how fault displacement may contribute to mechanical disruption of the WP and DS. In this analysis, estimates of very low probability fault displacement are compared with the dimensions of the EBS features. Potential damage to the EBS is estimated, and the results are used to create an abstraction for TSPA.	10 CFR 63.311 10 CFR 63.331	DLL
Drift Seepage Submodel Modifications for Seismic Disruption 6.6.2.1	Epistemic: \Input_Params_Epistemic\Epistemic_Params_Events\Epistemic_Params_Seismic Aleatory: \Input_Params_Aleatory\Aleatory_Params_Events\Input_Params_Seismic_Uncert \Input_Params_Aleatory\Aleatory_Params_Events\Input_Params_Seismic_FD_Uncert EBS: \Time_Zero\EBS_PS_Loop\Static_Calcs_PS_Loop\Static_Calcs_Events\Seismic_Fault_Displacement \Global_Inputs_and_Calcs\Global_Ev	1.2.03.02.0D Seismic-induced drift collapse alters in-drift thermohydrology	Postclosure ground motion in lithophysal rock could result in substantial or complete drift collapse affecting the hydrologic and thermal environment in the EBS. The potential for drift collapse and its thermal-hydrologic consequences are addressed in by the Multiscale Thermohydrologic Model implemented in TSPA. Changes in seepage behavior caused by seismically induced drift collapse are included in calculations for the lithophysal host rock only. A seepage abstraction is used to represent the range from intact (uncollapsed) to fully collapsed openings. The approach interpolates linearly between the uncollapsed and collapsed abstractions using rockfall volume as modeled in seismic consequence abstraction to define the extent of collapse. Both MSTHM and seismic consequence abstraction are implemented in the TSPA-LA model.	10 CFR 63.311 10 CFR 63.331	DLL
		2.1.08.02.0A Enhanced influx at the repository	The impact of an underground opening on the unsaturated flow field (including capillary barrier effect and the related flow diversion around the drifts) and its relevance for seepage is explicitly captured in the seepage calibration model and seepage model for performance assessment, which provide the basis for the drift seepage abstraction implementation in the TSPA-LA Model The drift seepage abstraction provides a seepage abstraction look-up table for enhanced seepage due to drift collapse as a result of seismic ground motions.	10 CFR 63.311 10 CFR 63.331	DLL

Table I-2. Model Implementation for Included Features, Events, and Processes (Continued)

Submodel implemented in the TSPA-LA Model and Section Number	Path in GoldSim Model File	FEPs Included in the Submodel	TSPA Inclusion Explanation	Performance Assessment Standard[a]	TSPA-LA Model Implementation
EBS TH Environment Submodel Modifications for Seismic Disruption 6.6.2.2	ents\Seismic_Scenario	1.2.03.02.0D Seismic-induced drift collapse alters in-drift thermohydrology	Drift collapse can occur due to seismic-induced large peak ground velocity. Drift collapse can act like backfill and alter the in-drift thermal-hydrologic conditions. This effect is captured explicitly by MSTHM process model simulations. These simulations are used to develop TH abstractions implemented in the TSPA for the Seismic Scenario Class.	10 CFR 63.311 10 CFR 63.331	GSM
Human Intrusion Submodel 6.7	Aleatory: \Input_Params_Aleatory\Aleatory_Params_Events\Aleatory_Params_HI EBS: \Time_Zero\EBS_PS_Loop\Static_Calcs_PS_Loop\Static_Calcs_Events\Human_Intrusion_Events \Global_Inputs_and_Calcs\Global_Events\Human_Intrusion Other: \TSPA_Model\UZ_Transport\UZ_Transport_Calculations\HI_Borehole_Transport	1.4.04.00.0A Drilling activities (human intrusion)	These FEPs are included in a stylized TSPA assessment that is consistent with the requirements described for the human intrusion stylized scenario defined in 10 CFR 63.322 [DIRS 180319] and proposed rule 10 CFR 63.321 [DIRS 178394]. This assessment addresses drilling activities, inadvertent human intrusion and effects of drilling.	10 CFR 63.321	GSM
		1.4.04.01.0A Effects of drilling intrusion		10 CFR 63.321	GSM/MA/ DLL
		1.4.02.02.0A Inadvertent human intrusion		10 CFR 63.321	GSM/MA/ DLL

Table I-2. Model Implementation for Included Features, Events, and Processes (Continued)

Submodel implemented in the TSPA-LA Model and Section Number	Path in GoldSim Model File	FEPs Included in the Submodel	TSPA Inclusion Explanation	Performance Assessment Standard[a]	TSPA-LA Model Implementation
Human Intrusion Submodel 6.7	Aleatory: \Input_Params_Aleatory\Aleatory_Params_Events\Aleatory_Params_HI EBS: \Time_Zero\EBS_PS_Loop\Static_Calcs_PS_Loop\Static_Calcs_Events\Human_Intrusion_Events \Global_Inputs_and_Calcs\Global_Events\Human_Intrusion Other: \TSPA_Model\UZ_Transport\UZ_Transport_Calculations\HI_Borehole_Transport	2.1.03.01.0B General corrosion of drip shields	In the case of human intrusion, the rate of general corrosion is used to determine the earliest time at which intrusion would not be recognized by the drillers. The TSPA-LA Model for general corrosion is the only DS corrosion mechanism modeled. This process is modeled as being independent of temperature and relative humidity and is initiated at the time of repository closure. Because of the low corrosion rate of titanium alloy used for the DSs, the initial breaches of the DSs are not expected to occur until well after 10,000 years.	10 CFR 63.321	GSM/MA/ DLL
		2.1.03.11.0A Physical form of waste package and drip shield	The rate of general corrosion is used to determine the earliest time at which human intrusion would not be recognized by the drillers. The TSPA-LA model for general corrosion is the only drip shield corrosion mechanism modeled. This process is modeled independent of temperature and relative humidity, but is dependent on the specific forms of the drip shields, waste packages, and internal waste containers that are proposed for the Yucca Mountain repository.	10 CFR 63.321	GSM/MA/ DLL
TSPA FEPs	\Model	0.1.02.00.0A Timescales of concern	The simulation durations are set to 20,000 years and 1,000,000 years to cover the regulatory time periods of 10,000 years and 1,000,000 years and to evaluate uncertainties in results after 10,000 years and before 20,000 years.	10 CFR 63.311 10 CFR 63.331 10 CFR 63.321	GSM/MA/ DLL
		0.1.03.00.0A Spatial domain of concern	The spatial domain encompassed and evaluated explicitly in the TSPA and GoldSim model file extends from the land surface through the UZ, through the repository, into the SZ, and laterally away from the repository to the location of the RMEI and to a representative volume of water in the accessible environment	10 CFR 63.311 10 CFR 63.331 10 CFR 63.321	GSM/MA/ DLL

Table I-2. Model Implementation for Included Features, Events, and Processes (Continued)

Submodel implemented in the TSPA-LA Model and Section Number	Path in GoldSim Model File	FEPs Included in the Submodel	TSPA Inclusion Explanation	Performance Assessment Standard[a]	TSPA-LA Model Implementation
TSPA FEPs (continued)	\Model	0.1.09.00.0A Regulatory requirements and exclusions	This is intrinsically included throughout the TSPA-LA Model because these regulations provided requirements for model development. One example of how this FEP was implemented is comparing the mean biosphere dose with the established regulatory limit.	10 CFR 63.311 10 CFR 63.331 10 CFR 63.321	GSM/MA/ DLL
		0.1.10.00.0A Model and data issues	Model and data requirements are addressed specifically at 10 CFR 63.114 [DIRS 178394] and are included in the GoldSim model file. This FEP is very broad in nature and also includes information covered in Sections 5, 6, 7, and 8 of this document.	10 CFR 63.311 10 CFR 63.331 10 CFR 63.321	GSM/MA/ DLL
		1.1.07.00.0A Repository design	This FEP is implemented in many locations in the TSPA-LA Model. Model components reflect the physical dimensions, material characteristics, and evolution of the in-drift environment, all of which stem directly from design considerations. The data element Drift_Diameter is one example of repository design implementation. The dimensions of the invert are another example of the design implementation.	10 CFR 63.311 10 CFR 63.331 10 CFR 63.321	GSM/MA/ DLL
		1.1.13.00.0A Retrievability	Retrievability is implicitly addressed in the TSPA-LA Model through the implementation of the repository design (FEP 1.1.07.00.0A). Particularly applicable to this FEP are the model components for the EBS, WP and DS degradation, waste form degradation and mobilization, and EBS flow and transport. Retrievability is thereby implicitly included in the TSPA.	10 CFR 63.311 10 CFR 63.331 10 CFR 63.321	GSM/MA/ DLL
		1.1.09.00.0A Schedule and planning	Schedule and planning is one of several initial conditions set for the TSPA-LA Model. For example, the waste emplacement schedule and closure of the repository are tied to the TSPA via the assumed post-emplacement ventilation duration and the radiation decay and thermal decay that takes place during preclosure and is accounted for in radionuclide inventories and thermal-hydrological inputs that are provided to TSPA.	10 CFR 63.311 10 CFR 63.331 10 CFR 63.321	GSM/MA/ DLL

Table I-2. Model Implementation for Included Features, Events, and Processes (Continued)

Submodel implemented in the TSPA-LA Model and Section Number	Path in GoldSim Model File	FEPs Included in the Submodel	TSPA Inclusion Explanation	Performance Assessment Standard[a]	TSPA-LA Model Implementation
TSPA FEPs (continued)	\Model	2.1.01.04.0A Repository-scale spatial heterogeneity of emplaced waste	Waste form heterogeneity is addressed through several approaches: (1) the waste form physical, chemical, and radiological properties are addressed through the degradation models for the CSNF waste form, the DSNF waste form, and the HLW form; (2) WP radionuclide inventory heterogeneity is addressed through uncertainty parameters; and (3) effects of WP heterogeneity as a result of differing waste form contents is addressed in the In-Package Chemistry submodel.	10 CFR 63.311 10 CFR 63.331 10 CFR 63.321	GSM

[a] 10 CFR 63.311 Individual Protection (70 FR 53313 [DIRS 178394])

10 CFR 63.331 Groundwater Protection (10 CFR 63 [DIRS 180319])

10 CFR 63.321 Human Intrusion (70 FR 53313 [DIRS 178394])